JOANNA MELISSA RIBEIRO GONÇALVES

EMERGING

Environmental **M**ixtures of **E**merging Contaminants **R**epercussions on **G**onads and **I**mpact on **N**ext **G**enerations

UNIVERSITY OF ALGARVE
FACULTY OF SCIENCE AND TECHNOLOGY

2024

JOANNA MELISSA RIBEIRO GONÇALVES

EMERGING

Environmental **M**ixtures of **E**merging Contaminants **R**epercussions on **G**onads and **I**mpact on **N**ext **G**enerations

PhD in Marine, Earth, and Environmental Sciences
Branch of Environmental Sciences and Technologies

This work was developed under the supervision of
Full Professor Doctor Maria João Bebianno.

UNIVERSITY OF ALGARVE
FACULTY OF SCIENCE AND TECHNOLOGY

2024

EMERGING - **E**nvironmental **M**ixtures of **E**merging Contaminants **R**epercussions on **G**onads and **I**mpact on **N**ext **G**enerations

Declaração de autoria de trabalho

Declaro ser o autor deste trabalho, que é original e inédito. Autores e trabalhos consultados estão devidamente citados no texto e constam da listagem de referências incluída.

This PhD was supported by:

- The Foundation of Science and Technology (FCT) through the PhD grant (UI/ BD/150758/2020)
- FCT through the project EMERGEMIX ([ALG-01-0145-FEDER-030922] PTDC/BIA-BMA/30922/ 2017) and RESPONSE (FCT JPIOCEANS/0005/2020)

- The Centre for Marine and Environmental Research (CIMA) through the funds attributed to the Centre by FCT (UI/MAR/00350/2020).

- The Associate Laboratory ARNET through the funds granted by FCT under the project (LA/P/0069/2020)

ACKNOWLEDGEMENTS

First and foremost, I'd like to thank CIMA (Centro de Investigação Marinha e Ambiental) for selecting me for one of their PhD scholarships and for all the support the whole faculty and institution have given me during the past four years.

I would like to extend my heartfelt thanks to my supervisor, Professor Dr. Maria João Bebianno, for her invaluable advice, support, and wisdom over the past six years of my life. Thank you for always being there professionally and personally when I needed you. I am grateful for all the motivation, scientific guidance, and encouragement throughout these years. I could not have chosen a better mentor!

I would like to thank all the master's students I supervised—Clara Beckmann, Rachel Acker, and Emma Ventura—for their invaluable assistance in the lab and for the support they offered me while I assisted them with their master's theses.

I would also like to thank my lab group, particularly Tainá Fonseca, Juliano Vilke, and Maria Costa, for their companionship, invaluable advice, and patience when I felt stressed. Thank you to Vania Sousa for teaching and helping me characterise the nanoparticles, and to Catarina Sousa, CIMA's secretary, for all the help and for going out of your way to help solve situations when problems popped up.

Thank you to all my friends for distracting me when I needed a break and cheering me on; you know who you are!

The next people I'd like to thank mean the world to me! I extend my heartfelt thanks to my parents, Celeste and Victor Gonçalves, for always supporting me, being there for me, loving me unconditionally, and helping me reach where I am today. Without you, I wouldn't be the person I am now or have achieved all I have. Thank you for supporting me every step of the way!

To my brother, Tiago Gonçalves, for helping me with all computer-related difficulties and sharing your computer genius! Without you, I don't think I would have been able to sort out some of the computer hiccups I encountered throughout the four years (in the lab and out).

Thank you to my life partner, Antero Martins, for navigating all the ups and downs, uplifting me and helping me believe in myself. Thank you for always cheering me on and supporting me every step of the way.

Lastly, I would like to thank my daughter, Ellie Gonçalves Martins. I spent the last two years of my PhD pregnant and relishing life with you. You have bestowed upon me a strength I never realised I possessed, and I dedicate this thesis to you. You are my everything, and I hope to provide you with all that my parents have given me and more.

GENERAL ABSTRACT

Contaminants of emerging concern (CECs) represent an increasing threat to marine ecosystems, underscoring the need to comprehend their interactions and toxicity. Among these, nanoplastics (NPs), particularly secondary NPs, are prevalent and pose ecological risks. Other contaminants, such as 5-Fluorouracil (5-FU), a cytostatic drug resulting from wastewater discharge, and silver nanoparticles (nAg), further exacerbate ocean pollution. Mussels, which reproduce in the water column, expose their gametes to these contaminants, making it essential to evaluate their impact on reproductive success and ecological balance. This thesis evaluates the toxic effects of polystyrene (PS) NPs (50 nm; 10 µg/L), 5-FU (10 ng/L), and nAg (20 nm; 10 µg/L) individually and in mixtures in *Mytilus galloprovincialis*, with a focus on reproductive organs and sex-specific differences. It employs genotoxicity, neurotoxicity, cytotoxicity, antioxidant enzymes, lipid peroxidation, proteomic analyses, and a weight-of-evidence approach to assess hazard levels and synergistic and antagonistic interaction effects. PS-NP impacts on gametes and embryo-larval development were also examined. PS-NP interactions with abiotic and biotic factors influence their toxicity, affecting marine organisms at multiple levels. Mussels ingest PS-NPs, leading to tissue-specific accumulation, oxidative stress, neurotoxicity, and reproductive impairments, particularly in females. Disruptions in gonadal protein expression impact gametes and reproductive success, reducing oocyte and spermatozoa counts while compromising oocyte integrity. Larval development suffers, especially when gametes are exposed pre-fertilisation, resulting in smaller, malformed larvae with greater contaminant accumulation. 5-FU induces genotoxicity and oxidative stress, and its combination with PS-NPs and nAg leads to synergistic toxicity. The mixture of PS-NPs and 5-FU is the most harmful. Contaminant mixtures exacerbate reproductive harm and threaten biodiversity. Understanding these combined effects is essential for environmental management, as their interactions amplify toxicity and long-term ecological risks.

RESUMO GERAL

Os contaminantes emergentes (CECs) representam uma nova ameaça ao meio marinho, tornando essencial compreender as interações e a potencial toxicidade das misturas de CECs quando entram no oceano. Os nanoplásticos, especialmente os nanoplásticos secundários, são abundantes no ambiente marinho e apresentam riscos ecológicos significativos. Para além dos nanoplásticos, contaminantes emergentes como o 5-Fluorouracilo (5-FU), um fármaco citostático, que entra nos ecossistemas marinhos devido ao tratamento inadequado de águas residuais, assim como as nanopartículas de prata (nAg) são uma preocupação para a saúde do oceano. Os mexilhões reproduzem-se na coluna de água e, caso a gametogénese seja bem-sucedida, os gametas ficam expostos aos contaminantes presentes no ambiente marinho. Compreender as repercussões que estes contaminantes podem ter nos gametas e no desenvolvimento embrionário-larval é fundamental, uma vez que o sucesso reprodutivo garante gerações futuras viáveis, assegurando assim o equilíbrio ecológico e a biodiversidade.

As interações dos PS-NPs com fatores abióticos e bióticos influenciam as suas propriedades e toxicidade, afetando os organismos marinhos em vários níveis tróficos. Consequentemente, esta tese avalia os efeitos tóxicos dos nanoplásticos de poliestireno (50 nm; 10 µg/L), 5-FU (10 ng/L) e nAg (20 nm; 10 µg/L), tanto individualmente como em misturas, no mexilhão do Mediterrâneo *Mytilus galloprovincialis*, com foco nos efeitos da acumulação nas brânquias, glândula digestiva, e no orgão reprodutivo bem como diferenças entre machos e fêmeas. Foram analisados vários efeitos biológicos como genotoxicidade, neurotoxicidade, citotoxicidade, enzimas antioxidantes e peroxidação lipídica e proteómica. Além disso, a caracterização das nanopartículas e a ingestão de PS-NPs também foram avaliadas. Foi, também, utilizada uma abordagem de Weight of Evidence para avaliar o nível de risco, e calcularam-se os efeitos sinérgicos e antagónicos. Os efeitos dos PS-NPs nos gâmetas e no desenvolvimento embrionário-larval do mexilhão também foram avaliados.

M. galloprovincialis ingere PS-NPs, resultando em acumulação específica em determinados tecidos, sendo as gonadas as mais prejudicadas, e como resultado leva ao stress oxidativo, neurotoxicidade e impactos na reprodução, sobretudo nas fêmeas. As alterações na expressão proteica nas gónadas masculinas e femininas afetam os gametas e o sucesso reprodutivo. A exposição a PS-NPs resultou numa redução significativa no número de oócitos e espermatozoides, comprometendo a integridade dos oócitos. O desenvolvimento larvar foi negativamente afetado, especialmente quando os gametas foram expostos antes da fertilização,

resultando em larvas menores e malformadas, com maior acumulação de contaminantes nos gametas do que nos embriões.

O 5-FU induz genotoxicidade e stress oxidativo nos mexilhões e, quando combinado com PS-NPs e nAg, ocorrem efeitos tóxicos sinergéticos, sendo a mistura de PS-NPs e 5-FU mais prejudicial do que a mistura terciária. A exposição a misturas destes contaminantes induz danos reprodutivos, comprometendo a gametogénese e reduzindo o sucesso da fertilização, ameaçando assim a dinâmica populacional e a biodiversidade. Os efeitos combinados dos contaminantes emergentes requerem atenção científica urgente, uma vez que as suas interações amplificam a toxicidade e representam riscos ecológicos a longo prazo. É fundamental aprofundar a investigação sobre os seus mecanismos, especialmente no que diz respeito à saúde reprodutiva e à estabilidade dos ecossistemas, para uma gestão ambiental e decisões políticas mais informadas.

INDEX

FIGURE INDEX

TABLE INDEX

ABBREVIATIONS

5-FU – 5-Fluorouracil

CECs – contaminants of emerging concern

DLB – 1 – fish cell line of *Dicentrarchus labrax*

DNA – deoxyribonucleic acid

dTMP – deoxythymidine monophosphate

EC_{50} – half-maximal effective concentration

FdUMP – fluorodeoxyuridine monophosphate

FdUTP – fluorodeoxyuridine triphosphate

FUTP – fluorouridine triphosphate

HDPE – high-density polyethylene

IARC – International Agency for Research on Cancer

LC_{50} – half-maximal lethal concentration

LDPE – low-density polyethylene

MoA – mode of action

mRNA – messenger ribonucleic acid

nAg – silver nanoparticles

NOM – Natural organic matter

NPs – nanoplastics

OD_{600} – optical density

PAHs – polycyclic aromatic hydrocarbons

PCBs – polychlorinated biphenyls

PE – polyethylene

PET – polyethylene terephthalate

PMMA – poly(methyl methacrylate)

PMMA-COOH – poly(methyl methacrylate) with a carboxyl group attached

POPs – persistent organic pollutants

PP – polypropylene

PS – polystyrene

PS-COOH – polystyrene with a carboxyl group attached

PS-NH_2 – polystyrene with an amide group attached

PS-NPs – polystyrene nanoplastics

PUR – polyurethane

PVC – polyvinyl chloride

RNA – ribonucleic acid

ROS – reactive oxygen species

SAF – 1 – fish cell line of *Sparus aurata*

SW – seawater

UTP – uridine triphosphate

WTTP – wastewater treatment plant

CHAPTER I

General Introduction

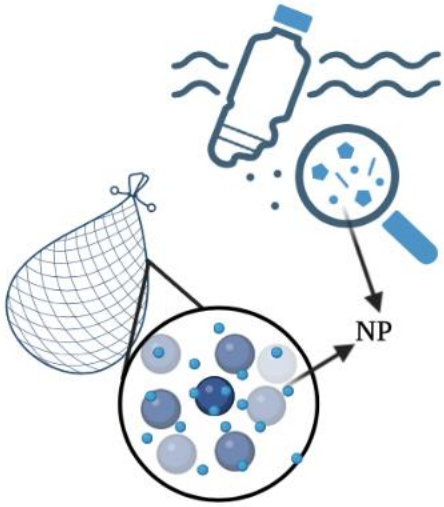

Mytilus galloprovincialis

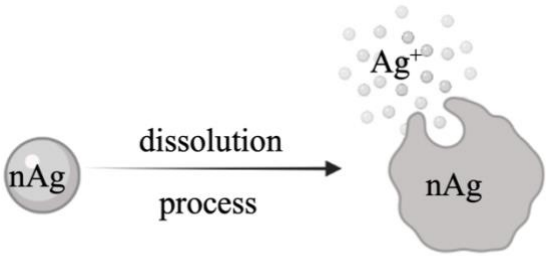

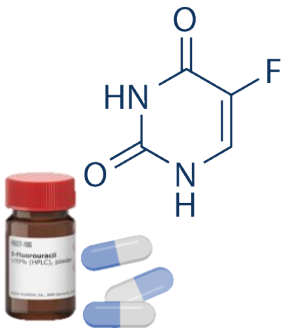

This chapter has been published in:

- Gonçalves, J. M., & Bebianno, M. J. (2021). Nanoplastics impact on marine biota: A review. *Environmental Pollution*, *273*. https://doi.org/10.1016/j.envpol.2021.116426

- Alkimin, G. D. de, Gonçalves, J. M., Nathan, J., & Bebianno, M. J. (2022). Impact of Micro and Nanoplastics in the Marine Environment. In *Assessing the Effects of Emerging Plastics on the Environment and Public Health* (pp. 172–225). https://doi.org/10.4018/978-1-7998-9723-1.ch009

And submitted to:

- Gonçalves, J. M., & Bebianno, M.J. (2025) 5-Fluorouracil's effects on aquatic organisms: a review. *Impacts of Pollutants of Emerging Concern on Ecosystems and Human Health* (Publisher: Elsevier)

1.1. Contaminants of emerging concern

Contaminants of emerging concern (CECs) are a range of chemical compounds (anthropogenic and naturally occurring) that are not routinely monitored in the environment (Larroze et al., 2021). CECs must fall within two criteria: environmental persistence and harmfulness and ecotoxicological effects (Pastorino & Ginebreda, 2021). Polycyclic aromatic hydrocarbons (PAHs), pesticides, metals, environmental oestrogens, (micro)plastics and phthalates, nanoparticles, medications, personal care items, UV filters, flame retardants, and disinfection byproducts are among the CECs (Larroze et al., 2021). Besides other sources, such as waste mismanagement and landfill dumping, wastewater treatment plants (WTTP) are the primary source as they need the correct techniques or strategies for removing CECs, leading to an inevitable release into our Oceans.

1.2. Nanoplastics impact on marine biota: A review

Emerging contaminants, such as nanoplastics, are gaining a vast interest within the scientific community. Most of the plastic debris found in the marine environment originates from land-based sources, and once in the marine environment, plastic can be degraded into smaller fragments. Nanoplastics fall within the definition of other nanoparticles (1 to 100 nm in size) and may be divided into primary or secondary nanoplastics. Primary nanoplastics enter the environment in their original small size associated with specific applications and consumer products, whilst secondary nanoplastics are a consequence of macro/microplastic degradation. The formation of nanoplastics changes the physical-chemical characteristics of the particle; thus, at a nanoscale, it is expected that the nanoparticles' strength, conductivity, and reactivity will differ substantially from macro/micro-sized particles. To date, the toxicity nanoplastics may pursue on marine biota is still scarce.

1.2.1. Plastics: What are nanoplastics?

An ongoing worldwide environmental concern is plastic debris pollution, whereby in 2022, global plastic production reached 400.3 million tons (PlasticsEurope, 2023). In Europe, plastics production almost reached 58.7 million tons, whilst China alone produced 32% of the world’s plastics (Plastics Europe, 2023). Plastics are synthetic organic polymers with high durability, are lightweight, and can easily be moulded into any shape or product (Worm et al., 2017). Plastic chemical stability, persistence and bioaccumulation have caused plastic pollution to become increasingly prominent (Shen et al., 2019; Hu et al., 2020). The wide use of plastic

in a variety of applications increases its release into the marine environment, whereby most of the plastic debris found in the marine environment originates from land-based sources (Bouder & Friot, 2007; Jambeck et al., 2015). Plastics are quite resistant to decomposition. Therefore, sizeable plastic litter will break into meso-plastics (5-40 mm), microplastics (1-5000 μm) (Thompson et al., 2004), and nanoplastics (NPs) (1-100 nm) (Gigault et al., 2018) before decomposing completely. NPs fall within the definition of other nanoparticles (1 to 100 nm in size) (Koelmans et al., 2015; Gigault et al., 2018) and may be divided into primary or secondary NPs. Primary NPs are those that enter the environment in their original small size associated with specific applications and consumer products (e.g., cosmetics, clothing fibres, drug delivery, ink for 3D printers) (Bergami et al., 2016; Canesi et al., 2015; Bessa et al., 2018; Tamminga et al., 2018; Wang et al., 2018), whilst secondary NPs are a consequence of macro/microplastics degradation (Andrady, 2011; Cole et al., 2011). However, Koelmans et al. (2015) establish that the time required to reach nano-sized particles depends on the size of the initial plastic.

NP formation leads to alterations in the physical-chemical characteristics of the particle, surface area and size, wherein, at a nanoscale, the strength, conductivity and reactivity will differ substantially from macro/micro-sized particles (Klaine et al., 2012; Mattsson et al., 2015, 2018). As the size of the plastic particle decreases, biological reactivity, on the other hand, increases, thus being crucial to comprehend the burden of nanoplastic availability and its biological impact on marine biota (Mattsson et al., 2018; Ferreira et al., 2019). The fate, mobility and resilience of NPs are highly dependent on their stability and feasibility in forming aggregates. The NP aggregation mechanism is critical as aggregates sediment or immobilise, whereas dispersed NPs can diffuse, be more mobile, bioavailable, and potentially more harmful (Ramirez et al., 2019). Natural organic matter (NOM), inorganic colloids, weathering, UV-radiation, and biodegradation are all factors that affect the composition, stability, formation of NP aggregates, and the particle's nano-specific properties (Andrady, 2011; Oriekhova & Stoll, 2018; Shen et al., 2019). Weathering, for instance, increases the crystallinity of plastic debris, acquiring carbonyl functionalities inclusive of negative surface charges because of oxidation (Fotopoulou & Karapanagioti, 2012; Rouillon et al., 2016). Likewise, NOM and inorganic colloids lead to the aggregation of NPs (Oriekhova & Stoll, 2018), consequently becoming less bioavailable and less prone to enter biological membranes. Adsorbed NOM convey a negative charge and alters the surface characteristics of NPs by raising their absolute surface potential (Zhang et al., 2009). Nonetheless, high NOM concentrations can reverse the surface charge of NPs, facilitating the stabilisation of NPs (Ramirez et al., 2019). Therefore, the charge

neutralisation of the isoelectric point is a prerequisite for the creation of large aggregates composed of NPs, thus a crucial mechanism for managing environmental nanoplastics identification, as well as incrementing the importance of NPs surface charge neutralisation (Oriekhova & Stoll, 2018).

Herein, another issue to be addressed is plastic polymers with adsorbed toxic compounds such as polycyclic aromatic hydrocarbons (PAHs), persistent organic pollutants (POPs), polychlorinated biphenyls (PCBs) and other chemical constituents (i.e., metals) (Rios et al., 2007; Teuten et al., 2009; Lee et al., 2014; Rochman et al., 2016; Davranche et al., 2019). NP's high surface area favours this sorption by binding chemicals hydrophobically (Liu et al., 2016), which in turn also increases the potential toxicity of the nanoparticle towards marine biota because of the possible release of these sorbates and constituent chemicals. This increases the importance of establishing the mode of action of NPs with sorption of pollutants in the marine environment, how they behave as vectors, and the toxicity they may pursue on marine biota.

Plastic particle toxicity to marine organisms depends on particle size, concentration and exposure period, where the toxicity of NPs is also affected by pollutants, food availability, species and their developmental stage (Kogel et al., 2020). Decreased growth rate, energy and movement, stress, inflammation and malformations are associated with nanoplastic toxicity towards marine biota (Kogel et al., 2020). The smaller the particle size, the more prone marine organisms are to toxicity by these NPs as the surface area increases, and so does the possibility of passing through biological membranes. On the grounds of their nano-size, NPs have an increased ability to pass through cellular boundaries and accumulate within organisms, easily entering the food web and possibly escalating trophic levels up to human beings (Mattsson et al., 2015, 2018; Worm et al., 2017; Peng et al., 2020). The knowledge of NP's effects on marine biota is still scarce. This review's purpose is to gather all information on nanoplastics toxicity available on marine biota to date.

1.2.2. Effects of nanoplastics in marine biota

According to the Plastics Europe Fact sheet (2023), the leading plastic polymers are polypropylene (PP [15.4%]), low-density and high-density polyethylene (LDPE [13.4%] & HDPE [8.7%]), polyvinyl chloride (PVC [9.1%]), polystyrene (PS [5.4%]), polyurethane (PUR [5.3%]) and polyethylene terephthalate (PET [5.0%]). These plastic polymers are employed in many industries, such as electronics, personal health care, food packaging, housing insulation, and medical equipment and devices (PlasticsEurope, 2023).

Though nanoplastics have not yet been quantified in the marine environment, Halle et al. (2017) obtained a nanoplastic portion from the North Atlantic subtropical gyre, wherein PVC, PET, PS and polyethylene (PE) were the plastic polymers present at a nanoscale. Although the quantification of NPs in the marine environment has yet to be explored, Halle et al. (2017) provided evidence for the existence of plastic debris in the nano-fraction in the marine environment. Nevertheless, NPs effect on marine organisms at environmentally relevant concentrations are still being determined due to the lack of quantification of NPs in the marine environment. Moreover, accurately measuring the concentration of NPs is a major challenge as several analytical methods are required for various types of NP polymers as well as for various complex matrices (soil, sediments, turbid waters and tissues) (Halle et al., 2017).

With regards to the evaluation of nanoplastic toxicity in marine biota, a summary of the data available in the literature for the species evaluated to date can be found in Figure 1.2.1. Figure 1.2.1. the crustacean *A. fransiscana* and the mollusc *Mytilus galloprovincialis* are the species most evaluated in the scientific literature on NP exposure. With relation to the groups of marine biotas presented in Figure 1.2.1., a wide array of species from primary producers to primary/secondary consumers have been studied, providing an insight into the effects of NPs at various levels of the marine ecosystem, wherein crustaceans and molluscs, again, are highly used in ecotoxicological assessments of NPs.

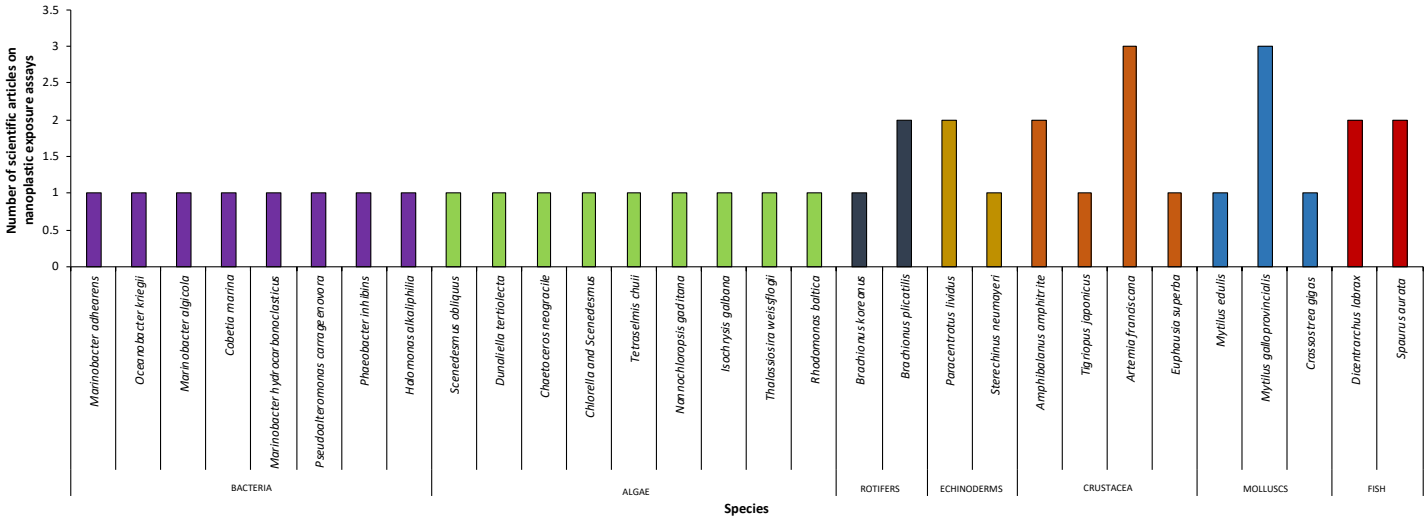

Figure 1.2.1. Type of species evaluated for NP exposure *vs* number of scientific publications

Figure 1.2.2. shows that PS NPs and poly(methyl methacrylate) (PMMA) were the only NPs frequently used to evaluate the effects in biota with either an amide-group or a

carboxyl-group attached, focusing on how negatively charged and positively charged particles toxicity differ, but PS-NH_2 was the type of PS NPs predominately used in comparison with other chemical groups attached to PS or types of nanoplastic polymers.

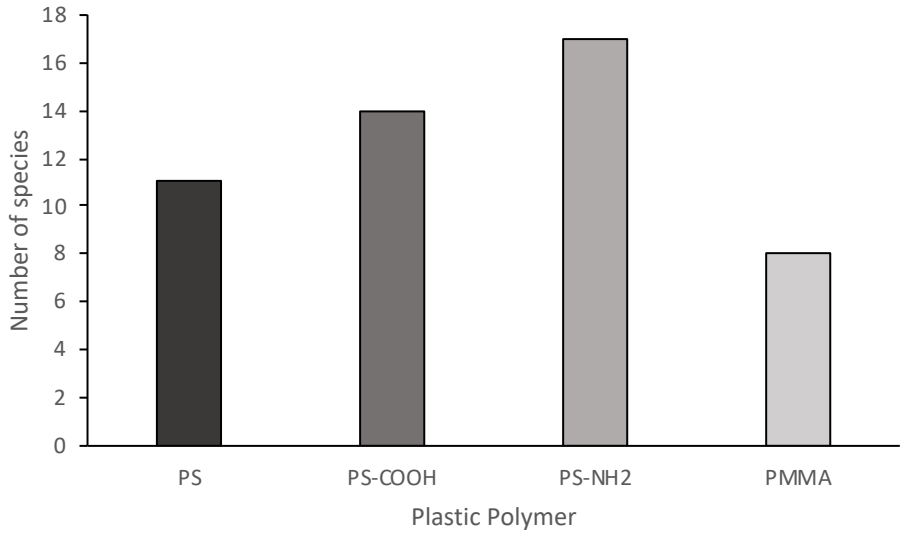

Figure 1.2.2. Type of NP polymers used in ecotoxicological assessments *vs* number of species whereby the effects of NP polymers have been assessed.

Moreover, Figure 1.2.3 presents the percentage of the different nanoparticle sizes for each polymer type. As can be seen in Figure 1.2.3., Different size range percentages were used for each NP polymer, making it difficult to compare the effects. Furthermore, in this review, the effects of nanoplastics on marine biota are characterised below, initiating with bacteria and ascending through the trophic levels. A summary of the effects of nanoplastics evaluated in marine biota to date can be found in Tables 1.2.1. – 1.2.4.

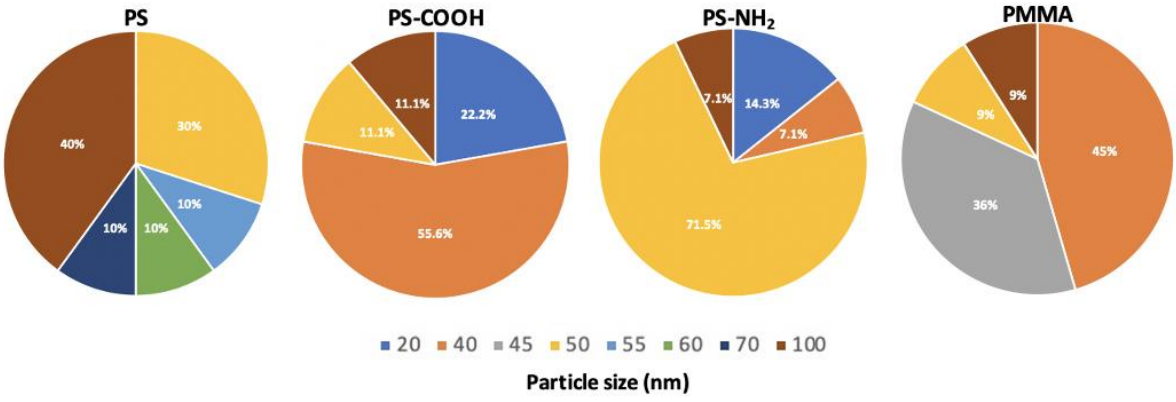

Figure 1.2.3. Percentage of nanoparticle size (nm) for each type of polymer used. PS – polystyrene; PS-COOH – anionic carboxylated polystyrene; PS-NH_2 – cationic amino polystyrene; PMMA – poly(methyl methacrylate).

1.2.2.1. Bacteria

Bacteria are an important component of marine ecosystems, and microbial community alterations due to the presence of environmental contaminants, such as nanoplastics, may have significant effects on biogeochemical cycling as well as other critical ecosystem services (Rotini et al., 2017). Bacteria exposed to several polymers of PS-NPs of different sizes and exposure times are summarised in Tables 1.2.1. – 1.2.3. Recently, Okshevsky et al. (2020) observed that marine bacteria formation of biofilm on PS NPs is impacted by both concentrations and surface functionalisation of PS NPs, suggesting that species interaction along with surface properties and concentrations of plastic NPs are determining factors on how NPs impact marine bacteria biofilm formation. For instance, PS-NH_2 at the highest concentration (200 ppm; 20 nm; 5 days) led to an increase in aggregation in all species studied whilst generating a decrease in both growth rate and optical density (OD_{600}) (Okshevsky et al., 2020). PS-NH_2 also prompted a decrease in the biofilm formation of all bacteria species except for *Oceanobacter kriegii* (Okshevsky et al., 2020). On the other hand, negatively charged NPs (PS-COOH; 200 ppm; 20 nm; 5 days) promoted biofilm formation of some bacteria species (*Marinobacter adherens, Marinobacter algicola, Cobetia marina* and *O. kriegii*), whilst causing a decrease in others (*Phaeobacter inhibins*) (Okshevsky et al., 2020). PS-COOH additionally, increased growth rate, OD_{600} and aggregation of *C. marina*, as well as aggregation of *Pseudoalteromonas carrageenovora*, and a decrease in growth rate and OD_{600} of *O. kriegii* (Okshevsky et al., 2020). Undoubtedly, the surface properties of NPs have contrasting effects on a battery of bacteria, making it imperative to understand the kinetics of toxicity of differently charged nanoplastics. In the marine bacterium *Halomonas alkaliphile*, a bacterium which thrives in high salt concentrations, exposed to cationic amino PS nanoparticles (PS-NH_2; 50 nm) and to PS nanobeads (PS-beads; 55 nm) for 2 hours at different concentrations (20, 80, 160 and 320 μg/mL) affected cell growth, and influenced the chemical composition and ammonia conversion efficiencies at 80 μg/L (Sun et al., 2018). Furthermore, PS-NH_2 induce higher oxidative stress towards bacteria when compared to PS-beads, as these positively charged NPs adhere to the cell surface by the action of electrostatic activity, promoting higher toxicity by these NPs (Sun et al., 2018). Overall, NPs with an amide group have more toxic effects in bacterial communities than NPs with a carboxyl group. After that, the NP toxicity is dependent on functionalised NP surface charge and size.

Table 1.2.1. The effects of polystyrene nanoparticles (PS; ≤100 nm) on marine biota according to size, concentration and exposure period. Abbreviations include: ↑ - increased; ↓ - decreased; ⊥ - inhibited; ⊤ - induced; ▵ - altered; ROS - Reactive oxygen species; LC/EC_x – Lethal or sublethal concentration causing x% of effect.

Phylum	Test species	Particle type	Particle size (nm)	Concentration (µg/mL)	Exposure time (h)	Effects	Reference
Bacteria	*Halomonas alkaliphilia*	PS (beads)	55	20 - 320	2	↓ growth rate; (32% at 320 µg/mL)	Sun et al., 2018
Algae	*Dunaliella tertiolecta*		50	250	72	↓ 45% cell density; ↓ 57% growth rate	Sjollema et al., 2016
Rotifers	*Brachionus koreanus*	PS	50	10	24	↑ mortality; NSW → EC50 = 6.62 ± 0.87 µg/mL; RSW → EC50 = 2.75 ± 0.67 µg/mL	Manfra et al., 2017
Crustacea	*Amphibalanus amphitrite* (II stage of nauplius)		100	0.5 - 10	24 and 48	↑ expression of *clap* and *cstb*; ↑ nº of molts (48h)	Bergami et al., 2017b
	Artemia franciscana (1st instar larvae)			0.001 - 10	24 and 48	⊥ swimming speed (24h); ⊥ swimming speed ↑ post 48h (1 and 10 µg/mL); Ingested and accumulated PS in gut	Gambardella et al., 2017
	Trigriopus japonicus		50	0.125 - 25	96	↓ fecundity; ↑ embryo malformations; ↑ mortality larvae; mortality of parents at 25 µg/mL	Lee et al., 2013
Molluscs	*Mytilus edulis*		30	100, 200 and 300	8	⊤ production of pseudofaeces → ↑ proportionally to concentration	Wegner et al., 2012
	Mytilus galloprovincialis	PS	106 ± 10	0.5 - 50	96	↓ enzymatic activity; ⊥ neurotransmission; ↑oxidative stress; ↑ LPO; ↑ genotoxicity; ▵ gene expression	Brandts et al., 2018b
		PS with carbamazepine (Cbz)		0.5 + 6.3 µg/L of Cbz		↑ genotoxicity; ↓gene expression	
Fish	*Dicentrarchus labrax* (DLB-1)	PS	100	0.001 - 10	24	↓ cell viability (66%) (0.001 µg/mL); minimum viability = 64% (1 µg/mL)	Almeida et al., 2019
	Spaurus aurata (SAF-1)			0.001 - 10	24	↓ cell viability (25%) (0.001 µg/mL); mild effects at higher concentrations	

1.2.2.2. Algae

Algae, as primary producers, are key organisms in sustaining a healthy aquatic environment, as they are the base of food webs, source of oxygen production as well as other nutrients (Mao et al., 2018). The use of algal assays for ecotoxicological assessment of emerging contaminants is mainly linked to their high-sensitivity response, enabling the detection of toxic effects at lower concentrations that are not detectable by other marine organisms (Palumo & Mingazzini, 2011). The ecotoxicological assessment of NPs on marine algae has been investigated in some species (Sjollema et al., 2016; Bergami et al., 2017; Venâncio et al., 2019; González-Fernández et al., 2020; Gomes et al., 2020) (*see* Table 1.2.1. – 1.2.4.). An inhibitory effect on growth and development of the microalgae *Dunaliella tertiolecta* exposed to PS beads (50 nm) at 250 µg/mL for 72 hours (Sjollema et al., 2016) and exposed to PS-NH_2 (50 nm) and PS-COOH (40 nm) for the same time (Bergami et al., 2017) was observed, wherein PS-COOH showed no effects, though PS-COOH were adsorbed on microalgae (Bergami et al., 2017). PS-NH_2, on the other hand, inhibited cell growth (Bergami et al., 2017), and PS beads led to a reduction of 45% in cell density and cellular growth was affected by 57% after exposure (Sjollema et al., 2016). There is a higher affinity of positively charged NPs (PS-NH_2) in comparison to negatively charged NPs (PS-COOH). This may be

due to the electrostatic interactions between the positively charged particles and cellulose, the major component of cell walls in algae, as shown by Bhattacharya et al. (2010) in the freshwater single-celled algae *Chlorella* and multi-celled algae *Scenedesmus* (PS-COOH and PS-NH_2; 20 nm; 0.08 – 0.8 µg/mL; 2 h).

A battery of microalgae, *Tetraselmis chuii*, *Nannochloropsis gaditana*, *Isochrysis galbana*, and the marine diatom *Thalassiosira weissflogii*, after 96 hours of exposure to PMMA (40 nm; 0 – 304.1 mg/L for microalgae and 0 – 293.0 mg/L for marine diatom) had significant impacts on growth rates of all microalgae (Venâncio et al., 2019). *T. chuii* presented the highest median effective concentration (EC_{50} = 132.5 mg/L), whereas *T. weissflogii* showed to be the most sensitive microalgae (EC_{50} = 83.4 mg/L) (Venâncio et al., 2019). In the marine diatom *Chaetoceros neogracile*, after 96 h of exposure to PS-NH2 (50 nm; 0.05 µg/mL and 5 µg/mL), pigment and lipid compositions of diatoms were affected (González-Fernández et al., 2020). Re-adjustment of lipid classes and fatty acids were noteworthy at both growth phases, whereby thylakoid membrane structure and cellular energy reserves of diatoms were observed after PS-NH_2 exposure. Highest concentrations of PS-NH_2 lead to impairment of long-chain fatty acids, particularly at exponential cultures (González-Fernández et al., 2020). In the red microalgae, *Rhodomonas baltica*, exposed to PMMA and PMMA-COOH (50 nm; 0.5 – 100 µg/mL; 72 h), both NPs were found to be toxic, wherein the interaction of NPs with microalgae was particle behaviour dependent (Gomes et al., 2020). A greater effect on cellular and physiological parameters was caused by PMMA exposure. Meanwhile, PMMA-COOH inhibition of microalgae growth was associated with cell cycle and cell viability (Gomes et al., 2020). A decrease in photosynthetic performance was also an outcome of both NPs, increasing the importance of comprehending the toxicity of NPs in algae, as its effects on the photosystems of primary consumers consequently affect the entire ecosystem.

The information below suggests that these particles' nanotoxicity impacts algae's cell wall and pigmentation, possibly inactivating the photosystems and hindering photosynthesis. Nonetheless, the available data shows that PS-NH_2 has more pronounced effects than PS-COOH. Moreover, algae's uptake of nanoplastics depends on particle charge and surface functionalisation. Still, NPs appear to cause physiological distress once within the algal metabolism.

Table 1.2.2. The effects of anionic carboxylated polystyrene nanoparticles (PS-COOH; ≤100 nm) on marine biota according to size, concentration and exposure period. Abbreviations are: ↑ - increased; ↓ - decreased; ⊥ - inhibited; ⊤ - induced; ROS - Reactive oxygen species; LC/EC_x – Lethal or sublethal concentration causing x% of effect; OD_{600} – optical density at 600 nm.

Phylum	Test species	Particle type	Particle size (nm)	Concentration (µg/mL)	Exposure time (h)	Effects	Reference
Bacteria	*Marinobacter adhearens*	PS-COOH	20	0 - 200	5*	< 20 µg/mL → no impact on biofilm formation, growth rate, OD600 200 µg/mL → no impact on living/dead ratio; ↑ biofilm formation	Okshevsky et al., 2020
	Oceanobacter kriegii					< 20 µg/mL → no impact on biofilm formation, growth rate, OD600 200 µg/mL → no impact on living/dead ratio; ↑ biofilm formation; ↓ growth rate; ↓ OD600	
	Cobetia marina					< 20 µg/mL → no impact on biofilm formation, growth rate, OD600 200 µg/mL → no impact on living/dead ratio; ↑ biofilm formation; ↑ growth rate; ↑ OD600; ↑ aggregation	
	Marinobacter algicola					< 20 µg/mL → no impact on biofilm formation, growth rate, OD600 200 µg/mL → no impact on living/dead ratio; ↑ biofilm formation	
	Pseudoalteromonas carrageenovora					< 20 µg/mL → no impact on biofilm formation, growth rate, OD600 200 µg/mL → no impact on living/dead ratio; ↑ aggregation	
	Phaeobacter inhibins					< 20 µg/mL → no impact on biofilm formation, growth rate, OD600 200 µg/mL → no impact on living/dead ratio; ↓ biofilm formation	
	Marinobacter hydrocarbonoclasticus					< 20 µg/mL → no impact on biofilm formation, growth rate, OD600 200 µg/mL → no impact on living/dead ratio	
Algae	*Dunaliella tertiolecta*		50	250	72	no effects	Bergami et al., 2017a
Rotifers	*Brachionus plicatilis*		40	0.5 - 50	24 and 48	no effects on mortality; ↑ gut retention of PS-COOH	Manfra et al., 2017
Echinoderms	*Paracentrotus lividus*			2.5 - 50	6, 24, 48 hpf	Accumulated in embryos; no malformations	Della Torre et al., 2014
	Sterechinus neumayeri			1 and 5	6 and 24	in vitro assay; ↑ antioxidant response; ↑ apoptosis; ↑ phagocytic capacity; ☒ modulation of genes related to external challenges; ↑ inflammatory response	Bergami et al., 2019
Crustacea	*Artemia franciscana*			0.5 - 10	24 and 48	no effects	Bergami et al., 2017b
	- upto instar III nauplius			5 - 100	72 and 14*	Accumulated and retained in gut lumen	Bergami et al., 2016
	Euphausia superba		60	2.5	48	No mortality; active swimming; waterbourne ingestion and egestion	Bergami et al., 2020
Molluscs	*Crassostrea gigas (gametes)*		100	0.1 - 100	1 to 5	↑ cell size; ↑ spermatozoa complexity; ↓ nº spermatozoa; ↑ ROS (dose-response)	González-Fernández et al., 2018
*days ** mins							

1.2.2.3. Rotifers

Rotifers are primary and secondary consumers of high importance and relevance as zooplankton members in several aquatic trophic webs (Wallace et al., 2006), playing an important role in marine ecosystems as they transfer energy from the bottom of the food chain to species higher up (Jeong & Choi, 2019). The small size and sensitivity, as well as ease of culture and exponential growth, are favourable characteristics of rotifers as test models in ecotoxicological studies (Dahms et al., 2011). Data on the effects of NPs on rotifers are scarce (see Tables 1.2.1. – 1.2.4.). The rotifer *Brachionus plicatilis* exposed to PS-COOH and PS-NH_2 (40 and 50 nm, respectively) at concentrations between 0.5 – 50 mg/L for 24-48 h, PS-

COOH had no acute toxicity, whilst PS-NH_2 nanoplastics, on the other hand, showed high mortality (Manfra et al., 2017). Also, in *B. plicatilis*, after exposure to PMMA (40 nm; 96 h; 4.7 – 75.0 mg/L), at 48 h into the exposure, the survival rate was highly affected in both L-type and S-type rotifers (LC_{50} = 13.3 mg/L and LC_{50} = 37.6 mg/L, respectively) (Venâncio et al., 2019). In *Brachionus koreanus* exposed to two different sizes of PS microplastics (500 and 6000 nm, 10 µg/mL) and a PS nanoplastics (50 nm) for 24 h at a concentration of 10 µg/mL, the accumulation of NPs was higher than microplastics and associated with oxidative stress-induced damage to lipid membranes (Jeong & Choi, 2019). Rotifers' survival is highly affected after exposure to NPs, wherein NP toxicity is dependent on both polymer type and size. Although further studies are necessary, particularly those related to different NP sizes, positively charged NPs present a more toxic effect on rotifers than negatively charged NPs, as seen in algae and bacteria.

1.2.2.4. Echinoderms

Considering echinoderms, sea urchins are highly considered excellent tools to assess the toxicity of many chemical compounds and environmental stressors, especially during embryonic life stages, as sea urchins have high sensitivity to low concentrations of contaminants (Sugni et al., 2007). The effects of exposure to rotifers are presented in Tables 1.2.1. – 1.2.4. *Paracentrotus lividus* embryos and larvae exposed to PS-COOH (40 nm; 50 µg/mL) and PS-NH_2 (50 nm; 10 µg/mL) for 6, 24 and 48 hours lead to accumulation of both NPs, whereby PS-NH_2 induced higher toxicity that was unseen by PS-COOH (Della Torre et al., 2014). The half-maximum effective concentration (EC_{50}) of PS-NH_2 at 24 hpf and 48 hpf were 3.82 µg/mL and 2.61 µg/mL, respectively, wherein malformations of skeletal rods and arms, as well as undeveloped embryos, were some of the effects encountered after exposure to PS-NH_2 (Della Torre et al., 2014). Pinsino et al. (2017) also showed that *P. lividus* exposed to 3 and 4 µg/mL of PS-NH_2 (50 nm) simultaneously induced skeletal rods and arms malformations at 4 µg/mL. Therefore, the impact of skeletal rods and arms can be a specific effect of NPs, but more data is necessary to confirm this. Moreover, in an *in vitro* assay of PS-COOH and PS-NH_2 exposure to the sea urchin *Sterechinus neumayeri* (40 and 50 nm, respectively; 6 and 24 h; 1 and 5 µg/mL), both NPs affected cellular phagocytosis, engendered inflammatory responses towards oxidative stress and provoked apoptosis at a molecular level (Bergami et al., 2019). Once more, Bergami et al. (2019) findings establish that different surface-charged NPs are challenging for *S. neumayeri* immune cells. Comparatively, PS-NH_2 possess a more toxic effect towards echinoderms than PS-COOH, as seen in bacteria, algae and

rotifers. Predominately associated with the lack of toxicity of PS-COOH is the electrostatic cell membrane repulsion (Bhattacharya et al., 2010), as well as the consequent loss of nanoscale properties and reactivity due to NP agglomeration in SW (Bergami et al., 2017). Therefore, NPs' toxicity towards echinoderms is particle size and type dependent.

Table 1.2.3. The effects of cationic amino polystyrene nanoparticles (PS-NH_2; ≤100 nm) affect marine biota according to size, concentration and exposure period. Abbreviations are: ↑ - increased; ↓ - decreased; ⊥ - inhibited; ☒ - affected; ⊤ - induced; ROS - Reactive oxygen species; LC/EC_x – Lethal or sublethal concentration causing x% of effect; OD_{600} – optical density at 600 nm.

Phylum	Test species	Particle type	Particle size (nm)	Concentration (µg/mL)	Exposure time (h)	Effects	Reference
Bacteria	*Marinobacter adhearens*	PS-NH_2	20	0 - 200	5*	< 20 µg/mL → no impact on biofilm formation, growth rate, OD600 200 µg/mL → ↑ aggregation; ↓ growth rate; ↓ OD600	Okshevsky et al., 2020
	Oceanobacter kriegii					< 20 µg/mL → no impact on biofilm formation, growth rate, OD600 200 µg/mL → ↑ biofilm formation; ↑ aggregation; ↓ growth rate; ↓ OD600	
	Cobetia marina					< 20 µg/mL → no impact on biofilm formation, growth rate, OD600 200 µg/mL → ↓ biofilm formation; ↑ aggregation; ↓ growth rate; ↓ OD600	
	Marinobacter algicola					< 20 µg/mL → no impact on biofilm formation, growth rate, OD600 200 µg/mL → ↓ biofilm formation; ↑ aggregation; ↓ growth rate; ↓ OD600	
	Pseudoalteromonas carrageenovora					< 20 µg/mL → no impact on biofilm formation, growth rate, OD600 200 µg/mL → ↓ biofilm formation; ↑ aggregation; ↓ growth rate; ↓ OD600	
	Phaeobacter inhibins					< 20 µg/mL → no impact on biofilm formation, growth rate, OD600 200 µg/mL → ↓ biofilm formation; ↑ aggregation; ↓ growth rate; ↓ OD600	
	Marinobacter hydrocarbonoclasticus					< 20 µg/mL → no impact on biofilm formation, growth rate, OD600 200 µg/mL → ↓ biofilm formation; ↑ aggregation; ↓ growth rate; ↓ OD600	
	Halomonas alkaliphilia		50	20 - 320	2	⊥ growth rate; ↓ chlorophyll content; ↑ oxidative damage	Sun et al., 2018
Algae	*Dunaliella tertiolecta*		40	250	72	⊥ growth rate (EC50 = 12.97 ± 0.57 µg/mL)	Bergami et al., 2017a
	Chaetoceros neogracile		50	0.05 and 5	96	↓ cellular energy reserves; ↓ pigment composition; re-adjustment of galactolipids & triacylglycerol; ☒ thylakoid membrane structures	González-Fernández et al., 2020
Rotifers	*Brachionus plicatilis*			0.5 - 50	24 and 48	↑ mortality; NSW → EC50 = 6.62 ± 0.87 µg/mL; RSW → EC50 = 2.75 ± 0.67 µg/mL	Manfra et al., 2017
Echinoderms	*Paracentrotus lividus*			1 - 50	6, 24, 48 hpf	⊤ malformations in larvae; 24 hpf → EC50 = 3.82 µg/mL; 48 hpf → EC50 = 2.61 µg/mL	Della Torre et al., 2014
				3 and 4	24 and 48	⊥ skeletal elongation (3 µg/mL); ⊤ malformations of skeletal rods and arms	Pinsino et al., 2017
	Sterechinus neumayeri			1 and 5	6 and 24	in vitro assay; ↓ phagocytic capacity; ↓ gene modulation; ↑ cellular debris at 5 µg/mL (24h); ↑ inflammatory response; ↑ apoptosis	Bergami et al., 2019
Crustacea	*Artemia franciscana*			0.5 - 10	24 and 48	↑ expression of *clap* and *cstb*; ↑ nº of molts (48h)	Bergami et al., 2017b
	- upto instar III nauplius			5 - 100	72 and 14*	Accumulated and retained in gut lumen; most toxic	Bergami et al., 2016
	Euphausia superba			2.5	48	no mortality; ↑ exuviae production (12.6 ± 1.31); ↓ swimming activity	Bergami et al., 2020
Molluscs	*Crassostrea gigas (gametes)*		100	0.1 - 100	1 to 5	↑ cell size; ↑ spermatozoa complexity; ↓ nº spermatozoa	González-Fernández et al., 2018
	Mytilus galloprovincialis		50	0.0001 - 20	48	↑ malformations D-larvae; ↑ delay in development (2.5 - 10 µg/mL); ↓ 20 - 30% shell length (48h); EC50 = 0.142 µg/mL	Balbi et al., 2017
	- haemocytes			1 - 50	30**	↓ lysosomal membrane stability; ↑ ROS; ⊤ cellular damage	Canesi et al., 2016
*days ** mins							

1.2.2.5. Crustacea

Benthic and planktonic marine crustaceans are useful in ecotoxicological assays, as small crustaceans are a crucial link within the food web, as they play an important role as primary and sometimes also as secondary consumers (Luigi et al., 2012). They connect the energetic fluxes between primary producers (e.g., algae) and consumers found at higher levels (e.g., fish) and, therefore, are placed at a key level within the food web (Luigi et al., 2012). Thus, the effects of NPs are present in Table 1.2.1. – 1.2.4. are important to assess possible trophic transfer. In the brine shrimp *Artemia franciscana* exposed to PS-COOH (40 nm) and PS-NH_2 (50 nm) particles (0.5 – 10 µg/mL; 24 – 48 h), exposure to PS-NH_2 (1 µg/mL) leads to an increase in the expression of cathepsin L-associated protein (*clap*) and cathepsin B (*cstb*), two genes connected to growth. This increased after 48 hours and was related to an increase in the number of moults (Bergami et al., 2017). On the other hand, organisms exposed to PS-COOH had no effects; however, they did accumulate NPs (Bergami et al., 2017). In *A. franciscana* (up to instar III nauplis) exposed to the same NPs (5 – 100 µg/mL), a growth inhibition test (72 h) and a long-term sublethal test (14 d) showed NPs were accumulated and retained inside the gut lumen (Bergami et al., 2017). PS-NH_2 particles were more toxic than PS-COOH (Bergami et al., 2016). PS nanoparticles (100 nm; 0.001 – 10 µg/mL) exposed to the first instar larvae of *A. franciscana* and II stages of nauplii of the acorn barnacle *Amphibalanus amphitrite* ingested and accumulated NPs in the gut after 24 and 48 h of exposure. PS particles affected organisms' swimming speed, wherein *A. amphitrite* exposed to higher concentrations showed mobility inhibition after 48 h. On the other hand, *A. franciscana* swimming speed was inhibited at 24 h and increased inhibition at higher concentrations (Gambardella et al., 2017). The acorn barnacle *A. Amphitrite,* after a chronic exposure test to PMMA (45 nm; 5-25ppm; 24 h), bioaccumulation of NPs occurred in barnacles and persisted in the body throughout the stages of growth and development (nauplius to juvenile barnacle) posing a potential long-term effect of NPs on invertebrate communities (Bhargava et al., 2018). The effects of PS (50 nm) in a marine copepod, *Tigriopus japonicus,* exposed to NPs caused a significant decrease in fecundity, malformations of embryo development, and high mortality of larvae, wherein the highest concentrations of PS nanoplastics lead to parent's death (Lee et al., 2013). More recently, the effects of NPs on Antarctic krill juveniles, *Euphausia superba*, were assessed (Bergami et al., 2020). Exposure to PS-COOH (48 h; 2.5 µg/L; 62 nm) had no adverse effects, in contrast, PS-NH_2 (48 h; 2.5 µg/L; 50 nm) reduced swimming activity of krill and increased moulting (Bergami et al., 2020). Antarctic krill is a keystone species and plays a central role in the Antarctic food chains and carbon cycle, increasingly impacting the future

effect of NPs on Antarctic pelagic ecosystems and the biogeochemical cycle (Bergami et al., 2020).

In summary, crustaceans ingest and accumulate NPs, where at high concentrations, mobility is affected, as is growth and development, in all NPs assessed. A clear distinction between PS-COOH and PS-NH_2 toxicity is also noticeable, wherein PS-NH_2 has more severe effects on crustaceans, as shown in bacteria, algae, rotifers and echinoderms. Further investigation is necessary to understand the effects other types of NPs pursue on crustaceans, such as copepods, brine shrimps, barnacles, and amphipods. Furthermore, within crustaceans, copepods are extremely valuable in ecotoxicological evaluations, whereby the use of a combination of whole-animal bioassays and gene expression studies indicates that copepods, such as *Tigriopus* spp., may serve as excellent tools to evaluate the impacts of marine pollution throughout coastal regions (Raisuddin et al., 2007).

Table 1.2.4. The effects of poly(methyl methacrylate) nanoparticles (PMMA; ≤100 nm) on marine biota according to size, concentration and exposure period. Abbreviations stand for: ↑ - increased; ↓ - decreased; ⊥ - inhibited; ☒ - affected; ⊤ - induced; ROS - Reactive oxygen species; LC/EC_x – Lethal or sublethal concentration causing x% of effect; OD_{600} – optical density at 600 nm.

Phylum	Test species	Particle type	Particle size (nm)	Concentration (µg/mL)	Exposure time (h)	Effects	Reference
Algae	*Tetraselmis chuii*	PMMA	40	0 - 304.1	96	↓ growth rates (>150 µg/mL); EC50 = 132.5 µg/mL; EC20 = 117.4 µg/mL	Venâncio et al., 2019
	Nannochloropsis gaditana					↓ growth rates (>150 µg/mL)	
	Isochrysis galbana					↓ growth rates (≥ 213.6 µg/mL)	
	Thalassiosira weissflogii			0 - 293.0		⊥ growth rates (≥ 18.8 µg/mL); EC50 = 83.4 µg/mL; EC20 = 48.9 µg/mL	
	Rhodomonas baltica	PMMA	50	0.5 - 100	72	↓ cell viability, ↑ cell size & complexity; ↑ ROS; ↑ LPO; ↓ DNA content; ↓ photosynthetic capacity; hyperpolarization of mitocondrial membrane; membrane integrity loss; overproduction of pigments	Gomes et al., 2020
		PMMA-COOH				↓ growth; ⊥ cell cycle; ↓ cell viability; ↓ metabolic activity; ↓ photosynthetic capacity	
Rotifers	*Brachionus plicatilis*	PMMA	40	4.7 - 75.0	96	☒ survival (48 h; L-type > S-type); L-type → EC50 = 13.3 µg/mL; S-type → EC50 = 37.6 µg/mL	Venâncio et al., 2019
Crustacea	*Amphibalanus amphitrite*		45	25	24	↑ bioaccumulation	Bergami et al., 2017b
Fish	*Spaurus aurata*			0 - 10	24 and 96	↑ antioxidant defences; ⊤ alterations in lipid metabolism pathways; ↑ genotoxicity in blood cells; ↑ cholesterol and triglycerides in plasma; ↑ Erythrocytic nuclear abnormalities	Brandts et al., 2021
	Dicentrarchus labrax			0 - 20	96	↑ abundance of mRNA transcript; ⊥ fish immune system	Brandts et al., 2018
			100	0.001 - 10	24	⊥ immune system; ↑ abundance of mRNA transcript; ☒ molecular signalling & pathways	Almeida et al., 2019

1.2.2.6. Molluscs: Bivalvia

As sessile filter-feeding organisms, bivalves can accumulate many NPs in the surrounding environment, empowering measurements of stress levels in their tissues. Their wide geographical distribution and presence at different latitudes are some of the characteristics that make bivalves excellent sentinel organisms for ecotoxicological evaluations. However, the effects of NP exposure to bivalves are still scarce (see Tables 1.2.1. – 1.2.4). In the blue mussel *Mytilus edulis*, PS nanoparticles (30 nm; 100 – 300 µg/mL) induced the production of pseudofaeces, increasing with the increase in NP concentration, wherein results suggested that PS particles were recognised as non or low-nutritional food (Wegner et al., 2012). In the Mediterranean mussel, *Mytilus galloprovincialis*, haemocytes exposed to PS-NH_2 (50 nm; 1 – 50 mg/L), after 30 mins, PS-NH_2 causes a decrease in lysosomal membrane stability and an increment in oxyradical generation, leading to rapid cellular harm such as membrane blebbing and misfortune of filopodia (Canesi et al., 2015). Additionally, the generation of the protein corona in haemolymph serum was observed with the existence of PS-NH_2 (Canesi et al., 2015). In early embryo development of the mussel *M. galloprovincialis*, after exposure to PS-NH_2 (50 nm; 0.001 – 20 mg/L), malformations of D-veligers were observed at concentrations more than or equal to 2.5 mg/L (Balbi et al., 2017). A dose-dependent delay concerning the development of larvae was also observed, with an increase in embryos encountered at the pre-veliger stage and a stable proportion found still at the trochophore stage (EC_{50} = 0.142 mg/L). The highest concentration (20 mg/L) of PS-NH_2 led to complete inhibition of D-shaped veliger, whereby 90% of larvae remained at the trochophore stage (Balbi et al., 2017). In gametes of the oyster *Crassostrea gigas*, exposed to PS-COOH and PS-NH_2 (100 nm; 0.1 – 100 mg/L), NPs caused an increase in relative cell size as well as the complexity of spermatozoa (González-Fernández et al., 2018). Moreover, a dose-response increase in reactive oxygen species production was observed in organisms exposed to PS-COOH but not to PS-NH_2. Oocytes were found to be less related to different cell membranes (González-Fernández et al., 2018). In gametes and embryo-larval development of *C. gigas* exposed to PS beads, PS-COOH and PS-NH_2 (50 nm; 0.1 – 25 µg/mL), all NPs significantly impaired the fertilisation yield in a dose-response manner at concentrations between 1 and 25 µg/mL, wherein PS-NH_2 exhibited the strongest toxicity, inducing a significant reduction in fertilisation yield associated at an EC_{50} of 4.9 ± 0.9 µg/mL (Tallec et al., 2018). D-larval yield also decreased significantly after exposure to all NPs at 10 and 25 µg/mL, wherein the highest toxicity observed was also by PS-NH_2, presenting a decrease of 6.4% in D-larval yield at the lowest concentration (0.1 µg/mL). Embryo-larval development success was completely inhibited (100% reduction) at an EC_{50} of 0.15 ± 0.4

µg/mL (Tallec et al., 2018). Tallec et al. (2018) highlight that NP exposures may have detrimental effects on planktonic stages of bivalves, seemingly interacting with biological membranes, leading to cytotoxicity and genotoxicity, potentially impairing reproductive success. Undoubtedly, NP toxicity in bivalves is extremely concerning, as data have shown that NPs are recognised as a low-nutritional food and are taken up by these filter feeders. In addition, after exposure to NPs, the integrity of their immune response is compromised by decreasing the stability of the lysosomal membrane in addition, bivalve gametes are also vulnerable to NP toxicity, as is embryo-larval development, thereby jeopardising future populations and disrupting the surrounding environment. Therefore, it is important to assess if other types of NPs induce the same type of effects.

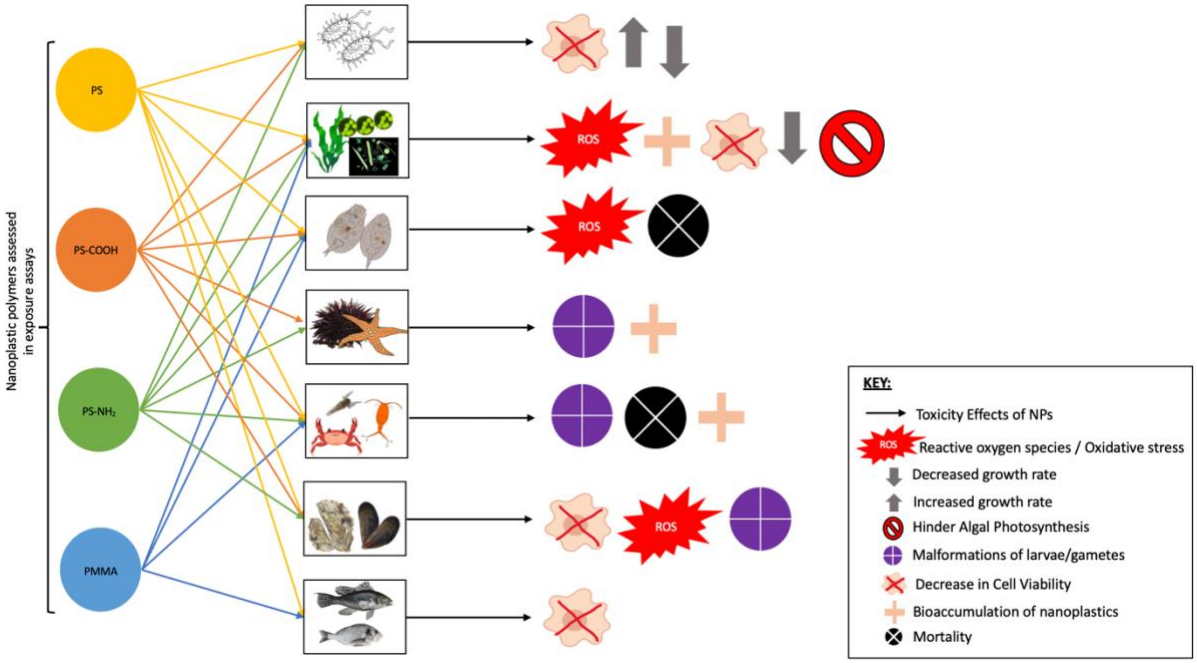

Figure 1.2.4. Illustration of different NP polymer's effects on marine biota.

1.2.2.7. Fish

Very few studies on the effects of NPs on marine fish have been encountered (see Tables 1.2.1. and 1.2.4.). Most of the data available are focused on the effects on freshwater fish (Mattsson et al., 2015, 2017; Chen et al., 2017; Skjolding et al., 2017; Chae et al., 2018; Pitt et al., 2018; Lee et al., 2019). Recently, marine continuous fish cell lines have been developed to aid in the study of molecular and physiological responses to stressors (Langner et al., 2011; Villalba et al., 2017). Fish cell lines have become a crucial tool for understanding the effects of emerging

contaminants (e.g., NPs) at a molecular level (Morcillo et al., 2017; Pannetier et al., 2018) as well as avoiding the use of animals in experiments as recommended by the European Union (Directive 2010/63 EU).

In two fish cell lines of the seabream *Sparus aurata* and the seabass *Dicentrarchus labrax*, SAF – 1 and DLB – 1, respectively, exposed to PS NPs (100 nm; 0.001 – 10 mg/L) for 24 h, in SAF – 1, though not significant, there was a slight decrease (25%), in cell viability at lowest concentrations (Table 1.2.1.). However, at higher concentrations, mild effects were present on this cell line (Almeida et al., 2019). In DLB – 1, a decrease in cell viability was observed, whereby at 0.001 mg/L, cell viability was 66%, showing oscillation at higher concentrations within the minimum viability of 64% at 1 mg/L (Almeida et al., 2019).

More recently, short-term exposure of PMMA to the seabream *S. aurata* (45 nm; 0 – 10 µg/mL; 24 and 96 h) resulted in upregulation of the mRNA levels of essential lipid metabolism-related genes, showing a global increase in plasma cholesterol and triglycerides (Brandts et al., 2021). Antioxidant enzymatic response increased throughout the exposure period, exceptionally with a decrease in total antioxidant capacity after 96 h. PMMA nanoparticles activated antioxidant defences, induced alterations in lipid metabolism pathways and genotoxicity in *S. aurata* blood cells (Brandts et al., 2021). Similarly, in the seabass *D. labrax* after exposure to the same NP and size (PMMA; 45 nm; 0 – 20 mg/L; 96 h) also led to an increase in abundance of mRNA transcript as well as the impairment of the fish's immune system (Brandts et al., 2018). In *D. labrax*, NPs change molecular signalling pathways and potentially interfere with lipid metabolism, as seen in *S. aurata* (Brandts et al., 2018, 2021) (Table 1.2.4). Consequently, regarding all data available on fish exposed to NPs, mRNA transcript is highly affected, increasing the possibility of mutations, as well as cellular malfunctions.

NPs can disrupt fish immune systems, induce oxidative stress, compromise lipid metabolism, and decrease cell viability. However, more studies need to be conducted with other types of NPs to understand how their toxicity affects fish entirely. It is also imperative to evaluate different species and understand how different NP polymers can affect the quality of aquaculture quality and their effects on fisheries and, consequently, human beings.

Considering all the above, a summary of nanoplastics' effects on marine biota to date is illustrated in Figure 1.2.4. As can be seen, the information about the effects on marine organisms is still very limited and NPs, along with their nano-specific properties, are of major concern as they fundamentally differ from those of the same polymer type in bulk form and are

size-dependent (Klaine et al., 2012). Moreover, it is crucial to develop methods that accurately measure NP concentrations in the different components of the marine environment and biota. In addition, the concentrations used need to be environmentally relevant so that data can be harmonised, thus making it possible to compare the effects of NPs in marine biota.

1.3. Nanotechnology: Silver nanoparticles

Silver nanoparticles (nAg) are primarily employed in the textile, antimicrobial coating, personal care, and photonics industries due to the development of nanotechnology and the increasing use of engineered nanomaterials in nano-functionalized consumer goods (Lee & Jun, 2019; Maillard & Hartemann, 2013; Pereira et al., 2020). Because of its antimicrobial, antibacterial, antifungal, antiviral, anti-inflammatory, and anticancer properties, the production of nAg products has increased dramatically over the years (Khan et al., 2018). The global nAg market is expected to reach a value of over USD 4.53 billion by 2030, with a revenue of over USD 2.68 billion in 2023 (Grandview Research, 2024). Its applications in implant technology, biomarkers, tissue engineering, biosensors, nanomedicine and nanorobots, and image enhancement devices have also increased demand from the pharmaceutical industry (Grandview Research, 2024). Since wastewater treatment facilities (WTTP) are ineffective at removing or treating nAg, it is predicted that nAg levels in the environment will be between 0.03 and 0.08 mg/L (Fernandes et al., 2017). In the WWTP, for example, nAg will mostly partition to the sludge (Bolaños-Benítez et al., 2020). Ag may reach the marine environment by leaching and surface runoff, and sludge may be dumped in landfills or used as fertiliser for crops (Blaser et al., 2008). The harmful effects of nAg on marine life have been extensively studied (Auguste et al., 2018; Gomes et al., 2013; Lorusso et al., 2022; McCarthy et al., 2013; Rezvani et al., 2019), and its mode of action (MoA) harms cell membranes directly; nAg can release Ag+ ions, and both Ag+ and nAg produce reactive oxygen species (ROS) (Ghobashy et al., 2021). The microbial community in soils are also affected by the presence of nAg (Kusi et al., 2020; Oca-Vásquez et al., 2020; Tortella et al., 2020), though in the presence of PS-NPs, for instance, can ease the inhibition of denitrification induced by nAg (Jiao et al., 2022). The effects of nAg in marine organisms in the presence of other emerging contaminants remain scarce, and its properties may be enhanced or diminished, making an evaluation critical.

1.4. Cytotoxic drugs: 5-Fluorouracil

Chemotherapeutic agents like 5-fluorouracil (5-FU) are commonly used in the treatment of cancer, particularly colorectal cancer and other solid tumours. As it is classified as an emerging contaminant, its presence in European waters has sparked concern. 5-FU's mode of action, misincorporating its fluoronucleotides into RNA and DNA, is deemed toxic to aquatic organisms like algae, invertebrates and fish. Concerns regarding bioaccumulation of 5-FU in aquatic organisms are the potential impacts of biomagnification within the ecosystem and, consequently, on human health through seafood and fish consumption. Most studies have focused on the effects of 5-FU on freshwater species, with the effects on marine species remaining scarce. This review aims to gather all the available information on the ecotoxicological effects of 5-FU in freshwater and marine species.

1.4.1. 5-Fluorouracil and its medical use.

Unfortunately, the diagnosis of cancer in patients has increased over the years and continues to do so. As a chemotherapeutical treatment, cytostatic drugs are commonly used as they effectively destroy cancerous cells, but the downside is that they do not distinguish between cancerous and healthy ones. Fluorouracil, sometimes referred to as 5-fluorouracil or 5-FU, is a member of the chemotherapeutic medication class used to treat a variety of neoplasms. 5-FU is used in the treatment of gastric, pancreatic, breast, and colorectal adenocarcinomas, and topical 5-FU (usually at 5%) for dermatological diseases such as numerous actinic or solar keratoses and superficial basal cell carcinomas (Mahnik et al., 2007; Casale & Patel, 2024*)*. In Europe, it is highly recommended that before patients are treated with 5-FU, they should be evaluated for any deficiency or lack of the dihydropyrimidine dehydrogenase enzyme (DPD), as the lack of this enzyme, if treated with 5-FU will increase the risk of severe and life-threatening side effects (EMA/367286/2020). The International Agency for Research on Cancer (IARC) classifies 5-FU under class 3, meaning its carcinogenicity is not classifiable towards humans (IARC monographs, 1987). As a pyrimidine analogue of uracil with a fluorine atom replacing hydrogen in the C-5 position, it can misincorporate itself into RNA and DNA, causing a release of cytochrome *c* from the mitochondria and promoting the generation of reactive oxygen species (ROS) (Vermorken et al., 2007; Matuo et al., 2009; Cairns et al., 2011). Through the uracil transportation system, three metabolites are formed as 5-FU enters the cell by active transportation: fluorodeoxyuridine monophosphate (FdUMP), fluorodeoxyuridine triphosphate (FdUTP) and fluorouridine triphosphate (FUTP) (Fig. 1.4.1).

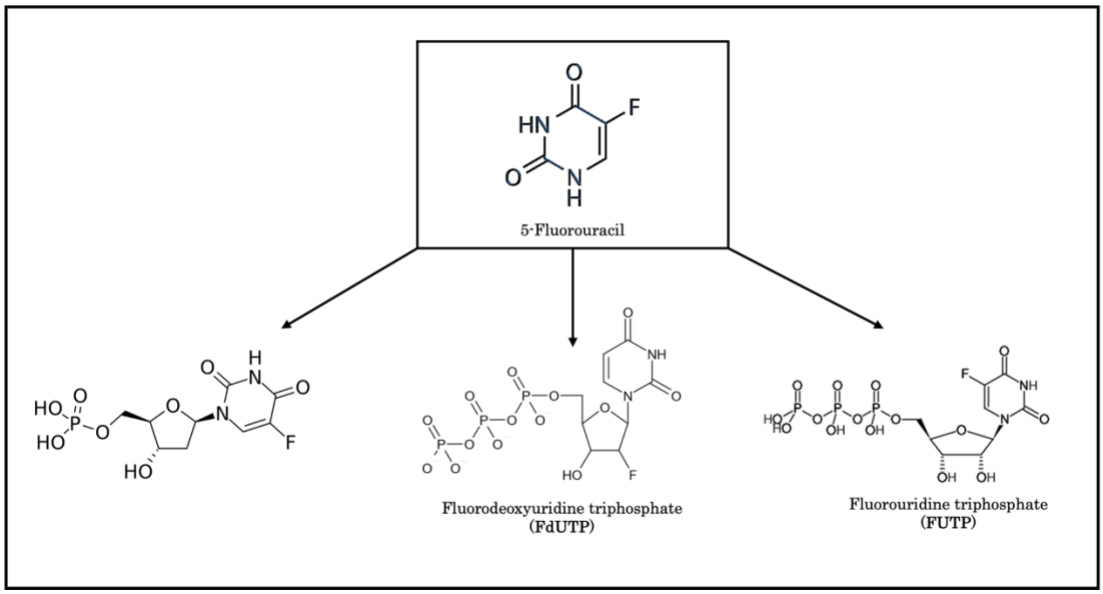

Figure 1.4.1. 5-Fluouracil and its metabolites.

FdUMP suppresses the function of thymidylate synthase and inhibits the production of deoxythymidine monophosphate (dTMP). dTMP is essential for DNA replication and repair, and the depletion of dTMP leads to an imbalance in intracellular nucleotides, which generates double-stranded DNA breaks assisted by the enzyme endonuclease (Zhang et al., 2008). FdUTP directly induces DNA damage. FUTP combines itself into RNA rather than uridine triphosphate (UTP), causing RNA damage (Ghafouri-Fard et al., 2021) (Fig. 1.4.2).

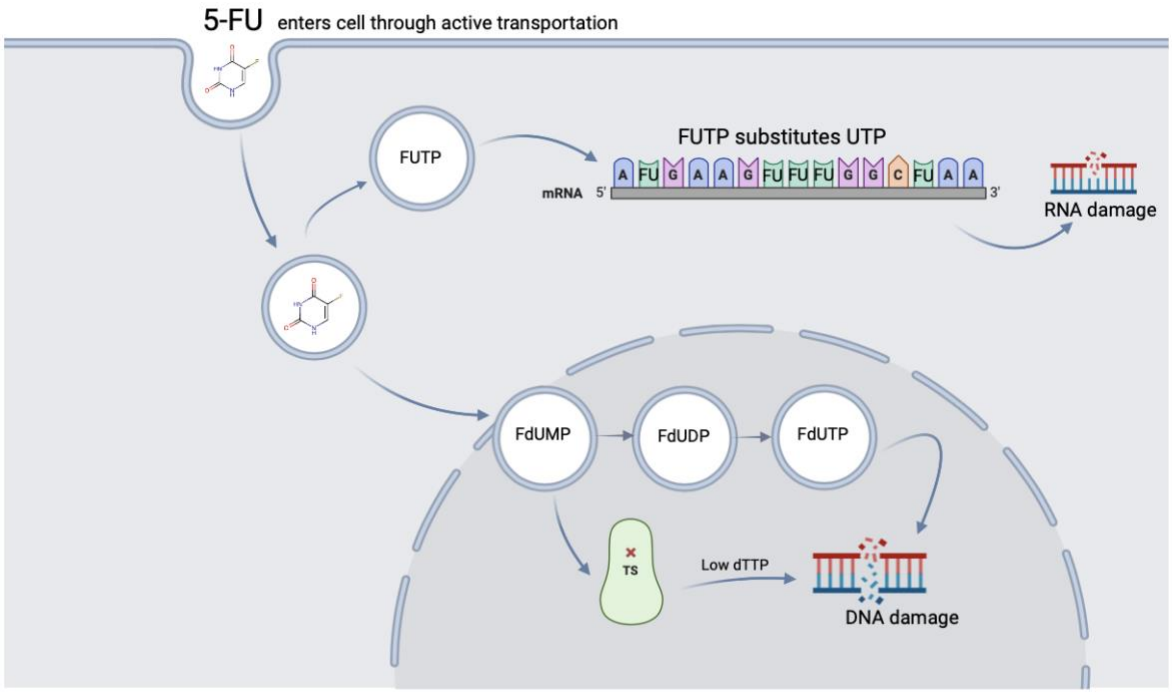

Figure 1.4.2. 5-Fluorouracil mode of action within the cell (adapted from Gonçalves et al., 2022 [Chapter 4])

In Europe, 5-FU is administered intravenously (Fig. 1.4.3.A) and used in creams for cutaneous use in different countries (Fig. 1.4.3.B) to treat a variety of neoplasms mentioned previously, where France (8%), Germany (10%), Portugal (7%) and the United Kingdom (8%) have the highest percentage of administration (Fig. 4) (Infarmed, 2023). The most common dosage used in these representative countries is 50 mg/mL of 5-FU intravenously (Fig. 1.4.4.), although high dosages are also administered.

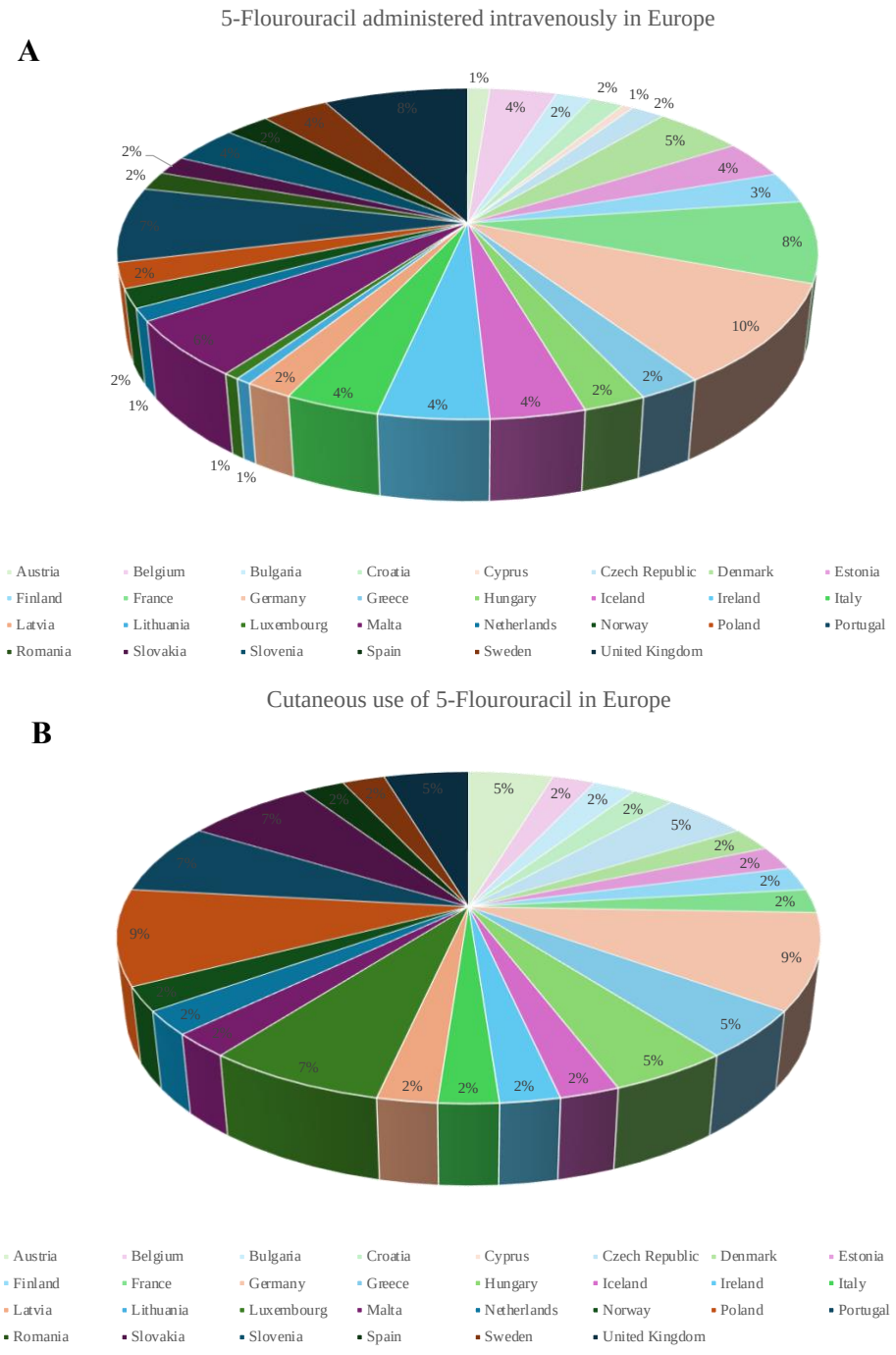

Figure 1.4.3. Percentage of 5-Fluorouracil administrated intravenously (**A**) and for cutaneous use (**B**) in Europe (Infarmed, 2023).

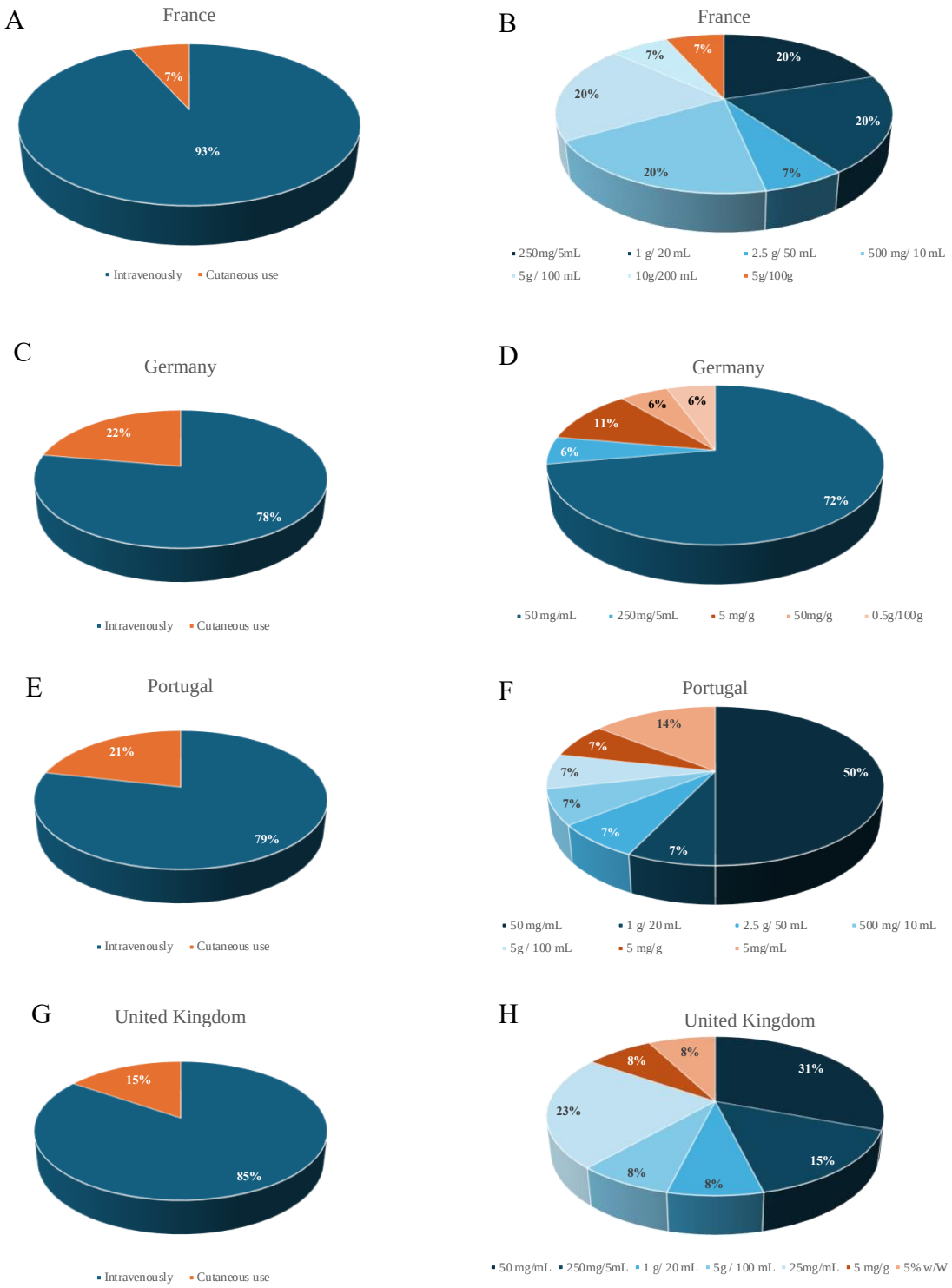

Figure 1.4.4. Percentage of types of 5-Fluorouracil administration (A, C, E, G) and dosages (B, D, F, H) authorised in the four most representative countries in Europe (Infarmed, 2023)

1.4.2. Levels of 5-FU in the aquatic environment

When administrated to patients, pharmaceuticals do not fully metabolise and end up exiting the body through urine, entering hospital and urban wastewater effluents and

undergoing treatment for the breakdown or removal of this pharmaceutical before being released into the freshwater or marine ecosystems (Fig. 1.4.5.). The wastewater treatment plants are not available in some parts of the world and the ones available do not yet have the correct technology to remove residual pharmaceuticals such as 5-FU, which is highly persistent in wastewater, as its use as a chemotherapeutical agent continues to increase, entering the aquatic ecosystem. For instance, 6.7 µg/L of 5-FU has been reported in hospital effluents in France (Castastini et al., 2007) and 123.5 µg/L in Austrian wastewater effluents, 4.7 to 14.0 ng/L in municipal wastewaters in Slovenia (Kosjek et al., 2013), and 0.01 – 41 ng/L of predicted environmental concentrations in surface waters (Misík et al., 2019). Moreover, in European waters, the levels of 5-FU have been estimated to range between 0.3 ng/L to 2.5 ng/L (Heath & Isidori, 2020), whilst, in other regions of the world, 5-FU has been estimated to be detected between 6.2 ng/L (Taipei region) and 160 ng/L (Gaoping river) (Lin et al., 2014). Many other factors come into play when considering the effects of 5-FU in the marine environment, as aquatic conditions change and can affect the behaviour of 5-FU. The reactions of 5-FU with O_3 and •OH in seawater can alter the molecule and, in turn, change its toxic properties towards marine biota. A theoretical study of the degradation effects of 5-FU by O_3 and •OH showed that some transformation products (Fig. 6) containing nitrous groups and a carbonyl urea structure would still have toxic effects on marine organisms. Some products' developmental toxicity and mutagenicity remain active, prejudging human health (Li et al., 2020). Additionally, cytostatic drugs such as 5-FU are known to have cytotoxic, genotoxic, mutagenic, and carcinogenic effects on non-target organisms (Kümmerer & Henninger, 2003), incrementing the importance of understanding how 5-FU's presence can affect aquatic biota. This review aims to gather all information available on the effects of 5-FU on freshwater and marine species.

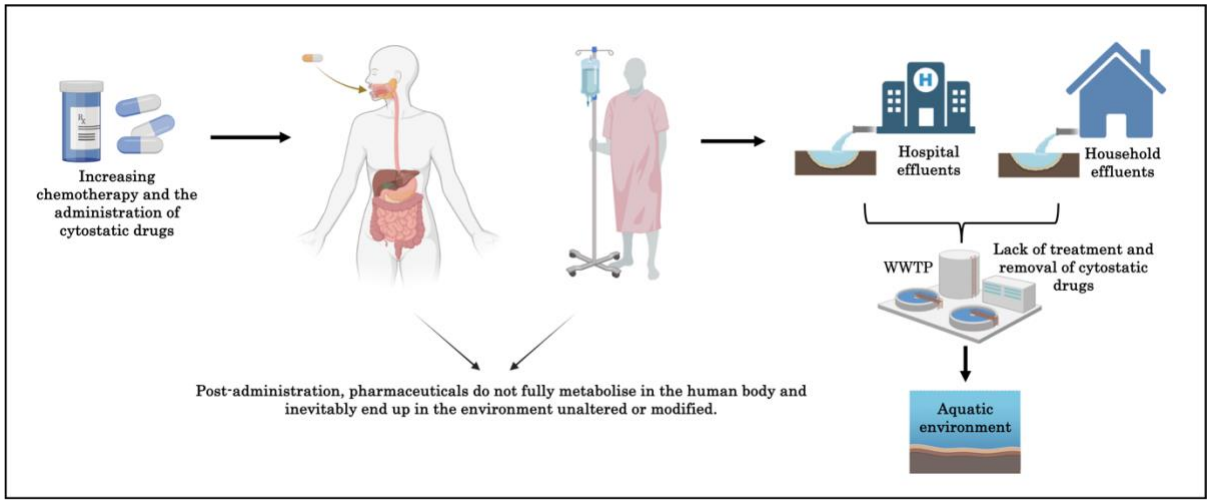

Figure 1.4.5. How cytostatic drugs end up in the aquatic environment.

1.4.3. 5-FU effects on freshwater species

Freshwater habitats, such as rivers, lakes, marshes, and streams, are essential to sustain life and preserve ecological balance. With runoffs, improper disposals, and primarily wastewater effluent, freshwater ecosystems are the first to encounter any residual 5-FU. Thus, the toxic effects of 5-FU on freshwater species are concerning. A summary of the impact of 5-FU on freshwater species can be found in *Table* 1.4.1. In the oligochaeta *Limnodrilus udekemianus,* an exposure to 5-FU (0.004 – 40 µM) led to a loss of 70% cellular viability and a significant increase of DNA damage after 96h (Kračun-Kolarević et al., 2015). The integration of 5-FU in DNA and RNA was observed after 72h of exposure (5.87 – 187.7 mg/L) in the algae *Scenedesmus vacuolatus,* compromising growth and accumulating within the organism (Asad et al., 2012). Another alga, *Raphiodocelis subcapitata*, was exposed to a minor concentration of 5-FU, 0.005–0.492 mg/L, for 72h and submitted to ecotoxicity assays insufficient to calculate EC_{50} for yield and growth inhibition. In the green hydra (*Hydra viridissima*), EC_{50} obtained for mortality and feeding after 96h of exposure to a concentration range of 0.0504 - 3.226 mg/mL was 0.0554 and 0.0679 mg/mL, respectively (Venâncio et al., 2023). Meanwhile, the exposure of zebrafish, *Danio rerio* to 0.806-8.452 mg/mL of 5-FU for 96h led to hatching abnormalities with LC_{50} and $EC_{50,}$ equalling 4.546, 4.1 and 2.459 mg/mL, respectively (Venâncio et al., 2023). In freshwater mussels, a decrease in lipid peroxidation in both the digestive gland and gonads was observed in *Elliptio complanata* after 96 h of exposure to 5-FU (0, 4, 20 and 100 µg/L), along with a decrease in DNA strand break repair activity, being the two relatable (Kleinert et al., 2021). Toxicity testing carried out in several organisms at the bottom of the food chain has also been reported. 5-FU was found to be highly toxic to

Microbacterium sp., *Pseudomonas fluorescens, Kurhtia gibsonii and Enterococcus casseliflavus* after 16 and 18 hours with EC_{50} of 37.3, 8.3, 3.6 and 11.8 µg/L, respectively (Załęska-Radziwiłł et al., 2014). In the water flea, *Daphnia magna,* immobilisation (48 h) and reproduction (21 days) were targets for toxicity testing of 5-FU. EC_{50} for immobilisation of *D. magna* was found to be 36 mg/L and 20.84 mg/L in two different studies (Załęska-Radziwiłł et al., 2014; Parella et al., 2014). Toxicity testing for the effect of 5-FU on the reproduction of *D. magna* showed EC_{50} to be equal to 0.03 mg/L (Parella et al., 2014). In other arthropods, 5-FU caused an EC_{50} of 0.003 mg/L in the reproduction of *Ceriodaphnia dubia* after 7 days, and an EC_{50} of 0.32 mg/L was obtained for the inhibition of population growth of *Brachionus calyciflorus* after 48 h (Parella et al., 2014). Furthermore, toxicity testing of 5-FU was carried out in fish embryos and adults. For *D. rerio,* 5-FU led to an EC_{50} of 2610 mg/L for embryo mortality and > 100 mg/L in adult mortality (Kovács et al., 2016). In the species *Xenopus laevis*, EC_{50} was reported as 80 mg/L for embryo malformation and 400 mg/L in *Pimephales promelas* (De Young et al., 1996). According to published results, 5-FU is deemed more toxic to embryos in fish species than adults. Considering the environmental predicted concentrations, these EC_{50}'s are higher than the ng/L range for European waters. However, Załęska-Radziwiłł and colleagues (2014), as well as Parella and colleagues (2014), do calculate EC_{50} within the range of 5-FU found in wastewater and hospital effluents. A more thorough evaluation with a lower set starting concentration of 5-FU to understand its toxicity within the ng/L range should be carried out so a more concise comparison with environmentally detected concentrations can be made.

Table 1.4.1. Effect of 5-FU on freshwater species

Phylum	Test species	Concentration (mg/mL)	Exposure time	Effects	Reference
Bacteria	*Microbacterium* sp.		18h	Toxicity testing: EC_{50} = 37.3 µg/L; reported as extremely toxic	Załęska-Radziwiłł *et al.,* 2014
	Pseudomonas fluorescens		16h	Toxicity testing in relation to growth: EC_{50} = 8.3 µg/L; reported as extremely toxic	
	Kurhtia gibsonii		18h	Toxicity testing in relation to growth: EC_{50} = 3.6 µg/L; reported as extremely toxic	
	Enterococcus casseliflavus			Toxicity testing in relation to growth: EC_{50} = 11.8 µg/L; reported as extremely toxic	
Annelida	*Limnodrilus udekemianus*	0.000520312 ; 0.00520312; 0.0520312; 0.520312 and 5.203120	96 h	Comet assay: cell viability < 70% for highest 3 concentrations and induce an increase of DNA damage	Kračun-Kolarević *et al.,* 2015
Algae	*Scenedesmus vacuolatus*	0.00587 - 0.1877	72 h	Integrates into DNA and RNA. Acute toxicity and compromises growth. Accumulates within organism with a bioaccumulation factor of $1.84 \times 10^{4.}$	Asad *et al.,* 2012
	Raphiodocelis subcapitata			Toxicity testing: EC_{50} = 0.07 mg/L	Białk-Bielinska *et al.,* 2017
		5.0×10^{-6} - 0.000492		Toxicity testing: EC_{50} not computable	Venâncio *et al.*, 2023
Magnoliophyta	*Lemna minor*		7 days	Toxicity testing: EC_{50} = 2.45 mg/L	Białk-Bielinska *et al.,* 2017
Cnidaria	*Hydra viridissima*	0.0504 - 3.226	96 h	EC_{50} mortality and feeding were 0.0554 and 0.0679 mg/mL	Venâncio *et al.*, 2023
Anthropoda	*Daphnia magna*		48h	**Immobilisation** toxicity testing: EC_{50} = 36 mg/L	Zounková *et al.*, 2007
				Immobilisation toxicity testing: EC_{50} = 20.84 mg/L	Parella *et al.,* 2014
			21 days	**Reproduction (neonates number)** toxicity testing: EC_{50} = 0.03 mg/L	
	Ceriodaphnia dubia		7 days	**Reproduction (neonates number)** toxicity testing: EC_{50} = 0.003 mg/L	
	Brachionus calyciflorus		48h	**Population growth inhibition** toxicity testing: EC_{50} = 0.32 mg/L	
Mollusca	*Elliptio complanata*	0, 4.0×10^{-6}, 2.0×10^{-5} and 0.0001	96 h (at 15ºC)	LPO ↓ in digestive gland and gonads ; ↓ DNA strand breaks (repair activity) in digestive gland and gonads ; DNA damage related with LPO for digestive gland and gonads	Kleinert *et al.,* 2021
Fish	*Danio rerio*	0.806 - 8.452	96h	LC_{50} and EC_{50} for hatching and abnormalities were 4.546, 4.1 and 2.459 mg/mL, respectively.	Venâncio *et al.*, 2023
				Embryo mortality toxicity testing: EC_{50} = 2610 mg/L	Kovács *et al.,* 2016
				Adult mortality toxicity testing: EC_{50} = >100 mg/L	
	Xenopus laevis		120h	**Embryo malformation** toxicity testing: EC_{50} = 80 mg/L	DeYoung *et al.,* 1996
	Pimephales promelas			**Embryo malformation** toxicity testing: EC_{50} = 400 mg/L	

1.4.4. 5-FU effects on marine species

So far, the effects of 5-FU have yet to be widely evaluated in the marine environment and require more attention. A summary of the effects known to date can be found in *Table* 1.4.2. The toxicity assessment based on the EU Directive 93/67/EEC showed that 5-FU is harmful and highly toxic to the growth and bioluminescence of the marine bacterium *Aliivibrio fischeri* (Załęska-Radziwiłł et al., 2014). It is of uttermost importance to gather more information on the effects of 5-FU on marine organisms.

Table 1.4.2. Effect of 5-FU on marine species

Phylum	Test species	Concentration (mg/mL)	Exposure time	Effects	Reference
Bacteria	*Aliivibrio fischeri*		24h	For growth: EC_{50} = 10421.8 µg/L and NOEC = 6100 µg/L considered as harmful by the toxicity assessment EU Directive 93/67/EEC.	Załęska-Radziwiłł *et al.*, 2014
				For bioluminescence: EC_{50} = 16.0 µg/L and NOEC = 1.5 µg/L considered as extremely toxic by the toxicity assessment EU Directive 93/67/EEC.	
Mollusca	*Mytilus galloprovincialis*	1.0×10^{-8}	21 days	↑ DNA damage in mussel haemolymph. Antioxidant enzymes counteracted ROS generation and no LPO observed in gills, and a slight ↑ in LPO in the digestive gland. 5FU more toxic towards both tissues in a mixture of contaminants (mixed with polystyrene nanoplastics (50nm) and silver nanoparticles (20nm) as there are synergistic interactions observed.	Gonçalves *et al.*, 2022
				In mussel gonads, all antioxidant enzymes ↑ after 3 days of exposure, followed by ⊥ at 14 and 21 days. 5FU more toxic in a mixture of contaminants (mixed with polystyrene nanoplastics (50nm) and silver nanoparticles (20nm), leading to a 57-fold ↑ in LPO, with synergistic interactions.	Gonçalves *et al.*, 2023

1.4.5. 5-FU and other contaminants

A primary concern within the scientific community is how these cytostatic drugs behave in the presence of other contaminants in the environment. Other emerging contaminants, such as nanoparticles, and in particular interest the plastic pollution problem, whether looking at microplastic or nanoplastics, a concern of how it can potentiate the toxic effects of cytostatic drugs, as well as other pharmaceuticals when they interact with these particles is crucial to understand their impact. As there is a need for more information concerning these mixtures, this thesis intends to evaluate the effect of the mixture of 5-FU with other emerging contaminants, particularly nanoplastics.

1.5. *Mytilus galloprovincialis*: a key species in ecotoxicology

Bivalves are sessile filter-feeding organisms with a wide geographical distribution at different latitudes and are found in high densities and stable populations, facilitating sampling and maintenance under laboratory conditions. Because of their early responsiveness to environmental stressors and filtering behaviour, bivalve molluscs are frequently considered ideal model species for marine-coastal monitoring programs (Dellali et al., 2021), such as the "Mussel Watch Program". As sessile filter-feeding organisms, mussels can accumulate contaminants present in their environment, and any shift in populational dynamics can be a sign of the hazard of the presence of these contaminants, making them excellent sentinel organisms for ecotoxicological studies.

The marine mussel *Mytilus galloprovincialis* (Lamark, 1819) (Figure 1.5.1.), commonly known as the "Mediterranean mussel", vastly populates the Portuguese coast and has a high market value in the Mediterranean diet. Economically valuable and used in aquaculture (Provenza et al., 2022), the mussel *M. galloprovincialis* was primarily cultivated in the coastal waters of Galicia (NW Spain) (FAO, 2024). Between 2020 and 2021, the annual aquaculture

production average for *M. galloprovincialis* was 86 117 tonnes (FAO, 2023). The seasonal variations in temperature, food availability, and gametogenic cycle affect mussels condition index and fatty acid profile (Araújo et al., 2024). There is a noticeable decline in the winter and a recovery in the spring, where the condition index declines following the early spring spawning cycle and rises later in the summer (Araújo et al., 2024).

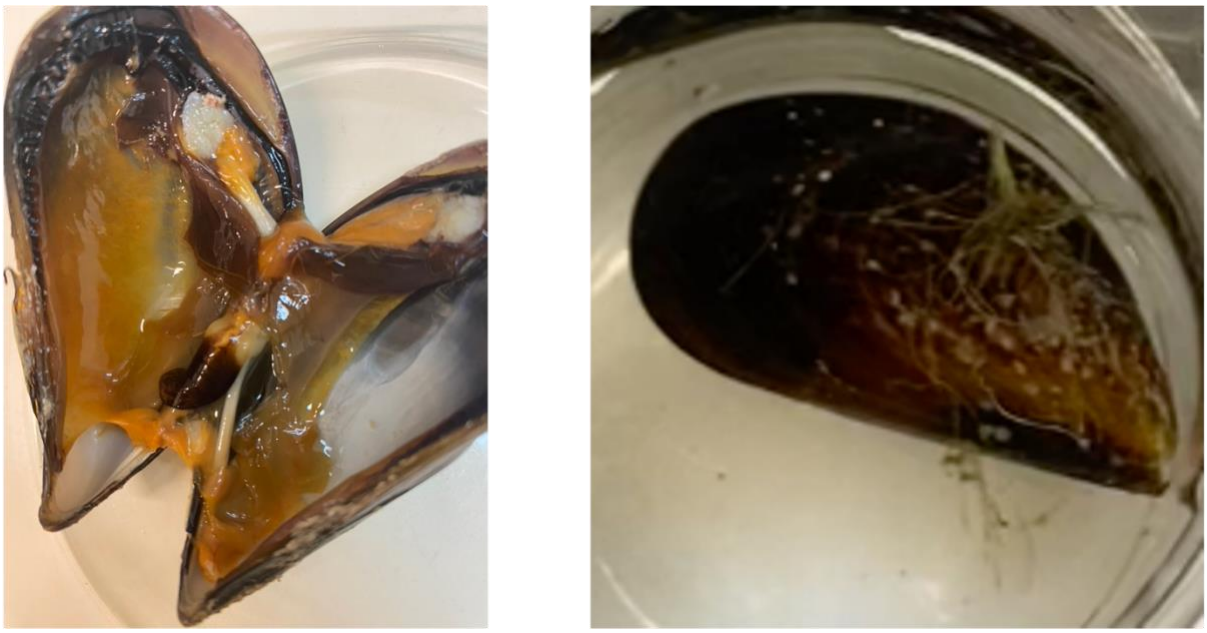

Figure 1.5.1. *Mytilus galloprovincialis,* Lamark 1819.

1.6. Gametogenesis and the reproductive cycle of *M. galloprovincialis*

The spawning cycle for *M. galloprovincialis* commences in early spring, and a second cycle occurs later in the summer. The life cycle of *M. galloprovincialis* is represented in Figure 1.6.1. During the gametogenic cycle, the mussel's reproductive organ undergoes several steps for gonad development and gamete release into the water column. Gametogenesis starts in the first period, which produces mature gametes in one or more cycles and ends with their expulsion each time. As the energy reserves required to initiate a new gametogenesis build-up, the second phase is known as sexual repose (Bhaby et al., 2014). During these stages, a vast amount of energy is required, and contaminants can disrupt energy storage to counteract toxic effects. In this case, the gametogenic cycle and reproductive success can be compromised and jeopardise future populations, causing an unsettling imbalance in the whole ecosystem. An important focus on how contaminants affect

the reproductive organs of *M. galloprovincialis* is imperative to comprehend the effects that can be brought upon future generations.

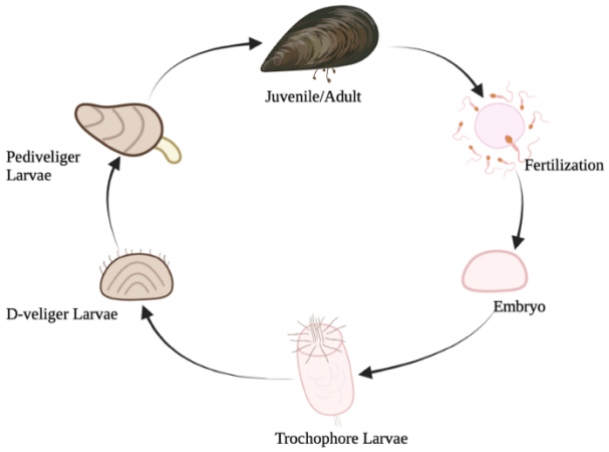

Figure 1.6.1. The life cycle of the Mediterranean mussel, *M. galloprovincialis*. (Image made with Biorender).

1.7. Objectives and outline

The scientific community is increasingly evaluating CECs, and it is critical to establish their harmfulness and ecotoxicological effects alone and in mixtures. Once in the Ocean, CECs are omnipresent, and therefore, the aim of this thesis relies on understanding their toxic effects alone and in secondary and tertiary mixtures.

Moreover, reproductive success is crucial for the generation of viable future populations, and the Mediterranean mussel is the perfect sentinel organism to help understand variations that the presence of CECs can cause.

In this thesis, an evaluation of ecotoxicological effects of polystyrene nanoplastics (50 nm), 5-Fluorouracil and silver nanoparticles (20 nm) was carried out using a multi-biomarker approach to assess the effects of the mixture of these CECs in the gills, the digestive gland, and the gonads with and without sex differentiation, as well as an evaluation of the effects in spermatozoa and oocytes of *M. galloprovincialis*. For that purpose, characterisation of nanoparticles, toxicity assays, cell viability, neurotoxicity, DNA damage, oxidative stress, oxidative damage, ingestion, proteomic analysis, synergistic and antagonistic evaluation of the mixtures, and a weight of evidence model has been accomplished to evaluate the effects of these CECs.

Chapter 1 addresses the question of what contaminants of emerging concern are and details of the three contaminants that will be focused on in this thesis. It also discusses the importance of evaluating the chosen emerging contaminants and reviewing the data available on their effects on marine biota. The chapter also discusses the importance of the Mediterranean mussel and its reproduction.

In **Chapter 2**, a toxicity assay of PS-NPs was used to calculate EC_{50}, *in vitro* assays were carried out to assess cytotoxicity in mussel haemolymph after exposure to PS-NPs, and the toxic effects on neurotoxicity in the gills of *M. galloprovincialis* and the ingestion of PS-NPs in the gills, digestive gland and gonads of *M. galloprovincialis*

Chapter 3 focuses on the effects of PS-NP exposure in the gills and the digestive glands of *M. galloprovincialis*. The behaviour of PS-NP was characterised in fresh and seawater. Genotoxicity was evaluated in mussel haemolymph, and the antioxidant capacity was assessed in terms of antioxidant enzymes and oxidative damage.

Chapter 4 evaluates the effects of 5-Fluorouracil alone and in a mixture with polystyrene nanoplastics and silver nanoparticles in the gills and the digestive gland of *M. galloprovincialis.* Genotoxicity was evaluated in mussel haemolymph, and the antioxidant enzymes and oxidative damage in the gills and the digestive glands, as well as synergistic and antagonistic interactions between this mixture of contaminants.

In **Chapter 5**, the effects of PS-NP, 5-FU and nAg individually and as a tertiary mixture are evaluated in the gonads of *M. galloprovincialis.* The antioxidant capacity was analysed regarding the antioxidant enzymes, and oxidative damage and synergistic and antagonistic interactions between these contaminants were evaluated.

Chapter 6 evaluates gender differences in the effects of PS-NP and 5-FU individually and as a mixture in the gonads of *M. galloprovincialis*. The ingestion of PS-NP in male and female gonads was evaluated. The antioxidant capacity in terms of the antioxidant enzymes, oxidative damage and synergistic and antagonistic interactions between contaminants in the mixture were assessed. A weight-of-evidence model was also used to evaluate the harmfulness of the individual contaminants and as a mixture in both male and female mussels.

In **Chapter 7,** a proteomic approach was used to evaluate changes in protein expression at the biological, cellular, and molecular levels in male and female mussels when exposed to PS-NP.

Chapter 8 assesses the effects of PS-NP on spermatozoa, oocyte and embryo-larval development of *M. galloprovincialis*.

Chapter 9 concludes with a comprehensive review of the findings from the earlier chapters, outlines general conclusions, and suggests further research.

CHAPTER II

Polystyrene nanoplastics in the marine mussel *Mytilus galloprovincialis*

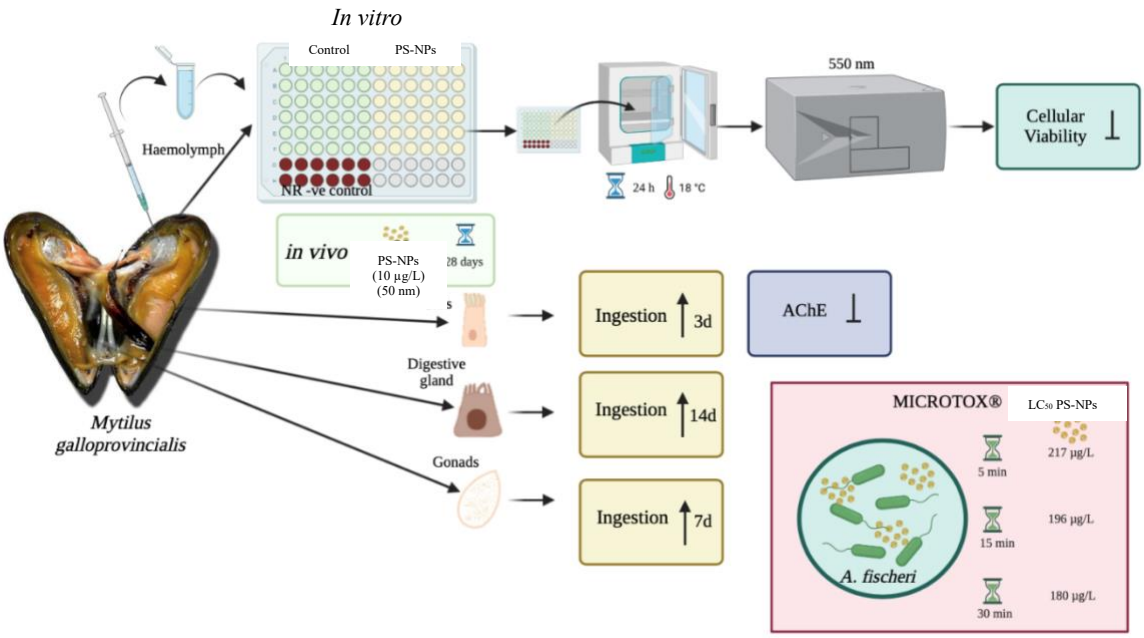

This chapter has been published in:

- Gonçalves, J. M., Benedetti, M., Errico, G., Regoli, F., & Bebianno, M. J. (2023). Polystyrene nanoplastics in the marine mussel *Mytilus galloprovincialis*. ☆. Environmental Pollution, 333(June), 122104. https://doi.org/10.1016/j.envpol.2023.122104

This chapter was presented at the international conference:

- **Micro2022 (14th – 18th November 2022): POSTER**
  →Neurotoxicity of polystyrene nanoplastics and their ingestion in the marine mussel *Mytilus galloprovincialis.* Joanna M. Gonçalves and Maria João Bebianno, Centre for Marine and Environmental Research, (CIMA) University of Algarve, Faro/Portugal

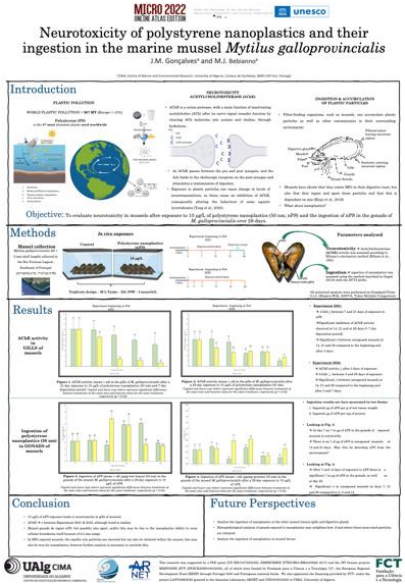

- **Encontro com a Ciência e a Tecnologia em Portugal 2023 (5th – 7th July 2023)– FCT: POSTER Presentation - Toxicity assessment of polystyrene nanoparticles in the bacteria Allivibrio fischeri and its ingestion in the marine mussel *Mytilus galloprovincialis*.** Joanna M. Gonçalves, Centre for Marine and Environmental Research, (CIMA) University of Algarve, Faro/Portugal

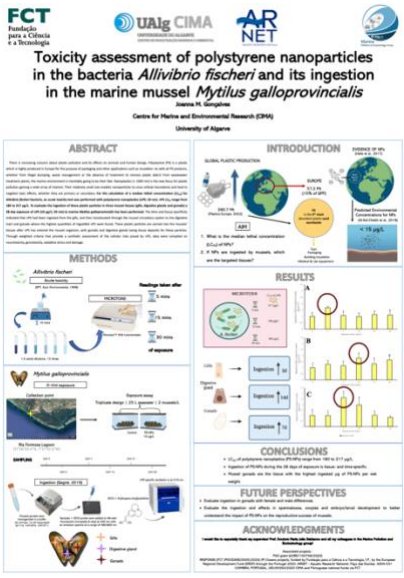

Abstract

Concerns about plastic pollution and its toxicity to animals and humans are increasing. Polystyrene (PS) is a plastic polymer that is extensively produced in Europe for packaging and building insulation, among other uses. Regardless of their source—illegal dumping, inadequate waste management, or insufficient treatment for removing plastic debris from wastewater treatment plants—PS products ultimately end up in the marine environment. Nanoplastics (< 1000 nm) have become the new focus of plastic pollution and are attracting significant interest. Whether primary or secondary, their small size enables nanoparticles to cross cellular boundaries, consequently resulting in adverse toxic effects. An *in vitro* assay of *Mytilus galloprovincialis* haemocytes exposed to 10 µg/L of polystyrene nanoplastics (PS-NPs; 50 nm) for 24 hours was conducted to assess cellular viability, along with the luminescence inhibition (LC_{50}) of *Aliivibrio fischeri* bacteria to evaluate acute toxicity. The cellular viability of mussel haemocytes significantly decreased after a 24-hour exposure, with PS-NPs LC_{50} ranging from 180 to 217 µg/L. Furthermore, a 28-day exposure of the marine bivalve *M. galloprovincialis* to PS-NPs (10 µg/L; 50 nm) was carried out to assess neurotoxic effects and the uptake of these plastic particles in three bivalve tissues (gills, digestive gland, and gonads). The ingestion of PS-NPs was both time- and tissue-specific, indicating that PS-NPs are taken in through the gills and then translocated via the mussel's bloodstream to the digestive gland and gonads, where the highest accumulation of ingested PS-NPs was observed. The presence of ingested PS-NPs may compromise the digestive glands' essential metabolic function and impair the mussels' gametogenic and reproductive success. Data on acetylcholinesterase inhibition, along with previously gathered information on a wide range of cellular biomarkers, were analysed through weighted criteria, providing a comprehensive assessment of cellular hazard from PS-NPs.

2.1.Introduction

Concerns have been raised regarding plastic pollution and its dangers to people and wildlife. Global plastic production (GPP) increased to 390.7 Mt in 2021 (PlasticEurope, 2022) and, among the consequences of illegal littering and dumping, waste mismanagement, as well as a low percentage of recycled plastics (8.3%) compared to fossil-based plastics (90.2%), the aquatic environment is the inevitable fate of these materials. In Europe, plastic production was equivalent to 15% of GPP (57.2 Mt), with applications such as packaging and building and construction composing 39.1 and 21.3% of Europe's plastic demands, respectively (PlasticEurope, 2022). In 2021, the European Union adopted a directive banning all single-use plastics, except bottles and fishing gear, which account for 70% of marine litter (Directive (EU) 2019/904).

Polystyrene (PS) is a plastic polymer highly produced for packaging, building insulation, medical equipment, toys, and single-use plastics (PlasticEurope, 2022). Besides being inexpensive and readily available, PS is known for its incredible dimensional stability and water resistance, permitting it to remain consistent in size and shape and certified as safe for use in food and beverages (Block et al., 2017). For example, PS can be found in day-to-day products, such as disposable cutlery, food containers, plates, cups, automotive and electrical components, and household items. However, not all plastic and PS products are recyclable (The Waste and Resources Action Programme, 2023). With PS products placed in waste bins, waste mismanagement and illegal dumping, and wastewater treatment plants (WWTP) also lacking the correct technique or method for plastic debris removal, the marine environment will be the endpoint for these PS particles. Field has reported seventeen million tons/year of generated PS global waste (Yuan et al., 2022). Once in the ocean, plastics undergo five main processes—hydrolysis, mechanical/physical degradation, thermal-oxidative degradation, photo-degradation, and biodegradation (Andrady, 2011) — that break down and fragment plastics into smaller sizes. After much focus on microplastics (> 1µm to 5 mm), nanoplastics (< 1000 nm; PS-NPs) are gradually gaining priority as nano-sized plastic particles may cross cellular boundaries, increasing their potential toxicity towards marine organisms (Peng et al., 2020). PS-NPs in the aquatic environment can be either primary or secondary. Primary PS-NPs enter the environment already in the nano-size range, and they are found in daily-use products such as cosmetics, clothing fibres, drug delivery and 3D ink printers (Bergami et al., 2016; Bessa et al., 2018; Canesi et al., 2015; Dong et al., 2019; Tamminga et al., 2018; Wang et al., 2018). The breakdown and

fragmentation of macroplastics (> 5 mm) and microplastics (< 5 mm) generate secondary PS-NPs. Although techniques for detecting and quantifying PS-NPs in the ocean are still challenging, evidence exists of plastics in the nano-size range. In the North Atlantic Gyre, a segment of nanoplastic containing PS in the nano-size range, along with polyethylene, polyvinyl chloride, and polyethylene terephthalate, was discovered. After simulating coastal activities on a PS cup and lid, nano-sized particles were released after just 5 minutes (Ekvall et al., 2019).

The toxic effects of PS-NPs in marine organisms have been evaluated (Auguste et al., 2020; Capolupo et al., 2021; Ferreira et al., 2019; Gonçalves & Bebianno, 2021; Gonçalves et al., 2022; Kihara et al., 2021) (Chapters 1, 3), demonstrating that PS-NP-mediated toxicity influences cell growth, larval development, embryonic malformation, inflammation, and the potential inactivation of algal photosystems (Gonçalves & Bebianno, 2021; Kögel et al., 2020) (Chapter 1). In the marine mussel *Mytilus galloprovincialis,* PS-NPs induce oxidative stress and damage (10 µg/L; 50 nm; 21 days) (Gonçalves et al., 2022; Chapter 3) and lysosomal destabilisation (1.5 – 150 ng/L; 50 nm; 21 days) (Capolupo et al., 2021). Additionally, in the mussel *Mytilus coruscus,* oxidative stress and a reduction in amylase activity were observed following exposure to PS-NPs (80 nm; 15 days; 0.26 mg/L). Although the ingestion and translocation of MPs have been evaluated, determining whether PS-NP toxicity is solely due to their ability to cross cellular boundaries or whether these nanoparticles are ingested, accumulated, and translocated between tissues remains challenging. In comparing MPs/PS-NP uptake, Wang et al. (2021) found that the ingestion of PS-NPs (70 nm and 500 nm) was greater than that of MPs (5, 10 and 100 µm) in the digestive tract of *M. coruscus* and noted translocation of the particles into the gonads (3-, 15- and 87-hours exposure, followed by 87 hours depuration). Consequently, this study conducted a combination of *in vitro* and *in vivo* experiments to assess both acute toxicity and chronic effects of PS-NPs on key model species. An *in vitro* assay on *M. galloprovincialis* haemocytes was performed to evaluate cellular viability after 24 hours of exposure to 10 µg/L of PS-NPs (50 nm), and acute toxicity was further characterised through the Microtox® bioassay (LC_{50}). An *in vivo* 28-day exposure of mussels was performed at the same concentration of PS-NPs to evaluate both the ingestion of nanoparticles in gills, digestive glands, and gonads and the onset of neurotoxicity in gills. These data were further integrated with those previously reported on a broad selection of cellular biomarkers; their overall elaboration through weighted criteria was expected to evaluate the toxicological hazard of PS-NPs better.

2.2.Materials and Methods

2.2.1. Polystyrene nanoplastics (PS-NPs)

Fluoresbrite® Plain YG spherical polystyrene nanoplastics of 50 nm in size (CAS 9003-53-6) were purchased from Polysciences, Inc. (Germany). 50 nm particles packed as 2.5% aqueous suspension, with 3.64×10^{14} particles/mL in ultrapure water (7732-18- 5) (CV = 15%, Excitation max. = 441 nm, Emission max. = 486 nm). Gonçalves et al. (2022) provides a comprehensive description of the characterisation of PS-NPs and demonstrates that the hydrodynamic diameter of PS-NPs increases when dispersed in FSW (852 ± 103 nm), indicating that the high salt content in seawater contributes to aggregation/agglomeration kinetics (Chapter 3). A concentration of 10 µg/L was employed for exposure assays.

2.2.2. Acute toxicity assay

The solid phase Microtox® bioassay (SPT, Azur Environmental, 1998) was employed to assess the acute toxicity of polystyrene nanoplastics (PS-NPs; 50 nm) in the bioluminescent marine bacterium *Aliivibrio fischeri,* according to ISO 1134-3: 2007 and ISO 21338: 2010, following the methodology outlined by Gambardella et al. (2019). All reagents and lyophilised *A. fischeri* bacteria (NRRL B-11177) were sourced from Modern Water Ltd (USA). The tests were conducted at 15ºC in the provided Microtox diluent. The initial concentration of PS-NPs used was 3724 µg/L, and a 1:2 serial dilution was performed 13 times, with the lowest concentration of PS-NPs tested being 0.45 µg/L. The acute toxicity of PS-NPs was evaluated in terms of relative bioluminescence using a Microtox™ 500 luminometer after 5, 15, and 30 minutes of incubation. Bioluminescence inhibition was determined using the Microtox®FX equipment**,** and the data were analysed with the MicrotoxOmni software. The median lethal concentration (LC_{50}) was defined as the concentration that resulted in a 50% reduction in light after 5, 15, and 30 minutes of exposure for the bacteria.

2.2.3. *In vitro* assay

Fifteen mussels *M. galloprovincialis* (60 ± 5 mm) were collected from an offshore aquaculture site in Lagos, Southeast Portugal (A: 37º04’200” N 8º42,800” W, B: 37º04’200” N 8º41’000” W, C: 37º03’400” N 8º41’000” W, D: 37º03’400” N 8º42’800” W; Testa & Cunhas Ltd) and transported alive to the laboratory. Mussels (2 mussels/L)

were placed into a 10 L tank with 7.5 L of seawater (S: 36 ± 1) and left to acclimatise for 48 hours. Then, mussel haemolymphs were extracted from the posterior adductor muscle of mussels with a sterile hypodermic syringe (1 mL; 25 G needle) under aseptic conditions in a vertical laminar airflow cabinet and kept on ice. Cell extraction and incubation methods were based on the modifications of protocols developed by Gómez-Mendikute & Cajaraville (2003) and Katsumiti et al. (2014). Five pools of three mussels per pool were used. Firstly, 10 µL of pooled haemolymph was diluted in an anti-aggregation solution (171mM NaCl; 0.2M Tris; 0.15% v/v HCl 1 N; 24mM EDTA) to avoid clumping and aggregation of cells (Katsumiti et al., 2014). Trypan blue dye (0.4% in physiological solution; v/v) was added for cell staining in a 1:2 ratio (cell suspension: Trypan Blue 0.4%). Using a Neubauer chamber (200 cells per specimen), along with a haemocytometer and light microscopy (Compound Light Microscopy; 400x), cell viability was determined by the following equation:

$$Concentration\ (cells\ mL^{-1}) = \frac{nº\ cells\ \times\ 10\,000}{nº\ squares}\ \times\ dilution\ factor$$

Cell suspensions were diluted to a 2 x 10^5 haemocyte cells/mL density following cellular viability in an anti-aggregation solution. A volume of 100 µL was seeded into 96-well microplates (six replicates per pool) containing Dulbecco's Modified Eagle Medium (DMEM, pH 7.4) and exposed to 10 µg/L of PS-NPs. The microplates were incubated for 24 hours at 18 °C. After this incubation period, the culture media was discarded, and the neutral red (NR) assay was performed, adapted from the protocol described by Katsumiti et al. (2014). The culture medium from the wells was carefully removed, and the state of the cells was examined under light microscopy (Compound Light Microscopy; 400x). Subsequently, 50 µL of neutral red working solution (0.4%, pH 7.3-7.4) was added to each well, including empty wells for the negative control, and incubated for 1 hour in the dark. The microplate was then centrifuged at 270 *g* for 10 minutes at 4°C, after which the supernatant was removed, and the wells were gently washed with PBS. The dye was extracted from the viable cells using an acetic acid/ethanol solution (1:100), following sample transfer to U-bottom 96-well microplates and centrifugation at 270 *g* for 10 minutes at 4 °C. The supernatants were subsequently placed in flat bottom microplates, and absorbance was measured at 550 nm using the Infinite M200 Pro, TECAN®.

2.2.4. *In vivo* assay

Mussels *M. galloprovincialis* Lamarck, with a shell size of 60 ± 5 mm, were collected from the Ria Formosa Lagoon in Southeast Portugal (37°00'30.6"N 7°59'39.6"W) and transported alive to the laboratory. Following a four-day acclimatisation period, 50 mussels were placed into each 30 L tank containing 25 L of seawater in a triplicate design to achieve a ratio of 2 mussels per litre. Mussels were exposed to 10 µg/L of polystyrene nanoparticles (PS-NPs; 50 nm) for 28 days. Seawater was exchanged every two days, and nanoparticles were re-dosed. No mortality was observed in either treatment.

Mussels were collected at the beginning of the experiment and after 3, 7, 14, 21, and 28 days of exposure. They were weighed, and the gills, digestive glands, and gonads were dissected. Then, they were instantly frozen in liquid nitrogen and stored at -80°C for subsequent investigation of neurotoxicity (AChE) in the gills and the ingestion of PS-NPs in the three tissues.

2.2.5. Quality control and assessment

Each tank was covered in glass to reduce airborne pollution, and glass pipettes were used to administer aeration to prevent plastic contamination. To prevent further plastic contamination, no gloves, plastic instruments, or plastic materials were used during tissue dissection. Furthermore, haemolymph extraction and cell cultures were performed under aseptic conditions in a vertical laminar airflow cabinet.

2.2.6. Acetylcholinesterase activity (AChE)

AChE activity was only assessed in the gills of *M. galloprovincialis* (n=5 per treatment and time of exposure) following a modification of Ellman's colourimetric method (Ellman et al., 1961). This method relies on the reaction between acetylthiocholine (ATC) and 5,5'-dithiobis(2-nitrobenzoic acid) (DTNB), resulting in the formation of a yellow product, 5-thio-2-nitrobenzoic acid (TNB) ion. Initially, the gills were individually homogenised in 5 mL of Tris-HCl buffer (100 mM, pH 8) and 50 µL of Triton X-100 (0.1%). After centrifugation (12 000 x *g*, 4ºC, 30 min), the supernatant was collected and stored at -80ºC until further analysis.

AChE activity was determined by adding DTNB (0.75 mM) to the samples, which were left to incubate at room temperature for 5 mins. Then, an ATC solution (3 mM) was added to trigger the reaction. The absorbance was read at 412 nm using a Tecan (Infinite 200 Pro)

microplate reader for 5 mins with 30-second intervals. AChE activity is expressed as nmol ATC min^{-1} mg $protein^{-1}$.

2.2.7. Total protein

AChE activity was standardised to determine total protein concentrations using the Bradford (1976) method. Total protein concentrations (mg protein g^{-1} tissue) were calculated using bovine serum albumin (BSA) as a standard and optimised for the microplate reader.

2.2.8. Ingestion

Following the method described by Gagné (2019), the ingestion of PS-NPs was evaluated using a fluorescence-based methodology with the molecular rotor probe 9-(dicyanovinyl)-julolidine (DCVJ). Firstly, individual tissues (gills, digestive glands, and gonads) (n=6 per treatment, per time of exposure) from mussels were homogenised at 20% (w/v) in an ice-cold buffer solution (50 mM NaCl, 10 mM Hepes – NaOH [pH 7.4], 1 mM EDTA, and 1 mM DTT), utilising a VWR Star-Beater (5 min, 20/s shaking, with grinding balls). Samples were centrifuged for 20 minutes (2ºC, 15,000 *g*) to isolate the cytosolic fraction, and the resulting supernatant was immediately frozen at -80ºC until further analysis. Samples were then analysed using a spectrofluorometric microplate reader (Berthold Tristar 5) with excitation at 450 nm and emission spectra ranging from 400 to 800 nm. The wavelength corresponding to PS-NPs was 510 nm. Results are expressed as PS-NPs µg/g wet weight relative to controls.

2.2.9. Statistical Analysis

The significance of the differences between treatments and time was determined using the Shapiro-Wilk test for data distribution and variance homogeneity, alongside either parametric tests (ANOVA, followed by Tukey's post hoc test) or non-parametric equivalent tests (Kruskal-Wallis and a two-tailed multiple comparisons test). The results were deemed significant if $p < 0.05$. GraphPad Prism version 9.4.1 (GraphPad Software, Inc. CA) was utilised for the statistical analysis. Furthermore, the relationship between treatments (not exposed and exposed to PS-NPs) and the examined tissues (gills, digestive gland, and gonads) was assessed using Principal Component Analysis (PCA) [Statistica 7.0 software (Statsoft Inc., 2005; USA)].

2.2.10. Weight of Evidence (WOE)

In addition to results on acetylcholinesterase, data on cellular biomarkers (superoxide dismutase SOD, catalase CAT, glutathione peroxidase GPx, glutathione S-transferases GST, lipid peroxidation LPO and DNA damage) were also obtained from Gonçalves et al. (2022) (Chapter 3) who exposed mussels to the same exposure to PS-NPs as described in the present work (10 µg/L of PS-NPs 50 nm for 21 days). The overall biomarkers results were elaborated through a quantitative Weight Of Evidence model (WOE, Sediqualsoft) that provides a synthetic hazard index based on a specifically developed algorithm and mathematical procedure (Regoli et al., 2019). For each analysed biomarker, the magnitude of the observed variation is compared to a specific threshold, corrected for the toxicological relevance of the biological endpoint (weight) and the statistical significance of the difference concerning controls. Whole calculations, detailed flow charts, and the rationale for weights, thresholds, and expert judgements have been previously described in detail (Regoli et al., 2019).

2.3.Results

2.3.1. PS-NPs Acute Toxicity

The EC_{50} (µg/L) for luminescence inhibition of *A. fischeri* after 5, 15, and 30 minutes of exposure to PS-NPs was 217, 196, and 180 µg/L, respectively (Table 2.1).

Table 2.1. LC_{50} concentration (µg/L) of polystyrene nanoplastics

LC_{50} (µg/L)		
5 mins	15 mins	30 mins
217	196	180

2.3.2. *In vitro* assay

In *M. galloprovincialis* haemocytes, exposure to PS-NPs (10 µg/L) for 24 hours caused a significant reduction in cell viability compared to unexposed cells ($p < 0.05$) (Fig. 2.1.).

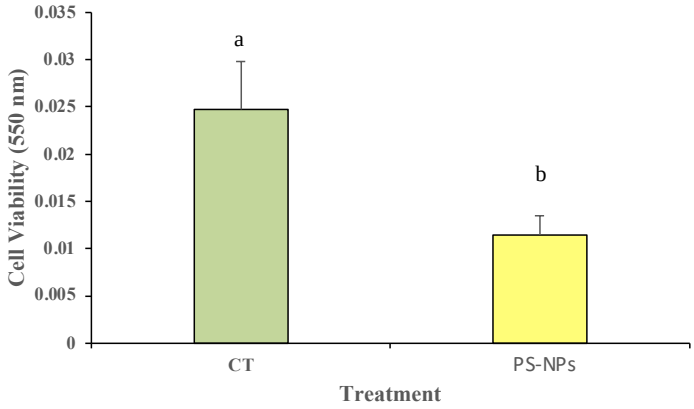

Figure 2.1. *M. galloprovincialis* cell viability (mean ± sd) using Neutral Red dye in unexposed haemocytes (CT) and those exposed to 10 µg/L of PS-NPs after 24 h. Different letters indicate significant differences between treatments ($p < 0.05$).

2.3.3. AChE activity

Significant differences in unexposed mussels were observed on days 14, 21, and 28 compared to the beginning, while the effects of PS-NPs became particularly evident after 3 and 7 days of exposure ($p < 0.05$; Fig 2.2). In the gills of mussels exposed to PS-NPs, a substantial decrease in AChE activity was recorded after 3 days of exposure ($p < 0.05$), with an additional two-fold decrease measured between 3 and 28 days ($p < 0.05$).

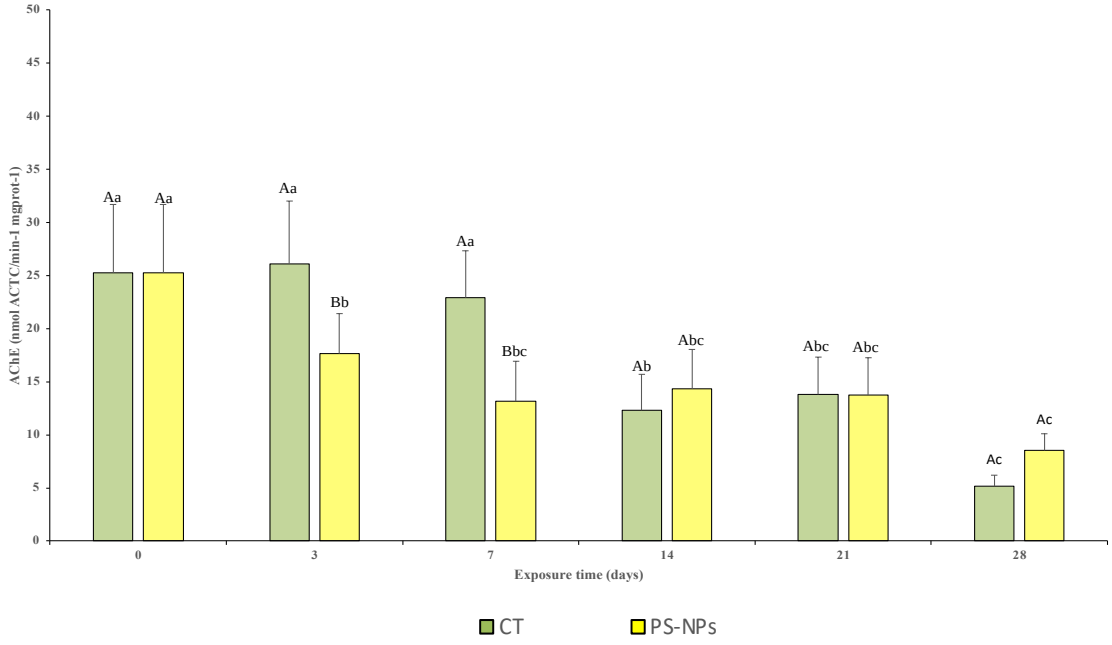

Figure 2.2. Acetylcholinesterase activity (AChE) in gills of *M. galloprovincialis* (mean ± sd) unexposed (CT) and exposed to 10 µg/L of PS-NPs after 28-d. Different upper- and lower-case letters indicate significant differences between treatments for the same time and between times for the same treatments, respectively ($p < 0.05$).

2.3.4. Ingestion

Mussel gills showed substantial ingestion of PS-NPs (1.7 ± 0.01 µg/w.w.), equating to 6.75 x 10^8 particles/mL (Fig. 2.3A) after 3 days of exposure, compared to other durations ($p < 0.05$). In the digestive glands, there was a notable increase in PS-NP ingestion after 14 days of exposure ($p < 0.05$), amounting to 5.5 x 10^{10} particles/mL (Fig. 2.3B). In comparison to gills and digestive glands, the highest levels of PS-NP ingestion were observed in the gonads after 7 and 14 days of exposure, with values of 2.6 ± 0.5 and 2.0 ± 0.6 µg PS-NPs/g w.w., representing 2.9 x 10^{10} and 2.1 x 10^{10} particles/mL, respectively ($p < 0.05$), as shown in Fig. 2.3C.

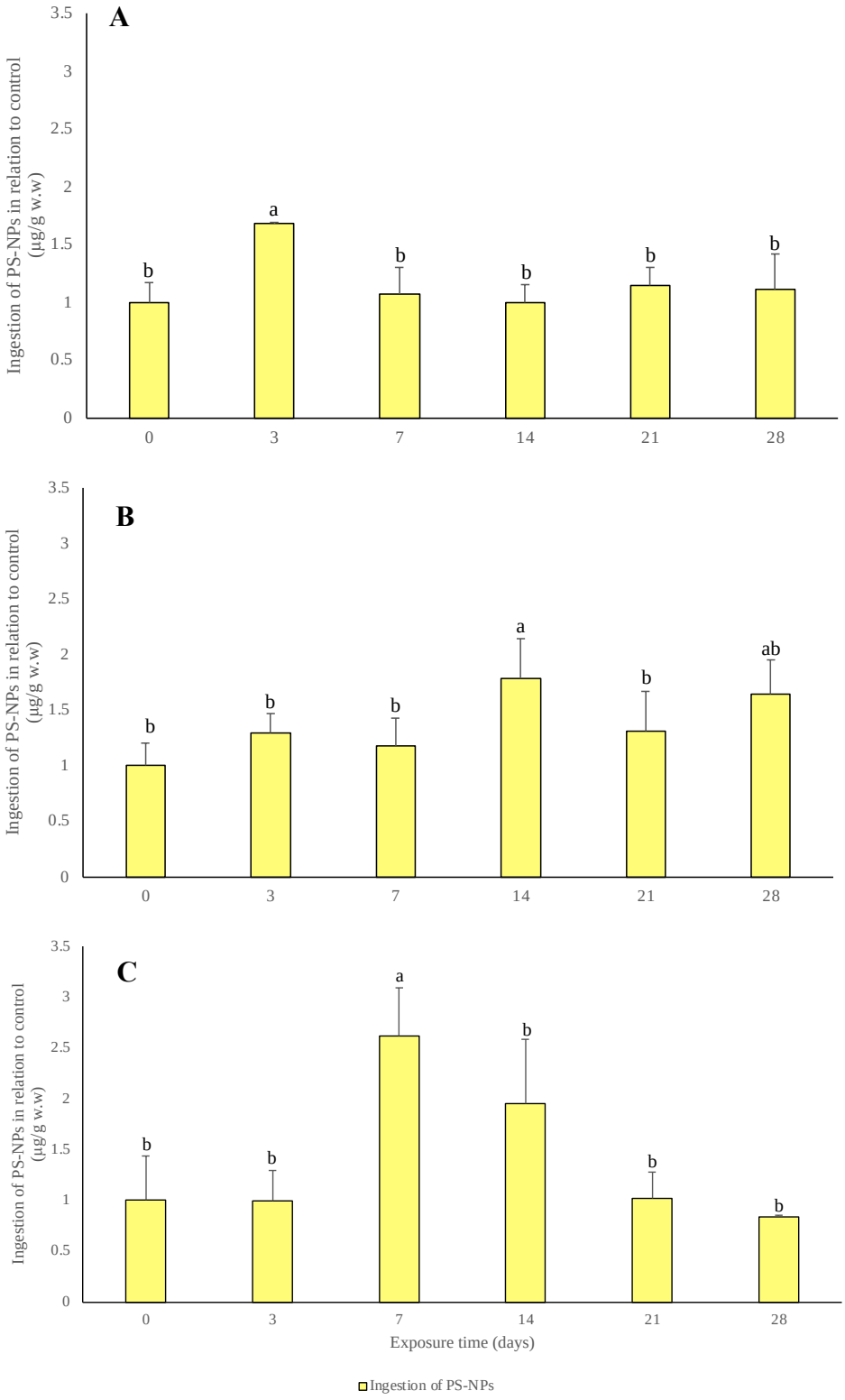

Figure 2.3. Ingestion of PS-NPs relative to controls (µg/g w.w) in *M. galloprovincialis* **(A)** gills, **(B)** digestive glands, and **(C)** gonads (mean ± sd) after 28-d to 10 µg/L of PS-NPs (50 nm). Different lower-case letters indicate significant differences between times for the same treatments ($p < 0.05$).

2.3.5. Principal Component Analysis (PCA)

The ingestion of PS-NPs in the three mussel tissues (gills, digestive gland, and gonads) was described using PCA, which was applied to all the data collected at each time point throughout the 28 days of exposure (Fig. 2.4). The two principal components (PC1 and PC2) accounted for 74.2% of the overall variation (PC1 = 50.37%, PC2 = 23.82%; Fig. 2.4). There is a distinct separation between the mussel gills and the other evaluated tissues, as well as a differentiation between the unexposed mussels and those exposed to polystyrene nanoplastics. The first principal component exhibits significant positive associations with the digestive gland and gonads of mussels, in addition to days 7, 14, and 21 of exposure to PS-NPs. Relative to the second component, significant associations are evident in the digestive gland of mussels and on days 14 and 28 of exposure to PS-NPs. Therefore, the PCA (Fig. 2.4) corroborates the ingestion of PS-NPs observed in the digestive gland and gonads of mussels (Fig. 2.3.B and 2.3.C), supporting the notion that 7, 14, and 21 days of exposure are the most critical for this species. Thus, the PCA confirms that the ingestion of PS-NPs in *M. galloprovincialis* is both tissue- and time-dependent.

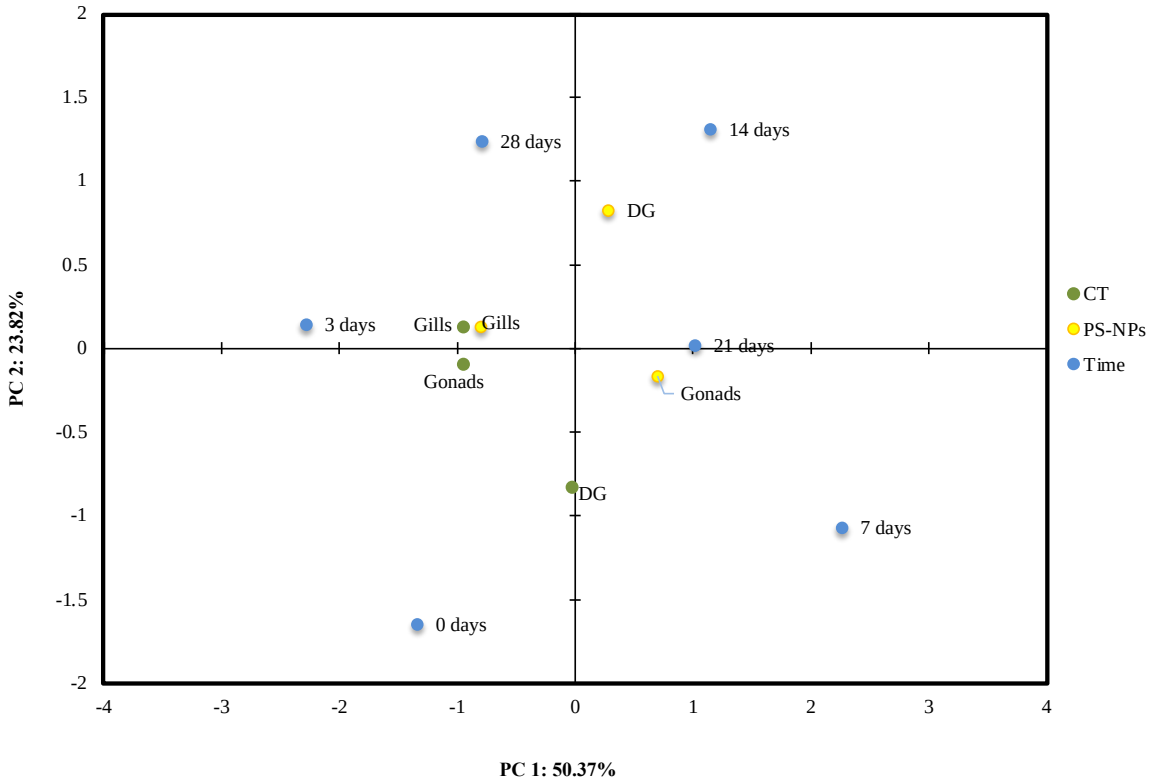

Figure 2.4. Principal component analysis of ingestion in the gills, digestive glands, and gonads of *M. galloprovincialis* in unexposed and exposed to 10 µg/L of PS-NPs for 28-d ($p < 0.05$).

2.3.6. WOE

The overall WOE elaboration of biomarker results (Table 2.2) indicated an increase in cellular hazard after 3 days (Moderate) and even more so after 7 and 14 days (Major), while it returned to a Slight level by day 21. The parameters that primarily contributed to the time-course hazard increase were the antioxidant enzymes (SOD, CAT, GPx, and GST), further evidenced by significant variations in oxidative damage concerning DNA and lipid peroxidation.

Table 2.2. Weight of Evidence (WOE) of 10 µg/L of PS-NPs

Sample code	Data	N. param in class ABSENT	N. param in class SLIGHT	N. param in class MODERATE	N. param in class MAJOR	N. param in class SEVERE	Level of hazard for biomarkers	
PS-NPs-0	14.07.2020	17	0	0	0	0	ABSENT	
PS-NPs-3	14.07.2020	10	3	2	1	1	MODERATE	
PS-NPs-7	14.07.2020	8	1	2	4	1	MAJOR	
PS-NPs-14	14.07.2020	10	0	3	3	1	MAJOR	
PS-NPs-21	14.07.2020	12	4	0	0	0	SLIGHT	

2.4. Discussion

The haemolymph of mussels reports the functional condition of the organs it perfuses and extensive information on the animals' overall physiological status (Digilio et al., 2016). The viability of haemocyte cells in *M. galloprovincialis* haemolymph was affected by the exposure to PS-NPs (10 µg/L; 50 nm; Fig. 2.1.). *M. galloprovincialis* haemocytes exposed to 50 µg/mL of PS-NH_2 PS-NPs (50 nm) also caused cytotoxicity [30 min; (Canesi et al., 2015)], although the concentration is much higher than the one used in this study, cytotoxicity results may reflect increased toxicity of virgin PS-NPs compared to functionalised PS-NPs (i.e. PS-COOH and PS-NH_2). Moreover, PS-COOH and PS-NH_2 have been shown to alter immune parameters in the haemolymph of *M. galloprovincialis*, such as phagocytosis, lysosome activity, reactive oxygen species (ROS) and nitric oxide (NO) production (Auguste et al., 2018; Auguste et al., 2020; Canesi et al., 2015). They should be evaluated for virgin PS-NPs to assess whether they are more hazardous than functionalised PS-PS-NPs. Additionally, increased DNA damage in *M. galloprovincialis* haemolymph was caused by exposure to PS-NPs [10 µg/L; 50 nm; 14-d (Gonçalves et al., 2022; Chapter 3) and 0.05 – 50 mg/L; 106 ± 10 nm; 96 h (Brandts et al., 2018)]. The

translocation of PS-NPs from tissues to cells was evaluated, demonstrating that the internalisation of PS-NPs in haemocytes is size-dependent, with 50 nm PS-NPs mostly internalised compared to 100 nm and 1 µm polystyrene particles (Sendra et al., 2020a). Therefore, PS-NPs of 50 nm in size induce cytotoxicity and may have more severe implications for the overall physiological status of *M. galloprovincialis*.

Regarding acute toxicity, no effects of microplastics were demonstrated at environmentally relevant concentrations (Booth et al., 2016; Gagné, 2017; Gambardella et al., 2019), while exposure of the luminescent bacteria, *A. fischeri*, to PS-NPs (0.45 to 3724 µg/L; 50 nm) caused toxic effects after 5, 15 and 30 mins of exposure (Table 2.1.). After 30 mins, LC_{50} for PS-NPs (50 nm) was evaluated here to have a much lower value, 180 µg/L, compared to 1000 mg/L of 2-poly(methylmethacrylate) NPs [86 to 125 nm; 0.01 – 1000 mg/L; PMMA-NPs; (Booth et al., 2016)] and 1000 µg/mL polyethyleneimine PS-NPs [55 and 110 nm; 3 – 1000 µg/mL; PS-PEI-PS-NPs; (Casado et al., 2013)]. Therefore, it is deducible that PS-NPs are more toxic than PMMA-NPs and PS-PEI-NPs. Gambardella et al. (2019) suggested that particles smaller than 1µm would be more toxic as the pore size of cell walls prevents larger particles from entering the bacterium (PE-MPs; 1 – 500 µm; 25 mg/L), thus confirming the ability of nano-sized particles to cross cellular boundaries. Moreover, PE-MPs did not affect *A. fischeri* luminescence (Gambardella et al., 2019). With effects on cellular viability, growth, and potential internalisation of PS-NPs, nano-sized plastic particles pose a greater risk than micro-sized ones, with unpredictable consequences for trophic transfer and overall ecosystem impacts.

In the gills of mussels, neurotoxicity occurred after 3 days of exposure to 10 µg/L of PS-NPs (50 nm). Despite the differences observed in controls, a decrease in AChE activity was noticeable throughout the 21-d exposure. A 15 ng/L exposure of PS-NPs (50 nm) for 21 days also caused a decrease in AChE activity in the *M. galloprovincialis* gills (Capolupo et al., 2021), while no neurotoxicity was observed in the freshwater clam *Corbicula fluminea* after exposure to PS-NPs (80 nm; 0.1 – 5 mg/L; 96 h) (Li et al., 2020). On the other hand, microfibres of PET caused a dose-dependent increase of AChE activity in the gills of *M. galloprovincialis* (PET-MFs; 100 µm; 0.0005 – 100 mg/L, Choi et al., 2021) suggesting that PS-NPs have a more significant on AChE, causing adverse effects to the neurological and sensory systems of mussels. Acetylcholine, a key neurotransmitter in the neurological and sensory systems, is broken down by AChE to convey impulses at cholinergic synapses, essential for neurotransmitter release and synaptic plasticity (Picciotto et al., 2012). Therefore, it can be deduced that as the size of PS-NPs decreases,

they exert more neurotoxic effects on mussels, which are more pronounced in seawater than in freshwater.

To the best of our knowledge, this is the first data set on the ingestion of polystyrene nanoplastics (50 nm), using the method developed by Gagné (2019), in the three tissues of *M. galloprovincialis* (gills, digestive gland, and gonads) after a 10 µg/L exposure for 28 days. Considering the pathways of PS-NP intake for a filter-feeder organism like *M. galloprovincialis*, these particles can directly enter the organism through the gills or their ability to cross cellular boundaries due to their small size. With biological reactivity increasing with decreasing particle size (Peng et al., 2020), the relationship between PS-NP ingestion and toxicity towards organisms is crucial. After 28 days of exposure to 10 µg/L of PS-NPs (50 nm), *M. galloprovincialis* gills, digestive gland and gonads presented time-specific ingestion rates. As filter-feeding organisms, the increase in PS-NP ingestion by the gills after 3 days of exposure is expected, as this is the first tissue to encounter contaminants in the surrounding environment. Looking at the same experimental conditions (10 µg/L PS-NPs; 50 nm; 21-d), the gills of *M. galloprovincialis* after 3 days of exposure led to a significant decrease of antioxidant enzyme activity until the 14th day, leading to oxidative damage (Gonçalves et al., 2022; Chapter 3). Results suggested that the internalisation of PS-NPs in the gills has a prolonged toxic effect, although an adaptive response was observed after 21 days. In another study, PS-NPs (50 nm) were also found in *M. galloprovincialis* gills. However, larger PS-NPs (100 nm and 1µm) were more abundant after 24h of exposure (Sendra et al., 2020b); this was partly expected as larger particles have similar sizes to food sources and are often mistaken as non or low-nutritional food (PS-NPs; 30 nm; 0.1 – 0.3 g/L; 8 h) (Wegner et al., 2012). However, in the gills of the mussel *Mytilus coruscus*, intake and ingestion of PS-NPs were seen as unstable, with intake levels of smaller PS-NPs (70 nm) higher than bigger tested PS-MNPs (0.5, 5, 10 and 100 µm) [0.2 mg/L; 3h and 24h; (Wang et al., 2021)]. Therefore, further evaluation is necessary to comprehend how different sizes of PS-NPs are ingested and accumulated in the gills of mussels.

The digestive gland of mussels is responsible for vital metabolic functions, such as food intracellular uptake/digestion and as a storage for reserve substances (Faggio et al., 2018). Here, the mussel's digestive gland shows a significant intake of PS-NPs after 14 days of exposure ($p < 0.05$). This suggests that after initial ingestion of the gills at day 3, PS-NPs translocate to the digestive gland and remain stored until the end of the experiment. The seventh day was most critical for mussel digestive glands after 21 days of exposure to 10

µg/L (50 nm), causing inhibition of CAT and GPx activity and consequently leading to oxidative damage (Gonçalves et al., 2022; Chapter 3). In this instance, the results suggest that although not significant, the presence of PS-NPs at day 7 is critical for this tissue and that the increase in ingestion after this time point truly overwhelms the antioxidant defence system of the mussel.

Moreover, Sendra et al. (2020) suggest that the digestive gland of *M. galloprovincialis* was the expected destination for PS-NPs (50 nm; 3 and 24h), being these particles were observed in the stomach lumen, epithelia of the stomach and the lumen of digestive tubules. Also, glitter particles (62.5 particles/L; 7-d) ingested by *M. galloprovincialis* accumulated in the digestive tract of mussels as the ingested glitter increased with the decrease in particle size (Provenza et al., 2022). Findings confirm that the smaller the size of the nanoplastic, the greater the accumulation of these particles in the digestive system of mussels. Wang et al. (2021) found that most ingested PS-MNPs (70 nm, 0.5, 5, 10, and 100 µm; 87h exposure followed by 87h depuration) in *M. coruscus* were in the digestive gland of the mussels, being dependent on particle ingestion size, with a higher ingestion of 70 nm PS-NPs. This confirms the role of the mussel's digestive gland as a reservoir and substantiates that the ingestion of PS-NPs is size-dependent.

Gonads of mussels showed the highest levels of PS-NPs among those measured in the three tissues, mainly after 7 and 14 days of exposure (2.6 ± 0.5 and 2.0 ± 0.6 µg PS-NPs/g w.w., respectively; $p < 0.05$). Considering the anatomy of mussels, a hypothesis is that PS-NPs, due to their small size and ability to cross cellular boundaries, may 'diffuse' across tissues besides being transported to different tissues via the haemolymph. A translocation study from cells to tissue showed that internalisation of PS-NPs (50 nm, 100 nm and 1µm; 3 – 24 h) into haemocytes was size–dependent, with PS-NPs of 50 nm being the most internalised (Sendra et al., 2020b). Therefore, the observed ingestion of PS-NPs (50 nm) in gonads may be due to their translocation by the mussel's bloodstream. However, their ability to cross cellular boundaries (Peng et al., 2020) should not be excluded. Wang et al. (2021) also observed that in *M. coruscus*, translocation of PS-MNPs to gonads occurred (70 nm, 0.5, 5, 10, and 100 µm; 87h exposure followed by 87h depuration). However, the ingestion of PS-NPs by gonads was much lower than in the digestive gland. This study observed the opposite; thus, smaller PS-NPs seem more hazardous for mussel gonads. However, the antioxidant defence mechanism of *M. galloprovincialis* exposed to 10 µg/L of PS-NPs (50 nm) for 21 days was able to counteract PS-NPs toxicity, and no oxidative damage was observed (Gonçalves & Bebianno, 2023; Chapter 5). Still, further analysis

with sex-differentiating effects is crucial to understanding how ingested PS-NPs can affect the reproductive organs of mussels. During the gametogenesis cycle, lipid content has been shown to increase with the maturation of female gonads and to be used as an energy source during gametogenesis and embryo-larval development (Martinez-Pita et al., 2012). The gonads of mussels and their development are essential for reproductive success and may be compromised with the increase in ingested PS-NPs, affecting spermatozoa mobility and robustness of oocytes; however, further investigation is necessary to confirm this. More concerning, as PS-NPs of 50 nm internalise haemocytes, spermatozoa and oocytes may also be at risk. In *Crassostrea gigas*, the fertilisation rate decreased after gametes were exposed to PS-NPs (50 nm; 1.5 h) (Tallec et al., 2018), and sperm mobility and fertilisation success was impaired, as agglomerates of nanoparticles were found attached to spermatozoa and the jelly coating of oocytes (PS-COOH and PS-NH_2; 0.1 to 100 mg/L; 1, 3 and 5 h) (González-Fernández et al., 2018). In *M. galloprovincialis,* malformations of D-larvae were found after embryos were exposed to PS-NPs (50 nm; 10 µg/L; 48 hpf) (Auguste et al., 2021), suggesting that the high levels of ingested PS-NPs in mussel gonads may pose a significant threat to the reproduction of these organisms.

In the present study, the biological significance of the results observed in this and a previous study (Gonçalves et al., 2022; Chapter 3) was summarised in specific hazard indices, allowing an easier qualitative and quantitative comparison of the effects of PS-NPs at different exposure times. The applied elaboration considers the toxicological relevance (weight) of measured endpoints' and the number and magnitude of variations normalised to specific thresholds. This model has been validated in several case studies aimed at evaluating biological and environmental risk assessment, providing the possibility to integrate large datasets of heterogeneous data and better interpret asynchronous variations of complex pathways (Mezzelani et al., 2021; Nardi et al., 2022; Pittura et al., 2018; Regoli et al., 2014). The weighted assessment of biomarker results confirmed the involvement of oxidative stress in modulating the toxicity of nanoparticles, revealing a clear time-dependent trend, as previously outlined in the discussion of individual results (Table 2.2). The cellular hazard increased to moderate after 3 days, further rising on days 7 and 14, and at this point, the observed variations were classified as major hazards. Following this peak, a counteracting response to the oxidative challenge is evident in the return to a slightly hazardous condition.

2.5.Conclusion

This dataset provides evidence of the ingestion of polystyrene nanoplastics in the marine mussel *M. galloprovincialis*, as well as neurotoxicity and *in vitro* effects on mussel haemolymph. PS-NPs induce neurotoxicity in mussel gills and reduce viable haemocytes in the mussel's haemolymph. Ingestion in mussels is tissue and time-specific, with the highest levels of ingested PS-NPs found in mussel gonads. The amount of ingested PS-NPs may elucidate biochemical alterations in mussel tissues; however, further investigation is required. Additionally, the effects of ingested PS-NPs in the gonads of mussels need further examination to understand how they may influence gametogenesis, fertilisation success, and embryo-larval development. Finally, the impacts of consuming PS-NPs contaminated shellfish batches could pose adverse effects on human health and should be considered for future analysis.

CHAPTER III

Chronic toxicity of polystyrene nanoparticles in the marine mussel *Mytilus galloprovincialis*

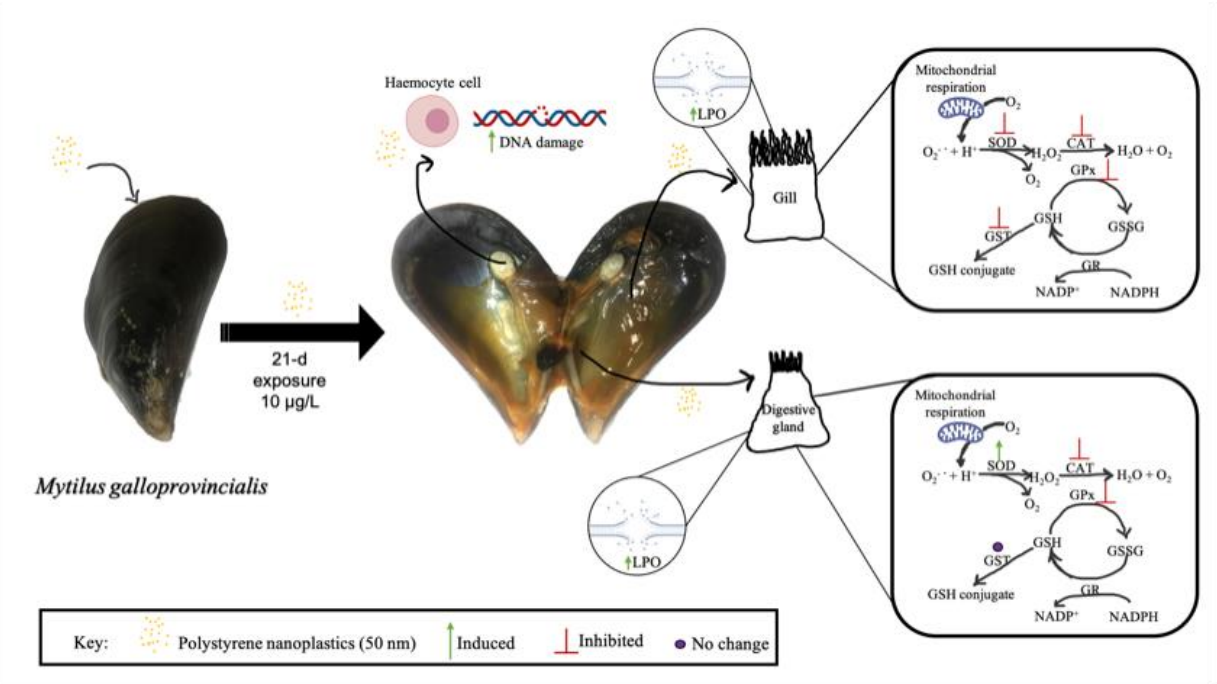

This chapter has been published in:

- Gonçalves, J. M., Sousa, V. S., Teixeira, M. R., & Bebianno, M. J. (2022). Chronic toxicity of polystyrene nanoparticles in the marine mussel *Mytilus galloprovincialis*. Chemosphere, 287(January 2022), 132356. https://doi.org/10.1016/j.chemosphere.2021.132356

This chapter was presented at the international conferences:

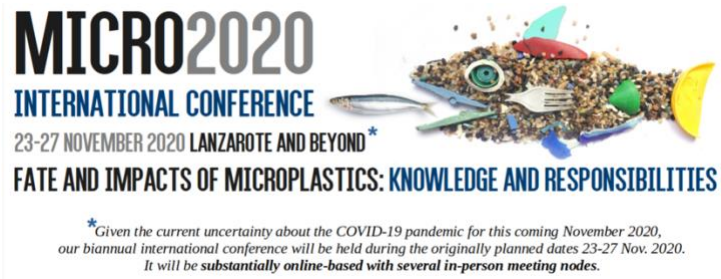

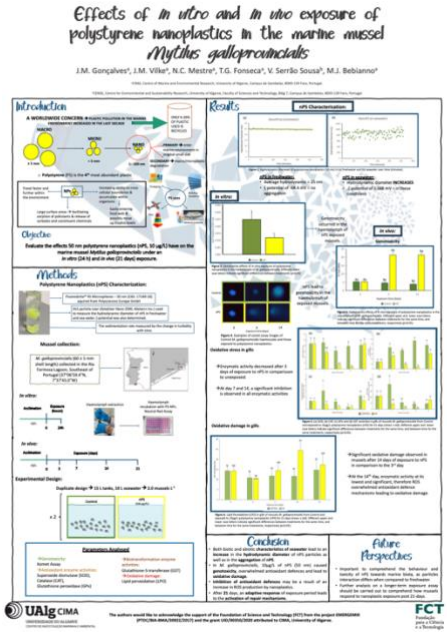

- **Micro2020** (23rd – 27th November 2020): **POSTER**
  Gonçalves, J. M., Vilke, J. M., Mestre, N. C., Fonseca, T. G., Serrão Sousa, V., Bebianno, M. J. (2020). Effects of *in vitro* and *in vivo* exposure of polystyrene nanoplastics in the marine mussel *Mytilus galloprovincialis*.

- **CICTA2021** (29th November – 2nd December 2021): **ORAL PRESENTATION**

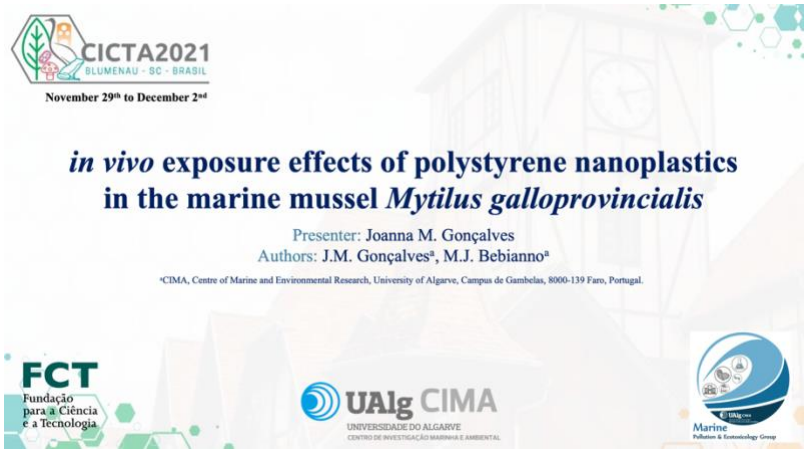

Abstract

Nanoplastics (NP) (1 – 100 nm) are a growing global concern, and their adverse effects on marine organisms are still scarce. This study evaluated the impact of polystyrene nanoplastics (10 µg/L; 50 nm PS-NPs) in the marine mussel *Mytilus galloprovincialis* after a 21–day exposure. Over time, the hydrodynamic diameter and zeta potential of PS-NPs were analysed in seawater and ultrapure water. A multi-biomarker approach (genotoxicity (the comet assay) was assessed in mussel haemocytes, and the antioxidant enzymes (superoxide dismutase (SOD), catalase (CAT), glutathione peroxidase (GPx)), biotransformation enzyme (glutathione – *S* – transferase (GST)), and oxidative damage (LPO)) was assessed in gills and digestive glands to evaluate the toxicity of PS-NPs towards mussels. In seawater, aggregation of PS-NPs is favoured, and consequently, the hydrodynamic diameter increases. Genotoxicity was highly noticeable in mussels exposed to PS-NPs, presenting a higher % tail DNA when compared to controls. Antioxidant enzymes are overwhelmed after PS-NP exposure, leading to oxidative damage in both tissues. Results showed that mussel tissues are incapable of dealing with the effects that this emerging stressor pursues towards the organism. The Integrated Biomarker Response index, used to summarise the biomarkers analysed into one index, shows that PS-NP toxicity towards mussels is both tissue- and time-dependent since gills are the most compromised tissue.

3.1 Introduction

Nanoplastics (NP) (1 – 100 nm) (Gigault et al., 2018) in the marine environment primarily originate from the degradation of macro/microplastics (Andrady, 2011; Cole et al., 2011) but can also enter the marine environment in their initial small size, having been intentionally manufactured to a specific size for applications found in consumer products (e.g., cosmetics, clothing fibres, drug delivery, etc.) (Bessa et al., 2018; Tamminga et al., 2018; Wang et al., 2018). These pose an increasing global concern, and the time required to produce nano-sized plastic particles depends on the size of the original plastic (Koelmans et al., 2015). Once in the marine environment, plastic particles undergo two primary breakdown processes: fragmentation and degradation (Mattsson et al., 2018). Following the fragmentation of larger plastic polymer chains into smaller fragments, the polymer itself remains unaltered; however, degradation processes render plastic polymers vulnerable to bond-breaking mechanisms, thus altering the polymer properties (Andrady, 2011). Regarding plastic degradation, five main processes can occur in the marine environment: hydrolysis, mechanical/physical and thermo-oxidative degradation, photodegradation, and biodegradation (Andrady, 2011). Once plastic

polymers undergo degradation into nano-sized particles, the surface area increases, enhancing their potential biological impact (Mattsson et al., 2018; Ferreira et al., 2019). Furthermore, at the nanoscale, plastic particles exhibit novel physical properties that facilitate their penetration through biological barriers, leading to accumulation in tissues and consequently affecting the organism's metabolism and behaviour (Worm et al., 2017; Mattsson et al., 2018; Ramirez et al., 2019). Compared to microplastics, the more significant health alterations in mussels have recently been linked to PS-NP exposure (Capolupo et al., 2021). Therefore, it is crucial to comprehend the burden of nanoplastic presence and its biological effects on marine biota.

The presence of plastic waste at the nanoscale in marine environments is established; however, detecting realistic concentrations of nanoplastics (NP) remains challenging, as several analytical methods are needed to measure NP concentrations accurately across various types of NP polymers and complex matrices (Halle et al., 2017). In the North Atlantic subtropical gyre, Halle and colleagues (2017) succeeded in obtaining a nanoplastic segment containing nano-scaled plastic polymers such as polyvinyl chloride (PVC), polyethylene terephthalate (PET), polyethylene (PE), and polystyrene (PS). Additionally, styrene oligomers have been identified along global water shorelines and in sand, and due to their widespread spatial distribution, they are regarded as a global contaminant in sandy beaches (Kwon et al., 2015). PS is the fourth most abundant plastic in the world and is extensively utilised in building insulation, plastic cutlery and glasses, packaging, toys, and medical equipment (PlasticsEurope, 2019). The degradation of PS products released into the environment is likely to result in styrene oligomers (Ekvall et al., 2019). Furthermore, Ekvall et al. (2019) demonstrated that nano-scaled PS particles were generated after five minutes of mechanical breakdown of PS coffee cup lids and polystyrene foams, simulating processes that occur along coastlines globally. Therefore, PS is a significantly important plastic polymer to evaluate at the nanoscale, as its potential release into the marine environment is increasingly high, particularly in coastal shorelines.

When acknowledging NP toxicity towards marine organisms, factors such as the plastic particle polymer, size, concentration, and exposure time must be considered, along with the fact that their toxicity is also influenced by the presence of other contaminants, food availability, species, and species developmental stages (Kögel et al., 2020). Decreases in growth rates, energy, stress, inflammation, and malformations are all linked to NP toxicity and its effects on marine biota (Kögel et al., 2020). Recent reviews have examined the effects of NP in the aquatic environment (Haegerbaeumer et al., 2019; Ferreira et al., 2019; Peng et al., 2020; Gonçalves & Bebianno, 2021; Kihara et al., 2021) (Chapter 1). In the marine context,

the impacts of NP on bacteria, algae, rotifers, nematodes, crustaceans, echinoderms, bivalves, and fish have been assessed (Ferreira et al., 2019; Gonçalves & Bebianno, 2021; Kihara et al., 2021; Capulupo et al., 2021) (Chapter 1). Most of the available data are based on PS PS-NPs with functionalised groups (amide or carboxyl groups) rather than on virgin PS nanoparticles, as it has been found that those with an amide group are more toxic than PS-NPs with a carboxyl group (Gonçalves & Bebianno, 2021; Chapter 1). PS-NPs have been shown to affect cell growth, larvae development, embryo malformations, oxidative stress-induced damage to lipid membranes, and potential inactivation of photosystems in algae (Gonçalves & Bebianno, 2021; Chapter 1). Ekvall et al. (2019) discovered that nanosized polystyrene particles were formed after mechanical breakdown, where PS-NPs exhibited either negative or neutral surface charges, highlighting the need to assess virgin PS-NP exposure. However, it is also vital to comprehend the toxic effects of PS-NPs without functionalised groups, namely virgin PS-NPs. Furthermore, due to mechanical abrasion from waves, winds, sand, and rocks, the PS-NPs produced encompass various types of PS-NPs (Ekvall et al., 2019).

Bivalves are regarded as excellent sentinel organisms for ecotoxicological assessments due to their wide geographical distribution and sessile filter-feeding habits, which enable them to accumulate nanoplastics (NP) from the surrounding environment, making them crucial species for assessing the effects of polystyrene nanoplastics (PS-NPs). Chronic exposure to NP in bivalves, considering the potential for reactive oxygen species (ROS) generation leading to oxidative stress and tissue-specific damage, remains relatively rare. Consequently, the primary aim of the present study is to understand the effects of PS NP (10 µg/L) in the marine mussel *Mytilus galloprovincialis through* a multi-biomarker approach. This study evaluates genotoxicity (comet assay) in the mussel's haemolymph, effects on antioxidant enzyme activities (superoxide dismutase – SOD, catalase – CAT, glutathione peroxidase – GPx), biotransformation enzyme activity (glutathione S-transferases – GST), and oxidative damage (lipid peroxidation – LPO) in the gills and digestive gland following a 21-day exposure. Although environmentally relevant concentrations of NP are still limited, for microplastics (< 5 mm), concentrations range from 0.008 µg/L (Desforges et al., 2014) to 10 µg/L (Ivar Do Sul et al., 2014) in coastal regions. Thus, a concentration of 10 µg/L of polystyrene nanoplastics was chosen.

3.2.Materials and methods

3.2.1. Polystyrene nanoplastics (PS-NPs)

Fluoresbrite® Plain YG 0.05 Micron Microspheres (9003-53-6) were obtained from Polysciences, Inc. (Germany). These 0.05 µm particles are packaged as a 2.5% aqueous suspension, containing 3.64 x 10^14 particles/mL in water (7732-18-5), with a coefficient of variation of 15%. The excitation maximum is 441 nm, and the emission maximum is 486 nm. A concentration of 10 µg/L was realised by adding 3 µL of PS-NPs to 10 L of seawater.

3.2.2. Characterisation of PS-NPs

Commercially available PS-NPs (from Polysciences, Inc., LOT#A780141) were analysed using a DLS particle sizer (ZetaSizer Nano ZS90, Malvern Inc.) to measure the hydrodynamic diameter of PS-NPs in both ultrapure water [7732-18-5] and filtered seawater (FSW). Zeta potential values of the NPs were determined through electrophoresis mobility measurements at 25°C, employing the same equipment, in a disposable polycarbonate capillary cell (1x1x1, DTS1061, Malvern Inc.). Time-resolved DLS measurements were implemented to assess aggregation kinetics, with samples measured over a period ranging from 2 to 12 hours. The estimated time interval between the onset of aggregation and data collection was 50 seconds.

3.2.3. Experimental Design

Mussels *M. galloprovincialis* Lam. (50 ± 5 mm shell length) were handpicked from the Ria Formosa Lagoon (Portugal) (37°00'30.6"N 7°59'39.6" W) and transported alive to the laboratory. All mussels were scrap–cleaned and placed into 10 L glass tanks (2 mussels/L) containing natural seawater (S: 35 ± 1) on a 12 h/12 h light/dark cycle, kept under constant aeration. The mussels were acclimatised for four days. After acclimatisation, mussels were exposed to 10 µg/L of PS-NPs alongside a control group maintained in clean seawater, arranged in a duplicate design (2 tanks per treatment) for 21 days. The seawater was changed every other day, with the redosing of PS-NP concentration. Seawater quality was analysed daily by measuring salinity (36.5 ± 0.75), temperature (24.5 ± 1.5°C), pH (7.9 ± 0.2), and oxygen saturation (100 ± 1.7%). The mussels were solely fed with the plankton present in the natural seawater. Mortality was observed in mussels subjected to PS-NP exposure on day 1 (one dead mussel) and day 3 (one dead mussel). No mortality was noted among the unexposed mussels. In this experiment, five mussels from both control and PS-NPs tanks were removed at the

beginning and after 3, 7, 14, and 21 days of exposure, during which the water volume, on exchange days, and repositioning of PS-NP contamination was adjusted to the number of mussels in each tank to maintain the ratio of 2 mussels/L. At each sampling point, mussels from each experimental condition were collected, dissected into gills and digestive glands, and immediately frozen in liquid nitrogen before being stored at -80°C until further use. Additionally, five mussel haemolymphs were collected on days 0, 3, and 14 of exposure for genotoxicity (comet assay). For condition index purposes, mussels were sampled on days 0, 7, and 14. A battery of biomarkers, consisting of antioxidant enzymes (SOD, CAT, GPx), a biotransformation enzyme (GST), and oxidative damage (LPO), was employed to assess the effects of PS-NPs in the gills and digestive glands of *M. galloprovincialis*.

3.2.4. Quality control quality assessment

To eliminate plastic contamination, glass pipettes and glass tanks with supported aeration were enclosed, thus preventing aerial plastic contamination. Furthermore, no gloves or plastic materials/equipment were utilised during tissue dissection to avoid additional plastic contamination.

3.2.5. Condition Index

The condition index (CI) was assessed in mussels (five per treatment and exposure duration) to determine their physiological status at the beginning (day 0) and after 7 and 21 days of exposure. The CI was calculated as the percentage (%) of the ratio of the total mussel weight (tissue and shell) (g) to the wet weight (g) of the soft tissues (Gomes et al., 2013).

3.2.6. Genotoxicity assay

DNA damage was assessed using the alkaline comet assay, adapted from Singh et al. (1988) and Gomes et al. (2013). Haemolymph from five mussels, collected after 0, 3, and 14 days of exposure to PS-NPs, as well as from five unexposed mussels, was extracted from the posterior adductor muscle with a sterile hypodermic syringe (1 mL, 25 G needle). For each experimental condition, 100 µL of subsample was stained with 100 µL of trypan blue to evaluate cell viability, where the percentage of live cells was determined by randomly counting 100 cells. For DNA damage assessment, microscopic slides were cleaned beforehand in ethanol/ether (1:1) and coated with 0.65% normal melting point agarose (NMA) in Tris-acetate EDTA. Upon collection, mussel haemolymph cells were centrifuged at 3000 *rpm* for 3 minutes (4°C), and the pellets containing isolated cells were suspended in 0.65% low melting point

agarose (LMA, in Kenny's salt solution) and cast onto the microscopic slides. Slides with embedded cells were then immersed in a lysis buffer (2.5 M NaOH, 100 mM EDTA, 10 mM Tris, 1% Triton X-100, 10% dimethyl sulfoxide, 1% sarcosine, pH 10, 4°C) for 1 hour, allowing the diffusion of cellular components and immobilisation of DNA in agarose. After the lysis stage, slides were carefully placed in an electrophoresis chamber containing electrophoresis buffer (300 mM NaOH, 1 mM EDTA, adjusted pH 13, 4°C). Electrophoresis was then performed for 5 minutes at 25 V and 300 mA. Once completed, the slides were removed, soaked in a neutralising solution (0.4 mM Tris, pH 7.5), rinsed with bi-distilled water, and left to dry overnight. Afterwards, slides were stained with 4,6-diamidino-2-phenylindole (DAPI, one µg/mL), and the presence of comets was analysed using an optical fluorescence microscope (Axiovert S100) coupled to a camera (Sony). With a total magnification of ×400, the Komet 5.5 image analysis system was employed to score 50 randomly selected cells for each slide (200 cells scored per group), following the determination of the amount of DNA in the tail. Results are expressed as mean ± standard deviation.

3.2.7. Tissue preparation for enzyme activities analysis

The gills and digestive gland of the mussel were individually homogenised in 5 mL of 20 mM Tris-sucrose buffer (0.5 M sucrose, 0.075 M KCl, 1 mM DTT, 1 mM EDTA, pH 7.6) in an ice bath for 2 minutes, following the protocol described by Geret et al. (2002). The homogenates were then centrifuged (500 *g*, 15 minutes, 4°C), and the resulting supernatant was re-centrifuged (12,000 *g*, 45 minutes, 4°C) to obtain the cytosolic fraction. Aliquots (150 µL) of the cytosolic fraction were separated for the determination of the activities of each antioxidant enzyme (SOD, CAT, GPx) and the biotransformation enzyme (GST).

In addition, total protein concentrations (mg protein g^{-1} tissue), adapted for microplate readers using bovine serum albumin (BSA) as a standard, were determined using Bradford's (1976) method.

3.2.7.1. Superoxide dismutase (SOD) activity

SOD activity was evaluated in the gills and digestive gland by calculating the decrease in absorption of the substrate cytochrome *c* at 550 nm, using the xanthine oxidase/hypoxanthine system. The results are expressed as U mg^{-1} protein (McCord & Fridovich, 1969).

3.2.7.2. Catalase (CAT) activity

The quantitative determination of CAT activity in the gills and digestive gland of mussels followed the procedure defined by Greenwald (1985) and is based on measuring the consumption of hydrogen peroxide (H_2O_2) at 240 nm spectrophotometrically. Results are expressed as mmol min^{-1} mg $protein^{-1}$.

3.2.7.3.Glutathione peroxidase (GPx) activity

GPx activity in the gills and digestive gland was measured at 340 nm, using cumene hydroperoxide as the substrate at 28°C, with a microplate reader (Infinite® 200, Pro-Tecan), based on the method adapted from McFarland et al. (1999). Outcomes are presented as mmol min^{-1} mg $protein^{-1}$.

3.2.7.4.Glutathione-*S*-transferases (GST) activity

The biotransformation enzyme GST was measured in the gills and the digestive gland by conjugating 0.2 mM reduced glutathione (GSH) with 0.2 mM 1-chloro-2,4-dinitrobenzene (CDNB) in a reaction mixture of 0.2 M KH_2PO_4/K_2HPO_4 buffer (pH 7.9) at 340 nm using a microplate reader (Infinite® 200, Pro-Tecan), following the method adapted from Habig et al. (1974). Results are expressed as µmol CDNB min^{-1} mg^{-1} protein.

3.2.8. Lipid Peroxidation (LPO)

Mussel gills and digestive glands were individually homogenised on ice with 5 mL of 0.02 M Tris-HCl buffer (pH 8.6) and butylated hydroxytoluene (BHT) in a 1:10 ratio. Homogenates (3 mL) were centrifuged at 30,000 *g* for 45 minutes (4°C), and the resulting supernatant was used to determine total protein concentrations (Bradford, 1976) and LPO levels. LPO levels were assessed by measuring the absorbance of malondialdehyde (MDA) and (2 E)-4-hydroxy-2-nonenal (HNE) at 540 nm, following the method adapted from Erdelmeier et al. (1998). Results are presented as nmol/mg protein.

3.2.9. Integrated Biomarker Response Index

The integrated biomarker response index (IBR) is an effective tool for visualising the biological effects of pollutants and simplifying the interpretation of the relationship between the suite of biomarkers and contamination levels (Devin et al., 2014). Therefore, the biomarker data from the gills and digestive gland of *M. galloprovincialis* exposed to polystyrene PS-NPs were integrated using biomarker response index version 2 (IBR) proposed by Sanchez et al. (2013), which modified the IBR index defined by Beliaeff & Burgeot (2002) and described in Serafim et al. (2011). The IBR facilitates the integration of different biomarker responses into a numeric value. A concept of reference deviation is based on disturbed and undisturbed states, where the IBR index was developed to eliminate the dependency of the IBR result on the arrangement of the biomarkers, as well as the induction and inhibition of each biomarker (Sanchez et al., 2013). The IBR represents a sum of the deviation between unexposed and PS-NPs on each sampling day.

Briefly, the combined data of each biomarker (X_i) was compared to the data (X_0) of each biomarker from the control group and log transformed (Y_i) to reduce variance [$Y_i = \log (X_i / X_0)$]. The mean (μ) and standard deviation (σ) for Y_i were calculated, and the data of each parameter were further standardised according to the following equation:

$$Z_i = \frac{(Y_i - \mu)}{\sigma}$$

To create a baseline centred on controls and represent parameter variation relative to this baseline, the mean of the standardised biomarker response (Z_i) and the mean of the unexposed biomarker (Z_0) were used to define a biomarker deviation index (A):

$$A = Z_i - Z_0$$

Lastly, to obtain the IBR index, the absolute value of A was calculated for each parameter in each experimental condition and summed:

$$IBRv2 = \sum |A_i|$$

3.2.10. Statistical analysis

The significant differences between treatments and time were evaluated using parametric tests (ANOVA followed by Tukey's post-hoc test) or non-parametric equivalents (Kruskal-Wallis and a two-tailed multiple comparisons test), depending on data distribution and homogeneity of variances (Shapiro-Wilk test). Results were deemed significant when $p < 0.05$. A Principal Component Analysis (PCA) was also employed to assess the relationship

between treatments (unexposed and exposed to PS-NPs) and the analysed parameters [antioxidant and biotransformation enzymes (SOD, CAT, GPx, GST) activities and oxidative damage (LPO)] in the gills and digestive gland of mussels throughout the exposure period (21 days). These statistical analyses were conducted using R software (R Core Team, 2017) and Statistica 7.0 software (Statsoft Inc., 2005, USA). For IBR, statistical differences were assessed using a t-test on Microsoft Excel (Microsoft Corporation, 2018. *Microsoft Excel*, Available at: https://office.microsoft.com/excel), with results considered significant when $p < 0.05$.

3.3.Results

3.3.1. PS-NPs characterisation

The hydrodynamic diameter and zeta potential (ζ-potential) of polystyrene nanoplastics (PS-NPs; 50 nm) were studied over a period of 2 to 12 hours, with measurements taken every 50 seconds in ultrapure water (Fig. 3.1. A) and filtered seawater (FSW; Fig. 3.1. B). The results indicated that in ultrapure water, the size of PS-NPs remained constant over time, suggesting that no aggregation of PS-NPs occurred under these conditions. According to Fig. 3.1. A, the average size of PS-NPs is approximately 25 nm, which is less than the size reported by the manufacturer. This discrepancy is typical, as it often relates to the methods used for measuring the size of these particles. The hydrodynamic diameter of PS-NPs in ultrapure water is consistent with the ζ-potential, which indicates that under these conditions, the ζ-potential is approximately -68.8 ± 0.66 mV, significantly distant from zero. Consequently, PS-NPs are stable, and no aggregation takes place. Conversely, when PS-NPs are dispersed in FSW, the size increases to (852 ± 103 nm), indicating that aggregation or agglomeration occurs due to the high concentration of salts in seawater (Fig. 3.1. B). The ζ-potential under these conditions further demonstrates that aggregation or agglomeration is favoured, as the ζ-potential is nearly zero (-0.068 ± 0.23 mV).

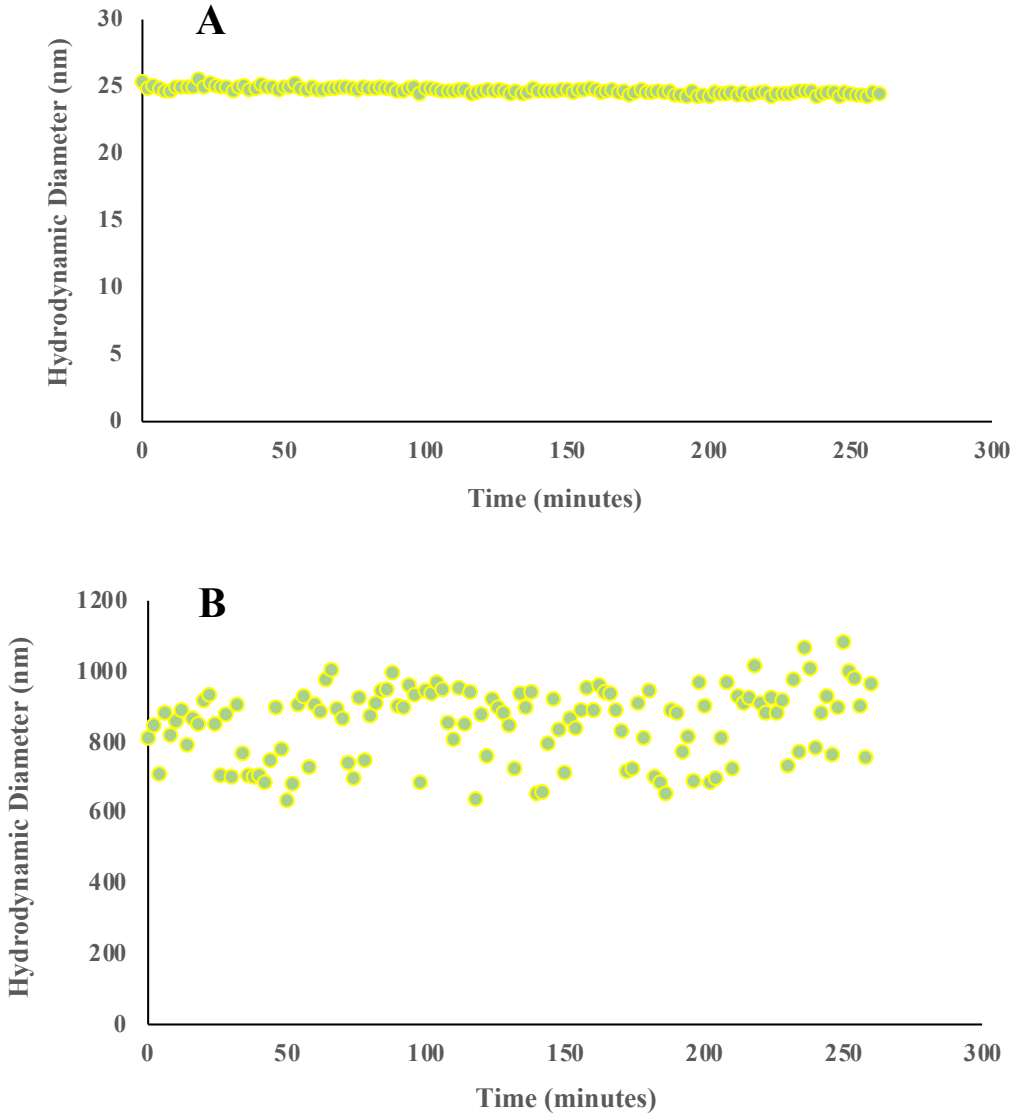

Figure 3.1. The hydrodynamic diameter of polystyrene nanoplastics (50 nm) in **(A)** ultrapure water and **(B)** seawater over time (minutes).

3.3.2. Condition Index

There were no significant variations in the condition index of *M. galloprovincialis* between treatments or exposure times, with values ranging from 37.30 ± 2.81 to 42.93 ± 1.90 % ($p > 0.05$) (Table 3.1).

Table 3.1. Condition index (mean ± S.D.) of *M. galloprovincialis* exposed to PS-NPs at the beginning and end of the exposure.

Time (day)	CT	PS-NPs
0	37.30 ± 2.81	
7	40.67 ± 8.16	41.66 ± 5.54
21	37.22 ± 3.03	42.93± 1.90

3.3.3. Genotoxicity

DNA damage was assessed in the haemocytes of unexposed and PS-NP-exposed mussels by measuring the comet parameter of % tail DNA at the beginning of the experiment and after 3 and 14 days of exposure (Fig. 3.2). No significant differences were observed during each exposure period in the haemocytes of unexposed mussels ($p > 0.05$). However, DNA damage in mussels exposed to PS-NPs was significantly higher (by fourfold) than in unexposed mussels on both exposure days ($p < 0.05$). Examples of comets in mussel haemocytes from both the control and the PS-NP-exposed groups are documented in Fig. 3.3. The haemocytes of *M. galloprovincialis* from controls exhibited a nucleoid core with no DNA migrating into the tail region at 0, 3, and 14 days, whereas in PS-NP-exposed mussels, the nucleoid core displayed broken DNA fragments or damaged DNA migrating into the tail region after 3 and 14 days of exposure. Therefore, exposure to PS-NPs leads to genotoxicity in the haemolymph of the exposed mussels.

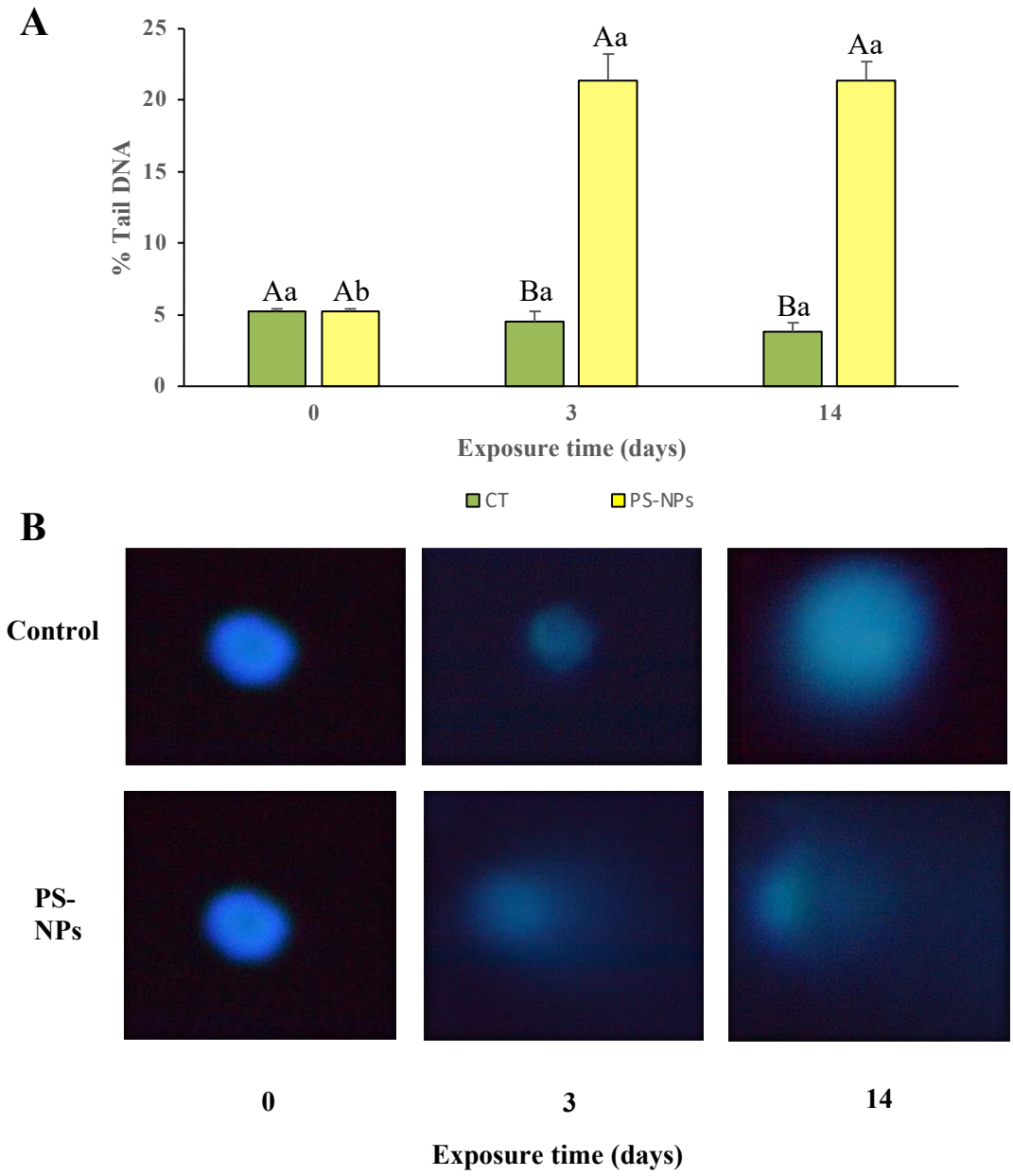

Figure 3.2. (A) Genotoxicity effects of *in vivo* exposure of polystyrene PS-NPs in the haemolymph of *M. galloprovincialis* and **(B)** examples of comet assay images of unexposed *M. galloprovincialis* haemocytes and those exposed to polystyrene PS-NPs. Different upper- and lower-case letters indicate significant differences between treatments for the same time and between times for the same treatment, respectively (p<0.05).

3.3.4. Enzymatic activity

Antioxidant enzyme activities in tissues of unexposed mussels remained unchanged over time ($p > 0.05$; Fig. 3.3. A – H), with exceptions noted in CAT (gills, $p < 0.05$; Fig. 3.3. C), GPx (gills, $p < 0.05$; Fig. 3.3. E), and GST activities (gills, $p < 0.05$; Fig. 3.3. G).

In the gills, a significant decreasing trend in SOD activity is observed after 3, 7, and 14 days in mussels exposed to PS-NPs, when compared to unexposed mussels ($p < 0.05$; Fig. 3.3 A). SOD activity in mussels after 14 days of exposure to PS-NPs shows significant differences when compared to PS-NPs-exposed mussels after 21 days and to unexposed mussels ($p < 0.05$). Conversely, in the digestive gland, SOD activity increased after 3 and 7 days in PS-NPs-exposed mussels ($p < 0.05$; Fig. 3.3 B), while in PS-NPs-exposed mussels, a significant decrease at 14 days is evident when compared to unexposed mussels and those exposed for 21 days ($p < 0.05$).

CAT activity in the gills of mussels exposed to PS-NPs significantly differed from that of unexposed mussels throughout the exposure period ($p < 0.05$; Fig. 3.3. C). A decrease in CAT activity is notable in PS-NPs-exposed mussels after 7 days of the bioassay, and a significant difference was observed between mussels after 14 days when compared to those at 3 and 21 days of exposure ($p < 0.05$). In the digestive glands of PS-NPs-exposed mussels, a general decline in CAT activity was noted until the end of the exposure period, with this decrease being significant between unexposed and exposed mussels at both 3 and 21 days of exposure ($p < 0.05$; Fig. 3.3. D). Furthermore, after 14 and 21 days of exposure to PS-NPs, the digestive glands of the mussels exhibited a significant decrease compared to the beginning of the exposure ($p < 0.05$).

In the gills of mussels, GPx activity decreased significantly after 3, 7, and 14 days of exposure to PS-NPs compared to unexposed mussels ($p < 0.05$; Fig. 3.3. E). However, no significant differences were observed among the exposure times for mussels subjected to PS-NPs. A decrease in GPx activity was also noted in the digestive gland of mussels exposed to PS-NPs after 3 days, which was significantly different from control mussels at 7, 14, and 21 days of exposure ($p < 0.05$; Fig. 3.3. E). In terms of exposure time, the GPx activity in mussels exposed to PS-NPs is significantly different at 7 and 14 days compared to the beginning of the experiment ($p < 0.05$).

The activities of the biotransformation enzyme (GST) also decreased in the gills of mussels exposed to PS-NPs after 3, 7, and 14 days of exposure compared to the unexposed group ($p < 0.05$; Fig. 3.3. G). After 14 days of exposure to PS-NPs, the gill activity was

significantly lower in PS-NP exposed mussels than at both the beginning and the end of the exposure period ($p < 0.05$). Conversely, in the digestive glands of PS-NP exposed mussels, no significant differences were observed compared to the unexposed group ($p > 0.05$; Fig. 3.3. H). However, significant differences were noted within the PS-NP exposed mussels at 21 days of exposure when compared to the start of the experiment ($p < 0.05$).

Overall, enzymatic activities in gills decreased after 3 days of exposure to PS-NPs, whereas in the digestive glands, the reduction in enzymatic activity is particularly notable after 7 days of exposure, with exceptions for SOD and GST activities. The duration of exposure to PS-NPs is critical for mussel gills at 7 and 14 days, whereas in the digestive glands, prolonged exposure to PS-NPs leads to more adverse effects (14 and 21 days).

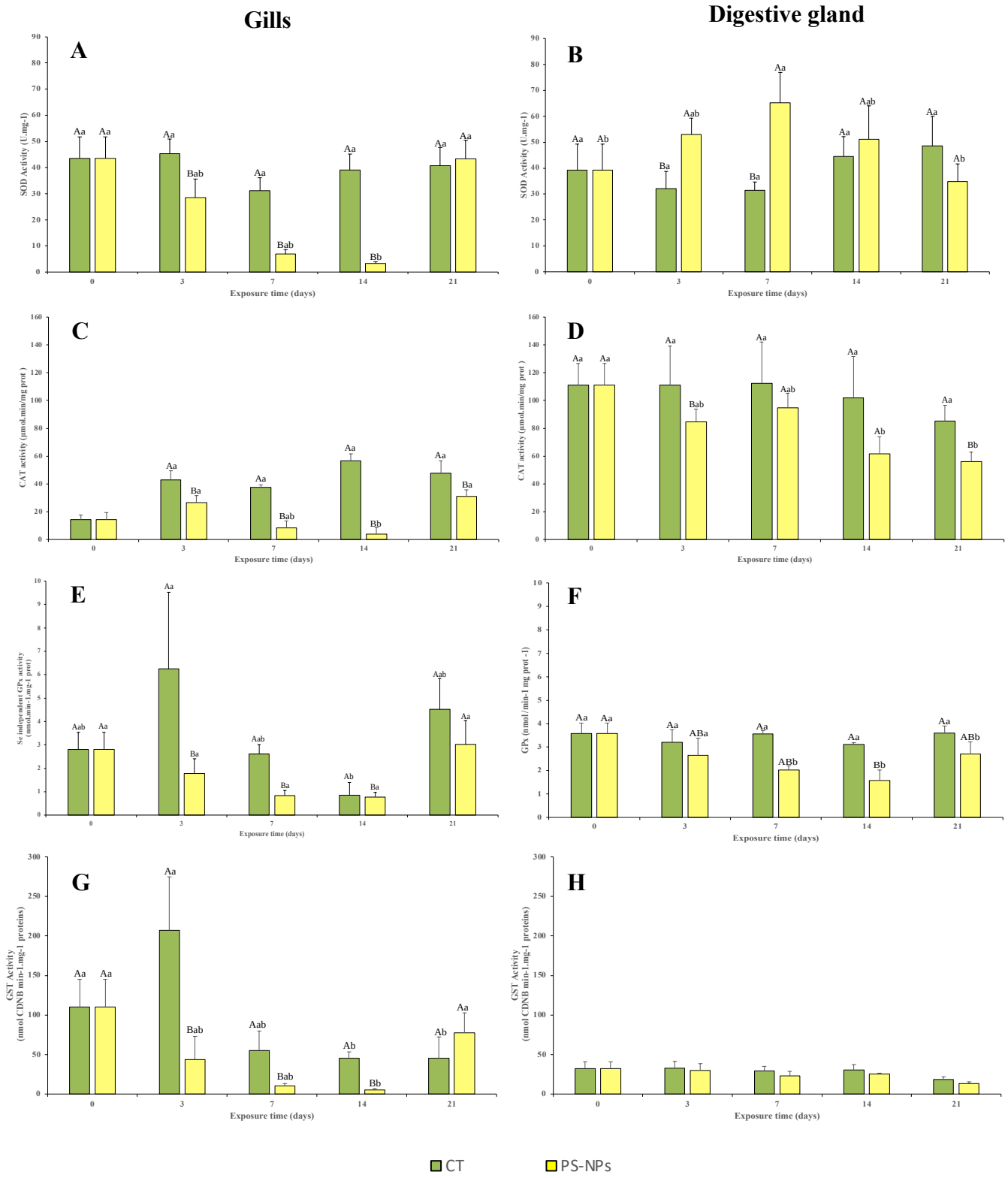

Figure 3.3. Superoxide dismutase (SOD) (A-B), catalase (CAT) (C-D), glutathione peroxidase (GPx) (E-F) and glutathione-S-transferase (GST) (G-H) activities (mean ± std) in the gills and digestive gland of mussels *M. galloprovincialis* from controls and exposed to 10 µg/L PS-NPs for 21 days. Different upper- and lower-case letters indicate significant differences between treatments for the same time and between times for the same treatments, respectively (p<0.05).

3.3.5. Oxidative damage

Oxidative damage in both tissues of unexposed mussels remained unchanged throughout the exposure ($p > 0.05$; Fig. 3.4 A – B). In the gills of mussels exposed to PS-NPs, LPO levels increased significantly at 14 days of exposure compared to the control ($p < 0.05$; Fig. 3.4 A), with LPO levels in PS-NPs-exposed mussels at 3 days significantly lower than those recorded after 14 days of exposure ($p < 0.05$). In the digestive glands, a significant rise in LPO levels was observed earlier, at 7 days of exposure to PS-NPs, when compared to the gills ($p < 0.05$; Fig. 3.4 B), and this also showed significant differences from all other exposure times of both PS-NPs-exposed and unexposed mussels at the same time point ($p < 0.05$). After 3 days of exposure to PS-NPs, the digestive glands of mussels exhibited lower LPO levels than those of unexposed mussels ($p < 0.05$).

Predominately, LPO occurred earlier in the digestive glands of PS-NPs-exposed mussels than in gills.

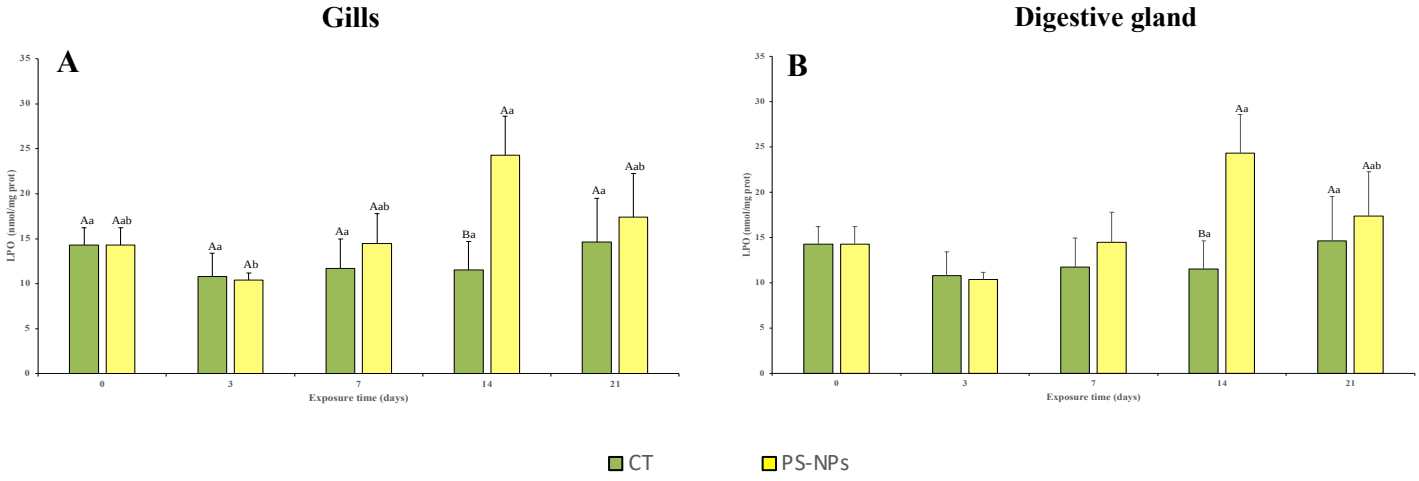

Figure 3.4. Lipid Peroxidation (LPO) in gills (A) and digestive gland (B) of mussels *M. galloprovincialis* from control and exposed to 10 µg/L PS-NPs for 21 days (mean ± std). Different upper- and lower-case letters indicate significant differences between treatments for the same time and between times for the same treatments, respectively ($p<0.05$).

3.3.6. Principal component analysis (PCA)

PCA was applied to all data collected from both tissues (gills and digestive gland) of mussels in order to describe the impact of PS-NPs on the response of biomarkers (SOD, CAT, GPx, GST activities, and LPO; Fig. 3.5. A – B). The two principal components account for 82.5% and 83.5% of the total variance in gills (PC1 = 62.9%, PC2 = 19.5%; Fig. 3.5. A) and digestive glands (PC1 = 59.0%, PC2 = 24.4%; Fig. 3.5. B) of mussels, respectively.

In mussels, the gills and digestive glands exhibited differing responses to exposure to PS-NPs; thus, the toxicity of PS-NPs appears to be tissue-specific. This may be attributed to the ability of these nano-sized plastic particles to penetrate cellular boundaries. In conclusion, in both tissues, LPO was found to be positively correlated with PS-NP exposure, while the remaining enzymatic activities (SOD, CAT, GPx, and GST) demonstrated a negative correlation with PS-NP exposed mussels and a positive association with controls, except for SOD activity in the digestive gland. Additionally, the PCA results for both tissues indicate that exposure time also plays a significant role, presenting PS-NP toxicity as chronic (greater than 7 days).

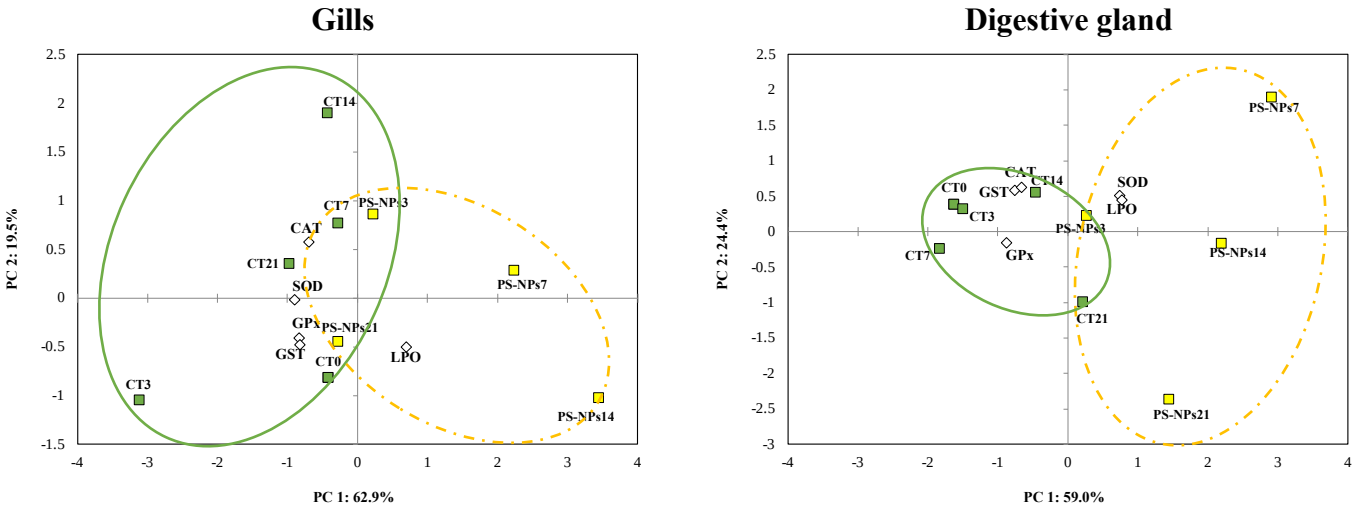

Figure 3.5. Principal component analysis (PCA) of a battery of biomarkers (SOD, CAT, GPx, GST activities and LPO) in gills and digestive glands of mussels *M. galloprovincialis* from controls (CT) exposed to PS-NPs for 21 days ($p < 0.05$).

3.3.7. Integrated Biomarker Response

The Integrated Biomarker Response (version 2) (IBR) was calculated for the gill and digestive gland biomarker data from all exposure times to PS-NPs. Graphical representations of the IBR and star plots for both mussel tissues are shown in Figure 6. The IBR pattern was dependent on tissue type and exposure duration. No significant differences were observed in the digestive gland ($p > 0.05$) (Fig. 3.6.A), although a linear increase was noted. In the gills, significant differences in exposure times were observed. The IBR value in the gills after 14 days of exposure to PS-NPs is significantly higher compared to other sampling days ($p < 0.05$)

(Fig. 3.6.A). The IBR value for the gills after 3 days of exposure is significantly lower than at other exposure times ($p < 0.05$) (Fig. 3.6.A). No significant differences were found between 7 days and 21 days of exposure in mussel gills ($p > 0.05$) (Fig. 3.6.A). Star plots indicated that changes in biomarkers were also dependent on tissue type and exposure duration (Fig. 3.6.B). The IBR plot reveals that the seventh day of exposure was critical for the digestive glands of mussels, making LPO the primary contributor to the overall IBR score. For the gills, the 14th day is the most significant, with SOD and GST, followed by CAT and LPO, all contributing to the overall calculated IBR score.

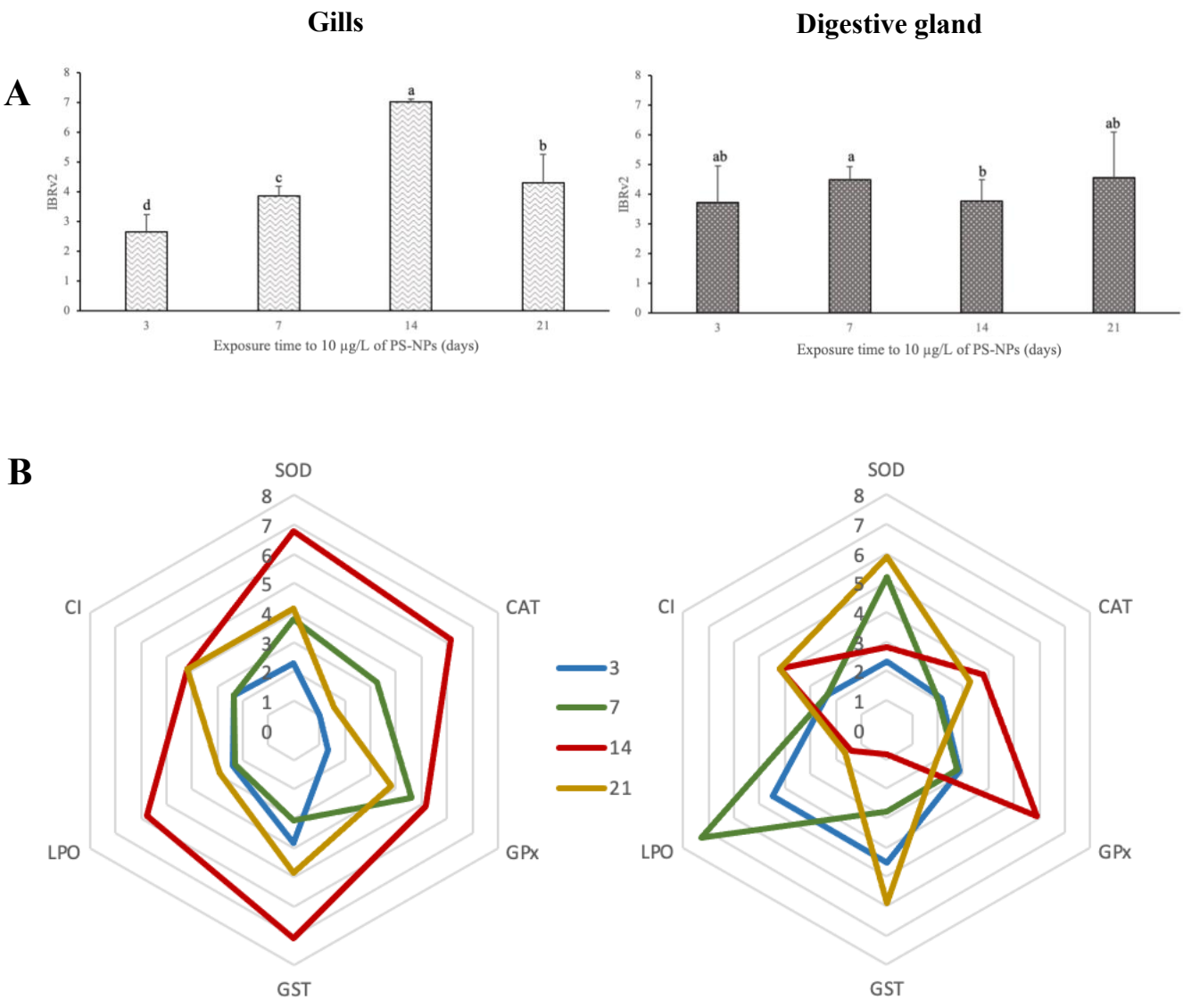

Figure 3.6. (A) Integrated biomarker response index version 2 (IBR) (mean ± S.D) and **(B)** star plots of the gills and digestive glands of *M. galloprovincialis* exposed to polystyrene nanoplastics for 21 days. Lowercase letters indicate significant differences between exposure times ($p < 0.05$).

3.4.Discussion

Plastic pollution in the marine environment, particularly at the nanoscale, is a significant concern, and the toxicity of these particles in bivalves is deeply troubling. Data has shown that PS-NPs are recognised and consumed by these filter feeders as a low-nutritional food source, compromising the integrity of the bivalve immune system and impairing fertilisation and the development of embryo-larvae (Wegner et al., 2012; Canesi et al., 2015; Balbi et al., 2017; Brandts et al., 2018; González-Fernández et al., 2018; Tallec et al., 2018; Rist et al., 2019; Auguste et al., 2020; Baudrimont et al., 2020; Cole et al., 2020; Li et al., 2020; Sendra et al., 2020a,b; Capolupo et al., 2021). In light of this, this study aimed to assess the effects of genotoxicity, antioxidant responses, and oxidative damage following chronic exposure to PS-NPs in the Mediterranean mussel *M. galloprovincialis*.

Results demonstrate that PS-NPs at a low concentration (10 µg/L), when compared to other studies evaluating the effects of PS-NPs on mussels (Brandts et al., 2018; Auclair et al., 2020; Capolupo et al., 2021), significantly affect both the gills and the digestive gland of *M. galloprovincialis*, with PS-NPs mediated toxicity found to be tissue-specific and time-dependent.

In terms of PS-NP characterisation, FSW aggregation/agglomeration was preferred, possibly due to the high salt concentrations. This is supported by an increased hydrodynamic diameter and zeta potential, which is close to zero. Natural organic matter (NOM), inorganic colloids, and ultraviolet (UV) radiation are recognised as factors that modify the nano-specific properties, structure, cohesion, and aggregation of particles (Andrady, 2011; Oriekhova & Stoll, 2018; Shen et al., 2019). Therefore, the characterisation of PS-NPs indicates that their behaviour under FSW conditions differs markedly from that in ultrapure water, consequently leading to greater aggregation/agglomeration kinetics of PS-NPs. Additionally, compared to polystyrene microplastics (PS-MPs; 20 µm), the zeta potential in seawater (SW) significantly differs from that of PS-NPs (50 nm). Ribeiro et al. (2017) noted a zeta potential value of -12.4 ± 2.36 mV for PS-MPs (20 µm). In contrast, PS-NPs exhibit values that are nearly zero (-0.068 ± 0.23 mV), indicating a higher propensity for aggregation/agglomeration than PS-MPs. Although the initial size of the plastic particles was unknown, El Hadri and colleagues (2020) demonstrated that for PS-NPs, the zeta potential was -44 ± 2 mV (at 25ºC, pH = 6.7 ± 0.3), with a size distribution of 306 ± 15 nm. Comparatively, PE and PE+PP at the nanoscale displayed zeta potentials of -36 ± 3 and -30 ± 2 mV, along with size distributions of 129 ± 7 and 460 ± 23 nm, respectively (El Hadri et al., 2020). Moreover, Sendra et al. (2020b) observed

differences in the behaviour of NP particles (50 and 100 nm), with and without fluorescence, across different media. In this study, the zeta potential was negative in all media, with the differences between fluorescent and non-fluorescent PS-NPs (50 nm) showing non-fluorescent particles possessing zeta potential values closer to zero in FSW. Conversely, in ultrapure water, the opposite trend was noted (Sendra et al., 2020b). The 50 nm NP evaluated in Sendra et al. (2020b) aligns with the present data, where the fluorescent dye has been incorporated internally, as this dye is highly hydrophobic and remains trapped within the particle in aqueous environments (Polyscience Inc., 2018). Nonetheless, minor differences in particle zeta potential were observed between fluorescent PS-NPs and PS-NPs without fluorescence in FSW (-24.8 and -13.3 mV, respectively) (Sendra et al., 2020b). Thus, it is essential to consider the chemical composition and size of each nanoparticle, as well as their interactions with NOM, inorganic colloids, UV radiation, salinity, pH, and O_2 levels within SW.

The antioxidant defence system of mussels exposed to PS-NPs exhibited alterations, showing time-dependent and tissue-specific toxicity. A continuous increase in antioxidant enzyme activity may demand energy that could detract from energy allocated to growth and reproduction (Trestrail et al., 2020).

The antioxidant defence system, regulated by the enzymes studied here, aids in minimising the effects of ROS within the cell. However, when ROS is overproduced, the antioxidant defence system can be overwhelmed and not counteract the effects, leaving mussels' innate immune system compromised and leading to oxidative damage. This is observed in the gills, where the first line of defence, SOD, was unable to counteract ROS production mediated by PS-NPs exposure. On the other hand, in the digestive gland, the increase in SOD activity suggests that superoxide radicals generated by PS-NPs exposure were counteracted in this tissue. As filter-feeding organisms, mussel's gills are a primary route for mussels to uptake xenobiotics (Jorgensen, 1996), and this observation can be a consequence of this factor. On the contrary, in mussels, *M. edulis* (PS-NPs - 50 nm; 500 µg/L; 24h) (Cole et al., 2020) and *Mytilus* spp. (polyethylene (PE) and polypropylene (PP) microplastics - < 400 µm; 10 – 100 µg/L; 10 days) (Revel et al., 2019) and in the clam *Scrobicularia plana* (PS microplastics - 20 µm; 1000 µg/L; 14 days) (Ribeiro et al., 2017), SOD activity increased in both tissues, wherein Cole et al. (2020) SOD activity in the digestive gland returned to control values after 7 days of exposure to PS-NPs. A similar pattern was observed in this study. This was also observed in the digestive gland of *M. coruscus* after exposure to PS microspheres (2 µm; 10, 10^4 and 10^6 particles/L; 14 days) (Wang et al., 2020). Alternatively, after exposure to PS-NPs (70 nm; 3.64×10^3 particles/L; 14 days), no significant changes were observed in

SOD activity in the digestive gland of *M. coruscus* (Wang et al., 2021). Therefore, while SOD acts as the first line of defence against ROS associated with PS-NPs toxicity in the digestive gland, it becomes overwhelmed in the gills.

Comparatively, CAT activity was also overwhelmed in both tissues of *M. galloprovincialis*, where the inhibition observed represents the incapability to eliminate hydrogen peroxide generated due to PS-NP exposure. Conversely, data from other species revealed either no alterations or an increase in CAT activity. In *M. coruscus* (PS-NPs; 70 nm; 3.64×10^3 particles/L; 14 days), no significant changes were observed in the digestive gland (Wang et al., 2021), and Ribeiro et al. (2017) found similar results in the clam *S. plana* after exposure to microplastics (PS; 20 µm; 1000 µg/L; 14 days). Meanwhile, PS microspheres (2 µm; 10, 10^4, and 10^6 particles/L; 7 days) and polyethylene (PE) and polypropylene (PP) microplastics (< 400 µm; 10 days) led to an increase in CAT activity in *M. coruscus* (Wang et al., 2020) and in the gills and digestive gland of *Mytilus* spp. (Revel et al., 2019). These comparisons substantiate the differences in the toxicity of nano and micro-sized plastic particles, suggesting that smaller plastic particle sizes are more toxic to bivalves. Additionally, the concentrations employed may play a significant role in the toxicity that plastic particles exert on bivalves, as higher concentrations increase the likelihood of aggregation/agglomeration within seawater, resulting in larger aggregate sizes and potentially decreasing the capacity of these aggregates to be ingested by the organisms.

GPx activity is particularly susceptible to the early onset of the pro-oxidant crisis, even at low levels of environmental disruption (Regoli & Giuliani, 2014). In the current data, GPx activity was unable to manage the excess hydrogen peroxide induced by PS-NP-mediated toxicity, which was evident in both tissues. The inhibition of GPx activity occurs after 3 days of exposure, with the lowest activity observed at 7 and 14 days. Interestingly, a slight increase in GPx activity is notable in both tissues after 21 days, suggesting a potential adaptive response. Studies evaluating the effects of plastic particles in bivalves have reported either no significant alterations in either tissue of *M. edulis* (PS microspheres; 2 µm; 10, 10^4, and 10^6 particles/L; 7 days) (Wang et al., 2020), or an increase in GPx activity before 3 days of exposure to PS microplastics (20 µm; 1000 µg/L; 14 days) in both the gills and digestive glands of the clam *S. plana* (Ribeiro et al., 2017).

In comparison, PS-NP exposure leads to an overproduction of ROS, which exceeds GPx's capacity to catalyse the reaction, converting hydrogen peroxide into water. As a result, mussel tissues struggle to cope with the detrimental effects of this stressor. However, before the 21-day mark, the activation of an adaptive response may account for the slight increase

observed. Wegner et al. (2012) demonstrate that these filter-feeding organisms recognise and ingest plastic nanoparticles as a low-nutritional food source. Given this, an adaptive response of the mussel to PS-NP toxicity may involve the upregulation of autophagy, typically associated with nutrient scarcity and other stressors (Moore et al., 2006). Autophagy serves to sequester and recycle oxidatively damaged proteins and organelles, providing a selective advantage for cellular survival (Moore et al., 2006). The adaptive response noted in the gills for all enzymatic activities assessed and in the digestive gland for GPx activity after 21 days of exposure to PS-NPs suggests that mechanisms such as autophagy can facilitate the recovery of the mussels' tissues.

The biotransformation enzyme GST promotes the binding of glutathione and mercapto-transferase to form glutathione peroxidase, effectively degrading hydrogen peroxide (Yu et al., 2018). Following an observed inhibition in GPx activity, it is anticipated that GST will intervene to protect the organism from ROS generated after PS-NP exposure, although this is not the case here. GST activity in the gills exhibited a similar pattern to the other enzymes assessed, whereas GST activity remained at control values in the digestive gland. Conversely, GST activity increased in the gills of *S. plana* and decreased in the digestive gland following PS microplastic exposure (20 µm; 1000 µg/L; 14 days) (Ribeiro et al., 2017). Nevertheless, this underscores the importance of evaluating plastic particles at the nanoscale, as their behaviour and mediated toxicity differ from larger-sized particles. Another reason for these differences may be attributed to the fact that mussels preferentially ingest smaller particles (Wang et al., 2021).

Furthermore, the ingestion of these PS-NPs was found to be favourable in the digestive tract; however, over time, particles translocate to the mantle, as the gills are not typical tissues for accumulation (Wang et al., 2021). Thus, through filter-feeding habits, PS-NPs enter the gills and translocate to the digestive tract of the mussel, thereby explaining the tissue-dependent and time-dependent toxicity observed. Overall, in both tissues, the results suggest that these enzymes are unable to counteract the negative effects of this stressor, leading to oxidative damage, as confirmed by the results of LPO.

When the antioxidant defence system is overwhelmed, membrane lipids are not salvaged from attacks by residual reactive oxygen species (ROS), leading to lipid peroxidation (LPO). Oxidative damage occurred in both tissues of the marine mussel *M. galloprovincialis*, with the highest significant levels of LPO recorded in the gills and the digestive gland at different times of exposure. PS-NPs induce oxidative stress following exposure to 0.05 mg/L of PS-NPs with an attached amide group (100 ± 6.9 nm; 96 h) in *M. galloprovincialis*, where

LPO levels increased significantly in the digestive gland, although no significant changes were found in the gills (Brandts et al., 2018). Wang et al. (2021) demonstrated that LPO was induced in the digestive glands of *M. coruscus* after exposure to PS-NPs (70 nm3.64×10^3 particles/L; 14 days). In the gills and digestive glands of *M. edulis* exposed to 500 µg/L of PS-NPs (50 nm; 24 h and 7 days), no significant differences in oxidative damage were observed, except for an initial decrease noted in the gills after 24 h of exposure, with no subsequent LPO occurring (Cole et al., 2020). In the clam *S. plana,* after exposure to PS microplastics (20 µm; 1000 µg/L; 14 days), LPO levels decreased in the gills, and a tendency for increase was observed in the digestive gland at 7 days of exposure, though not significant (Ribeiro et al., 2017).

Furthermore, no signs of LPO were observed in *Mytilus* spp. before 7 days of exposure to PS microplastics (2 and 6 µm; 2000 microbeads mL^{-1} day^{-1}; 7 days), although a significant increase in ROS was found in the haemocytes of the mussels' digestive gland (Paul-Pont et al., 2016). Our results contradict previous studies, as the gills and digestive glands exhibit oxidative damage, opposing the suggestion made by Li et al. (2020) that the gills of *M. galloprovincialis* do not display a greater antioxidant capacity compared to the digestive gland. Therefore, the LPO results indicate that the production of ROS overwhelmed the effectiveness of the antioxidant enzymes in the cells of the gills and digestive glands to maintain redox balance, leading to oxidative damage of membrane lipids. The PCA and IBR results (Figures 5 - 6) further confirm that both mussel tissues are vulnerable to changes in their antioxidant defence mechanisms following exposure to PS-NPs, with the gills being primarily affected by the presence of PS-NPs throughout the exposure period. IBR shows that the critical exposure duration for the gills is 14 days, as evidenced by the lowest enzymatic activities and highest oxidative damage observed at this time. The PCA also supports the findings of IBR. Moreover, the results for the digestive glands align with both the PCA and IBR, as 7 days represents the most critical exposure time to PS-NPs, further validated by the oxidative damage noted at this juncture.

In unexposed mussels, cells exhibited an average DNA fragmentation of 5.26%, which falls well within the normal levels for *Mytilus* (Mitchelmore et al., 1998). The findings indicated that polystyrene PS-NPs are genotoxic to the immune system of mussels, as DNA damage increased after three exposures and remained at similar levels for up to 14 days (Figure 2). Consequently, the DNA damage observed in the haemolymph of mussels is independent of exposure duration. However, this requires confirmation with a longer exposure period. This genotoxic damage may result from physical interactions between cell nuclei and PS-NPs, as

well as the production of a high concentration of reactive oxygen species (ROS). Nevertheless, the underlying mechanism has yet to be established. The integrity of DNA in *M. galloprovincialis declined*, evidenced by increased DNA damage after a 96-hour exposure to PS-NPs (106 ± 10 nm; 0.05 – 50 mg/L) (Brandts et al., 2018).

Similarly, *in vivo* acute toxicity exposure (96-h; 50 nm; 10 µg/L) of PS-NPs with an amide group attached adversely affects the immune defence capacity of *M. galloprovincialis* (Auguste et al., 2020). After exposure to microplastic, microfibre, and NP, Cole et al. (2020) noted that in *M. edulis,* exposed to similar-sized PS-NPs, a higher concentration and shorter duration (50 nm; 24-h and 7-d; 500 µg/L) *resulted in* no significant DNA damage. In the study by Cole et al. (2020), PS-NPs exposed mussels exhibited 3% DNA damage, whereas this study observed 21.4% DNA damage. Comparing the concentrations used in Cole et al. (2020) to those in this study, there are more available NP particles at 500 µg/L than at 10 µg/L, which in turn form larger aggregates, thereby reducing the likelihood of physical interactions between cell nuclei and NP particles as they are unlikely to span cellular boundaries due to their size. Furthermore, although no significant changes in DNA damage were detected, a significant increase in the number of micronuclei per one thousand cells was found with regard to exposure duration (Cole et al., 2020). Thus, an increase in micronuclei formation and a decrease in haemocyte cells circulating in the haemolymph may be potential genotoxic consequences of NP exposure. Results indicate that the DNA integrity of mussels is compromised following both acute and chronic exposure to PS-NPs, potentially due to the inadequacy of the mussel's antioxidant defence mechanisms to mitigate any ROS generated by exposure to PS-NPs, leaving excess ROS to attack the DNA bases through oxidation of the molecules, thereby causing oxidative damage. The percentage of tail DNA observed (Figure 2) may be attributed to the relentless assaults of free radicals formed, rendering DNA non-viable and disrupting the flow of information, thus undermining the mussel's immune system.

Furthermore, the immediate translocation of PS-NPs in haemocytes was confirmed, as well as the primary uptake route in *M. galloprovincialis* (PS-NPs; 50 nm; 10 mg/L; 3h) (Sendra et al., 2020b). This internalisation of PS-NPs in haemocyte cells also prompted changes in the immune response of mussels (Sendra et al., 2020b). Although the parameters analysed by Auguste et al. (2020) differ from those examined here, PS-NPs resulted in an increase in extracellular ROS production. Consequently, they may have contributed to the oxidative stress and DNA damage observed in the current results. Enhanced oxyradical generation through the interaction of NP particles with cellular boundaries may be a primary effect of genotoxicity; however, further investigation is required to achieve a deeper understanding. Regarding the

characterisation of NP particles in the marine environment, the results suggest that the lower the concentration, the lesser the formation of aggregates, thus increasing the likelihood of crossing cellular boundaries and, in turn, augmenting genotoxicity and oxidative damage to these particles.

It is understood that PS-NPs enter the internal structure of mussels through ingestion during feeding processes and are predominantly sorted in the gills. In contrast, larger PS-NPs and aggregates are redirected to the digestive gland, where they accumulate and/or partially translocate to the haemolymph, subsequently distributing to other tissues (Faggio et al., 2018; Sendra et al., 2020b). Moreover, the uptake of PS-NPs can disrupt the internal organisation of cells, interfering with the enzymatic activity involved in energy metabolism (Auclair et al., 2020). In conclusion, it can be hypothesised that after PS-NPs reach the digestive gland cells and induce lipid peroxidation following a week of exposure, PS-NPs are redistributed via the haemolymph to other tissues, such as the gills, overwhelming any possible defence managed by antioxidant enzymes and resulting in the oxidative damage observed after two weeks of exposure, which may also explain the genotoxicity detected in the haemolymph of mussels.

3.5.Conclusion

The present study provides evidence that PS-NP toxicity is tissue-specific and time-dependent. The abiotic and biotic characteristics of seawater result in an increased hydrodynamic diameter and aggregation of polystyrene nanoplastics. In *M. galloprovincialis*, 10 µg/L of 50 nm polystyrene PS-NPs induced genotoxicity, overwhelmed antioxidant defences, and caused oxidative damage to both tissues. The inhibition and induction of antioxidant defences may stem from reactive oxygen species generated by NP toxicity, which may be linked to the ingestion, translocation, and accumulation of nanoplastics. In the gills of mussels, an adaptive response appears to trigger the activation of repair mechanisms, such as autophagy, although further studies are needed to fully understand this activation. Moving forward, it is crucial to deepen our understanding of the behaviour and toxicity of PS-NPs towards marine biota and their mode of action, as particle interactions vary significantly compared to ultrapure water. Additionally, further analysis of extended exposure periods is vital to understanding how mussels react to nanoplastic exposure beyond 21 days.

CHAPTER IV

Assessing the effects of the cytostatic drug 5-Fluorouracil alone and in a mixture of emerging contaminants on the mussel *Mytilus galloprovincialis*

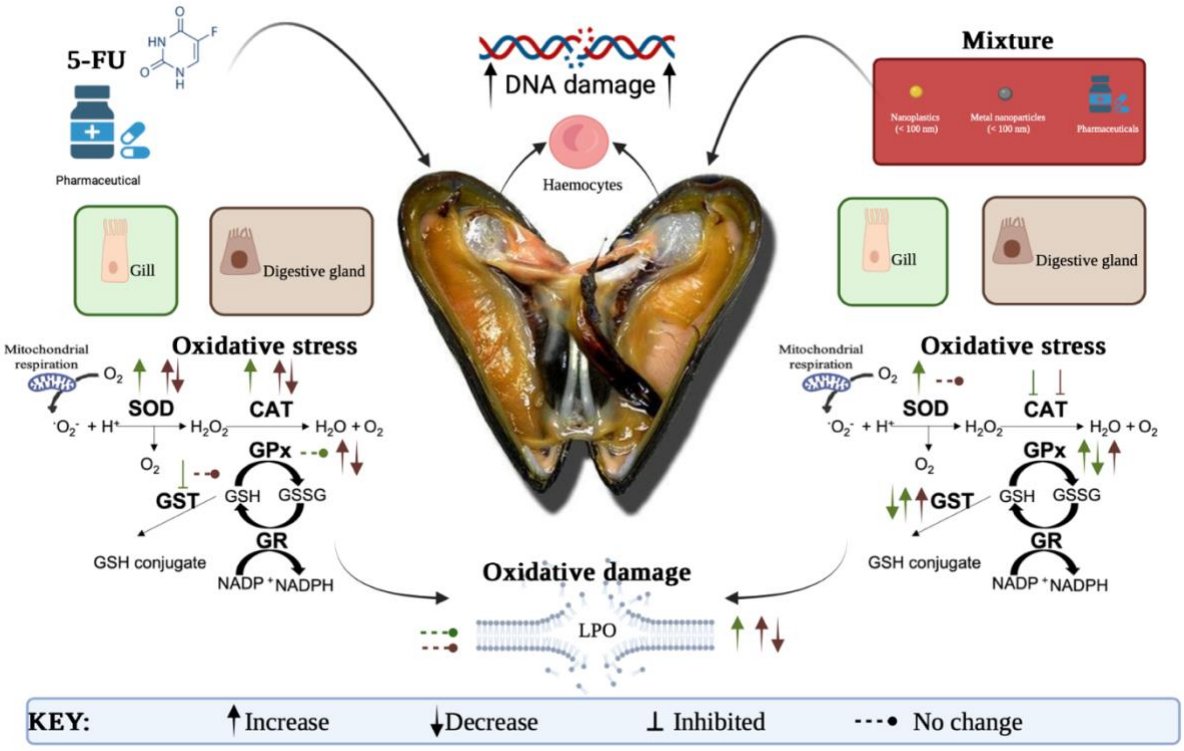

This chapter has been published in:

- Gonçalves, J. M., Beckmann, C., & Bebianno, M. J. (2022). Assessing the effects of the cytostatic drug 5-Fluorouracil alone and in a mixture of emerging contaminants on the mussel *Mytilus galloprovincialis*. Chemosphere, 305(June), 135462. https://doi.org/10.1016/j.chemosphere.2022.135462

This chapter was presented at the international conference:

CICTA 2021 (29th November – 2nd December 2021): **ORAL PRESENTATION**

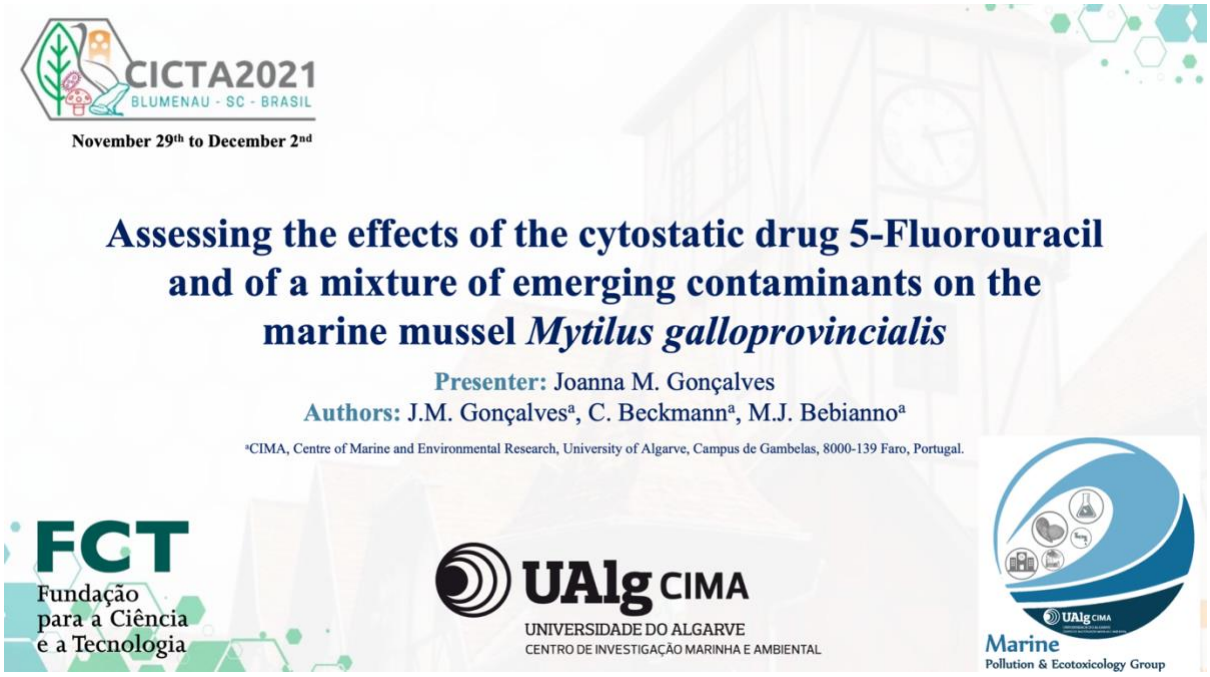

Abstract

The assessment of contaminants of emerging concern, both individually and in mixtures, and their effects on marine biota requires attention. 5-Fluorouracil is a category 3 cytostatic anti-cancer medication (IARC) used to treat various cancers, including colon, pancreatic, and breast cancer. In the presence of other pollutants, this pharmaceutical can interact and form mixtures of contaminants, such as adhering to plastics and interacting with metal nanoparticles. This study aimed to comprehend the effects of 5-Fluorouracil (5-FU; 10 ng/L) and a mixture of emerging contaminants (Mix): silver nanoparticles (nAg; 20 nm; 10 µg/L), polystyrene nanoparticles (PS-NPs; 50 nm; 10 µg/L), and 5-FU (10 ng/L), in an *in vivo* (21 days) exposure of the mussel *Mytilus galloprovincialis.* A multi-biomarker approach, including genotoxicity, the antioxidant defence system (superoxide dismutase (SOD), catalase (CAT), glutathione peroxidases (GPx), glutathione S-transferases (GST) activities), and oxidative damage (LPO), was employed to assess the effects in the gills and digestive gland of mussels. Both treatments caused genotoxicity in the mussel's haemolymph, and antagonism between contaminants was observed in the Mix. The observed genotoxicity confirms 5-FU's mode of action (MoA) by causing DNA damage. The antioxidant defence system of mussels exposed to 5-FU activated, countering the reactive oxygen species (ROS) generated during the exposure, though this was not observed in mussels exposed to the mixture. Mussels could withstand the effects of the single compound but not those of the Mix. Regarding oxidative stress and damage, the interactions of the components of the mixture demonstrated a synergistic effect.

4.1. Introduction

5-Fluorouracil (5-FU), a cytostatic agent (IARC Class 3), is among the most frequently prescribed cancer drugs for the treatment of solid tumours, as well as colorectal, pancreatic, and breast cancer (Mahnik et al., 2007). 5-FU is a pyrimidine analogue of uracil, distinguished by a fluorine atom substituted for hydrogen at the C-5 position (Vermorken et al., 2007). Its primary mode of action (MoA) in mammals involves the misincorporation of its fluoro-nucleotides into DNA (Matuo et al., 2009) and the release of cytochrome *c* from the mitochondria, which promotes the formation of reactive oxygen species (ROS), ultimately leading to the generation of superoxide radicals and oxidative stress (Cairns et al., 2011). 5-FU enters the cell via active transport through the uracil transport system. Three metabolites are formed: 1 – Fluorodeoxyuridine monophosphate (FdUMP), which suppresses the function of thymidylate synthase, thereby inhibiting the production of deoxythymidine monophosphate (dTMP); 2 – Fluorodeoxyuridine triphosphate (FdUTP), which can directly induce DNA damage; and 3 – Fluorouridine triphosphate (FUTP), which can integrate into RNA instead of uridine triphosphate (UTP), leading to RNA damage (Ghafouri-Fard et al., 2021). While this is the case for mammalian cells, the MoA of 5-FU remains unknown in invertebrates, such as mussels.

Pharmaceuticals are a significant group of contaminants of emerging concern (CECs), yet cytostatic drugs have received insufficient attention. The number of patients undergoing chemotherapy treatments involving cytostatic drugs, whether in hospitals or at home, is troubling, as these agents rarely fully metabolise and are eventually discharged into the water either unaltered or modified (Trombini et al., 2016). Furthermore, wastewater treatment plants (WWTPs) lack the necessary processes to effectively remove or break down pharmaceuticals. Additionally, other sources such as surface runoff and aquaculture also contribute to these contaminants entering rivers and the ocean, leaving aquatic life constantly exposed to them (Thiagarajan et al., 2021). Cytostatic drugs are not effectively eliminated and are highly persistent in WWTPs (Bürge et al., 2006; Mahnik et al., 2007). Moreover, this class of pharmaceuticals is recognised for having cytotoxic, genotoxic, mutagenic, and carcinogenic effects on non-target organisms (Kümmerer & Henninger, 2003). In the marine environment, the effects of 5-FU remain largely unknown; however, for instance, in freshwater systems, 5-FU has been demonstrated to cause acute toxicity and hinder the growth of the green microalgae, *Scenedesmus vacuolatus* (5.87 to 187.7 mg/L; 72h) (Asad et al., 2012), and to induce DNA damage in the aquatic oligochaete *Limnodrilus udekemianus* at environmentally relevant concentrations (0.004 µM; 96 h) (Kračun-Kolarević et al., 2015). Therefore, the

widespread use of the not readily biodegradable 5-FU (Kummerer & Al-Ahmad, 1997) and its effects on non-target marine organisms should be thoroughly investigated, as the physical-chemical parameters of the marine environment may influence the behaviour of 5-FU and its metabolites.

In European waters, concentrations of 5-FU have been estimated to fall within the range between 0.3 ng/L to 2.5 ng/L (Heath & Isidori, 2020) , while in the Taipei region, concentrations of 6.2 ng/L were detected, with levels reaching a maximum of 160 ng/L in the Gaoping River (Lin et al., 2014). 5-FU appears to be quite persistent in the water and likely remains in the sediments (Besse et al., 2012). Mahnik et al. (2007) proposed a strategy for removing this pharmaceutical through membrane reactor systems and demonstrated that 24 hours can almost completely eradicate 5-FU due to biotransformation. However, according to Li et al. (2021), mixtures of anticancer medications seem to have additive effects in marine species, or possibly even synergistic effects. Precautionary mitigation measures should be implemented to prevent the increasing and continuous discharge of these toxic residues into the marine environment, and some promising treatment technologies have already been identified (Zhang et al., 2013).

Pharmaceuticals are not the only emerging contaminants entering the ocean. Contaminants within the nano-sized range are also increasing, including nanomaterials and nanoplastics. Attention is rapidly turning towards the mixtures of CECs within the scientific community, focusing on how and if they interact and whether they will have more severe toxic effects on non-target marine organisms. CECs are defined as a range of chemical compounds, whether anthropogenic or naturally occurring, that are not routinely monitored in the marine environment. They are classified based on their persistence in the marine environment as well as their harmfulness and ecotoxicological effects. Pharmaceuticals are known as “classical” CECs, and although microplastics and nanoplastics are not yet included in this list, nanomaterials and nanoparticles have been added (EPA, 2008; Gatz, 2021). Despite this, CECs have the potential to reach and damage ecosystems, resulting in adverse effects on humans and/or ecology (Nawaz & Sengupta, 2019). Their fate in the marine environment is influenced by both land-based and ocean-based sources, such as waste mismanagement, accidents (i.e., spills), antifouling agents, and fishing gear. As previously mentioned, effluents and WTTP are the primary sources of CECs from pharmaceuticals. Not only do pharmaceuticals inevitably end up in the ocean, but products such as plastics, metals, and industrial effluents (Holmes et al., 2012) also accumulate in the marine environment, creating mixtures of compounds that

may be toxic. The concern regarding these mixtures is growing, and there is a pressing need to enhance our understanding of how they behave.

There has been a rapid increase in the applications of nanoparticles and nanomaterials (1 – 100 nm), with silver nanoparticles (nAg) accounting for more than 50% of global nanomaterial consumer products (Pulit-Prociak & Banach, 2016). nAg is frequently used in personal care products, antimicrobial coatings, photonic devices, and the textile industry (Maillard & Hartemann, 2013; Lee & Jun, 2019; Pereira et al., 2020), and a significant amount of nAg in the environment originates from its release from consumer products. Once released into sewer systems, nAg subsequently enters wastewater treatment plants (WWTP) and ultimately reaches the aquatic environment, where it poses a serious environmental risk due to the potential toxicity of these nanoparticles (Wang et al., 2018; Vilela et al., 2018). The mode of action (MoA) of nAg is known to damage cell membranes and directly generate reactive oxygen species (ROS), either by the nanoparticles themselves or through the release of Ag^+ ions, creating a "trojan horse" effect (Ghobashy et al., 2021). In marine organisms, nAg has been shown to promote oxidative stress responses by impairing the capacity of the antioxidant enzyme defence system (Gomes et al., 2014; Walters et al., 2016; Bouallegui et al., 2017). However, the effects of nAg on marine organisms in a "cocktail" of emerging contaminants remain unclear.

Moreover, plastic pollution is a significant and ongoing issue that the scientific community has committed to understanding its potential toxicity. From macro- to microplastics, numerous studies have assessed their effects on the marine environment (Lu et al., 2016; Ribeiro et al., 2017; Calderon et al., 2019; Vasanthi et al., 2021), yet one class of plastics not fully understood is nanoplastics. Nanoplastics arise from the degradation of macro- and microplastics (primary nanoplastics) and range from 1 to 100 nm in size (Gigault et al., 2018); they also enter the marine environment in their manufactured nano-sized form (secondary nanoplastics) (Andrady, 2011; Cole et al., 2011; Bessa et al., 2018; Tamminga et al., 2018). During the synthesis of nano-sized plastics, changes occur in the physical-chemical characteristics of the plastic particles, with their surface area, size, intensity, conductivity, and reactivity differing significantly from those of macro- and micro-sized particles (Klaine et al., 2012; Mattsson et al., 2015, 2018). A major concern regarding nanoplastics is that their size allows these particles to pass through cellular boundaries, underscoring the importance of understanding this size class of plastics, given that biological reactivity increases with decreasing size (Mattsson et al., 2018; Ferreira et al., 2019; Peng et al., 2020). Furthermore, plastics may serve as vectors for other contaminants present in the aquatic environment through

sorption mechanisms, which vary depending on the type of plastic polymer, highlighting the need to investigate these processes (Thiagarajan et al., 2021). Despite the challenges in quantifying nanoplastics in the marine environment, examples of nanoscale plastic polymers include polyvinyl chloride (PVC), polyethylene terephthalate (PET), polyethylene (PE), and polystyrene (PS), which have been found in the nanoplastic segment of the subtropical North Atlantic gyre (Ter Halle et al., 2017). Additionally, just five minutes of mechanical abrasion simulating coastal activity on a PS cup and lid resulted in the formation of plastic in the nano-range (Ekvall et al., 2019). PS is the fourth most commonly used plastic polymer worldwide (PlasticsEurope, 2021), and extensive data is available regarding their effects on marine organisms such as bivalves (Tallec et al., 2018; Cole et al., 2020; Sendra et al., 2021) and fish (Mattsson et al., 2015; Bessa et al., 2018; Maaghloud et al., 2021), while limited information exists about the effects of nanoplastics in their virgin form (Gonçalves & Bebianno, 2021; Chapter 1). *M. galloprovincialis* exposed to PS nanoplastic (PS-NPs) at a concentration of 10 µg/L (PS-NPs; 50 nm; 21-d) exhibited inhibition of the antioxidant defence system, leading to oxidative damage, particularly affecting the mussel gills, and causing genotoxicity in the mussel haemolymph (Gonçalves et al., 2022; Chapter 3). In comparison to PS microplastics (PS-MPs), exposure to PS-NPs in *M. galloprovincialis* (50 nm; 1.5 – 150 ng/L; 21-d) resulted in more pronounced effects on lysosomal indicators of general stress, indicating a related pattern of increased antioxidant activity in the mussel gills (Capolupo et al., 2021).

It is crucial to understand how these CECs affect marine organisms individually to comprehend their potential interactions as a mixture. For instance, if an organism simultaneously ingests more than one contaminant, various interaction possibilities may arise; the combination might lead to the toxic effect of one contaminant being added to that of another (additive or non-interaction), or the harmful effects of the combination may be significantly less than those of a single contaminant (antagonism), or the hazardous effects of the combination might be considerably greater than those of the individual compounds (synergism) (Stenersen, 2004). It is known that pharmaceuticals and nanomaterials interact with micro- and nanoplastics through adsorption, and the interaction between plastics and other CECs can cause substantial changes to surface properties, as well as influence the uptake and accumulation in exposed organisms (Zhou et al., 2021). Although the method of interaction for pharmaceuticals has been addressed, there is limited data available on the interaction of nanomaterials such as metals (Holmes et al., 2012, 2014; Thiagarajan et al., 2021). For these, two methods of sorption can be observed: a period of rapid sorption followed by a tendency towards equilibrium, or a more prolonged phase of gradual sorption (Holmes et al., 2012). Therefore, the presence of

CECs and their effects is significant in investigating the safety of seafood consumers. Consequently, this study aimed to evaluate the effects of 5-FU (10 ng/L) both alone and in a mixture with silver nanoparticles (nAg; 10 µg/L; 20 nm) and polystyrene nanoplastics (PS-NPs; 10 µg/L; 50 nm) on the marine mussel *Mytilus galloprovincialis* during a 21-day *in vivo* exposure. A multi-biomarker approach was employed to assess genotoxicity, oxidative stress, and oxidative damage.

4.2. Materials and methods

4.2.1. Experimental Design

Mussels *Mytilus galloprovincialis* Lamarck, with an average shell size of 50 mm ± 5 mm, were collected from the Ria Formosa Lagoon in Southeast Portugal (37°00'30.6"N 7°59'39.6" W) and transported to the laboratory. After an acclimatisation period of four days, 20 mussels were placed in duplicate designs within 15 L tanks containing 10 L of seawater. The mussels were contaminated with 10 ng/L of 5-FU and a corresponding mixture comprising 10 ng/L of 5-FU, 10 µg/L of nAg, and 10 µg/L of PS-NPs. They were exposed to these treatments for a duration of 21 days, with re-dosing of contaminants and seawater exchanges conducted every two days. Mortality was noted in mussels exposed to 5-FU, with six mussels dead by day 3 and two by day 10 of exposure. Mussels were collected on days 0, 3, 7, 14, and 21 for multi-biomarker analysis. They were weighed, and their gills and digestive glands were dissected, quickly frozen in liquid nitrogen, and stored at -80°C until further analysis.

4.2.2. Condition Index

The condition index (CI) was employed to assess the physiological status of mussels (5 per treatment and exposure period) at the beginning (day 0), as well as at 7 and 21 days following exposure. The percentage of the ratio between the total mussel weight (including tissue and shell) (g) and the wet weight (g) of the soft tissues was utilised to determine the CI (Gomes et al., 2013).

4.2.3. Genotoxicity assay

The alkaline comet test was used to measure DNA damage as developed by Singh et al. (1988) and Gomes et al. (2013). Haemolymph from mussels was collected using a sterile hypodermic syringe (1 mL) with a 25 G needle, retrieved from the posterior adductor muscle of five mussels after 0, 3, and 14 days of exposure to 5-FU and Mix, alongside five unexposed mussels. A 100 µL sub-sample from each experimental condition was stained with 100 µL of trypan blue to assess cell viability, and the percentage of living cells was calculated by counting 100 randomly selected cells.

For the comet assay, microscopic slides were cleaned with ethanol/ether (1:1) and coated with 0.65% normal melting point agarose (NMA) in Tris-acetate EDTA for DNA damage assessment. Mussel haemolymph cells were then centrifuged at 3000 rpm for 3 minutes (4°C) to extract cells, which were subsequently suspended in 0.65% low melting point agarose (LMA, in Kenny's salt solution) and cast onto the microscopic slides. Slides containing embedded cells were then immersed in a lysis solution (2.5 M NaOH, 100 mM EDTA, 10 mM Tris, 1% Triton X-100, 10% dimethyl sulfoxide, 1% sarcosine, pH 10, 4°C) for 1 hour to allow cellular components to diffuse into the agarose and the DNA to be immobilised. Following the lysis step, the slides were gently placed in electrophoresis buffer (300 mM NaOH, 1 mM EDTA, adjusted pH 13, 4°C) and set aside for 15 minutes. Electrophoresis was then conducted for 5 minutes at 25 V and 300 mA. The slides were removed and immersed in a neutralising solution (0.4 mM Tris, pH 7.5) before being washed with bi-distilled water and allowed to dry overnight. The presence of comets was determined using an optical fluorescence microscope (Axiovert S100) attached to a camera (Sony) after the slides were stained with 4,6-diamidino-2-phenylindole (DAPI, 1 g/mL). Following assessing the proportion of DNA in the tail, the Komet 5.5 image analysis system was employed to score 50 randomly selected cells for each slide (200 cells assessed per group) at a total magnification of 400. The results are presented as the mean and standard deviation.

4.2.4. Tissue preparation and analysis of enzymatic activities

Individual mussel gills and digestive glands were homogenised in 5 mL of 20 mM Tris-Sucrose buffer (0.5 M Sucrose, 0.075 M KCl, 1 mM DTT, 1 mM EDTA, pH 7.6) in an ice bath for 2 minutes, as described by Geret et al. (2002). The cytosolic fraction was obtained after centrifuging the homogenates (500 g, 15 minutes, 4°C), and the supernatant was re-centrifuged (12,000 g, 45 minutes, 4°C). The activities of antioxidant enzymes (superoxide dismutase (SOD), catalase (CAT), glutathione peroxidases (GPx)) and the biotransformation enzyme (glutathione-S-transferases (GST)) were determined using aliquots (150 µL) of the cytosolic fraction.

In addition, total protein concentrations were determined using Bradford's (1976) method. These concentrations (mg protein g^{-1} tissue) were calculated using bovine serum albumin (BSA) as a standard and optimised for the microplate reader.

SOD activity was assessed in both tissues by measuring the decrease in cytochrome *c* absorption using the xanthine oxidase/hypoxanthine system at 550 nm, with the results expressed as U mg^{-1} protein (McCord & Fridovich, 1969).

The quantitative evaluation of CAT activity in both tissues follows Greenwald's (1985) method, which relies on the spectrophotometric detection of hydrogen peroxide (H_2O_2) consumption at 240 nm. The results are expressed in mmol min^{-1} mg $protein^{-1}$.

GPx activity in both tissues were measured using a microplate reader (Infinite® 200, Pro-Tecan) at 340 nm with cumene hydroperoxide as a substrate at 28°C, following a method developed by McFarland et al. (1999). The results are presented in mmol min^{-1}mg $protein^{-1}$.

The GST activity in both tissues was assessed by conjugating 0.2 mM reduced glutathione (GSH) with 0.2 mM 1-chloro-2,4-dinitrobenzene (CDNB) in a 0.2 M KH2PO4/K2HPO4 buffer (pH 7.9). Subsequently, the reaction mixture was measured at 340 nm using a microplate reader (Infinite® 200, Pro-Tecan), following the method outlined by Habig et al. (1974). The data are presented in mol CDNB min^{-1} mg^{-1} protein units.

4.2.5. Lipid Peroxidation (LPO)

Individual mussel gills and digestive glands were homogenised on ice with 5 mL of 0.02 M Tris-HCl buffer (pH 8.6) and a 1:10 ratio of butylated hydroxytoluene (BHT). The supernatant from homogenates (3 mL), centrifuged at 30,000 g for 45 minutes at 4°C, was used to assess total protein concentrations and LPO levels. The absorbance of malondialdehyde (MDA) and (2E)-4-hydroxy-2-nonenal (HNE) at 540 nm was employed to determine LPO levels using the technique derived from Erdelmeier et al. (1998). The results are expressed in nanomoles per milligram of protein.

4.2.6. Statistical Analysis

A student t-test was used to evaluate the condition index of mussels, and statistical analysis was conducted using Microsoft Excel (©Microsoft 2022). Two parametric tests were performed to determine whether significant differences exist between treatments and time. A two-way ANOVA with a confidence level of 95% and a post hoc Tukey test were utilised to compare the results pairwise. A Principal Component Analysis (PCA) was performed to examine the relationship between treatments (control, 5-FU, and Mix) and variables (antioxidant and biotransformation enzymes, oxidative damage). GraphPad Prism Version 9.1.1 was utilised for the statistical analyses (GraphPad Software, Inc. CA).

4.3. Results

4.3.1. Condition Index

There is no significant discrepancy in the condition index of *M. galloprovincialis* between treatments or times of exposure, except between controls and mussels exposed to 5-FU on the seventh day of exposure ($p < 0.05$). The values range from 37.30 ± 2.81 (controls), 34.91 ± 2.45 (5-FU), and 40.84 ± 3.82 (Mix) (*see* Table 4.1).

Table 4.1. Condition index (mean ± S.D.) (%) of *M. galloprovincialis* exposed to 5-FU and a mixture of emerging contaminants (10 µg/L of silver nanoparticles + 10 µg/L of polystyrene nanoplastics + 10 ng/L of 5-Fluorouracil) at the beginning, after 7 days, and at the end of the exposure.

Time (day)	CT	5-FU	Mix
0	37.30 ± 2.81		
7	40.67 ± 8.16	32.59 ± 4.35	31.45 ± 5.55
21	37.22 ± 3.03	34.91 ± 2.45	40.84 ± 3.82

4.3.2. Genotoxicity

Haemocytes of mussels, both unexposed and those exposed to 5-FU and Mix, were analysed for DNA damage at the start of the trial, as well as after 3 and 14 days of exposure, utilising the comet parameter % tail DNA (Fig. 4.1.). Figure 4.1.A displays a few examples of comets in mussel haemocytes from the control group and from those exposed to 5-FU and Mix. After 3 and 14 days of exposure, the nucleoid core of unexposed *M. galloprovincialis* haemocytes showed no broken DNA fragments or damaged DNA migrating towards the tail region. In contrast, the nucleoid core of mussels exposed to 5-FU and Mix presented broken DNA fragments or damaged DNA moving into the tail region (Fig. 4.1.A). At each exposure time, unexposed mussels displayed no significant differences in % tail DNA ($p > 0.05$; Fig. 4.1.B); however, a significant difference in DNA damage was observed in mussels exposed to 5-FU and Mix compared to the unexposed group ($p < 0.05$; Fig. 4.1.B). Furthermore, on the 3rd day of exposure, the % tail DNA in both treatments were considerably greater than on the 14th day (2-fold difference in both treatments) ($p < 0.05$; Fig. 4.1.B). Consequently, both 5-FU alone and combined with Mix cause genotoxicity in the haemolymph of the mussels (see Fig. 4.1.).

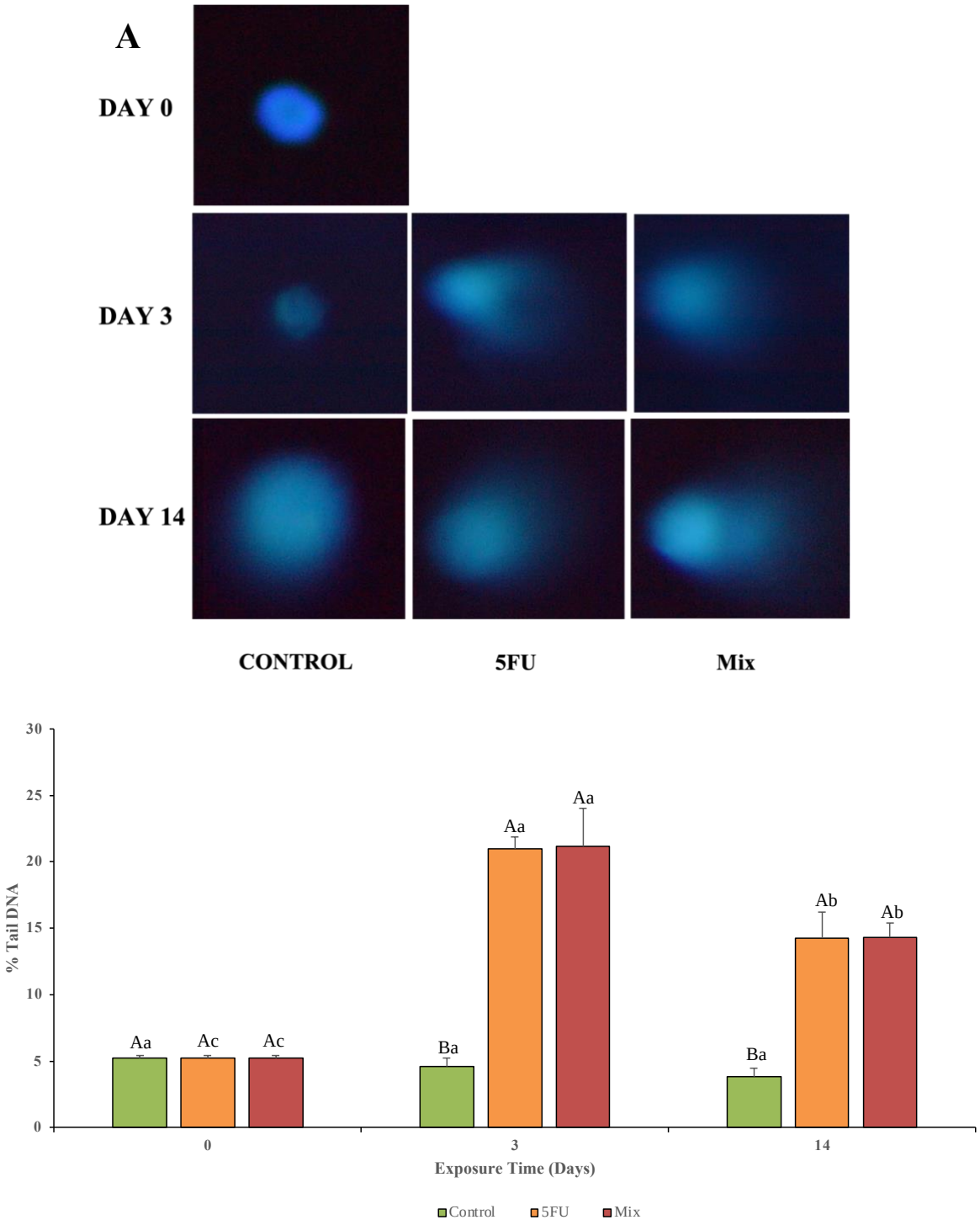

Figure 4.1. Genotoxicity effects of *in vivo* exposure of 5-Fluorouracil (10 ng/L) and a mixture of emerging contaminants (10 µg/L of silver nanoparticles + 10 µg/L of polystyrene nanoplastics + 10 ng/L of 5-Fluorouracil) in the haemolymph of *M. galloprovincialis.* (A) examples of comet assay images of unexposed *M. galloprovincialis* haemocytes and (B) DNA damage (% tail DNA). Different upper- and lower-case letters indicate significant differences between treatments for the same time and between times for the same treatment, respectively ($p < 0.05$).

4.3.3. Enzymatic activities

There were no significant differences in the various enzymatic activities recorded over time in the control group ($p > 0.05$, Fig. 4.2. A – J), apart from GST in the gills ($p < 0.05$, Fig. 4). The activities of all enzymes—SOD, CAT, GPx, and GST—altered following exposure to the different types of contamination.

Mussels exposed to 5-FU showed an increasing trend in SOD activity in their gills over time, with all exposure durations significantly differing from the beginning of the exposure when compared to controls and to Mix-exposed mussels on the 21st day ($p < 0.05$; Fig. 4.2.A). In the gills, after exposure to the mixture of contaminants, a significant increase in SOD activity was noted until day 14, returning to levels comparable to controls on day 21 ($p < 0.05$; Fig. 4.2.A). In the digestive gland, SOD activity significantly increased after 3 days compared to the start of the exposure for both treatments ($p < 0.05$; Fig. 4.2.B). In the digestive gland exposed to Mix, however, a significant rise in SOD, compared to unexposed mussels, is evident in the first week of exposure ($p < 0.05$). Overall, the rising SOD activity in both tissues after exposure to 5-FU or Mix is significantly different from controls after 7 days ($p < 0.05$), with this significance in the gills being maintained until the end of the exposure.

A significant increase in CAT activity is observed in the gills of mussels exposed to 5-FU compared to the beginning of exposure ($p < 0.05$); however, a slight decrease in activity is noted on day 14 (Fig. 4.2.C). A significant difference for 5-FU-exposed mussels is evident at all time points compared to control mussels ($p < 0.05$). In the gills of mussels subjected to the Mix, a noteworthy increase is recorded after 7 days, maintaining these levels on day 14, with both days showing significant differences from day 3 and the initial state of contamination ($p < 0.05$; Fig. 4.2.C). When comparing 5-FU and the Mix, it is evident that CAT activity in the gills is significantly higher from the 3rd to the 21st day of exposure to 5-FU. In the digestive gland of mussels, exposure to 5-FU resulted in a sharp, significant increase in CAT activity (2.4-fold) after 3 days, followed by a decline ($p < 0.05$; Fig. 4.2.D). In Mix-exposed mussels, a significant decrease in CAT activity occurs throughout the duration of exposure, with CAT activity on days 14 and 21 being significantly lower than at the other time points compared to unexposed mussels ($p < 0.05$; Fig. 4.2.D). A significant difference between 5-FU and Mix is also noticeable throughout the entire exposure period ($p < 0.05$; Fig. 4.2.D). A slight increase in activity throughout the experiment is detected for GPx activity in gills exposed to 5-FU. However, significant differences are only observed on the initial day compared to day 21 ($p < 0.05$; Fig. 4.2.E). The gills of 5-FU-exposed mussels significantly differed from the controls on days 3 and 14 ($p < 0.05$; Fig. 4.2.E). A steep, significant increase

in GPx activity in the gills of Mix-exposed mussels occurs until the seventh day (4.8-fold and 8.3-fold on days 3 and 7, respectively, $p < 0.05$), followed by a decrease in activity. Significant differences were noted throughout the exposure compared to the start of the exposure, with the highest significant activity recorded at 7 days ($p < 0.05$, Fig. 4.2.E). Significant differences between both treatments are also important during the first week of exposure ($p < 0.05$; Fig. 4.2.E). In the digestive gland of mussels, GPx activity showed no significant differences compared to the initial state of 5-FU exposure and unexposed mussels over time, except on day 21 ($p < 0.05$; Fig. 4.2.F). In the digestive glands of Mix-exposed mussels, a significant rise in activity is observed on day 3 and day 21 ($p < 0.05$; Fig. 4.2.F). In Mix-exposed mussels, GPx activity follows a similar pattern to that of 5-FU-exposed mussels' digestive glands, with significant differences noted on days 3 and 21 of exposure ($p < 0.05$; Fig. 4.2.F). Throughout the exposure, no significant differences in GPx activity were identified between 5-FU and Mix ($p > 0.05$, Fig. 4.2.F). Generally, GPx activity in the digestive glands displays low variation across all treatments, apart from the 3rd and 21st days for 5-FU- and Mix-exposed mussels.

Firstly, it is important to note that significant differences were observed in the gills of unexposed mussels on days 7, 14, and 21, where GST activity is significantly lower ($p < 0.05$) than the levels measured at days 0 and 3, indicating an overall decreasing trend (Fig. 4.2.G). This may result from cyclic behaviour, as lower GST activity during the summer months has been attributed to seasonal variations in temperature and the reproductive cycle (Borković et al., 2005). For gills exposed to 5-FU, notable inhibition of GST activity occurs after 3 days, with lower activity maintained compared to controls until the end of the exposure period ($p < 0.05$; Fig. 4.2.G). In the case of mussels exposed to Mix, a significant inhibition ($p < 0.05$; Fig. 4.2.G) of GST activity (9.7-fold) was recorded between the initial and third day, while after 14 and 21 days of exposure, a significant induction in GST activity was seen. A significant difference in GST activity was noted between the 5-FU and Mix treatments on days 14 and 21 of exposure ($p < 0.05$; Fig. 4.2.G). In contrast, GST activity in the digestive gland exhibits a completely different trend. Here, GST activity does not markedly differ from what was previously observed in the gills. A significant decrease in GST activity was only noted on day 14 for mussels exposed to 5-FU compared to the outset of the experiment ($p < 0.05$). There is no notable difference in GST activity within the digestive gland across times and treatments (Fig. 4.2.H). Nonetheless, there is a significant difference in Mix-exposed mussels compared to controls and 5-FU-exposed mussels after 14 and 21 days of exposure ($p < 0.05$).

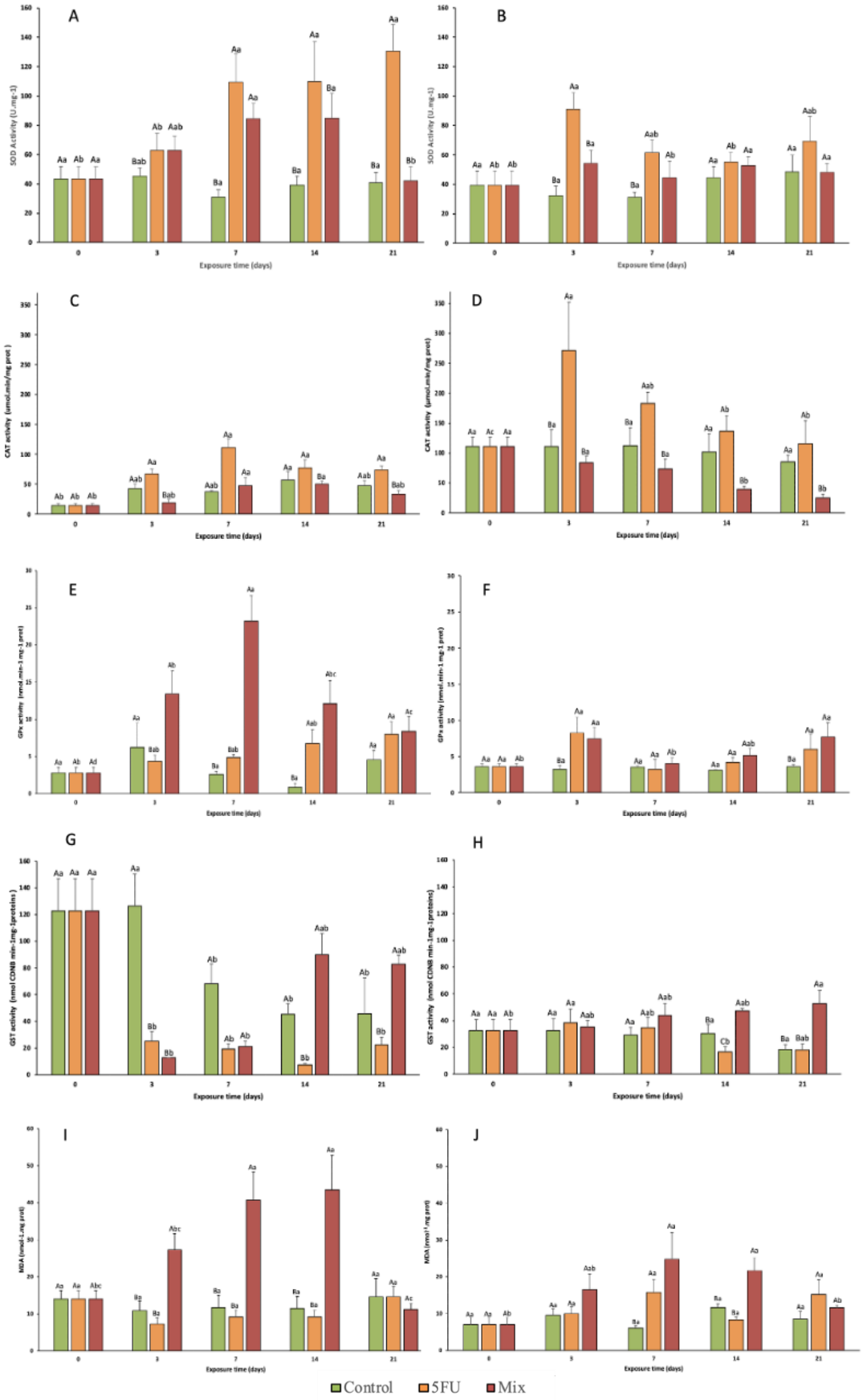

Figure 4.2. Biochemical markers in gills (A, C, E, G, I) and digestive gland (B, D, F, H, J) of *M. galloprovincialis* after a 21-day exposure to 5-Fluorouracil (10 ng/L) and a mixture of emerging contaminants (10 µg/L of silver nanoparticles + 10 µg/L of polystyrene nanoplastics + 10 ng/L of 5-

Fluorouracil). Different upper- and lower-case letters represent significant differences between treatments at the same time, and between times for the same treatment, respectively (p<0.05).

4.3.4. Oxidative damage: *Lipid Peroxidation*

LPO levels in both tissues (gills and digestive gland) of unexposed mussels did not change significantly throughout the 21 days of exposure (p > 0.05) (Fig. 4.2.I – J). No significant differences were found in LPO levels in the gills of mussels exposed to 5-FU (p > 0.05; Fig. 4.2.I). In the gills of mussels exposed to a Mix, a significant linear increase (y = 7.66x, r = 0.835) in LPO levels was detected from the third day until the 14th (p < 0.05; Fig. 4.2.I). The highest LPO levels were observed after 14 days of exposure. After 21 days, there was a sharp decrease of 3.9-fold, returning to control levels (Fig. 4.2.I). LPO levels for the gills of Mix-exposed mussels were significantly different from controls and 5-FU-exposed mussels on days 3, 7, and 14 (p < 0.05).

In the digestive gland of mussels exposed to 5-FU, LPO levels increased after one week, followed by a subsequent decrease and another increase after 14 and 21 days, respectively. Significant differences between unexposed and 5-FU-exposed mussels (p < 0.05; Fig. 4.2.J) were observed after one and two weeks of exposure. In the digestive gland, there was a significant increase (p < 0.05; 3.6-fold) in LPO levels after 7 days of exposure to Mix, followed by a decrease in control levels on day 21 (Fig. 4.2.J). Significant differences between Mix-exposed and 5-FU-exposed mussels were detected only on the 14th day of exposure. After 7 and 14 days of exposure, the results for the Mix were significantly different from controls (p < 0.05; Fig. 4.2.J).

4.3.5. Principal component analysis

PCA results applied to elucidate the effects of 5-FU and the mixture of contaminants on biomarker responses indicate a clear separation between unexposed individuals and those exposed to both types of exposure. The two principal components account for 82.0% of the variance in gills (PC1 = 47.7%, PC2 = 34.4%) and 78.2% in digestive glands (PC1 = 49.0%, PC2 = 29.2%) (Fig. 4.3.A – B). Overall, the results suggest that the effects in both tissues (gills and digestive gland) are time- and treatment-specific. Mussel responses appear to be dependent on time and tissue regarding 5-FU, as the prolonged exposure time (21st and 14th day) was most influential for gills and digestive glands, respectively. However, the seventh day proved to be most influential for both gills and digestive glands in mixed-exposed mussels. SOD and GPx

are the principal loadings influencing the first component in gills, whilst GST is negatively correlated (Fig. 4.3.A). Conversely, GST is the principal loading affecting the second component in the digestive gland (Fig. 4.3.B). This demonstrates that the different tissues exhibit varying responses to exposure, with mussel gills being the most compromised tissue.

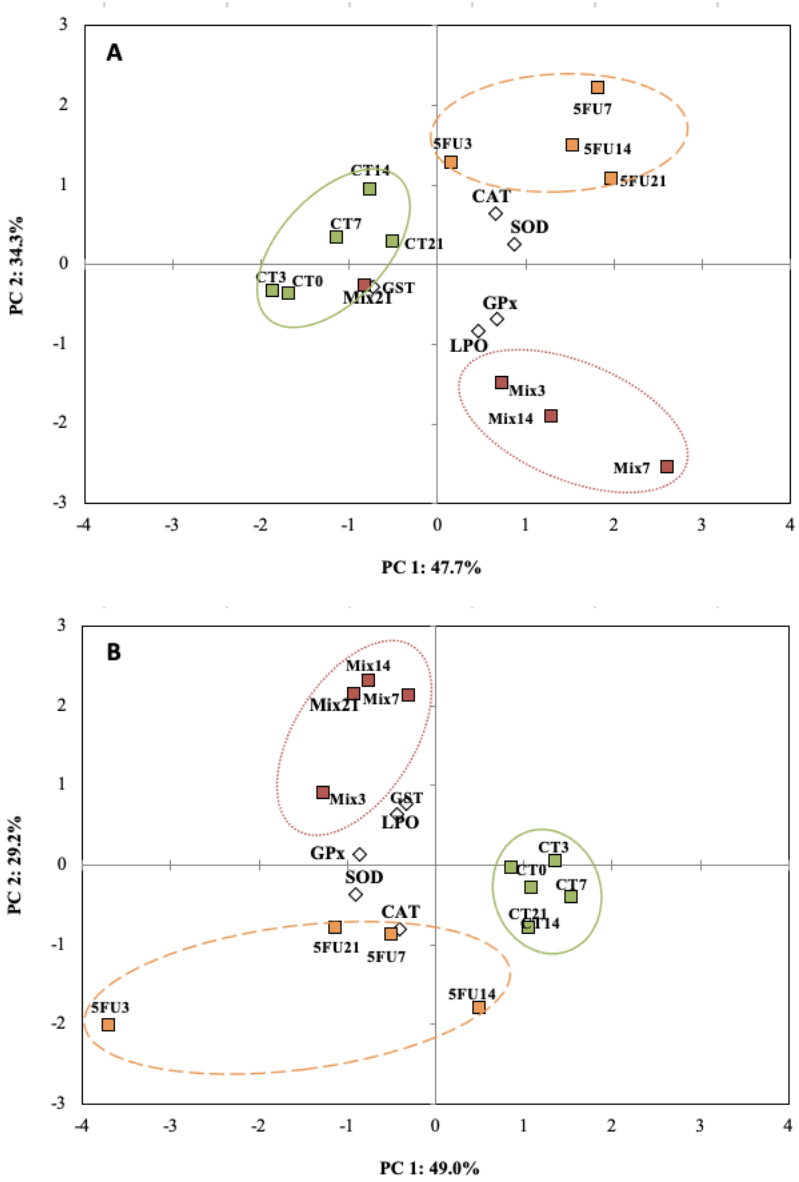

Figure 4.3. Principal Component Analysis (PCA) of a battery of biomarkers (SOD, CAT, GPx, GST and LPO) in the gills (A) and digestive gland (B) of mussels *M. galloprovincialis* from controls (CT) and after exposure to both treatments: 10 ng/L of 5-FU and a mixture of contaminants (10 µg/L of silver nanoparticles + 10 µg/L of polystyrene nanoplastics + 10 ng/L of 5-Fluorouracil) for 21 days ($p < 0.05$).

4.4. Discussion

Most of the data concerning the effects of 5-FU are limited to freshwater species (Gačić et al., 2014; Parrella et al., 2015; Kleinert et al., 2021). Therefore, to the best of our knowledge, this represents the first dataset on the effects of 5-FU alone, as well as in a mixture of contaminants, on the marine mussel *M. galloprovincialis. This was assessed* through the evaluation of biomarkers of genotoxicity, oxidative stress, and oxidative damage in two distinct tissues: the gills and the digestive gland, along with genotoxicity in the mussel's haemolymph. Exposure to these contaminants induces genotoxicity and oxidative stress.

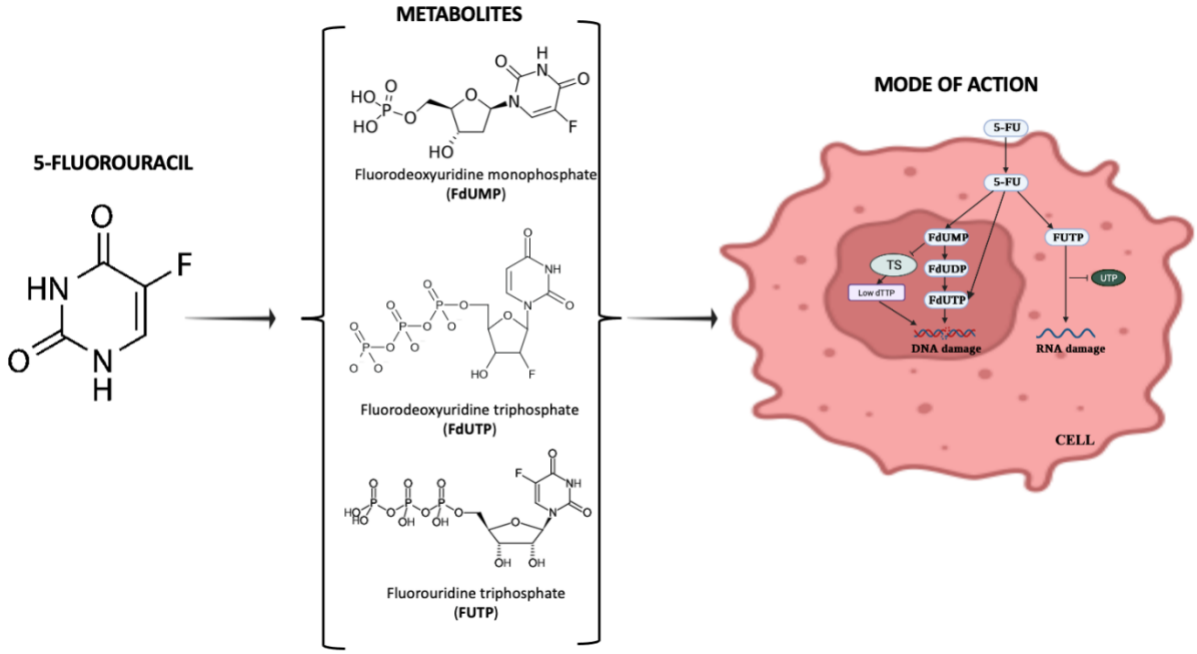

Figure 4.4. 5-Fluorouracil pyrimidine analogue, its metabolites and mode of action.

The mode of action (MoA) of 5-Fluorouracil is documented for mammalian cells (Fig. 4.4.), and a similar MoA for 5-FU is suggested by the genotoxicity observed in mussels (Fig. 4.1.). 5-FU is a uracil analogue with a fluorine atom at the C-5 position instead of a hydrogen atom (Vermorken et al., 2007). Once it enters the cell, 5-FU integrates into the DNA, inducing reactive oxygen species (ROS). The metabolites of 5-FU, namely FdUMP, FdUTP, and FUTP, are known to disrupt both DNA and RNA functions and processes. Although it cannot be confirmed definitively, the percentage of tail DNA observed in mussels exposed to 5-FU suggests that DNA damage is occurring. Haemocyte cells from unexposed mussels exhibited an average of DNA damage (5.3% fragmented DNA), which is typical for *Mytilus* (Mitchelmore et al., 1998). The most significant DNA damage noted in both treatments was detected on the third day of exposure, with a slightly lower yet still significant level of DNA

damage apparent after 14 days. Therefore, 5-FU and the Mix are genotoxic to the immune system of the mussel (Fig. 4.1.). In comparing mussels exposed to 5-FU and the Mix, similar levels of DNA damage were observed. However, this effect does not significantly differ from the damage observed with 5-FU alone. It has been established that nanoparticles (NPs) can adsorb and transport pharmaceutical compounds (Santana-Viera et al., 2021).

Moreover, the ionic strength significantly influences the sorption of 5-FU and other pharmaceuticals on the surface of plastic polymers, as the most substantial interactions have been observed in freshwater and low salinity conditions (Puckowski et al., 2021). To comprehend how nAg and PS-NPs interact with 5-FU, further investigation is required to confirm adsorption properties. In HeLa (human cell lines), a one-hour exposure to 5-FU was insufficient for DNA lesions to be recorded. However, a low % tail DNA was evident (Pinheiro, 2016). In the freshwater mussel *Elliptio complanata*, exposure to 5-FU resulted in a decrease in DNA strand breaks, while levels of lipid peroxidation (LPO) increased (Kleinert et al., 2021). In this study, the opposite was observed in 5-FU-exposed mussels, where DNA strand breaks increased while no significant levels of LPO were detected. Conversely, in mussels exposed to a mixture, DNA strand breaks and LPO were positively correlated in both tissues. Therefore, the physicochemical parameters of seawater compared to freshwater drastically impact the toxicity of 5-FU towards organisms, suggesting that 5-FU's toxicity is enhanced in the marine environment. Consequently, the genotoxicity observed in mussels exposed to the mixture warrants further investigation to better understand the interactions between pharmaceuticals, nanoplastics, and metal nanoparticles. According to the antagonistic or synergistic model developed by Ritz et al. (2021), the interactions of these contaminants within the mixture are antagonistic (*see Annex I*). Furthermore, the levels of the various parent compounds of 5-FU accumulated in mussel tissues require further study to assess the mechanisms of 5-FU in marine species.

The antioxidant defence mechanism of mussels was activated following exposure to 5-FU and a mixture of contaminants. After exposure to both treatments, the activity of SOD increased in the gills, with a minor increase noted in the digestive gland. The gills, as filter-feeding organisms, are the first tissues to encounter toxins in the water, leading them to filter and absorb these harmful substances (Jørgensen et al., 1996; Gonçalves et al., 2020). However, in the gills of *M. galloprovincialis* exposed to another anticancer drug—cisplatin (100 ng/L)—an inhibition of SOD was observed over the 14-day exposure period (Trombini et al., 2016). Nonetheless, a similar trend in the digestive gland (2.1–fold) was noted in mussels exposed to cisplatin (Trombini et al., 2016), as observed here for 5-FU. The metabolic role of SOD activity

is critical for removing superoxide radicals that are formed (Takahashi & Asada, 1983). As the first line of antioxidant defence (Li et al., 2009), it converts the superoxide anion ($\cdot O_2^-$) into hydrogen peroxide (H_2O_2). As more H_2O_2 is produced, CAT activity is expected to rise to facilitate H_2O_2 removal. Following the observed SOD activity, CAT activity in gills exposed to 5-FU presents a dumbbell-shaped pattern, whereas in the digestive gland, increased activity is observed after the first week. No changes were detected in the activity of CAT in mussels' gills exposed to cisplatin (100 ng/L); however, in the digestive gland, mussels display a similar activity level (272 µmol min/mg protein), confirming an increase in CAT activity due to exposure to anticancer drugs (Trombini et al., 2016). Although the increase in mussels exposed to cisplatin peaked on day 14 (Trombini et al., 2016), in this instance, the highest activity was achieved after 3 days, after which it declined throughout the experiment. CAT activity is more pronounced at higher concentrations of H_2O_2, signalling a substantial percentage of ROS generated in this tissue (Box et al., 2007). Exposure to 5-FU shows that GPx activity in the gills significantly increased by the end of the experiment, with a similar trend noted in *M. galloprovincialis* exposed to cisplatin (100 ng/L; 14 d) (Trombini et al., 2016). Conversely, the digestive gland of mussels exhibited a slight increase in GPx activity after exposure to 5-FU, whereas exposure of *M. galloprovincialis* to cyclophosphamide, another anticancer drug (CP) (1 ng/L, 14 d; Fernandes et al., 2020; and 100 and 1000 ng/L, 28 d, 21°C; Queirós et al., 2021), resulted in a significant increase in activity. It can be inferred that not all anticancer drugs act similarly and that the mussel's antioxidant defence response is dependent on the specific type of anticancer drug and its mode of action, as well as the concentration and behaviour of the pharmaceutical in seawater. A significant decrease in activity was noted for the biotransformation enzyme (GST) in the gills and digestive glands of mussels after exposure to 5-FU. Likewise, GST activity in the gills of *M. galloprovincialis* from northern Portugal, where most residues of pharmaceutically active compounds were detected, also diminished (3.16 µmol/min/mg protein) (Martínez-Morcillo et al., 2020). In the gills of *M. galloprovincialis* exposed to cisplatin (100 ng/L, 14 d), GST activity showed a dumbbell-shaped pattern, with an increase in GST activity in the digestive gland of mussels observed on the last day of exposure (Trombini et al., 2016). However, 5-FU resulted in inhibition of GST after 14 days of exposure. Similarly, GST activities in the digestive gland of *M. galloprovincialis* exposed to CP (1 µg/L, 14 d) diminished after 3 days (Fernandes et al., 2020), whilst Queirós et al. (2021) documented a significant increase in GST activity of mussels (*M. galloprovincialis*) exposed to CP (500 and 1000 ng/L, 17°C, 28 d). 5-FU induced oxidative stress in mussels, but the antioxidant defence system was able to mitigate the toxicity of 5-FU as no oxidative damage

was observed in either tissue. In contrast, Trombini et al. (2016) found an increase in lipid peroxidation (LPO) levels in the gills of *M. galloprovincialis* caused by cisplatin exposure (100 ng/L, 14 d), confirming oxidative damage through increased ROS production. Therefore, this indicates that the capacity of anticancer drugs to induce oxidative stress and damage is highly dependent on concentration and the drug's chemical composition. The PCA results (Fig. 4.3) further affirm the differences observed between 5-FU-exposed mussels and those exposed to the mixture. The response of 5-FU-exposed mussels is time- and tissue-dependent, with the critical time point for the gills noted at the end of the exposure period, while for the digestive glands, it is at 14 days. This confirms 5-FU's toxicity towards mussels despite the absence of oxidative damage, suggesting that prolonged exposure could compromise mussels' integrity and deserves further investigation.

Regarding mixtures of contaminants, exposure to a pharmaceutical-nanoplastic-metal nanoparticle mixture (Mix) resulted in an increase in SOD activity during the first two weeks of exposure in both the gills and digestive glands of *M. galloprovincialis*. Compared to 5-FU alone, the heightened SOD activity persists for an additional week in mussels exposed to Mix. In the gills of *M. galloprovincialis* exposed to gold nanoparticles with a zinc oxide corona (Au-ZnONP; 50 µg/L and 100 µg/L for 14 days) and to Diethyl 3-cyano-1-hydroxy-1-phenyl-2-methylpropylphosphate (PC, 100 µg/L), there was an increase in SOD activity. In contrast, the combination of both contaminants did not show significant differences from the control (Sellami et al., 2021). In other mixtures, the combined effects of micro-polystyrene (2 + 6 µm, 32 µg/L) and fluoranthene (FLU, 30 µg/L) on *Mytilus* spp. digestive glands demonstrated an increase in SOD activity within a similar range as reported by Paul-Pont et al. (2016). SOD activity also rose in the digestive gland of *M. edulis after exposure* to either 500 ng/mL of PS-MPs (20 µm) or 500 ng/mL of polyamide microfibres after 24 hours (Cole et al., 2020). In the Mix, the various contaminants had different impacts on SOD activity; for instance, PS-NPs (50 nm; 10 µg/L; 21 days) inhibited SOD activity in the gills of *M. galloprovincialis* (Gonçalves et al., 2022; Chapter 3) before also inhibiting it in the digestive gland. Conversely, nAg (< 100 nm; 10 µg/L; 15 days) resulted in an increase in SOD activity in both tissues (Gomes et al., 2014). This suggests an interaction between the components of the Mix. Generally, the gills of Mix-exposed mussels displayed significantly lower CAT activity, with increases noted between days 3 and 14. As CAT activity was inhibited, the Mix potentially amplified H_2O_2 production, and CAT could not mitigate the elevated reactive oxygen species (ROS) production, raising concerns about ROS toxicity towards *M. galloprovincialis*. A dumbbell-shaped pattern, analogous to that observed in mussels exposed solely to 5-FU, is evident in the gills of Mix-

exposed mussels. However, the activity values are markedly lower than those of 5-FU-exposed mussels. Similarly, CAT activity in *M. galloprovincialis* exposed to PS-NPs (15 ng/L for 21 days) exhibited a dumbbell-shaped pattern with a comparable decrease in activity (Capolupo et al., 2021), implying that this change may be attributable to the presence of PS-NPs within the Mix. However, CAT activity declined in both tissues of *M. galloprovincialis* after a 21-day exposure to PS-NPs (50 nm; 10 µg/L) (Gonçalves et al., 2022; Chapter 3), whereas exposure to nAg resulted in increased CAT activity in the gills and digestive glands (Gomes et al., 2014). This indicates a possible synergistic effect among the contaminants in the Mix. Within the digestive gland during Mix exposure, the reduction in CAT activity may stem from the transfer of contaminants onto plastics, as also observed by Paul-Pont et al. (2016) (micro-PS 2 + 6 µm, 32 µg/L and FLU 30 µg/L) in *Mytilus* spp. and by Almeida et al. (2019) (propanol and PS-NPs, 10 mg/L, 24 hours) in a fish cell line of *Sparus aurata.* These observations support the notion that a mixture of contaminants exhibits heightened toxicity compared to individual compounds and that plastics may serve as carriers for these contaminants. Nonetheless, we cannot discount the interaction of nAg within the mixture, as metal nanoparticle adsorption processes may also be at play. Glutathione peroxidase (GPx) may function as a compensatory mechanism for the deficiency in CAT activity. The activity of GPx in the gills of Mix-exposed mussels was induced, and a dumbbell-shaped pattern was noted. Thus, the increase in GPx activity in the gills, coinciding with inhibited CAT activity, suggests a critical dependence on GPx for ROS removal in these tissues (Regoli & Giuliani, 2014). Moreover, a noticeable rise in GPx activity was observed in the digestive glands of mussels after two weeks of exposure to the Mix. In contrast, GPx activity in mussels exposed to 5-FU decreased during this period. When considering the individual effects of the contaminants within the mixture, gills of *M. galloprovincialis* exposed to nAg (< 100 nm; 10 µg/L; 15 days) exhibited increased GPx activity exclusively (Gomes et al., 2014), while mussels exposed to PS-NPs alone (50 nm; 10 µg/L; 21 days) showed minimal GPx activity in both gills and digestive glands (Gonçalves et al., 2022; Chapter 3). Meanwhile, 5-FU indicated a declining trend in activity akin to unexposed mussels. As such, the interactions among the different particles within the Mix could elucidate the observed effects and suggest an enhanced ROS production, indicating that the toxicity of these compounds in the mixture is magnified. Consequently, the combined effects of the contaminants may yield synergistic consequences. GST activity similarly increased in the gills and digestive glands of mussels exposed to the Mix, significantly rising after two weeks of exposure. However, the gills exhibited GST inhibition during the initial week of exposure to the Mix. The decline in GST activity in the gills (on day 3) was directly

tied to increased LPO). Thus, the mussel's antioxidant response to the generated ROS proved insufficient to avert oxidative damage during the first week of exposure. Despite this, the observed upregulation of GST activity in the gills after 14 days correlates with a significant reduction in LPO on the 21st day. This suggests that mussels may manage the effects of exposure to the Mix after a prolonged duration. Additionally, the GST activity inhibition seen in mussels exposed solely to 5-FU might indicate the adsorption of 5-FU onto nAg or PS-NPs within the Mix, reducing the potency of 5-FU's toxicity. This could further explain the increase in the Mix relative to 5-FU alone. Further evaluation is essential to confirm this hypothesis. Moreover, a similar trend regarding GST activity elevation in the digestive glands of *Mytilus spp.* was noted after exposure to micro-PS and FLU (2 + 6 µm, 32 µg/L; 30g/L for 14 days) (Paul-Pont et al., 2016), suggesting an escalation of mixture toxicity over time. Results for mussels exposed to the Mix corroborate this pattern, reflected by initial increases in LPO levels in both tissues, albeit with a slight temporal difference, followed by decreased activity after 21 days. Exposure to other metal nanoparticles (e.g., nAg, nCuO) has been shown to increase oxidative stress in *M. galloprovincialis, with o*xidative damage being more pronounced in the gills compared to the digestive gland when exposed to nAg (10 µg/L for 15 days), indicating that the gills are more heavily affected by nAg (Gomes et al., 2013, 2014). A similar phenomenon is observed in this experiment. Furthermore, individual exposure to PS-NPs (50 nm; 10 µg/L; 21 days) resulted in oxidative damage in both tissues of *M. galloprovincialis*, with critical time-points for the gills and digestive glands noted at 14 days and 7 days, respectively (Gonçalves et al., 2022; Chapter 3). Exposure to 0.350 ppm of cadmium for 96 hours significantly influenced both the gills and digestive gland of *M. galloprovincialis*, as evidenced by increased LPO levels; however, LPO levels in the gills (10 nmol/mg protein) were twice those of the digestive gland (4.5 nmol/mg protein) (Santovito et al., 2021). These findings are consistent with those observed for Mix-exposure, where the gills exhibited the highest LPO levels (43.5 nmol/mg protein after 14 days). Additionally, Di Poi et al. (2018) noted that mixtures of contaminants (carbamazepine, methylparaben, aminomethylphosphonic acid; 0.96, 18.59, and 500 ng/L, respectively) are more toxic than individual compounds due to synergistic effects, although the individual compound toxicity remains unchanged. The overproduction of ROS overwhelmed the antioxidant enzyme system, leading to peroxidative damage to membrane lipids (Fernández et al., 2012). Consequently, it can be concluded that the Mix exerted a greater impact on LPO levels than 5-FU, indicating that mussels could endure the adverse effects of the individual compound but not those posed by the mixture. Di Poi et al. (2018) similarly concluded that binary and ternary mixtures (*C. gigas*, carbamazepine,

methylparaben, aminomethylphosphonic acid; 0.96, 18.59, 500 ng/L, and methylparaben, aminomethylphosphonic acid, respectively) exhibited greater toxicity than the individual compounds.

PCA results (Fig. 4.3.) further confirm the severity of mixtures of CECs and that mussel responses are mostly time-dependent, being 7 days of exposure, the most critical time point for both tissues. Therefore, the mixture of contaminants toxicity towards mussels is not tissue-specific, and compared to 5-FU-exposed mussels, mixtures are more toxic than their single compounds. Moreover, using the model defined by Ritz et al. (2021) to assess the antagonistic and synergistic effects of binary mixtures was adapted for tertiary mixtures, and the effects of pharmaceutical-nanoplastic-metal nanoparticle interactions can be found in the (see *Supplementary data*). A synergistic effect was confirmed in both tissues. Synergism was found in all biomarkers on the 14th day in mussel gills. In the digestive gland of mussels, apart from SOD and CAT, the effects of all other biomarkers were synergistic at days 14 and 21. This model is, therefore, a valuable tool to confirming antagonistic/synergistic effects, as suggested, and crucially, it demonstrates that prolonged exposure results in the observed synergistic effects, indicating that the duration of exposure is critical when considering the interactions of pharmaceuticals, nanoplastics, and metal nanoparticles.

4.5.Conclusions

The present data provides evidence that the adverse effects of 5-FU alone and in a mixture of contaminants in both mussel tissues are time and tissue-specific, differentiating in severity. *M. galloprovincialis* could counteract the toxicity of 5-FU, whilst the opposite was observed in Mix-exposed mussels, consequently leading to oxidative damage. An adaptive response observed in both tissues seems to be limited to GST activity, demonstrating the ability of this biotransformation enzyme to activate as a compensating mechanism to manage oxidative stress. Both 5-FU and Mix caused genotoxicity in mussel haemolymph, where the interactions between these emerging contaminants are antagonistic. Moreover, it is possible to conclude that single contaminant exposures are not as toxic as a mixture of different contaminants, and, on an important note, these interactions need to be further studied. Data suggests a synergistic effect in the interaction of a mixture of pharmaceutical-nanoplastic-metal nanoparticles concerning oxidative stress and oxidative damage.

CHAPTER V

Ecotoxicity of emerging contaminants in the reproductive organ of marine mussels *Mytilus galloprovincialis*

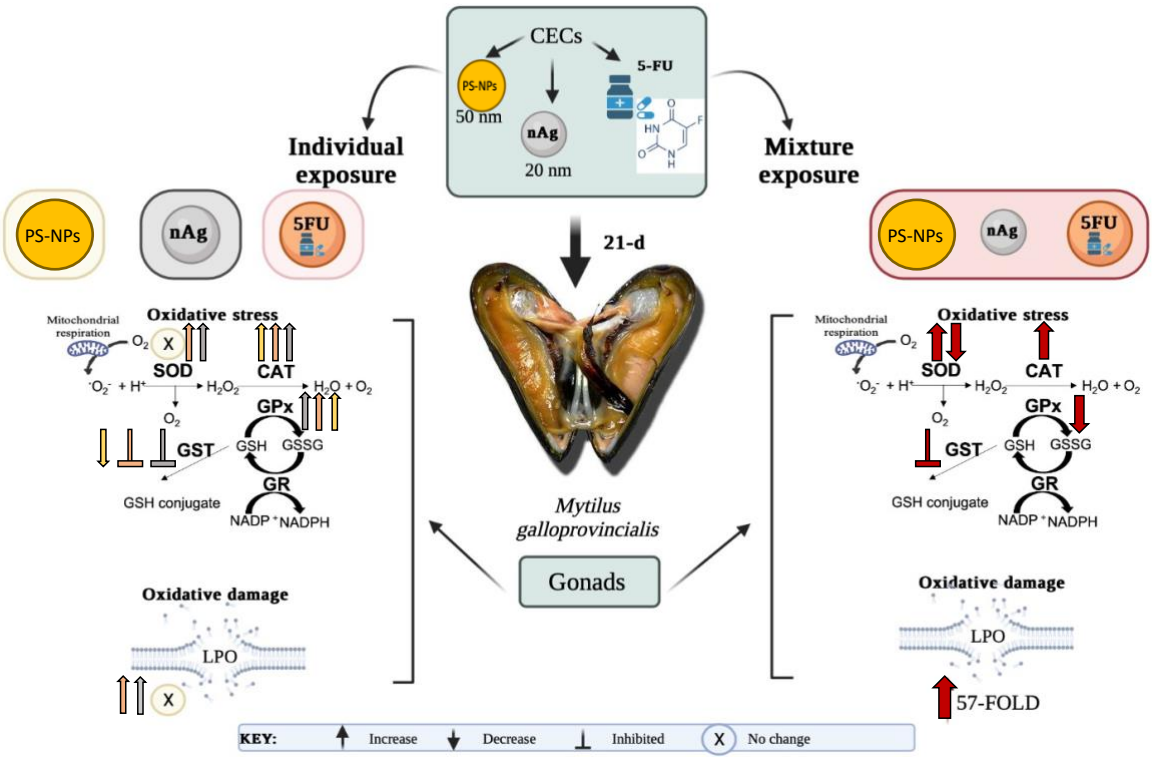

This chapter has been published in:

- Gonçalves, J. M., & Bebianno, M. J. (2023). Ecotoxicity of emerging contaminants in the reproductive organ of marine mussels *Mytilus galloprovincialis*. Science of the Total Environment, 881(April), 163486. https://doi.org/10.1016/j.scitotenv.2023.163486

This chapter has been presented at the international conference:

- **PRIMO'21 – Gothenburg, Sweden** (22nd – 25th May 2022): **ORAL Presentation - Ecotoxicity of emerging contaminants individually and as a mixture in the reproductive organ of marine mussels *Mytilus galloprovincialis.*** J.M. Gonçalves & M.J. Bebianno, CIMA, Centre of Marine and Environmental Research, University of Algarve, Campus de Gambelas, 8000-139 Faro, Portugal.

Abstract

Contaminants of emerging concern (CECs) pose a new threat to the marine environment, making it essential to comprehend CEC mixtures' interactions and potential toxicity once they enter the ocean. CECs—such as metal nanoparticles, nanoplastics, and pharmaceuticals—are contaminants that have been evaluated individually, yet their interactions as mixtures remain largely unexplored. Successful reproduction is crucial to secure a healthy and prosperous future generation; however, if compromised, population dynamics may be jeopardised, adversely affecting biodiversity. This study aimed to investigate the effects of silver (20 nm nAg, 10 µg/L), polystyrene nanoparticles (50 nm PS-NPs, 10 µg/L), and 5-fluorouracil (5-FU, 10 ng/L) both individually and in combination (10 µg/L of PS-NPs + 10 µg/L of nAg + 10 ng/L of 5-FU) in the gonads of *Mytilus galloprovincialis*. A multi-biomarker approach was employed, analysing the antioxidant defence system (ADS; superoxide dismutase, catalase, glutathione peroxidase, glutathione – *S* – transferase activities) and oxidative damage (OD; lipid peroxidation) in the mussel gonads. All exposure treatments after 3 days elevated enzymatic activity, followed by inhibition after 14 and 21 days. Consequently, the ADS became overwhelmed due to the generation of reactive oxygen species (ROS), leading to OD, except in mussels exposed to PS-NPs. The OD in mussels exposed to the mixture increased exponentially by 57-fold. When CEC mixtures interact, they can potentially be more harmful than their individual components, presenting a significant threat to marine species. A model was utilised to comprehend synergistic and antagonistic interactions, with antagonistic interactions evident in the evaluated biomarkers at all times, except for a synergistic interaction at day 3 concerning lipid peroxidation. Results indicate that the observed effects in the gonads of mussels exposed to the mixture primarily arise from the interaction between nAg and 5-FU rather than PS-NPs.

5.1. Introduction

Contaminants of emerging concern (CECs) have the scientific community rendered with the possible ecotoxicological effects they may have towards aquatic organisms and, consequently, human health. According to the criteria— persistence in the environment, and noxiousness and ecotoxicological effects— CECs are a variety of chemical substances (anthropogenic and/or naturally occurring) that are not frequently monitored in the environment (Pastorino & Ginebreda, 2021). These include pharmaceuticals and personal care products, endocrine-disrupting chemicals, nanomaterials and nanoparticles, and persistent organic pollutants (Kumar et al., 2022). The source of most CECs landing in our seas is primarily due to the lack of treatment and removal of these contaminants by wastewater treatment plants (WWTP). Inevitably, these CECs will end up all together in the ocean. Although it is crucially important to understand the toxicity these CECs pose to marine life, it is also of utmost importance to comprehend how their toxicity differs when the CECs are present all together. Mixtures of CECs are lately getting much attention; however, most data focus on mixtures of contaminants belonging to the same group (Affek et al., 2018; Brezovšek et al., 2014; Elersek et al., 2016; Mater et al., 2014; Novak et al., 2017)**,** whilst some focus on microplastics and pharmaceuticals interactions (Martín et al., 2022; Pashaei et al., 2022; Qu et al., 2018; Sellami et al., 2021), and others on micro/nanoplastic interaction with metals and metal nanoparticles (Davranche et al., 2019; Estrela et al., 2021; Yu et al., 2019). Consequently, the question arises of how toxic mixtures of differently classified CECs, such as engineered nanoparticles, nanoplastic pollution, and pharmaceuticals, impact the marine environment and whether these contaminants' interactions are more severe.

With the advancement of nanotechnology and engineered nanomaterials being most frequently utilised in nano-functionalized consumer goods, silver nanoparticles (nAg) are primarily used in personal care, antimicrobial coatings, photonic devices, and textile industries (Lee & Jun, 2019; Maillard & Hartemann, 2013; Pereira et al., 2020). Production of nAg products has rocketed throughout the years due to its properties — antimicrobial, antibacterial, antifungal, antiviral, anti-inflammatory, and anticancer (Khan et al., 2018) — the global nAg market size, with a revenue of over 2 billion USD in 2021, is projected to surpass 5 billion USD by 2029 (Market Research, 2022). The toxic effects of nAg towards marine organisms have been thoroughly evaluated (Auguste et al., 2018; Gomes et al., 2013; Lorusso et al., 2022; McCarthy et al., 2013; Rezvani et al., 2019) **,** and its mode of

action (MoA) is known to harm cell membranes directly; nAg can liberate Ag^{+} ions, and both nAg and Ag^{+} generate reactive oxygen species (ROS) (Ghobashy et al., 2021). nAg levels in the environment are anticipated to be between 0.03 and 0.08 mg L^{-1} (Fernandes et al., 2017), as WTTP are not effective in the removal or treatment of nAg. For instance, nAg will primarily partition to the sludge in WWTP (Bolaños-Benítez et al., 2020). Sludge may be sent to landfill/used as agricultural fertiliser, and through leaching and surface run-off, nAg may enter the marine environment (Blaser et al., 2008).

Moreover, WWTP needs to improve in the removal of plastic debris. As global plastic pollution is increasing ─ reports from 2021 show an increase in global plastic production to 390.7 million tons , 2022) ─ the possible adverse effects towards marine organisms are highly concerning. Europe, since 2020, has decreased plastic production by 4%, whilst China increased their production to almost a third of the world's plastics (PlasticEurope, 2022)**.** Polystyrene (PS), in Europe, accounts for 6.1% of plastic production, and its applications, such as packaging and building insulation, account for the world's two largest plastic markets, 44% and 18%, respectively (PlasticEurope, 2022). Nowadays, within plastic pollution, there is an increasing focus on nanoplastics, whether primary or secondary, as these nano-sized plastic particles could cross cellular boundaries, increasing their potential toxicity towards marine organisms — as the size of the particle decreases, the biological reactivity increases — (Peng et al., 2020). For instance, the antioxidant defence system of *M. galloprovincialis* was inhibited by exposure to PS nanoplastic (PS-NPs) at a dose of 10 µg/L (50 nm PS-NPs; 21 d), resulting in oxidative damage, with the mussel gills being the most severely affected tissue (Gonçalves, et al., 2022b; Chapter 3). Lysosomal indicators of general stress were more affected by PS-NPs exposure to *M. galloprovincialis* (50 nm; 1.5-150 ng/L; 21-d) than by PS-microplastics (PS-MPs), suggesting a connection between this trend and improved antioxidant production (Capolupo et al., 2021).

Moreover, when *M. galloprovincialis* were exposed to different types and shapes of plastic polymers in the micron size range (241.3 ± 32.7 to 3073.8 ± 21.7 1860.1 µm; 12.5 particles/L & 25 particles/L; polyamide, polyethylene, and polymethyl methacrylate; 7 days), the antioxidant defence in gills and the digestive gland was more overwhelmed by smaller particles, that were retained by the digestive tract compared to bigger ones (Provenza et al., 2022a). The glitter particles broke down into smaller and shorter particles, which resulted in higher levels of oxidative stress (Provenza et al., 2022a), increasing the

necessity to better understand the toxicity of NPs, as they differ from MPs. Given the absence of appropriate analytical techniques for determining the presence and concentration of NPs in marine matrixes, the detection of NPs in natural environments continues to remain tricky (Cai et al., 2021; L. Wang et al., 2021); however, Halle et al. (2017) collection from the North Atlantic Gyre, a nanoplastic segment containing four types of plastic polymers, including PS, all within the nano-size range, confirmed the presence of nanoplastics in the ocean.

Additionally, pharmaceuticals make up a significant subset of CECs, although anti-cancer drugs have yet to draw much attention. Concerningly, an increasing number of patients are getting cytostatic drug-based chemotherapy in hospitals or at home. Because these pharmaceutical compounds seldom entirely metabolise, they are eventually released into the water unchanged or modified (Trombini et al., 2016). One of the most popular pharmaceutical compounds for the treatment of solid tumours as well as colorectal, pancreatic, and breast cancer is 5-fluorouracil (5-FU), a cytostatic agent (IARC Class 3) (Mahnik et al., 2007). 5-FU is a pyrimidine analogue of uracil with a fluorine atom (Cairns et al., 2011), and the primary MoA of 5-FU in mammals is the incorrect incorporation of its fluoro-nucleotides into DNA (Matuo et al., 2009), as well as the release of cytochrome *c* from the mitochondria, promoting ROS and the production of superoxide radicals and oxidative stress (Gonçalves et al., 2022a; Chapter 4). According to estimates, 5-FU concentrations in European waterways range from 0.3 ng/L to 2.5 ng/L and below 160 ng/L in surface waters (Heath & Isidori, 2020). More recent information in the gills and digestive gland of the marine mussel *M. galloprovincialis* (10 ng/L; 21 d) showed that the antioxidant defence system (ADS) could counteract ROS production and prevent oxidative damage (Gonçalves et al., 2022a; Chapter 4). Conversely, due to the MoA of 5-FU, genotoxicity was observed in the haemolymph of *M. galloprovincialis* (Gonçalves, et al., 2022a; Chapter 4).

Bivalves are a class of species widely used in ecotoxicological assessment, and the Mediterranean mussel *M. galloprovincialis* is an excellent sentinel organism to help understand how these CECs can affect marine organisms. As sessile filter-feeders, *M. galloprovincialis* organisms are practical tools for evaluating the environmental quality because of their characteristics like susceptibility to contaminants, widespread geographic distribution, sedentary lifestyle, and ease of sampling (Provenza et al., 2022b). A more crucial aspect, which is seldom evaluated, is the impact these CECs may have on the mussel's reproductive organs, the gonads, as reproductive impairment or unsuccessful

larval-embryo development could consequently influence marine population dynamics. Therefore, this study aims to examine the effects of nAg (20 nm; 10 µg/L), PS-NPs (50 nm; 10 µg/L), 5-FU (10 ng/L), and a mixture of the three CECs (Mix: 10 µg/L of nAg + 10 µg/L of PS-NPs + 10 ng/L of 5-FU) on the gonads of *M. galloprovincialis* following a 21-day exposure assay, to evaluate whether the CECs are more toxic individually or as a mixture. A multi-biomarker approach was employed to assess oxidative stress and damage, quality indices, and to model the interactions occurring within the mixture.

5.2. Materials and Methods

5.2.1. Silver nanoparticles (nAg)

Silver dispersion – nanoparticles measuring 20 nm in size (TEM) in a 0.02 mg/mL aqueous buffer containing sodium citrate as a stabiliser were obtained from Sigma-Aldrich (730793) (JMGS, Portugal). A DLS particle sizer (ZetaSizer Nano ZS90, Malvern Inc.) was employed to measure the hydrodynamic diameter of nAg in both ultrapure water and filtered seawater (FSW), as well as to determine the electrophoretic mobility of nAg in a disposable polycarbonate capillary cell at 25 °C (DTS1061, Malvern Inc.) for the calculation of its zeta potential. The aggregation kinetics were evaluated using time-resolved DLS measurements. The size of the Ag nanoparticles was monitored over a duration of 2 to 12 hours. The hydrodynamic diameter (HD) of nAg remained stable in ultrapure water (34 ± 0.69 nm), with the ζ-potential under these conditions measuring (54.8 ± 1.62 mV), indicating no aggregation in ultrapure water. In contrast, the increase in HD in FSW (521.9 ± 87.42 nm) signifies aggregation of nAg in FSW. A concentration of 10 µg/L was employed for exposure assays.

5.2.2. Polystyrene nanoplastics (PS-NPs)

Fluoresbrite® Plain YG spherical polystyrene nanoplastics of 50 nm in size (CAS 9003-53-6) were purchased from Polysciences, Inc. (Germany). 50 nm particles packed as 2.5% aqueous suspension, with 3.64 × 1014 particles/mL in ultrapure water (7732-18- 5) (CV = 15%, Excitation max. = 441 nm, Emission max. = 486 nm). A concentration of 10 µg/L was used for exposure assays. Characterisation of PS-NPs is detailed Gonçalves et al. (2022b) (Chapter 3). It indicates that the hydrodynamic diameter of the PS-NPs increases when dispersed in FSW (852 ± 103 nm), suggesting that the high concentration of salts in seawater contributes to aggregation and agglomeration kinetics.

5.2.3. 5-Fluorouracil (5-FU)

5-FU (CAS 51-21-8) was procured from Sigma Aldrich, Inc. The experimental study was conducted using a class II biological safety cabinet and appropriate attire to ensure safe handling of medications (open-back, impervious chemotherapy protection gown, double powder-free latex gloves, and safety goggles). Sequential dilutions in ultrapure Milli-Q water were prepared to achieve a final concentration of 100 µg/L. Subsequently, a working solution of 10 ng/L of 5-FU was prepared in seawater.

5.2.4. Experimental Design

Mussels *M. galloprovincialis* Lamarck (50 mm ± 5 mm) were collected from the Ria Formosa Lagoon in southeast Portugal (37°00'30.6"N 7°59'39.6"W) during the reproductive phase (August 2020) and transported alive to the laboratory. Following a four-day acclimatisation period, 20 mussels were placed into each 15 L tank containing 10 L of seawater in a duplicated design. Mussels were exposed to 10 µg/L of nAg (20 nm), 10 µg/L of PS-NPs (50 nm), 10 ng/L of 5-FU, and the corresponding mixture (10 µg/L of both nAg and PS-NPs, alongside 10 ng/L of 5-FU) for 21 days. Seawater was exchanged every two days, and contaminants were re-dosed. Mortality was recorded in mussels exposed to nAg on day 6 (one dead mussel), to PS-NPs on day 1 (one dead mussel) and day 3 (one dead mussel), to 5-FU on day 3 (six dead mussels) and day 10 (two dead mussels), and to the mixture on day 0 (one dead mussel) and day 1 (one dead mussel) of exposure. Mussels were collected on days 0, 3, 7, 14, and 21 of exposure for a multi-biomarker analysis. The mussels were weighed, and their gonads were dissected and immediately frozen in liquid nitrogen. They were stored at -80°C for subsequent investigation into the effects of nAg, PS-NPs, 5-FU, and the mixture.

The availability of food resources permits mussels *M. galloprovincialis* to recuperate their gonads quickly. Therefore, spawning occurs throughout the year, with higher rates during summer (Ramos, 2017). In August specifically, the gonads were either ripe, spawning or in a late-spawning stage (Ramos, 2017).

5.2.5. Quality control and assessment

Each tank was equipped with a glass cover to minimise aerial pollution, and aeration was conducted using glass pipettes to avoid plastic contamination. During tissue dissection, no gloves, plastic tools, or materials were utilised to prevent any further plastic contamination.

5.2.6. Antioxidant enzymes

Gonads of mussels were individually homogenised in 5 mL of 20 mM Tris-Sucrose buffer (0.5 M Sucrose, 0.075 M KCl, 1 mM DTT, 1 mM EDTA, pH 7.6) utilising a VWR Star-Beater (5 min, 20/s shaking, with grinding balls), following Geret et al. (2002). after two centrifugations (1: 500 g, 15 minutes, 4°C; 2: 12,000 g, 45 minutes, 4°C), the cytosolic fraction was obtained. Aliquots were then employed to analyse the activities of the antioxidant enzymes: superoxide dismutase (SOD), catalase (CAT), glutathione peroxidases (GPx), and the activity of the biotransformation enzyme: glutathione-S-transferases (GST).

All enzymatic activities were standardised by determining total protein concentrations using the specified method Bradford (1976). Total protein concentrations (mg protein g^{-1} tissue) were calculated using bovine serum albumin (BSA) as a standard and optimised for a microplate reader.

SOD activity was measured by calculating the reduction in absorption of the substrate cytochrome c by the xanthine oxidase/hypoxanthine system at 550 nm, and the responses were represented as U mg^{-1} protein (McCord & Fridovich, 1969).

CAT activity was quantified using a spectrophotometric method for detecting hydrogen peroxide (H_2O_2) consumption at 240 nm. The results are given in mmol min^{-1}mg $protein^{-1}$.

Based on McFarland et al. (1999) the technique, GPx activity was assessed using a microplate reader (Infinite® 200, Pro-Tecan) at 340 nm, with cumene hydroperoxide as the substrate at 28°C. The results are presented in mmol min^{-1} mg $protein^{-1}$.

GST activity, based on Habig et al. (1974) the approach, was determined by conjugating 0.2 mM reduced glutathione (GSH) with 0.2 mM 1-chloro-2,4-dinitrobenzene (CDNB) in a reaction mixture of 0.2 M KH_2PO_4/K_2HPO_4 buffer (pH 7.9) and measured at 340 nm in a microplate reader (Infinite® 200, Pro-Tecan). Data is presented in mol CDNB min^{-1} mg^{-1} protein units.

5.2.7. Lipid peroxidation

Individual mussel gonads were homogenised with the aid of a VWR Star-Beater (5 min, 20/s shaking, with grinding balls) in 5 mL of a 1:10 ratio of butylated hydroxytoluene and 0.02 M Tris-HCl buffer (pH 8.6). (BHT). To measure total protein concentrations and LPO levels, homogenates (3 mL) were centrifuged at 30 000 *g* for 45 minutes at 4°C. Using a method adapted from Erdelmeier et al. (1998) the absorbance of malondialdehyde (MDA)

and (2 E)-4-hydroxy-2-nonenal (HNE) at 540 nm was used to determine the levels of LPO in units of nm/mg protein.

5.2.8. Integrated Biomarker Response (IBR)

An efficient index for visualising the biological consequences of contaminants and the relation between a battery of biomarkers and contamination levels is the integrated biomarker response index (IBR) (Devin et al., 2014). Thus, using a biomarker response index version 2 (IBR) proposed by Sanchez et al. (2013), which was modified from the IBR index defined by (Beliaeff & Burgeot, 2002) and described in Serafim et al. (2012) the biomarker data from gonads of *M. galloprovincialis* exposed to silver nanoparticles (nAg), polystyrene nanoplastics (PS-NPs), 5-fluorouracil (5-FU) and the mixture of the three contaminants (Mix) were assessed.

IBR enables the merging of various biomarker responses into a single numerical result. The IBR index was created to remove the IBR result dependent on the arrangement of the biomarkers and the induction and inhibition of each biomarker. It is based on a disturbed and undisturbed condition (Sanchez et al., 2013). IBR is the sum of the differences between control groups and groups exposed to nAg, PS-NPs, 5-FU, or Mix on each sampling day.

In contemplation of reducing variance, the combined data of each biomarker (X_i) were compared to the combined data (X_0) of each biomarker from the control group and log transformed (Y_i). Y_i's mean (μ) and standard deviation (σ) were computed, and the input for each parameter was further standardised using the equation:

$$Z_i = \frac{(Y_i - \mu)}{\sigma}$$

The mean of the standardised biomarker response (Z_i) and the mean of the unexposed biomarker (Z_0) were used to generate a baseline centred on controls and show parameter variation relative to this baseline:

$$A = Z_i - Z_0$$

Finally, the absolute value of A for each parameter in each experimental condition was calculated and added to obtain the IBR index:

$$IBRv2 = \sum |A_i|$$

5.2.9. Model for Synergistic or Antagonistic Effect

This method has been modified for tertiary combinations and is based on the single-dose factorial design described by Ritz et al. (2021) for binary mixtures. This approach

creates five treatments: control, nAg, PS-NPs, 5-FU, and a mixture of the three (Mix) by combining three factors (three contaminants) with two levels. The assertion of an opposing or complementary impact is only valid for the concentrations used in this evaluation [10 µg/L of nAg; 10 µg/L of PS-NPs; 10 ng/L of 5-FU, and Mix (10 µg/L of nAg +10 µg/L of PS-NPs +10 ng/L of 5-FU)]. Values were computed for all sampling times (0, 3, 7, 14, and 21 days), and all biomarkers (SOD, CAT, GPx, GST activities, and LPO levels) were examined using the following dose addition and independent action models:

5.2.9.1.Dose addition

$$E_{add} = (E_{5FU} - E_{control}) + (E_{nPS} - E_{control}) + (E_{nAg} - E_{control})$$

The difference (D_{da}) between the actual response (control) and the previously expected impact can characterise any antagonistic or synergistic effect. The following equation defines the difference:

$$D_{da} = E_{Mix} - E_{5FU} - E_{nPS} - E_{nAg} + E_{control}$$

5.2.9.2.Independent action

$$E_{ind} = \frac{E_{5FU} \times E_{nPS} \times E_{nAg}}{(E_{control})^2}$$

Under the presumption of independent action, every antagonistic or synergistic effect can be described as the difference (D_{ia}) between the observed and reference effects. The following equation defines the difference:

$$D_{ia} = E_{Mix} - E_{ind}$$

5.2.10. Statistical Analysis

According to data distribution and variance homogeneity (Shapiro-Wilk test), parametric tests (ANOVA, followed by Tukey's post-hoc test) or non-parametric equivalent tests (Kruskal-Wallis and a two-tailed multiple comparisons test) were used to assess the significant differences between treatments and time. If $p < 0.05$, the findings were significant. GraphPad Prism version 9.1.1 (GraphPad Software, Inc. CA) was used for the statistical analysis.

A Principal Component Analysis (PCA) was also used to assess the relationship between treatments (unexposed and exposed to nAg, PS-NPs, 5-FU, and Mix) and the

measured parameters [activities of antioxidant and biotransformation enzymes (SOD, CAT, GPx, GST) and oxidative damage (LPO)] in mussel gonads over the exposure period (21 days). The Statistica 7.0 programme achieved this (Statsoft Inc., 2005; USA).

For IBR, statistical differences were evaluated using a t-test on Microsoft Excel (*Microsoft Corporation*, 2018), and results were considered significant when $p < 0.05$.

5.3. Results

5.3.1. Antioxidant Enzyme Activities

The activities of antioxidant and biotransformation enzymes of unexposed mussel gonads did not alter throughout the exposure (21 days; $p > 0.05$; Fig. 5.1.A - D).

SOD activity in the gonads of mussels exposed to nAg and 5-FU shows an increasing trend, with activity observed at day 21 being significantly higher when compared to other treatments, as well as significantly different from nAg and 5-FU exposed gonads at other time points ($p < 0.05$; Fig. 5.1.A). In Mix-exposed mussel gonads, however, the activity of SOD exhibits a dumbbell-shaped pattern, indicating a significant increase on day 7 compared to the beginning and end of exposure, as well as compared to controls and gonads exposed to nAg and PS-NPs ($p < 0.05$). Conversely, no significant differences were found in the gonads of mussels exposed to PS-NPs throughout the exposure period, nor with controls ($p > 0.05$).

In all exposure treatments, the activity of CAT in mussel gonads increased significantly after 3 days of exposure compared to unexposed specimens and maintained high activity throughout the 14-day period ($p < 0.05$; Fig. 5.1.B). Mussels exposed to nAg and 5-FU exhibited the highest CAT activity at the end of the exposure period (21 days), whereas those exposed to PS-NPs and Mix showed a decrease in activity ($p < 0.05$).

A substantial increase in GPx activity is evident in mussel gonads exposed to Mix after 3 days of exposure, and an increase in GPx activity is also noteworthy in gonads exposed to nAg and 5-FU compared to unexposed ones at the same time point ($p < 0.05$; Fig. 5.1.C). However, gonads exposed to 5-FU and Mix exhibit a decrease in GPx activity on days 14 and 21. Conversely, those exposed to PS-NPs demonstrate a dumbbell-shaped pattern in GPx activity, showing a significant difference compared to controls from the seventh day of exposure until the end of the trial, and are significantly different from all treatment conditions on these days ($p < 0.05$). More significant differences are identified between treatments at each time point, with gonads exposed to Mix showing significantly higher levels than all treatment conditions on days 3 and 7 ($p < 0.05$), and notable differences are

also observed between PS-NPs-exposed and nAg and 5-FU-exposed mussel gonads ($p < 0.05$).

GST activity in all treatments decreased after 3 days of exposure, with the reduction in nAg, 5-FU, and Mix-exposed mussel gonads being significantly different from the controls and those exposed to PS-NPs ($p < 0.05$; Fig. 5.1.D). Low GST activity persists throughout the exposure period, as nAg, 5-FU, and Mix-exposed mussel gonads show significant differences from unexposed mussels at all time points. Additionally, the GST activity in PS-NPs-exposed mussels is significantly lower than in unexposed mussels on days 7 and 21 of exposure ($p < 0.05$).

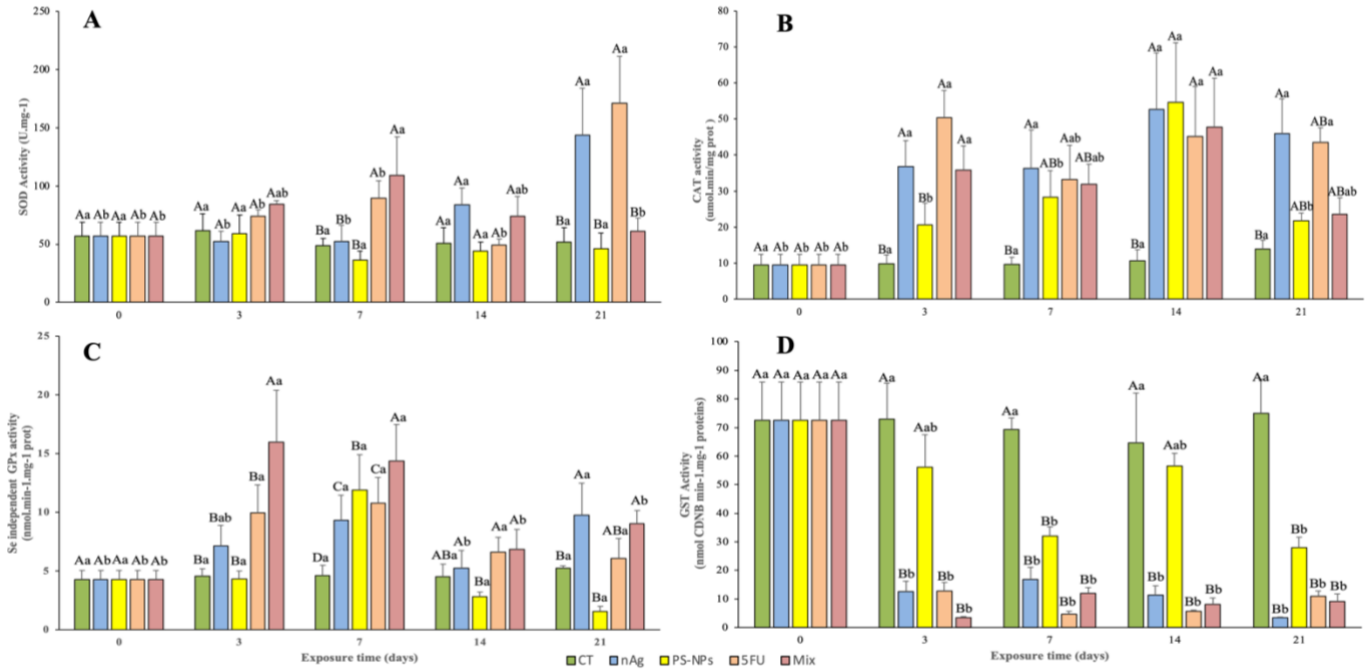

Figure 5.1. The activity of superoxide dismutase (SOD) (**A**), catalase (CAT) (**B**), glutathione peroxidase (GPx) (**C**), glutathione-*S*-transferase (GST) (**D**) (mean ± std) in gonads of *M. galloprovincialis* after a 21-day exposure to silver nanoparticles (10 µg/L), polystyrene nanoparticles (10 µg/L), 5-Fluorouracil (10 ng/L), and Mixture of the three contaminants (nAg + PS-NPs + 5-FU). Different upper- and lower-case letters indicate significant differences between treatments for the same time and between times for the same treatments, respectively (p<0.05).

5.3.2. Oxidative damage

Levels of LPO in unexposed mussel gonads did not change throughout the exposure period (21 days; $p > 0.05$). Aside from PS-NPs, all treatments exhibited levels of oxidative damage, with Mix-exposed mussels showing an exponentially higher level of LPO on day

3 compared to the other treatments, reflecting a 57-fold increase relative to unexposed mussels ($p < 0.05$; Fig. 5.2). On days 7, 14, and 21 of exposure, 5-FU-exposed mussel gonads exhibited the highest levels of oxidative damage, followed by nAg-exposed mussels on day 14 when compared to controls and PS-NPs-exposed mussels ($p < 0.05$).

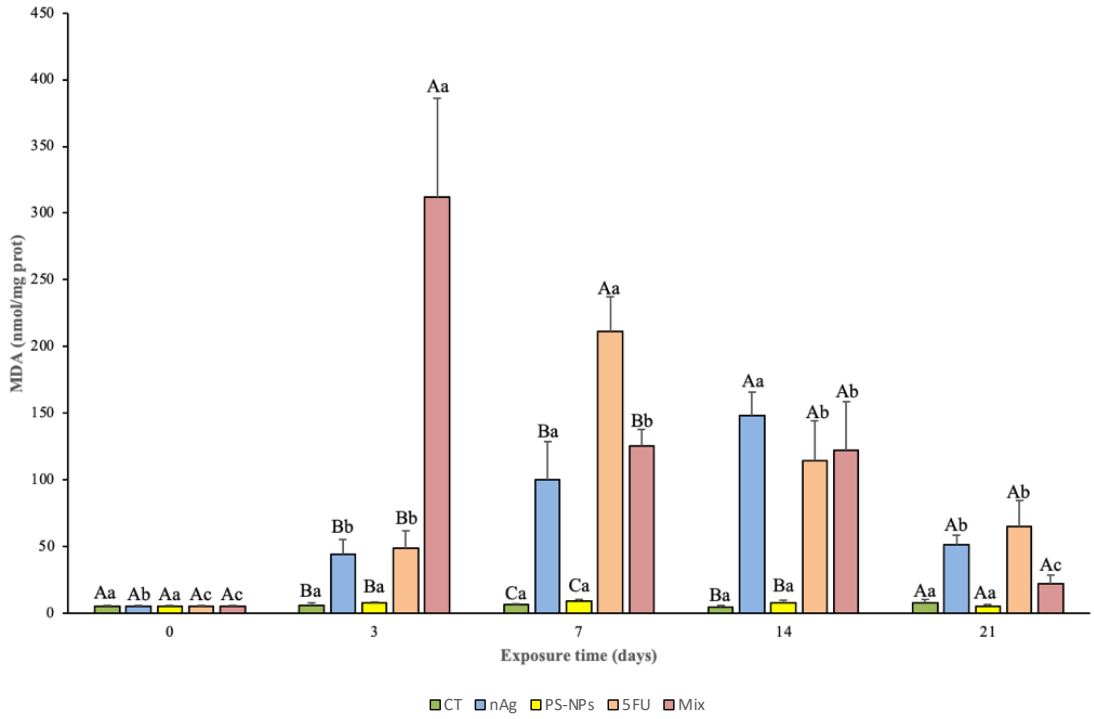

Figure 5.2. Lipid peroxidation (LPO) levels (mean ± std) in gonads of *M. galloprovincialis* after a 21-day exposure to silver nanoparticles (10 µg/L), polystyrene nanoparticles (10 µg/L), 5-Fluorouracil (10 ng/L), and Mixture of the three contaminants (nAg + PS-NPs + 5-FU). Different upper- and lower-case letters indicate significant differences between treatments for the same time and between times for the same treatments, respectively ($p<0.05$).

5.3.3. Principal component analysis (PCA)

The impact of nAg, PS-NPs, 5-FU, and Mix on the response of biomarkers (SOD, CAT, GPx, GST activities, and LPO) was described using PCA, which was applied to all the data collected from the gonads of mussels (Fig. 5.3). In mussel gonads, the two principal components account for 78.8% of the overall variation (PC1 = 58.8%, PC2 = 20.0%; Fig. 5.3). The PCA reveals a distinct difference between exposed and unexposed gonads, with unexposed mussel gonads positioned closely together and negatively correlated with both principal components. All periods of nAg exposure show a positive relationship with the 1st component (PC1) and a negative relationship with the 2nd (PC2). In contrast, in PS-NPs-exposed mussel gonads, all exposure times except day 7 exhibit a negative correlation with PC1, while days 7 and 14 are positively related to PC2, and days 3 and 21 are negatively related. Similar to nAg-exposed mussels, all sampling days for 5-FU and Mix-exposed mussel gonads are positively

correlated with PC1. The main difference between 5-FU and Mix is evident in PC2, where, in relation to exposure times, an opposing pattern is observed; days 3 and 21 in 5-FU are positively related, while days 7 and 14 for Mix-exposed mussel gonads are positively related, and days 7 and 14 for 5-FU-exposed gonads are negatively correlated, along with days 3 and 21 for Mix-exposed gonads. The principal biomarker loadings affecting PC1 are LPO, followed by GPx, whereas for PC2, it is SOD. This PCA indicates that nAg and 5-FU are the two contaminants that primarily influence the toxicity effects observed in mussel gonads exposed to Mix, with day 3 of exposure being the most critical time point.

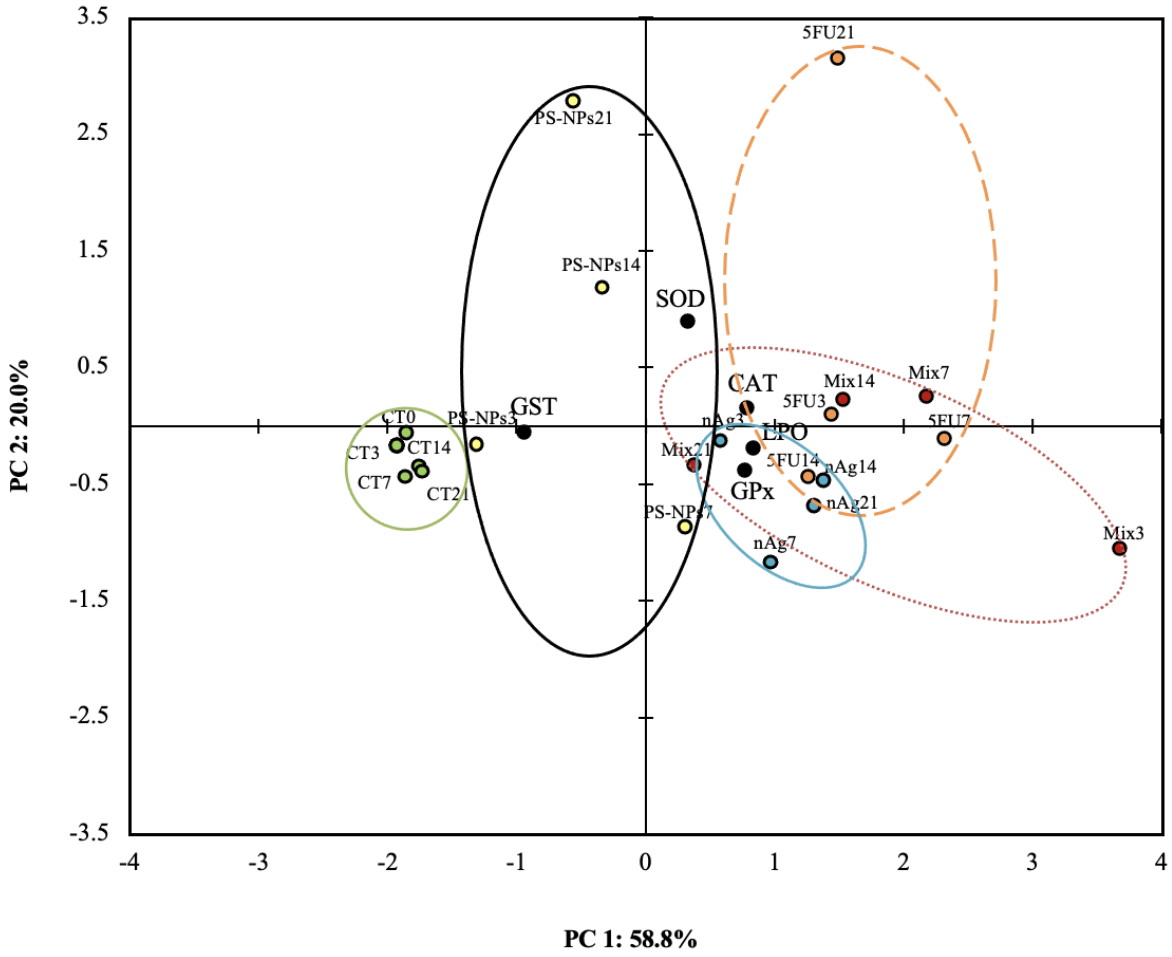

Figure 5.3. Principal Component Analysis (PCA) of biomarkers (SOD, CAT, GPx, GST activities and LPO) in the gonads of *M. galloprovincialis* from controls (CT) and those exposed to silver nanoparticles (nAg), polystyrene nanoplastics (PS-NPs), 5-fluorouracil (5-FU) and the mixture (Mix) for 21 days (p<0.05).

5.3.4. Integrated biomarker response (IBR)

The Integrated Biomarker Response (IBR) was calculated for the data on mussel biomarkers in the gonads at all exposure times to nAg, PS-NPs, 5-FU, and Mix. Fig. 4A—B shows a graphic representation of the IBR and star plots for all treatments.

The IBR pattern was both treatment-dependent and time-dependent. For nAg-exposed mussel gonads, an increasing trend in IBR scores is observed throughout the period of exposure, with the score on the 21st day being significantly different from the other time points ($p < 0.05$; Fig. 4A). The mussel gonads exposed to PS-NPs show a substantial increase from day 7 onwards, with the scores on days 7 and 21 significantly differing from those on day 14 ($p < 0.05$; Fig. 4A). The IBR score for the 5-FU-exposed mussel gonads rises on day 7 and begins to decline in the subsequent days ($p < 0.05$; Fig. 4A). In contrast, the IBR score for Mix-exposed mussels increases significantly on the 3rd day of exposure, followed by a decrease in score until the end of the experiment ($p < 0.05$; Fig. 4A). On day 3 of exposure, the Mix-exposed gonads have a significantly higher IBR score compared to the individual contaminant exposures, while on day 7, it is the PS-NPs-exposed gonads, and on day 21, the nAg and PS-NPs-exposed mussel gonads ($p < 0.05$; Fig. 4A). Star plots indicated that changes in biomarkers were also treatment and time-dependent (Fig. 4B). In nAg-exposed mussel gonads (Fig. 4B), the 21st day is the most critical, with SOD activity being the main contributor to the overall IBR score. There are three key time points for PS-NPs-exposed gonads: at 7 days, GPx activity and LPO levels are the leading contributors; at 14 days, CAT activity is the main contributor; and at 21 days, GPx and GST activities are the leading contributors to the total IBR score. The star plot for 5-FU-exposed mussel gonads reveals that the 21st day of exposure is the most critical, with SOD activity as its primary contributor, followed by day 7, where GPx activity and LPO levels significantly contribute to the overall IBR score. In mussel gonads exposed to Mix, day 3 is the most crucial, with GST activity, LPO, and GPx activity primarily contributing to the total IBR score.

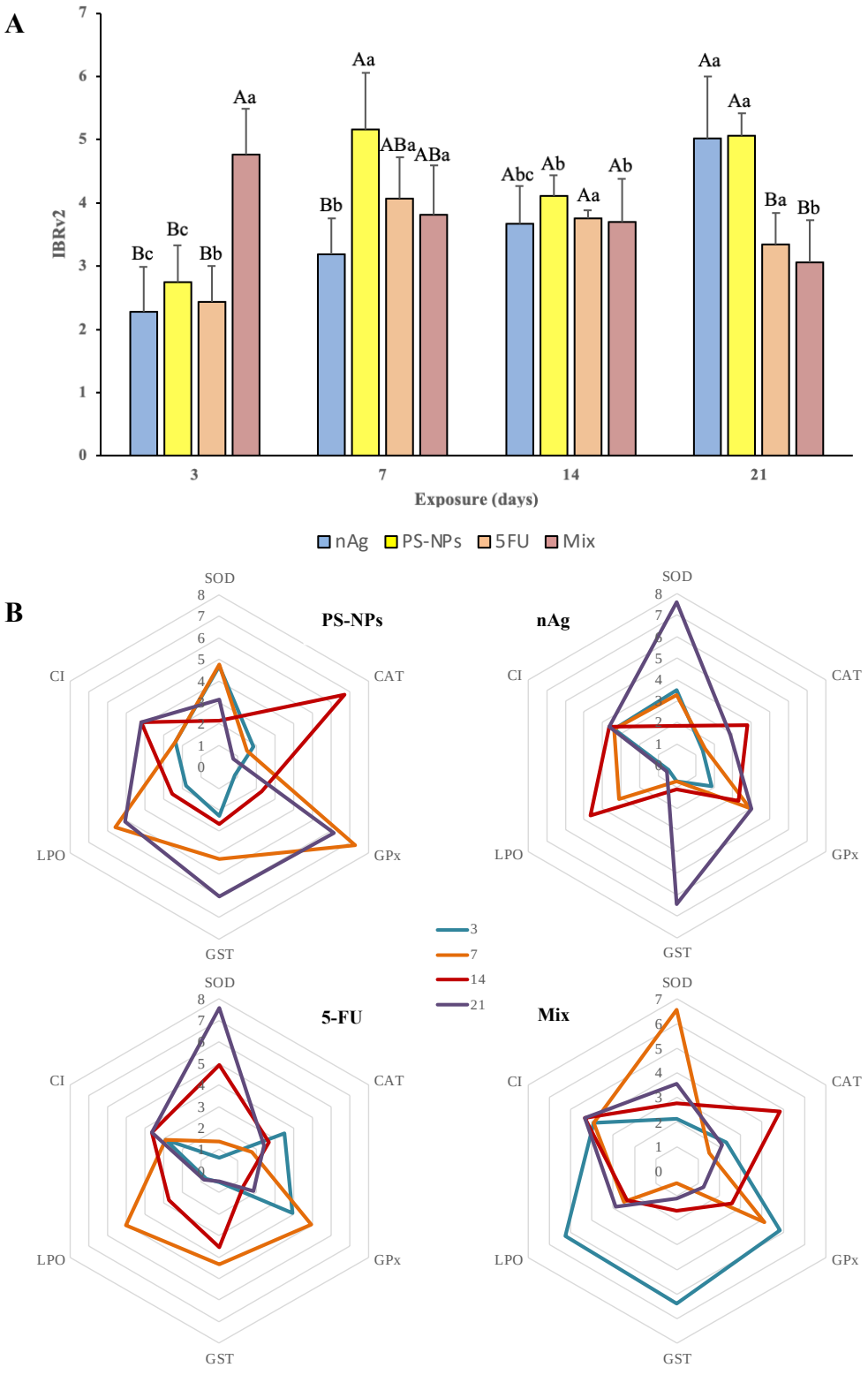

Figure 5.4. (**A**) Integrated biomarker response index version 2 (IBR) for all treatment exposures (nAg, PS-NPs, 5-FU and Mix) (mean ± SD), and (**B**) star plots of each treatment exposure in the gonads of *M. galloprovincialis*. Different upper- and lower-case letters indicate significant differences between treatments for the same time and between times for the same treatments, respectively (p<0.05)

5.3.5. Synergistic or Antagonistic effect

5.3.5.1. Difference of dose addition (D_{da})

The sum of differences relative to the control group for the contaminants when applied alone (assumption of dose addition; D_{da}) was conducted to understand better synergistic or antagonistic effects in mix-exposed mussel gonads (Table 5.1.). Following 3 days of exposure, the contaminants in the mixture exhibited synergistic interactions, particularly for LPO. An antagonistic effect is noted for LPO at the subsequent sampling time-point (day 7). On the 14th day of exposure, CAT activity is the primary enzyme displaying antagonistic interactions among contaminants in the mixture. In contrast, after 21 days of exposure, SOD activity becomes the main enzyme, and again the mix demonstrates antagonistic interactions.

Table 5.1. Antagonism or Synergism for tertiary mixtures: Difference of dose addition (D_{da}). *Dda* is under the assumption of dose addition (sum of differences relative to the control group) for the contaminants when applied alone (adapted from Ritz et al., 2021). If the difference in D_{da} is below or above 0, it indicates an antagonistic or synergistic effect.

Exposure time (days)	SOD	CAT	GPx	GST	LPO
0	0	0	0	0	0
3	-40	-62	-1	-5	217
7	-20	-56	-13	28	-188
14	31	-41	2	11	5
21	-104	-28	7	45	-40

5.3.5.2. Difference of independent action (D_{ia})

Furthermore, assuming there is independent action of the contaminants, a difference of independent action (D_{ia}) was also conducted for Mix-exposed mussel gonads to further understand any synergistic or antagonistic interactions between the contaminants (Table 5.2). Under this assumption, all days exhibit significantly higher negative values for D_{ia}, where both LPO and CAT activity demonstrate antagonistic interactions among the three contaminants in Mix-exposed mussel gonads from 3 to 14 days of exposure, with SOD activity showing the highest antagonistic effect on day 21.

Table 5.2. Antagonism or Synergism for tertiary mixtures: Difference of independent action (D_{ia}). D_{ia} is under the assumption of independent action of the contaminants (adapted from Ritz et al., 2021). If the difference in *Dia* is below or above 0, it indicates an antagonistic or synergistic effect.

Exposure time (days)	SOD	CAT	GPx	GST	LPO
0	0	0	0	0	0
3	-3	-392	-10	71	-448
7	13	-330	-40	3	-4278
14	39	-1116	10	11	-5801
21	-350	-179	3	8	-144

5.4. Discussion

Mixtures of CECs are attracting considerable attention; however, the interactions between metal nanoparticles, nanoplastics, and pharmaceuticals remain largely unexplored. Therefore, to our knowledge, this is the first dataset concerning the effects of nAg, PS-NPs, and 5-FU both individually and as a mixture (Mix) in the gonads of *M. galloprovincialis.*

The increase in the use of nAg in everyday life is mainly down to the properties these nanoparticles possess. In the last decade, the toxicity effects of nAg have been thoroughly evaluated in bivalves, with a focus on gills and digestive glands, haemocytes and even embryonic development (Auguste et al., 2018; Carrazco-Quevedo et al., 2019; Gomes et al., 2013; Ringwood et al., 2010). However, the effects of oxidative stress in the gonads of bivalves remain scarce. The primary mechanism of nAg toxicity when crossing cell membranes is the dissolution (McQuillan et al., 2012) and the release of antimicrobial silver ions that may interact with and influence the function of thiol-containing proteins found in the cell wall (Mikhailova, 2020). The reproductive organs of mussels prior to nAg exposure are susceptible to impaired gamete viability, reduced fertilisation success, and malformations of embryo-larval development, all possible outcomes of toxicity in mussel gonads. During the 21-day exposure to nAg, the ADS was activated, although the activities of GST (Fig. 5.1) and the GPx enzyme, which reduces lipid peroxides and protects against apoptosis, were inhibited.

Consequently, nAg exposure led to oxidative damage in mussel gonads (Fig. 5.2.). With mussel gonads compromised, gametogenesis and fertilisation success may be hindered. In the oyster, *Crassostrea virginica*, 1.6 µg/L of nAg (15 ± 6 nm) after a 48h exposure, a lysosomal destabilisation increase in oyster gonads, suggesting a high level of impaired gamete viability and reproductive failure, which was further supported by the decrease in embryonic development (Ringwood et al., 2010). Moreover, the spawning level success of female *M. galloprovincialis* fed with *Isochrysis galbana* exposed to 10 µg/L of PVP/PEI coated nAg (5.08 ± 2.03 nm; 21 d) was affected and triggered reproductive impairment that could impact populational fitness of mussels (Martínez, 2019)**.** According to the IBR score, the most problematic time of exposure, as well as the most compromising, is after 14 days for nAg-exposed gonads. Therefore, chronic exposure to nAg is concerning as the reproductive success of mussels is at stake. Additionally, this time-dependent response has been observed in other studies (Carrazco-Quevedo et al., 2019; Gomes et al., 2013). However, the primary mode of action of nAg remains unclear, and further assessments are needed to determine whether dissolved Ag^{+} ions released from nAg bind to organic matter present in the FSW.

Translocation of PS-NPs can occur through the bloodstream. However, due to the nano-size range, they may also cross cellular boundaries and be translocated to other mussel tissues (Sendra et al., 2020c), like the gonads. The ADS was not overwhelmed by PS-NP exposure and prevented oxidative damage from occurring. Compared to other tissues, in mussel's gills and digestive gland, ADS is compromised, and oxidative damage does occur, with gills the tissue most compromised (10 µg/L; 50 nm; 21 d) (Gonçalves et al., 2022b; Chapter 3). Oxidative damage also occurred in the digestive glands of *M. galloprovincialis* after 21 days of exposure to PS-NPs (50 nm; 150 ng/L) (Capolupo et al., 2021). IBR score for PS-NPs (Fig. 4) indicates that exposure durations of 7 and 21 days are the most critical time points for mussel gonads, relating to the activation and inhibition of the ADS. Furthermore, the PCA confirms that the effects of PS-NPs, when compared with other treatments, are negatively correlated (Fig. 5.3.).

5-FU is known to cause genotoxicity in mussel haemolymph (Gonçalves et al., 2022a; Chapter 4), and with its primary MoA being the substitution of the pyrimidine analogue uracil for its fluoro-nucleotides (Matuo et al., 2009), the damage in DNA is expected. However, in relation to the ADS and oxidative damage, the gills and digestive gland of *M. galloprovincialis* exposed to 10 ng/L for 21-d showed that the ADS could counteract ROS generation and led to no oxidative damage. Although the ADS activated in mussel gonads exposed to 5-FU, inhibition of GST activity was sufficient to see an increase in oxidative damage. Cellular membranes in the gonads are imperilled after exposure to 5-FU, suggesting that this toxicity may affect gonadal development and reproductive success. If robust oocytes and spermatozoa are unsuccessfully liberated into the water column, and embryo-larval development is jeopardised, a cascading effect in populational dynamics will be seen in future years. With the increase in the prescription of chemotherapeutical cytotoxic agents, being that breast (8567 cases), prostate (6912 cases) and colorectal cancer (5483 cases) were the most diagnosed cancers in Portugal in 2019 (Instituto Nacional de Estatística Statistics Portugal, 2021), the insufficient treatment and removal of cytotoxic agents by WTTP is highly concerning for the marine environment as well as for human health.

Mixtures of CECs in mussel gonads presented antagonistic and synergistic interactions (Table 1 – 2). After 3 days of exposure, synergistic interactions between nAg, PS-NPs and 5-FU are noted, coinciding with the 57-fold increase in oxidative damage compared to the individual exposures. However, on the remaining days of exposure, antagonistic interactions were found. This suggests that metal nanoparticle – nanoplastic – pharmaceutical interactions are severely hazardous towards the marine environment at sub-lethal exposures. Nonetheless, the insufficient effort from the ADS and the high levels of LPO indicate reproductive

impairment in mussel gonads, as a continuous increase in the ADS activity requires the energy typically directed towards growth and reproduction (Trestrail et al., 2020). IBR score for the Mix also confirms day 3 of exposure as the most jeopardising (Fig. 4). It is deducible from the PCA that the most influential contaminants in the toxicity of Mix are nAg and 5-FU (Fig. 5.3.). The antagonistic effects on the biomarkers assessed in mussel gonads exposed to Mix suggests that nAg anti-septic properties may be cancelling out the toxicity of 5-FU. However, binomial mixtures are necessary to establish this result fully. However, concerning genotoxicity, the ability of 5-FU to incorporate its fluoro-nucleotides is not diminished by the presence of either nAg or PS-NPs (Gonçalves et al., 2022a; Chapter 4). Knowingly as vectors (Xiang et al., 2022), the adsorption of other contaminants, such as pharmaceuticals and nanoparticles, by nanoplastics can explain the synergistic interaction encountered after acute exposure. Other studies have examined the interaction of CECs in a binomial complex (Almeida et al., 2019; Essawy et al., 2021; Sun et al., 2023). Almeida et al. (2019) found that effects on CAT activity were possibly due to the transfer of contaminants onto PS-NPs (propanol + PS-NPs, 10 mg/L, 24h) in a fish cell line of *Sparus aurata*.

On the other hand, antagonistic interactions between PS-NPs and nAg were noted in human undifferentiated Caco-2 cells (0 – 5 nAg µg/L + 0 – 100 PS-NPs µg/L; 24 h), whereby the nAg/PS-NPs complex modulated the cell's uptake of nAg and slightly changed nAg toxicity (Domenech et al., 2021). Whilst, synergistic interactions of biosynthesised nAg, rutin (R), and heliomycin (H) demonstrated a dose-dependent antimicrobial efficacy against two fish pathogens (*Aeromonas hydrophila* and *Pseudomonas fluorescens*) (24 h; 56 nm; 1 µg/L nAg + 64 – 512 µg/L of R and H) (Essawy et al., 2021). Therefore, understanding the interactions between metal nanoparticles, nanoplastics, and pharmaceuticals highly depends on the contaminant, concentration, size, and exposure time. Specifically, results suggest that mixtures at sub-lethal exposures were most toxic in mussel gonads, with CECs exhibiting synergistic toxicity. Furthermore, although antagonistic interactions were noted on the remaining exposure days, levels of oxidative damage remained elevated compared to controls and those exposed to PS-NPs. The implications for gonadal development, gamete viability, successful fertilisation, and embryo-larval development are concerning based on the current results. If verified, populational dynamics and ecosystem balance are at risk. Therefore, enhancing risk-assessment strategies and developing new technologies for treating and removing CECs in wastewater treatment plants is highly advisable. In Europe, mussels hold significant social and economic value. For instance, in Portugal, a 47.5% increase in mollusc aquaculture was reported in 2020 (9863 tons), with mussel aquaculture production rising by 37.7% (2007 tons)

(GRMV, 2021). In Portugal, mussel aquaculture primarily occurs in coastal areas, where CECs may be present in the surrounding waters. Consequently, not only may CEC mixtures affect the reproductive success of mussels and impact the aquaculture of mussels, but they can also have detrimental effects on marine biodiversity and human health from shellfish consumption.

5.5. Conclusion

The data set obtained herein suggests that the mixture of silver nanoparticles, polystyrene nanoplastics, and 5-fluorouracil is more toxic than its counterparts. The mixture exhibits high acute toxicity towards the reproductive organs of mussels, characterised by synergistic interactions, while antagonistic interactions between CECs occur during chronic exposures. However, oxidative damage is inevitable regardless of these synergistic or antagonistic interactions. Therefore, further investigation into complex mixtures and their toxicity is necessary to fully establish the mechanisms by which these CECs interact. Additionally, the toxic effects of CECs should be assessed in mussel gonads, accounting for female and male differences, to better understand how reproduction may be affected. Moreover, as the production of nanosilver-based consumer products, plastic pollution, and chemotherapeutic agents rise alongside increasing cancer diagnoses, the technologies for treating and removing CECs in WTTP need to be revised and enhanced. The development of novel risk–assessment strategies and regular monitoring of CECs is also advised.

CHAPTER VI

Gender effects of nanoplastics and emerging contaminants mixtures in *Mytilus galloprovincialis*.

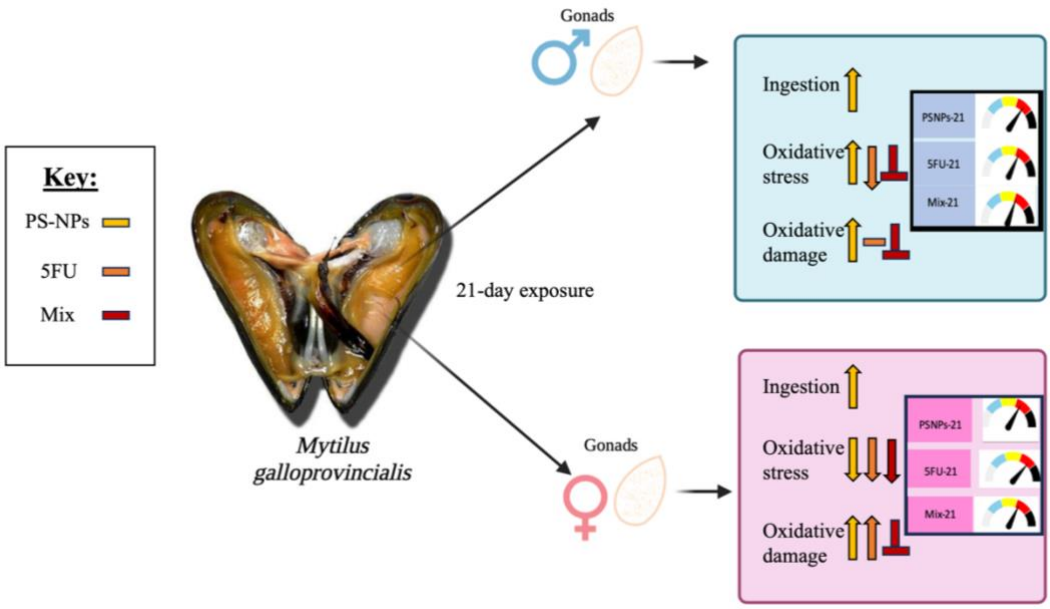

This chapter has been published in:

- Gonçalves, J. M., Benedetti, M., d'Errico, G., Regoli, F., & Bebianno, M. J. (2025). Gender effects of nanoplastics and emerging contaminants mixtures in *Mytilus galloprovincialis*. Aquatic Toxicology, 107219. https://doi.org/10.1016/J.AQUATOX.2024.107219

This chapter was presented at the international conference:

PRIMO22
26-29 MAY 2024
NANTES FRANCE

Gender differentiating effects of a mixture of emerging contaminants in the Mediterranean mussel *Mytilus galloprovincialis*

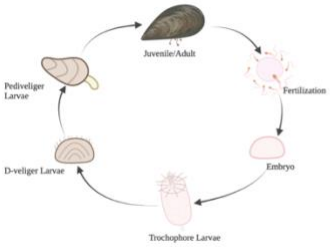

J.M. Gonçalves[1], M. Benedetti[2,3], G. d'Errico[2], F. Regoli[2,3] and M.J. Bebianno[1]

[1]CIMA, Centre of Marine and Environmental Research\ARNET - Infrastructure Network in Aquatic Research, University of Algarve, Campus de Gambelas, 8000-139 Faro, Portugal.

[2]Dipartimento di Scienze della Vita e dell'Ambiente, Università Politecnica delle Marche, Via Brecce Bianche, 60131 Ancona, Italy.

[3]National Future Biodiversity Centre (NFBC), Palermo, Italy

PRIMO22
26-29 MAY 2024
NANTES FRANCE

UAlg CIMA
UNIVERSIDADE DO ALGARVE
CENTRO DE INVESTIGAÇÃO MARINHA E AMBIENTAL

ARNET

Marine
Pollution & Ecotoxicology Group

FCT
Fundação para a Ciência e a Tecnologia

Abstract

The reproduction of mussels occurs within the water column, and if gametogenesis is successful, gametes are exposed to the surrounding contaminants. Nanoplastics and other emerging contaminants have been gaining vast attention; however, their effects on the reproductive tissues of mussels with sex differentiation are scarce. Here, the effects of polystyrene nanoparticles (50 nm; 10 µg/L), the cytotoxic drug 5-fluorouracil (10 ng/L), and a mixture of the two were evaluated in the gonads of *Mytilus galloprovincialis* after a 21-day exposure for a multi-biomarker assessment, and after 28 days for the ingestion of nanoplastics. The effects on the activity of superoxide dismutase, catalase, glutathione-*S*-transferase, and lipid peroxidation were evaluated. Moreover, synergistic and antagonistic interactions in the mixture were calculated. A weight of evidence model was also used to elaborate on the hazardous level of biomarker results relative to polystyrene nanoparticles alone and in the mixture. The ingestion of nanoplastics appeared gender and time-specific, with females mostly compromised. According to the data set, a synergistic interaction between the cytotoxic drug and the nanoplastics makes the combination far more dangerous than individual stressors. The Weight Of Evidence model also confirms that females are more compromised at chronic exposure times than males. This study shows that the uptake, fate, and impact of emerging contaminants of concern can be significantly influenced by sex.

6.1. Introduction

The marine mussel *Mytilus galloprovincialis* is an excellent sentinel organism for ecotoxicological studies and an essential species in the Mediterranean ecosystem. The reproduction of this species occurs within the water column. Once gametes are ripe, mussels liberate oocytes and spermatozoids into the ocean, and fertilisation occurs outside the organism. During gonad maturation, energy storage is crucial for both oocyte and spermatozoa development and release. The reproductive capacities of mussels, such as the quality of oocytes and spermatozoa, as well as embryo-larval development, are influenced by the availability of food sources (Fearman et al., 2009). Throughout the ripening of female gonads, lipid content increases as a source of energy during gametogenesis and the development of the embryo and larvae (Martínez-Pita et al., 2012). However, despite food availability, contaminants in the ocean can lead to adverse effects on the reproductive cycle of mussels; for example, if nanoplastics (NPs) are ingested by mussels, they can act as a low or non-nutritional food (Wegner et al., 2012). NPs (1 – 1000 nm) are a class of emerging contaminants, and their effects on the marine environment and consequences on reproduction are still elusive. In 2022, 390.7 million tons of global plastic production was reported (Plastics Europe, 2023). Plastic litter, along with the consequences of illegal dumping, waste mismanagement, and lack of treatment for the removal of plastic debris in wastewater treatment plants (WTTPs), make it necessary to evaluate not only the direct adverse effects on the overall organisms' health status but also how these particles can adversely affect the reproductive cycle of mussels. When contaminants negatively affect gonadal development and accumulate in gametes, this can substantially impact the ecosystem by reducing the population's ability to generate healthy offspring, reducing fertilisation success, impeding larval growth and, as a result, placing biodiversity at risk.

In the ocean, NPs can derive from the breakdown of larger plastic particles, classified as secondary NPs, or may be introduced already at the nanoscale, known as the primary NPs (Gonçalves & Bebianno, 2021; Chapter 1). Because of their small size, whether primary or secondary, NPs can cross cellular boundaries and is a significant concern, as not only can they enter the tissues and bloodstream of the mussels, but they can also enter spermatozoa and oocytes (González-Fernández et al., 2018; Tallec et al., 2018). In the case of spermatozoa, the infiltration of NPs can lead to a reduction of sperm release, inhibition of sperm motility, and DNA damage (Lewis & Ford, 2012). Oocytes are also in jeopardy, as NPs can cause a decrease in successful fecundity and numerous malformations, including total development arrest throughout the embryo-larval development (Tallec et al., 2018).

A mimicking of coastal activities on a polystyrene (PS) cup and lid revealed the formation of nanoscale particles after five minutes (Ekvall et al., 2019). Considering that PS is the fourth most abundant plastic produced (e.g. packaging, building and construction) and is not recyclable (The Waste and Resources Action Programme, 2023), it is fundamental to understand how PS nanoplastics (PS-NPs) affect the reproductive tissues of mussels. In the gonads of *M. galloprovincialis,* exposure to PS-NPs for 21 days caused oxidative stress, but no oxidative damage was observed (10 µg/L; 50 nm) (Gonçalves & Bebianno, 2023; Chapter 5). Evaluating if different effects occur on mussels' gender can help to shed light on how PS-NPs can affect the reproductive organs of mussels. Additionally, through sorption mechanisms, plastics can function as vectors for other contaminants in the ocean. NPs have larger surface areas than larger plastic particles, increasing their potential biological effect (Ferreira et al., 2019; Mattsson et al., 2018). Pharmaceuticals are listed as contaminants of emerging concern (Kumar et al., 2022). As the number of cancer patients receiving cytostatic drug-based chemotherapy increases, these chemicals are rarely fully metabolised and then released into the water system, barely modified (Trombini et al., 2016). The 5-fluorouracil (5-FU) (IARC Class 3) is one of the most widely used pharmaceutical compounds for treating colorectal, pancreatic, and breast cancer (Mahnik et al., 2007) tumours. As a pyrimidine analogue of uracil, 5-FU has a fluorine atom in its place, and the misincorporation of its fluoro-nucleotides into nucleic acids is a considerable concern for the aquatic environment. Moreover, 5-FU causes the release of cytochrome *c* from the mitochondria, promoting the production of reactive oxygen species and leading to oxidative stress (Gonçalves et al., 2022a; Chapter 4). In the gonads of *M. galloprovincialis*, a 21-day exposure to 10 ng/L of 5-FU caused a 33-fold increase in oxidative damage after 7 days (Gonçalves & Bebianno, 2023; Chapter 5).

These contaminants inevitably mix in the ocean, and 5-FU may be adsorbed onto the PS-NPs, leading to more adverse effects. For instance, extensive oxidative damage was seen in the gonads of *M. galloprovincialis,* with lipid peroxidation levels increasing 57–fold after three days of exposure to a mixture of emerging contaminants (10 ng/L of 5-FU, 10 µg/L of PS-NPs, and silver nanoparticles (50 and 20 nm, respectively) (Gonçalves & Bebianno, 2023; Chapter 5).

With the potential adsorption of 5-FU onto PS-NPs, the increase in toxicity is likely to cause more harm to female mussels than males, as females require twice the lipid content as an energy source during gametogenesis (Gao et al., 2022; Gonçalves et al., 2020). Consequently, malformation of oocytes can occur and disrupt the reproductive success of mussels. The concentrations of NPs in rivers, seas, and nature reserves in Asia, Europe, Antarctica, and the

Arctic Ocean vary from 0.3 to 488 µg/L (Shi et al., 2024). Predicted environmental concentrations of 5-FU range from 0.01 to 41 ng/L in surface waters (Misik et al., 2019). Therefore, this study aims to evaluate the gender-specific effects of polystyrene nanoplastics (PS-NPs, 50 nm, 10 µg/L) and 5-fluorouracil (5-FU, 10 ng/L) individually and as a mixture (10 µg/L of PS-NPs + 10 ng/L of 5-FU) in the reproductive tissues of *Mytilus galloprovincialis,* after 21-days of exposure. To comprehend these effects, antioxidant enzymatic activities and oxidative damage analysed the antioxidant capacity of male and female mussels, and the ingestion of PS-NPs was also evaluated (28 days) to understand whether there is sex-specificity towards the ingestion of these particles. Antagonistic and synergistic interactions were also calculated, and parameters were further integrated into a weight-of-evidence model to assess the biological risk of these compounds.

6.2. Materials and Methods

6.2.1. Polystyrene nanoplastics (PS-NPs)

Fluoresbrite® Plain YG spherical polystyrene nanoplastics with a size of 50 nm (CAS 9003-53-6) were provided by Polysciences, Inc. (Germany). The abundance of salt in fresh seawater triggers aggregation/agglomeration kinetics, increasing the hydrodynamic diameter of PS-NPs (852 ± 103 nm). Further details on PS-NP characterisation can be accounted for in Gonçalves et al. (2022b) (Chapter 3).

6.2.2. 5-Fluorouracil (5-FU)

The cytotoxic drug 5-FU (CAS 51-21-8) was purchased from Sigma Aldrich, Inc. A class II biological safety cabinet and the correct clothing equipment (double powder-free latex gloves, a protective lab coat with an open back resistant to chemotherapy, and safety goggles) were used to ensure the safety of this pharmaceutical. Successive dilutions were performed using Milli-Q water to reach a final exposure concentration of 10 ng/L.

6.2.3. Experimental Design

Mussels, *Mytilus galloprovincialis* (50 mm ± 5 mm), were sampled from the Ria Formosa Lagoon in the Southeast of Portugal (37°00'30.6"N 7°59'39.6" W), brought to the lab, scraped clean and placed into 30 L tanks (25 L of FSW) with a ratio of 2 mussels/L, in a triplicate design. After a four-day acclimatisation period, mussels were exposed to 10 µg/L of PS-NPs, 10 ng/L of 5-FU, and a mixture of 10 µg/L of PS-NPs and 10 ng/L of 5-FU, for a total

of 21 days. Contaminants and seawater were renewed every two days, concentrations were re-established, and mussels were sampled at 0, 3, 7, 14, and 21 days of exposure for consequent multi-biomarker evaluation. For ingestion purposes, unexposed mussels and those exposed to PS-NPs were exposed for an additional 7 days (sampling days = 0, 3, 7, 14, 21, and 28 days). On sampling days, the gonads of mussels were dissected and immediately frozen in liquid nitrogen and stored at -80ºC until further analysis.

6.2.4. Quality control and assessment

To bypass further plastic contamination, including airborne pollution, all tanks had a glass lid and glass pipettes for aeration, and no gloves or plastic equipment were used during tissue dissection.

6.2.5. Sex identification

For sex determination, an aliquot of each sample was analysed under an optical microscope (Compound Light Microscopy) at 400x magnification to determine whether oocytes or spermatozoa existed (Table 6.1.). To preserve the samples for later analysis, they were labelled according to gender and kept at -80ºC. Where possible, a sample size of *n*=5 males and n=5 females was used (Table 6.1.).

Table 6.1. Number of *M. galloprovincialis* mussels identified as male and female for analysis.

Time (days)	Treatment							
	CT		PS-NPs		5-FU		Mix	
	♂	♀	♂	♀	♂	♀	♂	♀
0	5	5	5	5	5	5	5	5
3	4	6	5	4	4	6	5	5
7	4	6	5	5	5	5	5	5
14	5	5	3	7	5	5	5	5
21	5	5	5	5	5	4	5	5

6.2.6. Ingestion

The ingestion of PS-NPs was assessed in mussel gonads exposed to 10 µg/L of PS-NPs utilising a fluorescence-based methodology using the molecular rotor probe 9-(dicyanovinyl)-julolidine (DCVJ), following Gagné (2019) method. First, male and female gonads of mussels were homogenised individually at 20% (w/v) in an ice-cold buffer solution (50 mM NaCl, 10

mM Hepes - NaOH [pH 7.4], 1 mM EDTA, and 1 mM DTT), using a VWR Star-Beater (5 min, 20/s shaking, with grinding balls). To separate the cytosolic fraction, samples were centrifuged for 20 min (2ºC, 15 000 *g*), and the resultant supernatant was immediately frozen (-80ºC) until further investigation. Then, samples were examined using a Berthold Tristar 5 spectrofluorometric microplate reader, with excitation at 450 nm and 400–800 nm emission spectra. PS-NPs have a wavelength of 510 nm, and results are compared to controls of PS-NPs g/g wet weight.

6.2.7. Antioxidant enzymes

Following Geret et al. (2002), male and female mussel gonads were homogenised in 5 mL of 20 mM Tris-Sucrose buffer (0.5 M Sucrose, 0.075 M KCl, 1 mM DTT, 1 mM EDTA, pH 7.6) using a VWR Star-Beater (5 min, 20/s shaking, with grinding balls). The cytosolic fraction was collected after two centrifugations (1°: 1,500 g for 15 minutes at 4°C; 2°: 12,000 g for 45 minutes at 4°C). The activities of the antioxidant enzymes superoxide dismutase (SOD), catalase (CAT), and the activity of the biotransformation enzyme glutathione-S-transferases (GST) were then examined in the aliquots.

Using the Bradford (1976) method, all enzymatic activities were standardised against total protein concentrations. Bovine serum albumin (BSA) was used as a reference to quantify total protein concentrations (mg protein g^{-1} tissue), which were then calibrated for a microplate reader.

The reduction in cytochrome c absorption by the xanthine oxidase/hypoxanthine system at 550 nm was used to calculate SOD activity, and the results were reported as U mg^{-1} protein (McCord & Fridovich, 1969).

Following Greenwald's (1985) methodology, CAT activity was measured by measuring hydrogen peroxide (H_2O_2) consumption at 240 nm using a spectrophotometric method. The data is expressed as mmol min^{-1}mg $protein^{-1}$.

Based on the method developed by Habig et al. (1974), the GST activity was measured using an Infinite® 200 microplate reader (Pro-Tecan) by conjugating 0.2 mM reduced glutathione (GSH) with 0.2 mM 1-chloro-2,4-dinitrobenzene (CDNB) in a reaction mixture of 0.2 M KH_2PO_4/K_2HPO_4 buffer (pH 7.9). Data is displayed in units of mol CDNB min^{-1} mg^{-1} protein.

6.2.8. Lipid peroxidation

Individual male and female mussel gonads were homogenised in 5 mL of a 1:10 ratio of butylated hydroxytoluene and 0.02 M Tris-HCl buffer (pH 8.6) using a VWR Star-Beater (5 min, 20/s shaking, with grinding balls). Homogenates (3 mL) were centrifuged at 30,000 *g* for 45 minutes at 4°C to determine the total protein and LPO amounts. The levels of LPO were calculated in units of nm/mg protein using a technique derived from Erdelmeier et al. (1998) using the absorbance of malondialdehyde (MDA) and (2 E)-4-hydroxy-2-nonenal (HNE) at 540 nm. Results are expressed as MDA (nmol/mg prot).

6.2.9. Model for Synergistic or Antagonistic Effect

Synergistic and antagonistic interactions were computed based on Ritz et al. (2021) single-dose factorial design for binary combinations. This method produces four treatments by combining two components (two contaminants) with two levels: control, PS-NPs, 5-FU, and a combination of the two (Mix). Only for the concentrations utilised in this evaluation—10 g/L of PS-NPs, 10 ng/L of 5-FU, and Mix (10 g/L of PS-NPs + 10 ng/L of 5-FU—is the declaration of an opposing or complementing influence valid. The following dose addition and independent action models were used to calculate values for all sampling intervals (0, 3, 7, 14, and 21 days) and all biomarkers (SOD, CAT, GST activity, and LPO levels) examined:

6.2.9.1. Dose addition

$$E_{add} = (E_{5FU} - E_{control}) + (E_{nPS} - E_{control})$$

The difference (D_{da}) between the actual response (control) and the previously expected impact can characterise any antagonistic or synergistic effect. The following equation defines the difference:

$$D_{da} = E_{Mix} - E_{5FU} - E_{nPS} + E_{control}$$

6.2.9.2. Independent action

$$E_{ind} = \frac{E_{5FU} \times E_{nPS}}{(E_{control})^2}$$

Under the presumption of independent action, every antagonistic or synergistic effect can be described as the difference (D_{ia}) between the observed and reference effects. The following equation defines the difference:

$$D_{ia} = E_{Mix} - E_{ind}$$

6.2.10. Statistical Analysis

The software program GraphPad Prism, version 9.4.1 (GraphPad Software, Inc. CA), was used for all statistical analyses. The significant differences between treatments, time, and sex were evaluated using parametric tests (ANOVA, followed by Tukey's posthoc test) or non-parametric equivalent tests (Kruskal-Wallis and a two-tailed multiple comparisons test), as determined by data distribution and variance homogeneity (Shapiro-Wilk test). The results were significant if $p < 0.05$.

The relationship between treatments (unexposed and exposed to PS-NPs, 5-FU, and Mix) and the measured parameters [activities of antioxidant and biotransformation enzymes (SOD, CAT, GST) and oxidative damage (LPO)] in mussel gonads over the exposure period (21 days) was also examined using a Principal Component Analysis (PCA). A t-test using Microsoft Excel (*Microsoft Corporation*, 2018) was used to analyse statistical differences for IBR, and findings were deemed significant when $p < 0.05$.

6.2.11. Weight of Evidence (WOE)

A quantitative Weight of Evidence model (WOE, Sediqualsoft) that provides a synthetic hazard index based on a specifically developed algorithm and mathematical procedure was used to elaborate the results from data on general cellular biomarkers (SOD, CAT, GST, and LPO) for male and female gonads exposed to different conditions (PS-NPs, 5-FU and Mix) over 21 days (Regoli et al., 2019). The size of the observed change for each biomarker under analysis is compared to a predetermined threshold after being adjusted for the biological endpoint (weight)'s toxicological relevance and the statistical significance of the difference from controls. In-depth descriptions of complete computations, intricate flow charts, the justification for weights, thresholds, and expert opinions have previously been provided (Regoli et al., 2019).

6.3. Results

6.3.1. Ingestion

The ingestion of PS-NPs in male and female mussels is significantly different after 14, 21 and 28 days of exposure, with higher levels of particles occurring in female gonads (Fig. 6.1.; $p<0.05$). Comparing the ingestion by males over time, there is a significant increase at 7,

14 and 21 days (p<0.05) compared to other time points. For females, there are more significant differences between exposure times, with an initial increase observed at 7 days and the highest and most significant increase in PS-NP ingestion occurring at 14 days of exposure (p<0.05).

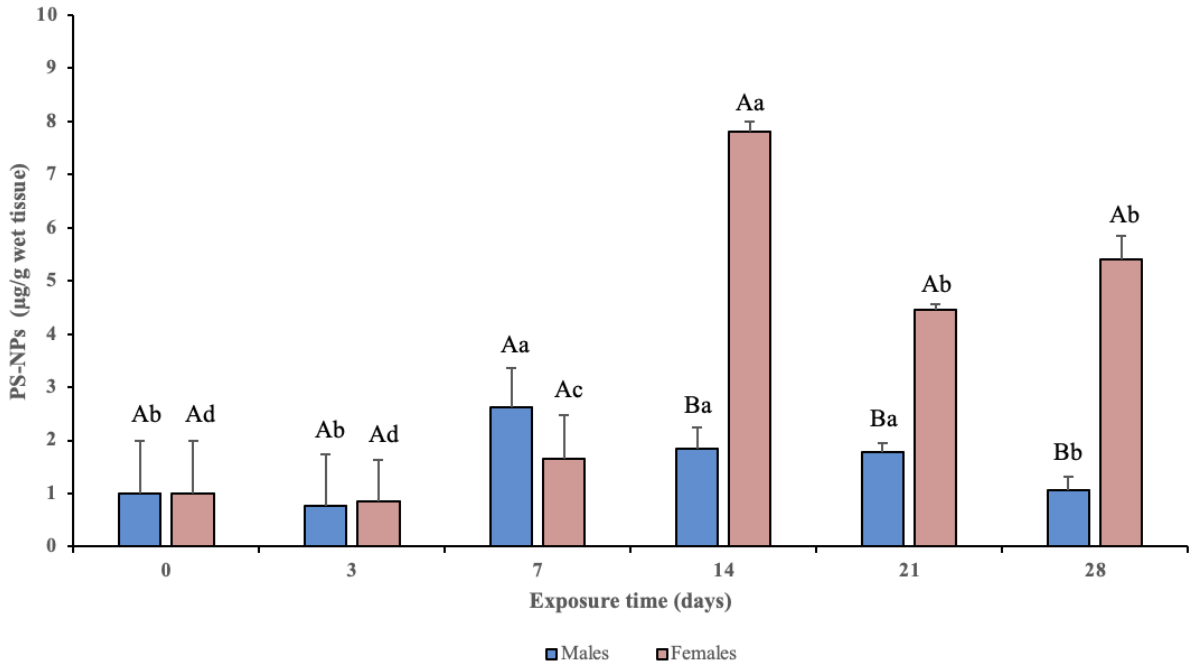

Figure 6.1. Ingestion of PS-NPs relative to controls (µg/g wet tissue) (mean ± std) in gonads of male (**blue**) and female (**red**) *M. galloprovincialis* and after 28 days of exposure to polystyrene nanoparticles (PS-NPs; 10 µg/L). Significant disparities between the sexes for the same time and between times for the same sex are indicated by different upper- and lower-case letters. (p<0.05).

6.3.2. Oxidative stress

Significant male and female differences are observed in the first line of defence of mussel's antioxidant system (SOD) after exposure to either treatment (Fig 6.2.A-B). A marked difference can be noted between unexposed male and female gonads at the beginning of the experiment (p<0.05), whereby female mussels have a significantly higher activity of SOD.

The SOD activity in males exposed to Mix significantly decreased after 3 days of exposure and is significantly different to females that present a higher activity, despite being significantly different from other treatment groups on that day (p<0.05, Fig 6.2.A-B). Furthermore, after 7 days of exposure, females exposed to 5-FU have a significant reduction in the activity of SOD compared to males. After 14 days, the same pattern is noticeable in Mix-exposed females (p<0.05). Observing male gonads individually, the most significant times of exposure and treatments are Mix-exposed gonads at 3 days and 5-FU-exposed males at 21 days

(p<0.05). Females, on the other hand, have a significant reduction of SOD activity in PS-NPs, 5-FU and Mix exposed gonads after 7 days, and low activity is observed until the end of exposure apart from the increase in activity observed in PS-NPs gonads at 21 days (p<0.05).

The activity of CAT after 21 days of exposure to various treatments is very different when looking at male and female results (Fig. 6.2.C-D). Apart from significant differences in unexposed males and females at 7 and 14 days (p<0.05), a significant inhibition of CAT activity is observed after 3 days in Mix-exposed males, at 7 days in PS-NPs exposed males and in the three exposure treatments at 21 days compared to females (p<0.05). Generally, males present a more significant decrease in CAT activity than females (p<0.05), except for PS-NPs exposed gonads at 21 days.

On the other hand, in both males and females, the biotransformation enzyme activity shows a similar pattern along the time of exposure (Fig. 6.2.E-F). The most noteworthy significant differences in GST activities between sexes are observed after 3 days of exposure in 5-FU-exposed mussels, with GST activity in male mussels decreasing in comparison to the increase observed in females (p<0.05) and at 21 days of exposure in PS-NPs gonads, being the increase in GST activity higher in females than that seen in males (p<0.05).

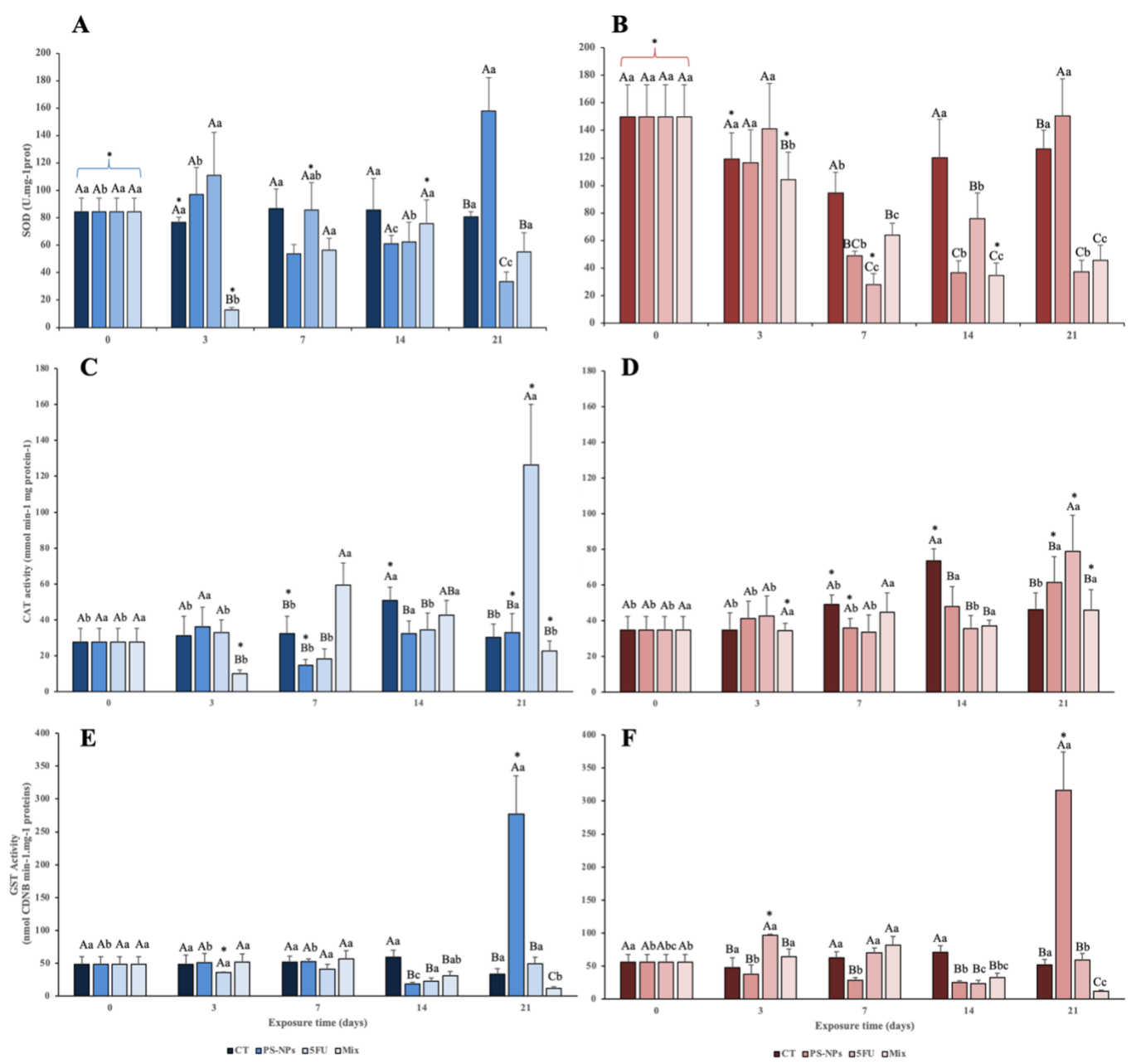

Figure 6.2. The activity of superoxide dismutase (SOD) (**A-B**), catalase (CAT) (**C-D**), glutathione-*S*-transferase (GST) (**E-F**) (mean ± std) in unexposed (CT) gonads of male (**blue**) and female (**red**) *M. galloprovincialis* and after 21 days of exposure to polystyrene nanoparticles (PS-NPs; 10 µg/L), 5-Fluorouracil (5-FU; 10 ng/L), and of a Mixture of the two contaminants (PS-NPs + 5-FU). Different upper- and lower-case letters indicate significant differences between treatments for the same time and between times for the same treatments, respectively (p<0.05). '*' indicates significant differences between sexes for the same time and treatments (p<0.05).

6.3.3. Oxidative damage

Lipid peroxidation levels in male and female mussels are significantly different, with a higher level of oxidative damage in female mussels (Fig. 6.3.). In comparison to other treatments and unexposed male gonads, there is a considerable increase in LPO levels after 3 days of PS-NP exposure. At this time, males are also considerably different from females. Compared to males, an increase in female LPO levels occurs after 14 days of exposure to PS-NPs and at 21 days in 5-FU-exposed gonads.

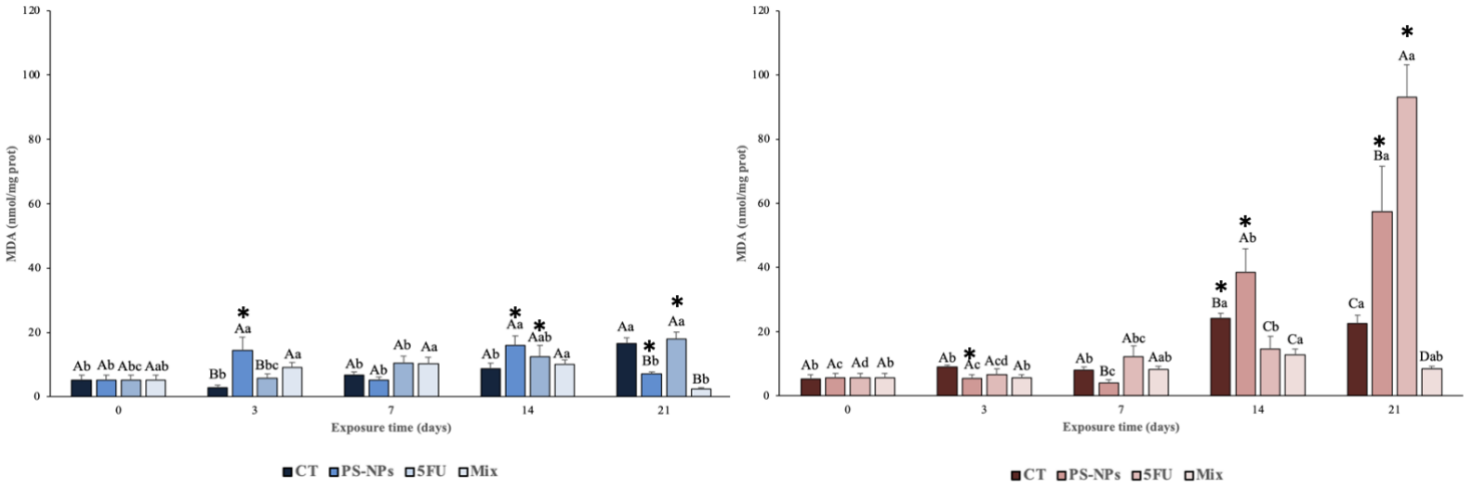

Figure 6.3. Lipid peroxidation levels (mean ± std) in unexposed (CT) gonads of male (**blue**) and female (**red**) *M. galloprovincialis* and after 21 days of exposure to polystyrene nanoparticles (PS-NPs; 10 µg/L), 5-Fluorouracil (5-FU; 10 ng/L), and of a Mixture of the two contaminants (PS-NPs + 5-FU). Different upper- and lower-case letters indicate significant differences between treatments for the same time and between times for the same treatments, respectively (p<0.05). '*' indicates significant differences between sexes for the same time and treatments (p<0.05).

6.3.4. Principal component analysis (PCA)

The impact of PS-NPs, 5-FU and a mixture of these two emerging contaminants (Mix) was evaluated in both male and female gonads of mussels' response in assessed biomarkers (SOD, CAT, GST and LPO) using PCA (Fig. 6.4.). In male gonads, the two principal components account for an overall variation of 79.5% (PC1 = 46.4%, PC2 = 33.1%, Fig. 6.4.A), whilst for female's the overall variation equal to 83.6% (PC1 = 47.1%, PC2 = 36.5%, Fig. 6.4.B). In both sexes, CAT and LPO are the principal biomarker loadings affecting PC1. In contrast, SOD, CAT, and GST are the primary biomarker loadings affecting PC2 in females, with the addition of LPO in males. A positive relationship of PS-NPs at 14 days is noticeable in both males and females in PC1; in PC2, a positive relationship is only noteworthy in male gonads at 3 and 14 days of exposure. For 5-FU exposed mussels, day 21 of exposure is positively related to both principal components analysed. The most time-points positively

related to PC1 are found in Mix-exposed mussels, as males are at 3, 7 and 14 days of exposure, with 3 days being the most influential. In contrast, females are at 7, 14 and 21 days, with 21 days having the most influence. Overall, mussels exposed 21 days to 5-FU are mostly compromised in male and female gonads. However, the mixture of the two emerging contaminants is the most prejudicial at several time points for both male and female mussels.

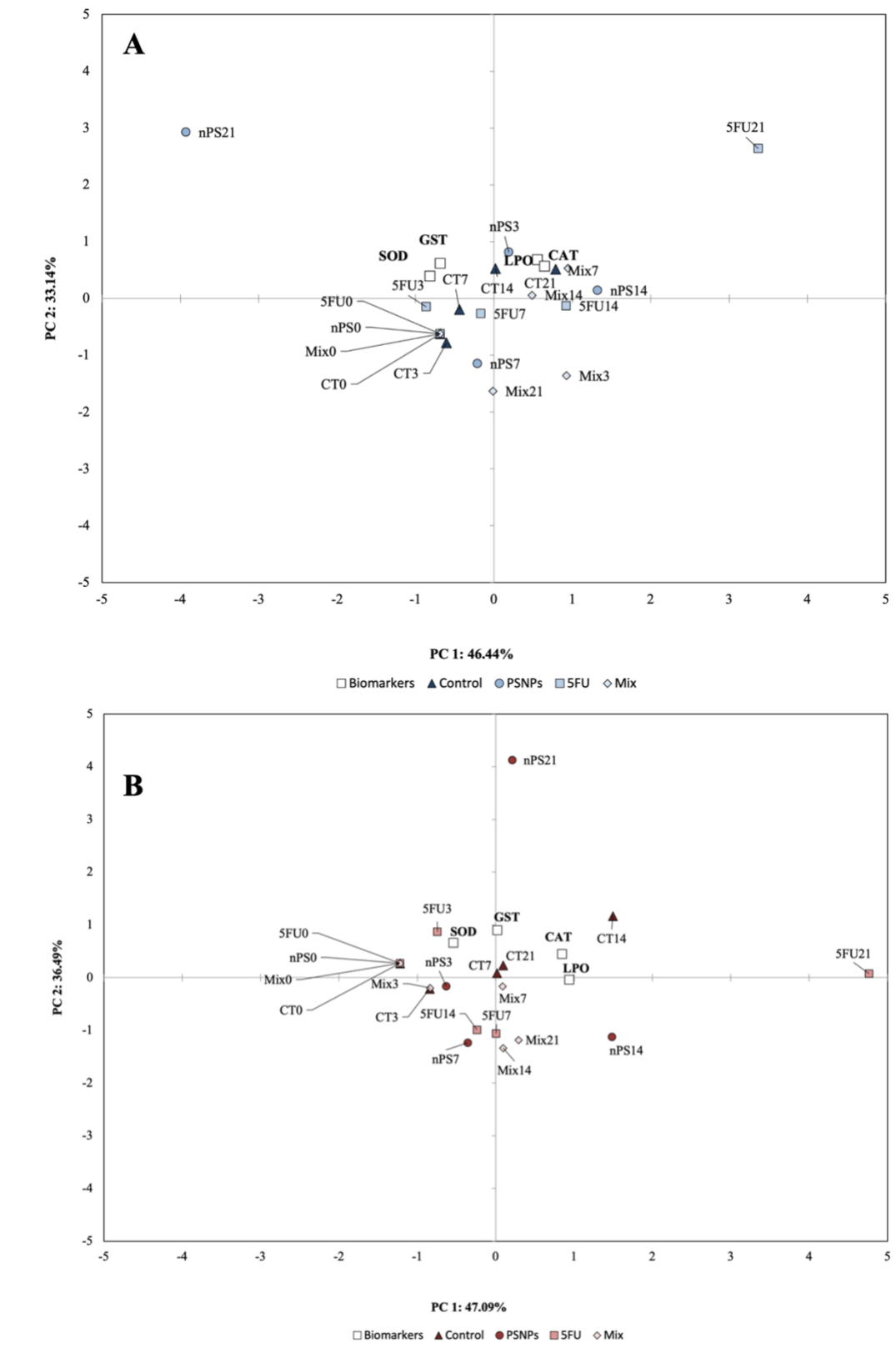

Figure 6.4. Principal component analysis (PCA) of biomarkers (SOD, CAT, GST activities and LPO) in (**A**) male gonads (*blue*) and (**B**) female gonads (*red*) of *M. galloprovincialis* from controls and those exposed to polystyrene nanoplastics (PSNPs), 5-Fluorouracil (5-FU) and a mixture of the two contaminants (Mix) for 21 days ($p<0.05$).

6.3.5. Synergistic or Antagonistic effect

Tables 6.2. and 6.3. show calculated synergistic and antagonistic interactions between PS-NPs and 5-FU in the mixture (Ritz et al., 2019).

According to the difference of dose addition (***D_{da}***) (Table 6.2.), antagonistic interactions are observable at 3 and 21 days of exposure when assuming a difference in dose addition and synergistic interactions at the other time points. On the other hand, when assuming the independent action (***D_{ia}***) of pollutants, the results of male and female gonads of synergistic and antagonistic effects differ slightly for each biomarker (Table 6.3.). However, a synergistic interaction is observable at all exposure times and in every biomarker evaluated, suggesting an adsorption mechanism of pharmaceuticals onto plastic particles, potentiating the toxic effects of 5-FU.

Table 6.2. Difference of dose addition (D_{da}). D_{da} is under the assumption of dose addition (sum of differences relative to the control group) for the contaminants when applied alone (adapted from Ritz et al., 2021). An antagonistic or synergistic effect is indicated when Dda is below or above 0.

Exposure time (days)	SOD		CAT		GST		LPO	
	♂	♀	♂	♀	♂	♀	♂	♀
3	-118	-34	-28	-15	12	-23	-8	3
7	4	82	59	24	15	46	1	0
14	38	42	27	27	49	54	-10	-16
21	-55	-15	-106	-48	-280	-311	-6	-119

Table 6.3. Difference of independent action (D_{ia}). D_{ia} is under the assumption of independent action of the contaminants (adapted from Ritz et al., 2021). An antagonistic or synergistic effect is indicated when Dia is below or above 0.

Exposure time (days)	SOD		CAT		GST		LPO	
	♂	♀	♂	♀	♂	♀	♂	♀
3	83	149	26	33	48	55	-5	5
7	12	104	10	34	51	63	8	5
14	56	64	59	45	56	82	8	7
21	75	34	38	35	19	26	10	2

6.3.6. Weight of Evidence (WOE)

The overall WOE elaboration of biomarker results (Tables 6.4. and 6.5.) indicated increased cellular hazard in both males and females. For male gonads, a Major hazard level is observed at 21 days of exposure to PS-NPs and 5-FU, whilst this Major hazard level is kept at 3 and 21 days in those exposed to the Mix. For females, on the other hand, a Major hazard level is observed in both exposure treatments (NPs and Mix)at 14 and 21 days of exposure, while in

mussels exposed to 5-FU, it is Major only at 21 days. For males, at 21 days of exposure to PS-NPs, SOD and GST are the biomarkers contributing to the Major and Severe effects established by the model, respectively. Again GST, SOD and CAT contributed to Major hazard levels in organisms exposed to 5-FU. Concerning the Mix exposure, after 3 days, SOD and CAT contribute to the Major hazard level and LPO as Severe, whilst after 21 days, LPO and GST both contribute to the Major hazardous level observed. In female mussels, the Major hazardous level noted after 14 days in PS-NPs is relative to SOD and GST and at 21 days to LPO, with the hazardous level reported for GST to be severe. Similarly, SOD and LPO contributed to the Major hazard level in 5-FU-exposed mussels. In mix-exposed females, SOD is the most contributing biomarker to the Major hazardous effect observed at both 14 and 21 days, with GST also contributing at 21 days of exposure.

Table 6.4. Weight of evidence (WOE) of 10 µg/L of PS-NPs, 10 ng/L of 5-FU and of a mixture of 10 µg/L of PS-NPs and 10 ng/L of 5-FU (Mix) in male gonads of *M. galloprovincialis* after 0, 3, 7, 14, and 21 days of exposure.

Sample code	N. param in class ABSENT	N. param in class SLIGHT	N. param in class MODERATE	N. param in class MAJOR	N. param in class SEVERE	Level of hazard for biomarkers	
PSNPs-0	4	0	0	0	0	ABSENT	
PSNPs-3	3	0	0	0	1 LPO	MODERATE	
PSNPs-7	2	0	2 CAT - SOD	0	0	MODERATE	
PSNPs-14	1	1 CAT	1 LPO	1 GST	0	MODERATE	
PSNPs-21	1	0	1 LPO	1 SOD	1 GST	MAJOR	
5FU-0	4	0	0	0	0	ABSENT	
5FU-3	3	0	1 LPO	0	0	SLIGHT	
5FU-7	2	1 LPO	1 CAT	0	0	SLIGHT	
5FU-14	2	1 CAT	1 GST	0	0	SLIGHT	
5FU-21	1	0	2 GST - SOD	0	1 CAT	MAJOR	
Mix-0	4	0	0	0	0	ABSENT	
Mix-3	1	0	0	2 SOD - CAT	1 LPO	MAJOR	
Mix-7	1	1 LPO	1 SOD	1 CAT	0	MODERATE	
Mix-14	3	0	1 GST	0	0	SLIGHT	
Mix-21	1	1 SOD	0	2 LPO - GST	0	MAJOR	

Table 6.5. Weight of evidence (WOE) of 10 µg/L of PSNPs, 10 ng/L of 5-FU and of a mixture of 10 µg/L of PS-NPs and 10 ng/L of 5-FU (Mix) in female gonads of *M. galloprovincialis* after 0, 3, 7, 14, and 21 days of exposure.

Sample code	N. param in class ABSENT	N. param in class SLIGHT	N. param in class MODERATE	N. param in class MAJOR	N. param in class SEVERE	Level of hazard for biomarkers	
PSNPs-0	4	0	0	0	0	ABSENT	
PSNPs-3	3	1 LPO	0	0	0	SLIGHT	
PSNPs-7	0	1 CAT	3 SOD - LPO - GST	0	0	MODERATE	
PSNPs-14	0	2 LPO - CAT	0	2 SOD - GST	0	MAJOR	
PSNPs-21	2	0	0	1 LPO	1 GST	MAJOR	
5FU-0	4	0	0	0	0	ABSENT	
5FU-3	3	0	0	1 GST	0	MODERATE	
5FU-7	2	1 CAT	0	1 SOD	0	MODERATE	
5FU-14	0	2 SOD - LPO	1 CAT	1 GST	0	MODERATE	
5FU-21	1	0	1 CAT	1 SOD	1 LPO	MAJOR	
Mix-0	4	0	0	0	0	ABSENT	
Mix-3	3	1 LPO	0	0	0	SLIGHT	
Mix-7	3	1 SOD	0	0	0	SLIGHT	
Mix-14	0	0	3 CAT - GST - LPO	1 SOD	0	MAJOR	
Mix-21	1	0	1 LPO	2 SOD - GST	0	MAJOR	

6.4. Discussion

A successful reproduction period is vital for the future of all the species. In mussels, many factors can influence reproduction after the release of gametes in the water column. Primarily, the success of gametogenesis is crucial to guarantee the release of viable gametes. Male gonads must be able to release viable spermatozoids without compromised swimming ability, whilst the robustness of oocytes released by females is essential for fecundity purposes. It is known that female mussels, throughout gametogenesis, require twice the energy content, where lipids are an important component (Gao et al., 2022; Gonçalves et al., 2020). Therefore, to our knowledge, this is the first dataset on male and female differences in *M. galloprovincialis* after exposure to PS-NPs, 5-FU and a mixture of these two emerging contaminants.

The ingestion of nanoplastics by filter-feeding organisms may compromise the immune systems and lead to more complications such as impaired fertilisation and embryo-larval development (Tallec et al., 2018; Auguste et al., 2021; Gonçalves et al., 2022b; Capolupo et al., 2021) (Chapter 3). The ingestion of PS-NPs (Fig. 6.1.) also provides evidence for the differentiation observed in male and female gonads of mussels. The higher effects observed in female oxidative damage are positively related to the ingestion of PS-NPs at 14 and 21 days. Male mussels, on the other hand, have higher ingestion of PS-NPs at 7 days of exposure, which was previously observed in the gonads of *M. galloprovincialis* with no sex differentiation (Gonçalves et al., 2023; Chapter 2), where translocation of PS-NPs was suggested between tissues after evaluating the ingestion in the gills, digestive glands, and gonads of mussels (10 µg/L; 28 days). This is highly concerning as in oysters, for instance, the fertilisation rate decreased after gametes were exposed to PS-NPs (10 µg/L; 50 nm; 1.5 h; *Crassostrea gigas*; Tallec et al., 2018). Moreover, a reduction in sperm motility and agglomerates of PS-NPs was encountered on the jelly-coatings of oocytes in *C. gigas* (PS-COOH and PS-NH_2; 0.1-100 mg/L; 1, 3 and 5 h; González-Fernández et al., 2018). Additionally, malformations of D-larvae after embryos of *M. galloprovincialis* were observed after exposure to PS-NPs (50 nm; 10 µg/L; 48 hours post fertilisation; Auguste et al., 2021). Exposure to 10 µg/L of PS-NPs (50 nm) (Fig. 6.2.A-B) significantly inhibits the first line of defence in the mussels' antioxidant defence system in both male and female gonads. However, this is not observed in gonads previously assessed with no sex differentiation (Gonçalves et al., 2023; Chapter 2). This increases the importance of evaluating the ecotoxicological effects of contaminants in the gonads of mussels with male and female differences. Also, this pattern is observable in other tissues, such as the gills and digestive glands subjected to the same exposure conditions (Gonçalves et al., 2022b; Chapter 3). Antioxidant enzyme activity can continuously rise, requiring energy that could

conflict with the energy required for development and reproduction (Trestrail et al., 2020). Nanoplastics decrease fertilisation success in the oyster *C. gigas* (PS-NPs; 50 nm; 25 µg/mL; Tallec et al., 2018) and cause malformations in embryo-larval development. Thus, when gonads are compromised from the beginning, gametogenesis is hindered, and the release of viable oocytes and spermatozoa may be jeopardised. Following the line of antioxidant defence, the same pattern is observable in male and female gonads CAT activity, and there is a significant difference between males and females after 7 and 21 days of exposure. Here, male gonads are mostly compromised by exposure to PS-NPs. On the other hand, the effects of PS-NPs (50 nm; 10 µg/L) in gonads with no sex differentiation significantly inhibited CAT activity after 14 and 21 days (Gonçalves et al., 2023; Chapter 2). In the digestive gland of *M. galloprovincialis* (50 nm; 150 ng/L; 21 days), there was a significant induction of CAT activity (Capolupo et al., 2021), suggesting that before the translocation of PS-NPs to gonads, an abundance of energy is being used to protect mussel's immune system from PS-NPs, consequently jeopardising energy used normally for growth and reproduction. However, in the gills and digestive glands of *M. galloprovincialis* exposed to 10 µg/L of PS-NPs (50 nm; 21 days), these nanoparticles caused an inhibitory effect of CAT activity throughout the exposure period (Gonçalves et al., 2022b; Chapter 3). Concentration, therefore, is an important factor when considering the toxicity of nanoplastics, as the higher the concentration, the more particles are available for aggregation/agglomeration (Gonçalves et al., 2022b; Chapter 3), shifting the overall particle size into the micro range. Thus, the bigger the particle aggregation, the less likely they are to cross cellular boundaries, whether the gonads or oocytes and spermatozoa. The biotransformation enzyme's activity, GST, also presented inhibition after exposure to PS-NPs in both male and female gonads, apart from increased activity on the 21st day, whereby gender differences are observed. This increase in activity was also noteworthy in the digestive glands of *M. galloprovincialis* exposed to 150 ng/L (21 days; 50 nm; Capolupo et al., 2021), though not in *M. galloprovincialis* exposed to 10 µg/L (21 days; 50 nm; Gonçalves et al., 2022b; Chapter 3). Oxidative damage in female mussels was significantly higher than in males after 14 and 21 days of exposure. The antioxidant system was overwhelmed by the presence of PS-NPs. Being that females need twice the lipid content as an energy source for gametogenesis, these levels of lipid peroxidation imply that the formation and liberation of viable oocytes into the water column for fecundity purposes are in jeopardy, leading to a possible decrease in the generation of future populations. The increase in oxidative damage was also seen in *M. galloprovincialis* gonads, without sex differentiation (50 nm; 10 µg/L; 21 days; Gonçalves et al., 2023; Chapter 2), as well as in other tissues ([50 nm; 150 ng/L; 21 days; Capolupo et al.,

2021] and [50 nm; 10 µg/L; 21 days; Gonçalves et al., 2022b; Chapter 3]). Thus, when gonads are chronically exposed, these effects may occur at an earlier stage throughout the gametogenic process, impairing the formation of viable oocytes and spermatozoa for release during reproductive periods, and further investigation is necessary to comprehend the severity nanoplastics can impose on the reproductive success of marine organisms. Additionally, an assessment of the exposure of nanoplastics at different gamete developmental stages will help unveil disparities in biomarker responses in both sexes, allowing the consideration of seasonal variation (Blanco-Rayón et al., 2020).

Considering mussels exposed to 5-FU, as a cytotoxic drug with a known mode of action being the misincorporation of its fluoro-nucleotides into DNA/RNA (Matuo et al., 2009), it is expected that inviable oocytes and spermatozoa arise from the gametogenic process, and that mal-formation of embryo-larval development occurs. Firstly, the antioxidant defence system in male gonads counterbalances any reactive oxygen species generated by 5-FU, as no oxidative damage is encountered; however, the opposite is observed in female gonads (Fig. 6.2. and 6.3.). The inhibition of SOD, CAT and GST observable at different times of exposure, as a consequence of the overwhelm of the antioxidant defence system in females, determine the oxidative damage increase at 21 days of exposure and is supported by the WOE. In other tissues of *M. galloprovincialis* (10 ng/L 5-FU; 21 days; Gonçalves et al., 2022a; Chapter 4), the exposure to 5-FU did not cause oxidative damage, whilst when analysing the gonads of *M. galloprovincialis* with no sex differentiation, this oxidative damage was observable after 7 days of exposure (10 ng/L; 21 days; Gonçalves & Bebianno, 2023; Chapter 5), whilst here the oxidative damage is significantly induced in females at 21 days. This suggests that the 5-FU's mode of action has a more severe effect on mussel gonads than other tissues and that 5-FU has a more severe effect on female gonads than males. Other pharmaceuticals evaluated with sex differentiation have been shown to have an endocrine-disrupting effect in the gonads of *M. galloprovincialis* (Gonzalez-Rey & Bebianno, 2012, 2013, 2014). Ibuprofen (250 ng/L; 15 days) had a more significant effect on male gonads, suggesting a possible impairment in mussels' reproductive fitness (Gonzalez-Rey & Bebianno, 2012), whereas diclofenac (250 ng/L; 15 days) exposure effects indicated alterations in the estrogenic activity and fluoxetine (75 ng/L; 14 days) and caused an inhibitory effect on alkali labile phosphate levels (Gonzalez-Rey & Bebianno, 2014). First and foremost, to comprehend the effects of 5-FU and other cytotoxic drugs, there is a need to evaluate protein expression with male and female differentiation exerting on the formation of oocytes and spermatozoa during the gametogenic stages and how this can affect their viability once released into the water column during the

reproductive stages. Moreover, further investigation into how the exposure of 5-FU affects marine biota is crucial with the increase in the use of this drug in chemotherapy treatments for breast, prostate, and colorectal cancer, as treatment and removal remain challenging for wastewater treatment plants.

As most contaminants end up in the ocean, the mixture of these two emerging contaminants is inevitable. A synergistic interaction between PS-NPs and 5-FU (Table 6.3.) suggests that there is an adsorption mechanism occurring, as seen before for other pharmaceutical compounds (Katsumiti et al., 2021; Zhou et al., 2021; Zhu et al., 2023), thus increasing the effects of 5-FU in the organism, as well as potentiating the entrance routes of 5-FU adsorbed onto PSNPs due to the nano-size range characteristic of these plastic particles, and facilitating the crossing of cellular boundaries (Peng et al., 2020). The antioxidant defence system's inhibitory effect is seen in male and female gonads exposed to the Mix, including oxidative damage. Therefore, results suggest that the Mix is highly potent and that in the gonads, both male and female mussels are compromised. Furthermore, the WOE supports that the Mix is majorly hazardous for both sexes at 21 days of exposure, suggesting that longer exposure times should be evaluated as, ultimately, the reproductive fitness of mussels may be impaired, jeopardising viable future generations and potentiating an unbalance in the ecosystem. Moreover, these effects can potentially reach humans through human shellfish batch consumption, as, to date, the removal/treatment in WWTPs remains difficult for these emerging contaminants. However, the adsorption mechanism between the pharmaceutical and nanoplastic may be a gateway to aid in developing methodologies to improve wastewater treatment plant protocols.

6.5. Conclusion

Emerging contaminants and their effects on the marine environment are gaining much attention; however, there is an urgent need to evaluate the effects on gender differentiation of marine organisms. This study provides evidence for the ingestion of PS-NPs being sex and time-specific, whereby females are the most compromised. Moreover, the data set provided here suggests that the complex mixture of nanoplastics and cytotoxic drugs, two emerging contaminants, are far more toxic than their counterparts, with a synergistic interaction calculated between them. The weighted elaboration biomarker results confirm that female mussels, compared to males, are majorly compromised at chronic exposure times, and this may lead to an impairment of robust oocyte formation throughout gametogenesis and affect reproductive success, with consequences for future generations. Nonetheless, males are also

majorly jeopardised by exposure to these emerging contaminants at acute and chronic exposure times, whereby spermatozoa motility and viability should be evaluated in future studies.

Overall, it is crucial to focus on how these emerging contaminants and others can affect marine organisms with sex differentiation and evaluate their possible effects on reproductive success to foresee the consequences they may bring on the whole ecosystem.

CHAPTER VII

Gender differences in protein expression after polystyrene nanoplastics exposure in mussels *Mytilus galloprovincialis.*

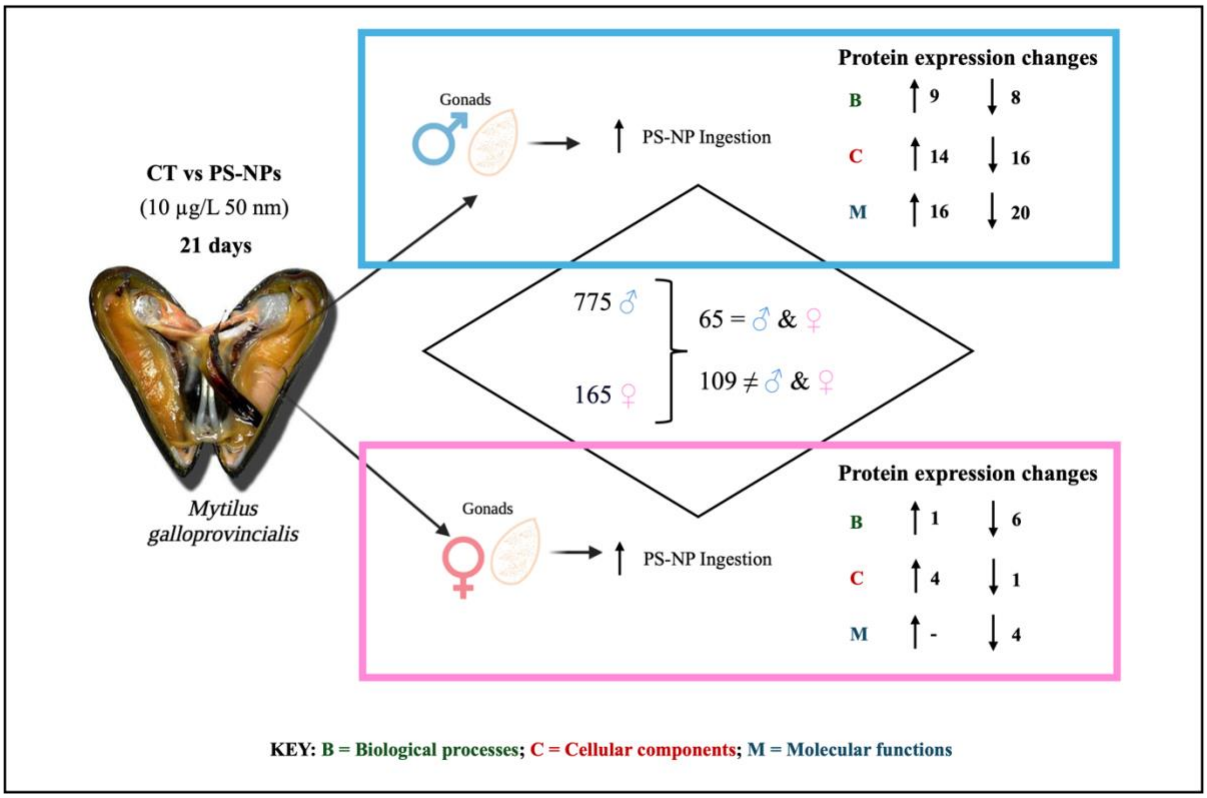

This chapter has been submitted to:

- The Journal of Hazardous Materials (February 2025)

Gonçalves, J. M, Mendes, V., Manadas, B., Bebianno, M.J. (*Submitted Feb 2025*). Gender differences in protein expression after polystyrene nanoplastics exposure in mussels *Mytilus galloprovincialis.* Journal of Hazardous Materials.

Abstract

Plastic pollution is a significant issue that the scientific community has been actively studying due to its harmful effects on aquatic ecosystems. Nanoplastics can pass through cellular barriers and enter the mussel's bloodstream. More worryingly, they can also penetrate sperm cells and oocytes, potentially impacting their motility and resilience. Reproductive success drives a shift in population dynamics and plays a vital role in maintaining a healthy ecosystem. Proteomics helps detect more protein changes caused by exposure to contaminants, such as nanoplastics, in marine organisms, providing deeper molecular-level insights into contamination-induced cellular pathways. Therefore, this study aimed to utilise a high-throughput proteomic approach to evaluate the impact of polystyrene nanoplastics (PS-NPs) on the gonads of male and female *M. galloprovincialis*, using a SWATH-MS analysis after 21 days of exposure to 10 µg/L of PS-NPs (50 nm). The accumulation of PS-NPs was also evaluated in male and female mussels. A comparison in protein expression of controls vs. those exposed in male and female mussel gonads and between males and females was evaluated. The findings indicate that PS-NP accumulation in male gonads alters protein expression more significantly than in females, interfering with protein synthesis, energy production, intracellular transport, and cellular homeostasis, possibly resulting in infertility. Female gonads exposed to PS-NPs revealed disruptions in proteins associated with translation, RNA processing and signalling, ribosome biogenesis, cell cycle regulation, and stress response. Protein folding, lipid metabolism, and calcium signalling pathways were also affected, leading to oogenesis, meiotic progression, intracellular transport, and energy metabolism impairments. These disruptions ultimately impact reproductive success and cellular homeostasis, leading to a decline in biodiversity.

7.1.Introduction

Plastic pollution is a significant problem the scientific community has been assessing because of its toxicity in aquatic ecosystems. A rise in global plastic production (400.3 Mt) was reported in 2022 compared to previous years; however, in Europe, there was a decrease of 1% compared to 2021 (PlasticsEurope, 2023). Nevertheless, despite programmes such as Operation Clean Sweep®, which promotes the containment of plastic pellets along the entire plastic value chain (www.opcleansweep.eu), plastics still find their way into the ocean. A particular concern is nanoplastics (NPs; < 100 nm), with concentrations ranging from 0.3 to 488 µg/L in seas, rivers, and nature reserves throughout Asia, Europe, Antarctica, and the

Arctic Ocean (Shi et al., 2024). Their small size and large surface area confer different toxic properties than larger plastic particles. In marine biota, NP toxicity is associated with reduced growth rates, energy and movement, stress, inflammation, and abnormalities (Kögel et al., 2020). Energy storage for processes such as gametogenesis is significantly influenced by food availability, and nanoplastics are misidentified as low-nutritional food sources by mussels (Wegner et al., 2012). NPs can cross cellular boundaries and enter the bloodstream of mussels, but more concerningly, they can invade spermatozoa and oocytes, potentially affecting motility and robustness. In the case of spermatozoa, specifically, NP contamination can lead to a decrease in sperm release, inhibition of sperm motility, and DNA damage (Lewis & Ford, 2012). This DNA damage can impair the sperm's ability to fertilise oocytes. The accumulation of NPs is gender- and time-specific in the marine mussel *M. galloprovincialis, with* more detrimental effects observed in females (polystyrene NPs [PS-NPs]; 10 µg/L, 28 days; Gonçalves et al., 2025; Chapter 6). A weight of evidence model confirms that NPs harm females under chronic exposure (Gonçalves et al., 2025; Chapter 6), potentially causing oocyte malformation, reducing successful fecundity, and leading to total developmental arrest during embryo-larval development (PS-NPs; 50 nm; 1.5 h; *Crassostrea gigas;* Tallec et al., 2018). Furthermore, a decrease in sperm motility, a reduction in sperm velocity, and unsuccessful embryogenesis in *C. gigas* was notable after exposure to PS-NPs with amine or carboxyl functional groups (1 h; 0.1-25 µg/mL; Tallec et al., 2020).

The Mediterranean mussel *Mytilus galloprovincialis* is found in high densities and relatively stable populations with a wide geographical distribution at different latitudes and adapted to various environmental parameters and stressors. As sessile filter-feeding organisms, mussels are capable of accumulating contaminants present, and any shift in populational dynamics can be a sign of the hazard of the presence of these contaminants. Gamete production and the energy that goes into it are essential for the reproductive success of mussels, such as *M. galloprovincialis,* as well as for larval survival and the recruitment of juveniles (Kautsky, 1982). Lipids are crucial, especially for female gonad development (Martínez-Pita et al., 2012), and play a key role in regulating the folding, organisation and final structure of all membrane proteins. Any interference or detour of energy to counterbalance any toxic effects from contaminants in the marine environment can cause unbalance and jeopardise gametogenesis and reproductive success. When ripe, mussels release spermatozoa and oocytes into the water column, where fertilisation occurs. In this sense, contaminants can interfere with the gametogenesis process and have toxic effects on the gametes released into the water column and larval development.

Reproductive success dictates the changes in populational dynamics and is crucial for a healthy ecosystem. Every species has its importance, and removing any level within the food chain can cause a massive downfall of biodiversity in a whole ecosystem. Therefore, understanding the effects of contaminants on species reproduction is vital to ensure that there will be future generations. A proteomic approach is crucial to acknowledge the impact that emerging contaminants, such as NPs, have at a biological, cellular and molecular level and the target toxicity they pursue. This approach enables the identification of a more significant number of protein alterations due to exposure to contaminants, like NPs, in marine organisms, giving access to a more excellent knowledge at a molecular level of those contamination-induced cellular pathways (López-Pedrouso et al., 2020).

In *M. galloprovincialis*, a male-associated polypeptide, MAP-39, was identified (Mikhailov et al., 1995). The expression of MAP-39 is associated with gonad development, maturation and spawning. The concentration of this polypeptide is 10% of total soluble proteins in mature male gonads, whilst only traces are attainable in female gonads (Mikhailov et al., 1995). In Zhong et al. (2020), an exposure to trichloropropyl phosphate (TCPP; 100 nmol/L; 42 days), a halogenated organophosphate ester widely used as flame retardants and plasticisers, 219 proteins were differentiated expressed between males and females *M. galloprovincialis*, where the gender-specific proteins were involved in protein synthesis and degradation, energy metabolism and the functions of the cytoskeleton and motor proteins. Proteomic responses after microplastic (MPs) exposure in the clam *Scrobicularia plana* caused cytoskeletal and cell structure alterations, disturbances in energy metabolism, oxidative stress, fatty acids, DNA binding and neurotransmission (polyethylene MPs [PE-MPs]; 11–13 µM; 1 mg/L; 14 days; Bebianno et al., 2022). With the adjacent BAP adsorbed onto MPs, a higher differentiation of protein expression was detected, where changes in glucose metabolism, RNA binding and apoptosis were also induced (Bebianno et al., 2022). *Mytilus edulis* exposed to high-density PE-MPs (25 µg/L; 0.5 – 330 µM) for 52 days caused alterations in the haemolymph proteome, and most proteins affected are involved in vital biological processes such as immune regulation, detoxification, metabolism and structural development (Green et al., 2019). Now, NPs induce more toxicity than MPs, causing more ROS production and higher total antioxidant capacity levels, with downregulation of specific genes involved in stress and immune response after transcriptomic sequencing in *Mytilus coruscus* (20 mg/L; PS-NPs 100 nm; PS-MPs 1 µM; Qi et al., 2023). As NPs are efficiently ingested by mussels (Qi et al., 2023), understanding the proteomic responses towards NP toxicity is of utmost importance. A SWATH-MS analysis

enables a deep proteome analysis by combining targeted and shotgun data extraction techniques (Anjo et al., 2015).

Therefore, this study aimed to use a high throughput proteomic approach to assess the effects of polystyrene NPs on the gonads of male and female *M. galloprovincialis*. To our knowledge, this is the first report about the effects of PS-NPs on mussel reproduction fitness.

7.2. Materials and Methods

7.2.1 Experimental Design

Firstly, Polysciences, Inc. (Germany) supplied Fluoresbrite® Plain YG spherical polystyrene nanoplastics (PS-NPs, 50 nm, CAS 9003-53-6). The hydrodynamic diameter of PS-NPs in seawater increases (852 ± 103 nm) as the salt present triggers aggregation/agglomeration kinetics. Additional information regarding PS-NP characterisation can be found in Gonçalves et al. (2022) (Chapter 3). Tanks were equipped with glass lids and aeration pipettes to prevent further plastic pollution, including airborne contamination. No gloves or plastic tools were used during tissue dissection.

Mussels, *M. galloprovincialis* (50 mm ± 5 mm), were collected from the Ria Formosa Lagoon in Southeast Portugal (37°00'30.6"N 7°59'39.6" W). They were cleaned and placed into 30 L tanks (25 L FSW) at two mussels per litre density in triplicate setups. Following a four-day acclimation, the mussels were exposed to 10 µg/L of PS-NPs for 21 days. Contaminants and seawater were refreshed every two days, with concentrations reset and samples taken in the beginning and after 21 days of exposure for PS-NP accumulation and proteomic analysis, where the mussels were dissected, gonads retrieved, followed by the determination of the sex for each sample. To achieve sex determination, an aliquot was examined using an optical microscope (Compound Light Microscopy) at 400× magnification to check for spermatozoa or oocytes. The samples were labelled appropriately and stored at -80°C to preserve them for further investigation.

7.2.2. PS-NP Accumulation

Using a fluorescence-based approach and the molecular rotor probe 9-(dicyanovinyl)-julolidine (DCVJ), the accumulation of PS-NPs was evaluated in mussel gonads subjected to 10 µg/L of PS-NPs, following the Gagné (2019) method. First, using a VWR Star-Beater, the male and female mussels' gonads were homogenised separately at 20% (w/v) in an ice-cold

buffer solution (50 mM NaCl, 10 mM Hepes-NaOH [pH 7.4], 1 mM EDTA, and 1 mM DTT) for 5 minutes while shaking at 20 rpm and utilising grinding balls. Samples were centrifuged for 20 minutes at 2°C and 15,000 *g* to isolate the cytosolic fraction. The supernatant was then promptly frozen at -80°C until it could be examined further. A Berthold Tristar 5 spectrofluorometric microplate reader was then used to analyse the samples, which had emission spectra from 400 to 800 nm and excitation at 450 nm**.** The wavelength of PS-NPs is 510 nm, and the outcomes have been compared with controls with the units of PS-NPs µg/g wet weight.

7.2.3. Sample preparation

Male and female gonads (n = 4 per sex and time) were homogenised in a Laemli solution (10% SDS, 30% glycerol, 0.6 M DTT, 0.012% bromophenol blue, and 0.5 M Tris HCl, pH 6.8). They were then sonicated slowly to prevent foam formation in a VWR Star-Beater (40 min, 5/s shaking, with grinding balls) and boiled at 95°C for 10 mins. The samples were then placed into labelled Eppendorf's and frozen at -80°C until further proteomic analysis.

7.2.4. LC-MS methodology

The total protein content was quantified using the Pierce™ 660 nm Protein Assay Kit (Thermo Scientific™). One pooled sample was prepared for each condition containing 70 µg of protein for the ion library generation. For relative protein quantification experiments (SWATH), 50 µg of protein from each sample was used for the following steps. An internal standard solution was added to each sample (including the pooled samples) containing green fluorescent protein (GFP) and Maltose/maltodextrin-binding periplasmic protein (MALE). After the denaturation step at 95°C for about 5 minutes, the protein content was separated by SDS-PAGE for about 17 minutes at 110 V (Short-GeLC Approach) (Anjo et al., 2015) and stained with Coomassie Brilliant Blue G-250. Each lane was divided into three separate gel fractions (5 fractions in pooled samples) for the destaining step using a 50 mM ammonium bicarbonate solution with 30% acetonitrile, followed by overnight protein digestion with trypsin. Peptide extraction from the gel was performed by incubating solutions containing different percentages of acetonitrile (30, 50, and 98%) with 1% formic acid. For protein identification, the five fractions were evaporated in a vacuum centrifuge, resuspended in 25 µL

of 2% ACN with 0.1% FA, and 10 µL were analysed by data-dependent acquisition (DDA). For relative protein quantification, the 3 fractions from each sample were joined, evaporated in a vacuum centrifuge, resuspended in 40 µL of 2% ACN with 0.1% FA, and 10 µL were analysed by data-independent acquisition (DIA/ SWATH-MS). Samples were analysed on a NanoLC™ 425 System (Eksigent) coupled to a Triple TOF™ 6600 mass spectrometer (Sciex) and the ionisation source (ESI DuoSpray™ Source). The chromatographic separation was performed on a Triart C18 Capillary Column 1/32" (12 nm, S-3µm, 150 × 0.3 mm, YMC) and using a Triart C18 Capillary Guard Column (0.5 × 5 mm, 3 µm, 12nm, YMC) at 50°C. The flow rate was set to 5 µL/min, and mobile phases A and B were 5% DMSO plus 0.1% formic acid in water and acetonitrile, respectively. The LC program was performed as follows: 5 – 30% of B (0 - 50 min), 30 – 98% of B (50 - 52 min), 98% of B (52 - 54 min), 98 - 5% of B (54 - 56 min), and 5% of B (56 - 65 min).

The ionisation source was operated in the positive mode set to an ion spray voltage of 5500 V, 25 psi for nebuliser gas 1 (GS1), 10 psi for nebuliser gas 2 (GS2), 25 psi for the curtain gas (CUR), and source temperature (TEM) at 100°C. For data-dependent acquisition (DDA) experiments, the mass spectrometer was set to scanning full spectra (m/z 350-1500) for 250 ms, followed by up to 100 MS/MS scans (m/z 100 – 2000) with 30 ms for the accumulation time. Candidate ions with a charge state between +1 and +5 and counts above a minimum threshold of 100 counts per second were isolated for fragmentation, and one MS/MS spectrum was collected before adding those ions to the exclusion list for 15 seconds (mass spectrometer-operated by Analyst® TF 1.8.1, Sciex®). The rolling collision energy was used with a collision energy spread of 5. For SWATH experiments, the mass spectrometer was operated in a looped product ion mode and precisely tuned to a set of 168 windows, covering the precursor mass range of 350-2250 m/z. A 50 ms survey scan (350-2250 m/z) was acquired at the beginning of each cycle, and SWATH-MS/MS spectra were collected from 100-2250 m/z for 19 ms, resulting in a cycle time of 3.29 seconds.

7.2.5 Ion-library from DDA information

A specific ion library of the precursor masses and fragment ions was created by combining all pool files in one protein identification search using the ProteinPilot™ software (v5.0, Sciex). The parameters of the paragon method were cysteine alkylation by acrylamide, digestion by trypsin, and gel-based ID. The protein identification search was conducted against the *Mytilus*

galloprovincialis database (UniProt), downloaded in May 2024. An independent False Discovery Rate (FDR) analysis, using the target-decoy approach provided by Protein Pilot™, was used to assess the quality of the identifications.

7.2.6 Relative quantification of proteins (SWATH-MS)

SWATH data were processed by the SWATH™ processing plug-in for PeakView™ (v2.0.01, Sciex®). Protein relative quantification was performed in all samples using the information from the protein identification search. Peptide relative quantification was obtained considering the FDR < 1% for at least three replicates in at least one of the conditions and by the sum of up to 5 fragments/peptide. Peptide relative peak areas were normalised for the total sum of fragment areas for the respective sample, and protein quantities were obtained by the sum of up to 15 peptides/protein.

7.2.7. Statistical analysis

Statistical analysis was conducted in MetaboAnalyst 6.0 (www.metaboanalyst.ca). The two-group comparisons were performed using the non-parametric Wilcoxon rank-sum test to select proteins with *p*-values below 0.05. Heatmap representations were performed considering the Euclidean distance and the Ward clustering algorithm. Venn diagrams were generated in the SRplot (Tang et al., 2023) platform using the module "proportional Venn" and jvenn (Bardou et al., 2014) for more than three groups. The functional analysis was performed by DAVID (Sherman et al., 2022; Huang et al., 2009) using the *Mytilus galloprovincialis* database as background. The enriched GO terms were represented for the number of genes by Heatmaps generated in the platform ImageGP (Tong Chen & Huang, 2022).

7.3. Results and discussion

7.3.1. PS-NP accumulation

After 21 days of exposure, the accumulation of PS-NPs in mussel female gonads is higher than in male gonads (*see* Table 7.1). This accumulation may weaken mussels' immune systems and cause additional prejudice towards gamete production, embryo-larval development and fertilisation (Tallec et al., 2018; Capolupo et al., 2021; Gonçalves et al., 2022, 2025) (Chapter 3, 6). After internalisation of PS-NPs, a decrease in fertilisation rate was

observed in oysters *Crassostrea gigas* (50 nm; 10 µg/L; 50 nm; 1.5 h; Tallec et al., 2018), as well as a reduction in sperm motility and the formation of PS-NPs agglomerates on jelly-coatings of oocytes as a result of PS- NPs exposure (PS-COOH and PS-NH_2; 0.1–100 mg L^{-1}; 1, 3, and 5 h; Gonzalez-Fernandez et al., 2018). Additionally, deformities in larval development have also been recorded in *M. galloprovincialis* (PS-NH_2; 50 and 100 nm; 10 µg/L; 48 h post fertilisation, Auguste et al., 2021), and the smaller PS-NPs have a more detrimental effect, whereby larvae exposed to PS-NH_2 nanoplastics demonstrate disruption of the molecular processes involved in shell formation (Auguste et al., 2021). PS-NP accumulation here is positively related to other outcomes analysed in Gonçalves et al. (2025) (Chapter 6), such as lipid peroxidation. Widespread cellular dysfunction brought on by PS-NP accumulation by male mussel gonads inhibits vital biological functions (protein synthesis, transport, energy metabolism, etc.). The harmful effects of oxidative stress and NP buildup cause this chain reaction of disturbances, making it more difficult for cells to maintain homeostasis and finish vital functions like reproductive and gonadal health. The cell manages the damage by upregulating stress adaption systems, such as antioxidants. However, stress can result in cell death or inability to reproduce if it surpasses the cell's ability to heal itself, causing impairment of spermatozoa motility and ability to fecund oocytes (Tallec et al., 2018; Gallo et al., 2021).

Table 7.1. Ingestion of PS-NPs (µg/g wet weight) relative to controls in male and female gonads of *M. galloprovincialis* after 21 days of exposure (mean ± std).

Time of exposure (days)	**PS-NPs µg/g wet weight**	
	♂	♀
0	1 ± 1	1 ± 1
21	1.78 ± 0.16	4.45 ± 0.10

Moreover, when female mussel gonads ingest PS-NPs, important cellular functions necessary for healthy cell function and reproduction are severely disrupted. Gonadal function and oocyte development are probably impacted when vesicle-mediated and intracellular protein transport is inhibited since this affects the distribution of vital proteins and organelles. Furthermore, genes essential for gonadal health, reproduction, and cell division are not properly expressed when mRNA processing and protein synthesis are disrupted. Also, spindle organisation and chromosome segregation, essential for meiosis and fertilisation, are hampered by microtubule malfunction, resulting in genomic instability and unsuccessful reproduction. Therefore, female mussels' ability to reproduce can be jeopardised by the combined impacts of

oxidative stress, protein degradation, and cellular dysfunction, leading to problems with oocyte viability and fertility. (Gallo et al., 2022; Zhang & Wu, 2023)

7.3.2. Protein relative quantification

Unexposed proteins of male and female gonads, as well as those differentially expressed because of exposure to PS-NPs, allowed the identification of 3865 proteins (considering 5% FDR against the *Mytilus galloprovincialis* from Uniprot), and 2128 proteins were further quantified. The list of proteins quantified is found in the supplementary material, Table S1. The exposure of male and female gonads to PS-NPs significantly altered the proteome of both genders ($p< 0.05$; Figures 7.1.- 7.4.). The Venn diagram (Figure 7.1.) shows the proteins differentially expressed in control males and females, between control and PS-NPs exposed males, between control and PS-NPs exposed females, between control male and female gonads, and between PS-NPs exposed male and female gonads, as well as the protein common among treatments and sex gonads ($p< 0.05$). As can be seen from Figure 1, the number of differentially expressed proteins was more significant in male gonads than in females after exposure to PS-NPs ($p< 0.05$). The differentially expressed proteins in male and female controls exposed to PS-NPs were hierarchically clustered, and heat maps of both conditions showing differential proteins up or down-regulated are presented in Figure 7.2. When mussels were exposed to PS-NPs, 775 proteins changed between controls and PS-NPs exposed male gonads ($p< 0.05$; Figures 7.1.- 7.2.A), while only 156 proteins were differentially expressed between controls and PS-NPs female gonads. ($p< 0.05$; Figures 7.1.- 7.2.B). Among these proteins, 65 were similar between male and female gonads ($p< 0.05$). However, when proteins were compared between control male and female gonads, 109 proteins were different ($p< 0.05$; Figures 7.1.- 7.3.A), but when exposed to PS-NPs, 118 proteins were differently expressed between male and female gonads ($p< 0.05$; Figure 7.3.B) with eight of these proteins similar between controls and PS-NPs exposed male and female gonads ($p< 0.05$). In zebrafish exposed to PS-NPs (1.0 mg L^{-1} for 21 days) of similar size (50 nm, 1 mg L^{-1}), NPs influence reproductive toxicity that is gender-specific (Li et al., 2024). When zebrafish are exposed to PS-NPs (70 nm), NPs can pass the blood barrier and accumulate in the gonads (Li et al., 2024). Zebrafish submitted to acute exposure of the same type of PS – NPs but with a smaller size (40 nm; 5 mg L^{-1}, 96h), NPs were able to penetrate the testicular barrier and be internalised in germ cell lines (Pujol et al., 2025). The exposure to high-density polyethylene (HPDE) microplastics also induced changes in the proteome of the haemolymph of *Mytilus edulis* (Green et al., 2019).

Gene Ontology (GO) enrichment analysis shows differences in protein expression related to putative biological processes (BP), cellular components (CC) and molecular functions (MF) between unexposed and PS-NPs exposure mussel male and female gonads (Figure 7.4.).

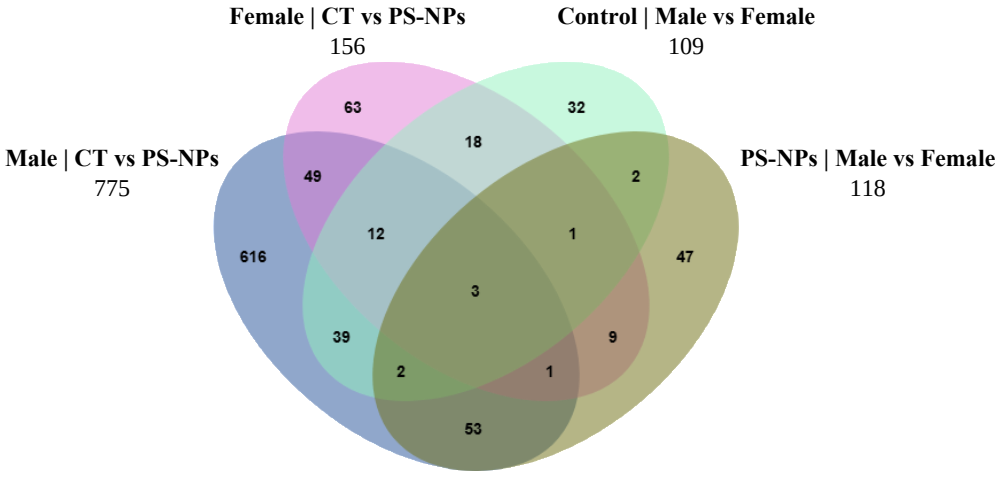

Figure 7.1. Venn diagram showing the number of specific and common differential proteins between controls (CT) vs PS-NPs contaminated gonads in male and female *M. galloprovincialis*, and male vs female *M.galloprovincialis* for CT and PS-NPs contaminated gonads after 21 days of exposure (Wilcoxon rank-sum test) (p<0.05).

7.3.3. Impact of PS-NP exposure on the proteome of unexposed and exposed mussel male gonads

GO analysis revealed that in control mussel male gonads compared to those exposed to PS-NPs, NPs affected proteins related to biological processes (9 proteins being upregulated and 8 proteins down-regulated) (p< 0.05; Figure 7.4.). In comparison, 14 proteins of the cellular components were upregulated, and 16 were downregulated (p< 0.05; Figure 7.4.). Regarding proteins related to molecular functions, 16 proteins were upregulated, and 20 proteins were downregulated (p< 0.05; Figure 7.4.).

The inhibition of these differentially expressed proteins because of the exposure to PS-NPs compared to control male gonads leads to changes in the following pathways: translation and ribosome biogenesis, protein folding and quality control, intracellular transport and vesicle trafficking, energy metabolism, RNA processing and tRNA charging, protein degradation, cytoskeletal dynamics and stress adaptation mechanisms. The reduction of the translation and maturation of LSU-rRNA affects the formation of the ribosome-mRNA complex, reducing protein synthesis, ribosomal assembly, and energy production. Other stress conditions, such as unfolded protein response, changes in cytoskeleton dynamics, oxidative damage and apoptosis,

can also occur. The inhibition of these proteins can severely compromise the ability of male mussel gonads to develop functional sperm, potentially leading to infertility. In the Pacific oyster *C. gigas* exposed to PS microplastics (6 µm; 0.023 mg L^{-1}), Sussarellu et al. (2016) showed that the exposure to this type of microplastics induced a decrease in the velocity of the sperm, compromising the ability to fertilise the oyster oocytes.

On the other hand, these interrelated processes represent the cell's integrated response to stress, particularly oxidative stress. In male mussel gonads exposed to PS-NPs (50 nm; 10 μgL^{-1}; 21 days; Gonçalves et al., 2025; Chapter 6), a significant increase in superoxide dismutase (SOD) and glutathione-S-transferase (GST) activity and a decrease in lipid peroxidation (LPO) were registered. Therefore, the cellular slowdown or inhibition of specific functions (like translation, ribosome biogenesis, and energy metabolism) can activate a protective antioxidant response, with increased SOD and GST activity and a reduction in LPO as part of the defence mechanism.

However, the upregulation of these proteins in male gonads induced changes in the following pathways: energy production microtubule-based processes, chromatin remodelling and DNA packaging, electron transport and oxidative stress response, nucleotide biosynthesis and motility and cell projection enhancing the need for energy and structural demand for spermatogenesis and sperm functionality. Moreover, the upregulation of the tricarboxylic acid cycle (TCA cycle), glycolysis, and mitochondrial electron transport chain and the induction of pyruvate dehydrogenase and acetyl-CoA biosynthetic processes highlights the need for high energy demand required for spermatogenesis and sperm motility.

When energy production is upregulated, cells may also need to upregulate their antioxidant response to counterbalance the oxidative stress induced by increased mitochondrial activity, explaining the observations detailed in Gonçalves et al. (2025) (Chapter 6) after male mussels were exposed to PS-NPs (10 µg/L of 50 nm for 21 days). Additionally, microtubules are essential for intracellular transport, cell division, and motility. Microtubule dynamics may be impacted by cell oxidative stress, which can interfere with motility and appropriate intracellular transport. However, as cells rearrange their cytoskeleton to support proper function under challenging circumstances, enhanced microtubule-based processes (such as polymerisation or stabilisation) may also be a stress reaction (Gurel et al., 2014). A stronger antioxidative response, including the increase of SOD and GST activity, may result from stimulation of microtubule dynamics in response to stress or energy needs (Dalle-Donne et al., 2001; Apraiz et al., 2006).

Nevertheless, energy generation, chromatin remodelling, microtubule-based processes, and other cellular functions are upregulated in response to stress and increased metabolic demand, which may increase ROS production. Cells respond to oxidative stress by increasing the activity of GST to detoxify lipid peroxidation products and other reactive intermediates and SOD to neutralise superoxide radicals formed. By maintaining membrane integrity and lowering LPO, this cellular adaptation ensures that vital functions like motility, DNA repair, and nucleotide biosynthesis run smoothly. Therefore, under stress, these systems' coordinated activation helps maintain homeostasis, prevent cellular damage, and manage the oxidative burden (Rangaswamy et al., 2024). In zebrafish (*Danio rerio)* males exposed in water to an acute concentration of PS-NPs (45 nm; 5 mg L^{-1} for 96h), NPs were able to penetrate the internal barrier of the spermatozoids and be internalised in germ cells, inducing the upregulation of several genes related to meiotic chromosomal assembly double-strand break and chromatic formation affecting sperm mobility (Pujol et al., 2025). Similarly, exposure for 28 days to PS-NPs (25, 50 and 100 nm; 5 mg ml^{-1}) indicates that PS-NPs decrease sperm concentration and viability and increase sperm abnormalities (Ma et al., 2024). Moreover, PS-NPs disrupt spermatogenesis in the testicular of male mice by inhibiting the expression of Pmfbp1/Ggn/Fsip2 and enabling Hsd3b5 protein expression to reduce dihydrotestosterone levels and affect sperm flagellar assembly by decreasing the expression of *Dnah8*/*Tekt5*/*Rsph6a* and the claudin family by destroying the tight junctions (Ma et al., 2024). PS-NPs also induce the expression of cathepsins (B/F/H), indicating that exposure to PS-NPs induces testicular cell apoptosis (Ma et al., 2024). However, in the present case, possible apoptosis needs to be confirmed.

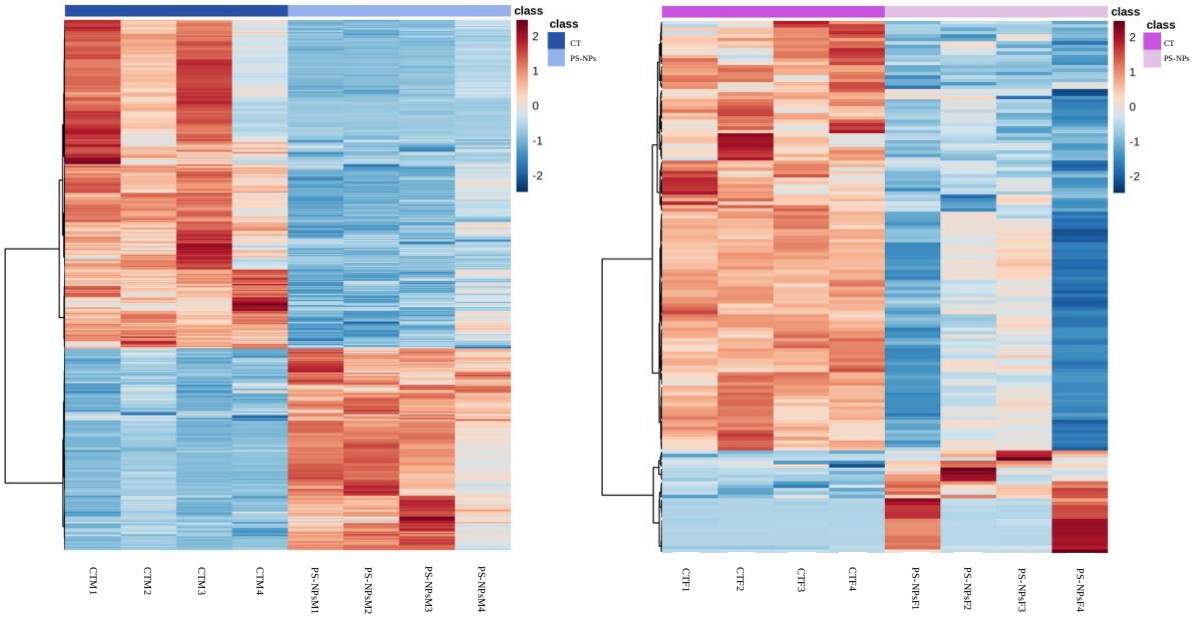

Figure 7.2. Heatmap of the 775 proteins differentially expressed (**A**) in male gonads and 156 proteins differentially expressed (**B**) in female gonads between controls (CT) and PS-NPs mussels exposed for 21 days (Wilcoxon rank-sum test) (p<0.05)

7.3.4. Impact of PS-NP exposure in non-exposed and exposed mussel female gonads

Opposite to the effect of NPs in mussel male gonads, the exposure of mussel female gonads to PS-NPs compared to controls induced fewer protein changes at BP, CC and MF levels (Figure 7.4.). This might be related to the variability observed in the gonads of mussel females exposed to PS-NPs. The exposure to PS-NPs induced changes in seven proteins involved in BP, six of which were downregulated, and one was upregulated, while with CC, four proteins were up-regulated. At the same time, only one was down-regulated, and four proteins related to MF were down-regulated (p< 0.05). Pujol et al. (2025) also found that in zebrafish (*Danio rerio*) exposed for 96h to a toxic concentration of the same type of NP (45 nm; 5 mgL^{-1} of), oocytes were not as severely affected by PS-NP exposure as the male gonads. This indicates that PS-NPs have a different impact on oocytes.

The exposure of mussel female gonads to PS-NPs inhibited the following proteins: vesicle-mediated transport, mRNA processing, establishment or maintenance of microtubule cytoskeleton polarity, intracellular protein transport, spindle organisation and microtubule polymerisation. Vesicle-mediated transport is crucial for the movement of proteins and lipids within the cell, especially between organelles like the endoplasmic reticulum (ER) and Golgi apparatus, and its inhibition could disrupt oocyte development by altering hormone signalling, nutrient storage, and protein secretion. The inhibition of mRNA processing affects gonad development and oocyte maturation by preventing protein translation required for cellular

function. The establishment or maintenance of microtubule cytoskeleton polarity is essential for the maintenance of cell shape, intracellular transport, and cell division. The inhibition of this protein disrupts cell division and positioning of organelles during oogenesis. The downregulation of intracellular protein transport disrupts energy production, meiotic progression, and hormone biosynthesis, and the inhibition of spindle organisation can lead to aneuploidy in oocytes, reduce fertility or cause developmental abnormalities in offspring. Moreover, inhibiting microtubule polymerisation by exposure to PS-NPs could impair meiotic progression, disrupt vesicle transport, and lead to oocyte or gonadal cell dysfunction. On the other hand, nucleosome assembly was induced to enhance the formation or restoration of nucleosomes, which can have several implications in different pathways, namely chromatin remodelling, gene transcription, and DNA damage repair. So, exposure to PS-NPs severely affects the meiotic cell cycle, cytoskeleton regulation, vesicle transport, mRNA processing, and hormonal signalling pathways.

The inhibition of these proteins affects the cytoskeleton organisation and dynamics, disrupting spindle formation and intracellular transport that are critical for oocyte maturation. The intracellular transport, vesicle-mediated transport pathway, spindle organisation, and chromosome segregation induce impaired spindle assembly that could disrupt meiosis. The inhibition of the energy metabolism and ATP-dependent processes pathway affects the ATPase and proton transport, which are critical for energy supply during oocyte development. The disruption of the GTPase-mediated signalling pathway affects the GTP-binding proteins that regulate vesicle trafficking and cytoskeleton assembly. GTPase activity activates the MAPk/ERK signalling pathway, which is involved in cell growth and differentiation and regulates actin polymerisation. Moreover, microtubule plus-end binding is crucial in cellular processes like mitosis, transport and cell shape maintenance. The impaired aminopeptidase activity could hinder protein turnover necessary for cellular remodelling, inducing changes in the aminopeptidase activity and protein degradation pathway. In Gonçalves et al. (2025) (Chapter 6), female gonads exposed to PS-NPs (50 nm; 10 μgL^{-1}; 21 days), the exponential increase in SOD, catalase (CAT), and GST activities did not prevent LPO. Cellular stress is caused mainly by disrupting protein homeostasis, organelle function, and DNA integrity caused by suppressing vesicle-mediated transport, mRNA processing, microtubule dynamics, protein transport, and spindle organisation. Reactive oxygen species (ROS) produced by these disturbances lead to oxidative stress. Antioxidant defence mechanisms, such as SOD, CAT, and GST, are upregulated by the cell to counteract ROS and detoxify reactive compounds (Gonçalves et al., 2025; Chapter 6).

Nevertheless, despite these efforts, LPO levels rise, indicating continuous oxidative damage, especially to cell membranes susceptible to ROS damage. The image shows a stressed cell strengthening its antioxidant defences to compensate for various dysfunctions. However, female gonads still suffer severe oxidative damage (Gonçalves et al., 2025; Chapter 6).

The exposure of PS-NPs in mussel female gonads induced an upregulation in the nucleosome assembly, which is involved in the deposition of histones onto DNA to form nucleosomes, the basic unit of chromatin that was also induced, highlighting the need for histone synthesis to package replicated DNA during oocyte maturation. The upregulation of nucleosome assembly and related proteins suggests enhanced chromatin remodelling, transcriptional regulation, and genome stability processes. These changes are pivotal for oocyte maturation, meiosis, and preparation for fertilisation. The increase in SOD, CAT, GST activity and LPO levels observed in female gonads exposed to PS-NPs for 21 days (50 nm; 10 μgL^{-1}; Gonçalves et al., 2025; Chapter 6) are indicators of oxidative stress caused by the exposure. The cell upregulates nucleosome assembly and associated proteins involved in DNA packing and chromatin remodelling in response to oxidative damage. This implies that to maintain healthy oocyte maturation and genome integrity, the cell is trying to shield its genome from the harmful effects of ROS and lipid peroxidation. While the upregulation of histone production and nucleosome assembly emphasises the cell's attempt to stabilise and repair the genome under this stressful exposure, the rise in antioxidant enzyme activity is part of the cell's attempt to combat oxidative damage (Pérez-Cremades et al., 2023).

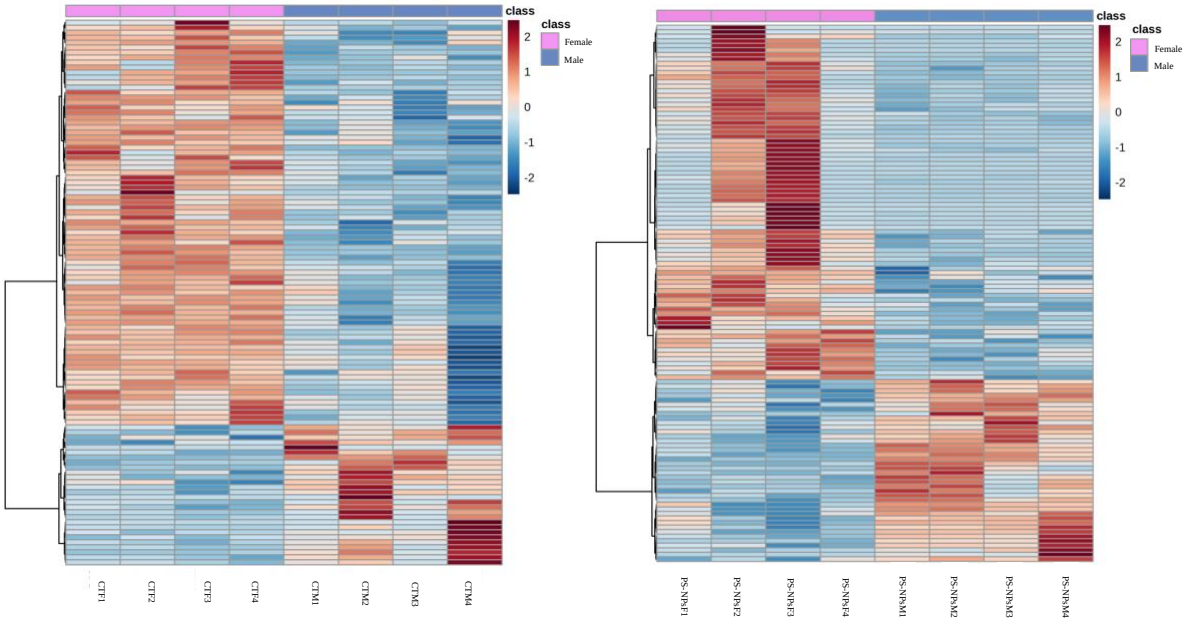

Figure 7.3. Heatmap of 109 proteins differentially expressed (**A**) between control male and female gonads and of 118 proteins differentially expressed (**B**) between PS-NPs exposed male and female gonads after 21 days of exposure (Wilcoxon rank-sum test) (p<0.05)

7.3.5. Differences in protein expression between mussels' male and female gonads exposed to PS-NPs

When comparing differential protein expression between mussel male and female gonads, three GO terms were expressed in males associated with the molecular function of the proteins namely: GTPase activity, GTP binding and ferric iron binding (p< 0.05; Figure 7.4.). GTPase activity controls processes that underline gametogenesis and maturation. At the same time, GTP binding hydrolysis into GDP regulates various molecular functions in the gonads, while ferric iron binding is related to cellular respiration, DNA synthesis and enzyme function. These proteins are indispensable for the metabolic and enzymatic processes needed for successful reproduction in mussels.

When male and female gonads were exposed to PS-NPs, six proteins were up-regulated in male mussels, namely, fucose metabolic process, alpha-L-fucosidase activity, lipid transporter activity, hydrolase activity, structural constituent of cytoskeleton, and cysteine-type peptidase activity (p< 0.05; Figure 7.4). This indicates that exposure to PS-NPs increases the fucosylation of proteins and lipids, enhancing cell communication and the immune system. On the other hand, alpha-L-fucosidase activity catalyses the hydrolysis of alpha-L-fucoside bonds, breaking down fucosylated glycoconjugates and causing lysosomal stress. In addition, the up-regulation of lipids transport activity and hydrolase activity increases energy production and membrane

synthesis. On the other hand, the structural constituent of cytoskeleton proteins maintains and regulates the structure and dynamics of the cytoskeleton (e.g., actin, tubulin) and its up-regulation promotes immune responses. Regarding cysteine-type peptidase activity, caspases and cathepsins use a cysteine residue to cleave peptide bonds and induce apoptosis.

On the other hand, PS-NP exposure induces the downregulation of the nitrogen compound metabolic process, nucleosome, structural constituent of chromatin and protein heterodimerisation activity ($p< 0.05$; Figure 7.4.). The downregulation of the nitrogen compound metabolic process involves the breakdown and recycling of nitrogen-containing compounds, like amino acids and nucleotides, impairing the amino acid metabolism, reducing growth and nucleotide synthesis and weakening cellular repair mechanisms by impacting DNA replication and RNA transcription, slowing cell proliferation and repair. The nucleosome and structural constituent of chromatin are the basic structural units comprising transcription and DNA wrapped around histone proteins. These two proteins are essential to organise and regulate DNA accessibility for replication and repair into a compact and functional structure of the cells. In male *D. rerio* gonads exposed to an acute concentration of PS-PNs (50 nm, 5 mg l^{-1}) for 96 h, abnormal sperm and clustering chromatin compact was observed that result in viable spermatozoids but with reduced motility that could lead to functional impairment that may be the result of oxidative stress and DNA damage (Pujol et al., 2025). Gene expression involved in reproduction and chromatin remodelling was also observed in *D. rerio* testis as well as in the immune system, indicating that PS-NPs induce an increase in the immune response to cope with the phagocytosis of this type of NP (Pujol et al., 2025). The downregulation of these proteins in male gonads due to PS-NP exposure can lead to DNA damage, mutations, and chromosomal abnormalities. In addition, the downregulation of protein heterodimerisation activity can affect cell growth and immune response and induce apoptosis. In male *D. rerio,* exposure to acute toxic concentrations of NPs (40 mn) induces caspase-3 levels, indicating that apoptosis occurred in prophase I (Pujol et al., 2025). These results indicate similar responses to the effects of PS-NPs at the genome and proteome level in zebrafish and *M. galloprovincialis* male gonads.

In summary, the exposure of PS-NPs in male gonads induces significant changes in the differential expression of these proteins, leading to an increase in energy production and immune responses, alterations in lipid metabolism and carbohydrate pathways, DNA damage, as well as apoptosis. The elevated levels of these proteins in male mussel gonads reflect the physiological and reproductive demands of continuous sperm production, chromatin

compaction, gamete motility, and metabolic regulation, responding to the effects induced by exposure to PS-NPs, which is more pronounced in males.

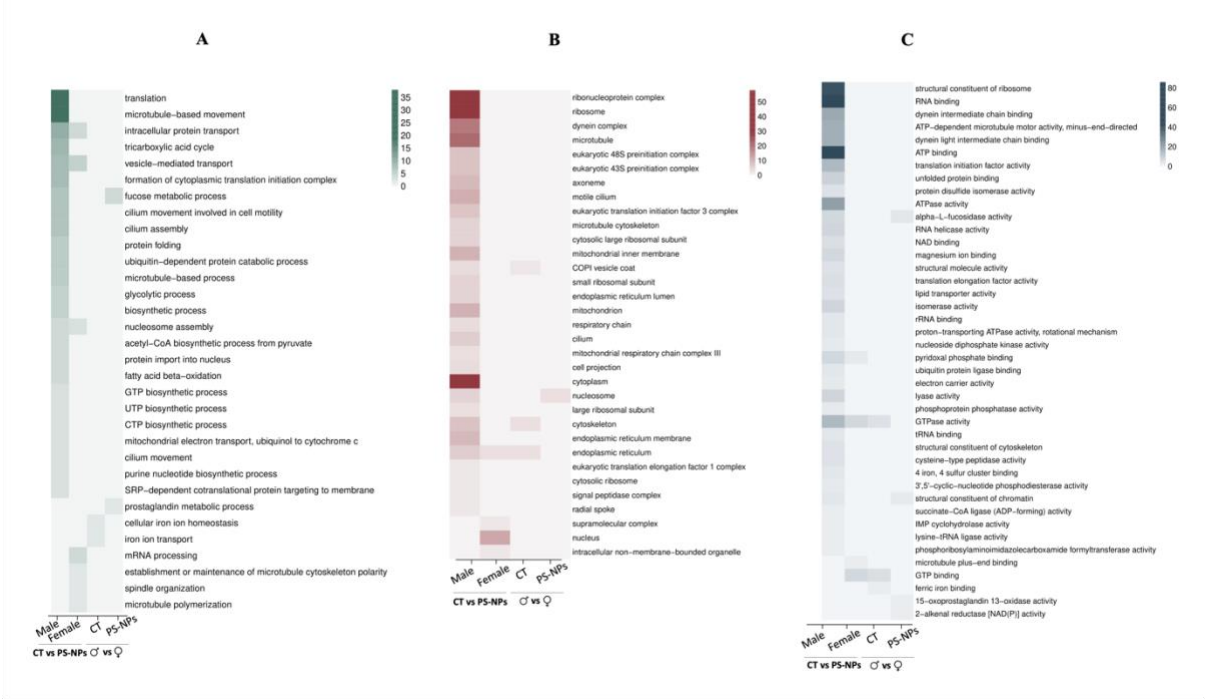

Figure 7.4. Functional identification in *M. galloprovincialis* gonads identified by DAVID GO enrichment analysis of (**A**) biological processes, (**B**) cellular components and (**C**) molecular function between controls and PS-NPs exposed mussels.

7.4. Conclusion

A quantitative proteomic analysis was conducted to assess the effects of PS-NPs in *M. galloprovincialis* male and female gonads. The results suggest that the accumulation of PS-NPs in male gonads affects more protein expression than in females, disrupting protein synthesis, energy production, intracellular transport, and cellular homeostasis, potentially leading to infertility. Regarding the effects of PS-NPs in female gonads, proteomic analysis revealed that exposure to PS-NPs disrupts proteins that are related to translation, RNA processing and signalling, ribosome biogenesis, cell cycle, and stress response, protein folding, lipid metabolism, and calcium signalling pathways impairing oogenesis, meiotic progression, intracellular trafficking, and energy metabolism affecting the reproductive success and cellular homeostasis. Therefore, with the increase of NPs expected to occur in the ocean, there is an urgent need to reduce the presence of NPs in the ocean because this emerging contaminant may be an additional source that can induce biodiversity loss.

CHAPTER VIII

Nanoplastic effects on spermatozoa, oocytes and larval development of the Mediterranean mussel *Mytilus galloprovincialis*

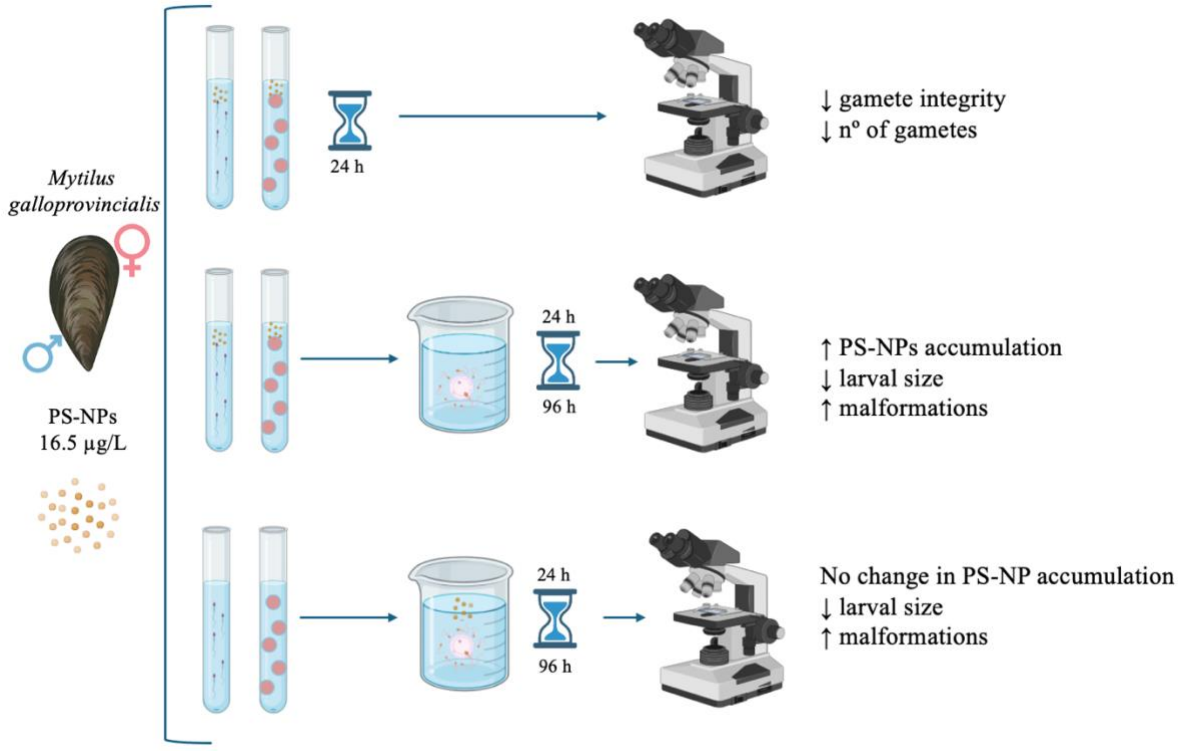

Abstract

Most bivalve species rely on external fertilisation for reproduction in the marine environment. Consequently, numerous risks threaten gametes and early life stages. Due to their increased surface area-to-volume ratio and potential ability to cross biological barriers, nanoplastics may pose greater dangers to marine life. Understanding the toxicity of these particles and their impact on successful reproduction is vital, as it can influence the survival of future generations and the equilibrium of entire ecosystems. This study aims to investigate the risks of exposure to PS-NPs (16.5 µg/L) for *Mytilus galloprovincialis* spermatozoa and oocytes prior to fertilisation, the detrimental effects on embryo-larval development following gamete exposure, and the consequences of exposure to PS-NPs (16.5 µg/L) post-fertilisation on embryo-larval development at 24- and 96-hours post-fertilisation (hpf). After 96 hpf, the effect of the PS-NPs was assessed in both exposure scenarios. The number of oocytes and spermatozoa decreased significantly, and the integrity of oocytes was compromised. Furthermore, larval development was adversely affected, particularly when gametes were exposed prior to fertilisation, leading to smaller and malformed larvae, with a higher accumulation observed in gametes than embryos.

8.1. Introduction

Nanoplastics (NPs; <1000 nm) and their effects on marine organisms are gaining a vast array of interest, as these tiny particles (<1000 nm) can potentially pass through biological barriers and, by having a higher surface area-to-volume ratio, are potentially more harmful and hazardous towards marine organisms than microplastics (1µm – 5mm) (Sharma et al., 2023). Although quantifying NPs in the environment remains challenging, they can enter the environment as primary or secondary NPs, entering the ocean in their manufactured small size or from degradation and mechanical abrasion of larger plastic particles, respectively. Global plastic production rose to 413.8 Mt in 2023, increasing from previous years. In contrast, Europe experienced a 4.7 Mt decline compared to 2022 (PlasticsEurope, 2024). Polystyrene (PS) accounts for 5.2% of the total global plastic production (PlasticsEurope, 2024), and primary PS-NPs are intentionally manufactured for use in scientific research to calibrate scientific instruments, as well as fluorescently labelled to evaluate absorption across biological membranes (Catarino et al., 2019). Among day-to-day products, PS can be found in CDs, Styrofoam cups and plates, toothbrushes, toys, food storage, etc. (Kik et al., 2020). To date, no studies have indicated the carcinogenic potential of PS-NPs; however, the PS monomer

(styrene) has been classified by the International Agency for Research on Cancer (IARC) as a potentially carcinogenic substance (B2). NPs are surrounded by a "protein corona" that allows them to penetrate cellular membranes and interact with cellular structures (Canesi et al., 2016; Auguste et al., 2021; Kik et al., 2022), increasing the potential toxicity of these particles. Bivalves, such as mussels, are excellent sentinel organisms for ecotoxicological studies and have shed some light on the effects NPs can have. Studies have shown that NPs lead to cytotoxicity, genotoxicity, neurotoxicity, oxidative stress and damage in the gills, digestive glands, and gonads of mussels (Capolupo et al., 2021; Gonçalves et al., 2022, 2023, 2025; Gonçalves & Bebianno, 2023) (Chapters 2, 3, 5 and 6). For example, exposure to PS-NPs at a concentration of 10 µg/L (50 nm nPS; 21 d) impaired the antioxidant defence system of *Mytilus galloprovincialis*, resulting in oxidative damage, with the mussel gills being the most seriously impacted tissue Gonçalves et al., 2022; Chapter 3). PS-NPs exposure to *M. galloprovincialis* (50 nm; 1.5–150 ng/L; 21–d) had a more significant impact on lysosomal markers of general stress than did PS-microplastics (PS-MPs), indicating a potential link between this trend and enhanced synthesis of antioxidants (Capolupo et al., 2021). The accumulation of PS-NPs has also been shown to be tissue and time-dependent after 28-day exposure to 10 µg/L of PS-NPs (50 nm), the highest accumulation recorded in the gonads of M. galloprovincialis Gonçalves et al., 2023; Chapter 2). Gametes exposed to PS-NPs (50 nm; 1.5 h) in *Crassostrea gigas* showed decreased fertilisation rates (Tallec et al., 2018). Agglomerates of nanoparticles were also found attached to spermatozoa and the jelly coating of oocytes (PS-COOH and PS-NH_2; 0.1–100 mg/L; 1, 3 and 5 h) (González-Fernández et al., 2018). After embryos were exposed to PS-NPs (50 nm; 10 µg/L; 48 hpf) in *M. galloprovincialis*, abnormalities of D-larvae were discovered (Auguste et al., 2021). Moreover, a decrease in spermatozoa motility and velocity, as well as an overall drop in successful embryogenesis, was encountered in *C. gigas* after exposure to PS-NPs with amine or carboxyl functions (1h; 0.1-25 µg/mL; Tallec et al., 2020). As bivalve reproduction occurs externally, the gametes and, with successful fertilisation, embryos and larvae are subjected to the contaminants in the surrounding environment, including NPs, and it is, therefore, crucial to understand the toxicity these particles have and their effects on successful reproduction, as it can dictate the viability of future generations and the balance of a whole ecosystem. Therefore, this study aimed to investigate the hazards of PS-NPs exposure (16.5 µg/L) on *M. galloprovincialis* spermatozoa and oocytes before fertilisation and the detrimental effects on embryo-larval development after gamete exposure, as well as the effects of PS-NPs exposure (16.5 µg/L) after fertilisation on embryo-larval development

after 24 and 96 hours post fertilisation (hpf). Furthermore, the accumulation of PS-NPs was also evaluated in both exposure conditions after 96 hpf.

8.2.Materials and Methods

8.2.1. Polystyrene nanoparticles (PS-NPs)

Polysciences, Inc. (Germany) supplied the Fluoresbrite® Plain YG spherical polystyrene nanoplastics, which have a size of 50 nm (CAS 9003-53-6). The hydrodynamic diameter of PS-NPs (852 ± 103 nm) increases due to aggregation/agglomeration kinetics triggered by the amount of salt in fresh seawater. Gonçalves et al. (2022) provide additional information regarding PS-NP characterisation (Chapter 3).

8.2.2. Gamete production and fertilisation

Mature *Mytilus galloprovincialis* (60 ± 5 mm), collected from offshore aquaculture between Sagres and Lagos, South Portugal (A: 37º04,200'N & 8º42,800'W; B: 37º04,200'N & 8º41,000'W; C: 37º03,400'N & 8º41,000'W; D: 37º03,400'N & 8º42,800'W) were induced to spawn by thermal stimulation (His et al., 1999) in separate beakers with 0.2 µm filtered seawater (FSW). As they begin to spawn, males and females are individually isolated in 150 mL of FSW to obtain a gamete-dense solution (Boukadida et al., 2019). Firstly, the oocytes and sperm of mussels are filtered through 100 µm and 50 µm, respectively. The quality of gametes is then assessed under an optical microscope, looking for regular oocytes and very mobile spermatozoa to select for the experiment. Then, oocytes are fertilised in a sperm-dense suspension with a ratio of 1:10 (oocyte: sperm). The appearance of a polar globule indicates fertilisation success (Boukadida et al., 2019). Fertilised eggs (ca. 150 eggs/mL) will be transferred into test tubes containing the experimental solutions (Boukadida et al., 2019).

8.2.3. Spermatozoa and oocyte count

In a Neubauer chamber, 10 µL aliquot of the obtained spermatozoids and oocytes from the total 150 mL was collected and used to obtain the total number of spermatozoids and oocytes released under an optical microscope (Zeiss, compound light microscopy). In 150 mL of sperm-dense solution, there was a total of 7,830,000 spermatozoids and 1,185,000 oocytes in 150 mL of oocyte-dense solution.

8.2.4. Experimental design

For experimental purposes, two sets of exposures were performed. For one of the exposure conditions, spermatozoa and oocytes were submitted to 16.5 µg/L of PS-NPs, and after 24h of exposure, oocytes were fertilised in a sperm-dense suspension (1:10 = oocyte: sperm). In the other exposure conditions, oocytes were fertilised in a sperm-dense suspension and only then exposed to 16.5 µg/L of PS-NPs. A replicate of six test tubes for each unexposed and exposed gametes/embryos was used in both experimental conditions.

8.2.5. Embryotoxicity

Larval development was checked in each treatment condition after 24 hpf. The percentage of abnormal larval formation was determined by directly observing 25 larvae under an optical microscope at a magnification of x40. Assays are validated if normal larval development is >80% in controls (Boukadida et al., 2016, 2019).

8.2.6. Accumulation

Using the molecular rotor probe 9-(dicyanovinyl)-julolidine (DCVJ) and a fluorescence-based methodology, the accumulation of PS-NPs in mussel larvae exposed to 16.5 µg/L of PS-NPs after 96 hpf was evaluated, following the Gagné (2019) method. First, using a VWR Star-Beater (5 min, 20/s shaking, with grinding balls), 2 mL of 96 hpf larvae solution (gametes previously exposed before fertilisation and embryos exposed post-fertilization) were homogenised in 5 mL of an ice-cold buffer solution (50 mM NaCl, 10 mM Hepes - NaOH [pH 7.4], 1 mM EDTA, and 1 mM DTT). Samples were centrifuged for 20 minutes at 2ºC and 15,000 *g* to extract the cytosolic fraction. The supernatant that was produced was promptly frozen at -80ºC until it could be further examined. After that, samples were analysed with a Berthold Tristar 5 spectrofluorometric microplate reader, which had emission spectra between 400 and 800 nm and excitation at 450 nm.

8.3. Results & Discussion

8.3.1. Spermatozoa & Oocytes: before and post-24 h exposure.

After 24 hours of exposure to PS-NPs, the number of spermatozoa and oocytes is reduced (Fig. 7.1 A—B). Furthermore, the integrity of oocytes (Fig. 7.1 B) is compromised following PS-NP exposure. Numerous studies have examined how PS-NPs affect the reproductive systems of mussels, emphasising spermatozoa and oocytes (González-Fernández et al., 2018; Tallec et al., 2018, 2020; Shi et al., 2022; Contino et al., 2023a; Romdhani et al.,

2024). Research indicates that PS-NPs adversely affect sperm function and fertilisation success, although there is scant direct evidence of a reduction in the quantity of these gametes. According to González-Fernández et al. (2018), PS-NPs can adhere to spermatozoa and oocyte jelly coatings to form agglomerates that hinder fertilisation. Due to this physical interference, less viable gametes may be available for successful reproduction. Exposure to environmental micro- and nano-plastics in *M. galloprovincialis* male gametes led to an overall decrease in viability, as it caused a decline in motility, DNA integrity, and changes to mitochondrial membrane potential and oxidative status while increasing apoptosis (1-100 µg/L; Romdhani et al., 2024). Moreover, in *M. galloprovincialis* exposed to PS-NPs (10 µg/L; 50 nm; 21 days), changes in protein expressions in male gonads also suggest oxidative damage and apoptosis due to PS-NPs (Chapter 7), which can have severe implications on viable spermatozoa, and therefore, reproductive success. In the case of females, the same exposure presented the suppression of intracellular protein transport that interferes with energy production, meiotic progression, and hormone synthesis (Chapter 7). Additionally, inhibiting spindle organisation may result in aneuploidy in oocytes, leading to reduced fertility or developmental abnormalities in offspring (Chapter 7), which supports the deformities in embryo-larval development seen here (*see section 8.2.2*).

Furthermore, the exposure to PS-NPs of the freshwater crustacean *Daphnia galeata* resulted in abnormal embryo development and reduced reproductive success (52nm; 5 mg/L; 5 days; Cui et al., 2017). The observed reproductive abnormalities raise the possibility of detrimental effects on gamete viability or function, even though the study did not measure changes in the number of gametes. These studies show that PS-NPs can negatively impact mussel reproduction by promoting abnormal embryo development, lowering fertilisation rates, and affecting sperm integrity. The known adverse effects on gamete function and reproductive outcomes imply that PS-NP exposure offers a serious risk to mussel reproductive health, even though there is little direct evidence of a decline in the number of spermatozoa and oocytes.

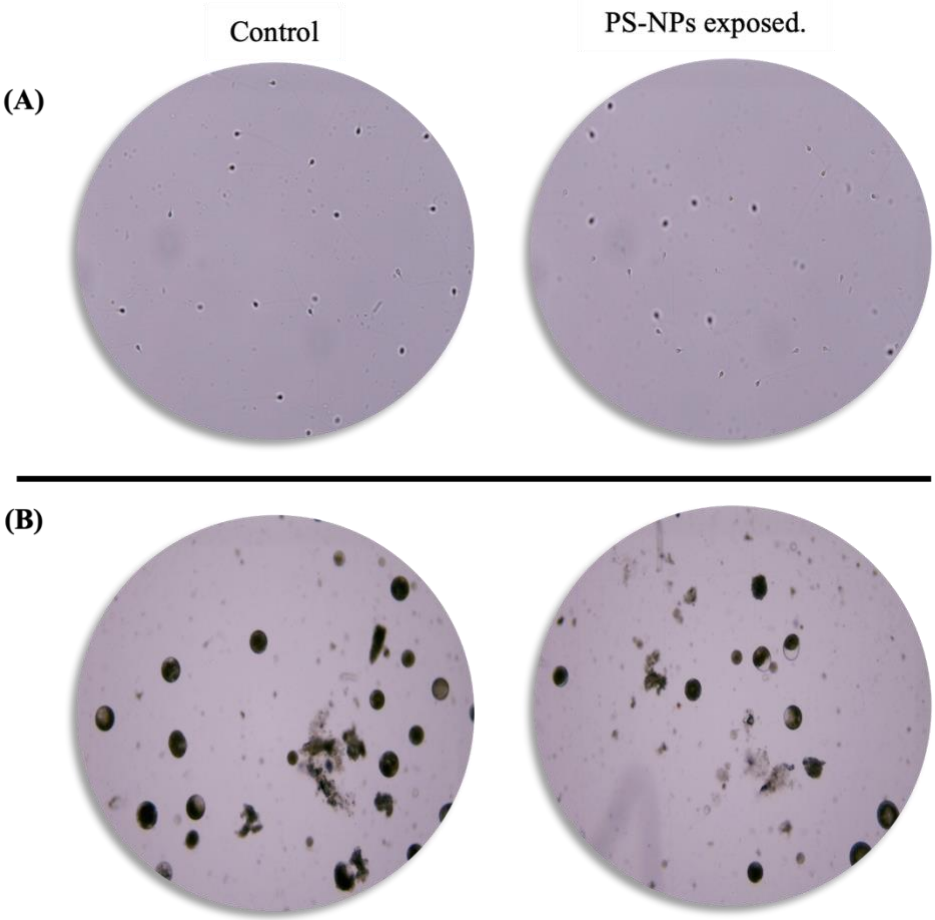

Figure 8.1. Microscopic images of *M. galloprovincialis* **(A)** spermatozoa **(B)** oocytes, at a magnification of x40, before control) and after a 24-hour exposure to 16.5 µg/L of PS-NPs.

8.3.2. Larval development

Larval development of embryos exposed to PS-NPs (Figure 7.2A) shows slightly reduced size and malformation compared to controls. Moreover, when gametes were exposed to PS-NPs before fertilisation (Fig. 7.2.B), the relative size of larvae from unexposed and exposed conditions decreased exponentially. Thus, gamete exposure seems to be more prejudicial for larval development in the case of successful fertilisation. However, more evaluation is necessary to confirm this. Although larval development was not evaluated, in the Pacific oyster (*C. gigas*), there was an increase in the relative size of spermatozoa and oocytes that resulted from the adhesion of PS-NPs (PS-COOH; PS-NH_2; 100 nm; 0.1-100 mg/L; 1, 3 and 5 h; González-Fernández et al., 2018).

An exposure to PS microplastic beads(0.5 µm and 5 µm; 0.26 mg/L and 0.69 mg/L) in the mussel *Tegillarca granosa* resulted in impaired sperm motility by reducing ATP production and cell viability, ultimately decreasing the likelihood of gamete collision (Shi et al., 2022). It

also led to disrupted ion transport in gametes by triggering oxidative stress, leading to the failure of gamete fusion and, therefore, hindering fertilisation success (Shi et al., 2022). In Contino et al. (2023b), the effects of amino-modified PS-NPs with diameters of 50 nm and 100 nm on embryonic development were assessed in *Artemia salina* (brine shrimp). The results showed that while hatching rates were not significantly affected, larvae exposed to these PS-NPs showed sublethal consequences such as increased oxidative stress, apoptosis, and gut and body size abnormalities. Adverse effects were more noteworthy at higher concentrations and smaller PS-NPs. PS-MPs impaired gamete quality and embryonic development in *C. gigas*, reducing fertilisation success rates and inducing abnormal larval development after oyster adults were exposed for 2 months (2 and 6 µm; 0.023 mg/L; Sussarellu et al., 2016).

Exposure to PS-NPs (30 nm; 100 mg/L; 96 hpf) has been linked to mortality in zebrafish embryos (*Danio rerio*) (Chantho et al., 2024). According to Chantho et al. (2024), the uptake of PS-NPs (30 nm) is predominately found in the digestive system of the larvae and is unseen in larger PS-NPs evaluated. They can also modulate the expression levels of genes linked to oxidative stress and apoptosis (Chantho et al., 2024). The size and concentration of PS-NPs frequently correlate with how severe these impacts are. Thus, exposure to PS-NPs following fertilisation may cause a variety of aquatic organisms to acquire deformities and experience mild reductions in larval size. Variables like nanoparticle size, concentration, and the species involved seem to determine the extent of these effects. Therefore, these findings suggest that PS-NPs can harm the early life stages of bivalves, potentially impacting successful reproduction and population dynamics.

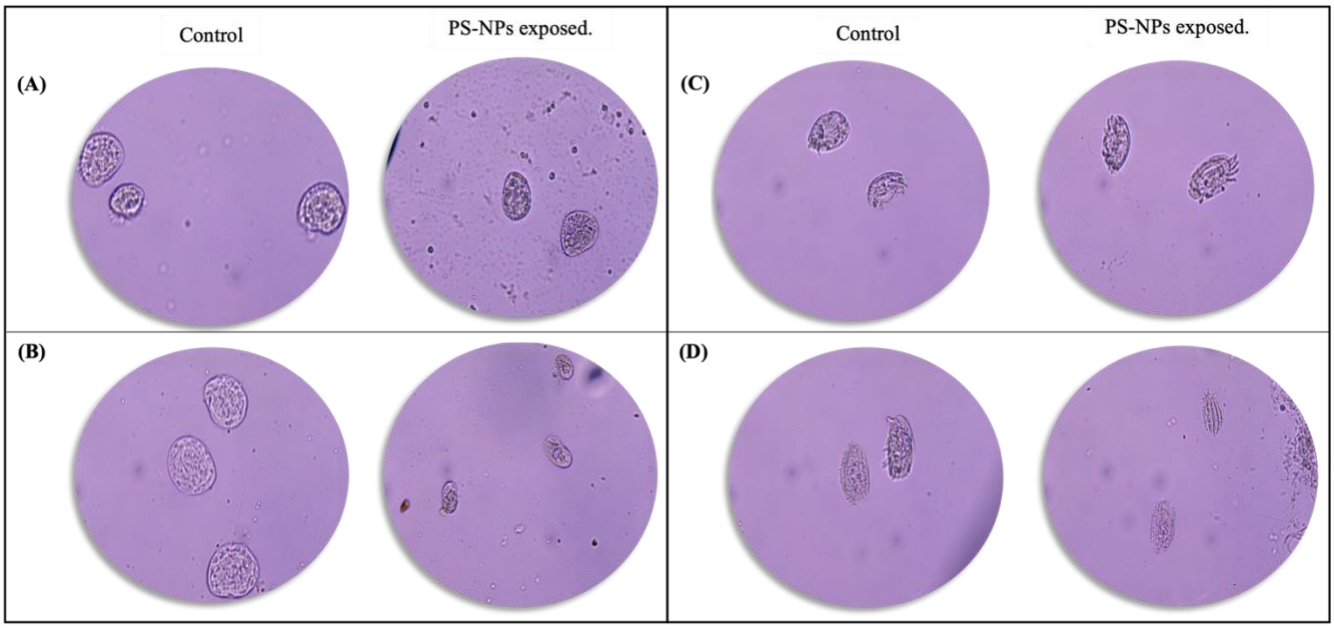

Figure 8.2. Microscopic images of *M. galloprovincialis* embryos **(A)** control and exposed post-fertilisation and **(B)** gametes control and exposed before fertilisation at 24 hpf, and embryos **(C)** control and exposed post-fertilisation and **(D)** gametes control and exposed before fertilisation at 96 hpf, at a magnification of 40x.

8.3.3. Accumulation

Accumulation of PS-NPs is significant in gametes compared to controls (p<0.05) (Fig. 7.3.A), whilst no significant differences are encountered in exposed embryos (p>0.05) (Fig. 7.3.B). In *C. gigas*, PS-NP accumulation in gametes adversely affected their function while also impacting embryonic development (PS-NPs, PS-COOH, PS-NH_2; 50 nm; 0-25 µg/mL; Tallec et al., 2018), and the exposure to PS-NH_2 was more toxic than the other PS-NPs studied. However, all PS-NPs significantly decreased fertilisation success and harmed embryo-larval development (Tallec et al., 2018).

In *Artemia franciscana*, PS-NPs were accumulated in the intestine, where differences were encountered in terms of locations, which depended on the type of PS-NPs (48 h; 40 nm PS-COOH, 50 nm PS-NH_2; 5-100 µg/mL; Bergami et al., 2016). PS-COOH was heavily retained in the larval gut lumen after 48 h, and PS-NH_2 (5–100 mg/ml) accumulated in larvae and adhered to sensory antennules and appendages, potentially impairing motility (Bergami et al., 2016). Contino et al. (2023a) reported similar findings in *A. salina* (PS-NH_2; 50 and 100 nm; 10 and 20 mg/L). On the contrary, Capolupo et al. (2021), after assessing the effects of PS-

MPs (virgin and loaded with chrysene; 23.67 ±2.46 ×103 MP/mL; 48 h) on gamete and embryonic development of *M. galloprovincialis*, found that PS-MPs did not significantly accumulate in mussel gametes or embryos, nor impact their development. Therefore, the size of the plastic particle, along with its concentration, are crucial factors in understanding the detrimental effects of nanoplastics towards gamete viability and reproductive success in species that rely on external fertilisation in the marine environment.

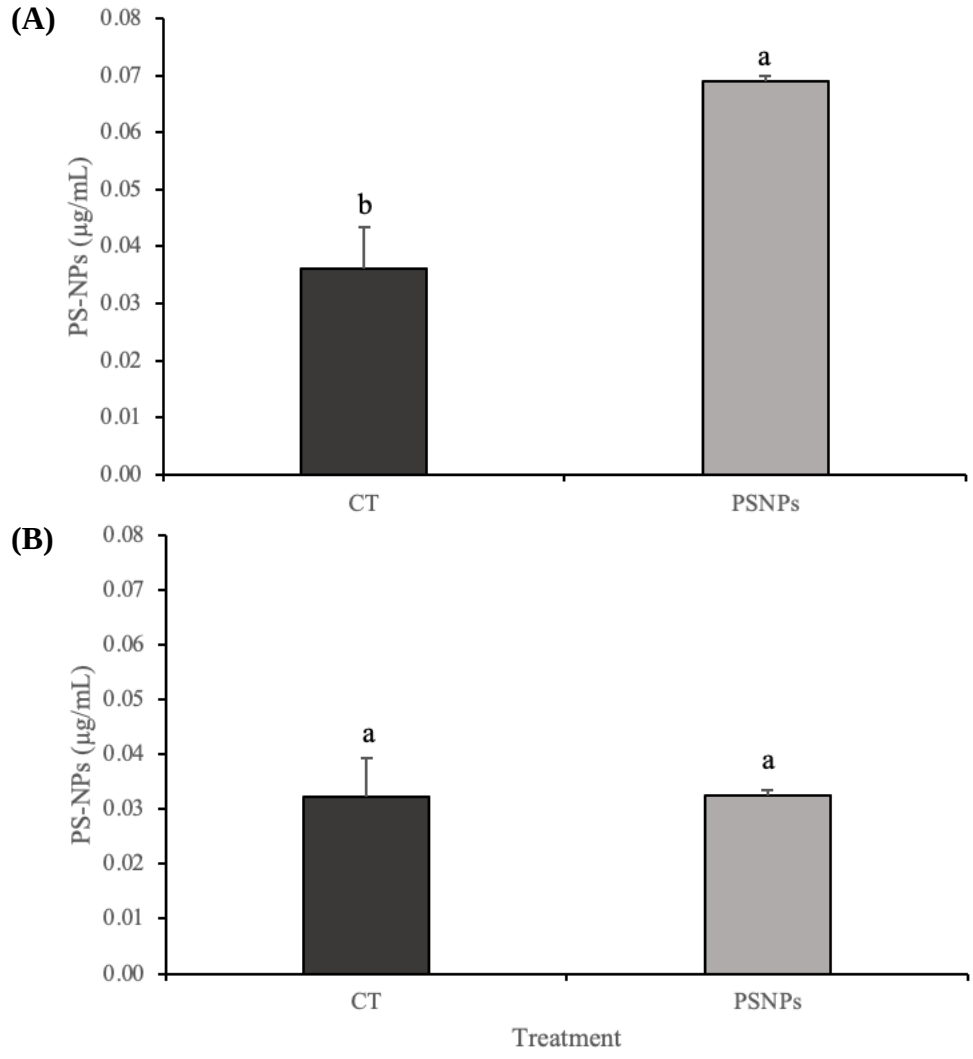

Figure 8.3. Accumulation of PS-NPs **(A)** to gametes before fertilisation and **(B)** after fertilisation after 16.5 µg/L exposure of PS-NPs.

8.4. Conclusion

This work highlights the detrimental effects of PS-NPs on mussel reproduction and early life stages. After a 24-hour exposure period, the quantity of spermatozoa and oocytes decreased dramatically, and the integrity of the oocytes was compromised. Further evaluation is necessary

to understand whether and how PS-NPs influence the number of gametes produced despite their impact on gamete function and fertilisation success. Larval development was also affected, particularly when gametes were exposed prior to fertilisation, resulting in reduced size and deformities. PS-NPs appear to primarily impact the reproductive cells, as evidenced by the significant accumulation of nanoplastics in gametes rather than embryos. Confirmation of long-term ecological effects necessitates further investigation.

CHAPTER IX

General Discussion, Conclusions and Future Perspectives

9. General Discussion and Conclusions

9.1. Effects of PS- NPs in *Mytilus galloprovincialis*

Nanoplastics are found in the marine environment either as primary nanoplastics or, more commonly, as secondary nanoplastics. Their fate is difficult to predict, as nanoplastics are an emerging contaminant of concern that interacts with their environmental surroundings. The effects of these interactions have not yet been fully clarified; however, available data indicate that nanoplastics significantly impact marine biota and ecosystems (Chapter 1, section 1.2.2; Gonçalves & Bebianno, 2021). Consequently, there is a growing interest within the scientific community regarding nanoplastics and their effects on the marine environment, as marine organisms can interact with and ingest this plastic debris due to its particle size and surface volume, potentially influencing seafood production and human health. In the marine environment, there is limited data on various types of virgin nanoplastics, primarily focusing on the effects of PS-NPs with a carboxyl group (-COOH) or an amide group ($-NH_2$) (Chapter 1, section 1.2.2; Gonçalves & Bebianno, 2021). Although not environmentally relevant, the surface properties of nanoparticles with -COOH or $-NH_2$ functionality serve as essential model molecules for evaluation as they provide insights into the different forms of toxicity associated with negatively and positively charged nanoparticles (Chapter 1, section 1.2.2; Gonçalves & Bebianno, 2021). Available data suggest that these nanoparticles exert toxic effects on marine biota, including bacterial communities, primary producers, primary and secondary consumers, and top consumers (Chapter 1, section 1.2.2; Gonçalves & Bebianno, 2021).

Furthermore, PS-NPs with an amide group exhibit greater toxicity than those with a carboxyl group, indicating that the charge of these NPs significantly influences their nanotoxicity (Chapter 1, section 1.2.2; Gonçalves & Bebianno, 2021). Additionally, certain marine organisms can accumulate NPs in specific tissues, leading to more detrimental effects on these organisms (Mattsson et al., 2015, 2018; Worm et al., 2017; Peng et al., 2020). Consequently, as many organisms ingest these particles and accumulate them within their tissues, this highlights the need for further research into the potentially toxic effects of exposure to various types and sizes of virgin NPs, along with different kinds and charged NPs. In a broader context, the extensive data identifying the many effects of NPs should aid decision-makers in considering both the production of nanomaterials and the breakdown of plastic consumer products as potential environmental issues. Notwithstanding the scientific duty to comprehend the toxicity of NPs and their ecological effects, the findings suggest that some NPs are less reactive than others, offering insights into the production of less potent nanomaterials (Chapter 1, section 1.2.2; Gonçalves & Bebianno, 2021).

To understand the effects of NPs (50 nm) in the ocean, the behaviour of NPs in seawater was assessed. When in seawater, PS-NPs of 50 nm aggregate, as indicated by the increased hydrodynamic diameter found in seawater compared to freshwater (Gonçalves et al., 2022b; Chapter 3). The abiotic and biotic characteristics of seawater, such as high salt content, natural organic matter (NOM), inorganic colloids, and ultraviolet (UV) radiation, influence the nano-specific properties, structure, cohesion, and aggregation of particles (Gonçalves et al., 2022b; Chapter 3). Therefore, the chemical composition and size of nanoplastics are essential considerations, as these factors, together with the abiotic and biotic characteristics of seawater, can all affect the hydrodynamic diameter of these particles. Following the behaviour of NPs in seawater, mussels *M. galloprovincialis* were exposed to NPs (50 nm; 10 µg/L) for 28 days. The marine mussel *M. galloprovincialis* ingests PS-NPs, which can be found in the gills, digestive glands, and gonads (Gonçalves et al., 2023, 2025; Chapters 2, 6). This ingestion is tissue- and time-specific, predominating in the gonads (Gonçalves et al., 2023; Chapter 2). These results lead us to examine gender differences. The uptake of PS-NPs in the gonads suggests that females are more adversely affected than males and that the ingestion patterns are also specific to sex (Gonçalves et al., 2025; Chapter 6).

Furthermore, the exposure to PS-NPs (50 nm; 10 µg/L; 21 days) induces neurotoxicity in the gills of mussels and reduces the number of viable haemocytes in the bloodstream of these organisms (Gonçalves et al., 2022b; Chapter 3). PS-NPs also cause mussels' genotoxicity, threatening their DNA's integrity (Gonçalves et al., 2022b; Chapter 3). Toxicity levels assessed through evaluations of oxidative stress and damage indicate that the antioxidant defence system in mussel tissues is overwhelmed by ROS generation due to PS-NP exposure, resulting in oxidative damage to the gills, digestive glands, and gonads of mussels, with females experiencing the highest levels of lipid peroxidation (Gonçalves et al., 2022b, 2023; Gonçalves & Bebianno, 2023; Chapters 2, 3, 5). It is understood that females require double the lipid content as an energy source during gametogenic stages, which may explain the observed sexual differences (Martínez-Pita et al., 2012). Focusing on the gills, this tissue shows an adaptive response, potentially activating repair mechanisms such as autophagy (Gonçalves et al., 2022b; Chapter 3). However, further investigation is necessary to understand how this adaptive response operates. A SWATH/MS proteomic analysis of the gills and digestive glands could illuminate the underlying biological processes, cellular components, and molecular functions contributing to this adaptive response to PS-NP exposure. Given the higher uptake in the gonads (Gonçalves et al., 2023, 2025; Chapter 2, 6), a quantitative proteomic approach was employed to gain a deeper understanding of the observed effects in male and female mussels

and to clarify the differences in the impact of NP exposure on gender. In the gonads of both male and female mussels, the quantitative proteomic analysis reveals numerous protein changes, with higher occurrences in males, affecting biological processes, cellular components, and molecular functions. This high-throughput analysis provides insights into the processes of ingestion, oxidative stress, and damage responses. PS-NP ingestion in male mussels significantly alters protein expression compared to females, disrupting protein synthesis, energy production, intracellular transport, and cellular homeostasis (Chapter 7).

Furthermore, the altered protein expressions in male mussels following exposure to PS-NPs (10 µg/L; 50 nm; 21 days) indicate oxidative damage, as detailed in Chapter 6 (section 6.3.3) (Gonçalves et al., 2025), and apoptosis (Chapter 7). This may lead to a decline in sperm viability and reproductive success. Further investigation into sperm viability and motility is crucial to decipher the effects of PS-NPs on male gametes. Nevertheless, all these changes may represent an adaptive response to ROS generation due to the presence of PS-NPs, enabling male mussels to counterbalance and maintain cellular homeostasis, as evidenced by the oxidative stress and damage observed here compared to females. The proteomic analysis revealed that, in female mussels, PS-NPs disrupt proteins associated with processes such as translation, RNA processing and signalling, ribosome biogenesis, the cell cycle, stress response, protein folding, lipid metabolism, and calcium signalling pathways, ultimately impairing oogenesis, meiotic progression, intracellular trafficking, and energy metabolism—factors that could negatively affect reproductive success (Chapter 7). Consequently, female mussels cannot counterbalance oxidative stress, suffer oxidative damage, and are thus at greater risk from exposure to PS-NPs. The Weight-of-Evidence model reinforces this assertion by providing a synthetic hazard index based on a specifically developed algorithm and mathematical procedure (Regoli et al., 2019).

Furthermore, following the evaluation of PS-NP effects on mussel gametes and early life stages, the number of spermatozoa and oocytes decreases, alongside compromised integrity of oocytes that can hinder the success of external fertilisation in mussels, thereby having a detrimental impact on biodiversity (Chapter 8). The upregulated and downregulated protein expressions from exposure to PS-NPs provide insight into the impacts on gametogenesis, gametes, and embryo-larval development. The effects observed on embryo-larval development were significantly more pronounced when gametes were exposed beforehand, as opposed to exposure following fertilisation. The reduced size and deformities relative to controls confirm this and suggest that PS-NPs are more hazardous during gametogenic stages and to gametes than to larvae (Chapter 8). This indicates that fertilisation and reproductive success are at risk,

necessitating confirmation of long-term ecological effects and further investigation. Nonetheless, these results highlight the importance of understanding the toxicity of nanoplastics to marine organisms, as their ability to accumulate and harm biota is highly concerning. Furthermore, the removal of nanoplastics from the aquatic environment remains unresolved, and these tiny plastic particles pose a significant threat to the marine ecosystem. Additionally, as shellfish are an essential part of the Mediterranean diet, humans are also at risk (Barboza et al., 2024).

9.2. Effects of mixture of CECs in *Mytilus galloprovincialis*

In the marine environment, several contaminants are present, and emerging contaminants such as nanoplastics, metal nanomaterials, and pharmaceutical compounds are a cause for concern due to their potentially detrimental effects on the health of marine biota. Consequently, this thesis assesses the effects of three emerging contaminants of concern (PS-NPs, 5-FU, and nAg) on the Mediterranean mussels *M. galloprovincialis,* analysed either individually or in combination, to evaluate the antagonistic, synergistic, or cumulative effects that these three contaminants may produce in this bivalve species (Gonçalves et al., 2022a; Gonçalves & Bebianno, 2023; Chapter 4, 5). The individual effects of PS-NPs are outlined in section 9.1 of this chapter.

The effects of 5-FU are crucial to assess, as it has been detected in seawater, with concentrations ranging from 0.01 to 41 ng/L in surface waters and 0.3 to 2.5 ng/L in European waters (Misík et al., 2019; Heath & Isidori, 2020). 5-FU is a straightforward chemotherapeutic agent for neoplasms, particularly in cases of breast, gastric, pancreatic, and colorectal adenocarcinoma (Mahnik et al., 2007; Casale & Patel, 2024). With the rising number of cancer patients and, consequently, the increased use of 5-FU (Infarmed, 2023) (Chapter 1, section 1.4.1; Gonçalves & Bebianno, 2021), this cytostatic drug inevitably ends up in hospital effluents, sewage systems, and surface run-offs, regardless of the dosage administered. Due to the inadequate removal of these pharmaceuticals in wastewater treatment plants (WWTPs), 5-FU and its metabolites inevitably enter aquatic environments, whether freshwater or marine; for this reason, it is considered a CEC. Another concern is the amplified toxic effects of 5-FU when it interacts with other emerging contaminants (Chapter 1, section 1.4.5; Chapter 4, 5, 6; Gonçalves et al., 2022a, 2025; Gonçalves & Bebianno, 2023). In summary, enhancing the treatment and/or removal of cytostatic drugs warrants substantial attention to reduce these pharmaceuticals' presence in aquatic environments, as decreasing administration among cancer patients is not a viable option.

Regrettably, WWTPs lack the technology to break down or remove CECs effectively. This eventually releases them into the aquatic environment, where they inevitably form mixtures. As contaminants interact, these mixtures can exhibit more pronounced toxic effects. For instance, plastic particles are known to adsorb pharmaceuticals, and depending on the type, size, and concentration of both the plastic particles and the pharmaceuticals involved, either synergistic or antagonistic toxic consequences may arise (Santana-Viera et al., 2021).

Due to their nature, cytostatic drugs in the marine environment, such as 5-FU, raise significant concerns; thus, mussels were exposed to 5-FU (10 µg/L) for 21 days. Its application as a chemotherapeutic agent and its mode of action induce genotoxicity in mussels, compromising DNA integrity (Matuo et al., 2009; Gonçalves et al., 2022a; Chapter 4). Nevertheless, when assessing oxidative stress and damage, the mussel's antioxidant defence system effectively countered ROS generation resulting from the presence of the pharmaceutical in the three tissues evaluated (Gonçalves et al., 2022a, 2025; Gonçalves & Bebianno, 2023; Chapters 4, 5, 6). However, these pharmaceuticals are not the only contaminants that enter the aquatic environment, and when analysing the cumulative effects in mixtures with other emerging contaminants such as PS-NPs and nAg, the severity of their toxicity amplifies (Gonçalves & Bebianno, 2023; Gonçalves et al., 2025; Chapters 5, 6).

Silver nanoparticles (nAg) account for over 50% of nanomaterials in consumer products worldwide (Pulit-Prociak & Banach, 2016). They are frequently found in personal care products, antimicrobial coatings, photonic devices, and the textile industry (Maillard & Hartemann, 2013; Lee & Jun, 2019; Pereirados et al., 2020). A considerable portion of nAg in the environment stems from its release through consumer products, with reported levels ranging from 0.03 to 0.08 mg/L (Fernandes et al., 2017). While the effects of nAg in the marine environment have been extensively studied, particularly in mussels *M. galloprovincialis,* and its mode of action is well understood (Auguste et al., 2018; Gomes et al., 2013; Lorusso et al., 2022; McCarthy et al., 2013; Rezvani et al., 2019), the impact on marine organisms exposed to a mixture of emerging contaminants remains unclear.

Mussels exposed to a mixture of PS-NPs, 5-FU, and nAg exhibited synergistic interactions, enhancing the toxicity of the assessed contaminants. The results indicate that the mixture induced mussels' time- and tissue-specific toxicity (Gonçalves et al., 2022a; Gonçalves & Bebianno, 2023; Chapters 4, 5). Of the three tissues evaluated, the gonads experienced the most damage, although synergistic interactions were evident during acute exposures, with prolonged exposure periods leading to antagonistic interactions among the contaminants. In this context, the properties of nAg play a critical role in diminishing the toxicity experienced

by mussels (Gonçalves & Bebianno, 2023; Chapter 5). This is further supported by findings from when mussels were exposed to a combination of PS-NPs and 5-FU (Gonçalves et al., 2025; Chapter 6).

In comparison to their counterparts, the analysis of the mixture of PS-NPs and 5-FU indicates that it is highly toxic to mussels, with synergistic interactions observed throughout the exposure period. This suggests that 5-FU is adsorbed onto PS-NPs, enhancing the toxicity of both contaminants and resulting in a more hazardous outcome for mussels (Gonçalves et al., 2025; Chapter 6). Considering gender differences, the WOE concludes that females are significantly more affected during prolonged exposure than males, jeopardising gonadal development, oogenesis, and, consequently, reproductive success. Nevertheless, males also experience adverse effects from exposure to these emerging contaminants, threatening spermatozoa motility and viability. Given the proteomic results for PS-NPs and the fact that the mixture of PS-NPs and 5-FU is considerably more toxic than the individual contaminants, it can be inferred that the upregulations and downregulations in protein expression are more pronounced in mussels exposed to the mixture. However, further investigation is required to confirm this assumption.

Overall, exposure to a mixture of CECs jeopardises mussels' health status, and they cannot counteract the toxic effects exacerbated by this “cocktail” of contaminants. More specifically, the reproductive organs of mussels are significantly more affected than the other assessed tissues, lacking the ability to rebound from the toxicity of these contaminants. As a result, gametogenesis and the release of viable gametes for external fertilisation are hindered. The gametes in the water column, which come into contact with these contaminants, suffer even greater harm, as their essential properties for successful reproduction are compromised. This situation indicates a decline in fertilisation success, leading to a loss of biodiversity.

In conclusion, the effects of emerging contaminants of concern in the marine environment require substantial attention from the scientific community. These contaminants evaluated here inevitably exist as mixtures, and their risks increase due to the potential amplification of their toxic properties through interactions. Focusing on these effects on reproductive organs and reproductive success is essential, as it can aid in understanding how population dynamics may be affected, given that reproduction is vital for a healthy ecosystem.

9.3. Future Perspectives

Based on the results obtained, further investigation is necessary to fully understand the effects of the CECs identified by the European Union. Therefore, for future research, several pathways are highlighted:

- Examine the effects of CECs on mussels during each gametogenic stage.
- Examine the impacts of CECs on gametes obtained from exposed adults and, consequently, the effects on the subsequent generation.
- Examine the effects of CECs on spermatozoa motility and viability alongside oocyte robustness and viability.
- Assess the effects of embryo-larval development, including ROS.
- Proteomic and genomic analysis of female and male mussels exposed to other CECs and mixtures of CECs.
- Gametes can be cryopreserved, reducing the number of animals used in experiments. The European Union is also concerned about this, which European legislation covers (Directive/2010/63/EU).
- 3D cell cultures can replace 2D cell cultures to more accurately analyse the toxic effects of CECs. They can mimic tissues and contribute to reducing the number of animals used in experiments.
- Restructuring and enhancing WWTPs is crucial to prevent CECs from entering aquatic environments. For instance, developing a mechanical mussel that uses its filter-feeding properties to remove nanoparticles from WWTPs is vital. This could represent an innovative solution to reducing the levels of these compounds entering the ocean.

REFERENCES

Affek, K., Załęska-Radziwiłł, M., Doskocz, N., & Dębek, K. (2018). Mixture toxicity of pharmaceuticals present in wastewater to aquatic organisms. Desalination and Water Treatment, 117, 15–20. https://doi.org/10.5004/dwt.2018.21964

Almeida, M., Martins, M. A., Soares, A. M. V., Cuesta, A., & Oliveira, M. (2019). Polystyrene nanoplastics alter the cytotoxicity of human pharmaceuticals on marine fish cell lines. Environmental Toxicology and Pharmacology, 69, 57–65. https://doi.org/10.1016/j.etap.2019.03.019

Alscher, R. G. (2002). Role of superoxide dismutases (SODs) in controlling oxidative stress in plants. Journal of Experimental Botany, 53(372), 1331–1341. https://doi.org/10.1093/jexbot/53.372.1331

Andrady, A. L. (2011). Microplastics in the marine environment. Marine Pollution Bulletin, 62(8), 1596–1605. https://doi.org/10.1016/j.marpolbul.2011.05.030

Anjo, S. I., Santa, C., & Manadas, B. (2015). Short GeLC-SWATH: A fast and reliable quantitative approach for proteomic screenings. Proteomics, 15(4), 757–762. https://doi.org/10.1002/pmic.201400221

Apraiz, I., Mi, J., & Cristobal, S. (2006). Identification of proteomic signatures of exposure to marine pollutants in mussels (*Mytilus edulis*). Molecular and Cellular Proteomics, 5(7), 1274–1285. https://doi.org/10.1074/mcp.M500333-MCP200

Araújo, J., Soares, F., Medeiros, A., Bandarrra, N., & Pousão-Ferreira, P. (2024). Mediterranean mussel (*Mytilus galloprovincialis*) offshore production at south Portugal. World Aquaculture Society. https://www.was.org/MeetingAbstracts/ShowAbstract/47413

Asad, U. D., Pfister, G., & Schramm, K. W. (2012). 5-Fluorouracil accumulation in green microalgae and its biogenetic transfer into ciliate protozoan. Bulletin of Environmental Contamination and Toxicology, 88(4), 548–554. https://doi.org/10.1007/s00128-012-0536-8

Auclair, J., Peyrot, C., Wilkinson, K. J., & Gagné, F. (2020). Biophysical effects of polystyrene nanoparticles on *Elliptio complanata* mussels. Environmental Science and Pollution Research, 27(20), 25093–25102. https://doi.org/10.1007/s11356-020-08920-z

Auguste, M., Balbi, T., Miglioli, A., Alberti, S., Prandi, S., Narizzano, R., Salis, A., Damonte, G., & Canesi, L. (2021). Comparison of different commercial nanopolystyrenes: Behavior in exposure media, effects on immune function and early larval development in the model bivalve *mytilus galloprovincialis.* Nanomaterials, 11(12). https://doi.org/10.3390/nano11123291

Auguste, M., Ciacci, C., Balbi, T., Brunelli, A., Caratto, V., Marcomini, A., Cuppini, R., & Canesi, L. (2018). Effects of nanosilver on *Mytilus galloprovincialis* hemocytes and early

embryo development. Aquatic Toxicology, 203, 107–116. https://doi.org/10.1016/j.aquatox.2018.08.005

Auguste, M., Lasa, A., Balbi, T., Pallavicini, A., Vezzulli, L., & Canesi, L. (2020). Impact of nanoplastics on hemolymph immune parameters and microbiota composition in *Mytilus galloprovincialis*. Marine Environmental Research, 159, 105017. https://doi.org/10.1016/j.marenvres.2020.105017

Balbi, T., Camisassi, G., Montagna, M., Fabbri, R., Franzellitti, S., Carbone, C., Dawson, K., & Canesi, L. (2017). Impact of cationic polystyrene nanoparticles (PS-NH2) on early embryo development of *Mytilus galloprovincialis*: Effects on shell formation. Chemosphere, 186, 1–9. https://doi.org/10.1016/j.chemosphere.2017.07.120

Bardou P, Mariette J, Escudié F, Djemiel C, Klopp C. jvenn: an interactive Venn diagram viewer. BMC Bioinformatics. 2014 Aug 29;15(1):293. doi: 10.1186/1471-2105-15-293. PMID: 25176396; PMCID: PMC4261873.

Baudrimont, M., Arini, A., Guégan, C., Venel, Z., Gigault, J., Pedrono, B., Prunier, J., Maurice, L., Ter Halle, A., & Feurtet-Mazel, A. (2020). Ecotoxicity of polyethylene nanoplastics from the North Atlantic oceanic gyre on freshwater and marine organisms (microalgae and filter-feeding bivalves). Environmental Science and Pollution Research, 27(4), 3746–3755. https://doi.org/10.1007/s11356-019-04668-3

Bebianno, M. J., Mendes, V. M., O'Donovan, S., Carteny, C. C., Keiter, S., & Manadas, B. (2022). Effects of microplastics alone and with adsorbed benzo(a)pyrene on the gills proteome of *Scrobicularia plana*. Science of the Total Environment, 842. https://doi.org/10.1016/j.scitotenv.2022.156895

Beliaeff, B., & Burgeot, T. (2002). Integrated biomarker response: A useful tool for ecological risk assessment. Environmental Toxicology and Chemistry, 21(6), 1316–1322. https://doi.org/10.1002/etc.5620210629

Bergami, E., Bocci, E., Vannuccini, M. L., Monopoli, M., Salvati, A., Dawson, K. A., & Corsi, I. (2016). Nano-sized polystyrene affects feeding, behaviour and physiology of brine shrimp *Artemia franciscana* larvae. Ecotoxicology and Environmental Safety, 123, 18–25. https://doi.org/10.1016/j.ecoenv.2015.09.021

Bergami, E., Krupinski Emerenciano, A., González-Aravena, M., Cárdenas, C. A., Hernández, P., Silva, J. R. M. C., & Corsi, I. (2019). Polystyrene nanoparticles affect the innate immune system of the Antarctic sea urchin *Sterechinus neumayeri*. Polar Biology, 42(4), 743–757. https://doi.org/10.1007/s00300-019-02468-6

Bergami, E., Manno, C., Cappello, S., Vannuccini, M. L., & Corsi, I. (2020). Nanoplastics affect moulting and faecal pellet sinking in Antarctic krill (*Euphausia superba*) juveniles. Environment International, 143, 105999. https://doi.org/10.1016/j.envint.2020.105999

Bergami, E., Pugnalini, S., Vannuccini, M. L., Manfra, L., Faleri, C., Savorelli, F., Dawson, K. A., & Corsi, I. (2017). Long-term toxicity of surface-charged polystyrene nanoplastics to marine planktonic species *Dunaliella tertiolecta* and *Artemia franciscana*. Aquatic Toxicology, 189, 159–169. https://doi.org/10.1016/j.aquatox.2017.06.008

Bessa, F., Barría, P., Neto, J. M., Frias, J. P. G. L., Otero, V., Sobral, P., & Marques, J. C. (2018). Occurrence of microplastics in commercial fish from a natural estuarine environment. Marine Pollution Bulletin, 128, 575–584. https://doi.org/10.1016/j.marpolbul.2018.01.044

Besse, J.-P., Latour, J.-F., & Garric, J. (2012). Anticancer drugs in surface waters. Environment International, 39(1), 73–86. https://doi.org/10.1016/j.envint.2011.10.002

Bhaby, S. , B. O. K. , E. A. (2014). *Mytilus galloprovincialis*; reproduction activity and mantle structure in a zone located in the Northwest of the Atlantic Ocean (Imessouane, Morocco). Journal of Marine Biology & Oceanography, 03(01). https://doi.org/10.4172/2324-8661.1000124

Bhargava, S., Chen Lee, S. S., Min Ying, L. S., Neo, M. L., Lay-Ming Teo, S., & Valiyaveettil, S. (2018). Fate of nanoplastics in marine larvae: A Case study using barnacles, *Amphibalanus amphitrite*. ACS Sustainable Chemistry & Engineering, 6(5), 6932–6940. https://doi.org/10.1021/acssuschemeng.8b00766

Bhattacharya, P., Lin, S., Turner, J. P., & Ke, P. C. (2010). Physical adsorption of charged plastic nanoparticles affects algal photosynthesis. Journal of Physical Chemistry C, 114(39), 16556–16561. https://doi.org/10.1021/jp1054759

Blanco-Rayón, E., Ivanina, A. v., Sokolova, I. M., Marigómez, I., & Izagirre, U. (2020). Sex and sex-related differences in gamete development progression impinge on biomarker responsiveness in sentinel mussels. Science of the Total Environment, 740. https://doi.org/10.1016/j.scitotenv.2020.140178

Blaser, S. A., Scheringer, M., MacLeod, M., & Hungerbühler, K. (2008). Estimation of cumulative aquatic exposure and risk due to silver: Contribution of nano-functionalized plastics and textiles. Science of the Total Environment, 390(2–3), 396–409. https://doi.org/10.1016/j.scitotenv.2007.10.010

Block, C., Brands, B., and Gude, T. (2022, September 02). Packaging Materials 2: Polystyrene for Food Packaging Applications. Updated Version. ILSI Europe Report Series. 2017, pp. 1–36. Commissioned by the Packaging Materials Task Force. Available online: https://ilsi.eu/publication/packaging-materials-2-polystyrene-for-food-packaging-applications-updated-version/.

Bolaños-Benítez, V., McDermott, F., Gill, L., & Knappe, J. (2020). Engineered silver nanoparticle (Ag-NP) behaviour in domestic on-site wastewater treatment plants and in sewage sludge amended-soils. Science of the Total Environment, 722, 137794. https://doi.org/10.1016/j.scitotenv.2020.137794

Booth, A. M., Hansen, B. H., Frenzel, M., Johnsen, H., & Altin, D. (2016). Uptake and toxicity of methylmethacrylate-based nanoplastic particles in aquatic organisms. Environmental Toxicology and Chemistry, 35(7), 1641–1649. https://doi.org/10.1002/etc.3076

Bouallegui Y, Ben Younes R, Turki F, Oueslati R. Impact of exposure time, particle size and uptake pathway on silver nanoparticle effects on circulating immune cells in *Mytilus*

galloprovincialis. Journal of Immunotoxicology. 2017, 14(1):116-124. doi: 10.1080/1547691X.2017.1335810. PMID: 28604134.

Boucher, J. and Friot D. (2017). Primary Microplastics in the Oceans: A Global Evaluation of Sources. Gland, Switzerland: IUCN. 43pp. dx.doi.org/10.2305/IUCN.CH.2017.01.en

Box, A., Sureda, A., Galgani, F., Pons, A., & Deudero, S. (2007). Assessment of environmental pollution at Balearic Islands applying oxidative stress biomarkers in the mussel *Mytilus galloprovincialis*. Comparative Biochemistry and Physiology Part C: Toxicology & Pharmacology, 146(4), 531–539. https://doi.org/10.1016/j.cbpc.2007.06.006

Bradford, M. M. (1976). A rapid and sensitive method for the quantitation of microgram quantities of protein utilizing the principle of protein-dye binding. Analytical Biochemistry, 72(1), 248–254. https://doi.org/https://doi.org/10.1016/0003-2697(76)90527-3

Brandts, I., Barría, C., Martins, M. A., Franco-Martínez, L., Barreto, A., Tvarijonaviciute, A., Tort, L., Oliveira, M., & Teles, M. (2021). Waterborne exposure of gilthead seabream (*Sparus aurata*) to polymethylmethacrylate nanoplastics causes effects at cellular and molecular levels. Journal of Hazardous Materials, 403, 123590. https://doi.org/10.1016/j.jhazmat.2020.123590

Brandts, I., Teles, M., Gonçalves, A. P., Barreto, A., Franco-Martinez, L., Tvarijonaviciute, A., Martins, M. A., Soares, A. M. V. M., Tort, L., & Oliveira, M. (2018). Effects of nanoplastics on *Mytilus galloprovincialis* after individual and combined exposure with carbamazepine. Science of the Total Environment, 643, 775–784. https://doi.org/10.1016/j.scitotenv.2018.06.257

Brandts, I., Teles, M., Tvarijonaviciute, A., Pereira, M. L., Martins, M. A., Tort, L., & Oliveira, M. (2018). Effects of polymethylmethacrylate nanoplastics on *Dicentrarchus labrax*. Genomics, 110(6), 435–441. https://doi.org/10.1016/j.ygeno.2018.10.006

Brezovšek, P., Eleršek, T., & Filipič, M. (2014). Toxicities of four anti-neoplastic drugs and their binary mixtures tested on the green alga *Pseudokirchneriella subcapitata* and the cyanobacterium *Synechococcus leopoliensis*. Water Research, 52, 168–177. https://doi.org/10.1016/j.watres.2014.01.007

Bürge, I. J., Buser, H.-R., Poiger, T., & Müller, M. D. (2006). Occurrence and fate of the cytostatic drugs cyclophosphamide and ifosfamide in wastewater and surface waters. Environmental Science & Technology, 40(23), 7242–7250. https://doi.org/10.1021/es0609405

Cai, H., Xu, E. G., Du, F., Li, R., Liu, J., & Shi, H. (2021). Analysis of environmental nanoplastics: Progress and challenges. Chemical Engineering Journal, 410, 128208. https://doi.org/10.1016/j.cej.2020.128208

Cairns, R. A., Harris, I. S., & Mak, T. W. (2011). Regulation of cancer cell metabolism. Nature Reviews Cancer, 11(2), 85–95. https://doi.org/10.1038/nrc2981

Calderon, E. A., Hansen, P., Rodríguez, A., Blettler, M. C. M., Syberg, K., & Khan, F. R. (2019). Microplastics in the digestive tracts of four fish species from the Ciénaga Grande de Santa Marta Estuary in Colombia. Water, Air, & Soil Pollution, 230(11), 257. https://doi.org/10.1007/s11270-019-4313-8

Canesi, L., Ciacci, C., Bergami, E., Monopoli, M. P., Dawson, K. A., Papa, S., Canonico, B., & Corsi, I. (2015). Evidence for immunomodulation and apoptotic processes induced by cationic polystyrene nanoparticles in the hemocytes of the marine bivalve *Mytilus*. Marine Environmental Research, 111, 34–40. https://doi.org/10.1016/j.marenvres.2015.06.008

Canesi, L., Ciacci, C., Fabbri, R., Balbi, T., Salis, A., Damonte, G., Cortese, K., Caratto, V., Monopoli, M. P., Dawson, K., Bergami, E., & Corsi, I. (2016). Interactions of cationic polystyrene nanoparticles with marine bivalve hemocytes in a physiological environment: Role of soluble hemolymph proteins. Environmental Research, 150, 73–81. https://doi.org/10.1016/j.envres.2016.05.045

Capolupo, M., Valbonesi, P., & Fabbri, E. (2021). A comparative assessment of the chronic effects of micro- and nano-Plastics on the physiology of the Mediterranean mussel *Mytilus galloprovincialis*. Nanomaterials, 11(3), 649. https://doi.org/10.3390/nano11030649

Carrazco-Quevedo, A., Römer, I., Salamanca, M. J., Poynter, A., Lynch, I., & Valsami-Jones, E. (2019). Bioaccumulation and toxic effects of nanoparticulate and ionic silver in *Saccostrea glomerata* (rock oyster). Ecotoxicology and Environmental Safety, 179, 127–134. https://doi.org/10.1016/j.ecoenv.2019.04.032

Casado, M. P., Macken, A., & Byrne, H. J. (2013). Ecotoxicological assessment of silica and polystyrene nanoparticles assessed by a multitrophic test battery. Environment International, 51, 97–105. https://doi.org/10.1016/j.envint.2012.11.001

Casale J, Patel P. Fluorouracil. [Updated 2024 Feb 16]. In: StatPearls [Internet]. Treasure Island (FL): StatPearls Publishing; 2025 Jan-. Available from: https://www.ncbi.nlm.nih.gov/books/NBK549808/

Catarino, A. I., Frutos, A., & Henry, T. B. (2019). Use of fluorescent-labelled nanoplastics (NPs) to demonstrate NP absorption is inconclusive without adequate controls. Science of the Total Environment, 670, 915–920. https://doi.org/10.1016/j.scitotenv.2019.03.194

Chae, Y., & An, Y. J. (2017). Effects of micro- and nanoplastics on aquatic ecosystems: Current research trends and perspectives. Marine Pollution Bulletin, 124(2), 624–632. https://doi.org/10.1016/j.marpolbul.2017.01.070

Chantho, V., Sillapaprayoon, S., Saenmuangchin, R., Pongkasem, J., Theanngern, K., Şeker, F. C. D., Aueviriyavit, S., & Pimtong, W. (2024). Effects of polystyrene nanoplastic size on zebrafish embryo development. Toxicology in Vitro, 99. https://doi.org/10.1016/j.tiv.2024.105868

Chen, Q., Yin, D., Jia, Y., Schiwy, S., Legradi, J., Yang, S., & Hollert, H. (2017). Enhanced uptake of BPA in the presence of nanoplastics can lead to neurotoxic effects in adult zebrafish. Science of the Total Environment, 609, 1312–1321. https://doi.org/10.1016/j.scitotenv.2017.07.144

Choi, J. S., Kim, K., Hong, S. H., Park, K. Il, & Park, J. W. (2021). Impact of polyethylene terephthalate microfiber length on cellular responses in the Mediterranean mussel *Mytilus galloprovincialis*. Marine Environmental Research, 168, 105320. https://doi.org/10.1016/j.marenvres.2021.105320

Cole, M., Liddle, C., Consolandi, G., Drago, C., Hird, C., Lindeque, P. K., & Galloway, T. S. (2020). Microplastics, microfibres and nanoplastics cause variable sub-lethal responses in mussels (*Mytilus* spp.). Marine Pollution Bulletin, 160, 111552. https://doi.org/10.1016/j.marpolbul.2020.111552

Cole, M., Lindeque, P., Halsband, C., & Galloway, T. S. (2011). Microplastics as contaminants in the marine environment: A review. Marine Pollution Bulletin, 62(12), 2588–2597. https://doi.org/10.1016/j.marpolbul.2011.09.025

Contino, M., Ferruggia, G., Indelicato, S., Pecoraro, R., Scalisi, E. M., Salvaggio, A., & Brundo, M. V. (2023a). Polystyrene nanoplastics in aquatic microenvironments affect sperm metabolism and fertilization of *Mytilus galloprovincialis* (Lamark, 1819). Toxics, 11(11). https://doi.org/10.3390/toxics11110924

Contino, M., Ferruggia, G., Indelicato, S., Pecoraro, R., Scalisi, E. M., Salvaggio, A., & Brundo, M. V. (2023b). Sublethal effects of polystyrene nanoplastics on the embryonic development of *Artemia salina* (Linnaeus, 1758). Animals, 13(19). https://doi.org/10.3390/ani13193152

Corsi, I., Cherr, G. N., Lenihan, H. S., Labille, J., Hassellov, M., Canesi, L., Dondero, F., Frenzilli, G., Hristozov, D., Puntes, V., Della Torre, C., Pinsino, A., Libralato, G., Marcomini, A., Sabbioni, E., & Matranga, V. (2014). Common strategies and technologies for the ecosafety assessment and design of nanomaterials entering the marine environment. ACS Nano, 8(10), 9694–9709. https://doi.org/10.1021/nn504684k

Cui, R., Kim, S. W., & An, Y. J. (2017). Polystyrene nanoplastics inhibit reproduction and induce abnormal embryonic development in the freshwater crustacean *Daphnia galeata*. *Scientific Reports*, *7*(1). https://doi.org/10.1038/s41598-017-12299-2

Dalle-Donne, I., Rossi, R., Milzani, A., di Simplicio, P., & Colombo, R. (2001). The actin cytoskeleton response to oxidants: from small heat shock protein phosphorylation to changes in the redox state of actin itself. Free Radical Biology and Medicine, 31(12), 1624–1632. https://doi.org/10.1016/S0891-5849(01)00749-3

Davranche, M., Veclin, C., Pierson-Wickmann, A. C., El Hadri, H., Grassl, B., Rowenczyk, L., Dia, A., Ter Halle, A., Blancho, F., Reynaud, S., & Gigault, J. (2019). Are nanoplastics able to bind significant amounts of metals? The lead example. Environmental Pollution, 249, 940–948. https://doi.org/10.1016/j.envpol.2019.03.087

Della Torre, C., Bergami, E., Salvati, A., Faleri, C., Cirino, P., Dawson, K. A., & Corsi, I. (2014). Accumulation and embryotoxicity of polystyrene nanoparticles at early stage of development of sea urchin embryos *Paracentrotus lividus*. Environmental Science and Technology, 48(20), 12302–12311. https://doi.org/10.1021/es502569w

Dellali, M., Hedfi, A., Ali, M. ben, Noureldeen, A., Darwish, H., Beyrem, H., Gyedu-Ababio, T., Dervishi, A., Karachle, P. K., & Boufahja, F. (2021). Multi-biomarker approach in *Mytilus galloprovincialis* and *Ruditapes decussatus* as a predictor of pelago-benthic responses after exposure to Benzo[a]Pyrene. Comparative Biochemistry and Physiology Part - C: Toxicology and Pharmacology, 249. https://doi.org/10.1016/j.cbpc.2021.109141

Desforges, J. P. W., Galbraith, M., Dangerfield, N., & Ross, P. S. (2014). Widespread distribution of microplastics in subsurface seawater in the NE Pacific Ocean. Marine Pollution Bulletin, 79(1–2), 94–99. https://doi.org/10.1016/j.marpolbul.2013.12.035

Devin, S., Burgeot, T., Giambérini, L., Minguez, L., & Pain-Devin, S. (2014). The integrated biomarker response revisited: Optimization to avoid misuse. Environmental Science and Pollution Research, 21(4), 2448–2454. https://doi.org/10.1007/s11356-013-2169-9

DeYoung, D., Bantle, J., Hull, M., & Burks, S. L. (1996). Differences in Sensitivity to Developmental Toxicants as Seen in *Xenopus* and *Pimephales* Embryos. Bulletin of Environmental Contamination and Toxicology 56, 143–150. https://doi.org/10.1007/s001289900021

Di Poi, C., Costil, K., Bouchart, V., & Halm-Lemeille, M.-P. (2018). Toxicity assessment of five emerging pollutants, alone and in binary or ternary mixtures, towards three aquatic organisms. Environmental Science and Pollution Research, 25(7), 6122–6134. https://doi.org/10.1007/s11356-017-9306-9

Digilio, G., Sforzini, S., Cassino, C., Robotti, E., Oliveri, C., Marengo, E., Musso, D., Osella, D., & Viarengo, A. (2016). Haemolymph from *Mytilus galloprovincialis:* Response to copper and temperature challenges studied by 1H-NMR metabonomics. Comparative Biochemistry and Physiology Part - C: Toxicology and Pharmacology, 183–184, 61–71. https://doi.org/10.1016/j.cbpc.2016.02.003

Domenech, J., Cortés, C., Vela, L., Marcos, R., & Hernández, A. (2021). Polystyrene nanoplastics as carriers of metals. Interactions of polystyrene nanoparticles with silver nanoparticles and silver nitrate, and their effects on human intestinal caco-2 cells. Biomolecules, 11(6). https://doi.org/10.3390/biom11060859

Dong, Z., Zhang, W., Qiu, Y., Yang, Z., Wang, J., & Zhang, Y. (2019). Cotransport of nanoplastics (PS-NPs) with fullerene (C60) in saturated sand: Effect of PS-NPs/C60 ratio and seawater salinity. Water Research, 148, 469–478. https://doi.org/10.1016/j.watres.2018.10.071

Ekvall, M. T., Lundqvist, M., Kelpsiene, E., Šileikis, E., Gunnarsson, S. B., & Cedervall, T. (2019). Nanoplastics formed during the mechanical breakdown of daily-use polystyrene products. Nanoscale Advances, 1(3), 1055–1061. https://doi.org/10.1039/c8na00210j

El Hadri, H., Gigault, J., Maxit, B., Grassl, B., & Reynaud, S. (2020). Nanoplastic from mechanically degraded primary and secondary microplastics for environmental assessments. NanoImpact, 17, 100206. https://doi.org/10.1016/j.impact.2019.100206

Elersek, T., Milavec, S., Korošec, M., Brezovsek, P., Negreira, N., Zonja, B., de Alda, M. L., Barceló, D., Heath, E., Ščančar, J., & Filipič, M. (2016). Toxicity of the mixture of

selected antineoplastic drugs against aquatic primary producers. Environmental Science and Pollution Research, 23(15), 14780–14790. https://doi.org/10.1007/s11356-015-6005-2

Ellman, G. L., Courtney, K. D., Andres, V., & Featherstone, R. M. (1961). A new and rapid colorimetric determination of acetylcholinesterase activity. Biochemical Pharmacology, 7(2), 88–95. https://doi.org/10.1016/0006-2952(61)90145-9

Environmental, A. (1998). Microtox acute toxicity test guide. *Users Manual, Carlsbad, USA*.

Erdelmeier, I., Gérard-Monnier, D., Yadan, J. C., & Chaudière, J. (1998). Reactions of N-methyl-2-phenylindole with malondialdehyde and 4- hydroxyalkenals. Mechanistic aspects of the colorimetric assay of lipid peroxidation. Chemical Research in Toxicology, 11(10), 1184–1194. https://doi.org/10.1021/tx970180z

Essawy, E., Abdelfattah, M. S., El-Matbouli, M., & Saleh, M. (2021). Synergistic effect of biosynthesized silver nanoparticles and natural phenolic compounds against drug-resistant fish pathogens and their cytotoxicity: An *in vitro* study. Marine Drugs, 19(1). https://doi.org/10.3390/md19010022

Estrela, F. N., Batista Guimarães, A. T., Silva, F. G., Marinho da Luz, T., Silva, A. M., Pereira, P. S., & Malafaia, G. (2021). Effects of polystyrene nanoplastics on *Ctenopharyngodon idella* (grass carp) after individual and combined exposure with zinc oxide nanoparticles. Journal of Hazardous Materials, 403. https://doi.org/10.1016/j.jhazmat.2020.123879

EU Directive 93/67/EEC. (1993). Official Journal of the European Communities.

European Medicines Agency (EMA/367286/2020). (2020). 5FU A31_2020-04_public health communication_post EC decision. www.ema.europa.eu/contact

Faggio, C., Tsarpali, V., & Dailianis, S. (2018). Mussel digestive gland as a model tissue for assessing xenobiotics: An overview. Science of the Total Environment, 636, 220–229. https://doi.org/10.1016/j.scitotenv.2018.04.264

FAO. 2024. *Mytilus galloprovincialis*. Cultured Aquatic Species Information Programme. Text by Figueras, A.. In: *Fisheries and Aquaculture*. [Cited Monday, December 2nd 2024]. https://www.fao.org/fishery/en/culturedspecies/mytilus_galloprovincialis/en

Fearman, J. A., Bolch, C. J. S., & Moltschaniwskyj, N. A. (2009). Energy storage and reproduction in mussels, *Mytilus galloprovincialis:* The influence of diet quality. Journal of Shellfish Research, 28(2), 305–312. https://doi.org/10.2983/035.028.0212

Fernandes, E., Fonseca, T. G., Carriço, T., Mestre, N., Tavares, Á., & Bebianno, M. J. (2020). Cytotoxic responses of the anticancer drug cyclophosphamide in the mussel *Mytilus galloprovincialis* and comparative sensitivity with human cells lines. Chemosphere, 261, 127678. https://doi.org/10.1016/j.chemosphere.2020.127678

Fernandes, J. P., Mucha, A. P., Francisco, T., Gomes, C. R., & Almeida, C. M. R. (2017). Silver nanoparticles uptake by salt marsh plants – Implications for phytoremediation

processes and effects in microbial community dynamics. Marine Pollution Bulletin, 119(1), 176–183. https://doi.org/10.1016/j.marpolbul.2017.03.052

Fernández, B., Campillo, J. A., Martínez-Gómez, C., & Benedicto, J. (2010). Antioxidant responses in gills of mussel (*Mytilus galloprovincialis*) as biomarkers of environmental stress along the Spanish Mediterranean coast. Aquatic Toxicology, 99(2), 186–197. https://doi.org/10.1016/j.aquatox.2010.04.013

Fernández, B., Campillo, J. A., Martínez-Gómez, C., & Benedicto, J. (2012). Assessment of the mechanisms of detoxification of chemical compounds and antioxidant enzymes in the digestive gland of mussels, *Mytilus galloprovincialis*, from Mediterranean coastal sites. Chemosphere, 87(11), 1235–1245. https://doi.org/10.1016/j.chemosphere.2012.01.024

Ferreira, I., Venâncio, C., Lopes, I., & Oliveira, M. (2019). Nanoplastics and marine organisms: What has been studied? Environmental Toxicology and Pharmacology, 67, 1–7. https://doi.org/10.1016/j.etap.2019.01.006

Fotopoulou, K. N., & Karapanagioti, H. K. (2012). Surface properties of beached plastic pellets. Marine Environmental Research, 81, 70–77. https://doi.org/10.1016/j.marenvres.2012.08.010

Gačić, Z., Kolarević, S., Sunjog, K., Kračun-Kolarević, M., Paunović, M., Knežević-Vukčević, J., & Vuković-Gačić, B. (2014). The impact of *in vivo* and *in vitro* exposure to base analogue 5-FU on the level of DNA damage in haemocytes of freshwater mussels *Unio pictorum* and *Unio tumidus*. Environmental Pollution, 191, 145–150. https://doi.org/10.1016/j.envpol.2014.04.024

Gagné, F. (2019). Detection of polystyrene nanoplastics in biological tissues with a fluorescent molecular rotor probe. Journal of Xenobiotics, 9, 7–9. https://doi.org/10.4081/xeno.2019.8147

Gallo, A., Esposito, M. C., Boni, R., & Tosti, E. (2022). Oocyte quality assessment in marine invertebrates: a novel approach by fluorescence spectroscopy. Biological Research, 55(1). https://doi.org/10.1186/s40659-022-00403-4

Gallo, A., Esposito, M. C., Tosti, E., & Boni, R. (2021). Sperm motility, oxidative status, and mitochondrial activity: Exploring correlation in different species. Antioxidants, 10(7). https://doi.org/10.3390/antiox10071131

Gambardella, C., Morgana, S., Ferrando, S., Bramini, M., Piazza, V., Costa, E., Garaventa, F., & Faimali, M. (2017). Effects of polystyrene microbeads in marine planktonic crustaceans. Ecotoxicology and Environmental Safety, 145, 250–257. https://doi.org/10.1016/j.ecoenv.2017.07.036

Gambardella, C., Piazza, V., Albentosa, M., Bebianno, M. J., Cardoso, C., Faimali, M., Garaventa, F., Garrido, S., González, S., Pérez, S., Sendra, M., & Beiras, R. (2019). Microplastics do not affect standard ecotoxicological endpoints in marine unicellular organisms. Marine Pollution Bulletin, 143, 140–143. https://doi.org/10.1016/j.marpolbul.2019.04.055

Gatz, L. (2021). Contaminants of Emerging Concern Under the Clean Water Act. Congretional Research Service, R45998. https://crsreports.congress.gov

Geret, F., Serafim, A., Barreira, L., & João Bebianno, M. (2002). Response of antioxidant systems to copper in the gills of the clam *Ruditapes decussatus*. Marine Environmental Research, 54(3–5), 413–417. https://doi.org/10.1016/S0141-1136(02)00164-2

Ghafouri-Fard, S., Abak, A., Tondro Anamag, F., Shoorei, H., Fattahi, F., Javadinia, S. A., Basiri, A., & Taheri, M. (2021). 5-Fluorouracil: A narrative review on the role of regulatory mechanisms in driving resistance to this chemotherapeutic agent. Frontiers in Oncology, 11, 1–21. https://doi.org/10.3389/fonc.2021.658636

Ghobashy, M. M., Elkodous, M. A., Shabaka, S. H., Younis, S. A., Alshangiti, D. M., Madani, M., Al-Gahtany, S. A., Elkhatib, W. F., Noreddin, A. M., Nady, N., & El-Sayyad, G. S. (2021). An overview of methods for production and detection of silver nanoparticles, with emphasis on their fate and toxicological effects on human, soil, and aquatic environment. Nanotechnology Reviews, 10(1), 954–977. https://doi.org/10.1515/ntrev-2021-0066

Gigault, J., Halle, A. ter, Baudrimont, M., Pascal, P.-Y., Gauffre, F., Phi, T.-L., El Hadri, H., Grassl, B., & Reynaud, S. (2018). Current opinion: What is a nanoplastic? Environmental Pollution, 235, 1030–1034. https://doi.org/10.1016/j.envpol.2018.01.024

Gomes, T., Almeida, A. C., & Georgantzopoulou, A. (2020). Characterization of cell responses in *Rhodomonas baltica* exposed to PMMA nanoplastics. Science of the Total Environment, 726, 138547. https://doi.org/10.1016/j.scitotenv.2020.138547

Gomes, T., Araújo, O., Pereira, R., Almeida, A. C., Cravo, A., & Bebianno, M. J. (2013). Genotoxicity of copper oxide and silver nanoparticles in the mussel *Mytilus galloprovincialis.* Marine Environmental Research, 84, 51–59. https://doi.org/10.1016/j.marenvres.2012.11.009

Gomes, T., Pereira, C. G., Cardoso, C., Sousa, V. S., Teixeira, M. R., Pinheiro, J. P., & Bebianno, M. J. (2014). Effects of silver nanoparticles exposure in the mussel *Mytilus galloprovincialis*. Marine Environmental Research, 101, 208–214. https://doi.org/10.1016/j.marenvres.2014.07.004

Gómez-Mendikute, A., & Cajaraville, M. P. (2003). Comparative effects of cadmium, copper, paraquat and benzo[a]pyrene on the actin cytoskeleton and production of reactive oxygen species (ROS) in mussel haemocytes. Toxicology in Vitro, 17(5–6), 539–546. https://doi.org/10.1016/S0887-2333(03)00093-6

Gonçalves, J. M., & Bebianno, M. J. (2021). Nanoplastics impact on marine biota: a review. Environmental Pollution, 273, 116426. https://doi.org/10.1016/j.envpol.2021.116426

Gonçalves, J. M., & Bebianno, M. J. (2023). Ecotoxicity of emerging contaminants in the reproductive organ of marine mussels *Mytilus galloprovincialis.* Science of the Total Environment, 881, 163486. https://doi.org/10.1016/j.scitotenv.2023.163486

Gonçalves, J. M., Beckmann, C., & Bebianno, M. J. (2022a). Assessing the effects of the cytostatic drug 5-Fluorouracil alone and in a mixture of emerging contaminants on the

mussel *Mytilus galloprovincialis*. Chemosphere, 305, 135462. https://doi.org/10.1016/j.chemosphere.2022.135462

Gonçalves, J. M., Benedetti, M., d'Errico, G., Regoli, F., & Bebianno, M. J. (2025). Gender effects of nanoplastics and emerging contaminants mixtures in *Mytilus galloprovincialis*. Aquatic Toxicology, 279, 107219. https://doi.org/10.1016/j.aquatox.2024.107219

Gonçalves, J. M., Rocha, T., Mestre, N. M., Fonseca, T. G., & Bebianno, M. J. (2020). Assessing cadmium-based quantum dots effects on the gonads of the marine mussel *Mytilus galloprovincialis*. Marine Environmental Research, 156, 104904. https://doi.org/10.1016/j.marenvres.2020.104904

Gonçalves, J. M., Sousa, V. S., Teixeira, M. R., & Bebianno, M. J. (2022b). Chronic toxicity of polystyrene nanoparticles in the marine mussel *Mytilus galloprovincialis*. Chemosphere, 287, 132356. https://doi.org/10.1016/j.chemosphere.2021.132356

González-Fernández, C., Le Grand, F., Bideau, A., Huvet, A., Paul-Pont, I., & Soudant, P. (2020). Nanoplastics exposure modulate lipid and pigment compositions in diatoms. Environmental Pollution, 262. https://doi.org/10.1016/j.envpol.2020.114274

González-Fernández, C., Tallec, K., le Goïc, N., Lambert, C., Soudant, P., Huvet, A., Suquet, M., Berchel, M., & Paul-Pont, I. (2018). Cellular responses of Pacific oyster (*Crassostrea gigas*) gametes exposed *in vitro* to polystyrene nanoparticles. Chemosphere, 208, 764–772. https://doi.org/10.1016/j.chemosphere.2018.06.039

Gonzalez-Rey, M., & Bebianno, M. J. (2012). Does non-steroidal anti-inflammatory (NSAID) ibuprofen induce antioxidant stress and endocrine disruption in mussel *Mytilus galloprovincialis*? Environmental Toxicology and Pharmacology, 33(2), 361–371. https://doi.org/10.1016/j.etap.2011.12.017

Gonzalez-Rey, M., & Bebianno, M. J. (2013). Does selective serotonin reuptake inhibitor (SSRI) fluoxetine affects mussel *Mytilus galloprovincialis*? Environmental Pollution, 173, 200–209. https://doi.org/10.1016/j.envpol.2012.10.018

Gonzalez-Rey, M., & Bebianno, M. J. (2014). Effects of non-steroidal anti-inflammatory drug (NSAID) diclofenac exposure in mussel *Mytilus galloprovincialis*. Aquatic Toxicology, 148, 818–831. https://doi.org/10.1016/j.aquatox.2014.01.011

Grandview Research. (2024). Silver nanoparticles market size, share & trends analysis report by application (electronics & electrical, healthcare, food & beverages, textiles, others), by Region, and segment forecasts, 2024 - 2030. Report ID: 978-1-68038-413-0. https://www.grandviewresearch.com/industry-analysis/silver-nanoparticles-market/toc

GraphPad Software Inc., CA. (2021). GraphPad Prism Version 9.1.1 for Windows, San Diego, California, USA. www.graphpad.com

Green, D. S., Colgan, T. J., Thompson, R. C., & Carolan, J. C. (2019). Exposure to microplastics reduces attachment strength and alters the haemolymph proteome of blue mussels (*Mytilus edulis*). Environmental Pollution, 246, 423–434. https://doi.org/10.1016/j.envpol.2018.12.017

Greenwald, R. A. (1985). Handbook Methods For Oxygen Radical Research. CRC Press. https://doi.org/10.1201/9781351072922

Gurel, P. S., Hatch, A. L., & Higgs, H. N. (2014). Connecting the cytoskeleton to the endoplasmic reticulum and Golgi. Current Biology 24(14), R660 - R672. https://doi.org/10.1016/j.cub.2014.05.033

Habig, W. H., & Jakoby, W. B. (1981). Assays for differentiation of glutathione S-Transferases. In Methods in Enzymology 77, 398–405. Elsevier. https://doi.org/10.1016/S0076-6879(81)77053-8

Habig, W. H., Pabst, M. J., & Jakoby, W. B. (1974). Glutathione S transferases. The first enzymatic step in mercapturic acid formation. Journal of Biological Chemistry, 249(22), 7130–7139. https://doi.org/10.1016/S0021-9258(19)42083-8

Haegerbaeumer, A., Mueller, M. T., Fueser, H., & Traunspurger, W. (2019). Impacts of micro- and nano-sized plastic particles on benthic invertebrates: A literature review and gap analysis. Frontiers in Environmental Science, 7. https://doi.org/10.3389/fenvs.2019.00017

Halle, A. Ter, Jeanneau, L., Martignac, M., Jardé, E., Pedrono, B., Brach, L., & Gigault, J. (2017). Nanoplastic in the North Atlantic Subtropical Gyre. Environmental Science and Technology, 51(23), 13689–13697. https://doi.org/10.1021/acs.est.7b03667

Hayes, J. D., Flanagan, J. U., & Jowsey, I. R. (2005). Glutathione transferases. Annual Review of Pharmacology and Toxicology, 45(1), 51–88. https://doi.org/10.1146/annurev.pharmtox.45.120403.095857

Heath, E., & Isidori, M. (2020). Fate and Effects of Anticancer Drugs in the Environment. In E. Heath, M. Isidori, T. Kosjek, & M. Filipič (Eds.), Fate and Effects of Anticancer Drugs in the Environment (1st ed.). Springer Cham. https://doi.org/10.1007/978-3-030-21048-9

Holmes, L. A., Turner, A., & Thompson, R. C. (2012). Adsorption of trace metals to plastic resin pellets in the marine environment. Environmental Pollution, 160, 42–48. https://doi.org/10.1016/j.envpol.2011.08.052

Holmes, L. A., Turner, A., & Thompson, R. C. (2014). Interactions between trace metals and plastic production pellets under estuarine conditions. Marine Chemistry, 167, 25–32. https://doi.org/10.1016/j.marchem.2014.06.001

Hu, E., Shang, S., Fu, Z., Zhao, X., Nan, X., Du, Y., & Chen, X. (2020). Cotransport of naphthalene with polystyrene nanoplastics (PSNP) in saturated porous media: Effects of PSNP/naphthalene ratio and ionic strength. Chemosphere, 245, 125602. https://doi.org/10.1016/j.chemosphere.2019.125602

Huang da W, Sherman BT, Lempicki RA. Systematic and integrative analysis of large gene lists using DAVID bioinformatics resources. Nature Protocols. 2009;4(1):44-57. doi: 10.1038/nprot.2008.211. PMID: 19131956.

IARC Monographs, I. A. for R. on C. (1987). 5-Fluorouracil (Group 3): Vol. Suppl. 7. http://publications.iarc.fr>media>download

INFARMED. (2024). Annex I List of nationally authorised medicinal products. https://www.infarmed.pt/documents/15786/3591726/Fluorouracilo_Anexos/24b80235-a077-88a3-56c3-62ba9c9bb4a5?version=1.2

Instituto Nacional de Estatística Statistics Portugal. (2021). Relatório e Contas - 2021 (I. P. A. A. J. de A. 1000-043 L. – P. Instituto Nacional de Estatística (Ed.)).

Ivar do Sul, J.A., Costa, M.F. & Fillmann, G. (2014)Microplastics in the pelagic environment around oceanic islands of the Western Tropical Atlantic Ocean. Water Air Soil Pollut 225(7), 2004. https://doi.org/10.1007/s11270-014-2004-z

Jambeck, J. R., Geyer, R., Wilcox, C., Siegler, T. R., Perryman, M., Andrady, A., Narayan, R., & Law, K. L. (2015). Plastic waste inputs from land into the ocean. Science, 347(6223), 768–771. https://doi.org/10.1126/science.1260352

Jeong, J., & Choi, J. (2019). Adverse outcome pathways potentially related to hazard identification of microplastics based on toxicity mechanisms. Chemosphere, 231, 249–255. https://doi.org/10.1016/j.chemosphere.2019.05.003

Jiao, K., Yang, B., Wang, H., Xu, W., Zhang, C., Gao, Y., Sun, W., Li, F., & Ji, D. (2022). The individual and combined effects of polystyrene and silver nanoparticles on nitrogen transformation and bacterial communities in an agricultural soil. Science of The Total Environment, 820, 153358. https://doi.org/10.1016/J.SCITOTENV.2022.153358

Johnson, A. C., Oldenkamp, R., Dumont, E., & Sumpter, J. P. (2013). Predicting concentrations of the cytostatic drugs cyclophosphamide, carboplatin, 5-fluorouracil, and capecitabine throughout the sewage effluents and surface waters of Europe: Cytostatic drug concentrations in European rivers. Environmental Toxicology and Chemistry, 32(9), 1954–1961. https://doi.org/10.1002/etc.2311

Jørgensen, C. B. (1996). Bivalve filter feeding revisited. Marine Ecology Progress Series, 142(1–3), 287–302. https://doi.org/10.3354/meps142287

Katsumiti, A., Gilliland, D., Arostegui, I., & Cajaraville, M. P. (2014). Cytotoxicity and cellular mechanisms involved in the toxicity of CdS quantum dots in hemocytes and gill cells of the mussel *Mytilus galloprovincialis.* Aquatic Toxicology, 153, 39–52. https://doi.org/10.1016/j.aquatox.2014.02.003

Katsumiti, A., Losada-Carrillo, M. P., Barros, M., & Cajaraville, M. P. (2021). Polystyrene nanoplastics and microplastics can act as Trojan horse carriers of benzo(a)pyrene to mussel hemocytes in vitro. Scientific Reports, 11(1), 1–17. https://doi.org/10.1038/s41598-021-01938-4

Kautsky, N. (1982) Growth and Size Structure in a Baltic *Mytilus edulis* Population. Marine Biology, 68, 117-133. http://dx.doi.org/10.1007/BF00397599

Khan, S. U., Saleh, T. A., Wahab, A., Khan, M. H. U., Khan, D., Khan, W. U., Rahim, A.,

Kamal, S., Khan, F. U., & Fahad, S. (2018). Nanosilver: New ageless and versatile biomedical therapeutic scaffold. International Journal of Nanomedicine, 13, 733–762. https://doi.org/10.2147/IJN.S153167

Kihara, S., Köper, I., Mata, J. P., & McGillivray, D. J. (2021). Reviewing nanoplastic toxicology: It's an interface problem. Advances in Colloid and Interface Science, 288, 102337. https://doi.org/10.1016/j.cis.2020.102337

Kik, K., Bukowska, B., & Sicińska, P. (2020). Polystyrene nanoparticles: Sources, occurrence in the environment, distribution in tissues, accumulation and toxicity to various organisms. Environmental Pollution, 262. https://doi.org/10.1016/j.envpol.2020.114297

Klaine, S. J., Koelmans, A. A., Horne, N., Carley, S., Handy, R. D., Kapustka, L., Nowack, B., & von der Kammer, F. (2012). Paradigms to assess the environmental impact of manufactured nanomaterials. Environmental Toxicology and Chemistry, 31(1), 3–14. https://doi.org/10.1002/etc.733

Kleinert, C., Poirier-Larabie, S., Gagnon, C., André, C., & Gagné, F. (2021). Occurrence and ecotoxicity of cytostatic drugs 5-fluorouracil and methotrexate in the freshwater unionid *Elliptio complanata*. Comparative Biochemistry and Physiology Part C: Toxicology & Pharmacology, 244, 109027. https://doi.org/10.1016/j.cbpc.2021.109027

Koelmans, A. A., Besseling, E., & Shim, W. J. (2015). Nanoplastics in the aquatic environment. Critical review. In M. Bergmann, L. Gutow, & M. Klages (Eds.), Marine Anthropogenic Litter, 325–340. Springer Cham. https://doi.org/10.1007/978-3-319-16510-3_12

Kögel, T., Bjorøy, Ø., Toto, B., Bienfait, A. M., & Sanden, M. (2020). Micro- and nanoplastic toxicity on aquatic life: Determining factors. Science of The Total Environment, 709, 136050. https://doi.org/10.1016/J.SCITOTENV.2019.136050

Kosjek, T., Perko, S., Žigon, D., & Heath, E. (2013). Fluorouracil in the environment: Analysis, occurrence, degradation and transformation. Journal of Chromatography A, 1290, 62–72. https://doi.org/10.1016/j.chroma.2013.03.046

Kovács, R., Bakos, K., Urbányi, B., Kövesi, J., Gazsi, G., Csepeli, A., Appl, Á. J., Bencsik, D., Csenki, Z., & Horváth, Á. (2016). Acute and sub-chronic toxicity of four cytostatic drugs in zebrafish. Environmental Science and Pollution Research, 23(15), 14718–14729. https://doi.org/10.1007/s11356-015-5036-z

Kračun-Kolarević, M., Kolarević, S., Atanacković, A., Marković, V., Gačić, Z., Paunović, M., & Vuković-Gačić, B. (2015). Effects of 5-Fluorouracil, Etoposide and CdCl2 in Aquatic Oligochaeta *Limnodrilus udekemianus* Claparede (Tubificidae) Measured by Comet Assay. Water, Air, and Soil Pollution, 226(8), 1–9. https://doi.org/10.1007/S11270-015-2511-6/FIGURES/4

Kumar, R., Qureshi, M., Vishwakarma, D. K., Al-Ansari, N., Kuriqi, A., Elbeltagi, A., & Saraswat, A. (2022). A review on emerging water contaminants and the application of sustainable removal technologies. Case Studies in Chemical and Environmental Engineering, 6, 100219. https://doi.org/10.1016/j.cscee.2022.100219

Kümmerer, K., & Henninger, A. (2003). Promoting resistance by the emission of antibiotics from hospitals and households into effluent. Clinical Microbiology and Infection, 9(12), 1203–1214. https://doi.org/10.1111/j.1469-0691.2003.00739.x

Kusi, J., Scheuerman, P. R., & Maier, K. J. (2020). Emerging environmental contaminants (silver nanoparticles) altered the catabolic capability and metabolic fingerprinting of microbial communities. Aquatic Toxicology, 228, 105633. https://doi.org/10.1016/J.AQUATOX.2020.105633

Kwon, B. G., Koizumi, K., Chung, S. Y., Kodera, Y., Kim, J. O., & Saido, K. (2015). Global styrene oligomers monitoring as new chemical contamination from polystyrene plastic marine pollution. Journal of Hazardous Materials, 300, 359–367. https://doi.org/10.1016/j.jhazmat.2015.07.039

Langner, S., Rakers, S., Ciba, P., Petschnik, A. E., Rapoport, D. H., & Kruse, C. (2011). New cell line from adipopancreatic tissue of Atlantic herring *Clupea harengus*. Aquatic Biology, 11(3), 271–278. https://doi.org/10.3354/ab00317

Lee, H., Shim, W. J., & Kwon, J. H. (2014). Sorption capacity of plastic debris for hydrophobic organic chemicals. Science of the Total Environment, 470–471, 1545–1552. https://doi.org/10.1016/j.scitotenv.2013.08.023

Lee, K. W., Shim, W. J., Kwon, O. Y., & Kang, J. H. (2013). Size-dependent effects of micro polystyrene particles in the marine copepod *Tigriopus japonicus*. Environmental Science and Technology, 47(19), 11278–11283. https://doi.org/10.1021/es401932b

Lee, S. H., & Jun, B. H. (2019). Silver Nanoparticles: Synthesis and Application for Nanomedicine. International Journal of Molecular Sciences 2019, 20(4), 865. https://doi.org/10.3390/IJMS20040865

Lee, S., Gounley, J., Randles, A., & Vetter, J. S. (2019). Performance portability study for massively parallel computational fluid dynamics application on scalable heterogeneous architectures. Journal of Parallel and Distributed Computing, 129, 1–13. https://doi.org/10.1016/j.jpdc.2019.02.005

Lewis, C., & Ford, A. T. (2012). Infertility in male aquatic invertebrates: A review. Aquatic Toxicology, 120–121, 79–89. https://doi.org/10.1016/j.aquatox.2012.05.002

Li, D., Chen, H., Liu, H., Schlenk, D., Mu, J., Lacorte, S., Ying, G.-G., & Xie, L. (2021). Anticancer drugs in the aquatic ecosystem: Environmental occurrence, ecotoxicological effect and risk assessment. Environment International, 153, 106543. https://doi.org/10.1016/j.envint.2021.106543

Li, J., Zhou, Y., Zhou, Z., Lin, C., Wei, J., Qin, Y., Xiang, Z., Ma, H., Zhang, Y., Zhang, Y., & Yu, Z. (2020). Comparative transcriptome analysis of three gonadal development stages reveals potential genes involved in gametogenesis of the fluted giant clam (*Tridacna squamosa*). BMC Genomics, 21(1). https://doi.org/10.1186/s12864-020-07276-5

Li, Z., Feng, C., Wu, Y., & Guo, X. (2020). Impacts of nanoplastics on bivalve: Fluorescence tracing of organ accumulation, oxidative stress and damage. Journal of Hazardous Materials, 392, 122418. https://doi.org/10.1016/j.jhazmat.2020.122418

Li, Z., Xian, H., Ye, R., Zhong, Y., Liang, B., Huang, Y., Dai, M., Guo, J., Tang, S., Ren, X., Bai, R., Feng, Y., Deng, Y., Yang, X., Chen, D., Yang, Z., & Huang, Z. (2024). Gender-specific effects of polystyrene nanoplastic exposure on triclosan-induced reproductive toxicity in zebrafish (*Danio rerio*). Science of the Total Environment, 932. https://doi.org/10.1016/j.scitotenv.2024.172876

Lin, A. Y.-C., Lin, Y.-C., & Lee, W.-N. (2014). Prevalence and sunlight photolysis of controlled and chemotherapeutic drugs in aqueous environments. Environmental Pollution, 187, 170–181. https://doi.org/10.1016/j.envpol.2014.01.005

Liu, L., Fokkink, R., & Koelmans, A. A. (2016). Sorption of polycyclic aromatic hydrocarbons to polystyrene nanoplastic. Environmental Toxicology and Chemistry, 35(7), 1650–1655. https://doi.org/10.1002/etc.3311

López-Pedrouso, M., Varela, Z., Franco, D., Fernández, J. A., & Aboal, J. R. (2020). Can proteomics contribute to biomonitoring of aquatic pollution? A critical review. Environmental Pollution, 267, 115473. https://doi.org/10.1016/J.ENVPOL.2020.115473

Lorusso, C., Calisi, A., Sarà, G., & Dondero, F. (2022). In-gel assay to evaluate antioxidant enzyme response to silver nitrate and silver nanoparticles in marine bivalve tissues. Applied Sciences, 12(6), 2760. https://doi.org/10.3390/app12062760

Lu, Y., Zhang, Y., Deng, Y., Jiang, W., Zhao, Y., Geng, J., Ding, L., & Ren, H. (2016). Uptake and accumulation of polystyrene microplastics in zebrafish (*Danio rerio*) and toxic effects in liver. Environmental Science & Technology, 50(7), 4054–4060. https://doi.org/10.1021/acs.est.6b00183

Luigi, P., Chiara, A., Elisabetta, G., Alessandra, S., & Gian, M. (2012). Utilization of Marine Crustaceans as Study Models: A New Approach in Marine Ecotoxicology for European (REACH) Regulation. Ecotoxicology. Ghousia Begum (Ed), vol. 91. https://doi.org/10.5772/28513

Ma, S., Wang, L., Li, S., Zhao, S., Li, F., & Li, X. (2024). Transcriptome and proteome analyses reveal the mechanisms involved in polystyrene nanoplastics disrupt spermatogenesis in mice. Environmental Pollution, 342, 123086. https://doi.org/10.1016/j.envpol.2023.123086

Maaghloud, H., Houssa, R., Bellali, F., El Bouqdaoui, K., Ouansafi, S., Loulad, S., & Fahde, A. (2021). Microplastic ingestion by Atlantic horse mackerel (*Trachurus trachurus*) in the North and central Moroccan Atlantic coast between Larache (35°30′N) and Boujdour (26°30′N). Environmental Pollution, 288, 117781. https://doi.org/10.1016/j.envpol.2021.117781

Mahnik, S. N., Lenz, K., Weissenbacher, N., Mader, R. M., & Fuerhacker, M. (2007). Fate of 5-fluorouracil, doxorubicin, epirubicin, and daunorubicin in hospital wastewater and their

elimination by activated sludge and treatment in a membrane-bio-reactor system. Chemosphere, 66(1), 30–37. https://doi.org/10.1016/j.chemosphere.2006.05.051

Maillard, J.-Y., & Hartemann, P. (2013). Silver as an antimicrobial: Facts and gaps in knowledge. Critical Reviews in Microbiology, 39(4), 373–383. https://doi.org/10.3109/1040841X.2012.713323

Manduzio, H., Rocher, B., Durand, F., Galap, C., Leboulenger, F. (2005). The point about oxidative stress in molluscs. Invertebrate Survival Journal, 2, 91–104. ⟨hal-01738557⟩

Manfra, L., Rotini, A., Bergami, E., Grassi, G., Faleri, C., & Corsi, I. (2017). Comparative ecotoxicity of polystyrene nanoparticles in natural seawater and reconstituted seawater using the rotifer *Brachionus plicatilis*. Ecotoxicology and Environmental Safety, 145, 557–563. https://doi.org/10.1016/j.ecoenv.2017.07.068

Mao, Y., Li, H., Huangfu, X., Liu, Y., & He, Q. (2020). Nanoplastics display strong stability in aqueous environments: Insights from aggregation behaviour and theoretical calculations. Environmental Pollution, 258, 113760. https://doi.org/10.1016/j.envpol.2019.113760

Market Research, M. (2022). Silver Nanoparticles Market – Forecast and Analysis (2022-2029) – by End Users and by Region. https://www.marketresearch.com/VPA-Research-v4245/Silver-Nanoparticles-Size-Share-Trends-34742743/

Martín, J., Santos, J. L., Aparicio, I., & Alonso, E. (2022). Microplastics and associated emerging contaminants in the environment: Analysis, sorption mechanisms and effects of co-exposure. Trends in Environmental Analytical Chemistry, 35, e00170. https://doi.org/10.1016/j.teac.2022.e00170

Martínez-Morcillo, S., Rodríguez-Gil, J. L., Fernández-Rubio, J., Rodríguez-Mozaz, S., Míguez-Santiyán, M. P., Valdes, M. E., Barceló, D., & Valcárcel, Y. (2020). Presence of pharmaceutical compounds, levels of biochemical biomarkers in seafood tissues and risk assessment for human health: Results from a case study in North-Western Spain. International Journal of Hygiene and Environmental Health, 223(1), 10–21. https://doi.org/10.1016/j.ijheh.2019.10.011

Martínez-Pita, I., Sánchez-Lazo, C., Ruíz-Jarabo, I., Herrera, M., & Mancera, J. M. (2012). Biochemical composition, lipid classes, fatty acids and sexual hormones in the mussel *Mytilus galloprovincialis* from cultivated populations in south Spain. Aquaculture, 358–359, 274–283. https://doi.org/10.1016/j.aquaculture.2012.06.003

Martínez-Pita, I., Sánchez-Lazo, C., Ruíz-Jarabo, I., Herrera, M., & Mancera, J. M. (2012). Biochemical composition, lipid classes, fatty acids and sexual hormones in the mussel *Mytilus galloprovincialis* from cultivated populations in south Spain. Aquaculture, 358–359, 274–283. https://doi.org/10.1016/j.aquaculture.2012.06.003

Martínez, N. D. (2019). An integrated study of molecular, cellular, tissue level and transgenerational effects of silver nanoparticles on dietarily exposed mussels at different seasons. https://addi.ehu.es/bitstream/handle/10810/42163/tesis_duroudier_martinez_nerea.pdf?s

equence=1&isallowed=y

Mater, N., Geret, F., Castillo, L., Faucet-Marquis, V., Albasi, C., & Pfohl-Leszkowicz, A. (2014). *In vitro* tests aiding ecological risk assessment of ciprofloxacin, tamoxifen and cyclophosphamide in range of concentrations released in hospital wastewater and surface water. Environment International, 63, 191–200. https://doi.org/10.1016/j.envint.2013.11.011

Mattsson, K., Ekvall, M. T., Hansson, L. A., Linse, S., Malmendal, A., & Cedervall, T. (2015). Altered behaviour, physiology, and metabolism in fish exposed to polystyrene nanoparticles. Environmental Science and Technology, 49(1), 553–561. https://doi.org/10.1021/es5053655

Mattsson, K., Jocic, S., Doverbratt, I., & Hansson, L. A. (2018). Nanoplastics in the Aquatic Environment. Microplastic Contamination in Aquatic Environments: An Emerging Matter of Environmental Urgency, Chapter 13, 379–399. https://doi.org/10.1016/B978-0-12-813747-5.00013-8

Mattsson, K., Johnson, E. V., Malmendal, A., Linse, S., Hansson, L. A., & Cedervall, T. (2017). Brain damage and behavioural disorders in fish induced by plastic nanoparticles delivered through the food chain. Scientific Reports, 7(1), 1–7. https://doi.org/10.1038/s41598-017-10813-0

Matuo, R., Sousa, F. G., Escargueil, A. E., Grivicich, I., Garcia-Santos, D., Chies, J. A. B., Saffi, J., Larsen, A. K., & Henriques, J. A. P. (2009). 5-Fluorouracil and its active metabolite FdUMP cause DNA damage in human SW620 colon adenocarcinoma cell line. Journal of Applied Toxicology, 29(4), 308–316. https://doi.org/10.1002/jat.1411

McCarthy, M. P., Carroll, D. L., & Ringwood, A. H. (2013). Tissue specific responses of oysters, *crassostrea virginica*, to silver nanoparticles. Aquatic Toxicology, 138–139, 123–128. https://doi.org/10.1016/j.aquatox.2013.04.015

McCord, J. M., & Fridovich, I. (1969). Superoxide Dismutase: an enzymic function for erythrocuprein (hemocuprein). Journal of Biological Chemistry, 244(22), 6049–6055. https://doi.org/10.1016/S0021-9258(18)63504-5

McFarland, V. A., Inouye, L. S., Lutz, C. H., Jarvis, A. S., Clarke, J. U., & McCant, D. D. (1999). Biomarkers of oxidative stress and genotoxicity in livers of field- collected brown bullhead, *Ameiurus nebulosus*. Archives of Environmental Contamination and Toxicology, 37(2), 236–241. https://doi.org/10.1007/s002449900510

McGillicuddy, E., Murray, I., Kavanagh, S., Morrison, L., Fogarty, A., Cormican, M., Dockery, P., Prendergast, M., Rowan, N., & Morris, D. (2017). Silver nanoparticles in the environment: Sources, detection and ecotoxicology. Science of The Total Environment, 575, 231–246. https://doi.org/10.1016/j.scitotenv.2016.10.041

McQuillan, J. S., Groenaga Infante, H., Stokes, E., & Shaw, A. M. (2012). Silver nanoparticle enhanced silver ion stress response in *Escherichia coli* K12. Nanotoxicology, 6(8), 857–866. https://doi.org/10.3109/17435390.2011.626532

Mezzelani, M., Nardi, A., Bernardini, I., Milan, M., Peruzza, L., d'Errico, G., Fattorini, D., Gorbi, S., Patarnello, T., & Regoli, F. (2021). Environmental pharmaceuticals and climate change: The case study of carbamazepine in *M. galloprovincialis* under ocean acidification scenario. Environment International, 146, 106269. https://doi.org/10.1016/j.envint.2020.106269

Mikhailov, A. T., Torrado, M., & Méndez, J. (1995). Sexual differentiation of reproductive tissue in bivalve molluscs: Identification of male associated polypeptide in the mantle of *Mytilus galloprovincialis* Lmk. The International Journal of Developmental Biology, 39(3), 545–548. PMID: 7577446.

Mikhailova, E. O. (2020). Silver nanoparticles: mechanism of action and probable bio-application. Journal of Functional Biomaterials, 11(4), 84. https://doi.org/10.3390/jfb11040084

Mišík, M., Filipic, M., Nersesyan, A., Kundi, M., Isidori, M., & Knasmueller, S. (2019). Environmental risk assessment of widely used anticancer drugs (5-fluorouracil, cisplatin, etoposide, imatinib mesylate). Water Research, 164, 114953. https://doi.org/10.1016/j.watres.2019.114953

Mitchelmore, C. L., Birmelin, C., Livingstone, D. R., & Chipman, J. K. (1998). Detection of DNA strand breaks in isolated mussel (*Mytilus edulis* L.) digestive gland cells using the "comet" assay. Ecotoxicology and Environmental Safety, 41(1), 51–58. https://doi.org/10.1006/eesa.1998.1666

Moore, M. N., Allen, J. I., & Somerfield, P. J. (2006). Autophagy: Role in surviving environmental stress. Marine Environmental Research, 62(1), 420–425. https://doi.org/10.1016/j.marenvres.2006.04.055

Morcillo, P., Chaves-Pozo, E., Meseguer, J., Esteban, M. Á., & Cuesta, A. (2017). Establishment of a new teleost brain cell line (DLB-1) from the European sea bass and its use to study metal toxicology. Toxicology in Vitro, 38, 91–100. https://doi.org/10.1016/j.tiv.2016.10.005

Nardi, A., Mezzelani, M., Costa, S., d'Errico, G., Benedetti, M., Gorbi, S., Freitas, R., & Regoli, F. (2022). Marine heatwaves hamper neuro-immune and oxidative tolerance toward carbamazepine in *Mytilus galloprovincialis*. Environmental Pollution, 300, 118970. https://doi.org/10.1016/j.envpol.2022.118970

Nawaz, T., & Sengupta, S. (2019). Contaminants of emerging concern: Occurrence, fate, and remediation. Satinder Ahuja (Ed.), In Advances in Water Purification Techniques: Meeting the Needs of Developed and Developing Countries, (pp. 67–114). Elsevier. https://doi.org/10.1016/B978-0-12-814790-0.00004-1

Novak, M., Žegura, B., Modic, B., Heath, E., & Filipič, M. (2017). Cytotoxicity and genotoxicity of anticancer drug residues and their mixtures in experimental model with zebrafish liver cells. Science of the Total Environment, 601–602, 293–300. https://doi.org/10.1016/j.scitotenv.2017.05.115

Oca-Vásquez, G. M., Solano-Campos, F., Vega-Baudrit, J. R., López-Mondéjar, R., Odriozola, I., Vera, A., Moreno, J. L., & Bastida, F. (2020). Environmentally relevant concentrations of silver nanoparticles diminish soil microbial biomass but do not alter enzyme activities or microbial diversity. Journal of Hazardous Materials, 391, 122224. https://doi.org/10.1016/j.jhazmat.2020.122224

Okshevsky, M., Gautier, E., Farner, J. M., Schreiber, L., & Tufenkji, N. (2020). Biofilm formation by marine bacteria is impacted by concentration and surface functionalization of polystyrene nanoparticles in a species-specific manner. Environmental Microbiology Reports, 12(2), 203–213. https://doi.org/10.1111/1758-2229.12824

Oriekhova, O., & Stoll, S. (2018). Heteroaggregation of nanoplastic particles in the presence of inorganic colloids and natural organic matter. Environmental Science: Nano, 5(3), 792–799. https://doi.org/10.1039/c7en01119a

Palumbo, M. T. & Mingazzini, M. (2011). Toxicity test with algae: Evaluation of the sensitivity related to the use of biomass versus growth rate endpoint. in 16th International MESAEP Symposium on Environmental Pollution. https://www.researchgate.net/publication/305217028_toxicity_test_with_algae_evaluation_of_the_sensitivity_related_to_the_use_of_biomass_versus_growth_rate_endpoint/citations

Pannetier, P., Fuster, L., Clérandeau, C., Lacroix, C., Gourves, P. Y., Cachot, J., & Morin, B. (2018). Usefulness of RTL-W1 and OLCAB-e3 fish cell lines and multiple endpoint measurements for toxicity evaluation of unknown or complex mixture of chemicals. Ecotoxicology and Environmental Safety, 150, 40–48. https://doi.org/10.1016/j.ecoenv.2017.12.027

Parrella, A., Lavorgna, M., Criscuolo, E., Russo, C., & Isidori, M. (2015). Eco-genotoxicity of six anticancer drugs using comet assay in daphnids. Journal of Hazardous Materials, 286, 573–580. https://doi.org/10.1016/j.jhazmat.2015.01.012

Parrella, A., Lavorgna, M., Criscuolo, E., Russo, C., Fiumano, V., & Isidori, M. (2014). Acute and chronic toxicity of six anticancer drugs on rotifers and crustaceans. Chemosphere, 115(1), 59–66. https://doi.org/10.1016/j.chemosphere.2014.01.013

Pashaei, R., Dzingelevičienė, R., Abbasi, S., Szultka-Młyńska, M., & Buszewski, B. (2022). Determination of the pharmaceuticals–nano/microplastics in aquatic systems by analytical and instrumental methods. In Environmental Monitoring and Assessment 194(2). https://doi.org/10.1007/s10661-022-09751-w

Pastorino, P., & Ginebreda, A. (2021). Contaminants of emerging concern (CECs): Occurrence and fate in aquatic ecosystems. International Journal of Environmental Research and Public Health, 18(24), 18–21. https://doi.org/10.3390/ijerph182413401

Paul-Pont, I., Lacroix, C., González Fernández, C., Hégaret, H., Lambert, C., Le Goïc, N., Frère, L., Cassone, A. L., Sussarellu, R., Fabioux, C., Guyomarch, J., Albentosa, M., Huvet, A., & Soudant, P. (2016). Exposure of marine mussels *Mytilus* spp. to polystyrene microplastics: Toxicity and influence on fluoranthene bioaccumulation. Environmental Pollution, 216, 724–737. https://doi.org/10.1016/j.envpol.2016.06.039

Pedrajas, J. R., Peinado, J., & López-Barea, J. (1995). Oxidative stress in fish exposed to model xenobiotics. Oxidatively modified forms of Cu,Zn-superoxide dismutase as potential biomarkers. Chemico-Biological Interactions, 98(3), 267–282. https://doi.org/10.1016/0009-2797(95)03651-2

Peng, L., Fu, D., Qi, H., Lan, C. Q., Yu, H., & Ge, C. (2020). Micro- and nano-plastics in marine environment: Source, distribution and threats — A review. Science of the Total Environment, 698, 134254. https://doi.org/10.1016/j.scitotenv.2019.134254

Pereira, A. K. dos S., Reis, D. T., Barbosa, K. M., Scheidt, G. N., da Costa, L. S., & Santos, L. S. S. (2020). Antibacterial effects and ibuprofen release potential using chitosan microspheres loaded with silver nanoparticles. Carbohydrate Research, 488, 107891. https://doi.org/10.1016/j.carres.2019.107891

Pérez-Cremades, D., Bueno-Betí, C., García-Giménez, J. L., Ibañez-Cabellos, J. S., Pallardó, F. v., Hermenegildo, C., & Novella, S. (2023). Extracellular histones trigger oxidative stress-dependent induction of the NF-kB/CAM pathway via TLR4 in endothelial cells. Journal of Physiology and Biochemistry, 79(2), 251–260. https://doi.org/10.1007/s13105-022-00935-z

Picciotto, M. R., Higley, M. J., & Mineur, Y. S. (2012). Acetylcholine as a neuromodulator: cholinergic signaling shapes nervous system function and behavior. Neuron, 76(1), 116–129. https://doi.org/10.1016/j.neuron.2012.08.036

Pinsino, A., Bergami, E., Torre, C. Della, Vannuccini, M. L., Addis, P., Secci, M., Dawson, K. A., Matranga, V., & Corsi, I. (2017). Amino-modified polystyrene nanoparticles affect signalling pathways of the sea urchin (*Paracentrotus lividus*) embryos. Nanotoxicology, 11(2), 201–209. https://doi.org/10.1080/17435390.2017.1279360

Pitt, J. A., Trevisan, R., Massarsky, A., Kozal, J. S., Levin, E. D., & Di Giulio, R. T. (2018). Maternal transfer of nanoplastics to offspring in zebrafish (*Danio rerio*): A case study with nanopolystyrene. Science of the Total Environment, 643, 324–334. https://doi.org/10.1016/j.scitotenv.2018.06.186

Pittura, L., Avio, C. G., Giuliani, M. E., d'Errico, G., Keiter, S. H., Cormier, B., Gorbi, S., & Regoli, F. (2018). Microplastics as vehicles of environmental PAHs to marine organisms: Combined chemical and physical hazards to the mediterranean mussels, *Mytilus galloprovincialis*. Frontiers in Marine Science, 5, 351215. https://doi.org/10.3389/fmars.2018.00103

Plastics Europe. (2023). *Plastics- the fast facts 2023*. https://plasticseurope.org/knowledge-hub/plastics-the-fast-facts-2023/

Plastics Europe. (2024). *Plastics - the fast Facts 2024*. https://plasticseurope.org/knowledge-hub/plastics-the-fast-facts-2024/

PlasticsEurope: (2022) *Plastics – The Facts 2022*. http://plasticseurope.org/knowledge-hub/plastics-the-fact.-2022/

PlasticsEurope. (2019). *Plastics - the Facts 2019*: An analysis of European plastics production, demand and waste data. https://www.plasticseurope.org/en/resources/market-data

PlasticsEurope. (2021). *Plastics - the Facts 2020*: An analysis of European plastics production, demand and waste data. https://www.plasticseurope.org/en/resources/market-data

Prabhu, K. S., Reddy, P. V., Jones, E. C., Liken, A. D., & Reddy, C. C. (2004). Characterization of a class alpha glutathione-S-transferase with glutathione peroxidase activity in human liver microsomes. Archives of Biochemistry and Biophysics, 424(1), 72–80. https://doi.org/10.1016/j.abb.2004.02.002

Provenza, F., Anselmi, S., Specchiulli, A., Piccardo, M., Barceló, D., Prearo, M., Pastorino, P., & Renzi, M. (2022a). Sparkling plastic: Effects of exposure to glitter on the Mediterranean mussel *Mytilus galloprovincialis.* Environmental Toxicology and Pharmacology, 96, 103994. https://doi.org/10.1016/j.etap.2022.103994

Provenza, F., Rampih, D., Pignattelli, S., Pastorino, P., Barceló, D., Prearo, M., Specchiulli, A., & Renzi, M. (2022b). Mussel watch program for microplastics in the Mediterranean sea: Identification of biomarkers of exposure using *Mytilus galloprovincialis*. Ecological Indicators, 142, 109212. https://doi.org/10.1016/j.ecolind.2022.109212

Puckowski, A., Cwięk, W., Mioduszewska, K., Stepnowski, P., & Białk-Bielińska, A. (2021). Sorption of pharmaceuticals on the surface of microplastics. Chemosphere, 263, 127976. https://doi.org/10.1016/j.chemosphere.2020.127976

Pujol, G., Marín-Gual, L., González-Rodelas, L., Álvarez-González, L., Chauvigné, F., Cerdà, J., Teles, M., Roher, N., & Ruiz-Herrera, A. (2025). Short-term polystyrene nanoplastic exposure alters zebrafish male and female germline and reproductive outcomes, unveiling pollutant-impacted molecular pathways. Journal of Hazardous Materials, 481, 136529. https://doi.org/10.1016/j.jhazmat.2024.136529

Pulit-Prociak, J. and Banach, M. (2016) Silver Nanoparticles—A Material of the Future...? Open Chemistry, 14, 76-91. https://doi.org/10.1515/chem-2016-0005

Qi, P., Qiu, L., Feng, D., Gu, Z., Guo, B., & Yan, X. (2023). Distinguish the toxic differentiations between acute exposure of micro- and nano-plastics on bivalves: An integrated study based on transcriptomic sequencing. Aquatic Toxicology, 254, 106367. https://doi.org/10.1016/j.aquatox.2022.106367

Qu, H., Ma, R., Wang, B., Zhang, Y., Yin, L., Yu, G., Deng, S., Huang, J., & Wang, Y. (2018). Effects of microplastics on the uptake, distribution and biotransformation of chiral antidepressant venlafaxine in aquatic ecosystem. Journal of Hazardous Materials, 359, 104–112. https://doi.org/10.1016/j.jhazmat.2018.07.016

Queirós, V., Azeiteiro, U. M., Barata, C., Santos, J. L., Alonso, E., Soares, A. M. V. M., & Freitas, R. (2021). Effects of the antineoplastic drug cyclophosphamide on the biochemical responses of the mussel *Mytilus galloprovincialis* under different temperatures. Environmental Pollution, 288, 117735. https://doi.org/10.1016/j.envpol.2021.117735

Raisuddin, S., Kwok, K. W. H., Leung, K. M. Y., Schlenk, D., & Lee, J. S. (2007). The copepod Tigriopus: A promising marine model organism for ecotoxicology and environmental genomics. Aquatic Toxicology, 83(3), 161–173. https://doi.org/10.1016/j.aquatox.2007.04.005

Ramirez, L., Gentile, S. R., Zimmermann, S., & Stoll, S. (2019). Behavior of TiO2 and CeO2 Nanoparticles and Polystyrene Nanoplastics in Bottled Mineral, Drinking and Lake Geneva Waters. Impact of Water Hardness and Natural Organic Matter on Nanoparticle Surface Properties and Aggregation. Water 2019, 11(4), 721. https://doi.org/10.3390/W11040721

Ramos, A. M. B. M. (2017). Reproductive strategy evaluation of mussel *Mytilus galloprovincialis* produced in longlines in two areas of Algarve coast. https://iconline.ipleiria.pt/bitstream/10400.8/2537/1/tese%202017%20final_com%20capa.pdf

Rangaswamy, B., An, J., & Kwak, I. S. (2024). Different recovery patterns of the surviving bivalve *Mytilus galloprovincialis* based on transcriptome profiling exposed to spherical or fibrous polyethylene microplastics. Heliyon, 10(10), e30858. https://doi.org/10.1016/j.heliyon.2024.e30858

Regoli, F., & Giuliani, M. E. (2014). Oxidative pathways of chemical toxicity and oxidative stress biomarkers in marine organisms. Marine Environmental Research, 93, 106–117. https://doi.org/10.1016/j.marenvres.2013.07.006

Regoli, F., d'Errico, G., Nardi, A., Mezzelani, M., Fattorini, D., Benedetti, M., Di Carlo, M., Pellegrini, D., & Gorbi, S. (2019). Application of a weight of evidence approach for monitoring complex environmental scenarios: The case-study of off-shore platforms. Frontiers in Marine Science, 6, 1–15. https://doi.org/10.3389/fmars.2019.00377

Regoli, F., Pellegrini, D., Cicero, A. M., Nigro, M., Benedetti, M., Gorbi, S., Fattorini, D., D'Errico, G., Di Carlo, M., Nardi, A., Gaion, A., Scuderi, A., Giuliani, S., Romanelli, G., Berto, D., Trabucco, B., Guidi, P., Bernardeschi, M., Scarcelli, V., & Frenzilli, G. (2014). A multidisciplinary weight of evidence approach for environmental risk assessment at the Costa Concordia wreck: Integrative indices from Mussel Watch. Marine Environmental Research, 96, 92–104. https://doi.org/10.1016/j.marenvres.2013.09.016

Revel, M., Lagarde, F., Perrein-Ettajani, H., Bruneau, M., Akcha, F., Sussarellu, R., Rouxel, J., Costil, K., Decottignies, P., Cognie, B., Châtel, A., & Mouneyrac, C. (2019). Tissue-specific biomarker responses in the blue mussel *Mytilus* spp. exposed to a mixture of microplastics at environmentally relevant concentrations. Frontiers in Environmental Science, 7, 1–14. https://doi.org/10.3389/fenvs.2019.00033

Rezvani, E., Rafferty, A., McGuinness, C., & Kennedy, J. (2019). Adverse effects of nanosilver on human health and the environment. Acta Biomaterialia, 94, 145–159. https://doi.org/10.1016/j.actbio.2019.05.042

Ribeiro, F., Garcia, A. R., Pereira, B. P., Fonseca, M., Mestre, N. C., Fonseca, T. G., Ilharco, L. M., & Bebianno, M. J. (2017). Microplastics effects in *Scrobicularia plana*. Marine Pollution Bulletin, 122(1–2), 379–391. https://doi.org/10.1016/j.marpolbul.2017.06.078

Ringwood, A. H., McCarthy, M., Bates, T. C., & Carroll, D. L. (2010). The effects of silver nanoparticles on oyster embryos. Marine Environmental Research, 69(S. 1), 10–12. https://doi.org/10.1016/j.marenvres.2009.10.011

Rios, L. M., Moore, C., & Jones, P. R. (2007). Persistent organic pollutants carried by synthetic polymers in the ocean environment. Marine Pollution Bulletin, 54(8), 1230–1237. https://doi.org/10.1016/j.marpolbul.2007.03.022

Rist, S., Baun, A., Almeda, R., & Hartmann, N. B. (2019). Ingestion and effects of micro- and nanoplastics in blue mussel (*Mytilus edulis*) larvae. Marine Pollution Bulletin, 140, 423–430. https://doi.org/10.1016/j.marpolbul.2019.01.069

Ritz, C., Streibig, J. C., & Kniss, A. (2021). How to use statistics to claim antagonism and synergism from binary mixture experiments. Pest Management Science, 77(9), 3890–3899. https://doi.org/10.1002/ps.6348

Romdhani, I., Gallo, A., Venditti, M., Abelouah, M. R., Varchetta, R., Najahi, H., Boukadida, K., Boni, R., Alla, A. A., Minucci, S., & Banni, M. (2024). Unveiling the impact of environmental microplastics on mussel spermatozoa: First evidence of prothymosin-α detection in invertebrate's male gametes. Journal of Hazardous Materials, 461. https://doi.org/10.1016/j.jhazmat.2023.132521

Rotini, A., Tornambè, A., Cossi, R., Iamunno, F., Benvenuto, G., Berducci, M. T., Maggi, C., Thaller, M. C., Cicero, A. M., Manfra, L., & Migliore, L. (2017). Salinity-based toxicity of CuO nanoparticles, CuO-bulk and Cu ion to *vibrio anguillarum*. Frontiers in Microbiology, 8, 2076. https://doi.org/10.3389/fmicb.2017.02076

Rouillon, C., Bussiere, P. O., Desnoux, E., Collin, S., Vial, C., Therias, S., & Gardette, J. L. (2016). Is carbonyl index a quantitative probe to monitor polypropylene photodegradation? Polymer Degradation and Stability, 128, 200–208. https://doi.org/10.1016/j.polymdegradstab.2015.12.011

Sanchez, W., Burgeot, T., & Porcher, J. M. (2013). A novel "Integrated Biomarker Response" calculation based on reference deviation concept. Environmental Science and Pollution Research, 20(5), 2721–2725. https://doi.org/10.1007/s11356-012-1359-1

Santana-Viera, S., Montesdeoca-Esponda, S., Torres-Padrón, M. E., Sosa-Ferrera, Z., & Santana-Rodríguez, J. J. (2021). An assessment of the concentration of pharmaceuticals adsorbed on microplastics. Chemosphere, 266, 1–6. https://doi.org/10.1016/j.chemosphere.2020.129007

Santovito, G., Trentin, E., Gobbi, I., Bisaccia, P., Tallandini, L., & Irato, P. (2021). Non-enzymatic antioxidant responses of *Mytilus galloprovincialis*: Insights into the physiological role against metal-induced oxidative stress. Comparative Biochemistry and Physiology Part C: Toxicology & Pharmacology, 240, 108909. https://doi.org/10.1016/j.cbpc.2020.108909

Sellami, B., Bouzidi, I., Hedfi, A., Almalki, M., Rizk, R., Pacioglu, O., Boufahja, F., Beyrem, H., & Sheehan, D. (2021). Impacts of nanoparticles and phosphonates in the behavior and oxidative status of the mediterranean mussels (*Mytilus galloprovincialis*). Saudi Journal

of Biological Sciences, 28(11), 6365–6374. https://doi.org/10.1016/j.sjbs.2021.07.017

Sendra, M., Saco, A., Yeste, M. P., Romero, A., Novoa, B., & Figueras, A. (2020). Nanoplastics: From tissue accumulation to cell translocation into *Mytilus galloprovincialis* hemocytes. resilience of immune cells exposed to nanoplastics and nanoplastics plus *Vibrio splendidus* combination. Journal of Hazardous Materials, 388, 121788. https://doi.org/10.1016/j.jhazmat.2019.121788

Sendra, M., Sparaventi, E., Blasco, J., Ignacio, M.-G., & V. M., A. C. (2020). Ingestion and bioaccumulation of polystyrene nanoplastics and their effects on the microalgal feeding of *Artemia franciscana*. Ecotoxicology and Environmental Safety, 188, 109853. https://doi.org/10.1016/j.ecoenv.2019.109853

Sendra, M., Sparaventi, E., Novoa, B., & Figueras, A. (2021). An overview of the internalization and effects of microplastics and nanoplastics as pollutants of emerging concern in bivalves. Science of The Total Environment, 753, 142024. https://doi.org/10.1016/j.scitotenv.2020.142024

Serafim, A., Company, R., Lopes, B., Fonseca, V. F., Frana, S., Vasconcelos, R. P., Bebianno, M. J., & Cabral, H. N. (2012). Application of an integrated biomarker response index (IBR) to assess temporal variation of environmental quality in two Portuguese aquatic systems. Ecological Indicators, 19, 215–225. https://doi.org/10.1016/j.ecolind.2011.08.009

Sharma, V. K., Ma, X., Lichtfouse, E., & Robert, D. (2023). Nanoplastics are potentially more dangerous than microplastics. Environmental Chemistry Letters 21(4), 1933–1936. https://doi.org/10.1007/s10311-022-01539-1

Shen, M., Zhang, Y., Zhu, Y., Song, B., Zeng, G., Hu, D., Wen, X., & Ren, X. (2019). Recent advances in toxicological research of nanoplastics in the environment: A review. Environmental Pollution 252, 511–521. https://doi.org/10.1016/j.envpol.2019.05.102

Sherman, B. T., Hao, M., Qiu, J., Jiao, X., Baseler, M. W., Lane, H. C., Imamichi, T., & Chang, W. (2022). DAVID: a web server for functional enrichment analysis and functional annotation of gene lists (2021 update). Nucleic Acids Research, 50(W1), W216–W221. https://doi.org/10.1093/NAR/GKAC194

Shi, C., Liu, Z., Yu, B., Zhang, Y., Yang, H., Han, Y., Wang, B., Liu, Z., & Zhang, H. (2024). Emergence of nanoplastics in the aquatic environment and possible impacts on aquatic organisms. Science of The Total Environment, 906, 167404. https://doi.org/10.1016/j.scitotenv.2023.167404.

Singh, N. P., McCoy, M. T., Tice, R. R., & Schneider, E. L. (1988). A simple technique for quantitation of low levels of DNA damage in individual cells. Experimental Cell Research, 175(1), 184–191. https://doi.org/https://doi.org/10.1016/0014-4827(88)90265-0

Sjollema, S. B., Redondo-Hasselerharm, P., Leslie, H. A., Kraak, M. H. S., & Vethaak, A. D. (2016). Do plastic particles affect microalgal photosynthesis and growth? Aquatic Toxicology, 170, 259–261. https://doi.org/10.1016/j.aquatox.2015.12.002.

Skjolding, L. M., Ašmonaitė, G., Jølck, R. I., Andresen, T. L., Selck, H., Baun, A., & Sturve, J. (2017). An assessment of the importance of exposure routes to the uptake and internal localisation of fluorescent nanoparticles in zebrafish (*Danio rerio*), using light sheet microscopy. Nanotoxicology, 11(3), 351–359. https://doi.org/10.1080/17435390.2017.1306128

Stenersen, J. (2004). Chemical pesticides mode of action and toxicology (1st ed.). CRC Press. https://doi.org/10.1201/9780203646830

Sugni, M., Mozzi, D., Barbaglio, A., Bonasoro, F., & Candia Carnevali, M. D. (2007). Endocrine disrupting compounds and echinoderms: New ecotoxicological sentinels for the marine ecosystem. Ecotoxicology, 16(1), 95–108. https://doi.org/10.1007/s10646-006-0119-8

Sun, N., Shi, H., Li, X., Gao, C., & Liu, R. (2023). Combined toxicity of micro/nanoplastics loaded with environmental pollutants to organisms and cells: Role, effects, and mechanism. Environment International, 171, 107711. https://doi.org/10.1016/j.envint.2022.107711

Sun, X., Chen, B., Li, Q., Liu, N., Xia, B., Zhu, L., & Qu, K. (2018). Toxicities of polystyrene nano- and microplastics toward marine bacterium *Halomonas alkaliphila*. Science of the Total Environment, 642, 1378–1385. https://doi.org/10.1016/j.scitotenv.2018.06.141

Sussarellu, R., Suquet, M., Thomas, Y., Lambert, C., Fabioux, C., Pernet, M. E. J., Goïc, N. le, Quillien, V., Mingant, C., Epelboin, Y., Corporeau, C., Guyomarch, J., Robbens, J., Paul-Pont, I., Soudant, P., & Huvet, A. (2016). Oyster reproduction is affected by exposure to polystyrene microplastics. Proceedings of the National Academy of Sciences of the United States of America, 113(9), 2430–2435. https://doi.org/10.1073/pnas.1519019113

Takahashi, M.-A., & Asada, K. (1983). Superoxide anion permeability of phospholipid membranes and chloroplast thylakoids. Archives of Biochemistry and Biophysics, 226(2), 558–566. https://doi.org/10.1016/0003-9861(83)90325-9

Tallec, K., Blard, O., González-Fernández, C., Brotons, G., Berchel, M., Soudant, P., Huvet, A., & Paul-Pont, I. (2020). Surface functionalization determines behavior of nanoplastic solutions in model aquatic environments. Chemosphere, 225, 639–646. https://doi.org/10.1016/j.chemosphere.2019.03.077

Tallec, K., Huvet, A., di Poi, C., González-Fernández, C., Lambert, C., Petton, B., le Goïc, N., Berchel, M., Soudant, P., & Paul-Pont, I. (2018). Nanoplastics impaired oyster free living stages, gametes and embryos. Environmental Pollution, 242, 1226–1235. https://doi.org/10.1016/j.envpol.2018.08.020

Tamminga, M., Hengstmann, E., & Fischer, E. K. (2018). Microplastic analysis in the South Funen Archipelago, Baltic Sea, implementing manta trawling and bulk sampling. Marine Pollution Bulletin, 128, 601–608. https://doi.org/10.1016/j.marpolbul.2018.01.066

Tang, D., Chen, M., Huang, X., Zhang, G., Zeng, L., Zhang, G., Wu, S., & Wang, Y. (2023). SRplot: A free online platform for data visualization and graphing. PloS One, 18(11). https://doi.org/10.1371/JOURNAL.PONE.0294236

Teuten, E. L., Saquing, J. M., Knappe, D. R. U., Barlaz, M. A., Jonsson, S., Björn, A., Rowland, S. J., Thompson, R. C., Galloway, T. S., Yamashita, R., Ochi, D., Watanuki, Y., Moore, C., Viet, P. H., Tana, T. S., Prudente, M., Boonyatumanond, R., Zakaria, M. P., Akkhavong, K., Yuko Ogata, Y., Hirai, H., Iwasa, S., Mizukawa, K., Hagino, Y., Imamura, A., Saha, M., & Takada, H. (2009). Transport and release of chemicals from plastics to the environment and to wildlife. Philosophical Transactions of the Royal Society B: Biological Sciences, 364(1526), 2027–2045. https://doi.org/10.1098/rstb.2008.0284

The Waste and Resources Action Programme. (2023). Recycle. https://www.recyclenow.com/recycle-an-item/polystyrene

Thiagarajan, V., Alex, S. A., Seenivasan, R., Chandrasekaran, N., & Mukherjee, A. (2021). Interactive effects of micro/nanoplastics and nanomaterials/pharmaceuticals: Their ecotoxicological consequences in the aquatic systems. Aquatic Toxicology, 232, 105747. https://doi.org/10.1016/j.aquatox.2021.105747

Thompson, R. C., Olson, Y., Mitchell, R. P., Davis, A., Rowland, S. J., John, A. W. G., McGonigle, D., & Russell, A. E. (2004). Lost at sea: Where is all the plastic? Science, 304(5672), 838. https://doi.org/10.1126/science.1094559/suppl_file/thompson.som.pdf

Tong Chen, Y.-X.L., Luqi Huang, ImageGP: An easy-to-use data visualization web server for scientific researchers. iMeta, 2022. 1(1).

Tortella, G. R., Rubilar, O., Durán, N., Diez, M. C., Martínez, M., Parada, J., & Seabra, A. B. (2020). Silver nanoparticles: Toxicity in model organisms as an overview of its hazard for human health and the environment. In Journal of Hazardous Materials (Vol. 390). Elsevier B.V. https://doi.org/10.1016/j.jhazmat.2019.121974

Trestrail, C., Nugegoda, D., & Shimeta, J. (2020). Invertebrate responses to microplastic ingestion: Reviewing the role of the antioxidant system. Science of the Total Environment, 734, 138559. https://doi.org/10.1016/j.scitotenv.2020.138559

Trombini, C., Garcia da Fonseca, T., Morais, M., Rocha, T. L., Blasco, J., & Bebianno, M. J. (2016). Toxic effects of cisplatin cytostatic drug in mussel *Mytilus galloprovincialis*. Marine Environmental Research, 119, 12–21. https://doi.org/10.1016/j.marenvres.2016.05.004

US. EPA. (2007). U. S. Environmental Protection Agency Nanotechnology White Paper.

Vasanthi, R. L., Arulvasu, C., Kumar, P., & Srinivasan, P. (2021). Ingestion of microplastics and its potential for causing structural alterations and oxidative stress in Indian green mussel *Perna viridis*– A multiple biomarker approach. Chemosphere, 283, 130979. https://doi.org/10.1016/j.chemosphere.2021.130979

Venâncio, C., Ferreira, I., Martins, M. A., Soares, A. M. V. M., Lopes, I., & Oliveira, M. (2019). The effects of nanoplastics on marine plankton: A case study with polymethylmethacrylate. Ecotoxicology and Environmental Safety, 184, 109632. https://doi.org/10.1016/j.ecoenv.2019.109632

Venâncio, C., Monteiro, B., Lopes, I., & Sousa, A. C. A. (2023). Assessing the risks of capecitabine and its active metabolite 5-fluorouracil to freshwater biota. Environmental Science and Pollution Research, 30(20), 58841–58854. https://doi.org/10.1007/s11356-023-26505-4

Vermorken, J. B., Remenar, E., van Herpen, C., Gorlia, T., Mesia, R., Degardin, M., Stewart, J. S., Jelic, S., Betka, J., Preiss, J. H., van den Weyngaert, D., Awada, A., Cupissol, D., Kienzer, H. R., Rey, A., Desaunois, I., Bernier, J., & Lefebvre, J.-L. (2007). Cisplatin, fluorouracil, and docetaxel in unresectable head and neck cancer. New England Journal of Medicine, 357(17), 1695–1704. https://doi.org/10.1056/nejmoa071028

Vilela, P., Liu, H., Lee, S., Hwangbo, S., Nam, K., & Yoo, C. (2018). A systematic approach of removal mechanisms, control and optimization of silver nanoparticle in wastewater treatment plants. Science of The Total Environment, 633, 989–998. https://doi.org/10.1016/j.scitotenv.2018.03.247

Villalba, M., Pérez, V., Herrera, L., Stepke, C., Maldonado, N., Fredericksen, F., Yáñez, A., & Olavarría, V. H. (2017). Infectious pancreatic necrosis virus infection of fish cell lines: Preliminary analysis of gene expressions related to extracellular matrix remodelling and immunity. Veterinary Immunology and Immunopathology, 193–194, 10–17. https://doi.org/10.1016/j.vetimm.2017.09.009

Wallace, R.L., Snell, T.W., Ricci, C., & Nogrady, T. (2006) Rotifera: Volume 1—Biology, Ecology and Systematics (2nd edn). Backhuys Publishers, 2006, 299 pp, ISBN 90-5782-178-8

Walters, C., Pool, E., Somerset, V., Walters, C., Pool, E., & Somerset, V. (2016). Nanotoxicity in Aquatic Invertebrates. Invertebrates - Experimental Models in Toxicity Screening. https://doi.org/10.5772/61715

Wang, L., Wu, W. M., Bolan, N. S., Tsang, D. C. W., Li, Y., Qin, M., & Hou, D. (2021). Environmental fate, toxicity and risk management strategies of nanoplastics in the environment: Current status and future perspectives. Journal of Hazardous Materials, 401, 123415. https://doi.org/10.1016/j.jhazmat.2020.123415

Wang, P., Menzies, N. W., Chen, H., Yang, X., McGrath, S. P., Zhao, F.-J., & Kopittke, P. M. (2018). Risk of silver transfer from soil to the food chain is low after long-term (20 Years) field applications of sewage sludge. Environmental Science & Technology, 52(8), 4901–4909. https://doi.org/10.1021/acs.est.8b00204

Wang, S., Hu, M., Zheng, J., Huang, W., Shang, Y., Kar-Hei Fang, J., Shi, H., & Wang, Y. (2021). Ingestion of nano/micro plastic particles by the mussel *Mytilus coruscus* is size dependent. Chemosphere, 263, 127957. https://doi.org/10.1016/j.chemosphere.2020.127957

Wang, W., Yuan, W., Chen, Y., & Wang, J. (2018). Microplastics in surface waters of Dongting Lake and Hong Lake, China. Science of the Total Environment, 633, 539–545. https://doi.org/10.1016/j.scitotenv.2018.03.211

Wang, X., Huang, W., Wei, S., Shang, Y., Gu, H., Wu, F., Lan, Z., Hu, M., Shi, H., & Wang, Y. (2020). Microplastics impair digestive performance but show little effects on antioxidant activity in mussels under low pH conditions. Environmental Pollution, 258, 113691. https://doi.org/10.1016/j.envpol.2019.113691

Wegner, A., Besseling, E., Foekema, E. M., Kamermans, P., & Koelmans, A. A. (2012). Effects of nanopolystyrene on the feeding behavior of the blue mussel (*Mytilus edulis* L.). Environmental Toxicology and Chemistry, 31(11), 2490–2497. https://doi.org/10.1002/etc.1984

Worm, B., Lotze, H. K., Jubinville, I., Wilcox, C., & Jambeck, J. (2017). Plastic as a Persistent Marine Pollutant. Annual Review of Environment and Resources, 42(1), 1–26. https://doi.org/10.1146/annurev-environ-102016-060700

Xiang, Y., Jiang, L., Zhou, Y., Luo, Z., Zhi, D., Yang, J., & Lam, S. S. (2022). Microplastics and environmental pollutants: Key interaction and toxicology in aquatic and soil environments. Journal of Hazardous Materials, 422, 126843. https://doi.org/10.1016/j.jhazmat.2021.126843

Yu, F., Yang, C., Zhu, Z., Bai, X., & Ma, J. (2019). Adsorption behavior of organic pollutants and metals on micro/nanoplastics in the aquatic environment. Science of the Total Environment, 694, 133643. https://doi.org/10.1016/j.scitotenv.2019.133643

Yu, P., Liu, Z., Wu, D., Chen, M., Lv, W., & Zhao, Y. (2018). Accumulation of polystyrene microplastics in juvenile Eriocheir sinensis and oxidative stress effects in the liver. Aquatic Toxicology, 200, 28–36. https://doi.org/10.1016/j.aquatox.2018.04.015

Yuan, Z., Nag, R., & Cummins, E. (2022). Ranking of potential hazards from microplastics polymers in the marine environment. Journal of Hazardous Materials, 429, 128399. https://doi.org/10.1016/j.jhazmat.2022.128399

Załeska-Radziwiłł, M., Affek, K., & Rybak, J. (2014). Ecotoxicity of chosen pharmaceuticals in relation to micro-organisms-risk assessment. Desalination and Water Treatment, 52(19–21), 3908–3917. https://doi.org/10.1080/19443994.2014.887503

Zhang, J., Chang, V. W. C., Giannis, A., & Wang, J.-Y. (2013). Removal of cytostatic drugs from aquatic environment: A review. Science of The Total Environment, 445–446, 281–298. https://doi.org/10.1016/j.scitotenv.2012.12.061

Zhang, W., & Wu, F. (2023). Effects of adverse fertility-related factors on mitochondrial DNA in the oocyte: a comprehensive review. Reproductive Biology and Endocrinology 21(1). BioMed Central Ltd. https://doi.org/10.1186/s12958-023-01078-6

Zhang, Y., Chen, Y., Westerhoff, P., Hristovski, K., & Crittenden, J. C. (2008). Stability of commercial metal oxide nanoparticles in water. Water Research, 42(8–9), 2204–2212. https://doi.org/10.1016/j.watres.2007.11.036

Zhong, M., Wu, H., Li, F., Shan, X., & Ji, C. (2020). Proteomic analysis revealed gender-specific responses of mussels (*Mytilus galloprovincialis*) to trichloropropyl phosphate

(TCPP) exposure. Environmental Pollution, 267, 115537. https://doi.org/10.1016/j.envpol.2020.115537

Zhou, X. X., Liu, R., Hao, L. T., & Liu, J. F. (2021). Identification of polystyrene nanoplastics using surface enhanced Raman spectroscopy. Talanta, 221, 121552. https://doi.org/10.1016/j.talanta.2020.121552

Zhu, S., Qin, L., Li, Z., Hu, X., & Yin, D. (2023). Effects of nanoplastics and microplastics on the availability of pharmaceuticals and personal care products in aqueous environment. Journal of Hazardous Materials, 458, 131999. https://doi.org/10.1016/j.jhazmat.2023.131999

ANNEX I

Chapter 4 – Assessing the effects of the cytostatic drug 5-Fluorouracil alone and in a mixture of emerging contaminants on the mussel *Mytilus galloprovincialis*

4.1. Following the single-dose factorial design explained by Ritz et al. (2021) for binary mixtures, this method has been adapted for tertiary mixtures. This design combines three factors (3 contaminants) with two levels, resulting in five treatments: control, 5FU, nPS, nAg and a mixture of the three (Mix = 5FU + nPS + nAg). The antagonistic or synergistic effect claim is only valid for the chosen concentrations evaluated here. Both dose addition and independent action models were used as follows, and values were calculated for all sampling times and all biomarkers analysed:

4.1.1. Dose addition

$$E_{add} = (E_{5FU} - E_{control}) + (E_{nPS} - E_{control}) + (E_{nAg} - E_{control})$$

Exposure time (days)	SOD		CAT		GPx		GST		LPO	
	Gill	DG	Gill	DG	Gill	DG	Gill	DG	Gill	DG
0	0	0	0	0	0	0	0	0	0	0
3	118	164	50	283	-2	5	-523	-16	-8	-6
7	181	116	149	159	1	-1	-114	3	1	157
14	116	69	70	18	9	2	-34	-53	10	88
21	166	85	123	42	13	5	46	-16	-11	128

Any antagonistic or synergistic effect can be defined as the difference (D_{da}) between the observed response (control) and the predicted effect. The following equation defines the difference:

$$D_{da} = E_{Mix} - E_{5FU} - E_{nPS} - E_{nAg} + E_{control}$$

Exposure time (days)	SOD		CAT		GPx		GST		LPO	
	Gill	DG	Gill	DG	Gill	DG	Gill	DG	Gill	DG
0										
3	-146	-174	-117	-421	9	-4	121	-14	13	4
7	-159	-134	-176	-309	17	-2	25	-18	16	-144
14	15	-9	26	-57	6	3	123	41	21	13
21	-92	-8	-24	-62	1	4	28	33	-2	-8

4.1.2. Independent effect

$$E_{ind} = \frac{E_{5FU} \times E_{nPS} \times E_{nAg}}{(E_{control})^2}$$

Exposure time (days)	SOD		CAT		GPx		GST		LPO	
	Gill	DG	Gill	DG	Gill	DG	Gill	DG	Gill	DG
0										
3	142	542	82	483	1	7	0	15	5	4
7	123	340	94	300	2	2	1	30	12	1392
14	26	136	15	102	13	4	1	1	18	75
21	396	130	162	113	24	8	70	5	4	341

Any antagonistic or synergistic effect can be defined as the difference (D_{ia}) between the observed and reference effects under the assumption of independent action. The following equation defines the difference:

$$D_{ia} = E_{Mix} - E_{ind}$$

Exposure time (days)	SOD		CAT		GPx		GST		LPO	
	Gill	DG	Gill	DG	Gill	DG	Gill	DG	Gill	DG
0										
3	-99	-503	-68	-372	1	-4	122	17	10	3
7	-60	-286	-75	-216	12	5	11	5	15	-1375
14	59	-92	33	-28	10	0	20	43	23	-50
21	-311	-77	-112	-73	-12	-3	20	43	39	-320

The exact process was carried out for genotoxicity in mussel haemolymph. The results are as follows:

Exposure time (days)	Genotoxicity			
	Eadd	Dda	Eind	Dia
0	0			
3	48	-36	415	-410
14	41	-17	358	-337

ANNEX II

Chapter 7 – Gender differences in protein expression after polystyrene nanoplastics exposure in mussels *Mytilus galloprovincialis.*

Complete list of Proteins identified

Protein	Uniprot accession	Protein Name	Number Peptides	P
tr|A0A8B6EYD8|A0A8B6EYD8_MYTGA	A0A8B6EYD8	Elongation factor 2	15	P0001
tr|A0A8B6EYF2|A0A8B6EYF2_MYTGA	A0A8B6EYF2	Uncharacterized protein	15	P0002
tr|A0A8B6FQW6|A0A8B6FQW6_MYTGA	A0A8B6FQW6	Transaldolase	14	P0003
tr|A0A8B6FU41|A0A8B6FU41_MYTGA	A0A8B6FU41	Hemicentin	14	P0004
tr|A0A8B6G8F3|A0A8B6G8F3_MYTGA	A0A8B6G8F3	Aubergine	14	P0005
tr|A0A8B6GA99|A0A8B6GA99_MYTGA	A0A8B6GA99	E1 ubiquitin-activating enzyme	14	P0006
tr|A0A8B6GAN9|A0A8B6GAN9_MYTGA	A0A8B6GAN9	guanylate cyclase	14	P0007
tr|A0A8B6GXC1|A0A8B6GXC1_MYTGA	A0A8B6GXC1	Clathrin heavy chain	14	P0008
tr|A0A8B6H3U1|A0A8B6H3U1_MYTGA	A0A8B6H3U1	Actinin alpha	14	P0009
tr|A0A8B6H576|A0A8B6H576_MYTGA	A0A8B6H576	Otoancorin	14	P0010
tr|A0A8B6H9R0|A0A8B6H9R0_MYTGA	A0A8B6H9R0	Heparan sulfate proteoglycan 2 (Perlecan)	14	P0011
tr|A0A8B6HT02|A0A8B6HT02_MYTGA	A0A8B6HT02	Armadillo repeat-containing protein 4	14	P0012
tr|C0Z203|C0Z203_MYTGA	C0Z203	Heat shock protein 90	14	P0013
tr|I1VYX3|I1VYX3_MYTGA	I1VYX3	Isocitrate dehydrogenase [NADP]	14	P0014
tr|A0A8B6CG53|A0A8B6CG53_MYTGA	A0A8B6CG53	phosphoenolpyruvate carboxykinase (GTP)	13	P0015
tr|A0A8B6CGD1|A0A8B6CGD1_MYTGA	A0A8B6CGD1	Staphylococcal nuclease domain-containing protein 1 (Frag	13	P0016
tr|A0A8B6CRC1|A0A8B6CRC1_MYTGA	A0A8B6CRC1	ATP synthase subunit alpha	13	P0017
tr|A0A8B6CYA7|A0A8B6CYA7_MYTGA	A0A8B6CYA7	Poly [ADP-ribose] polymerase	13	P0018
tr|A0A8B6DZ81|A0A8B6DZ81_MYTGA	A0A8B6DZ81	Glyceraldehyde-3-phosphate dehydrogenase	13	P0019
tr|A0A8B6EPK5|A0A8B6EPK5_MYTGA	A0A8B6EPK5	Heterogeneous nuclear ribonucleoprotein R	13	P0020
tr|A0A8B6F0P5|A0A8B6F0P5_MYTGA	A0A8B6F0P5	Talin	13	P0021
tr|A0A8B6F176|A0A8B6F176_MYTGA	A0A8B6F176	Vitellogenin	13	P0022
tr|A0A8B6FNH5|A0A8B6FNH5_MYTGA	A0A8B6FNH5	40S ribosomal protein S4	13	P0023
tr|A0A8B6H439|A0A8B6H439_MYTGA	A0A8B6H439	Transglutaminase-like domain-containing protein	13	P0024
tr|A0A8B6H7P1|A0A8B6H7P1_MYTGA	A0A8B6H7P1	Collagen, type VI, alpha	13	P0025
tr|A0A8B6H8X1|A0A8B6H8X1_MYTGA	A0A8B6H8X1	ATP synthase subunit beta (Fragment)	13	P0026
tr|A0A8B6BDM5|A0A8B6BDM5_MYTGA	A0A8B6BDM5	T-complex protein 1 subunit eta	12	P0027
tr|A0A8B6BVQ6|A0A8B6BVQ6_MYTGA	A0A8B6BVQ6	Dynein heavy chain, axonemal (Fragment)	12	P0028
tr|A0A8B6CKS3|A0A8B6CKS3_MYTGA	A0A8B6CKS3	Creatine kinase (Fragment)	12	P0029
tr|A0A8B6CW94|A0A8B6CW94_MYTGA	A0A8B6CW94	Alpha-1,4 glucan phosphorylase	12	P0030
tr|A0A8B6D196|A0A8B6D196_MYTGA	A0A8B6D196	Aminopeptidase	12	P0031
tr|A0A8B6DJC7|A0A8B6DJC7_MYTGA	A0A8B6DJC7	T-complex protein 1 subunit alpha	12	P0032
tr|A0A8B6DZ82|A0A8B6DZ82_MYTGA	A0A8B6DZ82	Heat shock 70kDa protein 5	12	P0033
tr|A0A8B6E7D7|A0A8B6E7D7_MYTGA	A0A8B6E7D7	T-complex protein 1 subunit gamma	12	P0034
tr|A0A8B6ES13|A0A8B6ES13_MYTGA	A0A8B6ES13	Uncharacterized protein	12	P0035
tr|A0A8B6EVV6|A0A8B6EVV6_MYTGA	A0A8B6EVV6	Importin N-terminal domain-containing protein	12	P0036
tr|A0A8B6EYE1|A0A8B6EYE1_MYTGA	A0A8B6EYE1	Uncharacterized protein	12	P0037
tr|A0A8B6F1U6|A0A8B6F1U6_MYTGA	A0A8B6F1U6	Cilia- and flagella-associated protein 52	12	P0038
tr|A0A8B6F498|A0A8B6F498_MYTGA	A0A8B6F498	Acyl-coenzyme A oxidase	12	P0039
tr|A0A8B6FPF3|A0A8B6FPF3_MYTGA	A0A8B6FPF3	Myosin heavy chain 6/7	12	P0040
tr|A0A8B6G0D3|A0A8B6G0D3_MYTGA	A0A8B6G0D3	Amine oxidase domain-containing protein	12	P0041
tr|A0A8B6GZC3|A0A8B6GZC3_MYTGA	A0A8B6GZC3	Cullin-associated NEDD8-dissociated protein 1	12	P0042
tr|A0A8B6H4C2|A0A8B6H4C2_MYTGA	A0A8B6H4C2	6-phosphogluconate dehydrogenase, decarboxylating	12	P0043
tr|A0A8B6C531|A0A8B6C531_MYTGA	A0A8B6C531	Receptor ligand binding region domain-containing protein	11	P0044
tr|A0A8B6C6W9|A0A8B6C6W9_MYTGA	A0A8B6C6W9	RNA helicase	11	P0045
tr|A0A8B6CDY5|A0A8B6CDY5_MYTGA	A0A8B6CDY5	T-complex protein 1 subunit theta	11	P0046
tr|A0A8B6CMG1|A0A8B6CMG1_MYTGA	A0A8B6CMG1	enoyl-CoA hydratase	11	P0047
tr|A0A8B6D126|A0A8B6D126_MYTGA	A0A8B6D126	Glycine--tRNA ligase	11	P0048
tr|A0A8B6D4C8|A0A8B6D4C8_MYTGA	A0A8B6D4C8	Cathepsin D	11	P0049
tr|A0A8B6DFY0|A0A8B6DFY0_MYTGA	A0A8B6DFY0	Spectrin beta chain	11	P0050
tr|A0A8B6DJL7|A0A8B6DJL7_MYTGA	A0A8B6DJL7	Vitellogenin domain-containing protein	11	P0051
tr|A0A8B6DY98|A0A8B6DY98_MYTGA	A0A8B6DY98	Patched 1	11	P0052
tr|A0A8B6E331|A0A8B6E331_MYTGA	A0A8B6E331	C-type lectin domain-containing protein	11	P0053
tr|A0A8B6E647|A0A8B6E647_MYTGA	A0A8B6E647	Uncharacterized protein	11	P0054
tr|A0A8B6EPI5|A0A8B6EPI5_MYTGA	A0A8B6EPI5	Aldehyde dehydrogenase (NAD+)	11	P0055
tr|A0A8B6EUI4|A0A8B6EUI4_MYTGA	A0A8B6EUI4	H(+)-transporting two-sector ATPase	11	P0056
tr|A0A8B6FH63|A0A8B6FH63_MYTGA	A0A8B6FH63	Uncharacterized protein	11	P0057
tr|A0A8B6G1S8|A0A8B6G1S8_MYTGA	A0A8B6G1S8	Protein disulfide-isomerase	11	P0058
tr|A0A8B6G3F1|A0A8B6G3F1_MYTGA	A0A8B6G3F1	Creatine kinase	11	P0059
tr|A0A8B6GAC6|A0A8B6GAC6_MYTGA	A0A8B6GAC6	Dynein heavy chain, axonemal	11	P0060
tr|A0A8B6GHQ1|A0A8B6GHQ1_MYTGA	A0A8B6GHQ1	Tektin	11	P0061
tr|A0A8B6H0J3|A0A8B6H0J3_MYTGA	A0A8B6H0J3	Uncharacterized protein	11	P0062
tr|A0A8B6H8Q8|A0A8B6H8Q8_MYTGA	A0A8B6H8Q8	Uncharacterized protein	11	P0063
tr|A0A8B6HCL2|A0A8B6HCL2_MYTGA	A0A8B6HCL2	Hemicentin	11	P0064
tr|A0A8B6HL13|A0A8B6HL13_MYTGA	A0A8B6HL13	Vitellinogen open beta-sheet domain-containing protein	11	P0065
tr|A0A8B6HNF8|A0A8B6HNF8_MYTGA	A0A8B6HNF8	VWFD domain-containing protein	11	P0066
tr|A0A8B6HSX3|A0A8B6HSX3_MYTGA	A0A8B6HSX3	proton-translocating NAD(P)(+) transhydrogenase	11	P0067
tr|A0A8B6BGH3|A0A8B6BGH3_MYTGA	A0A8B6BGH3	T-complex protein 1 subunit epsilon	10	P0068
tr|A0A8B6C556|A0A8B6C556_MYTGA	A0A8B6C556	threonine--tRNA ligase	10	P0069
tr|A0A8B6C763|A0A8B6C763_MYTGA	A0A8B6C763	Plastin-3	10	P0070
tr|A0A8B6CGX8|A0A8B6CGX8_MYTGA	A0A8B6CGX8	Importin subunit alpha	10	P0071
tr|A0A8B6CGZ3|A0A8B6CGZ3_MYTGA	A0A8B6CGZ3	Aconitate hydratase, mitochondrial	10	P0072
tr|A0A8B6D958|A0A8B6D958_MYTGA	A0A8B6D958	Spectrin alpha	10	P0073
tr|A0A8B6DKJ4|A0A8B6DKJ4_MYTGA	A0A8B6DKJ4	Uncharacterized protein	10	P0074
tr|A0A8B6DZW9|A0A8B6DZW9_MYTGA	A0A8B6DZW9	Kringle domain-containing protein	10	P0075
tr|A0A8B6EPW8|A0A8B6EPW8_MYTGA	A0A8B6EPW8	Myosin heavy chain	10	P0076
tr|A0A8B6F1F4|A0A8B6F1F4_MYTGA	A0A8B6F1F4	Coatomer subunit beta	10	P0077

Protein	Uniprot accession	Protein Name	Number Peptides	P
tr|A0A8B6F587|A0A8B6F587_MYTGA	A0A8B6F587	MICOS complex subunit MIC60	10	P0078
tr|A0A8B6F9J1|A0A8B6F9J1_MYTGA	A0A8B6F9J1	T-complex protein 1 subunit zeta	10	P0079
tr|A0A8B6FGC7|A0A8B6FGC7_MYTGA	A0A8B6FGC7	Ribonucleoside-diphosphate reductase subunit M1	10	P0080
tr|A0A8B6FGP7|A0A8B6FGP7_MYTGA	A0A8B6FGP7	Alpha-1,4 glucan phosphorylase	10	P0081
tr|A0A8B6FGV5|A0A8B6FGV5_MYTGA	A0A8B6FGV5	Dynein heavy chain, axonemal	10	P0082
tr|A0A8B6FH66|A0A8B6FH66_MYTGA	A0A8B6FH66	Elongation factor 1-gamma	10	P0083
tr|A0A8B6FRY3|A0A8B6FRY3_MYTGA	A0A8B6FRY3	Carbamoyl-phosphate synthase / aspartate carbamoyltransfe	10	P0084
tr|A0A8B6FSV1|A0A8B6FSV1_MYTGA	A0A8B6FSV1	Uncharacterized protein	10	P0085
tr|A0A8B6FUG8|A0A8B6FUG8_MYTGA	A0A8B6FUG8	26S proteasome non-ATPase regulatory subunit 13	10	P0086
tr|A0A8B6G4H0|A0A8B6G4H0_MYTGA	A0A8B6G4H0	Calcium-transporting ATPase	10	P0087
tr|A0A8B6G9Q8|A0A8B6G9Q8_MYTGA	A0A8B6G9Q8	Laminin, alpha 3/5	10	P0088
tr|A0A8B6GB76|A0A8B6GB76_MYTGA	A0A8B6GB76	Uncharacterized protein	10	P0089
tr|A0A8B6GBK5|A0A8B6GBK5_MYTGA	A0A8B6GBK5	C-1-tetrahydrofolate synthase, cytoplasmic	10	P0090
tr|A0A8B6GPC6|A0A8B6GPC6_MYTGA	A0A8B6GPC6	Laminin, gamma 1	10	P0091
tr|A0A8B6H8A8|A0A8B6H8A8_MYTGA	A0A8B6H8A8	NADH-ubiquinone oxidoreductase 75 kDa subunit, mitocho	10	P0092
tr|A0A8B6H9X2|A0A8B6H9X2_MYTGA	A0A8B6H9X2	Myosin heavy chain 6/7	10	P0093
tr|A0A8B6HB25|A0A8B6HB25_MYTGA	A0A8B6HB25	Serine/threonine-protein phosphatase 2A regulatory subuni	10	P0094
tr|A0A8B6HDB4|A0A8B6HDB4_MYTGA	A0A8B6HDB4	Actin-interacting protein 1	10	P0095
tr|A0A8B6HF54|A0A8B6HF54_MYTGA	A0A8B6HF54	Adducin	10	P0096
tr|A0A8B6BG90|A0A8B6BG90_MYTGA	A0A8B6BG90	Rab GDP dissociation inhibitor	9	P0097
tr|A0A8B6BI87|A0A8B6BI87_MYTGA	A0A8B6BI87	26S proteasome regulatory subunit T5	9	P0098
tr|A0A8B6BT14|A0A8B6BT14_MYTGA	A0A8B6BT14	Large subunit ribosomal protein L4e	9	P0099
tr|A0A8B6C847|A0A8B6C847_MYTGA	A0A8B6C847	Major vault protein	9	P0100
tr|A0A8B6C9A5|A0A8B6C9A5_MYTGA	A0A8B6C9A5	Alanine--tRNA ligase	9	P0101
tr|A0A8B6CAF7|A0A8B6CAF7_MYTGA	A0A8B6CAF7	D-3-phosphoglycerate dehydrogenase	9	P0102
tr|A0A8B6CB10|A0A8B6CB10_MYTGA	A0A8B6CB10	VWFA domain-containing protein	9	P0103
tr|A0A8B6CHQ8|A0A8B6CHQ8_MYTGA	A0A8B6CHQ8	TOG domain-containing protein	9	P0104
tr|A0A8B6CJ76|A0A8B6CJ76_MYTGA	A0A8B6CJ76	Isocitrate dehydrogenase [NAD] subunit, mitochondrial (Fra	9	P0105
tr|A0A8B6CNW7|A0A8B6CNW7_MYTGA	A0A8B6CNW7	Coatomer subunit beta	9	P0106
tr|A0A8B6D588|A0A8B6D588_MYTGA	A0A8B6D588	Exportin-1	9	P0107
tr|A0A8B6DV58|A0A8B6DV58_MYTGA	A0A8B6DV58	Aldehyde dehydrogenase domain-containing protein	9	P0108
tr|A0A8B6DZ60|A0A8B6DZ60_MYTGA	A0A8B6DZ60	isoleucine--tRNA ligase	9	P0109
tr|A0A8B6EBM4|A0A8B6EBM4_MYTGA	A0A8B6EBM4	Coatomer subunit alpha	9	P0110
tr|A0A8B6EC17|A0A8B6EC17_MYTGA	A0A8B6EC17	DNA replication licensing factor MCM2	9	P0111
tr|A0A8B6EC82|A0A8B6EC82_MYTGA	A0A8B6EC82	galactosylgalactosylxylosylprotein 3-beta-glucuronosyltrans	9	P0112
tr|A0A8B6EH82|A0A8B6EH82_MYTGA	A0A8B6EH82	Leucyl aminopeptidase	9	P0113
tr|A0A8B6EJ05|A0A8B6EJ05_MYTGA	A0A8B6EJ05	Ras GTPase-activating-like protein IQGAP1	9	P0114
tr|A0A8B6ELM7|A0A8B6ELM7_MYTGA	A0A8B6ELM7	VWFA domain-containing protein	9	P0115
tr|A0A8B6EU84|A0A8B6EU84_MYTGA	A0A8B6EU84	Na(+)/H(+) exchange regulatory cofactor NHE-RF1	9	P0116
tr|A0A8B6EVA6|A0A8B6EVA6_MYTGA	A0A8B6EVA6	UTP--glucose-1-phosphate uridylyltransferase	9	P0117
tr|A0A8B6FPY5|A0A8B6FPY5_MYTGA	A0A8B6FPY5	Tektin	9	P0118
tr|A0A8B6FT60|A0A8B6FT60_MYTGA	A0A8B6FT60	Radial spoke head protein 4A	9	P0119
tr|A0A8B6FW92|A0A8B6FW92_MYTGA	A0A8B6FW92	Molecular chaperone DnaK	9	P0120
tr|A0A8B6G5S6|A0A8B6G5S6_MYTGA	A0A8B6G5S6	Prohibitin	9	P0121
tr|A0A8B6G9A0|A0A8B6G9A0_MYTGA	A0A8B6G9A0	Aspartate aminotransferase	9	P0122
tr|A0A8B6GHX0|A0A8B6GHX0_MYTGA	A0A8B6GHX0	26S proteasome regulatory subunit N3	9	P0123
tr|A0A8B6GL71|A0A8B6GL71_MYTGA	A0A8B6GL71	Sperm-associated antigen 6	9	P0124
tr|A0A8B6GSX9|A0A8B6GSX9_MYTGA	A0A8B6GSX9	Chaperonin GroEL	9	P0125
tr|A0A8B6GZE3|A0A8B6GZE3_MYTGA	A0A8B6GZE3	Uncharacterized protein	9	P0126
tr|A0A8B6HQH7|A0A8B6HQH7_MYTGA	A0A8B6HQH7	Heat shock 70kDa protein 4 (Fragment)	9	P0127
tr|A0A8B6HSJ1|A0A8B6HSJ1_MYTGA	A0A8B6HSJ1	Trichohyalin	9	P0128
tr|Q6BD10|Q6BD10_MYTGA	Q6BD10	Elongation factor 1-alpha	9	P0129
tr|A0A8B6BJ49|A0A8B6BJ49_MYTGA	A0A8B6BJ49	Vinculin	8	P0130
tr|A0A8B6BRG0|A0A8B6BRG0_MYTGA	A0A8B6BRG0	Dynein heavy chain 1, cytosolic	8	P0131
tr|A0A8B6C281|A0A8B6C281_MYTGA	A0A8B6C281	Advillin	8	P0132
tr|A0A8B6CCJ8|A0A8B6CCJ8_MYTGA	A0A8B6CCJ8	26S proteasome regulatory subunit N6	8	P0133
tr|A0A8B6CP85|A0A8B6CP85_MYTGA	A0A8B6CP85	Selenium-binding protein 1	8	P0134
tr|A0A8B6CPS6|A0A8B6CPS6_MYTGA	A0A8B6CPS6	RuvB-like helicase	8	P0135
tr|A0A8B6CX88|A0A8B6CX88_MYTGA	A0A8B6CX88	Small ribosomal subunit protein eS1	8	P0136
tr|A0A8B6D042|A0A8B6D042_MYTGA	A0A8B6D042	Laminin, beta 1	8	P0137
tr|A0A8B6D4X4|A0A8B6D4X4_MYTGA	A0A8B6D4X4	Hypoxia up-regulated protein 1 (Fragment)	8	P0138
tr|A0A8B6DJ12|A0A8B6DJ12_MYTGA	A0A8B6DJ12	Outer dense fiber protein 3	8	P0139
tr|A0A8B6DJV9|A0A8B6DJV9_MYTGA	A0A8B6DJV9	Transitional endoplasmic reticulum ATPase	8	P0140
tr|A0A8B6DV07|A0A8B6DV07_MYTGA	A0A8B6DV07	RNA helicase	8	P0141
tr|A0A8B6E870|A0A8B6E870_MYTGA	A0A8B6E870	Calcium binding protein 39	8	P0142
tr|A0A8B6E942|A0A8B6E942_MYTGA	A0A8B6E942	Dynein heavy chain, axonemal	8	P0143
tr|A0A8B6EE91|A0A8B6EE91_MYTGA	A0A8B6EE91	Neural cell adhesion molecule	8	P0144
tr|A0A8B6EH32|A0A8B6EH32_MYTGA	A0A8B6EH32	Uncharacterized protein	8	P0145
tr|A0A8B6EIW3|A0A8B6EIW3_MYTGA	A0A8B6EIW3	alanine transaminase	8	P0146
tr|A0A8B6EPF5|A0A8B6EPF5_MYTGA	A0A8B6EPF5	Propionyl-CoA carboxylase beta chain, mitochondrial	8	P0147
tr|A0A8B6ETB5|A0A8B6ETB5_MYTGA	A0A8B6ETB5	Nucleolin	8	P0148
tr|A0A8B6F4R7|A0A8B6F4R7_MYTGA	A0A8B6F4R7	Adenylate kinase	8	P0149
tr|A0A8B6F7Q1|A0A8B6F7Q1_MYTGA	A0A8B6F7Q1	Collagen, type XVIII, alpha	8	P0150
tr|A0A8B6FIW7|A0A8B6FIW7_MYTGA	A0A8B6FIW7	Solute carrier family 25 (Mitochondrial phosphate transport	8	P0151
tr|A0A8B6FXU3|A0A8B6FXU3_MYTGA	A0A8B6FXU3	Protein disulfide-isomerase A6	8	P0152
tr|A0A8B6FYJ7|A0A8B6FYJ7_MYTGA	A0A8B6FYJ7	Armadillo repeat-containing protein 3	8	P0153
tr|A0A8B6G6U8|A0A8B6G6U8_MYTGA	A0A8B6G6U8	Core-binding (CB) domain-containing protein (Fragment)	8	P0154
tr|A0A8B6GFS3|A0A8B6GFS3_MYTGA	A0A8B6GFS3	Dynein heavy chain, axonemal (Fragment)	8	P0155
tr|A0A8B6GKE0|A0A8B6GKE0_MYTGA	A0A8B6GKE0	Aldehyde dehydrogenase (NAD+)	8	P0156
tr|A0A8B6GN57|A0A8B6GN57_MYTGA	A0A8B6GN57	DNA replication licensing factor MCM7	8	P0157
tr|A0A8B6GN87|A0A8B6GN87_MYTGA	A0A8B6GN87	Electron transfer flavoprotein subunit alpha	8	P0158
tr|A0A8B6H9Q9|A0A8B6H9Q9_MYTGA	A0A8B6H9Q9	Filamin	8	P0159
tr|A0A8B6HGI4|A0A8B6HGI4_MYTGA	A0A8B6HGI4	Gelsolin	8	P0160
tr|A0A8B6HLJ4|A0A8B6HLJ4_MYTGA	A0A8B6HLJ4	Vitellogenin domain-containing protein	8	P0161
tr|A0A8B6BJ80|A0A8B6BJ80_MYTGA	A0A8B6BJ80	AP-1 complex subunit gamma	7	P0162
tr|A0A8B6BMG3|A0A8B6BMG3_MYTGA	A0A8B6BMG3	Prolyl endopeptidase	7	P0163
tr|A0A8B6BSM2|A0A8B6BSM2_MYTGA	A0A8B6BSM2	Dynein heavy chain 1, cytosolic	7	P0164
tr|A0A8B6BSR2|A0A8B6BSR2_MYTGA	A0A8B6BSR2	Coatomer subunit gamma	7	P0165
tr|A0A8B6BVE0|A0A8B6BVE0_MYTGA	A0A8B6BVE0	Hydroxysteroid dehydrogenase-like protein 2	7	P0166
tr|A0A8B6BWH9|A0A8B6BWH9_MYTGA	A0A8B6BWH9	Fructose-bisphosphate aldolase	7	P0167
tr|A0A8B6BZS0|A0A8B6BZS0_MYTGA	A0A8B6BZS0	Ubiquitin carboxyl-terminal hydrolase 9/24	7	P0168
tr|A0A8B6C1U6|A0A8B6C1U6_MYTGA	A0A8B6C1U6	Proteasome subunit beta	7	P0169
tr|A0A8B6C2Y2|A0A8B6C2Y2_MYTGA	A0A8B6C2Y2	Malate dehydrogenase	7	P0170
tr|A0A8B6C6Z2|A0A8B6C6Z2_MYTGA	A0A8B6C6Z2	Peptidyl-prolyl cis-trans isomerase	7	P0171
tr|A0A8B6C8G8|A0A8B6C8G8_MYTGA	A0A8B6C8G8	Ribosomal protein S6 kinase	7	P0172
tr|A0A8B6CA44|A0A8B6CA44_MYTGA	A0A8B6CA44	Aspartate--tRNA ligase, cytoplasmic	7	P0173
tr|A0A8B6CCQ1|A0A8B6CCQ1_MYTGA	A0A8B6CCQ1	GDP-L-fucose synthase	7	P0174
tr|A0A8B6CGC3|A0A8B6CGC3_MYTGA	A0A8B6CGC3	Uncharacterized protein	7	P0175
tr|A0A8B6CV11|A0A8B6CV11_MYTGA	A0A8B6CV11	Flotillin	7	P0176
tr|A0A8B6D3Z8|A0A8B6D3Z8_MYTGA	A0A8B6D3Z8	Obscurin-RhoGEF	7	P0177
tr|A0A8B6D685|A0A8B6D685_MYTGA	A0A8B6D685	Dihydrolipoyllysine-residue succinyltransferase component	7	P0178
tr|A0A8B6D816|A0A8B6D816_MYTGA	A0A8B6D816	26S proteasome regulatory subunit 7	7	P0179
tr|A0A8B6DCE2|A0A8B6DCE2_MYTGA	A0A8B6DCE2	40S ribosomal protein S3	7	P0180
tr|A0A8B6DR79|A0A8B6DR79_MYTGA	A0A8B6DR79	glutamate dehydrogenase [NAD(P)(+)]	7	P0181
tr|A0A8B6DSL8|A0A8B6DSL8_MYTGA	A0A8B6DSL8	Adenosylhomocysteinase	7	P0182
tr|A0A8B6DZH2|A0A8B6DZH2_MYTGA	A0A8B6DZH2	Dolichyl-diphosphooligosaccharide--protein glycosyltransfe	7	P0183
tr|A0A8B6EC26|A0A8B6EC26_MYTGA	A0A8B6EC26	Septin 7	7	P0184
tr|A0A8B6ECQ5|A0A8B6ECQ5_MYTGA	A0A8B6ECQ5	Uncharacterized protein	7	P0185
tr|A0A8B6EJ43|A0A8B6EJ43_MYTGA	A0A8B6EJ43	Serine/threonine-protein phosphatase	7	P0186
tr|A0A8B6EKC0|A0A8B6EKC0_MYTGA	A0A8B6EKC0	Small ribosomal subunit protein uS2	7	P0187
tr|A0A8B6F1X3|A0A8B6F1X3_MYTGA	A0A8B6F1X3	Kelch-like protein 2/3	7	P0188
tr|A0A8B6F8A8|A0A8B6F8A8_MYTGA	A0A8B6F8A8	ATP synthase subunit O, mitochondrial	7	P0189
tr|A0A8B6FA55|A0A8B6FA55_MYTGA	A0A8B6FA55	phosphoglycerate mutase (2,3-diphosphoglycerate-depende	7	P0190
tr|A0A8B6FDB3|A0A8B6FDB3_MYTGA	A0A8B6FDB3	Ribonucleoside-diphosphate reductase	7	P0191
tr|A0A8B6FG53|A0A8B6FG53_MYTGA	A0A8B6FG53	Ropporin-1-like protein	7	P0192
tr|A0A8B6FRK3|A0A8B6FRK3_MYTGA	A0A8B6FRK3	Exportin-2	7	P0193
tr|A0A8B6FWX7|A0A8B6FWX7_MYTGA	A0A8B6FWX7	Electron transfer flavoprotein subunit beta	7	P0194

Protein	Uniprot accession	Protein Name	Number Peptides	P
tr|A0A8B6G0F4|A0A8B6G0F4_MYTGA	A0A8B6G0F4	phenylalanine 4-monooxygenase	7	P0195
tr|A0A8B6G0V7|A0A8B6G0V7_MYTGA	A0A8B6G0V7	C-type lectin domain-containing protein	7	P0196
tr|A0A8B6GCQ5|A0A8B6GCQ5_MYTGA	A0A8B6GCQ5	Dolichyl-diphosphooligosaccharide--protein glycosyltransfe	7	P0197
tr|A0A8B6GKK5|A0A8B6GKK5_MYTGA	A0A8B6GKK5	14-3-3 protein epsilon	7	P0198
tr|A0A8B6GLQ5|A0A8B6GLQ5_MYTGA	A0A8B6GLQ5	Aspartate aminotransferase, cytoplasmic	7	P0199
tr|A0A8B6GMH2|A0A8B6GMH2_MYTGA	A0A8B6GMH2	Ornithine aminotransferase	7	P0200
tr|A0A8B6GV47|A0A8B6GV47_MYTGA	A0A8B6GV47	ADP/ATP translocase	7	P0201
tr|A0A8B6GYJ9|A0A8B6GYJ9_MYTGA	A0A8B6GYJ9	Dyp-type peroxidase C-terminal domain-containing protein	7	P0202
tr|A0A8B6HNM7|A0A8B6HNM7_MYTGA	A0A8B6HNM7	S-(Hydroxymethyl)glutathione dehydrogenase / alcohol deh	7	P0203
tr|A0A8B6HP92|A0A8B6HP92_MYTGA	A0A8B6HP92	Uncharacterized protein (Fragment)	7	P0204
tr|A0A8B6HPY9|A0A8B6HPY9_MYTGA	A0A8B6HPY9	26S proteasome non-ATPase regulatory subunit 2	7	P0205
tr|A0A8B6HSL7|A0A8B6HSL7_MYTGA	A0A8B6HSL7	Dynein light intermediate chain, axonemal	7	P0206
tr|B6ZCB2|B6ZCB2_MYTGA	B6ZCB2	60S acidic ribosomal protein P0	7	P0207
tr|E0D7H4|E0D7H4_MYTGA	E0D7H4	RNA helicase	7	P0208
tr|A0A3L5TU74|A0A3L5TU74_MYTGA	A0A3L5TU74	Nucleolar protein 56 (Fragment)	6	P0209
tr|A0A8B6BE54|A0A8B6BE54_MYTGA	A0A8B6BE54	RIIa domain-containing protein	6	P0210
tr|A0A8B6BH70|A0A8B6BH70_MYTGA	A0A8B6BH70	Succinate dehydrogenase [ubiquinone] iron-sulfur subunit,	6	P0211
tr|A0A8B6BJW5|A0A8B6BJW5_MYTGA	A0A8B6BJW5	Prohibitin	6	P0212
tr|A0A8B6BM01|A0A8B6BM01_MYTGA	A0A8B6BM01	CH-like domain-containing protein (Fragment)	6	P0213
tr|A0A8B6BMF4|A0A8B6BMF4_MYTGA	A0A8B6BMF4	Long-chain-fatty-acid--CoA ligase	6	P0214
tr|A0A8B6BMX1|A0A8B6BMX1_MYTGA	A0A8B6BMX1	Proteasome subunit beta	6	P0215
tr|A0A8B6BNP8|A0A8B6BNP8_MYTGA	A0A8B6BNP8	Thioredoxin-like protein 1	6	P0216
tr|A0A8B6BWZ3|A0A8B6BWZ3_MYTGA	A0A8B6BWZ3	Histone H4	6	P0217
tr|A0A8B6C4P6|A0A8B6C4P6_MYTGA	A0A8B6C4P6	Lethal(2) giant larvae protein	6	P0218
tr|A0A8B6CEC6|A0A8B6CEC6_MYTGA	A0A8B6CEC6	UDP-glucose:glycoprotein glucosyltransferase	6	P0219
tr|A0A8B6CGB4|A0A8B6CGB4_MYTGA	A0A8B6CGB4	Large ribosomal subunit protein uL1	6	P0220
tr|A0A8B6CI49|A0A8B6CI49_MYTGA	A0A8B6CI49	116 kDa U5 small nuclear ribonucleoprotein component	6	P0221
tr|A0A8B6CP36|A0A8B6CP36_MYTGA	A0A8B6CP36	CTP synthase	6	P0222
tr|A0A8B6CT69|A0A8B6CT69_MYTGA	A0A8B6CT69	Importin-7	6	P0223
tr|A0A8B6CTY3|A0A8B6CTY3_MYTGA	A0A8B6CTY3	Atlastin	6	P0224
tr|A0A8B6CVL6|A0A8B6CVL6_MYTGA	A0A8B6CVL6	U5 small nuclear ribonucleoprotein 200 kDa helicase	6	P0225
tr|A0A8B6CY60|A0A8B6CY60_MYTGA	A0A8B6CY60	Tektin	6	P0226
tr|A0A8B6D0G8|A0A8B6D0G8_MYTGA	A0A8B6D0G8	Ribosome-binding protein 1	6	P0227
tr|A0A8B6D0L8|A0A8B6D0L8_MYTGA	A0A8B6D0L8	Gelsolin	6	P0228
tr|A0A8B6D2D4|A0A8B6D2D4_MYTGA	A0A8B6D2D4	Adenylyl cyclase-associated protein	6	P0229
tr|A0A8B6D2E0|A0A8B6D2E0_MYTGA	A0A8B6D2E0	Dynein heavy chain, axonemal	6	P0230
tr|A0A8B6D4L3|A0A8B6D4L3_MYTGA	A0A8B6D4L3	Eukaryotic translation initiation factor 3 subunit C	6	P0231
tr|A0A8B6D5A7|A0A8B6D5A7_MYTGA	A0A8B6D5A7	Succinate dehydrogenase (Ubiquinone) flavoprotein subunit	6	P0232
tr|A0A8B6D6E2|A0A8B6D6E2_MYTGA	A0A8B6D6E2	Palmitoyl-protein thioesterase 1	6	P0233
tr|A0A8B6D723|A0A8B6D723_MYTGA	A0A8B6D723	Moesin/ezrin/radixin homolog 1 (Fragment)	6	P0234
tr|A0A8B6D865|A0A8B6D865_MYTGA	A0A8B6D865	EH domain-containing protein 1	6	P0235
tr|A0A8B6DBA4|A0A8B6DBA4_MYTGA	A0A8B6DBA4	26S proteasome regulatory subunit 8	6	P0236
tr|A0A8B6DDL3|A0A8B6DDL3_MYTGA	A0A8B6DDL3	ubiquitinyl hydrolase 1	6	P0237
tr|A0A8B6DES3|A0A8B6DES3_MYTGA	A0A8B6DES3	Calponin-homology (CH) domain-containing protein	6	P0238
tr|A0A8B6DGQ6|A0A8B6DGQ6_MYTGA	A0A8B6DGQ6	Thymosin beta	6	P0239
tr|A0A8B6DJM9|A0A8B6DJM9_MYTGA	A0A8B6DJM9	AFG3 family protein	6	P0240
tr|A0A8B6DL53|A0A8B6DL53_MYTGA	A0A8B6DL53	VWFD domain-containing protein	6	P0241
tr|A0A8B6DP55|A0A8B6DP55_MYTGA	A0A8B6DP55	DnaJ homolog subfamily B member 11	6	P0242
tr|A0A8B6DR40|A0A8B6DR40_MYTGA	A0A8B6DR40	EF-hand domain-containing protein 1	6	P0243
tr|A0A8B6DRV5|A0A8B6DRV5_MYTGA	A0A8B6DRV5	Dihydrolipoyl dehydrogenase	6	P0244
tr|A0A8B6DRW1|A0A8B6DRW1_MYTGA	A0A8B6DRW1	Nidogen (Entactin) (Fragment)	6	P0245
tr|A0A8B6DZJ0|A0A8B6DZJ0_MYTGA	A0A8B6DZJ0	Cilia- and flagella-associated protein 43	6	P0246
tr|A0A8B6E034|A0A8B6E034_MYTGA	A0A8B6E034	Malic enzyme	6	P0247
tr|A0A8B6E2Z9|A0A8B6E2Z9_MYTGA	A0A8B6E2Z9	Glucosidase II subunit alpha	6	P0248
tr|A0A8B6EBF2|A0A8B6EBF2_MYTGA	A0A8B6EBF2	phenylalanine--tRNA ligase	6	P0249
tr|A0A8B6EE40|A0A8B6EE40_MYTGA	A0A8B6EE40	Uncharacterized protein	6	P0250
tr|A0A8B6EGI0|A0A8B6EGI0_MYTGA	A0A8B6EGI0	Actin-related protein 2	6	P0251
tr|A0A8B6EK85|A0A8B6EK85_MYTGA	A0A8B6EK85	Fascin	6	P0252
tr|A0A8B6ERX1|A0A8B6ERX1_MYTGA	A0A8B6ERX1	Cathepsin L	6	P0253
tr|A0A8B6EXQ9|A0A8B6EXQ9_MYTGA	A0A8B6EXQ9	Uncharacterized protein	6	P0254
tr|A0A8B6EYI6|A0A8B6EYI6_MYTGA	A0A8B6EYI6	Eukaryotic translation initiation factor 3 subunit A	6	P0255
tr|A0A8B6F3H4|A0A8B6F3H4_MYTGA	A0A8B6F3H4	Uncharacterized protein	6	P0256
tr|A0A8B6F6T7|A0A8B6F6T7_MYTGA	A0A8B6F6T7	FAS1 domain-containing protein	6	P0257
tr|A0A8B6F6Z5|A0A8B6F6Z5_MYTGA	A0A8B6F6Z5	RNA helicase	6	P0258
tr|A0A8B6FA66|A0A8B6FA66_MYTGA	A0A8B6FA66	Peroxiredoxin 6, 1-Cys peroxiredoxin	6	P0259
tr|A0A8B6FBK7|A0A8B6FBK7_MYTGA	A0A8B6FBK7	Obg-like ATPase 1 (Fragment)	6	P0260
tr|A0A8B6FC22|A0A8B6FC22_MYTGA	A0A8B6FC22	Microtubule-associated protein 1	6	P0261
tr|A0A8B6FHR5|A0A8B6FHR5_MYTGA	A0A8B6FHR5	Short-chain specific acyl-CoA dehydrogenase, mitochondria	6	P0262
tr|A0A8B6FQD5|A0A8B6FQD5_MYTGA	A0A8B6FQD5	26S proteasome regulatory subunit N2 (Fragment)	6	P0263
tr|A0A8B6FWA8|A0A8B6FWA8_MYTGA	A0A8B6FWA8	glutamine--tRNA ligase	6	P0264
tr|A0A8B6FY98|A0A8B6FY98_MYTGA	A0A8B6FY98	DNA topoisomerase 2	6	P0265
tr|A0A8B6FZ76|A0A8B6FZ76_MYTGA	A0A8B6FZ76	C2 domain-containing protein (Fragment)	6	P0266
tr|A0A8B6G0T1|A0A8B6G0T1_MYTGA	A0A8B6G0T1	Serine/threonine-protein kinase 31	6	P0267
tr|A0A8B6GEQ8|A0A8B6GEQ8_MYTGA	A0A8B6GEQ8	Eukaryotic translation initiation factor 3 subunit B	6	P0268
tr|A0A8B6GIB3|A0A8B6GIB3_MYTGA	A0A8B6GIB3	Myosin heavy chain 6/7 (Fragment)	6	P0269
tr|A0A8B6GIU1|A0A8B6GIU1_MYTGA	A0A8B6GIU1	NIMA (Never in mitosis gene a)-related kinase	6	P0270
tr|A0A8B6GKD8|A0A8B6GKD8_MYTGA	A0A8B6GKD8	Serine hydroxymethyltransferase	6	P0271
tr|A0A8B6GPN2|A0A8B6GPN2_MYTGA	A0A8B6GPN2	Tektin	6	P0272
tr|A0A8B6GQK5|A0A8B6GQK5_MYTGA	A0A8B6GQK5	thioredoxin-dependent peroxiredoxin	6	P0273
tr|A0A8B6GSE3|A0A8B6GSE3_MYTGA	A0A8B6GSE3	DNA replication licensing factor MCM5	6	P0274
tr|A0A8B6GU32|A0A8B6GU32_MYTGA	A0A8B6GU32	ATP synthase subunit gamma	6	P0275
tr|A0A8B6GY74|A0A8B6GY74_MYTGA	A0A8B6GY74	Cilia- and flagella-associated protein 57	6	P0276
tr|A0A8B6H328|A0A8B6H328_MYTGA	A0A8B6H328	Glucose-6-phosphate isomerase	6	P0277
tr|A0A8B6H6K8|A0A8B6H6K8_MYTGA	A0A8B6H6K8	Small ribosomal subunit protein uS4	6	P0278
tr|A0A8B6HBA9|A0A8B6HBA9_MYTGA	A0A8B6HBA9	Fumarylacetoacetase	6	P0279
tr|A0A8B6HD03|A0A8B6HD03_MYTGA	A0A8B6HD03	non-specific serine/threonine protein kinase	6	P0280
tr|A0A8B6HF71|A0A8B6HF71_MYTGA	A0A8B6HF71	Multifunctional fusion protein	6	P0281
tr|A0A8B6HL62|A0A8B6HL62_MYTGA	A0A8B6HL62	Small subunit ribosomal protein S19e	6	P0282
tr|A0A8B6HML0|A0A8B6HML0_MYTGA	A0A8B6HML0	VWFD domain-containing protein	6	P0283
tr|A0A8B6HQB3|A0A8B6HQB3_MYTGA	A0A8B6HQB3	alpha-L-fucosidase	6	P0284
tr|G9G141|G9G141_MYTGA	G9G141	TCTP	6	P0285
tr|A0A0K0YB29|A0A0K0YB29_MYTGA	A0A0K0YB29	LKD-rich protein-1	5	P0286
tr|A0A8B6BFV8|A0A8B6BFV8_MYTGA	A0A8B6BFV8	Ferritin	5	P0287
tr|A0A8B6BIH5|A0A8B6BIH5_MYTGA	A0A8B6BIH5	Peptidyl-prolyl cis-trans isomerase	5	P0288
tr|A0A8B6BRQ2|A0A8B6BRQ2_MYTGA	A0A8B6BRQ2	Beta-ureidopropionase	5	P0289
tr|A0A8B6BRW7|A0A8B6BRW7_MYTGA	A0A8B6BRW7	Link domain-containing protein	5	P0290
tr|A0A8B6BS10|A0A8B6BS10_MYTGA	A0A8B6BS10	40S ribosomal protein S7	5	P0291
tr|A0A8B6BSB5|A0A8B6BSB5_MYTGA	A0A8B6BSB5	Neutral ceramidase	5	P0292
tr|A0A8B6BTF8|A0A8B6BTF8_MYTGA	A0A8B6BTF8	long-chain-fatty-acid--CoA ligase	5	P0293
tr|A0A8B6C2G0|A0A8B6C2G0_MYTGA	A0A8B6C2G0	V-type H+-transporting ATPase subunit E	5	P0294
tr|A0A8B6C2P8|A0A8B6C2P8_MYTGA	A0A8B6C2P8	Myosin I	5	P0295
tr|A0A8B6C827|A0A8B6C827_MYTGA	A0A8B6C827	60S ribosomal protein L13	5	P0296
tr|A0A8B6CC47|A0A8B6CC47_MYTGA	A0A8B6CC47	glutathione transferase	5	P0297
tr|A0A8B6CDF0|A0A8B6CDF0_MYTGA	A0A8B6CDF0	Nucleolin	5	P0298
tr|A0A8B6CHV9|A0A8B6CHV9_MYTGA	A0A8B6CHV9	Aldehyde dehydrogenase (NAD+)	5	P0299
tr|A0A8B6CKQ4|A0A8B6CKQ4_MYTGA	A0A8B6CKQ4	Nucleophosmin 1	5	P0300
tr|A0A8B6CKU0|A0A8B6CKU0_MYTGA	A0A8B6CKU0	Proteasome subunit beta	5	P0301
tr|A0A8B6CMK8|A0A8B6CMK8_MYTGA	A0A8B6CMK8	DNA replication licensing factor MCM6	5	P0302
tr|A0A8B6CPA4|A0A8B6CPA4_MYTGA	A0A8B6CPA4	Bifunctional purine biosynthesis protein ATIC	5	P0303
tr|A0A8B6CT41|A0A8B6CT41_MYTGA	A0A8B6CT41	calcium/calmodulin-dependent protein kinase	5	P0304
tr|A0A8B6CT47|A0A8B6CT47_MYTGA	A0A8B6CT47	Dynamin 1-like protein	5	P0305
tr|A0A8B6CXQ1|A0A8B6CXQ1_MYTGA	A0A8B6CXQ1	Uncharacterized protein	5	P0306
tr|A0A8B6CYZ6|A0A8B6CYZ6_MYTGA	A0A8B6CYZ6	26S proteasome non-ATPase regulatory subunit 8 (Fragment	5	P0307
tr|A0A8B6D1I6|A0A8B6D1I6_MYTGA	A0A8B6D1I6	Microtubule-associated protein, RP/EB family	5	P0308
tr|A0A8B6D4T9|A0A8B6D4T9_MYTGA	A0A8B6D4T9	Uncharacterized protein	5	P0309
tr|A0A8B6D5A0|A0A8B6D5A0_MYTGA	A0A8B6D5A0	Large ribosomal subunit protein uL6	5	P0310
tr|A0A8B6D622|A0A8B6D622_MYTGA	A0A8B6D622	Large subunit ribosomal protein L3e	5	P0311

Protein	Uniprot accession	Protein Name	Number Peptides	P
tr|A0A8B6D6Q1|A0A8B6D6Q1_MYTGA	A0A8B6D6Q1	Hemicentin (Fragment)	5	P0312
tr|A0A8B6D7A5|A0A8B6D7A5_MYTGA	A0A8B6D7A5	Acetyltransferase component of pyruvate dehydrogenase co	5	P0313
tr|A0A8B6D9H8|A0A8B6D9H8_MYTGA	A0A8B6D9H8	W2 domain-containing protein	5	P0314
tr|A0A8B6DEG7|A0A8B6DEG7_MYTGA	A0A8B6DEG7	Sorting nexin-1/2	5	P0315
tr|A0A8B6DFV3|A0A8B6DFV3_MYTGA	A0A8B6DFV3	Peptidase M24 domain-containing protein	5	P0316
tr|A0A8B6DNA9|A0A8B6DNA9_MYTGA	A0A8B6DNA9	Cilia- and flagella-associated protein 58 central coiled coil d	5	P0317
tr|A0A8B6DP99|A0A8B6DP99_MYTGA	A0A8B6DP99	Fucolectin tachylectin-4 pentraxin-1 domain-containing pr	5	P0318
tr|A0A8B6DUV6|A0A8B6DUV6_MYTGA	A0A8B6DUV6	Betaine-homocysteine S-methyltransferase	5	P0319
tr|A0A8B6DVC9|A0A8B6DVC9_MYTGA	A0A8B6DVC9	Succinate--CoA ligase [ADP-forming] subunit beta, mitochon	5	P0320
tr|A0A8B6DXB5|A0A8B6DXB5_MYTGA	A0A8B6DXB5	Coiled-coil domain-containing protein 39	5	P0321
tr|A0A8B6DXE5|A0A8B6DXE5_MYTGA	A0A8B6DXE5	serine--tRNA ligase	5	P0322
tr|A0A8B6DZP1|A0A8B6DZP1_MYTGA	A0A8B6DZP1	Thioredoxin domain-containing protein	5	P0323
tr|A0A8B6E248|A0A8B6E248_MYTGA	A0A8B6E248	Coatomer subunit delta	5	P0324
tr|A0A8B6E2U4|A0A8B6E2U4_MYTGA	A0A8B6E2U4	Eukaryotic translation initiation factor 3 subunit E	5	P0325
tr|A0A8B6E3P4|A0A8B6E3P4_MYTGA	A0A8B6E3P4	Cyclin-dependent kinase 1	5	P0326
tr|A0A8B6E6J3|A0A8B6E6J3_MYTGA	A0A8B6E6J3	Uncharacterized protein	5	P0327
tr|A0A8B6E7A6|A0A8B6E7A6_MYTGA	A0A8B6E7A6	Heparan sulfate proteoglycan 2 (Perlecan)	5	P0328
tr|A0A8B6E9Q4|A0A8B6E9Q4_MYTGA	A0A8B6E9Q4	Large subunit ribosomal protein L7e	5	P0329
tr|A0A8B6EE65|A0A8B6EE65_MYTGA	A0A8B6EE65	Ig-like domain-containing protein	5	P0330
tr|A0A8B6EF95|A0A8B6EF95_MYTGA	A0A8B6EF95	Twitchin	5	P0331
tr|A0A8B6EJ00|A0A8B6EJ00_MYTGA	A0A8B6EJ00	Small subunit ribosomal protein S14e	5	P0332
tr|A0A8B6EJE5|A0A8B6EJE5_MYTGA	A0A8B6EJE5	Kinesin-like protein	5	P0333
tr|A0A8B6EPD3|A0A8B6EPD3_MYTGA	A0A8B6EPD3	Serine/threonine-protein phosphatase	5	P0334
tr|A0A8B6EQ31|A0A8B6EQ31_MYTGA	A0A8B6EQ31	Proteasome subunit alpha type	5	P0335
tr|A0A8B6ER63|A0A8B6ER63_MYTGA	A0A8B6ER63	Hydrocephalus-inducing protein	5	P0336
tr|A0A8B6EU46|A0A8B6EU46_MYTGA	A0A8B6EU46	Sperm-associated antigen 17	5	P0337
tr|A0A8B6EXG2|A0A8B6EXG2_MYTGA	A0A8B6EXG2	Acetyl-CoA hydrolase	5	P0338
tr|A0A8B6F3Z0|A0A8B6F3Z0_MYTGA	A0A8B6F3Z0	60S ribosomal protein L18a	5	P0339
tr|A0A8B6F4F8|A0A8B6F4F8_MYTGA	A0A8B6F4F8	Glucose-6-phosphate 1-dehydrogenase	5	P0340
tr|A0A8B6F7B4|A0A8B6F7B4_MYTGA	A0A8B6F7B4	Tropomyosin	5	P0341
tr|A0A8B6FAJ5|A0A8B6FAJ5_MYTGA	A0A8B6FAJ5	Uncharacterized protein	5	P0342
tr|A0A8B6FDZ1|A0A8B6FDZ1_MYTGA	A0A8B6FDZ1	EF-hand domain-containing protein	5	P0343
tr|A0A8B6FGX6|A0A8B6FGX6_MYTGA	A0A8B6FGX6	Arginyl-tRNA synthetase	5	P0344
tr|A0A8B6FI72|A0A8B6FI72_MYTGA	A0A8B6FI72	Uncharacterized protein (Fragment)	5	P0345
tr|A0A8B6FND3|A0A8B6FND3_MYTGA	A0A8B6FND3	T-complex protein 1 subunit delta	5	P0346
tr|A0A8B6FQN1|A0A8B6FQN1_MYTGA	A0A8B6FQN1	Eukaryotic translation initiation factor 3 subunit L	5	P0347
tr|A0A8B6FRC6|A0A8B6FRC6_MYTGA	A0A8B6FRC6	Ciliary microtubule inner protein 2A-C-like domain-containi	5	P0348
tr|A0A8B6FTE0|A0A8B6FTE0_MYTGA	A0A8B6FTE0	DNA replication licensing factor MCM4	5	P0349
tr|A0A8B6FTK4|A0A8B6FTK4_MYTGA	A0A8B6FTK4	CYRIA/CYRIB Rac1 binding domain-containing protein	5	P0350
tr|A0A8B6FTK6|A0A8B6FTK6_MYTGA	A0A8B6FTK6	Cytochrome b-c1 complex subunit 7	5	P0351
tr|A0A8B6G1F5|A0A8B6G1F5_MYTGA	A0A8B6G1F5	HECT-type E3 ubiquitin transferase	5	P0352
tr|A0A8B6G4G5|A0A8B6G4G5_MYTGA	A0A8B6G4G5	Pyruvate carboxylase	5	P0353
tr|A0A8B6G660|A0A8B6G660_MYTGA	A0A8B6G660	Lupus La protein	5	P0354
tr|A0A8B6G6A8|A0A8B6G6A8_MYTGA	A0A8B6G6A8	Nuclear pore complex protein Nup205	5	P0355
tr|A0A8B6GC26|A0A8B6GC26_MYTGA	A0A8B6GC26	Prefoldin subunit 3	5	P0356
tr|A0A8B6GLW0|A0A8B6GLW0_MYTGA	A0A8B6GLW0	Radial spoke head protein 9 homolog	5	P0357
tr|A0A8B6GP65|A0A8B6GP65_MYTGA	A0A8B6GP65	Vacuolar protein sorting-associated protein 13A/C	5	P0358
tr|A0A8B6GPV1|A0A8B6GPV1_MYTGA	A0A8B6GPV1	phosphoglucomutase (alpha-D-glucose-1,6-bisphosphate-de	5	P0359
tr|A0A8B6GYA0|A0A8B6GYA0_MYTGA	A0A8B6GYA0	CD109 antigen	5	P0360
tr|A0A8B6GZF7|A0A8B6GZF7_MYTGA	A0A8B6GZF7	Programmed cell death protein 4	5	P0361
tr|A0A8B6H2S7|A0A8B6H2S7_MYTGA	A0A8B6H2S7	Uncharacterized protein	5	P0362
tr|A0A8B6H4W7|A0A8B6H4W7_MYTGA	A0A8B6H4W7	glycylpeptide N-tetradecanoyltransferase	5	P0363
tr|A0A8B6H5E0|A0A8B6H5E0_MYTGA	A0A8B6H5E0	Eukaryotic peptide chain release factor subunit 1	5	P0364
tr|A0A8B6H6R5|A0A8B6H6R5_MYTGA	A0A8B6H6R5	26S proteasome regulatory subunit N5	5	P0365
tr|A0A8B6H7A5|A0A8B6H7A5_MYTGA	A0A8B6H7A5	DUF4476 domain-containing protein	5	P0366
tr|A0A8B6H7E1|A0A8B6H7E1_MYTGA	A0A8B6H7E1	Poly [ADP-ribose] polymerase	5	P0367
tr|A0A8B6H9T5|A0A8B6H9T5_MYTGA	A0A8B6H9T5	alpha-L-fucosidase	5	P0368
tr|A0A8B6HBZ6|A0A8B6HBZ6_MYTGA	A0A8B6HBZ6	leucine--tRNA ligase	5	P0369
tr|A0A8B6HHG6|A0A8B6HHG6_MYTGA	A0A8B6HHG6	Gelsolin	5	P0370
tr|A0A8B6HJD2|A0A8B6HJD2_MYTGA	A0A8B6HJD2	small monomeric GTPase	5	P0371
tr|A0A8B6HL24|A0A8B6HL24_MYTGA	A0A8B6HL24	ODAD1 central coiled coil region domain-containing protein	5	P0372
tr|A0A8B6HMA6|A0A8B6HMA6_MYTGA	A0A8B6HMA6	Dynein intermediate chain 2, axonemal	5	P0373
tr|A0A8B6HP91|A0A8B6HP91_MYTGA	A0A8B6HP91	3-hydroxyacyl-CoA dehydrogenase / 3a,7a,12a-trihydroxy-5	5	P0374
tr|A0A8B6HPY4|A0A8B6HPY4_MYTGA	A0A8B6HPY4	Small ribosomal subunit protein uS5	5	P0375
tr|A0A8B6HR88|A0A8B6HR88_MYTGA	A0A8B6HR88	Tektin	5	P0376
tr|A0A8B6HUT7|A0A8B6HUT7_MYTGA	A0A8B6HUT7	Proteasome subunit alpha type	5	P0377
tr|Q3S892|Q3S892_MYTGA	Q3S892	Malate dehydrogenase	5	P0378
tr|A0A8B6BEW3|A0A8B6BEW3_MYTGA	A0A8B6BEW3	Proteasome subunit beta	4	P0379
tr|A0A8B6BF89|A0A8B6BF89_MYTGA	A0A8B6BF89	4-hydroxyphenylpyruvate dioxygenase	4	P0380
tr|A0A8B6BFI3|A0A8B6BFI3_MYTGA	A0A8B6BFI3	NADH dehydrogenase [ubiquinone] flavoprotein 1, mitocho	4	P0381
tr|A0A8B6BL03|A0A8B6BL03_MYTGA	A0A8B6BL03	Ubiquinol-cytochrome c reductase core subunit 2	4	P0382
tr|A0A8B6BLQ6|A0A8B6BLQ6_MYTGA	A0A8B6BLQ6	Splicing factor 3B subunit 1 domain-containing protein	4	P0383
tr|A0A8B6BLZ7|A0A8B6BLZ7_MYTGA	A0A8B6BLZ7	DNA mismatch repair protein MSH2	4	P0384
tr|A0A8B6BMR3|A0A8B6BMR3_MYTGA	A0A8B6BMR3	RNA helicase (Fragment)	4	P0385
tr|A0A8B6BSD4|A0A8B6BSD4_MYTGA	A0A8B6BSD4	Counting factor associated protein D	4	P0386
tr|A0A8B6BT38|A0A8B6BT38_MYTGA	A0A8B6BT38	Thioredoxin domain-containing protein 5	4	P0387
tr|A0A8B6BTY3|A0A8B6BTY3_MYTGA	A0A8B6BTY3	Triosephosphate isomerase	4	P0388
tr|A0A8B6BUM1|A0A8B6BUM1_MYTGA	A0A8B6BUM1	Large ribosomal subunit protein eL30	4	P0389
tr|A0A8B6BV54|A0A8B6BV54_MYTGA	A0A8B6BV54	Calpain, invertebrate	4	P0390
tr|A0A8B6BVL5|A0A8B6BVL5_MYTGA	A0A8B6BVL5	Centrosomal protein CEP41	4	P0391
tr|A0A8B6BWA9|A0A8B6BWA9_MYTGA	A0A8B6BWA9	Very long-chain specific acyl-CoA dehydrogenase, mitochon	4	P0392
tr|A0A8B6BZ12|A0A8B6BZ12_MYTGA	A0A8B6BZ12	Reverse transcriptase domain-containing protein	4	P0393
tr|A0A8B6C045|A0A8B6C045_MYTGA	A0A8B6C045	Chloride intracellular channel protein	4	P0394
tr|A0A8B6C1F4|A0A8B6C1F4_MYTGA	A0A8B6C1F4	WSC domain-containing protein	4	P0395
tr|A0A8B6C2P9|A0A8B6C2P9_MYTGA	A0A8B6C2P9	Enolase	4	P0396
tr|A0A8B6C3J3|A0A8B6C3J3_MYTGA	A0A8B6C3J3	Uncharacterized protein	4	P0397
tr|A0A8B6C423|A0A8B6C423_MYTGA	A0A8B6C423	EF-hand domain-containing protein	4	P0398
tr|A0A8B6C6F3|A0A8B6C6F3_MYTGA	A0A8B6C6F3	Nucleoside-diphosphate kinase	4	P0399
tr|A0A8B6C964|A0A8B6C964_MYTGA	A0A8B6C964	Endonuclease/exonuclease/phosphatase domain-containing	4	P0400
tr|A0A8B6CC28|A0A8B6CC28_MYTGA	A0A8B6CC28	Annexin	4	P0401
tr|A0A8B6CCD5|A0A8B6CCD5_MYTGA	A0A8B6CCD5	14-3-3 protein epsilon	4	P0402
tr|A0A8B6CD05|A0A8B6CD05_MYTGA	A0A8B6CD05	Uncharacterized protein	4	P0403
tr|A0A8B6CDE6|A0A8B6CDE6_MYTGA	A0A8B6CDE6	tryptophan--tRNA ligase	4	P0404
tr|A0A8B6CES0|A0A8B6CES0_MYTGA	A0A8B6CES0	Small subunit ribosomal protein S5e	4	P0405
tr|A0A8B6CG35|A0A8B6CG35_MYTGA	A0A8B6CG35	Uncharacterized protein	4	P0406
tr|A0A8B6CG44|A0A8B6CG44_MYTGA	A0A8B6CG44	Alpha-galactosidase	4	P0407
tr|A0A8B6CHN3|A0A8B6CHN3_MYTGA	A0A8B6CHN3	C-type lectin domain-containing protein	4	P0408
tr|A0A8B6CNF8|A0A8B6CNF8_MYTGA	A0A8B6CNF8	FACT complex subunit	4	P0409
tr|A0A8B6CQ86|A0A8B6CQ86_MYTGA	A0A8B6CQ86	Tyrosine--tRNA ligase	4	P0410
tr|A0A8B6CSI5|A0A8B6CSI5_MYTGA	A0A8B6CSI5	Small subunit ribosomal protein S17e	4	P0411
tr|A0A8B6CT20|A0A8B6CT20_MYTGA	A0A8B6CT20	Adenylate kinase	4	P0412
tr|A0A8B6CTE1|A0A8B6CTE1_MYTGA	A0A8B6CTE1	Arp2/3 complex 34 kDa subunit	4	P0413
tr|A0A8B6CVU1|A0A8B6CVU1_MYTGA	A0A8B6CVU1	Cofilin	4	P0414
tr|A0A8B6D0R4|A0A8B6D0R4_MYTGA	A0A8B6D0R4	deoxyribose-phosphate aldolase	4	P0415
tr|A0A8B6D1D5|A0A8B6D1D5_MYTGA	A0A8B6D1D5	Saposin	4	P0416
tr|A0A8B6D2Y8|A0A8B6D2Y8_MYTGA	A0A8B6D2Y8	Sulfur dioxygenase	4	P0417
tr|A0A8B6D8K5|A0A8B6D8K5_MYTGA	A0A8B6D8K5	cAMP-dependent protein kinase regulator	4	P0418
tr|A0A8B6D9L9|A0A8B6D9L9_MYTGA	A0A8B6D9L9	glycine hydroxymethyltransferase	4	P0419
tr|A0A8B6DAP3|A0A8B6DAP3_MYTGA	A0A8B6DAP3	Mesencephalic astrocyte-derived neurotrophic factor homo	4	P0420
tr|A0A8B6DBB7|A0A8B6DBB7_MYTGA	A0A8B6DBB7	Nucleoside-diphosphate kinase	4	P0421
tr|A0A8B6DCF7|A0A8B6DCF7_MYTGA	A0A8B6DCF7	Protein DEK	4	P0422
tr|A0A8B6DDU4|A0A8B6DDU4_MYTGA	A0A8B6DDU4	Phosphoribosylaminoimidazole carboxylase / phosphoribos	4	P0423
tr|A0A8B6DGK2|A0A8B6DGK2_MYTGA	A0A8B6DGK2	Uncharacterized protein	4	P0424
tr|A0A8B6DHD7|A0A8B6DHD7_MYTGA	A0A8B6DHD7	H15 domain-containing protein	4	P0425
tr|A0A8B6DHE3|A0A8B6DHE3_MYTGA	A0A8B6DHE3	Cathepsin B	4	P0426
tr|A0A8B6DHI0|A0A8B6DHI0_MYTGA	A0A8B6DHI0	Histone-binding protein RBBP4	4	P0427
tr|A0A8B6DJD2|A0A8B6DJD2_MYTGA	A0A8B6DJD2	Carnitine O-acetyltransferase	4	P0428

Protein	Uniprot accession	Protein Name	Number Peptides	P
tr|A0A8B6DKT5|A0A8B6DKT5_MYTGA	A0A8B6DKT5	Tubulin beta chain	4	P0429
tr|A0A8B6DKX6|A0A8B6DKX6_MYTGA	A0A8B6DKX6	3,2-trans-enoyl-CoA isomerase, mitochondrial	4	P0430
tr|A0A8B6DQ79|A0A8B6DQ79_MYTGA	A0A8B6DQ79	Uncharacterized protein	4	P0431
tr|A0A8B6DTR6|A0A8B6DTR6_MYTGA	A0A8B6DTR6	Glycogen debranching enzyme	4	P0432
tr|A0A8B6DVU0|A0A8B6DVU0_MYTGA	A0A8B6DVU0	Proteasome activator subunit 3 (PA28 gamma)	4	P0433
tr|A0A8B6DW19|A0A8B6DW19_MYTGA	A0A8B6DW19	S-(hydroxymethyl)glutathione dehydrogenase	4	P0434
tr|A0A8B6DWS7|A0A8B6DWS7_MYTGA	A0A8B6DWS7	ATP-citrate synthase	4	P0435
tr|A0A8B6DXW2|A0A8B6DXW2_MYTGA	A0A8B6DXW2	Gastric intrinsic factor	4	P0436
tr|A0A8B6DYZ2|A0A8B6DYZ2_MYTGA	A0A8B6DYZ2	Proliferating cell nuclear antigen	4	P0437
tr|A0A8B6E1B2|A0A8B6E1B2_MYTGA	A0A8B6E1B2	Probable aminopeptidase NPEPL1	4	P0438
tr|A0A8B6E1R3|A0A8B6E1R3_MYTGA	A0A8B6E1R3	Uncharacterized protein	4	P0439
tr|A0A8B6E2C3|A0A8B6E2C3_MYTGA	A0A8B6E2C3	Dynein heavy chain, axonemal	4	P0440
tr|A0A8B6E375|A0A8B6E375_MYTGA	A0A8B6E375	Alanine-glyoxylate transaminase / (R)-3-amino-2-methylprop	4	P0441
tr|A0A8B6E3P5|A0A8B6E3P5_MYTGA	A0A8B6E3P5	Metalloendopeptidase	4	P0442
tr|A0A8B6E8V1|A0A8B6E8V1_MYTGA	A0A8B6E8V1	Dihydropteridine reductase	4	P0443
tr|A0A8B6EGF0|A0A8B6EGF0_MYTGA	A0A8B6EGF0	Cilia-and flagella-associated protein 96	4	P0444
tr|A0A8B6EL21|A0A8B6EL21_MYTGA	A0A8B6EL21	Propionyl-CoA carboxylase alpha chain, mitochondrial	4	P0445
tr|A0A8B6EM74|A0A8B6EM74_MYTGA	A0A8B6EM74	Collagen, type VI, alpha	4	P0446
tr|A0A8B6EMU2|A0A8B6EMU2_MYTGA	A0A8B6EMU2	Coronin-1B/1C/6	4	P0447
tr|A0A8B6ENC1|A0A8B6ENC1_MYTGA	A0A8B6ENC1	Uncharacterized protein	4	P0448
tr|A0A8B6EPE6|A0A8B6EPE6_MYTGA	A0A8B6EPE6	Glycine cleavage system P protein	4	P0449
tr|A0A8B6EV54|A0A8B6EV54_MYTGA	A0A8B6EV54	NAD(P)H oxidase (H2O2-forming)	4	P0450
tr|A0A8B6EVT8|A0A8B6EVT8_MYTGA	A0A8B6EVT8	Arachidonate 5-lipoxygenase	4	P0451
tr|A0A8B6EYH3|A0A8B6EYH3_MYTGA	A0A8B6EYH3	Coiled-coil domain-containing protein 40	4	P0452
tr|A0A8B6F3D1|A0A8B6F3D1_MYTGA	A0A8B6F3D1	2,4-dienoyl-CoA reductase [(3E)-enoyl-CoA-producing] (Frag	4	P0453
tr|A0A8B6F3E2|A0A8B6F3E2_MYTGA	A0A8B6F3E2	CCDC81 HU domain-containing protein	4	P0454
tr|A0A8B6F3N7|A0A8B6F3N7_MYTGA	A0A8B6F3N7	Glucosamine--fructose-6-phosphate aminotransferase (Isom	4	P0455
tr|A0A8B6F4T0|A0A8B6F4T0_MYTGA	A0A8B6F4T0	Dynein light intermediate chain	4	P0456
tr|A0A8B6F4X5|A0A8B6F4X5_MYTGA	A0A8B6F4X5	V-type proton ATPase subunit C	4	P0457
tr|A0A8B6F554|A0A8B6F554_MYTGA	A0A8B6F554	Neurotransmitter-gated ion-channel ligand-binding domain	4	P0458
tr|A0A8B6F7A2|A0A8B6F7A2_MYTGA	A0A8B6F7A2	Isochorismatase-like domain-containing protein	4	P0459
tr|A0A8B6F9T9|A0A8B6F9T9_MYTGA	A0A8B6F9T9	Spectrin beta	4	P0460
tr|A0A8B6FB32|A0A8B6FB32_MYTGA	A0A8B6FB32	Proteasome subunit beta	4	P0461
tr|A0A8B6FBS7|A0A8B6FBS7_MYTGA	A0A8B6FBS7	Uncharacterized protein	4	P0462
tr|A0A8B6FFY1|A0A8B6FFY1_MYTGA	A0A8B6FFY1	Phosphodiesterase	4	P0463
tr|A0A8B6FGA8|A0A8B6FGA8_MYTGA	A0A8B6FGA8	Dynein heavy chain, axonemal	4	P0464
tr|A0A8B6FHR2|A0A8B6FHR2_MYTGA	A0A8B6FHR2	Endoplasmic reticulum protein 29	4	P0465
tr|A0A8B6FIV8|A0A8B6FIV8_MYTGA	A0A8B6FIV8	Proline iminopeptidase	4	P0466
tr|A0A8B6FJ56|A0A8B6FJ56_MYTGA	A0A8B6FJ56	Pyruvate dehydrogenase E1 component subunit beta	4	P0467
tr|A0A8B6FJH4|A0A8B6FJH4_MYTGA	A0A8B6FJH4	Nucleosome assembly protein 1-like 1	4	P0468
tr|A0A8B6FJI3|A0A8B6FJI3_MYTGA	A0A8B6FJI3	Growth factor receptor-binding protein 2	4	P0469
tr|A0A8B6FMQ5|A0A8B6FMQ5_MYTGA	A0A8B6FMQ5	Dynein regulatory complex subunit 4	4	P0470
tr|A0A8B6FN32|A0A8B6FN32_MYTGA	A0A8B6FN32	Uncharacterized protein	4	P0471
tr|A0A8B6FPZ2|A0A8B6FPZ2_MYTGA	A0A8B6FPZ2	Translocon-associated protein subunit alpha	4	P0472
tr|A0A8B6FQ26|A0A8B6FQ26_MYTGA	A0A8B6FQ26	Uncharacterized protein	4	P0473
tr|A0A8B6FRR2|A0A8B6FRR2_MYTGA	A0A8B6FRR2	Succinate--CoA ligase [ADP/GDP-forming] subunit alpha, mit	4	P0474
tr|A0A8B6FUF6|A0A8B6FUF6_MYTGA	A0A8B6FUF6	Metabotropic glutamate receptor 2/3	4	P0475
tr|A0A8B6FWP8|A0A8B6FWP8_MYTGA	A0A8B6FWP8	DNA replication licensing factor MCM3	4	P0476
tr|A0A8B6FY69|A0A8B6FY69_MYTGA	A0A8B6FY69	fructose-bisphosphatase (Fragment)	4	P0477
tr|A0A8B6FYC3|A0A8B6FYC3_MYTGA	A0A8B6FYC3	Eukaryotic translation initiation factor 3 subunit G	4	P0478
tr|A0A8B6G3W0|A0A8B6G3W0_MYTGA	A0A8B6G3W0	Uncharacterized protein	4	P0479
tr|A0A8B6G690|A0A8B6G690_MYTGA	A0A8B6G690	26S proteasome regulatory subunit T4	4	P0480
tr|A0A8B6G720|A0A8B6G720_MYTGA	A0A8B6G720	Cilia- and flagella-associated protein 20	4	P0481
tr|A0A8B6GC79|A0A8B6GC79_MYTGA	A0A8B6GC79	Cullin-5	4	P0482
tr|A0A8B6GD52|A0A8B6GD52_MYTGA	A0A8B6GD52	dolichyl-diphosphooligosaccharide--protein glycotransferas	4	P0483
tr|A0A8B6GEI5|A0A8B6GEI5_MYTGA	A0A8B6GEI5	Uncharacterized protein	4	P0484
tr|A0A8B6GFA2|A0A8B6GFA2_MYTGA	A0A8B6GFA2	ATP synthase subunit b	4	P0485
tr|A0A8B6GGC2|A0A8B6GGC2_MYTGA	A0A8B6GGC2	Large subunit ribosomal protein L5e	4	P0486
tr|A0A8B6GI66|A0A8B6GI66_MYTGA	A0A8B6GI66	AP-1 complex subunit mu	4	P0487
tr|A0A8B6GMB0|A0A8B6GMB0_MYTGA	A0A8B6GMB0	Heterogeneous nuclear ribonucleoprotein U-like protein 1	4	P0488
tr|A0A8B6GN96|A0A8B6GN96_MYTGA	A0A8B6GN96	Hypoxanthine phosphoribosyltransferase	4	P0489
tr|A0A8B6GSK5|A0A8B6GSK5_MYTGA	A0A8B6GSK5	26S proteasome regulatory subunit N2	4	P0490
tr|A0A8B6GX49|A0A8B6GX49_MYTGA	A0A8B6GX49	Ras-related protein Rab-7A	4	P0491
tr|A0A8B6GYV7|A0A8B6GYV7_MYTGA	A0A8B6GYV7	Echinoderm microtubule-associated protein-like 1/2	4	P0492
tr|A0A8B6H346|A0A8B6H346_MYTGA	A0A8B6H346	cGMP-specific 3',5'-cyclic phosphodiesterase	4	P0493
tr|A0A8B6H3D1|A0A8B6H3D1_MYTGA	A0A8B6H3D1	Nuclear cap-binding protein subunit 1 (Fragment)	4	P0494
tr|A0A8B6H3W8|A0A8B6H3W8_MYTGA	A0A8B6H3W8	Heme-binding protein 2	4	P0495
tr|A0A8B6H615|A0A8B6H615_MYTGA	A0A8B6H615	aldehyde dehydrogenase (NAD(+)) (Fragment)	4	P0496
tr|A0A8B6H6J5|A0A8B6H6J5_MYTGA	A0A8B6H6J5	Glycerol-3-phosphate dehydrogenase [NAD(+)]	4	P0497
tr|A0A8B6H8S0|A0A8B6H8S0_MYTGA	A0A8B6H8S0	Galectin domain-containing protein	4	P0498
tr|A0A8B6H9V5|A0A8B6H9V5_MYTGA	A0A8B6H9V5	Ankyrin (Fragment)	4	P0499
tr|A0A8B6HCM0|A0A8B6HCM0_MYTGA	A0A8B6HCM0	Uncharacterized protein	4	P0500
tr|A0A8B6HDX4|A0A8B6HDX4_MYTGA	A0A8B6HDX4	Guanine nucleotide-binding protein G(s) subunit alpha	4	P0501
tr|A0A8B6HFA9|A0A8B6HFA9_MYTGA	A0A8B6HFA9	Mitochondrial 2-oxoglutarate/malate carrier protein	4	P0502
tr|A0A8B6HGE1|A0A8B6HGE1_MYTGA	A0A8B6HGE1	RNA helicase	4	P0503
tr|A0A8B6HIH7|A0A8B6HIH7_MYTGA	A0A8B6HIH7	methylmalonyl-CoA mutase	4	P0504
tr|A0A8B6HIV7|A0A8B6HIV7_MYTGA	A0A8B6HIV7	Uncharacterized protein	4	P0505
tr|A0A8B6HL18|A0A8B6HL18_MYTGA	A0A8B6HL18	Stress-induced-phosphoprotein 1	4	P0506
tr|A0A8B6HRA5|A0A8B6HRA5_MYTGA	A0A8B6HRA5	Methenyltetrahydrofolate synthase domain-containing prot	4	P0507
tr|A0A8B6HTL8|A0A8B6HTL8_MYTGA	A0A8B6HTL8	Cilia- and flagella-associated protein 157	4	P0508
tr|A0A8B6HU91|A0A8B6HU91_MYTGA	A0A8B6HU91	Uncharacterized protein	4	P0509
tr|F0V448|F0V448_MYTGA	F0V448	Putative C1q domain containing protein MgC1q11	4	P0510
tr|Q6WV89|Q6WV89_MYTGA	Q6WV89	Histone H2B	4	P0511
tr|Q8MUC3|Q8MUC3_MYTGA	Q8MUC3	glutathione transferase	4	P0512
tr|A0A0K0PUP6|A0A0K0PUP6_MYTGA	A0A0K0PUP6	Shell nacre collagen-like protein 1 (Fragment)	3	P0513
tr|A0A140H125|A0A140H125_MYTGA	A0A140H125	GTP-binding nuclear protein	3	P0514
tr|A0A3L5TR65|A0A3L5TR65_MYTGA	A0A3L5TR65	Uncharacterized protein (Fragment)	3	P0515
tr|A0A3L5TTA2|A0A3L5TTA2_MYTGA	A0A3L5TTA2	Uridylate-specific endoribonuclease (Fragment)	3	P0516
tr|A0A3R5TR15|A0A3R5TR15_MYTGA	A0A3R5TR15	peptidylprolyl isomerase (Fragment)	3	P0517
tr|A0A8B6BEU5|A0A8B6BEU5_MYTGA	A0A8B6BEU5	Adenylate kinase	3	P0518
tr|A0A8B6BFN0|A0A8B6BFN0_MYTGA	A0A8B6BFN0	Septin	3	P0519
tr|A0A8B6BFZ5|A0A8B6BFZ5_MYTGA	A0A8B6BFZ5	Speriolin C-terminal domain-containing protein	3	P0520
tr|A0A8B6BGR2|A0A8B6BGR2_MYTGA	A0A8B6BGR2	Translation initiation factor 3 subunit F	3	P0521
tr|A0A8B6BIV9|A0A8B6BIV9_MYTGA	A0A8B6BIV9	SWI/SNF-related matrix-associated actin-dependent regulat	3	P0522
tr|A0A8B6BJ82|A0A8B6BJ82_MYTGA	A0A8B6BJ82	Phosphoribosylformylglycinamidine synthase	3	P0523
tr|A0A8B6BK61|A0A8B6BK61_MYTGA	A0A8B6BK61	Uncharacterized protein	3	P0524
tr|A0A8B6BL85|A0A8B6BL85_MYTGA	A0A8B6BL85	Protein disulfide-isomerase	3	P0525
tr|A0A8B6BLG4|A0A8B6BLG4_MYTGA	A0A8B6BLG4	V-type proton ATPase subunit H	3	P0526
tr|A0A8B6BM75|A0A8B6BM75_MYTGA	A0A8B6BM75	Eukaryotic translation initiation factor 6	3	P0527
tr|A0A8B6BMP2|A0A8B6BMP2_MYTGA	A0A8B6BMP2	DUF4773 domain-containing protein	3	P0528
tr|A0A8B6BMV1|A0A8B6BMV1_MYTGA	A0A8B6BMV1	Ribose-phosphate pyrophosphokinase 1	3	P0529
tr|A0A8B6BQ12|A0A8B6BQ12_MYTGA	A0A8B6BQ12	Small nuclear ribonucleoprotein B and B	3	P0530
tr|A0A8B6BQZ3|A0A8B6BQZ3_MYTGA	A0A8B6BQZ3	Uncharacterized protein	3	P0531
tr|A0A8B6BR27|A0A8B6BR27_MYTGA	A0A8B6BR27	Heat shock protein 90kDa beta	3	P0532
tr|A0A8B6BRC4|A0A8B6BRC4_MYTGA	A0A8B6BRC4	Dynein light chain roadblock	3	P0533
tr|A0A8B6BT40|A0A8B6BT40_MYTGA	A0A8B6BT40	KH domain-containing, RNA-binding, signal transduction-as	3	P0534
tr|A0A8B6BTN1|A0A8B6BTN1_MYTGA	A0A8B6BTN1	DnaJ homolog subfamily C member 2	3	P0535
tr|A0A8B6BUC5|A0A8B6BUC5_MYTGA	A0A8B6BUC5	Translation initiation factor 5A	3	P0536
tr|A0A8B6BUY9|A0A8B6BUY9_MYTGA	A0A8B6BUY9	thioredoxin-disulfide reductase	3	P0537
tr|A0A8B6BW48|A0A8B6BW48_MYTGA	A0A8B6BW48	Mitochondria-eating protein C-terminal domain-containing	3	P0538
tr|A0A8B6BY54|A0A8B6BY54_MYTGA	A0A8B6BY54	Mitogen-activated protein kinase	3	P0539
tr|A0A8B6C153|A0A8B6C153_MYTGA	A0A8B6C153	Citrate synthase	3	P0540
tr|A0A8B6C1U1|A0A8B6C1U1_MYTGA	A0A8B6C1U1	Transforming growth factor-beta-induced protein	3	P0541
tr|A0A8B6C553|A0A8B6C553_MYTGA	A0A8B6C553	Protocadherin Fat 4	3	P0542
tr|A0A8B6C5C7|A0A8B6C5C7_MYTGA	A0A8B6C5C7	Large ribosomal subunit protein uL2	3	P0543
tr|A0A8B6C5U0|A0A8B6C5U0_MYTGA	A0A8B6C5U0	Uncharacterized protein	3	P0544
tr|A0A8B6C5W8|A0A8B6C5W8_MYTGA	A0A8B6C5W8	Ubiquitin carboxyl-terminal hydrolase	3	P0545

Protein	Uniprot accession	Protein Name	Number Peptides	P
tr|A0A8B6C603|A0A8B6C603_MYTGA	A0A8B6C603	Major vault protein	3	P0546
tr|A0A8B6C6U9|A0A8B6C6U9_MYTGA	A0A8B6C6U9	ELAV like protein 2/3/4	3	P0547
tr|A0A8B6C8D6|A0A8B6C8D6_MYTGA	A0A8B6C8D6	Heterogeneous nuclear ribonucleoprotein K	3	P0548
tr|A0A8B6CB06|A0A8B6CB06_MYTGA	A0A8B6CB06	Caspase 7	3	P0549
tr|A0A8B6CBF6|A0A8B6CBF6_MYTGA	A0A8B6CBF6	Sperm-associated antigen 16 protein	3	P0550
tr|A0A8B6CCQ9|A0A8B6CCQ9_MYTGA	A0A8B6CCQ9	Uncharacterized protein	3	P0551
tr|A0A8B6CDB6|A0A8B6CDB6_MYTGA	A0A8B6CDB6	NADPH2:quinone reductase	3	P0552
tr|A0A8B6CDI4|A0A8B6CDI4_MYTGA	A0A8B6CDI4	Poly [ADP-ribose] polymerase	3	P0553
tr|A0A8B6CEA7|A0A8B6CEA7_MYTGA	A0A8B6CEA7	ADF-H domain-containing protein	3	P0554
tr|A0A8B6CEW5|A0A8B6CEW5_MYTGA	A0A8B6CEW5	Large ribosomal subunit protein uL11	3	P0555
tr|A0A8B6CF87|A0A8B6CF87_MYTGA	A0A8B6CF87	Leucine-rich repeat-containing protein 40	3	P0556
tr|A0A8B6CHE6|A0A8B6CHE6_MYTGA	A0A8B6CHE6	Profilin	3	P0557
tr|A0A8B6CJ20|A0A8B6CJ20_MYTGA	A0A8B6CJ20	Dynein heavy chain, axonemal	3	P0558
tr|A0A8B6CJ29|A0A8B6CJ29_MYTGA	A0A8B6CJ29	kynurenine--oxoglutarate transaminase	3	P0559
tr|A0A8B6CJW3|A0A8B6CJW3_MYTGA	A0A8B6CJW3	Leucine-rich PPR motif-containing protein, mitochondrial	3	P0560
tr|A0A8B6CMT7|A0A8B6CMT7_MYTGA	A0A8B6CMT7	Collagen, type IV, alpha	3	P0561
tr|A0A8B6CNH5|A0A8B6CNH5_MYTGA	A0A8B6CNH5	Acyl-CoA dehydrogenase/oxidase N-terminal domain-contai	3	P0562
tr|A0A8B6CNQ4|A0A8B6CNQ4_MYTGA	A0A8B6CNQ4	sulfite oxidase	3	P0563
tr|A0A8B6CSF4|A0A8B6CSF4_MYTGA	A0A8B6CSF4	VWFA domain-containing protein	3	P0564
tr|A0A8B6CU81|A0A8B6CU81_MYTGA	A0A8B6CU81	Uncharacterized protein	3	P0565
tr|A0A8B6CXE3|A0A8B6CXE3_MYTGA	A0A8B6CXE3	Eukaryotic translation initiation factor 3 subunit H	3	P0566
tr|A0A8B6CXF7|A0A8B6CXF7_MYTGA	A0A8B6CXF7	Uncharacterized protein	3	P0567
tr|A0A8B6CYQ8|A0A8B6CYQ8_MYTGA	A0A8B6CYQ8	Glucosamine-6-phosphate isomerase	3	P0568
tr|A0A8B6CYY6|A0A8B6CYY6_MYTGA	A0A8B6CYY6	ODAD1 central coiled coil region domain-containing protein	3	P0569
tr|A0A8B6CZ28|A0A8B6CZ28_MYTGA	A0A8B6CZ28	Sulfotransferase domain-containing protein	3	P0570
tr|A0A8B6CZV8|A0A8B6CZV8_MYTGA	A0A8B6CZV8	Peptidase S9 prolyl oligopeptidase catalytic domain-contain	3	P0571
tr|A0A8B6D2D7|A0A8B6D2D7_MYTGA	A0A8B6D2D7	Carboxylic ester hydrolase	3	P0572
tr|A0A8B6D2R9|A0A8B6D2R9_MYTGA	A0A8B6D2R9	COP9 signalosome complex subunit 7	3	P0573
tr|A0A8B6D2T4|A0A8B6D2T4_MYTGA	A0A8B6D2T4	ADP-ribosylation factor	3	P0574
tr|A0A8B6D484|A0A8B6D484_MYTGA	A0A8B6D484	Dihydrolipoamide acetyltransferase component of pyruvate	3	P0575
tr|A0A8B6D5E9|A0A8B6D5E9_MYTGA	A0A8B6D5E9	lysozyme	3	P0576
tr|A0A8B6D7T2|A0A8B6D7T2_MYTGA	A0A8B6D7T2	Small ribosomal subunit protein uS15	3	P0577
tr|A0A8B6D901|A0A8B6D901_MYTGA	A0A8B6D901	Enolase-phosphatase E1	3	P0578
tr|A0A8B6D982|A0A8B6D982_MYTGA	A0A8B6D982	Uncharacterized protein	3	P0579
tr|A0A8B6D9E3|A0A8B6D9E3_MYTGA	A0A8B6D9E3	Programmed cell death 6-interacting protein	3	P0580
tr|A0A8B6DAY6|A0A8B6DAY6_MYTGA	A0A8B6DAY6	Nuclear pore complex protein Nup155	3	P0581
tr|A0A8B6DB68|A0A8B6DB68_MYTGA	A0A8B6DB68	AP-1 complex subunit beta-1 (Fragment)	3	P0582
tr|A0A8B6DCL3|A0A8B6DCL3_MYTGA	A0A8B6DCL3	Structural maintenance of chromosomes protein	3	P0583
tr|A0A8B6DCU4|A0A8B6DCU4_MYTGA	A0A8B6DCU4	Dolichyl-diphosphooligosaccharide--protein glycosyltransfe	3	P0584
tr|A0A8B6DCX7|A0A8B6DCX7_MYTGA	A0A8B6DCX7	Uncharacterized protein	3	P0585
tr|A0A8B6DES8|A0A8B6DES8_MYTGA	A0A8B6DES8	Uncharacterized protein	3	P0586
tr|A0A8B6DFH3|A0A8B6DFH3_MYTGA	A0A8B6DFH3	Large ribosomal subunit protein eL34	3	P0587
tr|A0A8B6DGB3|A0A8B6DGB3_MYTGA	A0A8B6DGB3	Eukaryotic translation initiation factor 5	3	P0588
tr|A0A8B6DHY5|A0A8B6DHY5_MYTGA	A0A8B6DHY5	ER-derived vesicles protein	3	P0589
tr|A0A8B6DI04|A0A8B6DI04_MYTGA	A0A8B6DI04	Suppressor of tumorigenicity protein 13	3	P0590
tr|A0A8B6DIA6|A0A8B6DIA6_MYTGA	A0A8B6DIA6	Histone H2A	3	P0591
tr|A0A8B6DJC1|A0A8B6DJC1_MYTGA	A0A8B6DJC1	Dynein regulatory complex subunit 3	3	P0592
tr|A0A8B6DJN5|A0A8B6DJN5_MYTGA	A0A8B6DJN5	WSC domain-containing protein	3	P0593
tr|A0A8B6DK71|A0A8B6DK71_MYTGA	A0A8B6DK71	Neurexin	3	P0594
tr|A0A8B6DLY5|A0A8B6DLY5_MYTGA	A0A8B6DLY5	Ubiquitin carboxyl-terminal hydrolase	3	P0595
tr|A0A8B6DM16|A0A8B6DM16_MYTGA	A0A8B6DM16	60S ribosomal protein L21	3	P0596
tr|A0A8B6DMR6|A0A8B6DMR6_MYTGA	A0A8B6DMR6	Vitellogenic carboxypeptidase-like protein	3	P0597
tr|A0A8B6DNE4|A0A8B6DNE4_MYTGA	A0A8B6DNE4	Enoyl-CoA hydratase, mitochondrial	3	P0598
tr|A0A8B6DQQ9|A0A8B6DQQ9_MYTGA	A0A8B6DQQ9	Uncharacterized protein	3	P0599
tr|A0A8B6DS00|A0A8B6DS00_MYTGA	A0A8B6DS00	Integrin beta	3	P0600
tr|A0A8B6DTD9|A0A8B6DTD9_MYTGA	A0A8B6DTD9	non-specific serine/threonine protein kinase	3	P0601
tr|A0A8B6DU64|A0A8B6DU64_MYTGA	A0A8B6DU64	IMP dehydrogenase	3	P0602
tr|A0A8B6DUG1|A0A8B6DUG1_MYTGA	A0A8B6DUG1	Cytosol aminopeptidase	3	P0603
tr|A0A8B6DVQ8|A0A8B6DVQ8_MYTGA	A0A8B6DVQ8	Exportin-7 (Fragment)	3	P0604
tr|A0A8B6DVZ6|A0A8B6DVZ6_MYTGA	A0A8B6DVZ6	MICOS complex subunit	3	P0605
tr|A0A8B6DZJ3|A0A8B6DZJ3_MYTGA	A0A8B6DZJ3	Phenylalanyl-tRNA synthetase beta chain	3	P0606
tr|A0A8B6E4M9|A0A8B6E4M9_MYTGA	A0A8B6E4M9	mRNA export factor	3	P0607
tr|A0A8B6E5K7|A0A8B6E5K7_MYTGA	A0A8B6E5K7	Peptidyl-prolyl cis-trans isomerase-like 6	3	P0608
tr|A0A8B6E7X0|A0A8B6E7X0_MYTGA	A0A8B6E7X0	Phosphoribosylaminoimidazolecarboxamide formyltransfer	3	P0609
tr|A0A8B6E7Z6|A0A8B6E7Z6_MYTGA	A0A8B6E7Z6	Type I protein arginine methyltransferase	3	P0610
tr|A0A8B6E847|A0A8B6E847_MYTGA	A0A8B6E847	Dynein heavy chain tail domain-containing protein	3	P0611
tr|A0A8B6E957|A0A8B6E957_MYTGA	A0A8B6E957	Phospholipid scramblase	3	P0612
tr|A0A8B6E9J1|A0A8B6E9J1_MYTGA	A0A8B6E9J1	Transgelin	3	P0613
tr|A0A8B6EBJ6|A0A8B6EBJ6_MYTGA	A0A8B6EBJ6	peptidylprolyl isomerase	3	P0614
tr|A0A8B6ECQ3|A0A8B6ECQ3_MYTGA	A0A8B6ECQ3	Pre-mRNA-processing factor 8	3	P0615
tr|A0A8B6ED05|A0A8B6ED05_MYTGA	A0A8B6ED05	Structural maintenance of chromosome 4	3	P0616
tr|A0A8B6ED11|A0A8B6ED11_MYTGA	A0A8B6ED11	S-formylglutathione hydrolase	3	P0617
tr|A0A8B6EDN1|A0A8B6EDN1_MYTGA	A0A8B6EDN1	Heat shock 70kDa protein 1/8	3	P0618
tr|A0A8B6EE00|A0A8B6EE00_MYTGA	A0A8B6EE00	Opine dehydrogenase domain-containing protein	3	P0619
tr|A0A8B6EE15|A0A8B6EE15_MYTGA	A0A8B6EE15	Formyltetrahydrofolate dehydrogenase	3	P0620
tr|A0A8B6EIF1|A0A8B6EIF1_MYTGA	A0A8B6EIF1	Carnitine O-palmitoyltransferase 2	3	P0621
tr|A0A8B6EIQ6|A0A8B6EIQ6_MYTGA	A0A8B6EIQ6	Protein sleepless	3	P0622
tr|A0A8B6EJH7|A0A8B6EJH7_MYTGA	A0A8B6EJH7	S-methyl-5'-thioadenosine phosphorylase	3	P0623
tr|A0A8B6EJT7|A0A8B6EJT7_MYTGA	A0A8B6EJT7	3-hydroxyisobutyrate dehydrogenase	3	P0624
tr|A0A8B6ELU9|A0A8B6ELU9_MYTGA	A0A8B6ELU9	Cytoplasmic polyadenylation element-binding protein	3	P0625
tr|A0A8B6ELY9|A0A8B6ELY9_MYTGA	A0A8B6ELY9	EF-hand domain-containing protein	3	P0626
tr|A0A8B6ENU1|A0A8B6ENU1_MYTGA	A0A8B6ENU1	rRNA 2'-O-methyltransferase fibrillarin	3	P0627
tr|A0A8B6EPU1|A0A8B6EPU1_MYTGA	A0A8B6EPU1	Delta(3,5)-Delta(2,4)-dienoyl-CoA isomerase	3	P0628
tr|A0A8B6EQ50|A0A8B6EQ50_MYTGA	A0A8B6EQ50	EF-hand domain-containing protein	3	P0629
tr|A0A8B6EQ84|A0A8B6EQ84_MYTGA	A0A8B6EQ84	glucose-6-phosphate 1-epimerase	3	P0630
tr|A0A8B6ERM7|A0A8B6ERM7_MYTGA	A0A8B6ERM7	Guanine nucleotide-binding protein G(I)/G(S)/G(T) subunit b	3	P0631
tr|A0A8B6ERS1|A0A8B6ERS1_MYTGA	A0A8B6ERS1	Actin beta/gamma 1	3	P0632
tr|A0A8B6ET55|A0A8B6ET55_MYTGA	A0A8B6ET55	Prenylcysteine oxidase / farnesylcysteine lyase	3	P0633
tr|A0A8B6EUH6|A0A8B6EUH6_MYTGA	A0A8B6EUH6	Leucine zipper transcription factor-like protein 1	3	P0634
tr|A0A8B6EY33|A0A8B6EY33_MYTGA	A0A8B6EY33	Actin beta/gamma 1	3	P0635
tr|A0A8B6EZ91|A0A8B6EZ91_MYTGA	A0A8B6EZ91	Eukaryotic translation initiation factor 2A	3	P0636
tr|A0A8B6EZB4|A0A8B6EZB4_MYTGA	A0A8B6EZB4	Importin subunit alpha	3	P0637
tr|A0A8B6EZJ9|A0A8B6EZJ9_MYTGA	A0A8B6EZJ9	Cytochrome b-c1 complex subunit 8	3	P0638
tr|A0A8B6F0P1|A0A8B6F0P1_MYTGA	A0A8B6F0P1	TNF family profile domain-containing protein	3	P0639
tr|A0A8B6F131|A0A8B6F131_MYTGA	A0A8B6F131	Arsenite methyltransferase	3	P0640
tr|A0A8B6F225|A0A8B6F225_MYTGA	A0A8B6F225	Glutamine synthetase	3	P0641
tr|A0A8B6F4D6|A0A8B6F4D6_MYTGA	A0A8B6F4D6	Myosin heavy chain	3	P0642
tr|A0A8B6F571|A0A8B6F571_MYTGA	A0A8B6F571	Small subunit ribosomal protein S10e	3	P0643
tr|A0A8B6F648|A0A8B6F648_MYTGA	A0A8B6F648	Small nuclear ribonucleoprotein Sm D2	3	P0644
tr|A0A8B6F652|A0A8B6F652_MYTGA	A0A8B6F652	Ribose-phosphate pyrophosphokinase	3	P0645
tr|A0A8B6F6I0|A0A8B6F6I0_MYTGA	A0A8B6F6I0	Complex I-49kD	3	P0646
tr|A0A8B6F9D5|A0A8B6F9D5_MYTGA	A0A8B6F9D5	Uncharacterized protein	3	P0647
tr|A0A8B6F9E9|A0A8B6F9E9_MYTGA	A0A8B6F9E9	Tropomyosin	3	P0648
tr|A0A8B6FA19|A0A8B6FA19_MYTGA	A0A8B6FA19	Double-stranded RNA-binding protein Staufen	3	P0649
tr|A0A8B6FAI5|A0A8B6FAI5_MYTGA	A0A8B6FAI5	Small nuclear ribonucleoprotein Sm D1	3	P0650
tr|A0A8B6FAS4|A0A8B6FAS4_MYTGA	A0A8B6FAS4	Eukaryotic translation initiation factor 3 subunit M	3	P0651
tr|A0A8B6FBV0|A0A8B6FBV0_MYTGA	A0A8B6FBV0	Xaa-Pro aminopeptidase (Fragment)	3	P0652
tr|A0A8B6FC70|A0A8B6FC70_MYTGA	A0A8B6FC70	Short-chain collagen C4-like	3	P0653
tr|A0A8B6FCA2|A0A8B6FCA2_MYTGA	A0A8B6FCA2	Alpha-mannosidase	3	P0654
tr|A0A8B6FI99|A0A8B6FI99_MYTGA	A0A8B6FI99	Proteasome subunit alpha type	3	P0655
tr|A0A8B6FIE8|A0A8B6FIE8_MYTGA	A0A8B6FIE8	RNA-binding protein 4	3	P0656
tr|A0A8B6FK09|A0A8B6FK09_MYTGA	A0A8B6FK09	thioredoxin-dependent peroxiredoxin	3	P0657
tr|A0A8B6FKZ2|A0A8B6FKZ2_MYTGA	A0A8B6FKZ2	asparagine--tRNA ligase	3	P0658
tr|A0A8B6FND0|A0A8B6FND0_MYTGA	A0A8B6FND0	Extended synaptotagmin-2	3	P0659
tr|A0A8B6FNL2|A0A8B6FNL2_MYTGA	A0A8B6FNL2	Carbonic anhydrase	3	P0660
tr|A0A8B6FPD4|A0A8B6FPD4_MYTGA	A0A8B6FPD4	Cytoskeleton-associated protein 5	3	P0661
tr|A0A8B6FQY4|A0A8B6FQY4_MYTGA	A0A8B6FQY4	Meiosis-specific nuclear structural protein 1	3	P0662

Protein	Uniprot accession	Protein Name	Number Peptides	P
tr|A0A8B6FRG0|A0A8B6FRG0_MYTGA	A0A8B6FRG0	E3 ubiquitin-protein ligase UBR4	3	P0663
tr|A0A8B6FT00|A0A8B6FT00_MYTGA	A0A8B6FT00	DnaJ homolog subfamily B member 5	3	P0664
tr|A0A8B6FU04|A0A8B6FU04_MYTGA	A0A8B6FU04	Dynein heavy chain, axonemal	3	P0665
tr|A0A8B6FUJ8|A0A8B6FUJ8_MYTGA	A0A8B6FUJ8	Uncharacterized protein	3	P0666
tr|A0A8B6FV92|A0A8B6FV92_MYTGA	A0A8B6FV92	Ubiquinol-cytochrome c reductase cytochrome c1 subunit	3	P0667
tr|A0A8B6FVC2|A0A8B6FVC2_MYTGA	A0A8B6FVC2	4a-hydroxytetrahydrobiopterin dehydratase	3	P0668
tr|A0A8B6FVT1|A0A8B6FVT1_MYTGA	A0A8B6FVT1	26S proteasome non-ATPase regulatory subunit 4 (Fragment	3	P0669
tr|A0A8B6FVU5|A0A8B6FVU5_MYTGA	A0A8B6FVU5	NADH dehydrogenase (Ubiquinone) 1 alpha subcomplex sub	3	P0670
tr|A0A8B6FXI7|A0A8B6FXI7_MYTGA	A0A8B6FXI7	Centractin	3	P0671
tr|A0A8B6FXY7|A0A8B6FXY7_MYTGA	A0A8B6FXY7	4-hydroxy-2-oxoglutarate aldolase, mitochondrial	3	P0672
tr|A0A8B6FZ84|A0A8B6FZ84_MYTGA	A0A8B6FZ84	Myosin light chain 6	3	P0673
tr|A0A8B6FZC7|A0A8B6FZC7_MYTGA	A0A8B6FZC7	Nuclear pore protein	3	P0674
tr|A0A8B6FZD9|A0A8B6FZD9_MYTGA	A0A8B6FZD9	Large subunit ribosomal protein L18e	3	P0675
tr|A0A8B6FZP1|A0A8B6FZP1_MYTGA	A0A8B6FZP1	Glutathione S-transferase	3	P0676
tr|A0A8B6GO24|A0A8B6GO24_MYTGA	A0A8B6GO24	Nucleoside phosphorylase domain-containing protein (Frag	3	P0677
tr|A0A8B6G0N3|A0A8B6G0N3_MYTGA	A0A8B6G0N3	Small ribosomal subunit protein uS13	3	P0678
tr|A0A8B6G0P4|A0A8B6G0P4_MYTGA	A0A8B6G0P4	Pumilio RNA-binding family	3	P0679
tr|A0A8B6G4A3|A0A8B6G4A3_MYTGA	A0A8B6G4A3	Pyruvate carboxylase	3	P0680
tr|A0A8B6G566|A0A8B6G566_MYTGA	A0A8B6G566	peptidylprolyl isomerase	3	P0681
tr|A0A8B6G855|A0A8B6G855_MYTGA	A0A8B6G855	DNA damage-binding protein 1	3	P0682
tr|A0A8B6GA85|A0A8B6GA85_MYTGA	A0A8B6GA85	UspA domain-containing protein	3	P0683
tr|A0A8B6GDF2|A0A8B6GDF2_MYTGA	A0A8B6GDF2	Ferritin	3	P0684
tr|A0A8B6GDR9|A0A8B6GDR9_MYTGA	A0A8B6GDR9	Syntaxin-binding protein 1	3	P0685
tr|A0A8B6GEX6|A0A8B6GEX6_MYTGA	A0A8B6GEX6	CSMD	3	P0686
tr|A0A8B6GFA5|A0A8B6GFA5_MYTGA	A0A8B6GFA5	NADAR domain-containing protein	3	P0687
tr|A0A8B6GGD0|A0A8B6GGD0_MYTGA	A0A8B6GGD0	Band 7 domain-containing protein	3	P0688
tr|A0A8B6GHR9|A0A8B6GHR9_MYTGA	A0A8B6GHR9	Guanine nucleotide-binding protein subunit alpha	3	P0689
tr|A0A8B6GHS8|A0A8B6GHS8_MYTGA	A0A8B6GHS8	Maestro heat-like repeat-containing protein family member	3	P0690
tr|A0A8B6GIM7|A0A8B6GIM7_MYTGA	A0A8B6GIM7	NADP-dependent oxidoreductase domain-containing protei	3	P0691
tr|A0A8B6GIW2|A0A8B6GIW2_MYTGA	A0A8B6GIW2	Ribosomal protein L15	3	P0692
tr|A0A8B6GJA5|A0A8B6GJA5_MYTGA	A0A8B6GJA5	Solute carrier family 25 (Mitochondrial phosphate transport	3	P0693
tr|A0A8B6GJD2|A0A8B6GJD2_MYTGA	A0A8B6GJD2	ZP domain-containing protein	3	P0694
tr|A0A8B6GK88|A0A8B6GK88_MYTGA	A0A8B6GK88	Prostaglandin reductase 1	3	P0695
tr|A0A8B6GKK6|A0A8B6GKK6_MYTGA	A0A8B6GKK6	Peroxiredoxin-5	3	P0696
tr|A0A8B6GPZ6|A0A8B6GPZ6_MYTGA	A0A8B6GPZ6	Eukaryotic peptide chain release factor GTP-binding subunit	3	P0697
tr|A0A8B6GQC1|A0A8B6GQC1_MYTGA	A0A8B6GQC1	Uncharacterized protein (Fragment)	3	P0698
tr|A0A8B6GTS1|A0A8B6GTS1_MYTGA	A0A8B6GTS1	Aldehyde dehydrogenase (NAD+)	3	P0699
tr|A0A8B6GTY8|A0A8B6GTY8_MYTGA	A0A8B6GTY8	Trans-1,2-dihydrobenzene-1,2-diol dehydrogenase	3	P0700
tr|A0A8B6GUZ7|A0A8B6GUZ7_MYTGA	A0A8B6GUZ7	Uncharacterized protein	3	P0701
tr|A0A8B6GV25|A0A8B6GV25_MYTGA	A0A8B6GV25	LIM zinc-binding domain-containing protein	3	P0702
tr|A0A8B6GV38|A0A8B6GV38_MYTGA	A0A8B6GV38	Ankyrin repeat and SOCS box protein 17	3	P0703
tr|A0A8B6GVE1|A0A8B6GVE1_MYTGA	A0A8B6GVE1	CD80-like immunoglobulin C2-set domain-containing prote	3	P0704
tr|A0A8B6GXZ3|A0A8B6GXZ3_MYTGA	A0A8B6GXZ3	Nuclear migration protein nudC	3	P0705
tr|A0A8B6H044|A0A8B6H044_MYTGA	A0A8B6H044	Dolichyl-diphosphooligosaccharide--protein glycosyltransfe	3	P0706
tr|A0A8B6H111|A0A8B6H111_MYTGA	A0A8B6H111	Endonuclease domain-containing 1 protein-like	3	P0707
tr|A0A8B6H1F3|A0A8B6H1F3_MYTGA	A0A8B6H1F3	mannose-1-phosphate guanylyltransferase	3	P0708
tr|A0A8B6H228|A0A8B6H228_MYTGA	A0A8B6H228	Endoplasmic reticulum resident protein 44	3	P0709
tr|A0A8B6H369|A0A8B6H369_MYTGA	A0A8B6H369	NCK-associated protein 1	3	P0710
tr|A0A8B6H3D0|A0A8B6H3D0_MYTGA	A0A8B6H3D0	Vesicle-associated membrane protein-associated protein A	3	P0711
tr|A0A8B6H459|A0A8B6H459_MYTGA	A0A8B6H459	Serine/threonine-protein phosphatase 6 regulatory subunit	3	P0712
tr|A0A8B6H4W1|A0A8B6H4W1_MYTGA	A0A8B6H4W1	Signal recognition particle subunit SRP68	3	P0713
tr|A0A8B6H4Z9|A0A8B6H4Z9_MYTGA	A0A8B6H4Z9	Uncharacterized protein	3	P0714
tr|A0A8B6H5B1|A0A8B6H5B1_MYTGA	A0A8B6H5B1	Carboxymethylenebutenolidase	3	P0715
tr|A0A8B6H6E9|A0A8B6H6E9_MYTGA	A0A8B6H6E9	Very low-density lipoprotein receptor	3	P0716
tr|A0A8B6H6V5|A0A8B6H6V5_MYTGA	A0A8B6H6V5	UspA domain-containing protein	3	P0717
tr|A0A8B6H753|A0A8B6H753_MYTGA	A0A8B6H753	Dynein axonemal heavy chain	3	P0718
tr|A0A8B6H785|A0A8B6H785_MYTGA	A0A8B6H785	Elongation factor 1-beta	3	P0719
tr|A0A8B6H7L7|A0A8B6H7L7_MYTGA	A0A8B6H7L7	Adenylate kinase 8	3	P0720
tr|A0A8B6H820|A0A8B6H820_MYTGA	A0A8B6H820	COP9 signalosome complex subunit 5	3	P0721
tr|A0A8B6H870|A0A8B6H870_MYTGA	A0A8B6H870	Myosin regulatory light chain 12	3	P0722
tr|A0A8B6H9E3|A0A8B6H9E3_MYTGA	A0A8B6H9E3	Dihydropyrimidinase	3	P0723
tr|A0A8B6HBC0|A0A8B6HBC0_MYTGA	A0A8B6HBC0	60S ribosomal protein L32	3	P0724
tr|A0A8B6HBF9|A0A8B6HBF9_MYTGA	A0A8B6HBF9	Dynein heavy chain, axonemal (Fragment)	3	P0725
tr|A0A8B6HCN8|A0A8B6HCN8_MYTGA	A0A8B6HCN8	Uncharacterized protein	3	P0726
tr|A0A8B6HD04|A0A8B6HD04_MYTGA	A0A8B6HD04	Dipeptidyl peptidase 1	3	P0727
tr|A0A8B6HDR2|A0A8B6HDR2_MYTGA	A0A8B6HDR2	inorganic diphosphatase	3	P0728
tr|A0A8B6HE85|A0A8B6HE85_MYTGA	A0A8B6HE85	Ankyrin repeat domain-containing protein 45	3	P0729
tr|A0A8B6HF22|A0A8B6HF22_MYTGA	A0A8B6HF22	BEACH-type PH domain-containing protein	3	P0730
tr|A0A8B6HF84|A0A8B6HF84_MYTGA	A0A8B6HF84	NADH dehydrogenase [ubiquinone] 1 alpha subcomplex sub	3	P0731
tr|A0A8B6HGT0|A0A8B6HGT0_MYTGA	A0A8B6HGT0	Serine/threonine-protein phosphatase	3	P0732
tr|A0A8B6HIA3|A0A8B6HIA3_MYTGA	A0A8B6HIA3	Solute carrier family 3 (Neutral and basic amino acid transpo	3	P0733
tr|A0A8B6HJY6|A0A8B6HJY6_MYTGA	A0A8B6HJY6	Integrin alpha 9	3	P0734
tr|A0A8B6HL60|A0A8B6HL60_MYTGA	A0A8B6HL60	Splicing factor, arginine/serine-rich 1/9	3	P0735
tr|A0A8B6HLV0|A0A8B6HLV0_MYTGA	A0A8B6HLV0	Golgi apparatus protein 1	3	P0736
tr|A0A8B6HN01|A0A8B6HN01_MYTGA	A0A8B6HN01	Leucine-rich repeat-containing protein 71	3	P0737
tr|A0A8B6HP01|A0A8B6HP01_MYTGA	A0A8B6HP01	phosphoenolpyruvate mutase	3	P0738
tr|A0A8B6HQ55|A0A8B6HQ55_MYTGA	A0A8B6HQ55	Methyltransferase domain-containing protein	3	P0739
tr|A0A8B6HRC5|A0A8B6HRC5_MYTGA	A0A8B6HRC5	5'-3' exoribonuclease	3	P0740
tr|A0A8B6HUT0|A0A8B6HUT0_MYTGA	A0A8B6HUT0	Engulfment and cell motility protein 1	3	P0741
tr|H6T4K6|H6T4K6_MYTGA	H6T4K6	Histone H2A	3	P0742
tr|A0A0N9FGL8|A0A0N9FGL8_MYTGA	A0A0N9FGL8	Carbonic anhydrase	2	P0743
tr|A0A126Q9B5|A0A126Q9B5_MYTGA	A0A126Q9B5	PAN2	2	P0744
tr|A0A140D2R8|A0A140D2R8_MYTGA	A0A140D2R8	CNOT1	2	P0745
tr|A0A3L5TQI8|A0A3L5TQI8_MYTGA	A0A3L5TQI8	Nedd8-activating x1 enzyme e1 regulatory subunit isoform (	2	P0746
tr|A0A3L5TRU1|A0A3L5TRU1_MYTGA	A0A3L5TRU1	Isoform a (Fragment)	2	P0747
tr|A0A3R5Q1J9|A0A3R5Q1J9_MYTGA	A0A3R5Q1J9	EF-hand domain-containing protein (Fragment)	2	P0748
tr|A0A8B6BF20|A0A8B6BF20_MYTGA	A0A8B6BF20	Glutathione S-transferase	2	P0749
tr|A0A8B6BFF4|A0A8B6BFF4_MYTGA	A0A8B6BFF4	Aspartate beta-hydroxylase	2	P0750
tr|A0A8B6BFG4|A0A8B6BFG4_MYTGA	A0A8B6BFG4	S-adenosylmethionine synthase	2	P0751
tr|A0A8B6BFS9|A0A8B6BFS9_MYTGA	A0A8B6BFS9	Alpha-soluble NSF attachment protein (Fragment)	2	P0752
tr|A0A8B6BG46|A0A8B6BG46_MYTGA	A0A8B6BG46	cathepsin X	2	P0753
tr|A0A8B6BGE7|A0A8B6BGE7_MYTGA	A0A8B6BGE7	26S proteasome regulatory subunit N5	2	P0754
tr|A0A8B6BH66|A0A8B6BH66_MYTGA	A0A8B6BH66	Alpha-aminoadipic semialdehyde synthase	2	P0755
tr|A0A8B6BHU6|A0A8B6BHU6_MYTGA	A0A8B6BHU6	EF-hand domain-containing protein	2	P0756
tr|A0A8B6BIK2|A0A8B6BIK2_MYTGA	A0A8B6BIK2	VWFA domain-containing protein (Fragment)	2	P0757
tr|A0A8B6BJ32|A0A8B6BJ32_MYTGA	A0A8B6BJ32	Catalase	2	P0758
tr|A0A8B6BJ56|A0A8B6BJ56_MYTGA	A0A8B6BJ56	Isocitrate dehydrogenase [NAD] subunit, mitochondrial	2	P0759
tr|A0A8B6BJA4|A0A8B6BJA4_MYTGA	A0A8B6BJA4	Uncharacterized protein	2	P0760
tr|A0A8B6BL01|A0A8B6BL01_MYTGA	A0A8B6BL01	Katanin p80 WD40 repeat-containing subunit B1	2	P0761
tr|A0A8B6BLR4|A0A8B6BLR4_MYTGA	A0A8B6BLR4	ATP-binding cassette, sub-family E, member 1	2	P0762
tr|A0A8B6BNK2|A0A8B6BNK2_MYTGA	A0A8B6BNK2	E2 ubiquitin-conjugating enzyme	2	P0763
tr|A0A8B6BPE2|A0A8B6BPE2_MYTGA	A0A8B6BPE2	Nicalin	2	P0764
tr|A0A8B6BQ10|A0A8B6BQ10_MYTGA	A0A8B6BQ10	Cortactin	2	P0765
tr|A0A8B6BQJ9|A0A8B6BQJ9_MYTGA	A0A8B6BQJ9	Uncharacterized protein	2	P0766
tr|A0A8B6BR73|A0A8B6BR73_MYTGA	A0A8B6BR73	NTR domain-containing protein	2	P0767
tr|A0A8B6BRE1|A0A8B6BRE1_MYTGA	A0A8B6BRE1	Isovaleryl-CoA dehydrogenase, mitochondrial	2	P0768
tr|A0A8B6BRR1|A0A8B6BRR1_MYTGA	A0A8B6BRR1	PDZ GRASP-type domain-containing protein	2	P0769
tr|A0A8B6BRR3|A0A8B6BRR3_MYTGA	A0A8B6BRR3	C1q domain-containing protein	2	P0770
tr|A0A8B6BSU6|A0A8B6BSU6_MYTGA	A0A8B6BSU6	Solute carrier family 25 (Mitochondrial dicarboxylate transp	2	P0771
tr|A0A8B6BTM5|A0A8B6BTM5_MYTGA	A0A8B6BTM5	Dynein assembly factor 5, axonemal	2	P0772
tr|A0A8B6BTV6|A0A8B6BTV6_MYTGA	A0A8B6BTV6	DnaJ homolog subfamily A member 1	2	P0773
tr|A0A8B6BU03|A0A8B6BU03_MYTGA	A0A8B6BU03	AMP-binding enzyme C-terminal domain-containing protein	2	P0774
tr|A0A8B6BU30|A0A8B6BU30_MYTGA	A0A8B6BU30	Phospholipid scramblase	2	P0775
tr|A0A8B6BU86|A0A8B6BU86_MYTGA	A0A8B6BU86	Dipeptidyl-peptidase III	2	P0776
tr|A0A8B6BVT6|A0A8B6BVT6_MYTGA	A0A8B6BVT6	Superoxide dismutase	2	P0777
tr|A0A8B6BVX9|A0A8B6BVX9_MYTGA	A0A8B6BVX9	Pyruvate dehydrogenase E1 component subunit alpha	2	P0778
tr|A0A8B6BWY3|A0A8B6BWY3_MYTGA	A0A8B6BWY3	Cystatin-A/B	2	P0779

Protein	Uniprot accession	Protein Name	Number Peptides	P
tr|A0A8B6BX65|A0A8B6BX65_MYTGA	A0A8B6BX65	High mobility group protein B1	2	P0780
tr|A0A8B6BXY5|A0A8B6BXY5_MYTGA	A0A8B6BXY5	Anaphase-promoting complex subunit 4-like WD40 domain	2	P0781
tr|A0A8B6BYA3|A0A8B6BYA3_MYTGA	A0A8B6BYA3	Protein LSM14	2	P0782
tr|A0A8B6BYL3|A0A8B6BYL3_MYTGA	A0A8B6BYL3	Translation initiation factor 4E	2	P0783
tr|A0A8B6BYL7|A0A8B6BYL7_MYTGA	A0A8B6BYL7	Lysine--tRNA ligase	2	P0784
tr|A0A8B6BYM8|A0A8B6BYM8_MYTGA	A0A8B6BYM8	Guanine nucleotide-binding protein G(O) subunit alpha	2	P0785
tr|A0A8B6BZA9|A0A8B6BZA9_MYTGA	A0A8B6BZA9	Apoptosis inhibitor 5 (Fragment)	2	P0786
tr|A0A8B6BZU0|A0A8B6BZU0_MYTGA	A0A8B6BZU0	26S proteasome regulatory subunit T3	2	P0787
tr|A0A8B6C0J3|A0A8B6C0J3_MYTGA	A0A8B6C0J3	Uncharacterized protein	2	P0788
tr|A0A8B6C1E0|A0A8B6C1E0_MYTGA	A0A8B6C1E0	Uncharacterized protein	2	P0789
tr|A0A8B6C284|A0A8B6C284_MYTGA	A0A8B6C284	Cytochrome c oxidase subunit 5A, mitochondrial	2	P0790
tr|A0A8B6C383|A0A8B6C383_MYTGA	A0A8B6C383	Dynein axonemal heavy chain	2	P0791
tr|A0A8B6C3A0|A0A8B6C3A0_MYTGA	A0A8B6C3A0	Eukaryotic translation initiation factor 4H	2	P0792
tr|A0A8B6C3H9|A0A8B6C3H9_MYTGA	A0A8B6C3H9	Tubulin alpha chain	2	P0793
tr|A0A8B6C3Q2|A0A8B6C3Q2_MYTGA	A0A8B6C3Q2	Perilipin-2	2	P0794
tr|A0A8B6C4B5|A0A8B6C4B5_MYTGA	A0A8B6C4B5	Twinfilin	2	P0795
tr|A0A8B6C4N8|A0A8B6C4N8_MYTGA	A0A8B6C4N8	protein-disulfide reductase	2	P0796
tr|A0A8B6C5I4|A0A8B6C5I4_MYTGA	A0A8B6C5I4	Kynurenine formamidase	2	P0797
tr|A0A8B6C797|A0A8B6C797_MYTGA	A0A8B6C797	Thioredoxin domain-containing protein 17	2	P0798
tr|A0A8B6C9P1|A0A8B6C9P1_MYTGA	A0A8B6C9P1	Intraflagellar transport protein 56	2	P0799
tr|A0A8B6CA14|A0A8B6CA14_MYTGA	A0A8B6CA14	Trichohyalin-plectin-homology domain-containing protein	2	P0800
tr|A0A8B6CA66|A0A8B6CA66_MYTGA	A0A8B6CA66	Protein kinase C and casein kinase substrate in neurons prot	2	P0801
tr|A0A8B6CA67|A0A8B6CA67_MYTGA	A0A8B6CA67	Tetraspanin	2	P0802
tr|A0A8B6CAW3|A0A8B6CAW3_MYTGA	A0A8B6CAW3	K Homology domain-containing protein	2	P0803
tr|A0A8B6CBN7|A0A8B6CBN7_MYTGA	A0A8B6CBN7	Uncharacterized protein	2	P0804
tr|A0A8B6CBV0|A0A8B6CBV0_MYTGA	A0A8B6CBV0	ADP-ribosylation factor-like protein 8	2	P0805
tr|A0A8B6CD17|A0A8B6CD17_MYTGA	A0A8B6CD17	Uncharacterized protein	2	P0806
tr|A0A8B6CDD6|A0A8B6CDD6_MYTGA	A0A8B6CDD6	Microtubule-associated protein Jupiter	2	P0807
tr|A0A8B6CE09|A0A8B6CE09_MYTGA	A0A8B6CE09	Enoyl reductase (ER) domain-containing protein	2	P0808
tr|A0A8B6CF20|A0A8B6CF20_MYTGA	A0A8B6CF20	Uncharacterized protein	2	P0809
tr|A0A8B6CF89|A0A8B6CF89_MYTGA	A0A8B6CF89	PID domain-containing protein	2	P0810
tr|A0A8B6CFZ5|A0A8B6CFZ5_MYTGA	A0A8B6CFZ5	Calponin-homology (CH) domain-containing protein	2	P0811
tr|A0A8B6CG13|A0A8B6CG13_MYTGA	A0A8B6CG13	Histone deacetylase	2	P0812
tr|A0A8B6CG91|A0A8B6CG91_MYTGA	A0A8B6CG91	SUEL-type lectin domain-containing protein	2	P0813
tr|A0A8B6CGB3|A0A8B6CGB3_MYTGA	A0A8B6CGB3	Rieske domain-containing protein	2	P0814
tr|A0A8B6CH94|A0A8B6CH94_MYTGA	A0A8B6CH94	Cytochrome b-c1 complex subunit Rieske, mitochondrial	2	P0815
tr|A0A8B6CIF3|A0A8B6CIF3_MYTGA	A0A8B6CIF3	Y-box-binding protein 1	2	P0816
tr|A0A8B6CII0|A0A8B6CII0_MYTGA	A0A8B6CII0	THO complex subunit 4	2	P0817
tr|A0A8B6CJD6|A0A8B6CJD6_MYTGA	A0A8B6CJD6	Eukaryotic translation initiation factor 3 subunit K	2	P0818
tr|A0A8B6CK18|A0A8B6CK18_MYTGA	A0A8B6CK18	Protein transport protein SEC24	2	P0819
tr|A0A8B6CKC8|A0A8B6CKC8_MYTGA	A0A8B6CKC8	Translin-associated factor X-interacting protein 1 N-termina	2	P0820
tr|A0A8B6CKQ9|A0A8B6CKQ9_MYTGA	A0A8B6CKQ9	EF-hand domain-containing protein	2	P0821
tr|A0A8B6CLB1|A0A8B6CLB1_MYTGA	A0A8B6CLB1	Collagen, type IV, alpha	2	P0822
tr|A0A8B6CLG9|A0A8B6CLG9_MYTGA	A0A8B6CLG9	Ubiquitin-conjugating enzyme E2 M	2	P0823
tr|A0A8B6CLS4|A0A8B6CLS4_MYTGA	A0A8B6CLS4	COP9 signalosome complex subunit 4 (Fragment)	2	P0824
tr|A0A8B6CMF8|A0A8B6CMF8_MYTGA	A0A8B6CMF8	Steroid 17alpha-monooxygenase / 17alpha-hydroxyprogest	2	P0825
tr|A0A8B6CN16|A0A8B6CN16_MYTGA	A0A8B6CN16	Sorting nexin-3/12	2	P0826
tr|A0A8B6CNV4|A0A8B6CNV4_MYTGA	A0A8B6CNV4	Kyphoscoliosis peptidase	2	P0827
tr|A0A8B6CPP0|A0A8B6CPP0_MYTGA	A0A8B6CPP0	Protocadherin Fat 4	2	P0828
tr|A0A8B6CPR1|A0A8B6CPR1_MYTGA	A0A8B6CPR1	Aurora kinase	2	P0829
tr|A0A8B6CPW3|A0A8B6CPW3_MYTGA	A0A8B6CPW3	VWFA domain-containing protein	2	P0830
tr|A0A8B6CQY3|A0A8B6CQY3_MYTGA	A0A8B6CQY3	Protein transport protein SEC61 subunit alpha	2	P0831
tr|A0A8B6CSC5|A0A8B6CSC5_MYTGA	A0A8B6CSC5	Beta-glucosidase	2	P0832
tr|A0A8B6CSE8|A0A8B6CSE8_MYTGA	A0A8B6CSE8	Fumarate hydratase, class I (Fragment)	2	P0833
tr|A0A8B6CTB8|A0A8B6CTB8_MYTGA	A0A8B6CTB8	Ras-related protein Rab-6A	2	P0834
tr|A0A8B6CUL3|A0A8B6CUL3_MYTGA	A0A8B6CUL3	protein-serine/threonine phosphatase	2	P0835
tr|A0A8B6CUP0|A0A8B6CUP0_MYTGA	A0A8B6CUP0	Aspartyl aminopeptidase	2	P0836
tr|A0A8B6CVA6|A0A8B6CVA6_MYTGA	A0A8B6CVA6	Membrane-associated progesterone receptor component	2	P0837
tr|A0A8B6CVW2|A0A8B6CVW2_MYTGA	A0A8B6CVW2	40S ribosomal protein S27	2	P0838
tr|A0A8B6CWI5|A0A8B6CWI5_MYTGA	A0A8B6CWI5	Tyrosine-protein phosphatase non-receptor type 11	2	P0839
tr|A0A8B6CWL2|A0A8B6CWL2_MYTGA	A0A8B6CWL2	Transgelin	2	P0840
tr|A0A8B6CWV3|A0A8B6CWV3_MYTGA	A0A8B6CWV3	Band 7 domain-containing protein	2	P0841
tr|A0A8B6CWY2|A0A8B6CWY2_MYTGA	A0A8B6CWY2	mitogen-activated protein kinase kinase	2	P0842
tr|A0A8B6CXA0|A0A8B6CXA0_MYTGA	A0A8B6CXA0	ATP-binding cassette, subfamily F, member 2	2	P0843
tr|A0A8B6CXP9|A0A8B6CXP9_MYTGA	A0A8B6CXP9	Transgelin	2	P0844
tr|A0A8B6CXZ8|A0A8B6CXZ8_MYTGA	A0A8B6CXZ8	Ciliary microtubule inner protein 2C	2	P0845
tr|A0A8B6CYK1|A0A8B6CYK1_MYTGA	A0A8B6CYK1	Proteasome subunit alpha type	2	P0846
tr|A0A8B6CZ75|A0A8B6CZ75_MYTGA	A0A8B6CZ75	Tetratricopeptide repeat protein 29	2	P0847
tr|A0A8B6D1E0|A0A8B6D1E0_MYTGA	A0A8B6D1E0	Uncharacterized protein	2	P0848
tr|A0A8B6D2Q9|A0A8B6D2Q9_MYTGA	A0A8B6D2Q9	E3 ubiquitin-protein ligase HUWE1	2	P0849
tr|A0A8B6D2W1|A0A8B6D2W1_MYTGA	A0A8B6D2W1	Heterogeneous nuclear ribonucleoprotein A1/A3	2	P0850
tr|A0A8B6D2Y9|A0A8B6D2Y9_MYTGA	A0A8B6D2Y9	RNA-binding protein Musashi	2	P0851
tr|A0A8B6D3I7|A0A8B6D3I7_MYTGA	A0A8B6D3I7	Protein NDRG3	2	P0852
tr|A0A8B6D420|A0A8B6D420_MYTGA	A0A8B6D420	Mitochondria-eating protein C-terminal domain-containing	2	P0853
tr|A0A8B6D4D9|A0A8B6D4D9_MYTGA	A0A8B6D4D9	Acid ceramidase	2	P0854
tr|A0A8B6D4L4|A0A8B6D4L4_MYTGA	A0A8B6D4L4	NADH dehydrogenase [ubiquinone] 1 beta subcomplex subu	2	P0855
tr|A0A8B6D521|A0A8B6D521_MYTGA	A0A8B6D521	DUF4201 domain-containing protein (Fragment)	2	P0856
tr|A0A8B6D557|A0A8B6D557_MYTGA	A0A8B6D557	Nucleolar protein 58 (Fragment)	2	P0857
tr|A0A8B6D5D3|A0A8B6D5D3_MYTGA	A0A8B6D5D3	peptidylprolyl isomerase	2	P0858
tr|A0A8B6D5Q5|A0A8B6D5Q5_MYTGA	A0A8B6D5Q5	Symplekin	2	P0859
tr|A0A8B6D8N2|A0A8B6D8N2_MYTGA	A0A8B6D8N2	Integrin beta	2	P0860
tr|A0A8B6D961|A0A8B6D961_MYTGA	A0A8B6D961	40S ribosomal protein S12	2	P0861
tr|A0A8B6D9Q5|A0A8B6D9Q5_MYTGA	A0A8B6D9Q5	Serine/arginine-rich splicing factor 2	2	P0862
tr|A0A8B6DBV9|A0A8B6DBV9_MYTGA	A0A8B6DBV9	Caspase 7	2	P0863
tr|A0A8B6DBX9|A0A8B6DBX9_MYTGA	A0A8B6DBX9	DnaJ homolog subfamily B member 13	2	P0864
tr|A0A8B6DCS1|A0A8B6DCS1_MYTGA	A0A8B6DCS1	Annexin	2	P0865
tr|A0A8B6DE11|A0A8B6DE11_MYTGA	A0A8B6DE11	Phosphoacetylglucosamine mutase	2	P0866
tr|A0A8B6DES1|A0A8B6DES1_MYTGA	A0A8B6DES1	Mannose-1-phosphate guanylyltransferase	2	P0867
tr|A0A8B6DEU6|A0A8B6DEU6_MYTGA	A0A8B6DEU6	Pre-mRNA-processing factor 19	2	P0868
tr|A0A8B6DEX3|A0A8B6DEX3_MYTGA	A0A8B6DEX3	Replication factor A protein 1	2	P0869
tr|A0A8B6DGU4|A0A8B6DGU4_MYTGA	A0A8B6DGU4	Dynein regulatry complex protein 1	2	P0870
tr|A0A8B6DH95|A0A8B6DH95_MYTGA	A0A8B6DH95	Arachidonate 5-lipoxygenase	2	P0871
tr|A0A8B6DHM6|A0A8B6DHM6_MYTGA	A0A8B6DHM6	Methyltransferase domain-containing protein	2	P0872
tr|A0A8B6DHU9|A0A8B6DHU9_MYTGA	A0A8B6DHU9	Integrin-linked kinase	2	P0873
tr|A0A8B6DIR2|A0A8B6DIR2_MYTGA	A0A8B6DIR2	Solute carrier family 25 (Mitochondrial carnitine/acylcarnit	2	P0874
tr|A0A8B6DJV6|A0A8B6DJV6_MYTGA	A0A8B6DJV6	Polypeptide N-acetylgalactosaminyltransferase	2	P0875
tr|A0A8B6DK78|A0A8B6DK78_MYTGA	A0A8B6DK78	Uncharacterized protein	2	P0876
tr|A0A8B6DKE5|A0A8B6DKE5_MYTGA	A0A8B6DKE5	Peptidase M14 carboxypeptidase A domain-containing prot	2	P0877
tr|A0A8B6DLG3|A0A8B6DLG3_MYTGA	A0A8B6DLG3	Alanine--glyoxylate aminotransferase	2	P0878
tr|A0A8B6DMV7|A0A8B6DMV7_MYTGA	A0A8B6DMV7	Cilia- and flagella-associated protein 70	2	P0879
tr|A0A8B6DMY0|A0A8B6DMY0_MYTGA	A0A8B6DMY0	Uncharacterized protein	2	P0880
tr|A0A8B6DN24|A0A8B6DN24_MYTGA	A0A8B6DN24	Uncharacterized protein	2	P0881
tr|A0A8B6DNK8|A0A8B6DNK8_MYTGA	A0A8B6DNK8	Eukaryotic translation initiation factor 2 subunit 1	2	P0882
tr|A0A8B6DNN5|A0A8B6DNN5_MYTGA	A0A8B6DNN5	UDP-N-acetylglucosamine diphosphorylase	2	P0883
tr|A0A8B6DP64|A0A8B6DP64_MYTGA	A0A8B6DP64	glutathione transferase	2	P0884
tr|A0A8B6DP80|A0A8B6DP80_MYTGA	A0A8B6DP80	3-hydroxyisobutyryl-CoA hydrolase, mitochondrial	2	P0885
tr|A0A8B6DQ42|A0A8B6DQ42_MYTGA	A0A8B6DQ42	C-type lectin domain-containing protein	2	P0886
tr|A0A8B6DQL6|A0A8B6DQL6_MYTGA	A0A8B6DQL6	Enolase	2	P0887
tr|A0A8B6DQM6|A0A8B6DQM6_MYTGA	A0A8B6DQM6	Phosphotransferase	2	P0888
tr|A0A8B6DQZ1|A0A8B6DQZ1_MYTGA	A0A8B6DQZ1	Serine/threonine-protein kinase SIK2	2	P0889
tr|A0A8B6DR67|A0A8B6DR67_MYTGA	A0A8B6DR67	Uncharacterized protein	2	P0890
tr|A0A8B6DTX0|A0A8B6DTX0_MYTGA	A0A8B6DTX0	Rootletin	2	P0891
tr|A0A8B6DU33|A0A8B6DU33_MYTGA	A0A8B6DU33	Glutathione reductase	2	P0892
tr|A0A8B6DVD9|A0A8B6DVD9_MYTGA	A0A8B6DVD9	Heterogeneous nuclear ribonucleoprotein L	2	P0893
tr|A0A8B6DWZ2|A0A8B6DWZ2_MYTGA	A0A8B6DWZ2	Tumor necrosis factor ligand superfamily member 10	2	P0894
tr|A0A8B6DX45|A0A8B6DX45_MYTGA	A0A8B6DX45	Cathepsin L	2	P0895
tr|A0A8B6DX85|A0A8B6DX85_MYTGA	A0A8B6DX85	DNA (cytosine-5)-methyltransferase	2	P0896

Protein	Uniprot accession	Protein Name	Number Peptides	P
tr|A0A8B6DY57|A0A8B6DY57_MYTGA	A0A8B6DY57	Flap endonuclease-1 (Fragment)	2	P0897
tr|A0A8B6DYC8|A0A8B6DYC8_MYTGA	A0A8B6DYC8	SMB domain-containing protein	2	P0898
tr|A0A8B6E023|A0A8B6E023_MYTGA	A0A8B6E023	Elongation factor 1-delta	2	P0899
tr|A0A8B6E0I5|A0A8B6E0I5_MYTGA	A0A8B6E0I5	Uncharacterized protein	2	P0900
tr|A0A8B6E1I5|A0A8B6E1I5_MYTGA	A0A8B6E1I5	CS domain-containing protein	2	P0901
tr|A0A8B6E1P9|A0A8B6E1P9_MYTGA	A0A8B6E1P9	Vitelline membrane outer layer 1-like protein	2	P0902
tr|A0A8B6E1T2|A0A8B6E1T2_MYTGA	A0A8B6E1T2	BTB domain-containing protein	2	P0903
tr|A0A8B6E240|A0A8B6E240_MYTGA	A0A8B6E240	Vacuolar proton pump subunit B (Fragment)	2	P0904
tr|A0A8B6E2A8|A0A8B6E2A8_MYTGA	A0A8B6E2A8	COP9 signalosome complex subunit 2 (Fragment)	2	P0905
tr|A0A8B6E381|A0A8B6E381_MYTGA	A0A8B6E381	C-type lectin domain-containing protein	2	P0906
tr|A0A8B6E3A2|A0A8B6E3A2_MYTGA	A0A8B6E3A2	Translocon-associated protein subunit beta	2	P0907
tr|A0A8B6E3S0|A0A8B6E3S0_MYTGA	A0A8B6E3S0	Profilin	2	P0908
tr|A0A8B6E560|A0A8B6E560_MYTGA	A0A8B6E560	Chitinase (Fragment)	2	P0909
tr|A0A8B6E653|A0A8B6E653_MYTGA	A0A8B6E653	Uncharacterized protein	2	P0910
tr|A0A8B6E7E0|A0A8B6E7E0_MYTGA	A0A8B6E7E0	Uncharacterized protein	2	P0911
tr|A0A8B6E8J5|A0A8B6E8J5_MYTGA	A0A8B6E8J5	Trypsin	2	P0912
tr|A0A8B6E910|A0A8B6E910_MYTGA	A0A8B6E910	Metalloendopeptidase (Fragment)	2	P0913
tr|A0A8B6E978|A0A8B6E978_MYTGA	A0A8B6E978	Heat shock 70kDa protein 1/8	2	P0914
tr|A0A8B6EA63|A0A8B6EA63_MYTGA	A0A8B6EA63	Large ribosomal subunit protein uL22	2	P0915
tr|A0A8B6EAL5|A0A8B6EAL5_MYTGA	A0A8B6EAL5	F-actin-capping protein subunit beta	2	P0916
tr|A0A8B6EB95|A0A8B6EB95_MYTGA	A0A8B6EB95	Acidic leucine-rich nuclear phosphoprotein 32 family membt	2	P0917
tr|A0A8B6EDA1|A0A8B6EDA1_MYTGA	A0A8B6EDA1	ER membrane protein complex subunit 4	2	P0918
tr|A0A8B6EEH7|A0A8B6EEH7_MYTGA	A0A8B6EEH7	Eukaryotic translation initiation factor 3 subunit D	2	P0919
tr|A0A8B6EEW7|A0A8B6EEW7_MYTGA	A0A8B6EEW7	Ganglioside GM2 activator	2	P0920
tr|A0A8B6EF06|A0A8B6EF06_MYTGA	A0A8B6EF06	Electron transfer flavoprotein-ubiquinone oxidoreductase (F	2	P0921
tr|A0A8B6EFL6|A0A8B6EFL6_MYTGA	A0A8B6EFL6	CUB domain-containing protein	2	P0922
tr|A0A8B6EG22|A0A8B6EG22_MYTGA	A0A8B6EG22	p24 family protein delta-1	2	P0923
tr|A0A8B6EG75|A0A8B6EG75_MYTGA	A0A8B6EG75	ATP receptor	2	P0924
tr|A0A8B6EGA6|A0A8B6EGA6_MYTGA	A0A8B6EGA6	Serine/threonine-protein phosphatase 2B regulatory subuni	2	P0925
tr|A0A8B6EGA8|A0A8B6EGA8_MYTGA	A0A8B6EGA8	Selenoprotein W-related protein	2	P0926
tr|A0A8B6EGG6|A0A8B6EGG6_MYTGA	A0A8B6EGG6	Myticin A protein	2	P0927
tr|A0A8B6EGX5|A0A8B6EGX5_MYTGA	A0A8B6EGX5	Blast:Synaptogenesis protein syg-2	2	P0928
tr|A0A8B6EH01|A0A8B6EH01_MYTGA	A0A8B6EH01	CUB domain-containing protein	2	P0929
tr|A0A8B6EHZ2|A0A8B6EHZ2_MYTGA	A0A8B6EHZ2	Uncharacterized protein	2	P0930
tr|A0A8B6EI55|A0A8B6EI55_MYTGA	A0A8B6EI55	Apolipoprotein D	2	P0931
tr|A0A8B6EIE1|A0A8B6EIE1_MYTGA	A0A8B6EIE1	Large ribosomal subunit protein eL6	2	P0932
tr|A0A8B6EJM8|A0A8B6EJM8_MYTGA	A0A8B6EJM8	omega-amidase	2	P0933
tr|A0A8B6EK28|A0A8B6EK28_MYTGA	A0A8B6EK28	5'-nucleotidase	2	P0934
tr|A0A8B6EKH9|A0A8B6EKH9_MYTGA	A0A8B6EKH9	Cullin 4	2	P0935
tr|A0A8B6EKI7|A0A8B6EKI7_MYTGA	A0A8B6EKI7	Proto-oncogene C-crk	2	P0936
tr|A0A8B6EKX5|A0A8B6EKX5_MYTGA	A0A8B6EKX5	Ribonuclease Z	2	P0937
tr|A0A8B6ELP9|A0A8B6ELP9_MYTGA	A0A8B6ELP9	Guanylate kinase (Fragment)	2	P0938
tr|A0A8B6EP64|A0A8B6EP64_MYTGA	A0A8B6EP64	Integrin alpha 6	2	P0939
tr|A0A8B6EPD9|A0A8B6EPD9_MYTGA	A0A8B6EPD9	Apextrin C-terminal domain-containing protein	2	P0940
tr|A0A8B6EPH2|A0A8B6EPH2_MYTGA	A0A8B6EPH2	Cullin 3	2	P0941
tr|A0A8B6EPP0|A0A8B6EPP0_MYTGA	A0A8B6EPP0	Calpain catalytic domain-containing protein	2	P0942
tr|A0A8B6EPU2|A0A8B6EPU2_MYTGA	A0A8B6EPU2	Secreted protein	2	P0943
tr|A0A8B6ES39|A0A8B6ES39_MYTGA	A0A8B6ES39	Uncharacterized protein	2	P0944
tr|A0A8B6ES98|A0A8B6ES98_MYTGA	A0A8B6ES98	Adenosine kinase	2	P0945
tr|A0A8B6ET84|A0A8B6ET84_MYTGA	A0A8B6ET84	SUMO-activating enzyme subunit	2	P0946
tr|A0A8B6ETA0|A0A8B6ETA0_MYTGA	A0A8B6ETA0	SCP domain-containing protein	2	P0947
tr|A0A8B6ETV5|A0A8B6ETV5_MYTGA	A0A8B6ETV5	Uncharacterized protein	2	P0948
tr|A0A8B6ETX6|A0A8B6ETX6_MYTGA	A0A8B6ETX6	Plasminogen activator inhibitor 1 RNA-binding protein (Frag	2	P0949
tr|A0A8B6EVB3|A0A8B6EVB3_MYTGA	A0A8B6EVB3	Speckle targeted PIP5K1A-regulated poly(A) polymerase	2	P0950
tr|A0A8B6EWX3|A0A8B6EWX3_MYTGA	A0A8B6EWX3	Phosphoribosylformylglycinamidine synthase	2	P0951
tr|A0A8B6EX80|A0A8B6EX80_MYTGA	A0A8B6EX80	Formyltetrahydrofolate dehydrogenase	2	P0952
tr|A0A8B6EXL9|A0A8B6EXL9_MYTGA	A0A8B6EXL9	NADH dehydrogenase [ubiquinone] 1 alpha subcomplex subu	2	P0953
tr|A0A8B6EXN2|A0A8B6EXN2_MYTGA	A0A8B6EXN2	RNA helicase	2	P0954
tr|A0A8B6EZW6|A0A8B6EZW6_MYTGA	A0A8B6EZW6	Cilia- and flagella-associated protein 45	2	P0955
tr|A0A8B6F080|A0A8B6F080_MYTGA	A0A8B6F080	CNOT1	2	P0956
tr|A0A8B6F1B6|A0A8B6F1B6_MYTGA	A0A8B6F1B6	Cadherin EGF LAG seven-pass G-type receptor 1	2	P0957
tr|A0A8B6F3H7|A0A8B6F3H7_MYTGA	A0A8B6F3H7	Cilia- and flagella-associated protein 161	2	P0958
tr|A0A8B6F3Y2|A0A8B6F3Y2_MYTGA	A0A8B6F3Y2	cysteine--tRNA ligase	2	P0959
tr|A0A8B6F4R8|A0A8B6F4R8_MYTGA	A0A8B6F4R8	Ig-like domain-containing protein	2	P0960
tr|A0A8B6F5I3|A0A8B6F5I3_MYTGA	A0A8B6F5I3	Uncharacterized protein	2	P0961
tr|A0A8B6F603|A0A8B6F603_MYTGA	A0A8B6F603	Golgi phosphoprotein 3	2	P0962
tr|A0A8B6F6Q8|A0A8B6F6Q8_MYTGA	A0A8B6F6Q8	Ig-like domain-containing protein	2	P0963
tr|A0A8B6F6S8|A0A8B6F6S8_MYTGA	A0A8B6F6S8	Uncharacterized protein	2	P0964
tr|A0A8B6F6T3|A0A8B6F6T3_MYTGA	A0A8B6F6T3	Serine/threonine-protein phosphatase	2	P0965
tr|A0A8B6F781|A0A8B6F781_MYTGA	A0A8B6F781	acetyl-CoA C-acetyltransferase	2	P0966
tr|A0A8B6F7I0|A0A8B6F7I0_MYTGA	A0A8B6F7I0	Nuclear pore complex protein Nup210	2	P0967
tr|A0A8B6F8N6|A0A8B6F8N6_MYTGA	A0A8B6F8N6	Cytoplasmic FMR1-interacting protein	2	P0968
tr|A0A8B6F900|A0A8B6F900_MYTGA	A0A8B6F900	NADH dehydrogenase [ubiquinone] 1 alpha subcomplex subu	2	P0969
tr|A0A8B6F906|A0A8B6F906_MYTGA	A0A8B6F906	Dehydrogenase/reductase SDR family member 4	2	P0970
tr|A0A8B6F942|A0A8B6F942_MYTGA	A0A8B6F942	RNA-binding protein 4	2	P0971
tr|A0A8B6F9E7|A0A8B6F9E7_MYTGA	A0A8B6F9E7	Large ribosomal subunit protein eL22	2	P0972
tr|A0A8B6F9L7|A0A8B6F9L7_MYTGA	A0A8B6F9L7	Translation initiation factor 2 subunit 3	2	P0973
tr|A0A8B6F9M4|A0A8B6F9M4_MYTGA	A0A8B6F9M4	Glycoside hydrolase family 38 N-terminal domain-containin	2	P0974
tr|A0A8B6FA82|A0A8B6FA82_MYTGA	A0A8B6FA82	tRNA (Cytosine34-C5)-methyltransferase (Fragment)	2	P0975
tr|A0A8B6FAQ9|A0A8B6FAQ9_MYTGA	A0A8B6FAQ9	Cytosolic nonspecific dipeptidase	2	P0976
tr|A0A8B6FBR9|A0A8B6FBR9_MYTGA	A0A8B6FBR9	Proteasomal ubiquitin receptor ADRM1	2	P0977
tr|A0A8B6FBZ7|A0A8B6FBZ7_MYTGA	A0A8B6FBZ7	RIB43A-like with coiled-coils protein 2	2	P0978
tr|A0A8B6FCA3|A0A8B6FCA3_MYTGA	A0A8B6FCA3	Uncharacterized protein (Fragment)	2	P0979
tr|A0A8B6FCP3|A0A8B6FCP3_MYTGA	A0A8B6FCP3	Ubiquitin-like domain-containing protein	2	P0980
tr|A0A8B6FD54|A0A8B6FD54_MYTGA	A0A8B6FD54	DnaJ homolog subfamily C member 13	2	P0981
tr|A0A8B6FD77|A0A8B6FD77_MYTGA	A0A8B6FD77	Uncharacterized protein	2	P0982
tr|A0A8B6FDI6|A0A8B6FDI6_MYTGA	A0A8B6FDI6	ZP domain-containing protein	2	P0983
tr|A0A8B6FDJ9|A0A8B6FDJ9_MYTGA	A0A8B6FDJ9	Cilia- and flagella-associated protein 77	2	P0984
tr|A0A8B6FDL4|A0A8B6FDL4_MYTGA	A0A8B6FDL4	peptidylprolyl isomerase	2	P0985
tr|A0A8B6FEK6|A0A8B6FEK6_MYTGA	A0A8B6FEK6	Uncharacterized protein	2	P0986
tr|A0A8B6FF49|A0A8B6FF49_MYTGA	A0A8B6FF49	Uncharacterized protein	2	P0987
tr|A0A8B6FFK3|A0A8B6FFK3_MYTGA	A0A8B6FFK3	Uncharacterized protein	2	P0988
tr|A0A8B6FGB3|A0A8B6FGB3_MYTGA	A0A8B6FGB3	Collagen, type II, alpha	2	P0989
tr|A0A8B6FGG3|A0A8B6FGG3_MYTGA	A0A8B6FGG3	WSC domain-containing protein	2	P0990
tr|A0A8B6FH33|A0A8B6FH33_MYTGA	A0A8B6FH33	Prominin 1	2	P0991
tr|A0A8B6FH65|A0A8B6FH65_MYTGA	A0A8B6FH65	Valacyclovir hydrolase	2	P0992
tr|A0A8B6FJ72|A0A8B6FJ72_MYTGA	A0A8B6FJ72	Glycerol-3-phosphate dehydrogenase	2	P0993
tr|A0A8B6FK68|A0A8B6FK68_MYTGA	A0A8B6FK68	Xylose isomerase	2	P0994
tr|A0A8B6FKX5|A0A8B6FKX5_MYTGA	A0A8B6FKX5	pyridoxal 5'-phosphate synthase (glutamine hydrolyzing)	2	P0995
tr|A0A8B6FKZ1|A0A8B6FKZ1_MYTGA	A0A8B6FKZ1	Uncharacterized protein	2	P0996
tr|A0A8B6FKZ3|A0A8B6FKZ3_MYTGA	A0A8B6FKZ3	Amidase	2	P0997
tr|A0A8B6FLW8|A0A8B6FLW8_MYTGA	A0A8B6FLW8	Choline dehydrogenase	2	P0998
tr|A0A8B6FM48|A0A8B6FM48_MYTGA	A0A8B6FM48	Ras-related protein Rab-11A	2	P0999
tr|A0A8B6FM52|A0A8B6FM52_MYTGA	A0A8B6FM52	dynamin GTPase	2	P1000
tr|A0A8B6FMU0|A0A8B6FMU0_MYTGA	A0A8B6FMU0	OCIA domain-containing protein	2	P1001
tr|A0A8B6FN07|A0A8B6FN07_MYTGA	A0A8B6FN07	Dynein heavy chain, axonemal	2	P1002
tr|A0A8B6FNK2|A0A8B6FNK2_MYTGA	A0A8B6FNK2	Protein SCO1/2	2	P1003
tr|A0A8B6FP69|A0A8B6FP69_MYTGA	A0A8B6FP69	Uncharacterized protein	2	P1004
tr|A0A8B6FP77|A0A8B6FP77_MYTGA	A0A8B6FP77	Intraflagellar transport protein 88	2	P1005
tr|A0A8B6FPN2|A0A8B6FPN2_MYTGA	A0A8B6FPN2	Fucolectin tachylectin-4 pentraxin-1 domain-containing pro	2	P1006
tr|A0A8B6FQQ2|A0A8B6FQQ2_MYTGA	A0A8B6FQQ2	Cleavage and polyadenylation specificity factor subunit 3	2	P1007
tr|A0A8B6FQQ4|A0A8B6FQQ4_MYTGA	A0A8B6FQQ4	Tudor domain-containing protein 1/4/6/7	2	P1008
tr|A0A8B6FQS1|A0A8B6FQS1_MYTGA	A0A8B6FQS1	Matrix metalloproteinase-14 (Membrane-inserted)	2	P1009
tr|A0A8B6FRC2|A0A8B6FRC2_MYTGA	A0A8B6FRC2	Phosphoinositide phospholipase C	2	P1010
tr|A0A8B6FRF5|A0A8B6FRF5_MYTGA	A0A8B6FRF5	Peptidyl-prolyl cis-trans isomerase	2	P1011
tr|A0A8B6FSK2|A0A8B6FSK2_MYTGA	A0A8B6FSK2	Uncharacterized protein	2	P1012
tr|A0A8B6FSL1|A0A8B6FSL1_MYTGA	A0A8B6FSL1	C1q domain-containing protein	2	P1013

Protein	Uniprot accession	Protein Name	Number Peptides	P
tr|A0A8B6FSW2|A0A8B6FSW2_MYTGA	A0A8B6FSW2	ADF-H domain-containing protein	2	P1014
tr|A0A8B6FT25|A0A8B6FT25_MYTGA	A0A8B6FT25	Profilin	2	P1015
tr|A0A8B6FUS2|A0A8B6FUS2_MYTGA	A0A8B6FUS2	Succinyl-CoA:3-ketoacid-coenzyme A transferase	2	P1016
tr|A0A8B6FVJ7|A0A8B6FVJ7_MYTGA	A0A8B6FVJ7	Aminomethyltransferase	2	P1017
tr|A0A8B6FVV4|A0A8B6FVV4_MYTGA	A0A8B6FVV4	2-oxoisovalerate dehydrogenase subunit alpha	2	P1018
tr|A0A8B6FW02|A0A8B6FW02_MYTGA	A0A8B6FW02	Uncharacterized protein	2	P1019
tr|A0A8B6FWT3|A0A8B6FWT3_MYTGA	A0A8B6FWT3	Inositol 1,4,5-trisphosphate receptor	2	P1020
tr|A0A8B6FWT9|A0A8B6FWT9_MYTGA	A0A8B6FWT9	NADH dehydrogenase [ubiquinone] 1 beta subcomplex subu	2	P1021
tr|A0A8B6FYM7|A0A8B6FYM7_MYTGA	A0A8B6FYM7	Dynein regulatory complex protein 10	2	P1022
tr|A0A8B6FYM9|A0A8B6FYM9_MYTGA	A0A8B6FYM9	Histone chaperone ASF1	2	P1023
tr|A0A8B6FZ88|A0A8B6FZ88_MYTGA	A0A8B6FZ88	Pantetheine hydrolase	2	P1024
tr|A0A8B6FZA3|A0A8B6FZA3_MYTGA	A0A8B6FZA3	Serpin domain-containing protein	2	P1025
tr|A0A8B6FZN1|A0A8B6FZN1_MYTGA	A0A8B6FZN1	Ras-related protein Rab-3C	2	P1026
tr|A0A8B6G0T4|A0A8B6G0T4_MYTGA	A0A8B6G0T4	Ras homolog gene family, member A	2	P1027
tr|A0A8B6G107|A0A8B6G107_MYTGA	A0A8B6G107	Phosphoglycerate kinase	2	P1028
tr|A0A8B6G1Q5|A0A8B6G1Q5_MYTGA	A0A8B6G1Q5	Uncharacterized protein	2	P1029
tr|A0A8B6G2E0|A0A8B6G2E0_MYTGA	A0A8B6G2E0	Sodium/potassium-transporting ATPase subunit beta	2	P1030
tr|A0A8B6G3I6|A0A8B6G3I6_MYTGA	A0A8B6G3I6	RNA helicase	2	P1031
tr|A0A8B6G4H2|A0A8B6G4H2_MYTGA	A0A8B6G4H2	Leucine-rich repeat-containing protein 23	2	P1032
tr|A0A8B6G4N0|A0A8B6G4N0_MYTGA	A0A8B6G4N0	26S proteasome regulatory subunit N8	2	P1033
tr|A0A8B6G4R4|A0A8B6G4R4_MYTGA	A0A8B6G4R4	Adenosylhomocysteinase	2	P1034
tr|A0A8B6G6D6|A0A8B6G6D6_MYTGA	A0A8B6G6D6	Protein ATP6V1FNB	2	P1035
tr|A0A8B6G6H2|A0A8B6G6H2_MYTGA	A0A8B6G6H2	Beta-galactosidase (Fragment)	2	P1036
tr|A0A8B6G6K2|A0A8B6G6K2_MYTGA	A0A8B6G6K2	dual-specificity kinase	2	P1037
tr|A0A8B6G6L1|A0A8B6G6L1_MYTGA	A0A8B6G6L1	Fibrinogen C-terminal domain-containing protein	2	P1038
tr|A0A8B6G795|A0A8B6G795_MYTGA	A0A8B6G795	Uncharacterized protein	2	P1039
tr|A0A8B6G7F6|A0A8B6G7F6_MYTGA	A0A8B6G7F6	Galectin	2	P1040
tr|A0A8B6G7J5|A0A8B6G7J5_MYTGA	A0A8B6G7J5	Large ribosomal subunit protein uL13	2	P1041
tr|A0A8B6G8E2|A0A8B6G8E2_MYTGA	A0A8B6G8E2	ATP-dependent DNA helicase 2 subunit 1	2	P1042
tr|A0A8B6G941|A0A8B6G941_MYTGA	A0A8B6G941	Ras-related protein Rab-35	2	P1043
tr|A0A8B6G9U4|A0A8B6G9U4_MYTGA	A0A8B6G9U4	Sulfotransferase domain-containing protein	2	P1044
tr|A0A8B6GB56|A0A8B6GB56_MYTGA	A0A8B6GB56	Sulfotransferase domain-containing protein	2	P1045
tr|A0A8B6GCK2|A0A8B6GCK2_MYTGA	A0A8B6GCK2	Serine/threonine-protein kinase PLK	2	P1046
tr|A0A8B6GF72|A0A8B6GF72_MYTGA	A0A8B6GF72	Vacuolar protein-sorting-associated protein 4	2	P1047
tr|A0A8B6GFI1|A0A8B6GFI1_MYTGA	A0A8B6GFI1	Tubulin-specific chaperone D	2	P1048
tr|A0A8B6GFL2|A0A8B6GFL2_MYTGA	A0A8B6GFL2	Uncharacterized protein	2	P1049
tr|A0A8B6GG39|A0A8B6GG39_MYTGA	A0A8B6GG39	Aldose 1-epimerase	2	P1050
tr|A0A8B6GGE1|A0A8B6GGE1_MYTGA	A0A8B6GGE1	Large subunit ribosomal protein L23Ae	2	P1051
tr|A0A8B6GGI6|A0A8B6GGI6_MYTGA	A0A8B6GGI6	ZP domain-containing protein	2	P1052
tr|A0A8B6GHH0|A0A8B6GHH0_MYTGA	A0A8B6GHH0	ZP domain-containing protein (Fragment)	2	P1053
tr|A0A8B6GI21|A0A8B6GI21_MYTGA	A0A8B6GI21	Acetyl-CoA carboxylase / biotin carboxylase 1	2	P1054
tr|A0A8B6GID5|A0A8B6GID5_MYTGA	A0A8B6GID5	Uncharacterized protein	2	P1055
tr|A0A8B6GIL6|A0A8B6GIL6_MYTGA	A0A8B6GIL6	Protein kinase A	2	P1056
tr|A0A8B6GIP4|A0A8B6GIP4_MYTGA	A0A8B6GIP4	galactokinase	2	P1057
tr|A0A8B6GJK9|A0A8B6GJK9_MYTGA	A0A8B6GJK9	Dynein intermediate chain 1, axonemal	2	P1058
tr|A0A8B6GJP2|A0A8B6GJP2_MYTGA	A0A8B6GJP2	F-box protein 36	2	P1059
tr|A0A8B6GKD6|A0A8B6GKD6_MYTGA	A0A8B6GKD6	Adenylate kinase	2	P1060
tr|A0A8B6GKF6|A0A8B6GKF6_MYTGA	A0A8B6GKF6	Protein lin-7 homolog	2	P1061
tr|A0A8B6GKP7|A0A8B6GKP7_MYTGA	A0A8B6GKP7	Tubulin beta chain	2	P1062
tr|A0A8B6GL55|A0A8B6GL55_MYTGA	A0A8B6GL55	Alanine-glyoxylate transaminase / (R)-3-amino-2-methylprop	2	P1063
tr|A0A8B6GMP6|A0A8B6GMP6_MYTGA	A0A8B6GMP6	Epidermal growth factor receptor kinase substrate 8	2	P1064
tr|A0A8B6GN58|A0A8B6GN58_MYTGA	A0A8B6GN58	26S proteasome regulatory subunit N8	2	P1065
tr|A0A8B6GN74|A0A8B6GN74_MYTGA	A0A8B6GN74	Cathepsin F	2	P1066
tr|A0A8B6GPF1|A0A8B6GPF1_MYTGA	A0A8B6GPF1	26S proteasome non-ATPase regulatory subunit 6 (Fragment	2	P1067
tr|A0A8B6GQ15|A0A8B6GQ15_MYTGA	A0A8B6GQ15	Kelch-like protein 1/4/5	2	P1068
tr|A0A8B6GQ68|A0A8B6GQ68_MYTGA	A0A8B6GQ68	Cytoplasmic polyadenylation element-binding protein	2	P1069
tr|A0A8B6GQ82|A0A8B6GQ82_MYTGA	A0A8B6GQ82	Citrate transport protein	2	P1070
tr|A0A8B6GR03|A0A8B6GR03_MYTGA	A0A8B6GR03	Blast:Protein FAM98A	2	P1071
tr|A0A8B6GS44|A0A8B6GS44_MYTGA	A0A8B6GS44	ER membrane protein complex subunit 1	2	P1072
tr|A0A8B6GTW9|A0A8B6GTW9_MYTGA	A0A8B6GTW9	EF-hand domain-containing protein	2	P1073
tr|A0A8B6GUF0|A0A8B6GUF0_MYTGA	A0A8B6GUF0	Aconitate hydratase	2	P1074
tr|A0A8B6GUP3|A0A8B6GUP3_MYTGA	A0A8B6GUP3	Dynein heavy chain 2, cytosolic	2	P1075
tr|A0A8B6GUR4|A0A8B6GUR4_MYTGA	A0A8B6GUR4	Tudor domain-containing protein 1/4/6/7 (Fragment)	2	P1076
tr|A0A8B6GVB7|A0A8B6GVB7_MYTGA	A0A8B6GVB7	DNA-directed RNA polymerase subunit beta	2	P1077
tr|A0A8B6GXA0|A0A8B6GXA0_MYTGA	A0A8B6GXA0	Ran-binding protein 3	2	P1078
tr|A0A8B6GXB1|A0A8B6GXB1_MYTGA	A0A8B6GXB1	Matrix metalloproteinase-14 (Membrane-inserted)	2	P1079
tr|A0A8B6GXN4|A0A8B6GXN4_MYTGA	A0A8B6GXN4	Ubiquitin fusion degradation protein 1	2	P1080
tr|A0A8B6GY64|A0A8B6GY64_MYTGA	A0A8B6GY64	Actin beta/gamma 1	2	P1081
tr|A0A8B6GZ97|A0A8B6GZ97_MYTGA	A0A8B6GZ97	very-long-chain enoyl-CoA reductase	2	P1082
tr|A0A8B6GZT3|A0A8B6GZT3_MYTGA	A0A8B6GZT3	Cysteine desulfurase	2	P1083
tr|A0A8B6GZZ4|A0A8B6GZZ4_MYTGA	A0A8B6GZZ4	Thioredoxin-like fold domain-containing protein	2	P1084
tr|A0A8B6H0Z6|A0A8B6H0Z6_MYTGA	A0A8B6H0Z6	Myosin VI	2	P1085
tr|A0A8B6H2X2|A0A8B6H2X2_MYTGA	A0A8B6H2X2	ATP synthase subunit e, mitochondrial	2	P1086
tr|A0A8B6H4A0|A0A8B6H4A0_MYTGA	A0A8B6H4A0	3-hydroxyanthranilate 3,4-dioxygenase	2	P1087
tr|A0A8B6H4S7|A0A8B6H4S7_MYTGA	A0A8B6H4S7	Protein phosphatase 1 regulatory subunit 7	2	P1088
tr|A0A8B6H4Y6|A0A8B6H4Y6_MYTGA	A0A8B6H4Y6	Sepiapterin reductase	2	P1089
tr|A0A8B6H5B3|A0A8B6H5B3_MYTGA	A0A8B6H5B3	START domain-containing protein	2	P1090
tr|A0A8B6H5R0|A0A8B6H5R0_MYTGA	A0A8B6H5R0	UspA domain-containing protein	2	P1091
tr|A0A8B6H751|A0A8B6H751_MYTGA	A0A8B6H751	Protein disulfide isomerase family A, member 5	2	P1092
tr|A0A8B6H758|A0A8B6H758_MYTGA	A0A8B6H758	Poly [ADP-ribose] polymerase	2	P1093
tr|A0A8B6H7G0|A0A8B6H7G0_MYTGA	A0A8B6H7G0	Uncharacterized protein	2	P1094
tr|A0A8B6H8E4|A0A8B6H8E4_MYTGA	A0A8B6H8E4	DNA replication licensing factor MCM3	2	P1095
tr|A0A8B6H8H9|A0A8B6H8H9_MYTGA	A0A8B6H8H9	Peroxin-19	2	P1096
tr|A0A8B6H8V2|A0A8B6H8V2_MYTGA	A0A8B6H8V2	RanBP-type and C3HC4-type zinc finger-containing protein 1	2	P1097
tr|A0A8B6H8W7|A0A8B6H8W7_MYTGA	A0A8B6H8W7	Tripeptidyl-peptidase 2	2	P1098
tr|A0A8B6H951|A0A8B6H951_MYTGA	A0A8B6H951	Myosin VII	2	P1099
tr|A0A8B6H989|A0A8B6H989_MYTGA	A0A8B6H989	Nuclear protein localization protein 4 homolog	2	P1100
tr|A0A8B6H9N7|A0A8B6H9N7_MYTGA	A0A8B6H9N7	AP-3 complex subunit mu	2	P1101
tr|A0A8B6H9Y1|A0A8B6H9Y1_MYTGA	A0A8B6H9Y1	small monomeric GTPase	2	P1102
tr|A0A8B6HAF5|A0A8B6HAF5_MYTGA	A0A8B6HAF5	Dihydrolipoamide acetyltransferase component of pyruvate	2	P1103
tr|A0A8B6HBD8|A0A8B6HBD8_MYTGA	A0A8B6HBD8	CSN12-like protein	2	P1104
tr|A0A8B6HBJ5|A0A8B6HBJ5_MYTGA	A0A8B6HBJ5	Lipase domain-containing protein	2	P1105
tr|A0A8B6HDM8|A0A8B6HDM8_MYTGA	A0A8B6HDM8	Phenylalanyl-tRNA synthetase beta chain	2	P1106
tr|A0A8B6HDX7|A0A8B6HDX7_MYTGA	A0A8B6HDX7	Dynein heavy chain tail domain-containing protein	2	P1107
tr|A0A8B6HEA1|A0A8B6HEA1_MYTGA	A0A8B6HEA1	Uncharacterized protein	2	P1108
tr|A0A8B6HEN9|A0A8B6HEN9_MYTGA	A0A8B6HEN9	alpha-L-fucosidase	2	P1109
tr|A0A8B6HEZ7|A0A8B6HEZ7_MYTGA	A0A8B6HEZ7	Small nuclear ribonucleoprotein Sm D3	2	P1110
tr|A0A8B6HF43|A0A8B6HF43_MYTGA	A0A8B6HF43	Protein transport protein SEC61 subunit beta	2	P1111
tr|A0A8B6HG14|A0A8B6HG14_MYTGA	A0A8B6HG14	Importin-4	2	P1112
tr|A0A8B6HIS2|A0A8B6HIS2_MYTGA	A0A8B6HIS2	14-3-3 protein epsilon	2	P1113
tr|A0A8B6HJR4|A0A8B6HJR4_MYTGA	A0A8B6HJR4	Dynein light chain	2	P1114
tr|A0A8B6HJS6|A0A8B6HJS6_MYTGA	A0A8B6HJS6	Elongin-C	2	P1115
tr|A0A8B6HL49|A0A8B6HL49_MYTGA	A0A8B6HL49	Ubiquitin-conjugating enzyme E2 L3	2	P1116
tr|A0A8B6HLR6|A0A8B6HLR6_MYTGA	A0A8B6HLR6	Thioredoxin	2	P1117
tr|A0A8B6HLV6|A0A8B6HLV6_MYTGA	A0A8B6HLV6	Rho GDP-dissociation inhibitor	2	P1118
tr|A0A8B6HLY7|A0A8B6HLY7_MYTGA	A0A8B6HLY7	Uncharacterized protein	2	P1119
tr|A0A8B6HMG6|A0A8B6HMG6_MYTGA	A0A8B6HMG6	4-trimethylaminobutyraldehyde dehydrogenase	2	P1120
tr|A0A8B6HND2|A0A8B6HND2_MYTGA	A0A8B6HND2	Ras-related protein Rab-1A	2	P1121
tr|A0A8B6HNG8|A0A8B6HNG8_MYTGA	A0A8B6HNG8	proline--tRNA ligase	2	P1122
tr|A0A8B6HNU7|A0A8B6HNU7_MYTGA	A0A8B6HNU7	VWFD domain-containing protein	2	P1123
tr|A0A8B6HNV5|A0A8B6HNV5_MYTGA	A0A8B6HNV5	Uncharacterized protein	2	P1124
tr|A0A8B6HP07|A0A8B6HP07_MYTGA	A0A8B6HP07	Glycogenin glucosyltransferase	2	P1125
tr|A0A8B6HP84|A0A8B6HP84_MYTGA	A0A8B6HP84	Phosphatidylinositol transfer protein	2	P1126
tr|A0A8B6HP87|A0A8B6HP87_MYTGA	A0A8B6HP87	NIPSNAP domain-containing protein	2	P1127
tr|A0A8B6HPM6|A0A8B6HPM6_MYTGA	A0A8B6HPM6	Iron-binding zinc finger CDGSH type domain-containing pro	2	P1128
tr|A0A8B6HT71|A0A8B6HT71_MYTGA	A0A8B6HT71	Uncharacterized protein	2	P1129
tr|A0A8B6HTD5|A0A8B6HTD5_MYTGA	A0A8B6HTD5	Troponin I	2	P1130

Protein	Uniprot accession	Protein Name	Number Peptides	P
tr|B6ZCB1|B6ZCB1_MYTGA	B6ZCB1	Large ribosomal subunit protein P2	2	P1131
tr|E5KXE3|E5KXE3_MYTGA	E5KXE3	Fibrinogen-related protein	2	P1132
tr|F0V449|F0V449_MYTGA	F0V449	Putative C1q domain containing protein MgC1q12	2	P1133
tr|F0V458|F0V458_MYTGA	F0V458	Putative C1q domain containing protein MgC1q21	2	P1134
tr|F0V464|F0V464_MYTGA	F0V464	Putative C1q domain containing protein MgC1q27	2	P1135
tr|F0V481|F0V481_MYTGA	F0V481	Putative C1q domain containing protein MgC1q44	2	P1136
tr|G0YL87|G0YL87_MYTGA	G0YL87	Apextrin-like protein	2	P1137
tr|G5D8W3|G5D8W3_MYTGA	G5D8W3	fructose-bisphosphate aldolase (Fragment)	2	P1138
tr|N0E3R7|N0E3R7_MYTGA	N0E3R7	Enkurin	2	P1139
tr|U3GM45|U3GM45_MYTGA	U3GM45	17 beta-hydroxysteroid dehydrogenase 10	2	P1140
tr|V9P9M1|V9P9M1_MYTGA	V9P9M1	MAP kinase p38-like protein	2	P1141
tr|W5XU87|W5XU87_MYTGA	W5XU87	Toll interacting protein	2	P1142
tr|A0A0C5PIV4|A0A0C5PIV4_MYTGA	A0A0C5PIV4	Allograft inflammatory factor-1	1	P1143
tr|A0A0C5PIY0|A0A0C5PIY0_MYTGA	A0A0C5PIY0	TNF ligand-like 1	1	P1144
tr|A0A0C5PRK9|A0A0C5PRK9_MYTGA	A0A0C5PRK9	MACPF domain-containing protein 7	1	P1145
tr|A0A0C5Q4H8|A0A0C5Q4H8_MYTGA	A0A0C5Q4H8	Stimulator of interferon protein 1	1	P1146
tr|A0A0K0PV08|A0A0K0PV08_MYTGA	A0A0K0PV08	Nacre apextrin-like protein 1	1	P1147
tr|A0A0K0YB43|A0A0K0YB43_MYTGA	A0A0K0YB43	Collagen-like protein-7 (Fragment)	1	P1148
tr|A0A0K0YB45|A0A0K0YB45_MYTGA	A0A0K0YB45	Transgelin-like protein-2	1	P1149
tr|A0A126Q9B1|A0A126Q9B1_MYTGA	A0A126Q9B1	MG_CNOT3	1	P1150
tr|A0A140D2S1|A0A140D2S1_MYTGA	A0A140D2S1	eIF4G (Fragment)	1	P1151
tr|A0A140D2S2|A0A140D2S2_MYTGA	A0A140D2S2	Polyadenylate-binding protein	1	P1152
tr|A0A3L5TR45|A0A3L5TR45_MYTGA	A0A3L5TR45	cystathionine gamma-lyase (Fragment)	1	P1153
tr|A0A3L5TRL7|A0A3L5TRL7_MYTGA	A0A3L5TRL7	Interferon-related developmental regulator N-terminal dom	1	P1154
tr|A0A3L5TS86|A0A3L5TS86_MYTGA	A0A3L5TS86	C-type lectin domain-containing protein (Fragment)	1	P1155
tr|A0A3L5TSE4|A0A3L5TSE4_MYTGA	A0A3L5TSE4	2-hydroxyacyl-CoA lyase 2 (Fragment)	1	P1156
tr|A0A3L5TTK6|A0A3L5TTK6_MYTGA	A0A3L5TTK6	Stomatin-like 2-like protein (Fragment)	1	P1157
tr|A0A3L5TUU9|A0A3L5TUU9_MYTGA	A0A3L5TUU9	Apextrin C-terminal domain-containing protein (Fragment)	1	P1158
tr|A0A3L5TVJ6|A0A3L5TVJ6_MYTGA	A0A3L5TVJ6	Tetratricopeptide repeat protein 38 (Fragment)	1	P1159
tr|A0A3R5SUI1|A0A3R5SUI1_MYTGA	A0A3R5SUI1	D-dopachrome decarboxylase	1	P1160
tr|A0A409V6S9|A0A409V6S9_MYTGA	A0A409V6S9	Uncharacterized protein (Fragment)	1	P1161
tr|A0A410GSX6|A0A410GSX6_MYTGA	A0A410GSX6	D-dopachrome decarboxylase	1	P1162
tr|A0A8B6BDY5|A0A8B6BDY5_MYTGA	A0A8B6BDY5	ubiquitinyl hydrolase 1	1	P1163
tr|A0A8B6BFJ2|A0A8B6BFJ2_MYTGA	A0A8B6BFJ2	GST N-terminal domain-containing protein	1	P1164
tr|A0A8B6BFM8|A0A8B6BFM8_MYTGA	A0A8B6BFM8	Cell division control protein 42	1	P1165
tr|A0A8B6BG31|A0A8B6BG31_MYTGA	A0A8B6BG31	Ras homolog enriched in brain	1	P1166
tr|A0A8B6BG61|A0A8B6BG61_MYTGA	A0A8B6BG61	Mitochondrial import inner membrane translocase subunit	1	P1167
tr|A0A8B6BGP5|A0A8B6BGP5_MYTGA	A0A8B6BGP5	Uncharacterized protein	1	P1168
tr|A0A8B6BHI6|A0A8B6BHI6_MYTGA	A0A8B6BHI6	Uncharacterized protein	1	P1169
tr|A0A8B6BHJ8|A0A8B6BHJ8_MYTGA	A0A8B6BHJ8	Glucosidase 2 subunit beta	1	P1170
tr|A0A8B6BHP5|A0A8B6BHP5_MYTGA	A0A8B6BHP5	BTB/POZ domain-containing protein 16	1	P1171
tr|A0A8B6BHT0|A0A8B6BHT0_MYTGA	A0A8B6BHT0	C1q domain-containing protein	1	P1172
tr|A0A8B6BI43|A0A8B6BI43_MYTGA	A0A8B6BI43	Wiskott-Aldrich syndrome protein	1	P1173
tr|A0A8B6BIF3|A0A8B6BIF3_MYTGA	A0A8B6BIF3	Signal recognition particle subunit SRP72	1	P1174
tr|A0A8B6BIR1|A0A8B6BIR1_MYTGA	A0A8B6BIR1	2-oxo-4-hydroxy-4-carboxy-5-ureidoimidazoline decarboxyl	1	P1175
tr|A0A8B6BJ63|A0A8B6BJ63_MYTGA	A0A8B6BJ63	Uncharacterized protein	1	P1176
tr|A0A8B6BJ87|A0A8B6BJ87_MYTGA	A0A8B6BJ87	Epimerase family protein SDR39U1	1	P1177
tr|A0A8B6BJL7|A0A8B6BJL7_MYTGA	A0A8B6BJL7	Cytochrome b5 heme-binding domain-containing protein	1	P1178
tr|A0A8B6BJM8|A0A8B6BJM8_MYTGA	A0A8B6BJM8	NAD(P)H-hydrate epimerase	1	P1179
tr|A0A8B6BJX7|A0A8B6BJX7_MYTGA	A0A8B6BJX7	Histone H1/5	1	P1180
tr|A0A8B6BK20|A0A8B6BK20_MYTGA	A0A8B6BK20	Laminin G domain-containing protein	1	P1181
tr|A0A8B6BKA3|A0A8B6BKA3_MYTGA	A0A8B6BKA3	Leucine-rich repeat-containing protein 16	1	P1182
tr|A0A8B6BKC9|A0A8B6BKC9_MYTGA	A0A8B6BKC9	Spermidine synthase	1	P1183
tr|A0A8B6BL09|A0A8B6BL09_MYTGA	A0A8B6BL09	Small ribosomal subunit protein eS24 (Fragment)	1	P1184
tr|A0A8B6BL13|A0A8B6BL13_MYTGA	A0A8B6BL13	Cilia- and flagella-associated protein 53	1	P1185
tr|A0A8B6BL78|A0A8B6BL78_MYTGA	A0A8B6BL78	Outer membrane protein insertion porin family	1	P1186
tr|A0A8B6BML0|A0A8B6BML0_MYTGA	A0A8B6BML0	Serine/arginine-rich splicing factor 2	1	P1187
tr|A0A8B6BNH3|A0A8B6BNH3_MYTGA	A0A8B6BNH3	Prefoldin subunit 2	1	P1188
tr|A0A8B6BNN2|A0A8B6BNN2_MYTGA	A0A8B6BNN2	histidine--tRNA ligase	1	P1189
tr|A0A8B6BNQ4|A0A8B6BNQ4_MYTGA	A0A8B6BNQ4	CH-like domain-containing protein	1	P1190
tr|A0A8B6BNW8|A0A8B6BNW8_MYTGA	A0A8B6BNW8	AIG1-type G domain-containing protein	1	P1191
tr|A0A8B6BPQ2|A0A8B6BPQ2_MYTGA	A0A8B6BPQ2	Minor histocompatibility antigen H13	1	P1192
tr|A0A8B6BPW4|A0A8B6BPW4_MYTGA	A0A8B6BPW4	DnaJ homolog subfamily C member 3	1	P1193
tr|A0A8B6BPZ6|A0A8B6BPZ6_MYTGA	A0A8B6BPZ6	Transmembrane 9 superfamily member (Fragment)	1	P1194
tr|A0A8B6BQ75|A0A8B6BQ75_MYTGA	A0A8B6BQ75	Band 7 domain-containing protein	1	P1195
tr|A0A8B6BQ82|A0A8B6BQ82_MYTGA	A0A8B6BQ82	5'-AMP-activated protein kinase, regulatory beta subunit	1	P1196
tr|A0A8B6BQB2|A0A8B6BQB2_MYTGA	A0A8B6BQB2	Tryptophan 2,3-dioxygenase	1	P1197
tr|A0A8B6BQK6|A0A8B6BQK6_MYTGA	A0A8B6BQK6	Ubiquitin-like 1-activating enzyme E1 A	1	P1198
tr|A0A8B6BQU4|A0A8B6BQU4_MYTGA	A0A8B6BQU4	C1q domain-containing protein	1	P1199
tr|A0A8B6BQU5|A0A8B6BQU5_MYTGA	A0A8B6BQU5	Uncharacterized protein	1	P1200
tr|A0A8B6BRF2|A0A8B6BRF2_MYTGA	A0A8B6BRF2	carbamoyl-phosphate synthase (glutamine-hydrolyzing) (Fra	1	P1201
tr|A0A8B6BRK1|A0A8B6BRK1_MYTGA	A0A8B6BRK1	MIR domain-containing protein	1	P1202
tr|A0A8B6BS24|A0A8B6BS24_MYTGA	A0A8B6BS24	PLAC domain-containing protein	1	P1203
tr|A0A8B6BS62|A0A8B6BS62_MYTGA	A0A8B6BS62	Lipocalin/cytosolic fatty-acid binding domain-containing pr	1	P1204
tr|A0A8B6BSE8|A0A8B6BSE8_MYTGA	A0A8B6BSE8	Solute carrier family 26, member 5	1	P1205
tr|A0A8B6BSP7|A0A8B6BSP7_MYTGA	A0A8B6BSP7	Phosphatidylinositol-4,5-bisphosphate 3-kinase	1	P1206
tr|A0A8B6BSQ3|A0A8B6BSQ3_MYTGA	A0A8B6BSQ3	Coiled-coil domain-containing protein 170	1	P1207
tr|A0A8B6BSW4|A0A8B6BSW4_MYTGA	A0A8B6BSW4	C-factor	1	P1208
tr|A0A8B6BSY8|A0A8B6BSY8_MYTGA	A0A8B6BSY8	Transmembrane 9 superfamily member	1	P1209
tr|A0A8B6BT26|A0A8B6BT26_MYTGA	A0A8B6BT26	1-phosphatidylinositol-5-phosphate 4-kinase	1	P1210
tr|A0A8B6BT61|A0A8B6BT61_MYTGA	A0A8B6BT61	DUF4515 domain-containing protein	1	P1211
tr|A0A8B6BTE6|A0A8B6BTE6_MYTGA	A0A8B6BTE6	Large ribosomal subunit protein P1	1	P1212
tr|A0A8B6BTQ2|A0A8B6BTQ2_MYTGA	A0A8B6BTQ2	Small ribosomal subunit protein uS10	1	P1213
tr|A0A8B6BU83|A0A8B6BU83_MYTGA	A0A8B6BU83	Uncharacterized protein	1	P1214
tr|A0A8B6BUZ7|A0A8B6BUZ7_MYTGA	A0A8B6BUZ7	WD repeat-containing protein 35	1	P1215
tr|A0A8B6BV11|A0A8B6BV11_MYTGA	A0A8B6BV11	Ras homolog gene family, member A	1	P1216
tr|A0A8B6BVJ9|A0A8B6BVJ9_MYTGA	A0A8B6BVJ9	Dehydrogenase/reductase SDR family member 1	1	P1217
tr|A0A8B6BWA7|A0A8B6BWA7_MYTGA	A0A8B6BWA7	Uncharacterized protein	1	P1218
tr|A0A8B6BWE2|A0A8B6BWE2_MYTGA	A0A8B6BWE2	Tubulin beta chain	1	P1219
tr|A0A8B6BWL8|A0A8B6BWL8_MYTGA	A0A8B6BWL8	Mediator of RNA polymerase II transcription subunit 14	1	P1220
tr|A0A8B6BX34|A0A8B6BX34_MYTGA	A0A8B6BX34	Uncharacterized protein	1	P1221
tr|A0A8B6BX68|A0A8B6BX68_MYTGA	A0A8B6BX68	Centrin-1	1	P1222
tr|A0A8B6BXM3|A0A8B6BXM3_MYTGA	A0A8B6BXM3	FYVE-type domain-containing protein	1	P1223
tr|A0A8B6BXQ6|A0A8B6BXQ6_MYTGA	A0A8B6BXQ6	RRM domain-containing protein	1	P1224
tr|A0A8B6BYG9|A0A8B6BYG9_MYTGA	A0A8B6BYG9	General vesicular transport factor p115	1	P1225
tr|A0A8B6BYT9|A0A8B6BYT9_MYTGA	A0A8B6BYT9	YidC/Oxa1 family membrane protein insertase	1	P1226
tr|A0A8B6BZ44|A0A8B6BZ44_MYTGA	A0A8B6BZ44	DNA excision repair protein ERCC-6-like	1	P1227
tr|A0A8B6BZ95|A0A8B6BZ95_MYTGA	A0A8B6BZ95	Signal peptidase complex catalytic subunit SEC11	1	P1228
tr|A0A8B6BZH3|A0A8B6BZH3_MYTGA	A0A8B6BZH3	ATP-dependent RNA helicase DOB1	1	P1229
tr|A0A8B6BZI3|A0A8B6BZI3_MYTGA	A0A8B6BZI3	DNA polymerase	1	P1230
tr|A0A8B6BZN7|A0A8B6BZN7_MYTGA	A0A8B6BZN7	Transmembrane protein 59	1	P1231
tr|A0A8B6BZS7|A0A8B6BZS7_MYTGA	A0A8B6BZS7	Tetratricopeptide repeat protein 5 OB fold domain-containi	1	P1232
tr|A0A8B6BZT7|A0A8B6BZT7_MYTGA	A0A8B6BZT7	RRM domain-containing protein	1	P1233
tr|A0A8B6C004|A0A8B6C004_MYTGA	A0A8B6C004	Bleomycin hydrolase	1	P1234
tr|A0A8B6C036|A0A8B6C036_MYTGA	A0A8B6C036	Ras-related protein Rab-18	1	P1235
tr|A0A8B6C0B6|A0A8B6C0B6_MYTGA	A0A8B6C0B6	Purine nucleoside phosphorylase	1	P1236
tr|A0A8B6C0H5|A0A8B6C0H5_MYTGA	A0A8B6C0H5	DNA polymerase delta subunit 2 (Fragment)	1	P1237
tr|A0A8B6C168|A0A8B6C168_MYTGA	A0A8B6C168	alpha-L-fucosidase	1	P1238
tr|A0A8B6C1D1|A0A8B6C1D1_MYTGA	A0A8B6C1D1	Ubiquitin-conjugating enzyme E2 variant (Fragment)	1	P1239
tr|A0A8B6C249|A0A8B6C249_MYTGA	A0A8B6C249	Receptor expression-enhancing protein	1	P1240
tr|A0A8B6C278|A0A8B6C278_MYTGA	A0A8B6C278	Lethal(2) giant larvae protein	1	P1241
tr|A0A8B6C295|A0A8B6C295_MYTGA	A0A8B6C295	Receptor expression-enhancing protein	1	P1242
tr|A0A8B6C2M5|A0A8B6C2M5_MYTGA	A0A8B6C2M5	U6 snRNA-associated Sm-like protein LSm2	1	P1243
tr|A0A8B6C3D2|A0A8B6C3D2_MYTGA	A0A8B6C3D2	Mitochondrial pyruvate carrier	1	P1244
tr|A0A8B6C3K4|A0A8B6C3K4_MYTGA	A0A8B6C3K4	mRNA m(6)A methyltransferase	1	P1245
tr|A0A8B6C3T8|A0A8B6C3T8_MYTGA	A0A8B6C3T8	Tyrosine-protein kinase	1	P1246
tr|A0A8B6C449|A0A8B6C449_MYTGA	A0A8B6C449	HIG1 domain-containing protein	1	P1247

Protein	Uniprot accession	Protein Name	Number Peptides	P
tr|A0A8B6C4I0|A0A8B6C4I0_MYTGA	A0A8B6C4I0	Myosin I	1	P1248
tr|A0A8B6C4L0|A0A8B6C4L0_MYTGA	A0A8B6C4L0	Band 7 domain-containing protein	1	P1249
tr|A0A8B6C4L7|A0A8B6C4L7_MYTGA	A0A8B6C4L7	Transcriptional coactivator p15 (PC4) C-terminal domain-co	1	P1250
tr|A0A8B6C4T2|A0A8B6C4T2_MYTGA	A0A8B6C4T2	Thyroglobulin type-1 domain-containing protein	1	P1251
tr|A0A8B6C511|A0A8B6C511_MYTGA	A0A8B6C511	Uncharacterized protein	1	P1252
tr|A0A8B6C541|A0A8B6C541_MYTGA	A0A8B6C541	Coatomer subunit epsilon	1	P1253
tr|A0A8B6C544|A0A8B6C544_MYTGA	A0A8B6C544	CD151 antigen	1	P1254
tr|A0A8B6C5E6|A0A8B6C5E6_MYTGA	A0A8B6C5E6	ADP-dependent glucokinase	1	P1255
tr|A0A8B6C5G7|A0A8B6C5G7_MYTGA	A0A8B6C5G7	Acetyl-CoA acyltransferase 2	1	P1256
tr|A0A8B6C5I5|A0A8B6C5I5_MYTGA	A0A8B6C5I5	Calpain-5	1	P1257
tr|A0A8B6C5K4|A0A8B6C5K4_MYTGA	A0A8B6C5K4	alpha-L-fucosidase	1	P1258
tr|A0A8B6C5R6|A0A8B6C5R6_MYTGA	A0A8B6C5R6	Lysosomal-associated membrane protein 1/2	1	P1259
tr|A0A8B6C639|A0A8B6C639_MYTGA	A0A8B6C639	Cleavage and polyadenylation specificity factor subunit 5	1	P1260
tr|A0A8B6C6D8|A0A8B6C6D8_MYTGA	A0A8B6C6D8	Tetratricopeptide repeat protein 21B	1	P1261
tr|A0A8B6C757|A0A8B6C757_MYTGA	A0A8B6C757	Large ribosomal subunit protein eL24	1	P1262
tr|A0A8B6C789|A0A8B6C789_MYTGA	A0A8B6C789	Beta-lactamase-related domain-containing protein	1	P1263
tr|A0A8B6C7M5|A0A8B6C7M5_MYTGA	A0A8B6C7M5	Large ribosomal subunit protein uL24 (Fragment)	1	P1264
tr|A0A8B6C7Q5|A0A8B6C7Q5_MYTGA	A0A8B6C7Q5	Isocitrate dehydrogenase [NADP]	1	P1265
tr|A0A8B6C7Y2|A0A8B6C7Y2_MYTGA	A0A8B6C7Y2	NACHT domain-containing protein	1	P1266
tr|A0A8B6C851|A0A8B6C851_MYTGA	A0A8B6C851	Fatty acid amide hydrolase 2	1	P1267
tr|A0A8B6C8M6|A0A8B6C8M6_MYTGA	A0A8B6C8M6	Secretory carrier-associated membrane protein	1	P1268
tr|A0A8B6C999|A0A8B6C999_MYTGA	A0A8B6C999	Gelsolin-like domain-containing protein	1	P1269
tr|A0A8B6C9J5|A0A8B6C9J5_MYTGA	A0A8B6C9J5	ADP-ribosyl cyclase/cyclic ADP-ribose hydrolase	1	P1270
tr|A0A8B6C9P6|A0A8B6C9P6_MYTGA	A0A8B6C9P6	DUF4455 domain-containing protein	1	P1271
tr|A0A8B6C9W6|A0A8B6C9W6_MYTGA	A0A8B6C9W6	Ribosomal protein L19 (Fragment)	1	P1272
tr|A0A8B6CA31|A0A8B6CA31_MYTGA	A0A8B6CA31	Arachidonate 5-lipoxygenase	1	P1273
tr|A0A8B6CAD3|A0A8B6CAD3_MYTGA	A0A8B6CAD3	Dual oxidase maturation factor 1	1	P1274
tr|A0A8B6CAQ7|A0A8B6CAQ7_MYTGA	A0A8B6CAQ7	RRM domain-containing protein	1	P1275
tr|A0A8B6CAT0|A0A8B6CAT0_MYTGA	A0A8B6CAT0	Ubiquitin carboxyl-terminal hydrolase 7	1	P1276
tr|A0A8B6CAT4|A0A8B6CAT4_MYTGA	A0A8B6CAT4	cellulase	1	P1277
tr|A0A8B6CAV0|A0A8B6CAV0_MYTGA	A0A8B6CAV0	ADP-ribosylhydrolase ARH3	1	P1278
tr|A0A8B6CAW2|A0A8B6CAW2_MYTGA	A0A8B6CAW2	TNF receptor-associated protein 1	1	P1279
tr|A0A8B6CB09|A0A8B6CB09_MYTGA	A0A8B6CB09	Uncharacterized protein	1	P1280
tr|A0A8B6CBH0|A0A8B6CBH0_MYTGA	A0A8B6CBH0	ADF-H domain-containing protein	1	P1281
tr|A0A8B6CBI6|A0A8B6CBI6_MYTGA	A0A8B6CBI6	alanine transaminase	1	P1282
tr|A0A8B6CC11|A0A8B6CC11_MYTGA	A0A8B6CC11	Uncharacterized protein	1	P1283
tr|A0A8B6CCB2|A0A8B6CCB2_MYTGA	A0A8B6CCB2	Delta-aminolevulinic acid dehydratase	1	P1284
tr|A0A8B6CCH6|A0A8B6CCH6_MYTGA	A0A8B6CCH6	Ferritin	1	P1285
tr|A0A8B6CCQ6|A0A8B6CCQ6_MYTGA	A0A8B6CCQ6	Apple domain-containing protein	1	P1286
tr|A0A8B6CD15|A0A8B6CD15_MYTGA	A0A8B6CD15	dTMP kinase	1	P1287
tr|A0A8B6CD16|A0A8B6CD16_MYTGA	A0A8B6CD16	2Fe-2S ferredoxin-type domain-containing protein	1	P1288
tr|A0A8B6CD57|A0A8B6CD57_MYTGA	A0A8B6CD57	CCR4-NOT transcription complex subunit 9	1	P1289
tr|A0A8B6CDJ8|A0A8B6CDJ8_MYTGA	A0A8B6CDJ8	Fatty acid-binding protein 7, brain	1	P1290
tr|A0A8B6CDM1|A0A8B6CDM1_MYTGA	A0A8B6CDM1	Calponin-homology (CH) domain-containing protein	1	P1291
tr|A0A8B6CDR3|A0A8B6CDR3_MYTGA	A0A8B6CDR3	14-3-3 protein gamma/eta	1	P1292
tr|A0A8B6CDS3|A0A8B6CDS3_MYTGA	A0A8B6CDS3	NADPH2:quinone reductase	1	P1293
tr|A0A8B6CDZ4|A0A8B6CDZ4_MYTGA	A0A8B6CDZ4	N-terminal acetyltransferase B complex non-catalytic subuni	1	P1294
tr|A0A8B6CEB8|A0A8B6CEB8_MYTGA	A0A8B6CEB8	ATP-dependent DNA helicase 2 subunit 2	1	P1295
tr|A0A8B6CEL3|A0A8B6CEL3_MYTGA	A0A8B6CEL3	Uncharacterized protein	1	P1296
tr|A0A8B6CEP5|A0A8B6CEP5_MYTGA	A0A8B6CEP5	Purple acid phosphatase	1	P1297
tr|A0A8B6CET6|A0A8B6CET6_MYTGA	A0A8B6CET6	LRP2-binding protein	1	P1298
tr|A0A8B6CEY4|A0A8B6CEY4_MYTGA	A0A8B6CEY4	Calcyclin-binding protein	1	P1299
tr|A0A8B6CF55|A0A8B6CF55_MYTGA	A0A8B6CF55	Uncharacterized protein	1	P1300
tr|A0A8B6CFG3|A0A8B6CFG3_MYTGA	A0A8B6CFG3	Cytosolic prostaglandin-E synthase	1	P1301
tr|A0A8B6CFI8|A0A8B6CFI8_MYTGA	A0A8B6CFI8	Sec1 family domain-containing protein 1	1	P1302
tr|A0A8B6CFM7|A0A8B6CFM7_MYTGA	A0A8B6CFM7	V-type H+-transporting ATPase S1 subunit	1	P1303
tr|A0A8B6CFP1|A0A8B6CFP1_MYTGA	A0A8B6CFP1	Protein kish	1	P1304
tr|A0A8B6CFP4|A0A8B6CFP4_MYTGA	A0A8B6CFP4	Cilia- and flagella-associated protein 69 ARM repeats domair	1	P1305
tr|A0A8B6CFT9|A0A8B6CFT9_MYTGA	A0A8B6CFT9	NADH dehydrogenase [ubiquinone] 1 beta subcomplex subu	1	P1306
tr|A0A8B6CFU8|A0A8B6CFU8_MYTGA	A0A8B6CFU8	Uncharacterized protein	1	P1307
tr|A0A8B6CGB8|A0A8B6CGB8_MYTGA	A0A8B6CGB8	ATP-binding cassette, subfamily F, member 3	1	P1308
tr|A0A8B6CGM4|A0A8B6CGM4_MYTGA	A0A8B6CGM4	La-related protein 1	1	P1309
tr|A0A8B6CGQ8|A0A8B6CGQ8_MYTGA	A0A8B6CGQ8	Uncharacterized protein	1	P1310
tr|A0A8B6CGY0|A0A8B6CGY0_MYTGA	A0A8B6CGY0	Lectin, mannose-binding 1 (Fragment)	1	P1311
tr|A0A8B6CGZ2|A0A8B6CGZ2_MYTGA	A0A8B6CGZ2	RNA helicase	1	P1312
tr|A0A8B6CGZ7|A0A8B6CGZ7_MYTGA	A0A8B6CGZ7	Suppressor of G2 allele of SKP1	1	P1313
tr|A0A8B6CH01|A0A8B6CH01_MYTGA	A0A8B6CH01	Vesicle-associated membrane protein 7	1	P1314
tr|A0A8B6CHF5|A0A8B6CHF5_MYTGA	A0A8B6CHF5	GDP-fucose protein O-fucosyltransferase 2 (Fragment)	1	P1315
tr|A0A8B6CIJ9|A0A8B6CIJ9_MYTGA	A0A8B6CIJ9	Phosphoglucomutase / phosphopentomutase	1	P1316
tr|A0A8B6CIS3|A0A8B6CIS3_MYTGA	A0A8B6CIS3	All-trans-retinol dehydrogenase (NAD+)	1	P1317
tr|A0A8B6CJ24|A0A8B6CJ24_MYTGA	A0A8B6CJ24	Uncharacterized protein (Fragment)	1	P1318
tr|A0A8B6CJE0|A0A8B6CJE0_MYTGA	A0A8B6CJE0	Chromo domain-containing protein	1	P1319
tr|A0A8B6CJU8|A0A8B6CJU8_MYTGA	A0A8B6CJU8	Uncharacterized protein	1	P1320
tr|A0A8B6CK63|A0A8B6CK63_MYTGA	A0A8B6CK63	40S ribosomal protein S21	1	P1321
tr|A0A8B6CL56|A0A8B6CL56_MYTGA	A0A8B6CL56	DNA primase small subunit	1	P1322
tr|A0A8B6CLT6|A0A8B6CLT6_MYTGA	A0A8B6CLT6	AP-2 complex subunit mu-1	1	P1323
tr|A0A8B6CM15|A0A8B6CM15_MYTGA	A0A8B6CM15	60S ribosomal protein L27	1	P1324
tr|A0A8B6CM37|A0A8B6CM37_MYTGA	A0A8B6CM37	Cysteine synthase A	1	P1325
tr|A0A8B6CM42|A0A8B6CM42_MYTGA	A0A8B6CM42	Uncharacterized protein	1	P1326
tr|A0A8B6CM73|A0A8B6CM73_MYTGA	A0A8B6CM73	Coronin	1	P1327
tr|A0A8B6CM89|A0A8B6CM89_MYTGA	A0A8B6CM89	SEL1 protein	1	P1328
tr|A0A8B6CMH0|A0A8B6CMH0_MYTGA	A0A8B6CMH0	U3 small nucleolar RNA-associated protein 19	1	P1329
tr|A0A8B6CMI5|A0A8B6CMI5_MYTGA	A0A8B6CMI5	polynucleotide adenylyltransferase	1	P1330
tr|A0A8B6CMJ9|A0A8B6CMJ9_MYTGA	A0A8B6CMJ9	Splicing factor, arginine/serine-rich 16	1	P1331
tr|A0A8B6CMR2|A0A8B6CMR2_MYTGA	A0A8B6CMR2	Dyskerin-like domain-containing protein	1	P1332
tr|A0A8B6CMS6|A0A8B6CMS6_MYTGA	A0A8B6CMS6	Agmatinase	1	P1333
tr|A0A8B6CNH6|A0A8B6CNH6_MYTGA	A0A8B6CNH6	Metalloendopeptidase	1	P1334
tr|A0A8B6CNP1|A0A8B6CNP1_MYTGA	A0A8B6CNP1	non-specific serine/threonine protein kinase	1	P1335
tr|A0A8B6CNQ7|A0A8B6CNQ7_MYTGA	A0A8B6CNQ7	Uncharacterized protein	1	P1336
tr|A0A8B6CNX2|A0A8B6CNX2_MYTGA	A0A8B6CNX2	Insulysin	1	P1337
tr|A0A8B6CP56|A0A8B6CP56_MYTGA	A0A8B6CP56	Nucleoporin NDC1	1	P1338
tr|A0A8B6CP63|A0A8B6CP63_MYTGA	A0A8B6CP63	Small nuclear ribonucleoprotein E	1	P1339
tr|A0A8B6CP94|A0A8B6CP94_MYTGA	A0A8B6CP94	Glycogen synthase kinase 3 beta	1	P1340
tr|A0A8B6CPB8|A0A8B6CPB8_MYTGA	A0A8B6CPB8	Uncharacterized protein	1	P1341
tr|A0A8B6CPH4|A0A8B6CPH4_MYTGA	A0A8B6CPH4	Nuclear pore complex protein Nup210 (Fragment)	1	P1342
tr|A0A8B6CPK8|A0A8B6CPK8_MYTGA	A0A8B6CPK8	EF-hand domain-containing protein (Fragment)	1	P1343
tr|A0A8B6CPP5|A0A8B6CPP5_MYTGA	A0A8B6CPP5	Tetratricopeptide repeat protein 30	1	P1344
tr|A0A8B6CQD8|A0A8B6CQD8_MYTGA	A0A8B6CQD8	COP9 signalosome complex subunit 6	1	P1345
tr|A0A8B6CQL0|A0A8B6CQL0_MYTGA	A0A8B6CQL0	Triokinase/FMN cyclase	1	P1346
tr|A0A8B6CQT8|A0A8B6CQT8_MYTGA	A0A8B6CQT8	Uncharacterized protein	1	P1347
tr|A0A8B6CQV7|A0A8B6CQV7_MYTGA	A0A8B6CQV7	Coiled-coil domain-containing protein 146	1	P1348
tr|A0A8B6CR00|A0A8B6CR00_MYTGA	A0A8B6CR00	Sperm-tail PG-rich repeat-containing protein 2	1	P1349
tr|A0A8B6CS94|A0A8B6CS94_MYTGA	A0A8B6CS94	Abhydrolase domain-containing protein 14	1	P1350
tr|A0A8B6CSD0|A0A8B6CSD0_MYTGA	A0A8B6CSD0	Rho GTPase-activating protein 17/44	1	P1351
tr|A0A8B6CSF1|A0A8B6CSF1_MYTGA	A0A8B6CSF1	Deltamethrin resistance protein prag01 domain-containing	1	P1352
tr|A0A8B6CSN9|A0A8B6CSN9_MYTGA	A0A8B6CSN9	N-acetyl-D-glucosamine kinase	1	P1353
tr|A0A8B6CT34|A0A8B6CT34_MYTGA	A0A8B6CT34	Phospholipase B-like	1	P1354
tr|A0A8B6CTD7|A0A8B6CTD7_MYTGA	A0A8B6CTD7	2-oxoisovalerate dehydrogenase E1 component beta subuni	1	P1355
tr|A0A8B6CTR2|A0A8B6CTR2_MYTGA	A0A8B6CTR2	VWFA domain-containing protein	1	P1356
tr|A0A8B6CTX1|A0A8B6CTX1_MYTGA	A0A8B6CTX1	Acetyl-coenzyme A synthetase	1	P1357
tr|A0A8B6CTY9|A0A8B6CTY9_MYTGA	A0A8B6CTY9	BTB/POZ domain-containing protein 7	1	P1358
tr|A0A8B6CUP1|A0A8B6CUP1_MYTGA	A0A8B6CUP1	Methionyl aminopeptidase	1	P1359
tr|A0A8B6CUP7|A0A8B6CUP7_MYTGA	A0A8B6CUP7	Ras-related protein Rab-14	1	P1360
tr|A0A8B6CUV3|A0A8B6CUV3_MYTGA	A0A8B6CUV3	IMP dehydrogenase	1	P1361
tr|A0A8B6CUX6|A0A8B6CUX6_MYTGA	A0A8B6CUX6	C-type lectin domain-containing protein	1	P1362
tr|A0A8B6CVG1|A0A8B6CVG1_MYTGA	A0A8B6CVG1	Dystroglycan 1	1	P1363
tr|A0A8B6CVJ0|A0A8B6CVJ0_MYTGA	A0A8B6CVJ0	CARD domain-containing protein	1	P1364

Protein	Uniprot accession	Protein Name	Number Peptides	P
tr|A0A8B6CVW7|A0A8B6CVW7_MYTGA	A0A8B6CVW7	Ricin B lectin domain-containing protein	1	P1365
tr|A0A8B6CW29|A0A8B6CW29_MYTGA	A0A8B6CW29	Actin related protein 2/3 complex, subunit 3	1	P1366
tr|A0A8B6CW59|A0A8B6CW59_MYTGA	A0A8B6CW59	MYND-type domain-containing protein	1	P1367
tr|A0A8B6CWA6|A0A8B6CWA6_MYTGA	A0A8B6CWA6	Uncharacterized protein	1	P1368
tr|A0A8B6CWT4|A0A8B6CWT4_MYTGA	A0A8B6CWT4	Tubulin alpha chain	1	P1369
tr|A0A8B6CWX9|A0A8B6CWX9_MYTGA	A0A8B6CWX9	Nucleoprotein TPR	1	P1370
tr|A0A8B6CXE7|A0A8B6CXE7_MYTGA	A0A8B6CXE7	Transgelin	1	P1371
tr|A0A8B6CXF0|A0A8B6CXF0_MYTGA	A0A8B6CXF0	Ras association domain-containing protein 2/4	1	P1372
tr|A0A8B6CXG1|A0A8B6CXG1_MYTGA	A0A8B6CXG1	Nucleoprotein TPR	1	P1373
tr|A0A8B6CXJ9|A0A8B6CXJ9_MYTGA	A0A8B6CXJ9	Heterogeneous nuclear ribonucleoprotein U-like protein 1	1	P1374
tr|A0A8B6CXX8|A0A8B6CXX8_MYTGA	A0A8B6CXX8	Antigen KI-67	1	P1375
tr|A0A8B6CY71|A0A8B6CY71_MYTGA	A0A8B6CY71	Protein RFT1 homolog	1	P1376
tr|A0A8B6CY79|A0A8B6CY79_MYTGA	A0A8B6CY79	Stathmin	1	P1377
tr|A0A8B6CYF0|A0A8B6CYF0_MYTGA	A0A8B6CYF0	2-oxoglutarate dehydrogenase, mitochondrial	1	P1378
tr|A0A8B6CYM8|A0A8B6CYM8_MYTGA	A0A8B6CYM8	Uncharacterized protein	1	P1379
tr|A0A8B6CYY9|A0A8B6CYY9_MYTGA	A0A8B6CYY9	TLDc domain-containing protein	1	P1380
tr|A0A8B6CZH3|A0A8B6CZH3_MYTGA	A0A8B6CZH3	C1q domain-containing protein	1	P1381
tr|A0A8B6CZM7|A0A8B6CZM7_MYTGA	A0A8B6CZM7	Calcium-transporting ATPase	1	P1382
tr|A0A8B6CZS1|A0A8B6CZS1_MYTGA	A0A8B6CZS1	Mitochondrial carrier	1	P1383
tr|A0A8B6D0B7|A0A8B6D0B7_MYTGA	A0A8B6D0B7	E2 ubiquitin-conjugating enzyme	1	P1384
tr|A0A8B6D0G2|A0A8B6D0G2_MYTGA	A0A8B6D0G2	Uncharacterized protein	1	P1385
tr|A0A8B6D0P0|A0A8B6D0P0_MYTGA	A0A8B6D0P0	Copper transport protein ATOX1	1	P1386
tr|A0A8B6D0Q7|A0A8B6D0Q7_MYTGA	A0A8B6D0Q7	ADP-ribosylation factor 1	1	P1387
tr|A0A8B6D0S5|A0A8B6D0S5_MYTGA	A0A8B6D0S5	C1q domain-containing protein	1	P1388
tr|A0A8B6D0S6|A0A8B6D0S6_MYTGA	A0A8B6D0S6	26S proteasome regulatory subunit N11	1	P1389
tr|A0A8B6D0T4|A0A8B6D0T4_MYTGA	A0A8B6D0T4	Cytochrome b5 heme-binding domain-containing protein	1	P1390
tr|A0A8B6D0W7|A0A8B6D0W7_MYTGA	A0A8B6D0W7	Mesenchyme-specific cell surface glycoprotein	1	P1391
tr|A0A8B6D100|A0A8B6D100_MYTGA	A0A8B6D100	Heterogeneous nuclear ribonucleoprotein A1/A3	1	P1392
tr|A0A8B6D1A2|A0A8B6D1A2_MYTGA	A0A8B6D1A2	C-type lectin domain-containing protein	1	P1393
tr|A0A8B6D1H1|A0A8B6D1H1_MYTGA	A0A8B6D1H1	Protein farnesyltransferase/geranylgeranyltransferase type-1	1	P1394
tr|A0A8B6D1V3|A0A8B6D1V3_MYTGA	A0A8B6D1V3	Uncharacterized protein	1	P1395
tr|A0A8B6D231|A0A8B6D231_MYTGA	A0A8B6D231	Thioredoxin domain-containing protein	1	P1396
tr|A0A8B6D255|A0A8B6D255_MYTGA	A0A8B6D255	Dimethylargininase	1	P1397
tr|A0A8B6D2J5|A0A8B6D2J5_MYTGA	A0A8B6D2J5	acetyl-CoA C-acetyltransferase	1	P1398
tr|A0A8B6D2M1|A0A8B6D2M1_MYTGA	A0A8B6D2M1	DUF885 domain-containing protein	1	P1399
tr|A0A8B6D2P0|A0A8B6D2P0_MYTGA	A0A8B6D2P0	Phospholipase A-2-activating protein	1	P1400
tr|A0A8B6D2R7|A0A8B6D2R7_MYTGA	A0A8B6D2R7	Fibrillin-2	1	P1401
tr|A0A8B6D2U0|A0A8B6D2U0_MYTGA	A0A8B6D2U0	Amine oxidase domain-containing protein	1	P1402
tr|A0A8B6D2W7|A0A8B6D2W7_MYTGA	A0A8B6D2W7	Alpha-N-acetylglucosaminidase (Fragment)	1	P1403
tr|A0A8B6D2Z8|A0A8B6D2Z8_MYTGA	A0A8B6D2Z8	RNA-binding protein Musashi	1	P1404
tr|A0A8B6D351|A0A8B6D351_MYTGA	A0A8B6D351	F-box and WD-40 domain protein 1/11	1	P1405
tr|A0A8B6D393|A0A8B6D393_MYTGA	A0A8B6D393	Uncharacterized protein	1	P1406
tr|A0A8B6D3G0|A0A8B6D3G0_MYTGA	A0A8B6D3G0	Annexin (Fragment)	1	P1407
tr|A0A8B6D3L1|A0A8B6D3L1_MYTGA	A0A8B6D3L1	Nicotinate phosphoribosyltransferase	1	P1408
tr|A0A8B6D3R9|A0A8B6D3R9_MYTGA	A0A8B6D3R9	Doublecortin domain-containing protein	1	P1409
tr|A0A8B6D406|A0A8B6D406_MYTGA	A0A8B6D406	Solute carrier family 9 (Sodium/hydrogen exchanger), memb	1	P1410
tr|A0A8B6D4F3|A0A8B6D4F3_MYTGA	A0A8B6D4F3	2'-5'-oligoadenylate synthetase 1 domain-containing protein	1	P1411
tr|A0A8B6D4G6|A0A8B6D4G6_MYTGA	A0A8B6D4G6	Heparan sulfate proteoglycan 2 (Perlecan)	1	P1412
tr|A0A8B6D4H3|A0A8B6D4H3_MYTGA	A0A8B6D4H3	TLDc domain-containing protein	1	P1413
tr|A0A8B6D4J4|A0A8B6D4J4_MYTGA	A0A8B6D4J4	Radial spoke head protein 1	1	P1414
tr|A0A8B6D4K7|A0A8B6D4K7_MYTGA	A0A8B6D4K7	NADH dehydrogenase [ubiquinone] 1 alpha subcomplex subu	1	P1415
tr|A0A8B6D4Q1|A0A8B6D4Q1_MYTGA	A0A8B6D4Q1	Solute carrier family 44 (Choline transporter-like protein), m	1	P1416
tr|A0A8B6D540|A0A8B6D540_MYTGA	A0A8B6D540	Zonadhesin	1	P1417
tr|A0A8B6D587|A0A8B6D587_MYTGA	A0A8B6D587	ATP-dependent Clp protease proteolytic subunit	1	P1418
tr|A0A8B6D5D2|A0A8B6D5D2_MYTGA	A0A8B6D5D2	Acylpyruvate hydrolase	1	P1419
tr|A0A8B6D5V2|A0A8B6D5V2_MYTGA	A0A8B6D5V2	peptide-methionine (R)-S-oxide reductase	1	P1420
tr|A0A8B6D5W8|A0A8B6D5W8_MYTGA	A0A8B6D5W8	glycine hydroxymethyltransferase (Fragment)	1	P1421
tr|A0A8B6D618|A0A8B6D618_MYTGA	A0A8B6D618	Large ribosomal subunit protein eL33	1	P1422
tr|A0A8B6D6Q9|A0A8B6D6Q9_MYTGA	A0A8B6D6Q9	Receptor-interacting serine/threonine-protein kinase 1	1	P1423
tr|A0A8B6D6W7|A0A8B6D6W7_MYTGA	A0A8B6D6W7	Deoxyribodipyrimidine photo-lyase	1	P1424
tr|A0A8B6D7H3|A0A8B6D7H3_MYTGA	A0A8B6D7H3	Alkylglycerone-phosphate synthase	1	P1425
tr|A0A8B6D7I5|A0A8B6D7I5_MYTGA	A0A8B6D7I5	Caprin-1	1	P1426
tr|A0A8B6D889|A0A8B6D889_MYTGA	A0A8B6D889	Fibroblast growth factor receptor 3	1	P1427
tr|A0A8B6D8T4|A0A8B6D8T4_MYTGA	A0A8B6D8T4	Armadillo repeat-containing protein 8	1	P1428
tr|A0A8B6D8T9|A0A8B6D8T9_MYTGA	A0A8B6D8T9	Plexin A	1	P1429
tr|A0A8B6D9K2|A0A8B6D9K2_MYTGA	A0A8B6D9K2	P-type domain-containing protein	1	P1430
tr|A0A8B6D9M7|A0A8B6D9M7_MYTGA	A0A8B6D9M7	tryptophan--tRNA ligase	1	P1431
tr|A0A8B6D9X9|A0A8B6D9X9_MYTGA	A0A8B6D9X9	Argininosuccinate lyase	1	P1432
tr|A0A8B6DA50|A0A8B6DA50_MYTGA	A0A8B6DA50	E3 UFM1-protein transferase 1 homolog	1	P1433
tr|A0A8B6DA95|A0A8B6DA95_MYTGA	A0A8B6DA95	Gamma-tubulin complex component	1	P1434
tr|A0A8B6DAA6|A0A8B6DAA6_MYTGA	A0A8B6DAA6	WAP domain-containing protein	1	P1435
tr|A0A8B6DAK2|A0A8B6DAK2_MYTGA	A0A8B6DAK2	Uncharacterized protein	1	P1436
tr|A0A8B6DAL8|A0A8B6DAL8_MYTGA	A0A8B6DAL8	Actin-related protein 2/3 complex subunit 5	1	P1437
tr|A0A8B6DAX4|A0A8B6DAX4_MYTGA	A0A8B6DAX4	LDLR chaperone MESD	1	P1438
tr|A0A8B6DB02|A0A8B6DB02_MYTGA	A0A8B6DB02	26S proteasome regulatory subunit T6	1	P1439
tr|A0A8B6DBP9|A0A8B6DBP9_MYTGA	A0A8B6DBP9	NadR/Ttd14 AAA domain-containing protein	1	P1440
tr|A0A8B6DBQ6|A0A8B6DBQ6_MYTGA	A0A8B6DBQ6	Uncharacterized protein	1	P1441
tr|A0A8B6DBY4|A0A8B6DBY4_MYTGA	A0A8B6DBY4	Growth hormone-inducible transmembrane protein	1	P1442
tr|A0A8B6DBZ7|A0A8B6DBZ7_MYTGA	A0A8B6DBZ7	Short/branched chain specific acyl-CoA dehydrogenase, mit	1	P1443
tr|A0A8B6DC48|A0A8B6DC48_MYTGA	A0A8B6DC48	V-type proton ATPase subunit a	1	P1444
tr|A0A8B6DC85|A0A8B6DC85_MYTGA	A0A8B6DC85	Template-activating factor I	1	P1445
tr|A0A8B6DCM1|A0A8B6DCM1_MYTGA	A0A8B6DCM1	GTP-binding protein SAR1	1	P1446
tr|A0A8B6DCW7|A0A8B6DCW7_MYTGA	A0A8B6DCW7	MAGUK p55 subfamily member 6	1	P1447
tr|A0A8B6DD76|A0A8B6DD76_MYTGA	A0A8B6DD76	Domain of unknown function with conserved HDNR motif d	1	P1448
tr|A0A8B6DDK2|A0A8B6DDK2_MYTGA	A0A8B6DDK2	GTPase KRas	1	P1449
tr|A0A8B6DE93|A0A8B6DE93_MYTGA	A0A8B6DE93	Splicing factor 3A subunit 1	1	P1450
tr|A0A8B6DED3|A0A8B6DED3_MYTGA	A0A8B6DED3	Uncharacterized protein	1	P1451
tr|A0A8B6DEQ8|A0A8B6DEQ8_MYTGA	A0A8B6DEQ8	EF-hand domain-containing protein	1	P1452
tr|A0A8B6DEW5|A0A8B6DEW5_MYTGA	A0A8B6DEW5	Guanylate cyclase	1	P1453
tr|A0A8B6DEY8|A0A8B6DEY8_MYTGA	A0A8B6DEY8	exodeoxyribonuclease III	1	P1454
tr|A0A8B6DFE7|A0A8B6DFE7_MYTGA	A0A8B6DFE7	Uncharacterized protein	1	P1455
tr|A0A8B6DFH9|A0A8B6DFH9_MYTGA	A0A8B6DFH9	acetate--CoA ligase	1	P1456
tr|A0A8B6DFJ0|A0A8B6DFJ0_MYTGA	A0A8B6DFJ0	Insulin-like growth factor 2 mRNA-binding protein 1	1	P1457
tr|A0A8B6DFQ1|A0A8B6DFQ1_MYTGA	A0A8B6DFQ1	acetate--CoA ligase (Fragment)	1	P1458
tr|A0A8B6DFS0|A0A8B6DFS0_MYTGA	A0A8B6DFS0	Rab5-interacting protein	1	P1459
tr|A0A8B6DFV1|A0A8B6DFV1_MYTGA	A0A8B6DFV1	Ras-related protein Rab-21	1	P1460
tr|A0A8B6DG82|A0A8B6DG82_MYTGA	A0A8B6DG82	glutaminyl-peptide cyclotransferase	1	P1461
tr|A0A8B6DGC7|A0A8B6DGC7_MYTGA	A0A8B6DGC7	CD109 antigen	1	P1462
tr|A0A8B6DGF4|A0A8B6DGF4_MYTGA	A0A8B6DGF4	Uncharacterized protein	1	P1463
tr|A0A8B6DGN4|A0A8B6DGN4_MYTGA	A0A8B6DGN4	Nuclear pore complex protein Nup85	1	P1464
tr|A0A8B6DH08|A0A8B6DH08_MYTGA	A0A8B6DH08	Uncharacterized protein	1	P1465
tr|A0A8B6DHA4|A0A8B6DHA4_MYTGA	A0A8B6DHA4	ATP-binding cassette, subfamily F, member 1	1	P1466
tr|A0A8B6DHH4|A0A8B6DHH4_MYTGA	A0A8B6DHH4	CS domain-containing protein	1	P1467
tr|A0A8B6DHI9|A0A8B6DHI9_MYTGA	A0A8B6DHI9	Serrate RNA effector molecule homolog	1	P1468
tr|A0A8B6DHK3|A0A8B6DHK3_MYTGA	A0A8B6DHK3	Lysyl-tRNA synthetase	1	P1469
tr|A0A8B6DHL6|A0A8B6DHL6_MYTGA	A0A8B6DHL6	Actin-related protein 2/3 complex subunit 4	1	P1470
tr|A0A8B6DHN4|A0A8B6DHN4_MYTGA	A0A8B6DHN4	5'-AMP-activated protein kinase, regulatory beta subunit (Fr	1	P1471
tr|A0A8B6DHP6|A0A8B6DHP6_MYTGA	A0A8B6DHP6	Protein disulfide isomerase family A, member 5	1	P1472
tr|A0A8B6DHS4|A0A8B6DHS4_MYTGA	A0A8B6DHS4	Phosphatidylinositol-binding clathrin assembly protein	1	P1473
tr|A0A8B6DHV7|A0A8B6DHV7_MYTGA	A0A8B6DHV7	Large subunit ribosomal protein L11e	1	P1474
tr|A0A8B6DHW2|A0A8B6DHW2_MYTGA	A0A8B6DHW2	Ubiquitin carboxyl-terminal hydrolase	1	P1475
tr|A0A8B6DI42|A0A8B6DI42_MYTGA	A0A8B6DI42	Sperm-associated antigen 1	1	P1476
tr|A0A8B6DIH3|A0A8B6DIH3_MYTGA	A0A8B6DIH3	Condensin complex subunit 1	1	P1477
tr|A0A8B6DIU6|A0A8B6DIU6_MYTGA	A0A8B6DIU6	SGNH hydrolase-type esterase domain-containing protein	1	P1478
tr|A0A8B6DIV7|A0A8B6DIV7_MYTGA	A0A8B6DIV7	CS domain-containing protein	1	P1479
tr|A0A8B6DJJ5|A0A8B6DJJ5_MYTGA	A0A8B6DJJ5	Uncharacterized protein	1	P1480
tr|A0A8B6DJX5|A0A8B6DJX5_MYTGA	A0A8B6DJX5	Calmodulin	1	P1481

Protein	Uniprot accession	Protein Name	Number Peptides	P
tr|A0A8B6DK06|A0A8B6DK06_MYTGA	A0A8B6DK06	Pericentriolar material 1 protein (Fragment)	1	P1482
tr|A0A8B6DK17|A0A8B6DK17_MYTGA	A0A8B6DK17	RNA-binding protein Nova	1	P1483
tr|A0A8B6DK24|A0A8B6DK24_MYTGA	A0A8B6DK24	Uncharacterized protein	1	P1484
tr|A0A8B6DKA1|A0A8B6DKA1_MYTGA	A0A8B6DKA1	GRAM domain-containing protein	1	P1485
tr|A0A8B6DKB2|A0A8B6DKB2_MYTGA	A0A8B6DKB2	Tetraspanin	1	P1486
tr|A0A8B6DKH8|A0A8B6DKH8_MYTGA	A0A8B6DKH8	D-lactate dehydratase	1	P1487
tr|A0A8B6DL23|A0A8B6DL23_MYTGA	A0A8B6DL23	D-fructose-1,6-bisphosphate 1-phosphohydrolase	1	P1488
tr|A0A8B6DL47|A0A8B6DL47_MYTGA	A0A8B6DL47	Copper acquisition factor BIM1-like domain-containing prot	1	P1489
tr|A0A8B6DL75|A0A8B6DL75_MYTGA	A0A8B6DL75	Filamin	1	P1490
tr|A0A8B6DLQ6|A0A8B6DLQ6_MYTGA	A0A8B6DLQ6	SH3-domain binding protein 2	1	P1491
tr|A0A8B6DM72|A0A8B6DM72_MYTGA	A0A8B6DM72	Filamin	1	P1492
tr|A0A8B6DM98|A0A8B6DM98_MYTGA	A0A8B6DM98	Dynein heavy chain AAA module D4 domain-containing prot	1	P1493
tr|A0A8B6DMF0|A0A8B6DMF0_MYTGA	A0A8B6DMF0	C2 domain-containing protein	1	P1494
tr|A0A8B6DML2|A0A8B6DML2_MYTGA	A0A8B6DML2	DNA-directed RNA polymerase II subunit RPB7	1	P1495
tr|A0A8B6DMU9|A0A8B6DMU9_MYTGA	A0A8B6DMU9	UMP-CMP kinase	1	P1496
tr|A0A8B6DN32|A0A8B6DN32_MYTGA	A0A8B6DN32	3-hydroxyacyl-CoA dehydrogenase	1	P1497
tr|A0A8B6DN37|A0A8B6DN37_MYTGA	A0A8B6DN37	Histone deacetylase 11	1	P1498
tr|A0A8B6DN62|A0A8B6DN62_MYTGA	A0A8B6DN62	Proteasome activator subunit 4	1	P1499
tr|A0A8B6DNP1|A0A8B6DNP1_MYTGA	A0A8B6DNP1	(S)-3-amino-2-methylpropionate transaminase	1	P1500
tr|A0A8B6DPA0|A0A8B6DPA0_MYTGA	A0A8B6DPA0	COP9 signalosome complex subunit 1	1	P1501
tr|A0A8B6DPQ0|A0A8B6DPQ0_MYTGA	A0A8B6DPQ0	SCO-spondin	1	P1502
tr|A0A8B6DPS1|A0A8B6DPS1_MYTGA	A0A8B6DPS1	Dynein heavy chain, axonemal	1	P1503
tr|A0A8B6DPV4|A0A8B6DPV4_MYTGA	A0A8B6DPV4	UspA domain-containing protein (Fragment)	1	P1504
tr|A0A8B6DQ01|A0A8B6DQ01_MYTGA	A0A8B6DQ01	Cadherin-like beta sandwich domain-containing protein	1	P1505
tr|A0A8B6DQ74|A0A8B6DQ74_MYTGA	A0A8B6DQ74	LHH domain-containing protein	1	P1506
tr|A0A8B6DQ86|A0A8B6DQ86_MYTGA	A0A8B6DQ86	phenylalanine 4-monooxygenase	1	P1507
tr|A0A8B6DQY3|A0A8B6DQY3_MYTGA	A0A8B6DQY3	EF-hand domain-containing protein	1	P1508
tr|A0A8B6DR02|A0A8B6DR02_MYTGA	A0A8B6DR02	VWFA domain-containing protein	1	P1509
tr|A0A8B6DRB8|A0A8B6DRB8_MYTGA	A0A8B6DRB8	Hydroxyacid-oxoacid transhydrogenase	1	P1510
tr|A0A8B6DRG1|A0A8B6DRG1_MYTGA	A0A8B6DRG1	DNA damage-inducible protein 1	1	P1511
tr|A0A8B6DRZ8|A0A8B6DRZ8_MYTGA	A0A8B6DRZ8	Protein transport protein SEC31	1	P1512
tr|A0A8B6DSF9|A0A8B6DSF9_MYTGA	A0A8B6DSF9	Uncharacterized protein	1	P1513
tr|A0A8B6DSH5|A0A8B6DSH5_MYTGA	A0A8B6DSH5	Rootletin	1	P1514
tr|A0A8B6DT66|A0A8B6DT66_MYTGA	A0A8B6DT66	RNA-binding protein 8A	1	P1515
tr|A0A8B6DTU3|A0A8B6DTU3_MYTGA	A0A8B6DTU3	Insulysin (Fragment)	1	P1516
tr|A0A8B6DTY9|A0A8B6DTY9_MYTGA	A0A8B6DTY9	SHSP domain-containing protein	1	P1517
tr|A0A8B6DUI6|A0A8B6DUI6_MYTGA	A0A8B6DUI6	Prostaglandin-H2 D-isomerase / glutathione transferase	1	P1518
tr|A0A8B6DV60|A0A8B6DV60_MYTGA	A0A8B6DV60	Heterogeneous nuclear ribonucleoprotein F/H	1	P1519
tr|A0A8B6DVC3|A0A8B6DVC3_MYTGA	A0A8B6DVC3	Serpin B	1	P1520
tr|A0A8B6DVH0|A0A8B6DVH0_MYTGA	A0A8B6DVH0	Aldoketomutase	1	P1521
tr|A0A8B6DVI4|A0A8B6DVI4_MYTGA	A0A8B6DVI4	EGF-like domain-containing protein	1	P1522
tr|A0A8B6DVK3|A0A8B6DVK3_MYTGA	A0A8B6DVK3	Protein MAK10 homolog	1	P1523
tr|A0A8B6DVT2|A0A8B6DVT2_MYTGA	A0A8B6DVT2	Small ribosomal subunit protein uS12	1	P1524
tr|A0A8B6DVV5|A0A8B6DVV5_MYTGA	A0A8B6DVV5	Leucine-rich repeat protein SHOC2	1	P1525
tr|A0A8B6DW57|A0A8B6DW57_MYTGA	A0A8B6DW57	ATP-binding cassette, subfamily B (MDR/TAP), member 1	1	P1526
tr|A0A8B6DWF4|A0A8B6DWF4_MYTGA	A0A8B6DWF4	Profilin	1	P1527
tr|A0A8B6DWN7|A0A8B6DWN7_MYTGA	A0A8B6DWN7	cAMP-dependent protein kinase regulator	1	P1528
tr|A0A8B6DX32|A0A8B6DX32_MYTGA	A0A8B6DX32	Leucine-rich repeat flightless-interacting protein 2	1	P1529
tr|A0A8B6DXB6|A0A8B6DXB6_MYTGA	A0A8B6DXB6	Protein transport protein SEC61 subunit gamma and related	1	P1530
tr|A0A8B6DXH9|A0A8B6DXH9_MYTGA	A0A8B6DXH9	DUF4200 domain-containing protein	1	P1531
tr|A0A8B6DXL8|A0A8B6DXL8_MYTGA	A0A8B6DXL8	Uncharacterized protein	1	P1532
tr|A0A8B6DXZ5|A0A8B6DXZ5_MYTGA	A0A8B6DXZ5	Transcription elongation factor SPT5	1	P1533
tr|A0A8B6DY83|A0A8B6DY83_MYTGA	A0A8B6DY83	Poly(A)-specific ribonuclease PARN	1	P1534
tr|A0A8B6DYJ0|A0A8B6DYJ0_MYTGA	A0A8B6DYJ0	F-actin-capping protein subunit alpha	1	P1535
tr|A0A8B6DYS6|A0A8B6DYS6_MYTGA	A0A8B6DYS6	AP-3 complex subunit sigma	1	P1536
tr|A0A8B6DYU2|A0A8B6DYU2_MYTGA	A0A8B6DYU2	Importin-4	1	P1537
tr|A0A8B6DZ40|A0A8B6DZ40_MYTGA	A0A8B6DZ40	WNT inhibitory factor 1	1	P1538
tr|A0A8B6DZF1|A0A8B6DZF1_MYTGA	A0A8B6DZF1	Nicotinamide mononucleotide adenylyltransferase	1	P1539
tr|A0A8B6DZP8|A0A8B6DZP8_MYTGA	A0A8B6DZP8	Nuclear autoantigenic sperm protein	1	P1540
tr|A0A8B6DZY1|A0A8B6DZY1_MYTGA	A0A8B6DZY1	Transcription factor BTF3	1	P1541
tr|A0A8B6E0F9|A0A8B6E0F9_MYTGA	A0A8B6E0F9	DEP domain-containing protein	1	P1542
tr|A0A8B6E0G8|A0A8B6E0G8_MYTGA	A0A8B6E0G8	Apextrin C-terminal domain-containing protein	1	P1543
tr|A0A8B6E0K7|A0A8B6E0K7_MYTGA	A0A8B6E0K7	THO complex subunit 6	1	P1544
tr|A0A8B6E1B8|A0A8B6E1B8_MYTGA	A0A8B6E1B8	Histone H1/5	1	P1545
tr|A0A8B6E1F6|A0A8B6E1F6_MYTGA	A0A8B6E1F6	Importin subunit alpha	1	P1546
tr|A0A8B6E1H1|A0A8B6E1H1_MYTGA	A0A8B6E1H1	DNA ligase	1	P1547
tr|A0A8B6E1M7|A0A8B6E1M7_MYTGA	A0A8B6E1M7	Uncharacterized protein	1	P1548
tr|A0A8B6E1N3|A0A8B6E1N3_MYTGA	A0A8B6E1N3	BAR domain-containing protein	1	P1549
tr|A0A8B6E1N7|A0A8B6E1N7_MYTGA	A0A8B6E1N7	ER lumen protein-retaining receptor	1	P1550
tr|A0A8B6E1R6|A0A8B6E1R6_MYTGA	A0A8B6E1R6	DNA replication complex GINS protein PSF3	1	P1551
tr|A0A8B6E1T6|A0A8B6E1T6_MYTGA	A0A8B6E1T6	von Willebrand factor A domain-containing protein 5A	1	P1552
tr|A0A8B6E1W6|A0A8B6E1W6_MYTGA	A0A8B6E1W6	Polyadenylate-binding protein	1	P1553
tr|A0A8B6E202|A0A8B6E202_MYTGA	A0A8B6E202	Betaine-homocysteine S-methyltransferase	1	P1554
tr|A0A8B6E227|A0A8B6E227_MYTGA	A0A8B6E227	Transportin-3	1	P1555
tr|A0A8B6E267|A0A8B6E267_MYTGA	A0A8B6E267	Glutathione S-transferase	1	P1556
tr|A0A8B6E2D1|A0A8B6E2D1_MYTGA	A0A8B6E2D1	Complex III subunit 9	1	P1557
tr|A0A8B6E2D9|A0A8B6E2D9_MYTGA	A0A8B6E2D9	WASH complex subunit strumpellin	1	P1558
tr|A0A8B6E2F1|A0A8B6E2F1_MYTGA	A0A8B6E2F1	N-acylethanolamine-hydrolyzing acid amidase	1	P1559
tr|A0A8B6E2U8|A0A8B6E2U8_MYTGA	A0A8B6E2U8	Ras-related protein Rab-10	1	P1560
tr|A0A8B6E3F6|A0A8B6E3F6_MYTGA	A0A8B6E3F6	L-fucose mutarotase	1	P1561
tr|A0A8B6E3G0|A0A8B6E3G0_MYTGA	A0A8B6E3G0	glutamate synthase (ferredoxin)	1	P1562
tr|A0A8B6E3K1|A0A8B6E3K1_MYTGA	A0A8B6E3K1	Lamin-B receptor (Fragment)	1	P1563
tr|A0A8B6E3V3|A0A8B6E3V3_MYTGA	A0A8B6E3V3	L-dopachrome isomerase	1	P1564
tr|A0A8B6E403|A0A8B6E403_MYTGA	A0A8B6E403	Piezo-type mechanosensitive ion channel component	1	P1565
tr|A0A8B6E406|A0A8B6E406_MYTGA	A0A8B6E406	Ribose-phosphate pyrophosphokinase N-terminal domain-c	1	P1566
tr|A0A8B6E4N6|A0A8B6E4N6_MYTGA	A0A8B6E4N6	Sialate O-acetylesterase	1	P1567
tr|A0A8B6E582|A0A8B6E582_MYTGA	A0A8B6E582	SMP-30/Gluconolactonase/LRE-like region domain-containi	1	P1568
tr|A0A8B6E5F5|A0A8B6E5F5_MYTGA	A0A8B6E5F5	Fused	1	P1569
tr|A0A8B6E5J9|A0A8B6E5J9_MYTGA	A0A8B6E5J9	Nucleolysin TIA-1/TIAR	1	P1570
tr|A0A8B6E6E9|A0A8B6E6E9_MYTGA	A0A8B6E6E9	N-terminal amino-acid N(alpha)-acetyltransferase NatA	1	P1571
tr|A0A8B6E6L9|A0A8B6E6L9_MYTGA	A0A8B6E6L9	Carboxypeptidase	1	P1572
tr|A0A8B6E721|A0A8B6E721_MYTGA	A0A8B6E721	FERM domain-containing protein	1	P1573
tr|A0A8B6E885|A0A8B6E885_MYTGA	A0A8B6E885	Gelsolin-like domain-containing protein	1	P1574
tr|A0A8B6E8G2|A0A8B6E8G2_MYTGA	A0A8B6E8G2	Mitochondria-eating protein	1	P1575
tr|A0A8B6E8H4|A0A8B6E8H4_MYTGA	A0A8B6E8H4	SH3 domain-binding glutamic acid-rich protein	1	P1576
tr|A0A8B6E8K1|A0A8B6E8K1_MYTGA	A0A8B6E8K1	non-specific serine/threonine protein kinase	1	P1577
tr|A0A8B6E8R1|A0A8B6E8R1_MYTGA	A0A8B6E8R1	Hsp90 chaperone protein kinase-targeting subunit	1	P1578
tr|A0A8B6E9E5|A0A8B6E9E5_MYTGA	A0A8B6E9E5	3'-phosphoadenosine 5'-phosphosulfate synthase	1	P1579
tr|A0A8B6E9I1|A0A8B6E9I1_MYTGA	A0A8B6E9I1	RRM domain-containing protein	1	P1580
tr|A0A8B6E9N0|A0A8B6E9N0_MYTGA	A0A8B6E9N0	Lipopolysaccharide-binding protein	1	P1581
tr|A0A8B6E9W8|A0A8B6E9W8_MYTGA	A0A8B6E9W8	Uncharacterized protein	1	P1582
tr|A0A8B6EA29|A0A8B6EA29_MYTGA	A0A8B6EA29	Ectoine hydroxylase	1	P1583
tr|A0A8B6EA34|A0A8B6EA34_MYTGA	A0A8B6EA34	Calponin-homology (CH) domain-containing protein	1	P1584
tr|A0A8B6EA93|A0A8B6EA93_MYTGA	A0A8B6EA93	Transmembrane protein 214	1	P1585
tr|A0A8B6EAE5|A0A8B6EAE5_MYTGA	A0A8B6EAE5	Uncharacterized protein	1	P1586
tr|A0A8B6EAP2|A0A8B6EAP2_MYTGA	A0A8B6EAP2	Domain of unknown function with conserved HDNR motif d	1	P1587
tr|A0A8B6EB99|A0A8B6EB99_MYTGA	A0A8B6EB99	Thiaminase-2/PQQC domain-containing protein	1	P1588
tr|A0A8B6EBF9|A0A8B6EBF9_MYTGA	A0A8B6EBF9	Upf1 domain-containing protein	1	P1589
tr|A0A8B6EBS6|A0A8B6EBS6_MYTGA	A0A8B6EBS6	C2 domain-containing protein	1	P1590
tr|A0A8B6EC67|A0A8B6EC67_MYTGA	A0A8B6EC67	Lamin B	1	P1591
tr|A0A8B6ECB0|A0A8B6ECB0_MYTGA	A0A8B6ECB0	Lectin, mannose-binding 2	1	P1592
tr|A0A8B6ECC5|A0A8B6ECC5_MYTGA	A0A8B6ECC5	U6 snRNA-associated Sm-like protein LSm6	1	P1593
tr|A0A8B6ECI2|A0A8B6ECI2_MYTGA	A0A8B6ECI2	UNC-45/Cro1/She4 central domain-containing protein	1	P1594
tr|A0A8B6ECL7|A0A8B6ECL7_MYTGA	A0A8B6ECL7	Anhydro-N-acetylmuramic acid kinase	1	P1595
tr|A0A8B6ECR6|A0A8B6ECR6_MYTGA	A0A8B6ECR6	Reticulon-like protein	1	P1596
tr|A0A8B6ECU5|A0A8B6ECU5_MYTGA	A0A8B6ECU5	Aminoacyl tRNA synthase complex-interacting multifunctio	1	P1597
tr|A0A8B6EDS8|A0A8B6EDS8_MYTGA	A0A8B6EDS8	RNA helicase	1	P1598

Protein	Uniprot accession	Protein Name	Number Peptides	P
tr|A0A8B6EE03|A0A8B6EE03_MYTGA	A0A8B6EE03	Leucyl aminopeptidase (Fragment)	1	P1599
tr|A0A8B6EE10|A0A8B6EE10_MYTGA	A0A8B6EE10	Vitellogenin domain-containing protein (Fragment)	1	P1600
tr|A0A8B6EE61|A0A8B6EE61_MYTGA	A0A8B6EE61	Protein kinase domain-containing protein	1	P1601
tr|A0A8B6EEC2|A0A8B6EEC2_MYTGA	A0A8B6EEC2	ZP domain-containing protein	1	P1602
tr|A0A8B6EEW0|A0A8B6EEW0_MYTGA	A0A8B6EEW0	DNA-dependent protein kinase catalytic subunit (Fragment)	1	P1603
tr|A0A8B6EEX1|A0A8B6EEX1_MYTGA	A0A8B6EEX1	Protein BCCIP homolog	1	P1604
tr|A0A8B6EF31|A0A8B6EF31_MYTGA	A0A8B6EF31	WSC domain-containing protein	1	P1605
tr|A0A8B6EF73|A0A8B6EF73_MYTGA	A0A8B6EF73	DUF885 domain-containing protein	1	P1606
tr|A0A8B6EFB1|A0A8B6EFB1_MYTGA	A0A8B6EFB1	Dynein heavy chain, axonemal	1	P1607
tr|A0A8B6EFJ6|A0A8B6EFJ6_MYTGA	A0A8B6EFJ6	Peroxisomal trans-2-enoyl-CoA reductase	1	P1608
tr|A0A8B6EG28|A0A8B6EG28_MYTGA	A0A8B6EG28	RING-type E3 ubiquitin transferase	1	P1609
tr|A0A8B6EG45|A0A8B6EG45_MYTGA	A0A8B6EG45	Anoctamin	1	P1610
tr|A0A8B6EG53|A0A8B6EG53_MYTGA	A0A8B6EG53	Large ribosomal subunit protein mL44 (Fragment)	1	P1611
tr|A0A8B6EGN9|A0A8B6EGN9_MYTGA	A0A8B6EGN9	Protein phosphatase 1 regulatory subunit 10	1	P1612
tr|A0A8B6EGY2|A0A8B6EGY2_MYTGA	A0A8B6EGY2	Endoplasmic reticulum-Golgi intermediate compartment pr	1	P1613
tr|A0A8B6EH57|A0A8B6EH57_MYTGA	A0A8B6EH57	C-type lectin domain-containing protein	1	P1614
tr|A0A8B6EHC8|A0A8B6EHC8_MYTGA	A0A8B6EHC8	Nuclear pore complex protein Nup153	1	P1615
tr|A0A8B6EHD1|A0A8B6EHD1_MYTGA	A0A8B6EHD1	Nuclear pore complex protein	1	P1616
tr|A0A8B6EHI7|A0A8B6EHI7_MYTGA	A0A8B6EHI7	H/ACA ribonucleoprotein complex subunit	1	P1617
tr|A0A8B6EHX6|A0A8B6EHX6_MYTGA	A0A8B6EHX6	Metalloendopeptidase	1	P1618
tr|A0A8B6EI89|A0A8B6EI89_MYTGA	A0A8B6EI89	Dynactin 1 (Fragment)	1	P1619
tr|A0A8B6EIA1|A0A8B6EIA1_MYTGA	A0A8B6EIA1	Protein quiver	1	P1620
tr|A0A8B6EIH9|A0A8B6EIH9_MYTGA	A0A8B6EIH9	Phosphotransferase	1	P1621
tr|A0A8B6EIJ7|A0A8B6EIJ7_MYTGA	A0A8B6EIJ7	Ig-like domain-containing protein	1	P1622
tr|A0A8B6EIX8|A0A8B6EIX8_MYTGA	A0A8B6EIX8	ADP-ribosylation factor 6	1	P1623
tr|A0A8B6EIZ7|A0A8B6EIZ7_MYTGA	A0A8B6EIZ7	RNA helicase (Fragment)	1	P1624
tr|A0A8B6EJ38|A0A8B6EJ38_MYTGA	A0A8B6EJ38	Carbonic anhydrase	1	P1625
tr|A0A8B6EJG8|A0A8B6EJG8_MYTGA	A0A8B6EJG8	Inter-alpha-trypsin inhibitor heavy chain H3-like	1	P1626
tr|A0A8B6EK00|A0A8B6EK00_MYTGA	A0A8B6EK00	Protein kinase C gamma type (Fragment)	1	P1627
tr|A0A8B6EK38|A0A8B6EK38_MYTGA	A0A8B6EK38	Prostaglandin E synthase 2	1	P1628
tr|A0A8B6EK60|A0A8B6EK60_MYTGA	A0A8B6EK60	Tubulin alpha chain	1	P1629
tr|A0A8B6EK77|A0A8B6EK77_MYTGA	A0A8B6EK77	Alcohol dehydrogenase-like C-terminal domain-containing p	1	P1630
tr|A0A8B6EKJ7|A0A8B6EKJ7_MYTGA	A0A8B6EKJ7	Arfaptin	1	P1631
tr|A0A8B6EKU7|A0A8B6EKU7_MYTGA	A0A8B6EKU7	Nucleoside diphosphate kinase	1	P1632
tr|A0A8B6EKY4|A0A8B6EKY4_MYTGA	A0A8B6EKY4	THO complex subunit 2	1	P1633
tr|A0A8B6EKZ3|A0A8B6EKZ3_MYTGA	A0A8B6EKZ3	Polycystin 2	1	P1634
tr|A0A8B6ELF4|A0A8B6ELF4_MYTGA	A0A8B6ELF4	ADP-ribosylation factor-like protein 3	1	P1635
tr|A0A8B6ELN6|A0A8B6ELN6_MYTGA	A0A8B6ELN6	Ciliogenesis-associated TTC17-interacting protein	1	P1636
tr|A0A8B6ELQ2|A0A8B6ELQ2_MYTGA	A0A8B6ELQ2	B3/B4 tRNA-binding domain-containing protein	1	P1637
tr|A0A8B6ELV7|A0A8B6ELV7_MYTGA	A0A8B6ELV7	Leucine-rich repeat-containing protein 59	1	P1638
tr|A0A8B6EM39|A0A8B6EM39_MYTGA	A0A8B6EM39	Signal recognition particle subunit SRP72	1	P1639
tr|A0A8B6EM47|A0A8B6EM47_MYTGA	A0A8B6EM47	CCHC-type zinc finger nucleic acid binding protein	1	P1640
tr|A0A8B6EM73|A0A8B6EM73_MYTGA	A0A8B6EM73	Signal recognition particle subunit SRP72	1	P1641
tr|A0A8B6EMD6|A0A8B6EMD6_MYTGA	A0A8B6EMD6	NADH dehydrogenase (Ubiquinone) 1 alpha subcomplex sub	1	P1642
tr|A0A8B6EMJ4|A0A8B6EMJ4_MYTGA	A0A8B6EMJ4	VWFA domain-containing protein	1	P1643
tr|A0A8B6EN17|A0A8B6EN17_MYTGA	A0A8B6EN17	60S ribosomal protein L35	1	P1644
tr|A0A8B6EN93|A0A8B6EN93_MYTGA	A0A8B6EN93	Phosphoinositide phospholipase C	1	P1645
tr|A0A8B6EP28|A0A8B6EP28_MYTGA	A0A8B6EP28	Selenide, water dikinase	1	P1646
tr|A0A8B6EP29|A0A8B6EP29_MYTGA	A0A8B6EP29	Large ribosomal subunit protein eL43	1	P1647
tr|A0A8B6EP93|A0A8B6EP93_MYTGA	A0A8B6EP93	UspA domain-containing protein	1	P1648
tr|A0A8B6EPB2|A0A8B6EPB2_MYTGA	A0A8B6EPB2	Kinesin light chain	1	P1649
tr|A0A8B6EPF3|A0A8B6EPF3_MYTGA	A0A8B6EPF3	CSD domain-containing protein	1	P1650
tr|A0A8B6EPJ8|A0A8B6EPJ8_MYTGA	A0A8B6EPJ8	EF-hand domain-containing protein	1	P1651
tr|A0A8B6EPT1|A0A8B6EPT1_MYTGA	A0A8B6EPT1	Tropomodulin	1	P1652
tr|A0A8B6EQA0|A0A8B6EQA0_MYTGA	A0A8B6EQA0	Uncharacterized protein	1	P1653
tr|A0A8B6EQG1|A0A8B6EQG1_MYTGA	A0A8B6EQG1	Tubulin beta chain	1	P1654
tr|A0A8B6EQG5|A0A8B6EQG5_MYTGA	A0A8B6EQG5	Fibrinogen C-terminal domain-containing protein	1	P1655
tr|A0A8B6EQJ7|A0A8B6EQJ7_MYTGA	A0A8B6EQJ7	Uncharacterized protein	1	P1656
tr|A0A8B6EQL7|A0A8B6EQL7_MYTGA	A0A8B6EQL7	DNA polymerase alpha subunit B	1	P1657
tr|A0A8B6EQS7|A0A8B6EQS7_MYTGA	A0A8B6EQS7	Cation-dependent mannose-6-phosphate receptor	1	P1658
tr|A0A8B6ER19|A0A8B6ER19_MYTGA	A0A8B6ER19	Ubiquitin-like modifier-activating enzyme 5	1	P1659
tr|A0A8B6ER88|A0A8B6ER88_MYTGA	A0A8B6ER88	Rhodanese domain-containing protein	1	P1660
tr|A0A8B6ERH4|A0A8B6ERH4_MYTGA	A0A8B6ERH4	HHIP-like protein 1	1	P1661
tr|A0A8B6ERN5|A0A8B6ERN5_MYTGA	A0A8B6ERN5	Eukaryotic translation initiation factor 4C	1	P1662
tr|A0A8B6ERW8|A0A8B6ERW8_MYTGA	A0A8B6ERW8	Spectrin beta	1	P1663
tr|A0A8B6ES21|A0A8B6ES21_MYTGA	A0A8B6ES21	Kynurenine formamidase	1	P1664
tr|A0A8B6ES22|A0A8B6ES22_MYTGA	A0A8B6ES22	Sorting nexin	1	P1665
tr|A0A8B6ET20|A0A8B6ET20_MYTGA	A0A8B6ET20	Importin-5	1	P1666
tr|A0A8B6ET28|A0A8B6ET28_MYTGA	A0A8B6ET28	Heat shock 70 kDa protein	1	P1667
tr|A0A8B6ET74|A0A8B6ET74_MYTGA	A0A8B6ET74	Uncharacterized protein	1	P1668
tr|A0A8B6ETI3|A0A8B6ETI3_MYTGA	A0A8B6ETI3	Protein OSCP1	1	P1669
tr|A0A8B6ETN4|A0A8B6ETN4_MYTGA	A0A8B6ETN4	C-type lectin domain-containing protein	1	P1670
tr|A0A8B6EUB2|A0A8B6EUB2_MYTGA	A0A8B6EUB2	Cytochrome P450, family 20, subfamily A	1	P1671
tr|A0A8B6EUJ4|A0A8B6EUJ4_MYTGA	A0A8B6EUJ4	Serine/threonine-protein phosphatase 2A regulatory subuni	1	P1672
tr|A0A8B6EUV2|A0A8B6EUV2_MYTGA	A0A8B6EUV2	Aldehyde dehydrogenase domain-containing protein	1	P1673
tr|A0A8B6EV33|A0A8B6EV33_MYTGA	A0A8B6EV33	DUF19 domain-containing protein	1	P1674
tr|A0A8B6EV53|A0A8B6EV53_MYTGA	A0A8B6EV53	Ig-like domain-containing protein (Fragment)	1	P1675
tr|A0A8B6EV71|A0A8B6EV71_MYTGA	A0A8B6EV71	Granulins domain-containing protein	1	P1676
tr|A0A8B6EVC3|A0A8B6EVC3_MYTGA	A0A8B6EVC3	Calcium uniporter protein (Fragment)	1	P1677
tr|A0A8B6EVJ7|A0A8B6EVJ7_MYTGA	A0A8B6EVJ7	Mitochondrial import receptor subunit TOM40	1	P1678
tr|A0A8B6EVK6|A0A8B6EVK6_MYTGA	A0A8B6EVK6	Importin-5	1	P1679
tr|A0A8B6EVM7|A0A8B6EVM7_MYTGA	A0A8B6EVM7	Uncharacterized protein	1	P1680
tr|A0A8B6EW25|A0A8B6EW25_MYTGA	A0A8B6EW25	Uncharacterized protein	1	P1681
tr|A0A8B6EW31|A0A8B6EW31_MYTGA	A0A8B6EW31	Erythrocyte band 7 integral membrane protein	1	P1682
tr|A0A8B6EWB6|A0A8B6EWB6_MYTGA	A0A8B6EWB6	IST1 homolog	1	P1683
tr|A0A8B6EWF3|A0A8B6EWF3_MYTGA	A0A8B6EWF3	glutamine--fructose-6-phosphate transaminase (isomerizing	1	P1684
tr|A0A8B6EWM2|A0A8B6EWM2_MYTGA	A0A8B6EWM2	long-chain-fatty-acid--CoA ligase	1	P1685
tr|A0A8B6EWX1|A0A8B6EWX1_MYTGA	A0A8B6EWX1	Signal transducer and activator of transcription 5B	1	P1686
tr|A0A8B6EX90|A0A8B6EX90_MYTGA	A0A8B6EX90	Uncharacterized protein	1	P1687
tr|A0A8B6EX98|A0A8B6EX98_MYTGA	A0A8B6EX98	Uncharacterized protein	1	P1688
tr|A0A8B6EXJ9|A0A8B6EXJ9_MYTGA	A0A8B6EXJ9	m7GpppX diphosphatase	1	P1689
tr|A0A8B6EXX3|A0A8B6EXX3_MYTGA	A0A8B6EXX3	Uncharacterized protein	1	P1690
tr|A0A8B6EXY4|A0A8B6EXY4_MYTGA	A0A8B6EXY4	RRM domain-containing protein	1	P1691
tr|A0A8B6EY18|A0A8B6EY18_MYTGA	A0A8B6EY18	Lysosomal-associated transmembrane protein	1	P1692
tr|A0A8B6EYL1|A0A8B6EYL1_MYTGA	A0A8B6EYL1	Cathepsin L	1	P1693
tr|A0A8B6EYQ6|A0A8B6EYQ6_MYTGA	A0A8B6EYQ6	Uncharacterized protein	1	P1694
tr|A0A8B6EYV0|A0A8B6EYV0_MYTGA	A0A8B6EYV0	Prolyl-tRNA synthetase	1	P1695
tr|A0A8B6EZ75|A0A8B6EZ75_MYTGA	A0A8B6EZ75	Ubiquilin	1	P1696
tr|A0A8B6EZM6|A0A8B6EZM6_MYTGA	A0A8B6EZM6	Homocysteine S-methyltransferase	1	P1697
tr|A0A8B6F0D6|A0A8B6F0D6_MYTGA	A0A8B6F0D6	UDP-glucose 4-epimerase	1	P1698
tr|A0A8B6F0L3|A0A8B6F0L3_MYTGA	A0A8B6F0L3	Histone H1/5	1	P1699
tr|A0A8B6F0T5|A0A8B6F0T5_MYTGA	A0A8B6F0T5	ADP-ribosylation factor-like protein 1	1	P1700
tr|A0A8B6F1F9|A0A8B6F1F9_MYTGA	A0A8B6F1F9	G-protein coupled receptor 158	1	P1701
tr|A0A8B6F1K9|A0A8B6F1K9_MYTGA	A0A8B6F1K9	NADPH2:quinone reductase	1	P1702
tr|A0A8B6F2E2|A0A8B6F2E2_MYTGA	A0A8B6F2E2	Small subunit ribosomal protein S30e	1	P1703
tr|A0A8B6F2W4|A0A8B6F2W4_MYTGA	A0A8B6F2W4	Uncharacterized protein	1	P1704
tr|A0A8B6F3A2|A0A8B6F3A2_MYTGA	A0A8B6F3A2	20S proteasome subunit alpha 1	1	P1705
tr|A0A8B6F3D4|A0A8B6F3D4_MYTGA	A0A8B6F3D4	Maestro heat-like repeat-containing protein family member	1	P1706
tr|A0A8B6F3Q0|A0A8B6F3Q0_MYTGA	A0A8B6F3Q0	PUA domain protein	1	P1707
tr|A0A8B6F3T1|A0A8B6F3T1_MYTGA	A0A8B6F3T1	5'-nucleotidase	1	P1708
tr|A0A8B6F3U8|A0A8B6F3U8_MYTGA	A0A8B6F3U8	Guanylate kinase-like domain-containing protein	1	P1709
tr|A0A8B6F4A1|A0A8B6F4A1_MYTGA	A0A8B6F4A1	Histone H2A	1	P1710
tr|A0A8B6F4M0|A0A8B6F4M0_MYTGA	A0A8B6F4M0	Endoplasmic reticulum transmembrane protein	1	P1711
tr|A0A8B6F5B4|A0A8B6F5B4_MYTGA	A0A8B6F5B4	EF-hand domain-containing protein	1	P1712
tr|A0A8B6F5I2|A0A8B6F5I2_MYTGA	A0A8B6F5I2	Uncharacterized protein	1	P1713
tr|A0A8B6F5U6|A0A8B6F5U6_MYTGA	A0A8B6F5U6	MAM domain-containing protein	1	P1714
tr|A0A8B6F5Y0|A0A8B6F5Y0_MYTGA	A0A8B6F5Y0	NADH dehydrogenase [ubiquinone] 1 beta subcomplex subu	1	P1715

Protein	Uniprot accession	Protein Name	Number Peptides	P
tr|A0A8B6F658|A0A8B6F658_MYTGA	A0A8B6F658	Uncharacterized protein	1	P1716
tr|A0A8B6F6K3|A0A8B6F6K3_MYTGA	A0A8B6F6K3	alpha-L-fucosidase	1	P1717
tr|A0A8B6F6S0|A0A8B6F6S0_MYTGA	A0A8B6F6S0	NADH dehydrogenase (Ubiquinone) Fe-S protein 8	1	P1718
tr|A0A8B6F7R2|A0A8B6F7R2_MYTGA	A0A8B6F7R2	S-phase kinase-associated protein 1	1	P1719
tr|A0A8B6F881|A0A8B6F881_MYTGA	A0A8B6F881	Pantetheine hydrolase	1	P1720
tr|A0A8B6F888|A0A8B6F888_MYTGA	A0A8B6F888	EF-hand domain-containing protein	1	P1721
tr|A0A8B6F8K4|A0A8B6F8K4_MYTGA	A0A8B6F8K4	C-type lectin domain family 10 member A	1	P1722
tr|A0A8B6F8T9|A0A8B6F8T9_MYTGA	A0A8B6F8T9	Peptidyl-prolyl cis-trans isomerase	1	P1723
tr|A0A8B6F8U6|A0A8B6F8U6_MYTGA	A0A8B6F8U6	FAD dependent oxidoreductase domain-containing protein	1	P1724
tr|A0A8B6F8X1|A0A8B6F8X1_MYTGA	A0A8B6F8X1	malate synthase	1	P1725
tr|A0A8B6F978|A0A8B6F978_MYTGA	A0A8B6F978	GDP-mannose 4,6-dehydratase	1	P1726
tr|A0A8B6F9G2|A0A8B6F9G2_MYTGA	A0A8B6F9G2	Cohesin complex subunit SA-1/2	1	P1727
tr|A0A8B6F9G8|A0A8B6F9G8_MYTGA	A0A8B6F9G8	Glutaredoxin-1	1	P1728
tr|A0A8B6F9R9|A0A8B6F9R9_MYTGA	A0A8B6F9R9	Phosphodiesterase	1	P1729
tr|A0A8B6F9Y3|A0A8B6F9Y3_MYTGA	A0A8B6F9Y3	Nascent polypeptide-associated complex subunit alpha	1	P1730
tr|A0A8B6FA18|A0A8B6FA18_MYTGA	A0A8B6FA18	Arp2/3 complex 41 kDa subunit	1	P1731
tr|A0A8B6FA40|A0A8B6FA40_MYTGA	A0A8B6FA40	Guanine nucleotide-binding protein subunit alpha-12	1	P1732
tr|A0A8B6FB74|A0A8B6FB74_MYTGA	A0A8B6FB74	Dynein heavy chain, axonemal (Fragment)	1	P1733
tr|A0A8B6FBA1|A0A8B6FBA1_MYTGA	A0A8B6FBA1	Serine/threonine-protein phosphatase 2A regulatory subuni	1	P1734
tr|A0A8B6FBT1|A0A8B6FBT1_MYTGA	A0A8B6FBT1	Sidoreflexin	1	P1735
tr|A0A8B6FBU3|A0A8B6FBU3_MYTGA	A0A8B6FBU3	Homogentisate 1,2-dioxygenase	1	P1736
tr|A0A8B6FBW2|A0A8B6FBW2_MYTGA	A0A8B6FBW2	Transforming growth factor beta-1-induced transcript 1 pro	1	P1737
tr|A0A8B6FCB1|A0A8B6FCB1_MYTGA	A0A8B6FCB1	Serine/threonine-protein kinase NIM1	1	P1738
tr|A0A8B6FCI7|A0A8B6FCI7_MYTGA	A0A8B6FCI7	ribose-5-phosphate isomerase (Fragment)	1	P1739
tr|A0A8B6FCM4|A0A8B6FCM4_MYTGA	A0A8B6FCM4	Lipocalin/cytosolic fatty-acid binding domain-containing pr	1	P1740
tr|A0A8B6FCR5|A0A8B6FCR5_MYTGA	A0A8B6FCR5	EF-hand domain-containing family member C2	1	P1741
tr|A0A8B6FD26|A0A8B6FD26_MYTGA	A0A8B6FD26	Transglutaminase 1	1	P1742
tr|A0A8B6FDM2|A0A8B6FDM2_MYTGA	A0A8B6FDM2	Signal peptidase complex subunit 3	1	P1743
tr|A0A8B6FDQ4|A0A8B6FDQ4_MYTGA	A0A8B6FDQ4	Structural maintenance of chromosomes protein	1	P1744
tr|A0A8B6FDU3|A0A8B6FDU3_MYTGA	A0A8B6FDU3	Dynein heavy chain, axonemal	1	P1745
tr|A0A8B6FF27|A0A8B6FF27_MYTGA	A0A8B6FF27	Histone H2A	1	P1746
tr|A0A8B6FFW8|A0A8B6FFW8_MYTGA	A0A8B6FFW8	Uncharacterized protein	1	P1747
tr|A0A8B6FGA4|A0A8B6FGA4_MYTGA	A0A8B6FGA4	Twinfilin	1	P1748
tr|A0A8B6FGE9|A0A8B6FGE9_MYTGA	A0A8B6FGE9	E2 ubiquitin-conjugating enzyme	1	P1749
tr|A0A8B6FGF4|A0A8B6FGF4_MYTGA	A0A8B6FGF4	Uncharacterized protein	1	P1750
tr|A0A8B6FGW8|A0A8B6FGW8_MYTGA	A0A8B6FGW8	Replication factor C subunit 3/5	1	P1751
tr|A0A8B6FH74|A0A8B6FH74_MYTGA	A0A8B6FH74	kynurenine--oxoglutarate transaminase	1	P1752
tr|A0A8B6FH76|A0A8B6FH76_MYTGA	A0A8B6FH76	LIM domain-binding protein 3	1	P1753
tr|A0A8B6FHM3|A0A8B6FHM3_MYTGA	A0A8B6FHM3	Tudor domain-containing protein 1/4/6/7	1	P1754
tr|A0A8B6FHP7|A0A8B6FHP7_MYTGA	A0A8B6FHP7	Myosin XVIII	1	P1755
tr|A0A8B6FHS9|A0A8B6FHS9_MYTGA	A0A8B6FHS9	Ribonuclease H2 subunit B	1	P1756
tr|A0A8B6FHV0|A0A8B6FHV0_MYTGA	A0A8B6FHV0	Niemann-Pick C1 protein	1	P1757
tr|A0A8B6FIC5|A0A8B6FIC5_MYTGA	A0A8B6FIC5	Pre-mRNA-splicing factor SYF1	1	P1758
tr|A0A8B6FJH9|A0A8B6FJH9_MYTGA	A0A8B6FJH9	glycogenin glucosyltransferase	1	P1759
tr|A0A8B6FJJ4|A0A8B6FJJ4_MYTGA	A0A8B6FJJ4	Aldehyde dehydrogenase domain-containing protein	1	P1760
tr|A0A8B6FJJ8|A0A8B6FJJ8_MYTGA	A0A8B6FJJ8	DUF1279 domain-containing protein	1	P1761
tr|A0A8B6FJK0|A0A8B6FJK0_MYTGA	A0A8B6FJK0	Protein phosphatase 1B	1	P1762
tr|A0A8B6FJM3|A0A8B6FJM3_MYTGA	A0A8B6FJM3	Sulfotransferase domain-containing protein	1	P1763
tr|A0A8B6FJP1|A0A8B6FJP1_MYTGA	A0A8B6FJP1	Sorting nexin-9/18/33	1	P1764
tr|A0A8B6FJR6|A0A8B6FJR6_MYTGA	A0A8B6FJR6	Protein YIPF (Fragment)	1	P1765
tr|A0A8B6FJS1|A0A8B6FJS1_MYTGA	A0A8B6FJS1	Cilia- and flagella-associated protein 299	1	P1766
tr|A0A8B6FKJ0|A0A8B6FKJ0_MYTGA	A0A8B6FKJ0	Hsp70-interacting protein	1	P1767
tr|A0A8B6FKT0|A0A8B6FKT0_MYTGA	A0A8B6FKT0	60S ribosomal protein L7a (Fragment)	1	P1768
tr|A0A8B6FL44|A0A8B6FL44_MYTGA	A0A8B6FL44	PNPLA domain-containing protein	1	P1769
tr|A0A8B6FLR3|A0A8B6FLR3_MYTGA	A0A8B6FLR3	NADH dehydrogenase [ubiquinone] 1 alpha subcomplex subu	1	P1770
tr|A0A8B6FLW2|A0A8B6FLW2_MYTGA	A0A8B6FLW2	U6 snRNA-associated Sm-like protein LSm3	1	P1771
tr|A0A8B6FMG5|A0A8B6FMG5_MYTGA	A0A8B6FMG5	Uncharacterized protein	1	P1772
tr|A0A8B6FMJ2|A0A8B6FMJ2_MYTGA	A0A8B6FMJ2	Ras suppressor protein 1	1	P1773
tr|A0A8B6FNI5|A0A8B6FNI5_MYTGA	A0A8B6FNI5	RAP domain-containing protein	1	P1774
tr|A0A8B6FNJ1|A0A8B6FNJ1_MYTGA	A0A8B6FNJ1	N-acetylgalactosamine kinase	1	P1775
tr|A0A8B6FNQ5|A0A8B6FNQ5_MYTGA	A0A8B6FNQ5	Transcription elongation factor	1	P1776
tr|A0A8B6FNW3|A0A8B6FNW3_MYTGA	A0A8B6FNW3	Transmembrane protein 33	1	P1777
tr|A0A8B6FNX0|A0A8B6FNX0_MYTGA	A0A8B6FNX0	Peroxisomal 3,2-trans-enoyl-CoA isomerase	1	P1778
tr|A0A8B6FNY1|A0A8B6FNY1_MYTGA	A0A8B6FNY1	Small ribosomal subunit protein eS28 (Fragment)	1	P1779
tr|A0A8B6FP56|A0A8B6FP56_MYTGA	A0A8B6FP56	Transcription elongation factor B, polypeptide 2	1	P1780
tr|A0A8B6FP60|A0A8B6FP60_MYTGA	A0A8B6FP60	C1q domain-containing protein	1	P1781
tr|A0A8B6FPE0|A0A8B6FPE0_MYTGA	A0A8B6FPE0	Cytoskeleton-associated protein 5	1	P1782
tr|A0A8B6FPG3|A0A8B6FPG3_MYTGA	A0A8B6FPG3	Uncharacterized protein	1	P1783
tr|A0A8B6FPG5|A0A8B6FPG5_MYTGA	A0A8B6FPG5	H-type lectin domain-containing protein	1	P1784
tr|A0A8B6FPM8|A0A8B6FPM8_MYTGA	A0A8B6FPM8	Uncharacterized protein	1	P1785
tr|A0A8B6FPV6|A0A8B6FPV6_MYTGA	A0A8B6FPV6	Succinate-semialdehyde dehydrogenase	1	P1786
tr|A0A8B6FPZ4|A0A8B6FPZ4_MYTGA	A0A8B6FPZ4	WD repeat-containing protein 63	1	P1787
tr|A0A8B6FQL0|A0A8B6FQL0_MYTGA	A0A8B6FQL0	Uncharacterized protein	1	P1788
tr|A0A8B6FQY8|A0A8B6FQY8_MYTGA	A0A8B6FQY8	Transcription elongation regulator 1	1	P1789
tr|A0A8B6FRE2|A0A8B6FRE2_MYTGA	A0A8B6FRE2	Uncharacterized protein	1	P1790
tr|A0A8B6FRG8|A0A8B6FRG8_MYTGA	A0A8B6FRG8	Vitellogenin receptor (Fragment)	1	P1791
tr|A0A8B6FRN6|A0A8B6FRN6_MYTGA	A0A8B6FRN6	EF-hand domain-containing protein	1	P1792
tr|A0A8B6FS13|A0A8B6FS13_MYTGA	A0A8B6FS13	Tubulin beta chain	1	P1793
tr|A0A8B6FS49|A0A8B6FS49_MYTGA	A0A8B6FS49	Chromobox protein 1	1	P1794
tr|A0A8B6FS62|A0A8B6FS62_MYTGA	A0A8B6FS62	Uncharacterized protein	1	P1795
tr|A0A8B6FSC2|A0A8B6FSC2_MYTGA	A0A8B6FSC2	Uncharacterized protein	1	P1796
tr|A0A8B6FSC3|A0A8B6FSC3_MYTGA	A0A8B6FSC3	Splicing factor, arginine/serine-rich 4/5/6	1	P1797
tr|A0A8B6FSM2|A0A8B6FSM2_MYTGA	A0A8B6FSM2	Lysosomal protein NCU-G1	1	P1798
tr|A0A8B6FSY5|A0A8B6FSY5_MYTGA	A0A8B6FSY5	Outer dense fiber protein 2	1	P1799
tr|A0A8B6FT49|A0A8B6FT49_MYTGA	A0A8B6FT49	Erythrocyte membrane protein band 4.1	1	P1800
tr|A0A8B6FTK5|A0A8B6FTK5_MYTGA	A0A8B6FTK5	Ubiquitin-ribosomal protein eL40 fusion protein (Fragment)	1	P1801
tr|A0A8B6FTP8|A0A8B6FTP8_MYTGA	A0A8B6FTP8	VWFA domain-containing protein	1	P1802
tr|A0A8B6FTT8|A0A8B6FTT8_MYTGA	A0A8B6FTT8	Copine-8	1	P1803
tr|A0A8B6FTT9|A0A8B6FTT9_MYTGA	A0A8B6FTT9	C-type lectin domain-containing protein	1	P1804
tr|A0A8B6FTW5|A0A8B6FTW5_MYTGA	A0A8B6FTW5	Peptidyl-prolyl cis-trans isomerase	1	P1805
tr|A0A8B6FU21|A0A8B6FU21_MYTGA	A0A8B6FU21	alpha-L-fucosidase	1	P1806
tr|A0A8B6FU44|A0A8B6FU44_MYTGA	A0A8B6FU44	coproporphyrinogen oxidase	1	P1807
tr|A0A8B6FU64|A0A8B6FU64_MYTGA	A0A8B6FU64	Fascin	1	P1808
tr|A0A8B6FUE6|A0A8B6FUE6_MYTGA	A0A8B6FUE6	NADH dehydrogenase (Ubiquinone) 1 beta subcomplex subu	1	P1809
tr|A0A8B6FUI6|A0A8B6FUI6_MYTGA	A0A8B6FUI6	CDK5 regulatory subunit-associated protein 3	1	P1810
tr|A0A8B6FUK2|A0A8B6FUK2_MYTGA	A0A8B6FUK2	GTPase-activating protein and VPS9 domain-containing prot	1	P1811
tr|A0A8B6FUQ1|A0A8B6FUQ1_MYTGA	A0A8B6FUQ1	UBC core domain-containing protein	1	P1812
tr|A0A8B6FUQ9|A0A8B6FUQ9_MYTGA	A0A8B6FUQ9	CCDC81 HU domain-containing protein	1	P1813
tr|A0A8B6FUY4|A0A8B6FUY4_MYTGA	A0A8B6FUY4	Regucalcin	1	P1814
tr|A0A8B6FV39|A0A8B6FV39_MYTGA	A0A8B6FV39	Sterol carrier protein 2	1	P1815
tr|A0A8B6FV87|A0A8B6FV87_MYTGA	A0A8B6FV87	Cystatin domain-containing protein	1	P1816
tr|A0A8B6FVI3|A0A8B6FVI3_MYTGA	A0A8B6FVI3	C1q domain-containing protein	1	P1817
tr|A0A8B6FVL8|A0A8B6FVL8_MYTGA	A0A8B6FVL8	Uncharacterized protein	1	P1818
tr|A0A8B6FVP7|A0A8B6FVP7_MYTGA	A0A8B6FVP7	OBG-type G domain-containing protein	1	P1819
tr|A0A8B6FVY9|A0A8B6FVY9_MYTGA	A0A8B6FVY9	Malonyl-CoA decarboxylase	1	P1820
tr|A0A8B6FW32|A0A8B6FW32_MYTGA	A0A8B6FW32	Carbohydrate sulfotransferase	1	P1821
tr|A0A8B6FWN5|A0A8B6FWN5_MYTGA	A0A8B6FWN5	Uncharacterized protein	1	P1822
tr|A0A8B6FX39|A0A8B6FX39_MYTGA	A0A8B6FX39	Phosphohistidine phosphatase	1	P1823
tr|A0A8B6FXK0|A0A8B6FXK0_MYTGA	A0A8B6FXK0	Cadherin domain-containing protein	1	P1824
tr|A0A8B6FY22|A0A8B6FY22_MYTGA	A0A8B6FY22	DNA replication licensing factor MCM5 (Fragment)	1	P1825
tr|A0A8B6FYB5|A0A8B6FYB5_MYTGA	A0A8B6FYB5	Small ribosomal subunit protein mS29	1	P1826
tr|A0A8B6FYC5|A0A8B6FYC5_MYTGA	A0A8B6FYC5	Inositol polyphosphate 5-phosphatase INPP5B/F	1	P1827
tr|A0A8B6FYQ7|A0A8B6FYQ7_MYTGA	A0A8B6FYQ7	alpha-L-fucosidase	1	P1828
tr|A0A8B6FYR2|A0A8B6FYR2_MYTGA	A0A8B6FYR2	H15 domain-containing protein	1	P1829
tr|A0A8B6FZD3|A0A8B6FZD3_MYTGA	A0A8B6FZD3	non-specific serine/threonine protein kinase	1	P1830
tr|A0A8B6FZI9|A0A8B6FZI9_MYTGA	A0A8B6FZI9	E2 ubiquitin-conjugating enzyme	1	P1831
tr|A0A8B6FZN2|A0A8B6FZN2_MYTGA	A0A8B6FZN2	Transportin-1	1	P1832

Protein	Uniprot accession	Protein Name	Number Peptides	P
tr|A0A8B6FZP6|A0A8B6FZP6_MYTGA	A0A8B6FZP6	Ras-related protein Rab-3C (Fragment)	1	P1833
tr|A0A8B6G050|A0A8B6G050_MYTGA	A0A8B6G050	EF-hand domain-containing protein (Fragment)	1	P1834
tr|A0A8B6G054|A0A8B6G054_MYTGA	A0A8B6G054	Glycogen [starch] synthase	1	P1835
tr|A0A8B6G0M5|A0A8B6G0M5_MYTGA	A0A8B6G0M5	Peptidase A2 domain-containing protein	1	P1836
tr|A0A8B6G0R1|A0A8B6G0R1_MYTGA	A0A8B6G0R1	Peptidase M16 N-terminal domain-containing protein	1	P1837
tr|A0A8B6G0Y1|A0A8B6G0Y1_MYTGA	A0A8B6G0Y1	ATP-dependent RNA helicase (Fragment)	1	P1838
tr|A0A8B6G142|A0A8B6G142_MYTGA	A0A8B6G142	Choline dehydrogenase	1	P1839
tr|A0A8B6G181|A0A8B6G181_MYTGA	A0A8B6G181	Proteasome subunit beta	1	P1840
tr|A0A8B6G210|A0A8B6G210_MYTGA	A0A8B6G210	Kindlin 2	1	P1841
tr|A0A8B6G3G3|A0A8B6G3G3_MYTGA	A0A8B6G3G3	Golgi integral membrane protein 4	1	P1842
tr|A0A8B6G424|A0A8B6G424_MYTGA	A0A8B6G424	Splicing factor, proline- and glutamine-rich	1	P1843
tr|A0A8B6G4D1|A0A8B6G4D1_MYTGA	A0A8B6G4D1	Translocon-associated protein subunit gamma	1	P1844
tr|A0A8B6G4H9|A0A8B6G4H9_MYTGA	A0A8B6G4H9	Ras-related protein R-Ras2	1	P1845
tr|A0A8B6G4K0|A0A8B6G4K0_MYTGA	A0A8B6G4K0	Low molecular weight phosphotyrosine protein phosphatas	1	P1846
tr|A0A8B6G5C9|A0A8B6G5C9_MYTGA	A0A8B6G5C9	FK506-binding protein 4/5	1	P1847
tr|A0A8B6G5G8|A0A8B6G5G8_MYTGA	A0A8B6G5G8	Large ribosomal subunit protein uL15	1	P1848
tr|A0A8B6G5Q9|A0A8B6G5Q9_MYTGA	A0A8B6G5Q9	DUF4795 domain-containing protein	1	P1849
tr|A0A8B6G713|A0A8B6G713_MYTGA	A0A8B6G713	Uncharacterized protein	1	P1850
tr|A0A8B6G756|A0A8B6G756_MYTGA	A0A8B6G756	Large ribosomal subunit protein eL14	1	P1851
tr|A0A8B6G777|A0A8B6G777_MYTGA	A0A8B6G777	Chitinase	1	P1852
tr|A0A8B6G7A8|A0A8B6G7A8_MYTGA	A0A8B6G7A8	EF-hand domain-containing protein	1	P1853
tr|A0A8B6G7C8|A0A8B6G7C8_MYTGA	A0A8B6G7C8	DUF4201 domain-containing protein	1	P1854
tr|A0A8B6G7D2|A0A8B6G7D2_MYTGA	A0A8B6G7D2	V-type proton ATPase subunit	1	P1855
tr|A0A8B6G7G7|A0A8B6G7G7_MYTGA	A0A8B6G7G7	Fragile X mental retardation protein	1	P1856
tr|A0A8B6G7X6|A0A8B6G7X6_MYTGA	A0A8B6G7X6	Dynein heavy chain, axonemal	1	P1857
tr|A0A8B6G851|A0A8B6G851_MYTGA	A0A8B6G851	Saccharopine dehydrogenase-like C-terminal domain-contai	1	P1858
tr|A0A8B6G8H6|A0A8B6G8H6_MYTGA	A0A8B6G8H6	Large ribosomal subunit protein eL31	1	P1859
tr|A0A8B6G8K4|A0A8B6G8K4_MYTGA	A0A8B6G8K4	aldehyde dehydrogenase (NAD(+))	1	P1860
tr|A0A8B6G8Y8|A0A8B6G8Y8_MYTGA	A0A8B6G8Y8	Uncharacterized protein	1	P1861
tr|A0A8B6G918|A0A8B6G918_MYTGA	A0A8B6G918	Mitochondrial cytochrome c oxidase subunit VIc/VIIs domai	1	P1862
tr|A0A8B6G980|A0A8B6G980_MYTGA	A0A8B6G980	Uncharacterized protein	1	P1863
tr|A0A8B6G9Y3|A0A8B6G9Y3_MYTGA	A0A8B6G9Y3	Uncharacterized protein	1	P1864
tr|A0A8B6GA24|A0A8B6GA24_MYTGA	A0A8B6GA24	Cilia- and flagella-associated protein 206	1	P1865
tr|A0A8B6GAC4|A0A8B6GAC4_MYTGA	A0A8B6GAC4	Dynein axonemal heavy chain	1	P1866
tr|A0A8B6GAM7|A0A8B6GAM7_MYTGA	A0A8B6GAM7	Pre-mRNA-processing factor 6	1	P1867
tr|A0A8B6GAN1|A0A8B6GAN1_MYTGA	A0A8B6GAN1	Dedicator of cytokinesis protein 1 (Fragment)	1	P1868
tr|A0A8B6GAR0|A0A8B6GAR0_MYTGA	A0A8B6GAR0	Far upstream element-binding protein	1	P1869
tr|A0A8B6GAX5|A0A8B6GAX5_MYTGA	A0A8B6GAX5	Nuclear pore complex protein Nup37	1	P1870
tr|A0A8B6GB01|A0A8B6GB01_MYTGA	A0A8B6GB01	Protein crumbs	1	P1871
tr|A0A8B6GBB8|A0A8B6GBB8_MYTGA	A0A8B6GBB8	Uncharacterized protein	1	P1872
tr|A0A8B6GBE6|A0A8B6GBE6_MYTGA	A0A8B6GBE6	ATP synthase-coupling factor 6, mitochondrial (Fragment)	1	P1873
tr|A0A8B6GBJ7|A0A8B6GBJ7_MYTGA	A0A8B6GBJ7	Malate dehydrogenase, mitochondrial	1	P1874
tr|A0A8B6GBM4|A0A8B6GBM4_MYTGA	A0A8B6GBM4	DnaJ homolog subfamily C member 17	1	P1875
tr|A0A8B6GBT4|A0A8B6GBT4_MYTGA	A0A8B6GBT4	E3 ubiquitin-protein ligase UBR4	1	P1876
tr|A0A8B6GC89|A0A8B6GC89_MYTGA	A0A8B6GC89	Uncharacterized protein	1	P1877
tr|A0A8B6GCA5|A0A8B6GCA5_MYTGA	A0A8B6GCA5	Translocon-associated protein subunit delta	1	P1878
tr|A0A8B6GCT4|A0A8B6GCT4_MYTGA	A0A8B6GCT4	Uncharacterized protein	1	P1879
tr|A0A8B6GCU5|A0A8B6GCU5_MYTGA	A0A8B6GCU5	Kynurenine 3-monooxygenase	1	P1880
tr|A0A8B6GD57|A0A8B6GD57_MYTGA	A0A8B6GD57	Hydrocephalus-inducing protein	1	P1881
tr|A0A8B6GD66|A0A8B6GD66_MYTGA	A0A8B6GD66	Ferritin	1	P1882
tr|A0A8B6GD99|A0A8B6GD99_MYTGA	A0A8B6GD99	Intraflagellar transport protein 74	1	P1883
tr|A0A8B6GEG5|A0A8B6GEG5_MYTGA	A0A8B6GEG5	Prostaglandin-H2 D-isomerase / glutathione transferase	1	P1884
tr|A0A8B6GEP1|A0A8B6GEP1_MYTGA	A0A8B6GEP1	EF-hand domain-containing protein	1	P1885
tr|A0A8B6GF37|A0A8B6GF37_MYTGA	A0A8B6GF37	TBC1 domain family member 9 (Fragment)	1	P1886
tr|A0A8B6GFC4|A0A8B6GFC4_MYTGA	A0A8B6GFC4	EGF-like domain-containing protein	1	P1887
tr|A0A8B6GG04|A0A8B6GG04_MYTGA	A0A8B6GG04	alpha-L-fucosidase	1	P1888
tr|A0A8B6GG94|A0A8B6GG94_MYTGA	A0A8B6GG94	Diazepam-binding inhibitor (GABA receptor modulator, acyl	1	P1889
tr|A0A8B6GGM7|A0A8B6GGM7_MYTGA	A0A8B6GGM7	Uncharacterized protein	1	P1890
tr|A0A8B6GGQ7|A0A8B6GGQ7_MYTGA	A0A8B6GGQ7	Medium-chain specific acyl-CoA dehydrogenase, mitochond	1	P1891
tr|A0A8B6GGW1|A0A8B6GGW1_MYTGA	A0A8B6GGW1	UspA domain-containing protein	1	P1892
tr|A0A8B6GGY4|A0A8B6GGY4_MYTGA	A0A8B6GGY4	Uncharacterized protein	1	P1893
tr|A0A8B6GH05|A0A8B6GH05_MYTGA	A0A8B6GH05	Striatin 1/3/4	1	P1894
tr|A0A8B6GH15|A0A8B6GH15_MYTGA	A0A8B6GH15	Retinol dehydrogenase 13	1	P1895
tr|A0A8B6GH19|A0A8B6GH19_MYTGA	A0A8B6GH19	Acetyl-CoA acyltransferase 1	1	P1896
tr|A0A8B6GH37|A0A8B6GH37_MYTGA	A0A8B6GH37	Vesicle-associated membrane protein 3	1	P1897
tr|A0A8B6GHG8|A0A8B6GHG8_MYTGA	A0A8B6GHG8	RNA-binding protein 39	1	P1898
tr|A0A8B6GHU1|A0A8B6GHU1_MYTGA	A0A8B6GHU1	EF-hand domain-containing protein	1	P1899
tr|A0A8B6GI23|A0A8B6GI23_MYTGA	A0A8B6GI23	Cytosolic Fe-S cluster assembly factor NUBP1 homolog	1	P1900
tr|A0A8B6GI34|A0A8B6GI34_MYTGA	A0A8B6GI34	B-cell receptor CD22	1	P1901
tr|A0A8B6GI86|A0A8B6GI86_MYTGA	A0A8B6GI86	Dynein light chain 1, axonemal	1	P1902
tr|A0A8B6GIJ2|A0A8B6GIJ2_MYTGA	A0A8B6GIJ2	Peroxiredoxin-like 2A	1	P1903
tr|A0A8B6GIT7|A0A8B6GIT7_MYTGA	A0A8B6GIT7	Glycine C-acetyltransferase	1	P1904
tr|A0A8B6GIW5|A0A8B6GIW5_MYTGA	A0A8B6GIW5	Uncharacterized protein	1	P1905
tr|A0A8B6GJA0|A0A8B6GJA0_MYTGA	A0A8B6GJA0	Ion transport domain-containing protein	1	P1906
tr|A0A8B6GJA1|A0A8B6GJA1_MYTGA	A0A8B6GJA1	Prostaglandin reductase 1	1	P1907
tr|A0A8B6GJD7|A0A8B6GJD7_MYTGA	A0A8B6GJD7	Methylmalonyl-CoA/ethylmalonyl-CoA epimerase	1	P1908
tr|A0A8B6GJJ0|A0A8B6GJJ0_MYTGA	A0A8B6GJJ0	Uncharacterized protein	1	P1909
tr|A0A8B6GJL8|A0A8B6GJL8_MYTGA	A0A8B6GJL8	ATP-dependent RNA helicase DDX1	1	P1910
tr|A0A8B6GK80|A0A8B6GK80_MYTGA	A0A8B6GK80	Phosphoinositide phospholipase C	1	P1911
tr|A0A8B6GKB3|A0A8B6GKB3_MYTGA	A0A8B6GKB3	Uroporphyrinogen decarboxylase	1	P1912
tr|A0A8B6GKB9|A0A8B6GKB9_MYTGA	A0A8B6GKB9	receptor protein-tyrosine kinase	1	P1913
tr|A0A8B6GKI2|A0A8B6GKI2_MYTGA	A0A8B6GKI2	Cleavage and polyadenylation specificity factor subunit 6 (Fr	1	P1914
tr|A0A8B6GL53|A0A8B6GL53_MYTGA	A0A8B6GL53	Kinesin-like protein	1	P1915
tr|A0A8B6GLA6|A0A8B6GLA6_MYTGA	A0A8B6GLA6	DNA damage-inducible protein 1	1	P1916
tr|A0A8B6GLG1|A0A8B6GLG1_MYTGA	A0A8B6GLG1	Beta-galactosidase	1	P1917
tr|A0A8B6GLG4|A0A8B6GLG4_MYTGA	A0A8B6GLG4	Prefoldin subunit 1	1	P1918
tr|A0A8B6GLM7|A0A8B6GLM7_MYTGA	A0A8B6GLM7	Semaphorin 6	1	P1919
tr|A0A8B6GM25|A0A8B6GM25_MYTGA	A0A8B6GM25	UspA domain-containing protein	1	P1920
tr|A0A8B6GM46|A0A8B6GM46_MYTGA	A0A8B6GM46	Small subunit ribosomal protein S35	1	P1921
tr|A0A8B6GM47|A0A8B6GM47_MYTGA	A0A8B6GM47	Vacuolar protein sorting-associated protein 13A/C	1	P1922
tr|A0A8B6GM94|A0A8B6GM94_MYTGA	A0A8B6GM94	ATP-dependent DNA helicase 2 subunit 2	1	P1923
tr|A0A8B6GMK6|A0A8B6GMK6_MYTGA	A0A8B6GMK6	EF-hand domain-containing protein (Fragment)	1	P1924
tr|A0A8B6GMW1|A0A8B6GMW1_MYTGA	A0A8B6GMW1	Ras GTPase-activating protein 1	1	P1925
tr|A0A8B6GMW3|A0A8B6GMW3_MYTGA	A0A8B6GMW3	Bromodomain adjacent to zinc finger domain protein 1A (Fr	1	P1926
tr|A0A8B6GN13|A0A8B6GN13_MYTGA	A0A8B6GN13	NADP-dependent oxidoreductase domain-containing protei	1	P1927
tr|A0A8B6GN51|A0A8B6GN51_MYTGA	A0A8B6GN51	NADH dehydrogenase [ubiquinone] 1 alpha subcomplex asse	1	P1928
tr|A0A8B6GNA6|A0A8B6GNA6_MYTGA	A0A8B6GNA6	ubiquitinyl hydrolase 1 (Fragment)	1	P1929
tr|A0A8B6GNF2|A0A8B6GNF2_MYTGA	A0A8B6GNF2	Cell wall hydrolase SleB domain-containing protein	1	P1930
tr|A0A8B6GNI6|A0A8B6GNI6_MYTGA	A0A8B6GNI6	ATP-dependent RNA helicase DOB1	1	P1931
tr|A0A8B6GNQ2|A0A8B6GNQ2_MYTGA	A0A8B6GNQ2	Radixin	1	P1932
tr|A0A8B6GPA0|A0A8B6GPA0_MYTGA	A0A8B6GPA0	Uncharacterized protein	1	P1933
tr|A0A8B6GPC3|A0A8B6GPC3_MYTGA	A0A8B6GPC3	SHSP domain-containing protein	1	P1934
tr|A0A8B6GPI6|A0A8B6GPI6_MYTGA	A0A8B6GPI6	Vesicle transport protein	1	P1935
tr|A0A8B6GPL4|A0A8B6GPL4_MYTGA	A0A8B6GPL4	c-Myc-binding protein	1	P1936
tr|A0A8B6GPT2|A0A8B6GPT2_MYTGA	A0A8B6GPT2	UBX domain-containing protein 1	1	P1937
tr|A0A8B6GRB0|A0A8B6GRB0_MYTGA	A0A8B6GRB0	Uncharacterized protein (Fragment)	1	P1938
tr|A0A8B6GRB2|A0A8B6GRB2_MYTGA	A0A8B6GRB2	Galectin	1	P1939
tr|A0A8B6GRE2|A0A8B6GRE2_MYTGA	A0A8B6GRE2	WD repeat and coiled-coil-containing protein	1	P1940
tr|A0A8B6GRI0|A0A8B6GRI0_MYTGA	A0A8B6GRI0	TOM1-like protein 2	1	P1941
tr|A0A8B6GRL5|A0A8B6GRL5_MYTGA	A0A8B6GRL5	Intraflagellar transport protein 172 (Fragment)	1	P1942
tr|A0A8B6GRW0|A0A8B6GRW0_MYTGA	A0A8B6GRW0	L-fuconate dehydratase	1	P1943
tr|A0A8B6GRZ3|A0A8B6GRZ3_MYTGA	A0A8B6GRZ3	Chaperonin GroES	1	P1944
tr|A0A8B6GS47|A0A8B6GS47_MYTGA	A0A8B6GS47	Dehydrogenase/reductase SDR family member 7	1	P1945
tr|A0A8B6GS64|A0A8B6GS64_MYTGA	A0A8B6GS64	WD repeat-containing protein 61	1	P1946
tr|A0A8B6GS71|A0A8B6GS71_MYTGA	A0A8B6GS71	Ca2+ transporting ATPase, plasma membrane	1	P1947
tr|A0A8B6GS96|A0A8B6GS96_MYTGA	A0A8B6GS96	Ciliary-associated calcium-binding coiled-coil protein 1	1	P1948
tr|A0A8B6GSS3|A0A8B6GSS3_MYTGA	A0A8B6GSS3	tRNA (Cytosine34-C5)-methyltransferase	1	P1949

Protein	Uniprot accession	Protein Name	Number Peptides	P
tr|A0A8B6GT04|A0A8B6GT04_MYTGA	A0A8B6GT04	AP-3 complex subunit delta	1	P1950
tr|A0A8B6GT15|A0A8B6GT15_MYTGA	A0A8B6GT15	Sm protein G	1	P1951
tr|A0A8B6GT63|A0A8B6GT63_MYTGA	A0A8B6GT63	tRNA (Cytosine34-C5)-methyltransferase	1	P1952
tr|A0A8B6GTN1|A0A8B6GTN1_MYTGA	A0A8B6GTN1	Phenazine biosynthesis-like domain-containing protein	1	P1953
tr|A0A8B6GTQ2|A0A8B6GTQ2_MYTGA	A0A8B6GTQ2	UV excision repair protein RAD23	1	P1954
tr|A0A8B6GTU9|A0A8B6GTU9_MYTGA	A0A8B6GTU9	Lysine-specific histone demethylase 1A	1	P1955
tr|A0A8B6GU25|A0A8B6GU25_MYTGA	A0A8B6GU25	HMG box domain-containing protein	1	P1956
tr|A0A8B6GU63|A0A8B6GU63_MYTGA	A0A8B6GU63	Cytosolic nonspecific dipeptidase	1	P1957
tr|A0A8B6GUK5|A0A8B6GUK5_MYTGA	A0A8B6GUK5	Glycoside hydrolase family 13 N-terminal domain-containin	1	P1958
tr|A0A8B6GUR0|A0A8B6GUR0_MYTGA	A0A8B6GUR0	Uncharacterized protein	1	P1959
tr|A0A8B6GUW4|A0A8B6GUW4_MYTGA	A0A8B6GUW4	MICOS complex subunit MIC13	1	P1960
tr|A0A8B6GV50|A0A8B6GV50_MYTGA	A0A8B6GV50	Enoyl reductase (ER) domain-containing protein	1	P1961
tr|A0A8B6GV58|A0A8B6GV58_MYTGA	A0A8B6GV58	non-specific serine/threonine protein kinase	1	P1962
tr|A0A8B6GVJ2|A0A8B6GVJ2_MYTGA	A0A8B6GVJ2	cathepsin X	1	P1963
tr|A0A8B6GVN1|A0A8B6GVN1_MYTGA	A0A8B6GVN1	Malate dehydrogenase	1	P1964
tr|A0A8B6GVP9|A0A8B6GVP9_MYTGA	A0A8B6GVP9	GMP synthase (Glutamine-hydrolysing)	1	P1965
tr|A0A8B6GVV3|A0A8B6GVV3_MYTGA	A0A8B6GVV3	Vacuolar protein sorting-associated protein 13A/C	1	P1966
tr|A0A8B6GWB0|A0A8B6GWB0_MYTGA	A0A8B6GWB0	arginine--tRNA ligase	1	P1967
tr|A0A8B6GWH0|A0A8B6GWH0_MYTGA	A0A8B6GWH0	VWFA domain-containing protein	1	P1968
tr|A0A8B6GX31|A0A8B6GX31_MYTGA	A0A8B6GX31	Lysosomal acid lipase/cholesteryl ester hydrolase	1	P1969
tr|A0A8B6GX76|A0A8B6GX76_MYTGA	A0A8B6GX76	NAD(P)H oxidase (H2O2-forming)	1	P1970
tr|A0A8B6GXC9|A0A8B6GXC9_MYTGA	A0A8B6GXC9	Uncharacterized protein	1	P1971
tr|A0A8B6GXF7|A0A8B6GXF7_MYTGA	A0A8B6GXF7	Renalase	1	P1972
tr|A0A8B6GYG8|A0A8B6GYG8_MYTGA	A0A8B6GYG8	Mitochondrial proton/calcium exchanger protein	1	P1973
tr|A0A8B6GYR0|A0A8B6GYR0_MYTGA	A0A8B6GYR0	Actin (Fragment)	1	P1974
tr|A0A8B6GZ56|A0A8B6GZ56_MYTGA	A0A8B6GZ56	Kynurenine formamidase	1	P1975
tr|A0A8B6GZ88|A0A8B6GZ88_MYTGA	A0A8B6GZ88	Actin beta/gamma 1	1	P1976
tr|A0A8B6GZN9|A0A8B6GZN9_MYTGA	A0A8B6GZN9	Eukaryotic translation initiation factor 4 gamma 2	1	P1977
tr|A0A8B6GZR7|A0A8B6GZR7_MYTGA	A0A8B6GZR7	Ficolin	1	P1978
tr|A0A8B6GZR8|A0A8B6GZR8_MYTGA	A0A8B6GZR8	mannose-6-phosphate isomerase	1	P1979
tr|A0A8B6H023|A0A8B6H023_MYTGA	A0A8B6H023	Fumarate hydratase, class II	1	P1980
tr|A0A8B6H0D6|A0A8B6H0D6_MYTGA	A0A8B6H0D6	Vacuolar protein sorting-associated protein 29	1	P1981
tr|A0A8B6H0E9|A0A8B6H0E9_MYTGA	A0A8B6H0E9	UPAR/Ly6 domain-containing protein (Fragment)	1	P1982
tr|A0A8B6H0M5|A0A8B6H0M5_MYTGA	A0A8B6H0M5	EF-hand domain-containing protein	1	P1983
tr|A0A8B6H0Q4|A0A8B6H0Q4_MYTGA	A0A8B6H0Q4	Small ribosomal subunit protein uS19	1	P1984
tr|A0A8B6H0R3|A0A8B6H0R3_MYTGA	A0A8B6H0R3	Methyltransferase domain-containing protein	1	P1985
tr|A0A8B6H114|A0A8B6H114_MYTGA	A0A8B6H114	Uncharacterized protein	1	P1986
tr|A0A8B6H139|A0A8B6H139_MYTGA	A0A8B6H139	Hexosyltransferase	1	P1987
tr|A0A8B6H151|A0A8B6H151_MYTGA	A0A8B6H151	Death-associated protein 1	1	P1988
tr|A0A8B6H1G0|A0A8B6H1G0_MYTGA	A0A8B6H1G0	WD40 repeat-containing protein SMU1	1	P1989
tr|A0A8B6H1K1|A0A8B6H1K1_MYTGA	A0A8B6H1K1	High mobility group protein B1	1	P1990
tr|A0A8B6H1Y6|A0A8B6H1Y6_MYTGA	A0A8B6H1Y6	C-terminal binding protein	1	P1991
tr|A0A8B6H2G9|A0A8B6H2G9_MYTGA	A0A8B6H2G9	Tetraspanin-18	1	P1992
tr|A0A8B6H2K2|A0A8B6H2K2_MYTGA	A0A8B6H2K2	Major facilitator superfamily associated domain-containing	1	P1993
tr|A0A8B6H2N7|A0A8B6H2N7_MYTGA	A0A8B6H2N7	Pre-mRNA-splicing factor CWC22	1	P1994
tr|A0A8B6H2P4|A0A8B6H2P4_MYTGA	A0A8B6H2P4	Charged multivesicular body protein 2a	1	P1995
tr|A0A8B6H2R0|A0A8B6H2R0_MYTGA	A0A8B6H2R0	Xaa-Pro dipeptidase	1	P1996
tr|A0A8B6H354|A0A8B6H354_MYTGA	A0A8B6H354	TPM domain-containing protein	1	P1997
tr|A0A8B6H362|A0A8B6H362_MYTGA	A0A8B6H362	Diaphanous 2	1	P1998
tr|A0A8B6H3F7|A0A8B6H3F7_MYTGA	A0A8B6H3F7	Metalloendopeptidase	1	P1999
tr|A0A8B6H3T7|A0A8B6H3T7_MYTGA	A0A8B6H3T7	Pre-mRNA-splicing factor CWC22	1	P2000
tr|A0A8B6H4P9|A0A8B6H4P9_MYTGA	A0A8B6H4P9	Mitochondrial import inner membrane translocase subunit	1	P2001
tr|A0A8B6H4R2|A0A8B6H4R2_MYTGA	A0A8B6H4R2	Enoyl-CoA hydratase	1	P2002
tr|A0A8B6H4V6|A0A8B6H4V6_MYTGA	A0A8B6H4V6	Granulins domain-containing protein	1	P2003
tr|A0A8B6H500|A0A8B6H500_MYTGA	A0A8B6H500	Uncharacterized protein	1	P2004
tr|A0A8B6H503|A0A8B6H503_MYTGA	A0A8B6H503	Flotillin-1 (Fragment)	1	P2005
tr|A0A8B6H5B8|A0A8B6H5B8_MYTGA	A0A8B6H5B8	Plasminogen receptor (KT)	1	P2006
tr|A0A8B6H5C3|A0A8B6H5C3_MYTGA	A0A8B6H5C3	Tubulin alpha chain	1	P2007
tr|A0A8B6H5L2|A0A8B6H5L2_MYTGA	A0A8B6H5L2	Major vault protein	1	P2008
tr|A0A8B6H5M0|A0A8B6H5M0_MYTGA	A0A8B6H5M0	GB1/RHD3-type G domain-containing protein	1	P2009
tr|A0A8B6H5P5|A0A8B6H5P5_MYTGA	A0A8B6H5P5	Dynein axonemal intermediate chain 4	1	P2010
tr|A0A8B6H5V4|A0A8B6H5V4_MYTGA	A0A8B6H5V4	Superoxide dismutase, Cu-Zn family	1	P2011
tr|A0A8B6H6L8|A0A8B6H6L8_MYTGA	A0A8B6H6L8	Uncharacterized protein	1	P2012
tr|A0A8B6H759|A0A8B6H759_MYTGA	A0A8B6H759	Ubiquitin-like 1-activating enzyme E1 A	1	P2013
tr|A0A8B6H771|A0A8B6H771_MYTGA	A0A8B6H771	C-type lectin domain-containing protein	1	P2014
tr|A0A8B6H792|A0A8B6H792_MYTGA	A0A8B6H792	Uncharacterized protein	1	P2015
tr|A0A8B6H7K9|A0A8B6H7K9_MYTGA	A0A8B6H7K9	RRM domain-containing protein	1	P2016
tr|A0A8B6H7L8|A0A8B6H7L8_MYTGA	A0A8B6H7L8	PFL domain-containing protein	1	P2017
tr|A0A8B6H7P5|A0A8B6H7P5_MYTGA	A0A8B6H7P5	Tubulin alpha chain	1	P2018
tr|A0A8B6H7R3|A0A8B6H7R3_MYTGA	A0A8B6H7R3	Serpin B	1	P2019
tr|A0A8B6H831|A0A8B6H831_MYTGA	A0A8B6H831	VPS35 endosomal protein-sorting factor-like	1	P2020
tr|A0A8B6H837|A0A8B6H837_MYTGA	A0A8B6H837	Uncharacterized protein	1	P2021
tr|A0A8B6H8M2|A0A8B6H8M2_MYTGA	A0A8B6H8M2	Sulfide:quinone oxidoreductase	1	P2022
tr|A0A8B6H8N6|A0A8B6H8N6_MYTGA	A0A8B6H8N6	Asparaginyl-tRNA synthetase	1	P2023
tr|A0A8B6H8P4|A0A8B6H8P4_MYTGA	A0A8B6H8P4	3-methylcrotonyl-CoA carboxylase beta subunit	1	P2024
tr|A0A8B6H8T4|A0A8B6H8T4_MYTGA	A0A8B6H8T4	Enolase 4	1	P2025
tr|A0A8B6H944|A0A8B6H944_MYTGA	A0A8B6H944	6-phosphofructokinase	1	P2026
tr|A0A8B6H945|A0A8B6H945_MYTGA	A0A8B6H945	Uncharacterized protein	1	P2027
tr|A0A8B6H982|A0A8B6H982_MYTGA	A0A8B6H982	Cullin 1	1	P2028
tr|A0A8B6H9B9|A0A8B6H9B9_MYTGA	A0A8B6H9B9	Troponin T, fast skeletal muscle	1	P2029
tr|A0A8B6H9D1|A0A8B6H9D1_MYTGA	A0A8B6H9D1	Low-density lipoprotein receptor-related protein 4	1	P2030
tr|A0A8B6H9Z8|A0A8B6H9Z8_MYTGA	A0A8B6H9Z8	Tensin	1	P2031
tr|A0A8B6HA03|A0A8B6HA03_MYTGA	A0A8B6HA03	Sulfide:quinone oxidoreductase	1	P2032
tr|A0A8B6HA48|A0A8B6HA48_MYTGA	A0A8B6HA48	C2 domain-containing protein	1	P2033
tr|A0A8B6HAG3|A0A8B6HAG3_MYTGA	A0A8B6HAG3	Caspase-3	1	P2034
tr|A0A8B6HAL9|A0A8B6HAL9_MYTGA	A0A8B6HAL9	Exportin-1/Importin-beta-like domain-containing protein	1	P2035
tr|A0A8B6HAR2|A0A8B6HAR2_MYTGA	A0A8B6HAR2	SH3 domain-containing protein	1	P2036
tr|A0A8B6HAT1|A0A8B6HAT1_MYTGA	A0A8B6HAT1	Amidohydrolase-related domain-containing protein	1	P2037
tr|A0A8B6HB26|A0A8B6HB26_MYTGA	A0A8B6HB26	Uncharacterized protein	1	P2038
tr|A0A8B6HBE5|A0A8B6HBE5_MYTGA	A0A8B6HBE5	UBX domain-containing protein	1	P2039
tr|A0A8B6HBX0|A0A8B6HBX0_MYTGA	A0A8B6HBX0	beta-N-acetylhexosaminidase	1	P2040
tr|A0A8B6HBX2|A0A8B6HBX2_MYTGA	A0A8B6HBX2	Lysosomal acid phosphatase	1	P2041
tr|A0A8B6HBZ2|A0A8B6HBZ2_MYTGA	A0A8B6HBZ2	Mannose receptor, C type	1	P2042
tr|A0A8B6HC44|A0A8B6HC44_MYTGA	A0A8B6HC44	Receptor ligand binding region domain-containing protein	1	P2043
tr|A0A8B6HCK0|A0A8B6HCK0_MYTGA	A0A8B6HCK0	CLIP-associating protein 1/2	1	P2044
tr|A0A8B6HCM2|A0A8B6HCM2_MYTGA	A0A8B6HCM2	Glutamate--cysteine ligase	1	P2045
tr|A0A8B6HD51|A0A8B6HD51_MYTGA	A0A8B6HD51	Kynurenine formamidase	1	P2046
tr|A0A8B6HDD1|A0A8B6HDD1_MYTGA	A0A8B6HDD1	Adenylyl cyclase-associated protein	1	P2047
tr|A0A8B6HDI0|A0A8B6HDI0_MYTGA	A0A8B6HDI0	Replication factor C subunit 2/4	1	P2048
tr|A0A8B6HDJ1|A0A8B6HDJ1_MYTGA	A0A8B6HDJ1	Aubergine	1	P2049
tr|A0A8B6HDV0|A0A8B6HDV0_MYTGA	A0A8B6HDV0	Oxysterol-binding protein 2	1	P2050
tr|A0A8B6HDV2|A0A8B6HDV2_MYTGA	A0A8B6HDV2	Arylsulfatase B	1	P2051
tr|A0A8B6HE47|A0A8B6HE47_MYTGA	A0A8B6HE47	Protein dpy-30 homolog	1	P2052
tr|A0A8B6HE67|A0A8B6HE67_MYTGA	A0A8B6HE67	Cleavage stimulation factor 50 kDa subunit	1	P2053
tr|A0A8B6HEF8|A0A8B6HEF8_MYTGA	A0A8B6HEF8	Protein DJ-1 (Fragment)	1	P2054
tr|A0A8B6HEG2|A0A8B6HEG2_MYTGA	A0A8B6HEG2	Poly [ADP-ribose] polymerase (Fragment)	1	P2055
tr|A0A8B6HEI8|A0A8B6HEI8_MYTGA	A0A8B6HEI8	Mitochondrial import receptor subunit TOM22 homolog	1	P2056
tr|A0A8B6HEL4|A0A8B6HEL4_MYTGA	A0A8B6HEL4	Regucalcin	1	P2057
tr|A0A8B6HEV7|A0A8B6HEV7_MYTGA	A0A8B6HEV7	Cysteine and glycine-rich protein	1	P2058
tr|A0A8B6HFG7|A0A8B6HFG7_MYTGA	A0A8B6HFG7	DNA mismatch repair protein	1	P2059
tr|A0A8B6HFP1|A0A8B6HFP1_MYTGA	A0A8B6HFP1	Actin-related protein 3	1	P2060
tr|A0A8B6HFT0|A0A8B6HFT0_MYTGA	A0A8B6HFT0	Inositol-1-monophosphatase (Fragment)	1	P2061
tr|A0A8B6HG48|A0A8B6HG48_MYTGA	A0A8B6HG48	Uncharacterized protein	1	P2062
tr|A0A8B6HGJ1|A0A8B6HGJ1_MYTGA	A0A8B6HGJ1	Coiled-coil-helix-coiled-coil-helix domain-containing protei	1	P2063
tr|A0A8B6HGP7|A0A8B6HGP7_MYTGA	A0A8B6HGP7	non-specific serine/threonine protein kinase	1	P2064
tr|A0A8B6HGZ8|A0A8B6HGZ8_MYTGA	A0A8B6HGZ8	Cilia-and flagella-associated protein 44 (Fragment)	1	P2065
tr|A0A8B6HH78|A0A8B6HH78_MYTGA	A0A8B6HH78	non-specific serine/threonine protein kinase	1	P2066

Protein	Uniprot accession	Protein Name	Number Peptides	P
tr|A0A8B6HH93|A0A8B6HH93_MYTGA	A0A8B6HH93	Uncharacterized protein (Fragment)	1	P2067
tr|A0A8B6HHF5|A0A8B6HHF5_MYTGA	A0A8B6HHF5	RNA helicase	1	P2068
tr|A0A8B6HHL6|A0A8B6HHL6_MYTGA	A0A8B6HHL6	Uncharacterized protein	1	P2069
tr|A0A8B6HHS6|A0A8B6HHS6_MYTGA	A0A8B6HHS6	C1q domain-containing protein	1	P2070
tr|A0A8B6HHU2|A0A8B6HHU2_MYTGA	A0A8B6HHU2	Splicing factor 3B subunit 3 (Fragment)	1	P2071
tr|A0A8B6HIA5|A0A8B6HIA5_MYTGA	A0A8B6HIA5	inositol-1,4-bisphosphate 1-phosphatase (Fragment)	1	P2072
tr|A0A8B6HIK5|A0A8B6HIK5_MYTGA	A0A8B6HIK5	Uncharacterized protein	1	P2073
tr|A0A8B6HIW0|A0A8B6HIW0_MYTGA	A0A8B6HIW0	Uncharacterized protein	1	P2074
tr|A0A8B6HJ30|A0A8B6HJ30_MYTGA	A0A8B6HJ30	SAP domain-containing ribonucleoprotein	1	P2075
tr|A0A8B6HJW7|A0A8B6HJW7_MYTGA	A0A8B6HJW7	3-hydroxybutyrate dehydrogenase	1	P2076
tr|A0A8B6HJY0|A0A8B6HJY0_MYTGA	A0A8B6HJY0	Cilia- and flagella-associated protein 126	1	P2077
tr|A0A8B6HK49|A0A8B6HK49_MYTGA	A0A8B6HK49	Protein kinase domain-containing protein	1	P2078
tr|A0A8B6HK58|A0A8B6HK58_MYTGA	A0A8B6HK58	Proteasome component ECM29 (Fragment)	1	P2079
tr|A0A8B6HKE5|A0A8B6HKE5_MYTGA	A0A8B6HKE5	Succinate dehydrogenase (Ubiquinone) cytochrome b560 su	1	P2080
tr|A0A8B6HKH5|A0A8B6HKH5_MYTGA	A0A8B6HKH5	UDPglucose 6-dehydrogenase (Fragment)	1	P2081
tr|A0A8B6HKT9|A0A8B6HKT9_MYTGA	A0A8B6HKT9	Nidogen (Entactin) (Fragment)	1	P2082
tr|A0A8B6HKX6|A0A8B6HKX6_MYTGA	A0A8B6HKX6	Annexin	1	P2083
tr|A0A8B6HLT9|A0A8B6HLT9_MYTGA	A0A8B6HLT9	U2 small nuclear ribonucleoprotein A	1	P2084
tr|A0A8B6HMM4|A0A8B6HMM4_MYTGA	A0A8B6HMM4	alpha-L-fucosidase	1	P2085
tr|A0A8B6HMQ1|A0A8B6HMQ1_MYTGA	A0A8B6HMQ1	Small subunit ribosomal protein S34	1	P2086
tr|A0A8B6HN84|A0A8B6HN84_MYTGA	A0A8B6HN84	DUF4200 domain-containing protein	1	P2087
tr|A0A8B6HNH4|A0A8B6HNH4_MYTGA	A0A8B6HNH4	Superoxide dismutase [Cu-Zn]	1	P2088
tr|A0A8B6HNS1|A0A8B6HNS1_MYTGA	A0A8B6HNS1	Aminopeptidase	1	P2089
tr|A0A8B6HNX5|A0A8B6HNX5_MYTGA	A0A8B6HNX5	Pre-mRNA-processing factor 39	1	P2090
tr|A0A8B6HP98|A0A8B6HP98_MYTGA	A0A8B6HP98	Solute carrier family 5 (Sodium/glucose cotransporter), mem	1	P2091
tr|A0A8B6HPS1|A0A8B6HPS1_MYTGA	A0A8B6HPS1	molybdopterin molybdotransferase	1	P2092
tr|A0A8B6HPZ2|A0A8B6HPZ2_MYTGA	A0A8B6HPZ2	Cysteine dioxygenase	1	P2093
tr|A0A8B6HQN1|A0A8B6HQN1_MYTGA	A0A8B6HQN1	3-methylcrotonyl-CoA carboxylase alpha subunit	1	P2094
tr|A0A8B6HQZ9|A0A8B6HQZ9_MYTGA	A0A8B6HQZ9	UBX domain-containing protein 1	1	P2095
tr|A0A8B6HRY8|A0A8B6HRY8_MYTGA	A0A8B6HRY8	Uncharacterized protein	1	P2096
tr|A0A8B6HRZ2|A0A8B6HRZ2_MYTGA	A0A8B6HRZ2	MANSC domain-containing protein	1	P2097
tr|A0A8B6HS14|A0A8B6HS14_MYTGA	A0A8B6HS14	Aubergine	1	P2098
tr|A0A8B6HSE0|A0A8B6HSE0_MYTGA	A0A8B6HSE0	DNA topoisomerase 2-associated protein PAT1	1	P2099
tr|A0A8B6HSQ9|A0A8B6HSQ9_MYTGA	A0A8B6HSQ9	Tyr recombinase domain-containing protein	1	P2100
tr|A0A8B6HSW4|A0A8B6HSW4_MYTGA	A0A8B6HSW4	Kindlin 2	1	P2101
tr|A0A8B6HT34|A0A8B6HT34_MYTGA	A0A8B6HT34	Maleylacetoacetate isomerase	1	P2102
tr|A4UDY5|A4UDY5_MYTGA	A4UDY5	Vitelline coat lysin M7 (Fragment)	1	P2103
tr|A7XP66|A7XP66_MYTGA	A7XP66	Myticin B	1	P2104
tr|B6ZCB0|B6ZCB0_MYTGA	B6ZCB0	Large ribosomal subunit protein P1	1	P2105
tr|E4Z7F7|E4Z7F7_MYTGA	E4Z7F7	Casein kinase II subunit alpha	1	P2106
tr|E4Z7F8|E4Z7F8_MYTGA	E4Z7F8	Casein kinase II subunit beta	1	P2107
tr|E5KXF1|E5KXF1_MYTGA	E5KXF1	Fibrinogen-related protein	1	P2108
tr|E6ZCD4|E6ZCD4_MYTGA	E6ZCD4	Fibrinogen-related protein 2	1	P2109
tr|E6ZCD5|E6ZCD5_MYTGA	E6ZCD5	Fibrinogen-related protein 3	1	P2110
tr|F0V440|F0V440_MYTGA	F0V440	Putative C1q domain containing protein MgC1q3	1	P2111
tr|F0V442|F0V442_MYTGA	F0V442	Putative C1q domain containing protein MgC1q5	1	P2112
tr|F0V452|F0V452_MYTGA	F0V452	Putative C1q domain containing protein MgC1q15	1	P2113
tr|G5D8W4|G5D8W4_MYTGA	G5D8W4	Cytochrome c oxidase subunit 4 (Fragment)	1	P2114
tr|H6BJK1|H6BJK1_MYTGA	H6BJK1	Myticin C	1	P2115
tr|H6BJQ4|H6BJQ4_MYTGA	H6BJQ4	Myticin C	1	P2116
tr|I6TK96|I6TK96_MYTGA	I6TK96	Thiredoxin	1	P2117
tr|Q0H9P8|Q0H9P8_MYTGA	Q0H9P8	Vitelline coat lysin M7 (Fragment)	1	P2118
tr|Q53IQ6|Q53IQ6_MYTGA	Q53IQ6	Heat shock protein 70	1	P2119
tr|Q5F0I9|Q5F0I9_MYTGA	Q5F0I9	ATP synthase subunit a	1	P2120
tr|Q5F0J6|Q5F0J6_MYTGA	Q5F0J6	Cytochrome c oxidase subunit 2	1	P2121
tr|Q5F1M4|Q5F1M4_MYTGA	Q5F1M4	Cytochrome c oxidase subunit 1	1	P2122
tr|Q5F1N0|Q5F1N0_MYTGA	Q5F1N0	Cytochrome c oxidase subunit 2	1	P2123
tr|Q5I2A7|Q5I2A7_MYTGA	Q5I2A7	HSP70	1	P2124
tr|Q9Y0B1|Q9Y0B1_MYTGA	Q9Y0B1	Mytilin B	1	P2125
tr|R4JGL3|R4JGL3_MYTGA	R4JGL3	Bax inhibitor-1 protein	1	P2126
tr|R4JJI2|R4JJI2_MYTGA	R4JJI2	Apoptosis regulator BAX	1	P2127
tr|U3GLV7|U3GLV7_MYTGA	U3GLV7	17 beta-hydroxysteroid dehydrogenase 12	1	P2128